

MicroRNA Analysis of the Invasive Margin of Glioblastoma Reveals Drugable Therapeutic Targets in Lipid Metabolism Pathways

Thesis submitted to the University of Nottingham for the degree of Doctor of Philosophy, July 2019

Huda Alfardus, 14260506

School of Medicine

Supervisors: Dr Stuart Smith, Dr Alan McIntyre, Prof. Richard Grundy

Abstract

Glioblastoma (GBM) is the most common type of adult brain tumour, representing 45.2% of all malignant brain and central nervous system tumours. It is also the most lethal, with a median post-therapy survival of 14 months, due to the high likelihood of tumour recurrence. Intratumour heterogeneity is thought to be a key contributor to GBM tumour recurrence, because treatments such as radiotherapy and chemotherapy typically only successfully target the core of the tumour. Due to its high visibility, this core is excised during surgery, but there is another more subtle region of the tumour, the invasive margin, which generally remains behind. This invasive margin is a mixture between normal brain and highly invasive tumour cells. If left over from surgery, these remaining tumour cells infiltrate the normal brain, and cause recurrence within 2cm of the original site. However, if surgeons are too vigorous in removing the invasive margin, they may cause unnecessary removal of healthy brain tissue, thereby causing other complications. This make developing specific methods to target the cancer cells in the invasive margin a priority area in GBM research.

In order to specifically target the invasive margin, we need to have a way of differentiating it reliably from the other regions. In this thesis, I investigated the role that micro RNAs (miRNAs), a type of small non-coding RNA, play in this intratumour heterogeneity. miRNAs act as post-transcriptional regulators of gene expression and can simultaneously suppress multiple genes within the same pathway, which makes them potentially valuable routes for therapy development.

I performed a miRNA microarray on tissue samples from three tumour regions (tumour core, rim, and invasive margin) and validated the results with qRT-PCR. I then performed computational predictions of gene targets of the differentially expressed miRNAs and validated them in cell lines and patient samples at both the mRNA (qRT-PCR) and protein (Western blot and immunohistochemistry) levels. I then performed a bi-phasic extraction of polar and non-polar metabolites and employed liquid chromatography-mass spectrometry (LC-MS) and tandem mass spectroscopy techniques to profile the intracellular metabolome and lipidome of U87 cells overexpressing miR-619-5p and miR-4793-3p. Transwell

invasion assays were performed to investigate the effect of each miRNA and its target on GBM cell invasion.

In this work, I found that two miRNAs, miR-619-5p and miR-4793-3p, are significantly downregulated in the invasive margin. Moreover, these miRNAs control the expression of genes that are involved in regulating lipid metabolism pathways. A second key finding was that the knockdown or pharmacological inhibition of the miR-619-5p target, CPT2, also significantly reduced the invasion of the cells in the invasive margin. Because CPT2 lies in the lipid metabolism pathway, my findings indicate that lipid metabolism may present a possible vulnerability of the GBM invasive cell population, and the understanding the function of miRNAs in regulating lipid homeostasis in GBM may provide novel avenues for GBM therapy.

Research Outputs

Papers

- **Alfardus** , H., McIntyre, A., Smith, S. "*MicroRNA Regulation of Glycolytic Metabolism in Glioblastoma*", BioMed Research International, vol. 2017, Article ID 9157370, 13 pages, 2017. doi:10.1155/2017/9157370. Available at: https://www.hindawi.com/journals/bmri/2017/9157370

- **Alfardus**, H., Estevez-Cebrero, M., Lourdusamy, A., Rowlinson, J., Grundy, R., McIntyre, A., Smith, S. *The Invasive Region of Glioblastoma Defined by 5-Aminolevulinic Acid Guided Surgery Has an Altered miRNA Expression Profile Compared to Central Tumour* [*Manuscript in Preparation]*

Conference Oral Presentations

- **Society for Neuro-Oncology Annual Meeting (Nov 2018)**

Marriot Hotel, New Orleans, LA, USA

- **British Neuro-Oncology Society Conference (Jul 2018)**

The University of Winchester, Winchester, UK

Conference Poster Presentations

- **The 13th Annual Meeting of the European Association for Neuro-Oncology (Oct 2018)**
  Waterfront Congress Centre, Stockholm, Sweden

- **The British Association for Cancer Research Tumour Microenvironment: Basic Science to Novel Therapies (Jun 2017)**
  Nottingham Conference Centre, Nottingham, UK

- **The 12th Annual Meeting of the European Association for Neuro-Oncology (Oct 2016)**
  Congress Centre Rosengarten, Mannheim, Germany

- **British Neuro-Oncology Society Conference 2016 (Jun 2016)**
  The University of Leeds, Leeds, UK

Acknowledgements

First and foremost, all praise and thanks is due to Allah (God), The Creator and The Sustainer of all the worlds. Without His support and assistance, none of this work would have been possible.

I will forever be indebted to my supervisors, Stuart Smith and Alan McIntyre, for their help, guidance, and tremendous support throughout this process. I am forever grateful to you both, thank you.

This work would not have been completed if it wasn't for the support of key members of the Children's Brain Tumour Research Centre who have always been there when I needed them, including Maria Estevez-Cebrero, Jonathan Rowlinson, Richard Grundy, Rumman Rahman, and Rebecca Chapman.

I'd also like to thank our project collaborators Dong-Hyun Kim, Salah Abdelrazig, and Catherine Ortori.

I'd also like to thank Rumman Khan, Tahsinur Khan, Abu Bakar Umar Bello and Abdulrahman Baki, who provided invaluable support during the stressful final stages -- I will never forget all of your kindnesses, thank you.

Finally, I must express my very profound gratitude to my husband, Ziyad Yehia, for providing me with unfailing support, and continuous encouragement throughout my years of life and through the process of researching and writing this thesis. This accomplishment would not have been possible without you.

Contents

Abstract 2

Research Outputs 5

Acknowledgements 6

Chapter 1: Introduction 32

1.1 Glioblastoma multiforme 33

1.1.1 Incidence 33

1.1.2 Treatment and prognosis 34

1.1.3 Molecular biology 35

1.1.4 Clinical and molecular classifications 38

1.1.5 *In vitro* cell cultures models of GBM 42

1.1.6 *In vivo* pre-clinical models of GBM 45

1.2 Cancer cell invasion 49

1.2.1 Molecular mechanisms of cancer cell invasion .. 50

1.2.2 Molecular regulation of GBM cell invasion 57

1.2.3 Cancer cell invasion strategies 59

1.2.4 Routes of GBM cell invasion 66

1.2.5 Modification of the brain ECM by GBM cells 69

1.2.6 Modification of the perivascular ECM by GBM cells 71

1.2.7 Clinical targeting of GBM cell invasion 75

1.2.8 *In vitro* assays to study GBM invasion 76

1.2.9 *In Vivo* Models to Study GBM Invasion 80

1.2.10 Ex Vivo Models to Study GBM Invasion 81

1.3 Cancer cell metabolic reprogramming 83

1.3.1 Advantages of metabolic reprogramming to cancer cells 83

1.3.2 Reprogrammed metabolic pathways in cancer, with a specific focus on GBM Lipid metabolism 89

1.3.3 Analytical profiling platforms to study cancer metabolism 116

1.3.4 Clinical targeting of cancer cell metabolism 123

1.3.5 Summary 133

1.4 MicroRNAs 135

1.4.1 microRNAs biogenesis and function 135

1.4.2 The role of miRNAs in cancer 138

1.4.3 miRNA regulation of GBM biology 139

1.4.4 miRNA Regulation of Glycolytic Transporters and Enzymes in GBM 149

1.4.5 miRNA Regulation of Glutamine Transporters in GBM 152

1.4.6 miRNA regulation of one-carbon metabolism in GBM 153

1.4.7 miRNA regulation of lipid metabolism in GBM . 155

1.4.8 miRNA regulation of GBM cell invasion 157

1.4.9 miRNAs targeting as a therapeutic approach for GBM. 161

1.5 Intra-tumour heterogeneity in cancer 174

1.5.1 Sources of intra-tumour heterogeneity 174

1.5.2 Genetic and phenotypic intra-tumour heterogeneity in GBM 175

1.5.3 Intra-tumour heterogeneity of cell metabolism in GBM and other cancers..... 178

1.5.4 Intra-tumour heterogeneity in GBM invasion .. 181

1.5.5 Intra-tumour heterogeneity in ECM remodelling by GBM cells..... 181

1.5.6 Intra-tumour heterogeneity in the expression of molecular regulators of GBM invasion 182

1.5.7 Clinical implications of GBM intra-tumour heterogeneity 186

Chapter 2: Materials and Methods 197

2.1 Clinical Samples..... 198

2.1.1 Patient Tissue Collection 198

2.1.2 Patient Cohort for Fluorescence-Activated Cell Sorting (FACS) Analysis 201

2.2 Cell Culture 201

2.2.1 Cell lines 201

2.2.2 Sub-culturing monolayer cells 202

2.2.3 Cell Counting 203

2.2.4 Snap Freezing Cell Pellets 204

2.2.5 Cryopreservation of Cells in Liquid Nitrogen Storage 204

2.2.6 Recovering cells from liquid nitrogen storage . 205

2.3 Gene-based Assays 205

2.3.1 Total RNA isolation 205

2.3.2 Spectrophotometric Analysis 208

2.3.3 miRNA Expression Analysis by microarray..... 209

2.3.4 Expression analysis of miRNAs by quantitative real-time polymerase chain reaction (qRT-PCR) 220

2.3.5 Gene expression analysis in cell line samples . 230

2.3.6 Gene Expression Analysis in Tissue Samples .. 239

2.4 Cell-based Assays 242

2.4.1 PrestoBlue Viability Assay 242

2.4.2 Transfection of GBM Cells with Small RNAs 243

2.4.3 Luciferase Assay 250

2.4.4 Pharmacological CPT2 Inhibitors Treatment ... 260

2.4.5 Nile Red 263

2.4.6 Transwell assay 264

2.5 Protein-based assays 265

2.5.1 Western Blotting 265

2.5.2 Immunohistochemical Analysis 271

2.6 Metabolomics and Lipidomics Analysis 276

2.6.1 Cells growth curve 276

2.6.2 Metabolites Extraction 276

2.6.3 Sample Preparation for LC-MS 277

2.6.4 LC-MS profiling of polar and non-polar metabolites 278

2.6.5 LC-MS profiling of non-polar metabolites 279

2.6.6 Pre-processing of LC-MS data 281

2.6.7 Statistical Analysis of LC-MS data 283

2.6.8 Clustering of LC-MS data 283

2.6.9 Metabolites identification and pathway analysis 284

Chapter 3: Evaluation of Intra-Tumour Heterogeneity of miRNA Expression in GBM 286

3.1 Introduction 287

3.2 Results 291

3.2.1 RNA yield and quality 291

3.2.2 miRNA microarray analysis 306

3.2.3 Molecular validation of GBM intra-tumour heterogeneity through qRT-PCR 316

3.2.4 Selection of miRNAs to be taken forward for functional analysis 335

3.2.5 miRNA expression in primary and commercial cell lines, according to microarray and qRT-PCR. 336

3.3 Discussion 340

3.4 Future work 345

3.5 Chapter Summary 345

Chapter 4: Evaluation of miR-619-5p and miR4793-3p gene targets in GBM 348

4.1 Introduction 349

4.2 Results 356

4.2.1 Optimisation of miRNA transient transfection conditions in a commercial GBM cell line 356

4.2.2 Evaluation of miRNA transient transfection conditions in a patient-derived primary GBM cell line... 364

4.2.3 Computational target prediction and pathway analysis 365

4.2.4 Validation of putative miR-619-5p and miR-4793-3p targets in U87 cells. 372

4.2.5 Selection of a subset of target genes for further analysis 375

4.2.6 Validation of three putative miR-619-5p and miR-4793-3p targets in GIN28 cells. 375

4.2.7 Confirming direct physical mRNA-miRNA interaction 377

4.2.8 Protein expression of putative miR-619-5p and miR-4793-3p targets 380

4.2.9 mRNA expression of putative miR-619-5p and miR-4793-3p targets in patient samples 383

4.2.10 Protein expression of putative miR-619-5p and miR-4793-3p targets in patient samples 385

4.3 Discussion 389

4.4 Future work 399

4.5 Chapter Summary 400

Chapter 5: Evaluation of Global Metabolic Alterations Following miR-619-5p and miR-4793-3p Overexpression in GBM Cells 403

5.1 Introduction 404

5.2 Results 407

5.2.1 Growth Curve of U87 and GIN28 following miRNA transfection for metabolomics analysis. 407

5.2.2 Metabolomics analysis of intra-cellular polar metabolites with LC-MS 409

5.2.3 Lipidomics analysis of intra-cellular polar metabolites with LC-tandem MS/MS 423

5.2.4 Lipid droplets (LD) analysis in U87 cells 426

5.2.5 LDs analysis in GBM patient samples 428

5.3 Discussion 432

5.4 Future work 445

5.5 Chapter summary 446

Chapter 6: miR-619-5p and miR-4793-3p regulate GBM cell invasion by targeting lipid metabolism enzymes 448

6.1 Introduction 449

6.2 Results 456

6.2.1 Optimisation of the transwell invasion model to test the invasion of the U87 cells 456

6.2.2 Transwell invasion assay following miR-619-5p and miR-4793-3p overexpression in U87 and GIN28 cells 461

6.2.3 Understanding the effect of CPT2 knockdown on GBM cell invasion 465

6.2.4 Understanding the effect of the pharmacological inhibition of CPT2 on GBM cell invasion 473

6.3 Discussion 484

6.3.1 FAO inhibition reduces GBM cell invasion 484

6.3.2 Technical considerations 499

6.4 Future work 501

6.5 Chapter Summary 502

Chapter 7: General Discussion, Final Conclusions, and Future Work 503

7.1 General Discussion 504

7.2 Final Conclusions 515

7.3 Future Projects 517

Chapter 8: Appendices 519

8.1 Detailed information of patient samples used in the project 520

8.2 Short Tandem Repeats (STRs) genotyping results. . 527

8.3 Raw microarray expression data of the five significantly expressed miRNAs between the three regions of the GBM tumour. 528

8.4 Alternative approach for differential expression analysis of miRNAs 533

8.5 Full tissue microarray (TMA) images from 36 adult GBM patients. 535

8.6 Metabolic profile of U87 cells 540

Chapter 9: References..... 543

List of Figures

Figure 1.1: Molecular classifications of GBM. 42

Figure 1.2: 5-step invasion model. 52

Figure 1.3: Routes of GBM cell invasion within the brain. 69

Figure 1.4: GBM-displacing astrocyte endfeet. 74

Figure 1.5: Glucose and Lipid metabolism in (A) normal and (B) cancer cells. 90

Figure 1.6: The process of fatty acid elongation. 93

Figure 1.7: Synthesis of lipid droplets in the endoplasmic reticulum. 94

Figure 1.8: Fatty acid oxidation (FAO) cycle. 99

Figure 1.9: TCA cycle in normal cells (green) and cancer (red). 108

Figure 1.10: Overview of the change in glutamate metabolism in IDH mutant cells 110

Figure 1.11: One-carbon metabolism - folate and methionine cycles. 116

Figure 1.12: miRNA biogenesis. 137

Figure 1.13: miRNA regulation of GBM biology 148

Figure 1.14: miRNA regulation of glycolytic transporters and enzymes in GBM. 150

Figure 2.1: Pre-operative MRI scans of a GBM patient's brain allow the selection of different regions of the tumour. 199

Figure 2.2: Intra-operative images of a GBM patient's tumour showing how 5-aminolevμlinic acid (5-ALA) can aid the surgery. 200
Figure 2.3: Preparation of the Agilent RNA NanoChip 210
Figure 2.4: The four reactions employed in the TaqMan™ Advance miRNA cDNA synthesis kit..... 222
Figure 2.5: The three chemical reactions employed in the TaqMan™ Advanced miRNA qRT-PCR Assay. 227
Figure 2.6: Primer Optimisation PCR Plates Layout. 234
Figure 2.7: Scatter plot of mean Ct values for the HILPDA primer pair at serially diluted concentrations of DNA template. 236
Figure 2.8: Amplification curve (left) and melting curve (right) for HILPDA from a serial dilution of control cDNA..... 238
Figure 2.9: Methods of small RNA transfection. 244
Figure 2.10: Schematic of pLightSwitch_3UTR vector..... 252
Figure 2.11: Typical tissue microarray layout. 272
Figure 3.1: Bioanalyser gel images of total RNA samples... 299
Figure 3.2: Boxplot of probe intensities distributions (n=72). 307
Figure 3.3: K-means clustering (n=72 arrays). 309
Figure 3.4: K-means clustering (n=71 arrays). 310

Figure 3.5: PCA of miRNA expression profiles based on GBM tumour regions. 312
Figure 3.6: Boxplot of differentially expressed miRNAs between the different GBM tumour regions. 315
Figure 3.7: Expression of housekeeping miRNAs..... 317
Figure 3.8: qRT-PCR validation of miRNA expression reported by microarray in the same patient cohort used for the microarray..... 322
Figure 3.9: qRT-PCR validation of miRNA expression reported by microarray in an independent GBM patient cohort. 324
Figure 3.10: qRT-PCR validation of miRNA expression reported by microarray in the FACS analysed samples. 327
Figure 3.11: qRT-PCR validation of miRNA expression reported by microarray in an independent GBM patient cohort in the FACS analysed invasive margin samples..... 329
Figure 3.12: 5-ALA cell population compared to tumour core and rim for patients 25, 30, and 31. 333
Figure 3.13: 5-ALA cell population compared to tumour core and rim for patients 32, 58, and 71 334
Figure 3.14: Expression of housekeeping miRNAs: (A) hsa-miR-361-5p and (B) hsa-miR-191-5p across GBM cell lines. 337
Figure 3.15: Expression of miRNAs in GBM cell lines by microarray (left panel) and by qRT-PCR (right panel). 339

Figure 4.1. Luciferase reporter system. 354
Figure 4.2. Comparison of U87 cell viability using PrestoBlue to assess the cytotoxicity of different dilutions of the DharmaFECT ™ transfection reagent after 24h. 358
Figure 4.3. U87 cells transfected with siGLO Green for 24h.360
Figure 4.4. Transfection efficiency assessed by counting siGlo Green positive U87 cells. 361
Figure 4.5. miRNA knock-in transfection in U87..... 362
Figure 4.6. miRNA knock-in transfection in GIN28. 365
Figure 4.7. Target prediction filtering scheme. 368
Figure 4.8. Graphical representation of significantly enriched pathways for miR-619-5p and miR-4793-3p targets. *P-values for each matched pathway was calculated from the z-score test (threshold was set to 0.05 following FDR correction). The colour shades from pink to black denotes different levels of statistical significance where pink is highly significant.* 369
Figure 4.9. mRNA expression of predicted gene targets 48h following miR-619-5p and miR-4793-3p overexpression in U87 cells..... 374
Figure 4.10. mRNA expression of predicted gene targets 48h following miR-619-5p and miR-4793-3p overexpression in GIN28 patient-derived cells. 376

Figure 4.11. Sequence alignment between miR-619-5p or miR-4793-3p and the 3'UTR of CPT2, ACOX1 and LDLR in human from TargetScan. 377
Figure 4.12. Luciferase activity in U87 cells. 379
Figure .4.13. Immunoblot of miR-619-5p and miR-4793-3p targets in U87 cells. 381
Figure 4.14. Immunoblot of miR-619-5p and miR-4793-3p targets in GIN28 cells. 382
Figure 4.15. mRNA expression in different regions of the GBM tumour..... 384
Figure 4.16. mRNA expression in 5-ALA sorted invasive margin samples. 385
Figure 4.17. Optimisation results of primary anti-CPT2 antibody on normal liver tissue. 386
Figure 4.18: Immunohistochemical staining pattern of CPT2 in GBM tumours. 388
Figure 5.1: Growth curve of U87 cells. 409
Figure 5.2: Representative peak alignment. 411
Figure 5.3: Representative normalisation. 412
Figure 5.4: Multivariate analysis for the U87 cell metabolome following miRNA transfection. 415
Figure 5.5: Hierarchical cluster analysis of differential metabolites in miR-619-5p, miR-4793-3p or miR-619-5p/ miR-

4793-3p co-transfections relative to non-targeting control (NT). 419

Figure 5.6: Graphical representation of significantly altered pathways following miR-619-5p and miR-4793-3p individual or co-transfection. 421

Figure 5.7: Abundance levels of significantly altered non-polar metabolites following (A) miR-619-5p and (B) miR-4793-3p transfections. 425

Figure 5.8: Confocal analysis of lipid droplets in U87 cells following miR-619-5p and miR-4793-3p individual or co-transfection. 427

Figure 5.9: Count of lipid droplets per cell in U87 cells following miR-619-5p and miR-4793-3p individual or co-transfection. 428

Figure 5.10: Optimisation results of primary anti-PLIN2 antibody on breast carcinoma tissue. 430

Figure 5.11 Immunohistochemical staining pattern of PLIN2 in GBM tumours. 431

Figure 6.1: Graphical illustration of the transwell invasion assay. 451

Figure 6.2 Optimisation of U87 cells invasion through collagen IV coated transwell inserts at a seeding density of 1×10^4 cells/well. 459

Figure 6.3 Optimisation of U87 cells invasion through collagen IV coated transwell inserts at a seeding density of 2 $\times 10^4$ cells/well. 460
Figure 6.4 Optimisation of U87 cells invasion through collagen IV coated transwell inserts at a seeding density of 5×10^4 cells/well. 461
Figure 6.5 Transwell invasion assays of U87 cells overexpressing miR-619-5p and/or miR-4793-3p. 463
Figure 6.6 Transwell invasion assays of GIN28 cells overexpressing miR-619-5p and/or miR-4793-3p. 464
Figure 6.7 Transfection efficiency of siRNA against CPT2 in U87 cells. 466
Figure 6.8 Transfection efficiency of siRNA against CPT2 in GIN28 cells. 467
Figure 6.9 Immunoblot of CPT2 following siRNA knockdown in GBM cells. 468
Figure 6.10 Growth curve of U87 and GIN28 cells following siRNA transfection. 469
Figure 6.11: Confocal analysis of lipid droplets in U87 and GIN28 cells after siCPT2 treatment. 470
Figure 6.12: Lipid droplet count in (A) U87 and (B) GIN28 cells following CPT2 knockdown by siRNA (siCPT2). 471

Figure 6.13 Effect of CPT2 knockdown on (A,B) U87 and (C,D) GIN28 cell invasion. 472
Figure 6.14 Determination of IC50 values for perhexiline and etomoxir in GBM cells. 475
Figure 6.15: Confocal analysis of lipid droplets in U87 and GIN28 cells after 72h of perhexiline treatment. 477
Figure 6.16: Lipid droplet count in (A) U87 and (B) GIN28 cells after perhexiline treatment. 478
Figure 6.17: Confocal analysis of lipid droplets in U87 and GIN28 cells after 72h of Etomoxir treatment. 479
Figure 6.18: Lipid droplet count in (A) U87 and (B) GIN28 cells after Etomoxir treatment. 480
Figure 6.19 Effect of Perhexiline on the invasion of (A,B) U87 and (C,D) GIN28 cells. 481
Figure 6.20 Effect of Etomoxir on the invasion of (A,B) U87 and (C,D) GIN28 cells. 483
Figure 8.1: Genotyping of GBM cell lines. 527
Figure 8.2: Volcano plots of miRNA expression profiles..... 534
Figure 8.3: TMA containing three tumour regions from GBM patients number 1-3 and 5-10 (N=9)..... 536
Figure 8.4: TMA containing three tumour regions from GBM patients 12, 13, 15, 17, 19, 20, 21, 25, and 26 (N=9). 537
Figure 8.5: TMA of nine GBM patients 27-33, 37-38 (N=9).538

Figure 8.6: TMA containing three tumour regions from GBM patients 39-42, 44-47, and 52 (N=9)..... 539
Figure 8.7: Total ion counts based on LC-MS metabolite analysis of U87 cells 540
Figure 8.8: Ion chromatograms of U87 cells co-transfected with miR-619-5p and miR-4793-3p analysed by LC-MS..... 541
Figure 8.9: Pie Chart of Metabolites that changed abundance as a result of miR-619-5p, miR-4793-3p, and co-transfection of both miRNAs, relative to the non-targeting control. 542

List of Tables

Table 2.1: Medium recipes for commercial and primary GBM cell lines. 202

Table 2.2: GeneChip® Affymetrix miRNA Array (version 4.1) human probe sets content. 212

Table 2.3: Target prediction algorithms features. 218

Table 2.4: TaqMan™ Advanced miRNA polyadenylation tailing reaction mixture composition and cycling conditions. 223

Table 2.5: TaqMan™ Advanced miRNA adaptor ligation mixture composition and cycling conditions. 223

Table 2.6: TaqMan™ Advanced miRNA RT reaction mixture composition and cycling conditions. 224

Table 2.7: TaqMan™ Advanced miRNA miR-Amp reaction mixture composition and cycling conditions. 224

Table 2.8: TaqMan™ Advanced miRNA Assay Probes..... 226

Table 2.9: TaqMan™ Advanced miRNA qRT-PCR Assay reaction mixture composition and cycling conditions. 229

Table 2.10: SYBR Green qRT-PCR reaction mixture composition and cycling conditions. 232

Table 2.11: Primers sequences and efficiencies for SYBR Green qRT-PCR..... 237

Table 2.12: TaqMan™ RNA-to-CT™ 1-Step qRT-PCR reaction mixture composition and cycling conditions. 241

Table 2.13: TaqMan™ Gene Expression Assay Probes and qRT-PCR Reaction Efficiencies. 242
Table 2.14: siGlo Green sequence information. 245
Table 2.15: siRNA sequence information. 245
Table 2.16: miRIDIAN miRNA mimics and hairpin inhibitors information. 246
Table 2.17: Transfection mixture based on cell culture vessel format. 249
Table 2.18: The sequences of 3'UTRs cloned into the pLightSwitch_3UTR vector. 253
Table 2.19: Co-transfection mixture per replicate 258
Table 2.20: LightSwitch Assay Solution mixture. 260
Table 2.21: Pharmacological CPT2 inhibitors information. .. 262
Table 2.22: Primary antibodies used in this project. 269
Table 2.23: Mobile phase gradient setting. 280
Table 3.1: Summary of Clinicopathological characteristics of adult GBM cases 291
Table 3.2: Patient-derived cell lines 292
Table 3.3: Quality and quantity of total RNA samples. 294
Table 3.4: Electropherogram results for total RNA samples that showed RNA degradation. 302
Table 3.5: Relative expression levels of differentially expressed miRNAs within the GBM tumour. 314

Table 4.1 Pathway enriched for the significantly changed metabolites following miRNA transfection. 370
Table 5.1: Normalisation factor multiplier that is applied to the abundance measurement of each ion in the sample. 412
Table 5.2: Fold change differences for identified differentially abundant metabolites. 420
Table 5.3: Metabolic pathway enriched for the significantly changed metabolites following miRNA transfection. 422
Table 5.4: Lipid classes of significantly altered lipid species before FDR correction in cells overexpressing miR-619-5p and miR-4793-3p. 424
Table 8.1: Tissue samples information 520
Table 8.2: hsa-miR-330-5p, ID: 20501275 528
Table 8.3: hsa-miR-215-3p, ID: 20500474 529
Table 8.4: hsa-miR-619-5p, ID: 20504364 530
Table 8.5: hsa-mir-4440, ID: 20536693 531
Table 8.6: hsa-miR-4793-3p, ID: 20519689 532

List of Common Abbreviations

αKG	α-Ketoglutarate
2-HG	2-hydroxyglutarate
5-ALA	5-Aminolevulinic acid
AKT	Protein kinase B
ANOVA	Analysis of Variance
APS	Ammonium persulfate
ATP	Adenosine 5’-triphosphate
BBB	Blood-brain barrier
cDNA	Complimentary DNA
CoA	Coenzyme A
CPT2	Palmitoyl-CoA transferase 2
Ct	Cycle threshold
DAG	Diacylglycerol
DMEM	Dulbecco’s modified eagle medium
DMSO	Dimethyl sulfoxide
ECM	Extra-cellular matrix
EGFR	Epidermal growth factor receptor
FACS	Fluorescence-Activated Cell Sorting
FAs	Fatty acids
FAO	Fatty acid oxidation
FBS	Foetal bovine serum
FDR	False discovery rate

FFPE	Formalin-fixed paraffin-embedded
FDA	Food and Drug Administration
GAPDH	Glyceraldehyde 3-phosphate dehydrogenase
GBM	Glioblastoma multiforme
GCE	Primary cells derived from the GBM core
GIN	Primary cells derived from the GBM invasive edge
HBSS	Hank's Balanced Salt Solution
IDH	Isocitrate dehydrogenase
IDH-mut	Isocitrate dehydrogenase mutant
IDH-wt	Isocitrate dehydrogenase wild type
IHC	Immunohistochemical analysis
LC-MS	Liquid chromatography-mass spectrometry
LDLR	Low-density lipoprotein receptor
LD/LDs	Lipid Droplet/Lipid Droplets
m/z	Mass-to-charge ratio
miRNA	MicroRNA
MMP	Matrix Metalloproteinase
mRNA	Messenger RNAs
NADH	Nicotinamide adenine dinucleotide
NADPH	Nicotinamide adenine dinucleotide phosphate
NFW	Nuclease-free water
NT	Non-targeting control

OAA	Oxaloacetate
OPLS-DA	Orthogonal partial least squares discriminant analysis
OXPHOS	Oxidative phosphorylation
PBS	Phosphate buffered saline
PCA	Principal component analysis
PDGFR	Platelet-derived growth factor receptor
PI3K	Phosphatidylinositol 3-kinase
PPP	Pentose phosphate pathway
PTEN	Phosphatase and tensin-homolog
QC	Quality control
RIN	RNA integrity number
ROS	Reactive oxygen species
RTK	Receptor tyrosine kinase
siRNA	Small interfering RNA
TBST	Tris buffered saline-Tween 20
TCA cycle	Tricarboxylic acid cycle
TCGA	The Cancer Genome Atlas
TGs	Triglycerides
TMZ	Temozolomide
U87	U87-MG Cell line
WHO	World Health Organisation

Chapter 1: Introduction

1.1 Glioblastoma multiforme

Glioblastoma multiforme (GBM) represents 12-15% of all intracranial tumours (Iacob and Dinca, 2009). GBM is the most common and aggressive form (World Health Organisation (WHO) grade IV) of glioma, an umbrella term for tumours thought to originate from glial progenitors such as astrocytomas (Louis *et al.*, 2007; Zong, Verhaak and Canoll, 2012). Primary GBM, which comprises 90% of all diagnosed GBM cases, arises *de novo*. Pre-existing low-grade gliomas, grade II (diffuse astrocytoma), can develop into high-grade gliomas, grade III (anaplastic astrocytoma), that give rise to secondary GBM. Secondary GBM constitutes the remaining 10% of the GBM cases (Louis *et al.*, 2007; Louis et al., 2016).

1.1.1 Incidence

Primary GBM is predominant in males, with a male: female incidence ratio of about 3:2 (Ohgaki *et al.*, 2004; Wöhrer *et al.*, 2009; Ostrom *et al.*, 2013a) and an age-specific incidence peaking between 70-74 and 75-79 years of age of for males and females respectively (Chakrabarti *et al.*, 2005). The peak incidence of secondary GBM is, however, in the fourth decade of life (Kleihues and Ohgaki, 1999; Cvetkoivč-Dožič D, Skender-

Gazibara M, 2004; Ohgaki *et al.*, 2004; Ohgaki and Kleihues, 2005b, 2009, 2013; Louis *et al.*, 2007). The most frequent anatomic location of GBM tumours in adult patients is in the supra-tentorial regions located above the tentorium cerebelli, which is an extension of the dura matter separating the occipital and temporal cerebral cortex from the cerebellum and infra-tentorial brainstem (Peter, Linet and Heineman, 1995). In general, GBM shows an increased incidence in the Caucasian population (Ohgaki and Kleihues, 2005a). In the UK and the United States alone, annual age-adjusted GBM incidence rate ranges between 4.64-5.26 per 100,000 people (Ostrom *et al.*, 2013b; Brodbelt *et al.*, 2015).

1.1.2 Treatment and prognosis

Until the introduction of adjuvant temozolomide (TMZ) in 2005, the standard of care for GBM patients consisted of maximal, but with invasive tumour deposits inevitably remaining, safe surgical resection followed by local radiotherapy (60 Gray) which costs around £17,000 per patient. The follow-up treatment with TMZ costs an extra £7,800 for an additional 2.5 quality-adjusted life-months. At a willingness-to-pay threshold of £30,000 per quality-adjusted life-year, the benefits of TMZ fall on the edge of acceptable, cost-effective therapies

(Wasserfallen *et al.*, 2005; Messali, Villacorta and Hay, 2014; Raizer *et al.*, 2014; Bernard-Arnoux *et al.*, 2016). Moreover, more than 90 % of GBM patients relapse after standard therapy in about 6.9 months (Stupp *et al.*, 2009; Minniti *et al.*, 2010; Scorsetti *et al.*, 2015). Glioma recurrence is often within 1-2cm from the resection margin appearing later on after the first diagnosis (metachronous lesions) or being already present at the time of surgery but difficult to remove (synchronous gliomas) (Lafitte *et al.*, 2001; Hou *et al.*, 2006). Therefore, GBM prognosis remains poor with a median overall survival of 14 months and a 5-year survival rate of less than 10% (Tran and Rosenthal, 2010; Koshy *et al.*, 2012).

1.1.3 Molecular biology

Comprehensive genomic analysis using 206 GBM patients performed by The Cancer Genome Atlas (TCGA) Network showed that genetic alterations, which are likely to be driver events in GBM, are frequently found in the receptor tyrosine kinase (RTK)/RAS/phosphatidylinositol 3-kinase (PI3K) (in 88% of the cases), P53/MDM2/MDM4 (87%), and retinoblastoma (RB)/ cyclin-dependent kinases (CDKs) (78%) pathways (Cancer Genome Atlas Research Network, 2008). Defects in all three pathways were observed in 74% GBMs, indicating that it

is probably a core requirement for gliomagenesis. Within the P53/MDM2/MDM4 pathway, the negative regulators of P53 (which is mutated in 35% of GBMs), MDM2 and MDM4 are found to be amplified in 14% and 7% of GBM cases, respectively. 52%, 47% and 2% of GBMs exhibited homozygous deletion of cyclin-dependent kinase inhibitor 2A/2B/2C (CDKN2A/B/C), which negatively regulate CDK4/2/6 in the RB/CDK pathway. CDK4/2/6, which are negative regulators of Rb (which is deleted in 11% of GBMs), are amplified in 18%, 2% and 1% of GBMs, respectively.

Within the RTK/RAS/PI3K pathway, the RTKs: hepatocyte growth factor receptor (encoded by the *c-Met* proto-oncogene) and platelet-derived growth factor receptor-α (PDGFRA), are aberrantly activated in 4% and 13% of GBMs, respectively. However, the gain of function mutations and/or amplification in the epidermal growth factor receptor (*EGFR*) are the most common in GBM (45% of GBM cases) (Cancer Genome Atlas Research Network, 2008). Active EGFR signals via multiple effector pathways, including RAS and PI3K signalling cascades. The cytoplasmic domain of activated EGFR recruits adaptor proteins to activate RAS (Lemmon and Schlessinger, 2010). Moreover, the activation of RAS signalling can be achieved

through losing the expression of the RAS antagonist, neurofibromin 1 (NF1), which is observed in about 18% of GBM cases (Dasgupta *et al.*, 2005; The Cancer Genome Atlas Research Network, 2008). RAS activates PI3K while PI3K can also be independently activated by the cytoplasmic domain of EGFR (Castellano and Downward, 2011; Mendoza, Er and Blenis, 2011; Yang *et al.*, 2012). On average, 15-25% of GBM patients carry activating mutations in PI3K (The Cancer Genome Atlas Research Network, 2008; Brennan *et al.*, 2013).

Activated PI3K catalyses the phosphorylation of phosphatidylinositol (4,5)-bisphosphate (PIP2) into phosphatidylinositol (3,4,5)-trisphosphate (PIP3), which can be reversed by the Phosphatase and tensin homolog (PTEN; deletions and mutations are found in 36% of GBMs) (Engelman, Luo and Cantley, 2006; Carracedo and Pandolfi, 2008; The Cancer Genome Atlas Research Network, 2008; Georgescu, 2010). Following the recruitment of protein kinase B (AKT) into the plasma membrane by the activated PIP3, AKT is phosphorylated by 3-phosphoinositide-dependent protein kinase 1 (PDK1) (Franke *et al.*, 1995; Frech *et al.*, 1997). Activation mutations in AKT are found in 2% of GBMs (Cancer Genome Atlas Research Network, 2008). Activated AKT

activates both the rapamycin-sensitive mTOR complex 1 (mTORC1) and the rapamycin-insensitive mTOR complex 2 (mTORC2) which activate downstream oncogenic signalling, such as the hypoxia-induced factor (*HIF*), under aerobic conditions and independent of hypoxia (Kaur *et al.*, 2005) and *c-Myc* (Masui *et al.*, 2013), which promote gliomagenesis.

1.1.4 Clinical and molecular classifications

Based on the clustering of the TCGA gene expression profiles, four molecular subtypes of GBM: classical, mesenchymal, proneural and neural have been proposed by Verhaak et al. (Verhaak et al., 2010) (Figure 1.1). Classical subtypes are characterised by EGFR overexpression and the lack of P53 mutations. The mesenchymal subtypes are characterised by deletions/mutations in the three tumour suppressors: *NF1, PTEN* and *P53*. Proneural GBMs, which are predominately found in younger patients, is characterised by the overexpression of PDGFRA and P53 mutations. Almost all secondary GBMs are considered proneural (Verhaak et al., 2010). Finally, patients with neural GBM subtype are the oldest and exhibit mutations in multiple genes that classify the other three GBM subtypes (Verhaak et al., 2010).

Based on WHO classification of GBM (2016), the mutation status of the isocitrate dehydrogenase-1 and -2 (IDH1 and IDH2) genes, encoding tricarboxylic acid (TCA) cycle enzymes, divides glioblastoma into two classes: IDH-wildtype and IDH-mutant GBMs (Louis et al., 2016). In the IDH-wildtype GBM class, there are three histological sub-variants, namely: giant cell GBM, epithelioid GBM and gliosarcoma according the 2016 WHO classification system (Louis et al., 2016). The IDH-mutant GBMs are predominately secondary GBMs c the proneural subtype while only 5% of primary GBM are found to carry IDH mutations (Dang et al., 2009; Kloosterhof et al., 2011; Jiao et al., 2012).

IDH1 is predominately mutated at arginine 132 (*R132*), while *IDH2* is often found to be mutated at arginine 172 (*R172*) (Fang *et al.*, 2011).

These mutations reside within the active site of the enzymes which enhance their catalytic activity to reduce α-ketoglutarate (α-KG) into 2-hydroxyglutarate (2-HG), which results in increased production of 2-HG in the cell (Dang *et al.*, 2009). 2-HG can competitively inhibit histone demethylases and 5-methylcytosine hydroxylases, thereby leading to extensive DNA methylation (hypermethylation) of CpG islands within multiple

promoter regions across a large number of loci (Xu *et al.*, 2011). Such genotype, referred to as glioma-CpG island methylator phenotype (G-CIMP), is considered as another distinct signature of proneural GBMs (Noushmehr *et al.*, 2010; Shinawi *et al.*, 2013).

In addition, the promoter methylation of the O6-Methylguanine-DNA Methyltransferase (*MGMT*) gene, encoding a DNA repair protein, mostly occurs in proneural secondary GBMs with G-CIMP-positive/ IDH1/2 mutant genotype (Hegi *et al.*, 2005; Dunn *et al.*, 2009; Thon, Kreth and Kreth, 2013; Wick *et al.*, 2014). MGMT can confer resistance to the alkylating chemotherapeutic agent, TMZ, by reversing mutagenic O6-alkyl-guanine back to guanine (Pegg, 1990; Verbeek *et al.*, 2008). However, the methylation of *MGMT* promoter causes transcriptional silencing of the gene and patients with *MGMT* methylation showed improved response to TMZ. As such, *MGMT* methylation, status can act as a prognostic biomarker that predicts improved response to TMZ (Hegi *et al.*, 2005; Dunn *et al.*, 2009; Reifenberger *et al.*, 2012; Thon, Kreth and Kreth, 2013; Wick *et al.*, 2014).

The glial proneural cell population, which is thought to give rise to astrocytic and oligodendroglial tumour lineages, can be distinguished by the alpha-thalassemia/mental retardation syndrome X-linked (*ATRX*) gene mutations, encoding a subunit of the chromatin remodelling complex, in astrocytomas and the mutually exclusive chromosomal 1p/19q co-deletions in oligodendrogliomas, which has a relatively better prognosis (Ohgaki and Kleihues, 2011; Jiao *et al.*, 2012) (Figure 1.1). More recently, a new classification tool has been developed by Capper et al. for routine molecular diagnostics of diffuse gliomas in the clinic (Capper *et al.*, 2018). Capper et al. used genome-wide DNA methylation profiles from a reference cohort consisting of 2,801 samples. The tool they developed, based on unsupervised clustering algorithm, clustered the samples into 91 methylation classes. These results were then validated with 1,155 diagnostic samples. For approximately 75% of the samples, the methylation class matched the result of the histopathological analysis, while in around 12% of the samples, the DNA methylation profile changed the histopathological diagnosis for patients (Capper *et al.*, 2018). Using this tool, clinicians can submit DNA-methylation profiles and request a classification of the samples to complement the classical diagnostic toolbox.

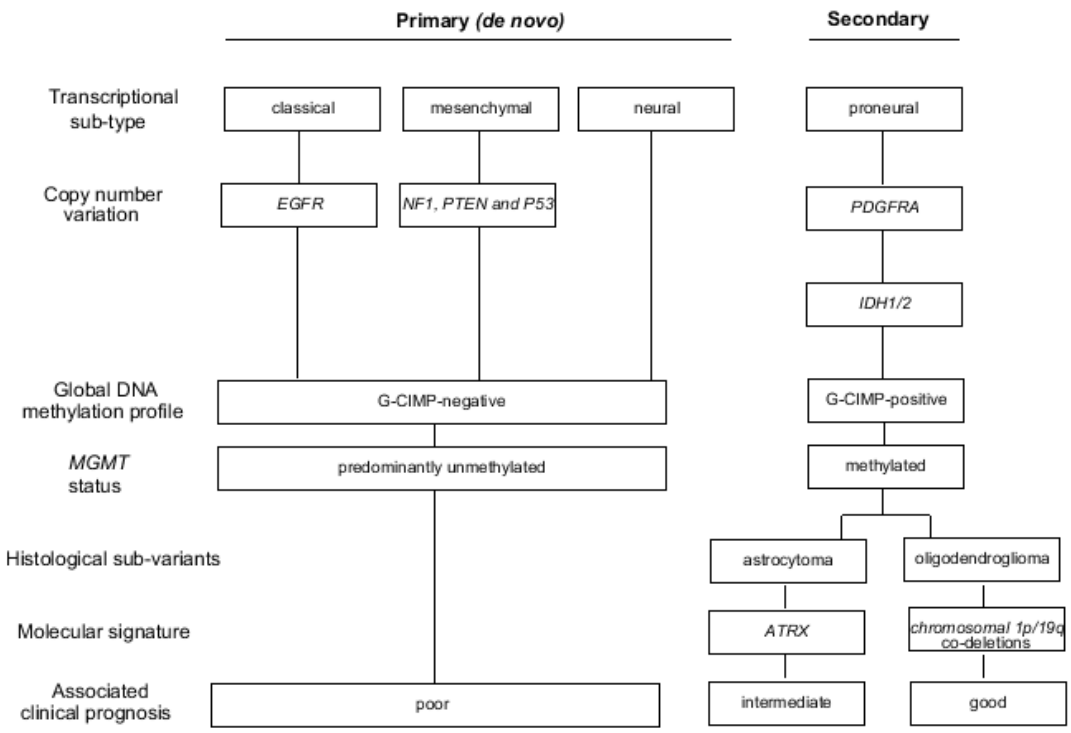


Figure 1.1: Molecular classifications of GBM.
GBM tumours are classified into four subtypes based on their transcriptional profiling. The proneural subtype is characterised by isocitrate dehydrogenase 1 and 2 (IDH/2) mutations, glioma-CpG island methylator phenotype (G-CIMP) and the promoter methylation of the O6-Methylguanine-DNA Methyltransferase (MGMT) gene.

1.1.5 *In vitro* cell cultures models of GBM

Cultured tumour cells are a central tool in cancer research used to identify genetic pathways and cellular functions that are altered by the disease. Classically, cells are grown in adherent monolayers to allow for rapid and reproducible testing of targeted drugs *in vitro* in a controlled and reproducible manner;

thereby serving as a pre-screen for further testing in *in vivo* pre-clinical models.

1.1.5.1 Patient-derived cell line models

Traditionally, the cell biology of GBM has been studied on the basis of established cell lines. The two most widely studied cell lines, U87-MG (U87; an abbreviation for Uppsala 87 Malignant Glioma) and U251-MG (U251), were established at Uppsala University, Sweden, more than 40 years ago from GBM patients (Westermark, Pontén and Hugosson, 1973; Pontén and Macintyre, 2009).

Of note, the recent genotyping of U87, which is now sourced from the American Type Culture Collection (ATCC) repository, has shown that the origin or genotype of these cells is different from that of the U87 cells established at Uppsala (Allen *et al.*, 2016). Although genetic aberrations from the original tumour are still retained, genetic drifts were acquired during decades of cell culture and as consequences of the standard practice of culturing the cells with fetal bovine serum (FBS) (Huszthy *et al.*, 2012; Torsvik *et al.*, 2014; Freedman *et al.*, 2015; Allen *et al.*, 2016). As such, many scientific journals now require

researchers to perform regular cell line authentication before publishing results with cell lines (Freedman *et al.*, 2015).

An alternative cell culture system is primary cells, which are isolated from individual human tumour specimens and cultured for a limited number of passages to ensure that they retain greater similarity to the primary tumour from which they are derived (Seidel, Garvalov and Acker, 2015). In contrast to U87, which were found not to fully recapitulate the invasive characteristic of GBM *in vivo* xenograft models, primary cells were found to depict the invasive morphology of GBM seen in patients, and thus may serve as better model *in vitro* models of GBM (Wong *et al.*, 2011).

1.1.5.2 Murine-derived cell line models

There are a number of *in vitro* cell lines that have been derived from rat GBM models including C6, 9L, T9, RG2, F98 and BT4C and RT-2 (Barth and Kaur, 2009). However, because these tumours are generated in different species, some of the mutations that are seen in human tumours are not detected in murine tumours. For example, murine models have not been

reported to develop *IDH1* mutations and efforts to create cell lines from transgenic mice, expressing IDH1R132H in nestin-positive neural progenitor cells, have been unsuccessful; therefore, these models are less relevant for the study of IDH mutant (IDH-mut) human gliomas (Bardella *et al.*, 2016).

1.1.6 *In vivo* pre-clinical models of GBM

Pre-clinical murine models of GBM facilitate the testing of novel therapies for GBM. There are many murine models that have been created, but the choice of which model to use is often based on the model having one or more of following factors: I) having relevant histological features and molecular alteration to those seen in patients tumours; II) recapitulating the intra-tumour heterogeneity; III) mimicking the tumour microenvironment; and IV) being readily reproducible and stable over time (Lenting *et al.*, 2017). The following section compares and contrasts different murine models in relation to these factors.

1.1.6.1 Ethyl-nitrosourea (ENU)-induced glioma models

This model was developed in the late 1970s and is based on the in utero exposure of rat embryos to ENU, which predominantly induces brain tumours (Russell *et al.*, 1979). The reason that

brain tumours are particularly induced is because DNA-repair mechanisms are less active in the brain than in other tissues (Mukherjee *et al.*, 2006). Induced tumours typically exhibit TP53 mutation, deletion of CDKN2A, and amplification of PDGFRA and EGFR (Zook, Simmens and Jones, 2000). An advantage of this model is the presence of an appropriate brain microenvironment, including an active immune system and an intact BBB. The main limitation of this model, however, is the poor reproducibility of tumour formation. In turn, high numbers of animals are required to be used to perform experiments with this model to improve the reliability of the results; thereby incurring high cost in terms of money and time (Reviewed in Friedl and Wolf, 2003).

1.1.6.2 Transgenic mouse models

The knowledge of the driver mutations that are involved in gliomagenesis has enabled the creation of genetically engineered mouse glioma models. An elegant example of a transgenic model is created by the administration of a vector expressing Cre-recombinase under the control of a glial cell-specific promoter, such as *GFAP*, into a LoxP transgenic mouse overexpressing *KRAS* and conditionally lacking *P53* or *PTEN* and *P16* (de Vries *et al.*, 2010). Such models would be useful to study the behaviours of genetically well-defined gliomas.

However, transgenic models tend to lack the intra-tumour genetic heterogeneity aspect as the mutated part of tumour grows more aggressively than the rest of tumour. Nonetheless, gliomas, in this model, form robustly and resemble human gliomas with respect to phenotype, and exist in the presence of immunity and BBB (Hambardzumyan *et al.*, 2011).

1.1.6.3 Allograft and xenograft models

In contrast to allograft models, where GBM cell lines of murine origin is intracranially injected into immunocompetent murine models (Beutler *et al.*, 1999), patient-derived xenograft models present a better model, as they involve transplanting freshly obtained surgical human specimens into the brain of immune-deficient murine models (Claes *et al.*, 2008; Luchman *et al.*, 2012; Klink *et al.*, 2013). Serial transplantation is then used to passage these tumours.

GBM xenografts can also be grown in the subcutaneous space to allow the growth of the tumour to be followed visually; thereby allowing rapid testing of treatment efficacy. However, subcutaneous GBM models lack the appropriate brain microenvironment, which limits their usability for testing drugs designed to disturb the tumour interaction with its

microenvironment, such as anti-angiogenic drugs or metabolic inhibitors (Wachsberger *et al.*, 2007).

One great advantage of using xenografts is that potential contamination coming from the host non-neoplastic tissue can be distinguished in the downstream analysis; for example, in RNA sequencing experiments, human and mouse transcripts can be distinguished.

A major drawback of such models though is that xenografting is performed in immune-deficient murine models. This places selection pressure on the fastest-growing cell clones, which in turn reduces the extent of intra-tumour heterogeneity. Moreover, xenografted murine models lack the presence of an intact immune system, which might affect tumour response to drugs. As such, these models are being further developed to mimic a human immune system. This would allow for the testing of more specific drugs, such as immune checkpoint inhibitors; however, this work has not yet proven successful (Morton *et al.*, 2016; Zitvogel *et al.*, 2016).

In conclusion, both *in vivo* and *in vitro* models have their advantages and drawbacks. New therapies are often tested on *in vitro* cell culture models, which are used as a pre-screen, before moving on to *in vivo* models. If drugs are shown to be promising as a proof-of-principle *in vivo*, then they can advance to clinical trials. Thus, GBM model systems are necessary tools for studying the biology of the tumour in a controlled lab environment, and each type of model plays its own part towards the development of a treatment for clinical use.

1.2 Cancer cell invasion

The highly infiltrative characteristic of GBM is the main source of recurrence (Reviewed in Demuth and Berens, 2004). GBM invades into the surrounding brain, and invasive cells can migrate far away from the original tumour (up to 2-4cm away) thereby rendering complete surgical resection of GBM impossible (Altieri *et al.*, 2015). Moreover, the application of radiotherapy is restricted to the area surrounding the GBM tumour in order to reduce radiation-induced injury to normal brain tissue after therapy. These invaded cells are not being targeted with radiotherapy. Moreover, GBM recurrence is seen even after the adjuvant treatment with TMZ, suggesting that invasive cells have resistance to alkylating chemotherapy, perhaps due to their slow proliferation rate. Therefore, understanding the biology of GBM invasion is of great

importance in order to develop novel therapeutic approaches to inhibiting cell invasion. Such a therapy would be particularly useful if used in conjunction with other therapies aimed at controlling cell proliferation.

1.2.1 Molecular mechanisms of cancer cell invasion

Tumour cells use invasion mechanisms that are similar, if not identical, to those used by normal healthy cells during physiological processes such as embryonic development and wound healing.

An interdependent five-step model has been established to describe cell invasion (Reviewed in Friedl and Wolf, 2003). In the first step (Step 1), the cell elongates and becomes polarised with a leading edge and a trailing edge each located at the opposite side of the cell body. The edges are formed by the extension of the cell membrane to form pseudopods (Figure 1.2). This process is initiated by actin polymerisation, which is mediated by the association of actin filaments with the two adaptor proteins, Arp2/3 complex and Wiskott-Aldrich syndrome protein (WASP), in order to connect to the clustered phosphoinositides (PIPs) at the inner leaflet of the plasma membrane (Rohatgi *et al.*, 1999). PIPs, in turn, can mediate

WASP activation by CDC42, a member of Rho-guanosine triphosphatase (Rho-GTPases) family, through the binding the CDC42 regulator, guanine-nucleotide exchange factor (GEF) (Cotteret and Chernoff, 2002). The resultant polymerised actin filaments at the inner leaflet of the plasma membrane are called cortical actin. Meanwhile, ARP2/3 complex can laterally interact with adjacent actin filaments and induce branching of cytoplasmic bundles and elongated cables of actin filaments to form what are known as stress fibres (Blanchoin *et al.*, 2000). The presence of the resulting polymerised actin filaments leads to the ruffling of the cell membrane and the formation of protrusions (Ridley *et al.*, 1992) (Figure 1.2).

In the second step (Step 2), the cell attaches to the extra-cellular matrix (ECM) via focal contacts (Figure 1.2). Cell protrusions bind to the ECM via adhesion transmembrane receptors, often from the integrin family (Richard O Hynes, 2002). Integrins are made of one of 18 different α-subunits that associate with one of eight different β-subunits to form αβ heterodimers. The combination of α and β subunits determines ligand specificity (Richard O. Hynes, 2002). Specific integrins bind specific ECM ligands including fibronectin (e.g., α5β1, αvβ3, α4β1), vitronectin (e.g., α6β1, α6β4, αvβ3), collagen (e.g.,

α1β1, α2β1), and laminin (e.g., α2β1, α3β1, α6β1) (Richard O. Hynes, 2002).

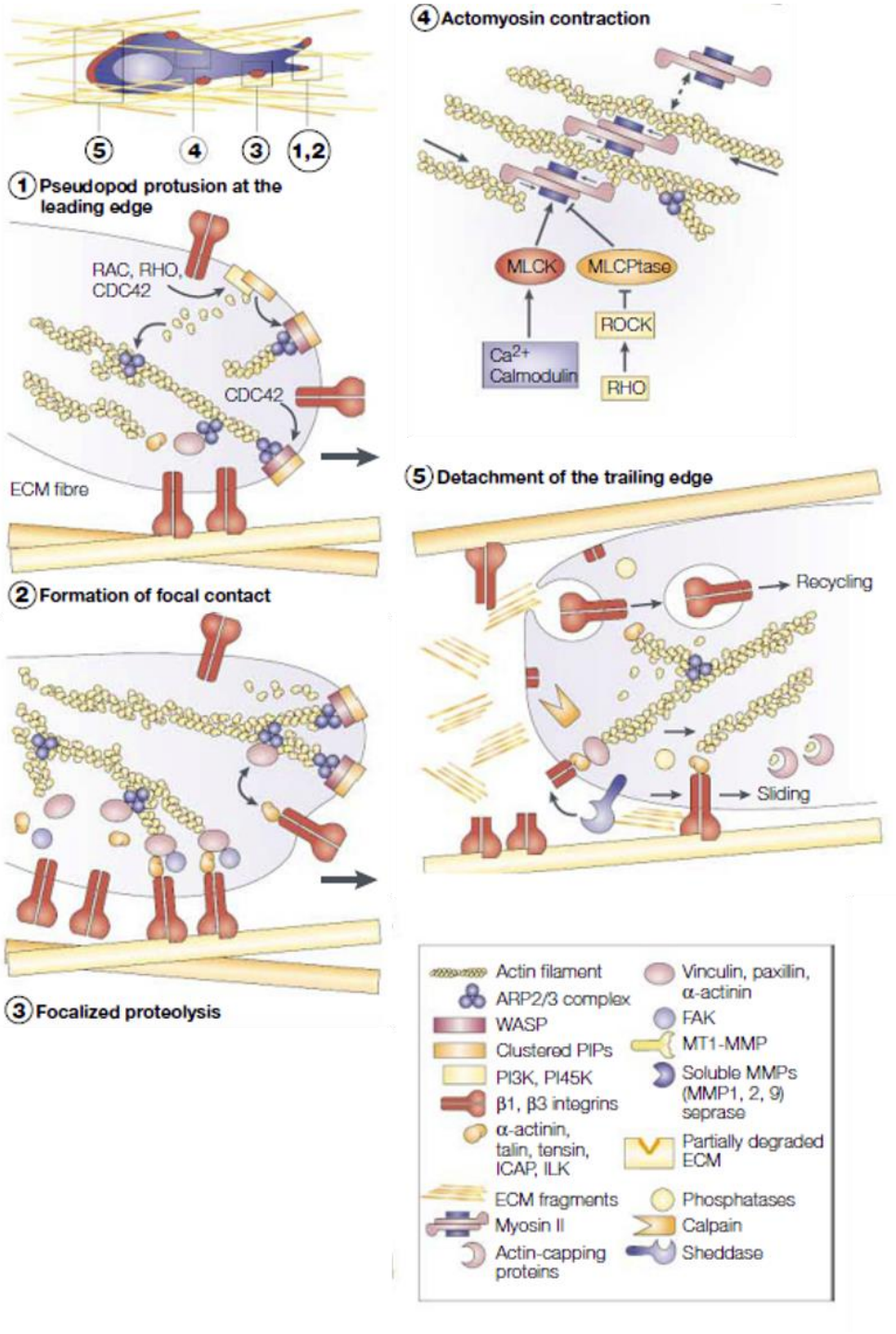


Figure 1.2: 5-step invasion model.
In step 1, the cell becomes polarised with a leading edge and a trailing edge as a result of actin polymerisation. In step 2, integrins come into contact with the extra-cellular matrix (ECM) and focal contact is formed. In step 3, proteases are recruited

to degrade ECM and create a path for invasion. In step 4, active myosin II binds to actin filaments (to form actomyosin) and initiates actomyosin contraction. In the final are (step 5), focal contact disassembly and actin de-polymerisation occurs at the trailing edge. Modified from (Friedl and Wolf, 2003 Review Paper).

The binding of integrins to their ligand leads to shifts in the distribution from diffused to localised clusters that develop into an initial small focal complex. The focal complex can then develop into a focal contact which spans approximately 20nm between the cell membrane and the ECM ligand, and covers an area of several μm on the cells surface with a length between 1–4 μm and a width between 0.5–2 μm (Friedl and Bröcker, 2000). Focal contacts allow the cell to stably adhere to, or slowly glide along, the particular ECM ligand as it moves forward (Regen and Horwitz, 1992; Smilenov *et al.*, 1999).

At the focal contact, integrins via their intracellular domains, interact with the adaptor protein, focal adhesion kinase (FAK) to recruit actin-binding crosslinking proteins, such as α-actinin, talin and vinculin. Vinculin, in turn, links the focal contact to the actin/ARP2/3 complex at the inner leaflet of the plasma membrane (DeMali, Barlow and Burridge, 2002).

Although the ECM molecules are important for attachment of cell protrusions, it can act as an obstacle for the invading cells.

Thus, the third step (Step 3) of the model of cell invasion involves the recruitment of proteases to degrade the ECM components that are near the cell surface to create a path for invasion (Figure 1.2). Integrins, and other non-integrin receptors such as hyaluronan receptors, can recruit cell-surface and soluble proteases to their ligand binding sites (Mueller *et al.*, 1999). For example, collagenases, such as matrix metalloproteinase 1 (MMP1) that binds to α2β1 (Dumin *et al.*, 2001), cleaves collagens into smaller fragments that are accessible to subsequent degradation by gelatinases, such as MMP2 (Dumin *et al.*, 2001) or MMP9 that bind αvβ3), or serine proteases such as, urokinase-type plasminogen activator (uPA) that binds αvβ3 or αVβ5.

uPA, along with another important collagenase, membrane-type matrix metalloproteinase-1 (MT1-MMP, aka MMP14), cleaves the pro-MMPs (pro-MMP1, pro-MMP2, and pro-MMP9) to create the active soluble MMPs (MMP1, MMP2, and MMP9). Cathepsin B, a lysosomal protease, as well as being able to degrade the ECM, activates pro-uPA, while its pro-form can itself be activated by uPA in a positive feedback loop. Cathepsin B also activates pro-MMPs via the inactivation of

Metallopeptidase Inhibitor 1 and 2 (TIMP1/2) (Kostoulas *et al.*, 1999).

The fourth step (Step 4) is characterised by the contraction of actin filaments, which promotes the shortening of the cell's length axis (Figure 1.2). Actin filaments contract upon the binding of the main motor protein in non-muscle cells, of active myosin II (then termed actomyosin). Myosin II induces actomyosin contraction when activated. Myosin II is activated by the myosin light chain kinase (MLCK) to mediate the contraction of the cortical actin. MLCK phosphorylates the myosin light chain (MLC), which activates myosin II. Distinctly, the RAC downstream effector, FAK, and the Rho-GTPase, Rho-A, through its downstream effector, Rho-associated protein kinase (ROCK) mediates stress-fibre contraction by activating the actin-binding LIM kinase (LIMK) (Kaibuchi, Kuroda and Amano, 1999; Katoh *et al.*, 2001). ROCK phosphorylates and inhibits the activity of the myosin light chain phosphatase (MLCP), a protein that counteracts MLCK activity (Kimura *et al.*, 1996; Solaro, 2000). This allows the cell to have separate control over the contractions of the stress fibre in the inner membrane and the cytoplasmic cortical actin to generate inward tension towards focal contacts at the outward edges.

Subsequently, the main cell body contracts, thereby generating traction force to drive the cell body, and its nucleus, and the trailing edge to glide forward (Regen and Horwitz, 1992; Smilenov *et al.*, 1999; Ballestrem *et al.*, 2001). As such, the fifth and final step (Step 5) of the cell invasion model is focal contact disassembly at the trailing edge to facilitate its detachment from the ECM and allow its forward gliding (Figure 1.2). The leading edge, however, remains attached to the ECM and further elongates (Palecek *et al.*, 1997; Ballestrem *et al.*, 2001; Ridley *et al.*, 2003). The accumulation of collagen fragments toward the trailing edge during the forward movement of the cell also weakens the focal contacts (Carragher *et al.*, 1999).

Focal contact disassembly occurs through proteolytic cleavage of both the extracellular portion and the intracellular domain of transmembrane adhesion receptors by the membrane-bound proteases, sheddases (Moss and Lambert, 2002), and cytoplasmic protease calpain (Potter *et al.*, 1998; Pfaff, Du and Ginsberg, 1999). Transmembrane adhesion receptors then become internalised via endocytosis to be recycled towards the leading edge (Bretscher, 1996). Alternatively, receptors get

deposited onto the ECM (Regen and Horwitz, 1992; Friedl *et al.*, 1997). Actin filaments are also recycled by gelsolin that caps actin filaments to sever their polymerisation and by cofilin, which inhibits LIMK and mediates actin filament depolymerisation (Wear, Schafer and Cooper, 2000). Actin filaments are also turned over by phosphatases which become upregulated to counteract the assembly of actomyosin (Zeng *et al.*, 2003)

1.2.2 Molecular regulation of GBM cell invasion

The expression levels of many genes that regulate the various steps of the five-step invasion model are differentially expressed in GBM cells to promote their invasion.

With relation to GTPases and their regulators, ECT2, VAV3, TRIO, SGEF, and SWAP-70 are five Rho GTPases regulators, GEFs, that have been described to promote GBM cell motility and are highly expressed in GBMs. Their expression is positively correlated to glioma grade (Salhia *et al.*, 2008; Seol *et al.*, 2009; Bralten *et al.*, 2011; Fortin Ensign *et al.*, 2013). Interestingly, GBM cells have been shown to differentially regulate the Rho GTPases depending on which route of invasion the cells take (Hirata *et al.*, 2012). Hirata et al. showed that the cells which are invading the brain parenchyma had lower RhoA

and higher Rac1 and Cdc42 activity than those invading perivascular space (Hirata *et al.*, 2012).

With regards to integrins, α2β1, α3/β1, α5β1, α6β1 and αvβ3 have all been reported to be upregulated in GBM compared to normal brain (Gingras *et al.*, 1995; Fukushima *et al.*, 1998; Riemenschneider *et al.*, 2005; Brown *et al.*, 2008).
With relation to FAK and the actin-binding crosslinking proteins that it recruits, *FAK* has been found to be overexpressed in GBMs, and its expression positively correlates with the tumour grade (Wang *et al.*, 2000; Hecker *et al.*, 2002; Gutenberg *et al.*, 2004). Similarly, *Talin-1* and *α-actinin* have both been found to be highly expressed in GBM (Sen, Ng and Kumar, 2012).

Finally, with regards to matrix proteases, several studies found that uPA/uPAR levels and activity were higher in GBM cells relative to lower-grade gliomas and normal brain (Yamamoto, Sawaya, Mohanam, Bindal, *et al.*, 1994; Yamamoto, Sawaya, Mohanam, Rao, *et al.*, 1994). Interestingly, *MMP14* was found to be upregulated in glioma-associated microglia, but not in GBM cells (Markovic *et al.*, 2009). GBM cells induce microglial MMP14 expression via releasing soluble factors that activate microglial toll-like receptor adapter protein MyD88 and

the p38 MAPK pathway (Markovic *et al.*, 2009). Activated microglial MMP14, in turn, results in the activation of pro-MMP2 and pro-MMP9 released by GBM cells (Markovic *et al.*, 2009). In addition, cytoplasmic MMP2 and MMP9 levels, as detected by IHC, have been shown to be significantly upregulated in patient GBM samples relative to lower-grade patient glioma samples and normal brain (Wang *et al.*, 2003). Furthermore, Choe et al. showed that active MMP9, as detected by gelatin zymography, was more elevated in primary than in the less aggressive secondary GBM patient samples (Choe *et al.*, 2002). Additionally, *AKT* can directly promote the expression of *MMP2* and *MMP9*, independent of β-catenin dependent pathways (Kubiatowski *et al.*, 2001). Moreover, β-catenin dependent pathways are implicated in the regulating of MMPs expression in GBM. Stable β-catenin translocates to the nucleus to interact with the lymphoid enhancer factor (LEF) transcription factor and drive the expression of its target genes, which include *MMP2* and *MMP9* in GBM (Liu *et al.*, 2012).

1.2.3 Cancer cell invasion strategies

There are two main strategies employed by cancer cells as they disseminate from the main tumour mass; namely, individual cell invasion or collective cell invasion. Individual cell invasion

can be either mesenchymal or amoeboid, while collective cell invasion can either be in protruding sheets/strands or detached cell clusters/cohorts. The choice of the strategy is determined by the degree of cell–ECM interaction, cell-cell adhesion and cell-cell communication (Reviewed in Lintz, Muñoz and Reinhart-King, 2017). In many tumours, both single cells and collectives are simultaneously present, though as a general observation leukaemias, lymphomas, sarcomas, and blastomas disseminate as single cells, while carcinomas use collective invasion (Verschueren, De Baetselier and Bereiter-Hahn, 1991; Paulus *et al.*, 1996; Wolf *et al.*, 2003). As such, the lower the differentiation state of the cancer, the more likely it is to invade as individual cells (Thiery, 2002).

Sometimes, tumour cells switch between strategies to evade therapies that target one particular strategy. For example, cells can undergo collective-amoeboid transition (CAT), as a response to integrin inhibitors, in order to switch from single-cell amoeboid to collective cell invasion where the cells develop epithelial phenotype (Lehmann *et al.*, 2017). Another example is the mesenchymal-amoeboid transition (MAT) where cells convert from collective to single-cell invasion with amoeboid features; this transition is used when stress-fibre formation

(through RAC action) is inhibited. (Taddei *et al.*, 2014). On the other hand, cadherin inhibitors can trigger epithelial-mesenchymal transition (EMT) marking a different type of transition from collective to single-cell invasion that is characterised by loss of cell-cell adhesion via loss-of-function mutations in cadherins. It is also characterised by the upregulation of protease that degrade cadherins and the loss of cytokeratins as well as the *de novo* expression of vimentin (Kalluri and Weinberg, 2009).

1.2.3.1 Strategy 1: individual cell invasion

Based on cell type, integrin engagement, cytoskeletal structure and protease production, single-cell invasion can occur in different morphological and functional variants. These variants include mesenchymal and amoeboid types of movements.

1.2.3.1.1 Mesenchymal movement

The five-step invasion model describes the molecular mechanisms of the mesenchymal type of individual cell invasion. Mesenchymal movement is predominately adopted by non-neoplastic cells such as fibroblasts and smooth muscle cells and

by cells from connective-tissue tumours, such as dedifferentiated epithelial cancers (Polette *et al.*, 1998; Tester *et al.*, 2000) fibrosarcomas (Wolf *et al.*, 2003), and GBM tumours (Paulus *et al.*, 1996). This movement is considered to be a slow 'gliding' type of movement with a low velocity of 0.1-2 μm/min (Friedl, Zänker and Bröcker, 1998). Moreover, tumour cells that use a mesenchymal type of invasion resemble a fibroblast-like spindle-shaped morphology and grow in adhesive cell culture conditions (Reviewed in Friedl and Wolf, 2003).

1.2.3.1.2 Amoeboid movement

The characteristics of the amoeboid movement have been established through studies of the single-cell amoeba, Dictyostelium discoideum. Amoeboid movement is used by healthy lymphocytes and neutrophils as well as by lymphomas, myeloid leukaemias (Verschueren, De Baetselier and Bereiter-Hahn, 1991), and small-cell lung and prostate carcinomas (Rintoul and Sethi, 2001); this movement allows cancer cells to undergo an early detachment and metastatic spread from a small primary tumour. The movement of these cells differs in several ways from mesenchymal migration. First, amoeboid cells have a short-lived and relatively low-affinity

binding to the ECM that is integrin-independent (Yumura, Mori and Fukui, 1984; Devreotes and Zigmond, 1988; Fey *et al.*, 2002). As such, these cells have low expression levels of *β1*and *β3 integrin*, which results in a low degree of adhesiveness for collagens (Falcioni *et al.*, 1994; JASPARS *et al.*, 1996; Rintoul and Sethi, 2001; Kraus *et al.*, 2002). Second, amoeboid cells grown in suspension have a round-shape with morphological ellipsoid features such as rapid cycles of contraction and expansion. Third, amoeboid cell movement is generated by cortical actin filaments, whereas stress fibres are lacking (Lewis, 1934; Entschladen *et al.*, 1997; Friedl, Borgmann and Bröcker, 2001) Due to their lack of focal contacts, amoeboid tumour cells use protease-independent invasive mechanisms to circumnavigate, rather than degrade, their ECM barriers (Lewis, 1934). The cells change their cytoplasmic flow to push forward (forward streaming) and form constriction rings to squeeze through narrow regions in the ECM (Lewis, 1934). As such, amoeboid movement is considered a fast 'gliding' type of movement and these cells can move at 10–30-fold higher velocities than mesenchymal tumour cells (Friedl, Zänker and Bröcker, 1998; Friedl, Borgmann and Bröcker, 2001).

1.2.3.2 Strategy 2: collective cell migration

In contrast to individual cell invasion, collective cell invasion is characterised by increased cell-cell adhesion, through expressing high levels of cadherins (*E-*, *N-*, *P-*, *VE-cadherins* and *cadherin-11*), as well as enhanced cell-cell communication, through overexpressing *connexions*, in order to facilitate the coordination of cytoskeletal activity (Hashizume *et al.*, 1996; Pishvaian *et al.*, 1999; Hsu *et al.*, 2000; Madhavan *et al.*, 2001). Cortical actin filaments form along cell junctions to create a larger-size multicellular contractile body (Hegerfeldt *et al.*, 2002). The body has three regions; namely leading margin, inner and trailing regions. The subset of cells in the leading margin region, which are termed path-generating cells, generate traction force via pseudopods (Reviewed in Khalil and Friedl, 2010). The anterior pseudopods facing toward the ECM engage and cluster integrins and overexpress *MMPs* to achieve polarised ECM degradation (Nabeshima *et al.*, 2000; Hegerfeldt *et al.*, 2002). The cells in the other two regions, inner and trailing, are dragged behind in a passive manner (Reviewed in Khalil and Friedl, 2010).

There are three main advantage of collective cell invasion: 1) cells in the inner regions can be protected from immunological and/or pharmacological assaults; 2) cells with heterogeneous clonal origin, e.g. apoptotic-resistant clones and invasive-clones, can form one functional unit that has different and/or complementary biological abilities, thereby increasing tumour survival probability; and finally 3) the large cell mass can produce high concentrations of pro-migratory factors and proteases to enhance invasion efficiency (Reviewed in Friedl and Wolf, 2003).

1.2.3.2.1 Protruding sheets/strands

The main feature of this morphological variant of collective cell invasion is that the cell maintains contact with the primary tumour site and generate local invasion. This type of cell invasion is commonly observed in epithelial cancers such as oral squamous cell carcinoma and mammary, colon, basal-cell carcinomas (Bell and Waizbard, 1986; PAGE and DL, 1987; Nabeshima *et al.*, 1999).

1.2.3.2.2 Detached cell clusters/cohorts

Epithelial cancers such as melanoma, ductal and lobular breast cancer, and epithelial prostate (Shimoyama *et al.*, 1989;

Hegerfeldt *et al.*, 2002; Harryman *et al.*, 2016; Khalil *et al.*, 2017) are known to invade in clusters/cohorts of cells. The key difference between tumour cell clusters/cohorts and sheets/strands is that clusters/cohorts detach from the primary tumour and can enter the lymphatic and blood vessels (Cheung *et al.*, 2016).

1.2.4 Routes of GBM cell invasion

Unlike other cancers, only 0.4-2% of GBMs metastasise outside of the brain to other organs (Beauchesne, 2011; Lun *et al.*, 2011; Hamilton *et al.*, 2014). A couple of reasons have been proposed to explain the rarity of extracranial metastasis in GBMs. First, GBM cells have been shown to lack the capacity to enter into the haematogenous and lymphatic vasculature; which are the two main routes used by metastatic cancer cells (Bernstein and Woodard, 1995). Second, the brain provides the necessary microenvironmental conditions to support GBM cell growth that might not be present outside of the brain (Reviewed in Cuddapah *et al.*, 2014). Thus, GBM cells preferentially invade intra-organ into the healthy brain tissue.

Interestingly, GBM cells invade using similar routes to those used by the neural stem cells (NSCs) during embryonic

development or repair processes in the damaged adult (Reviewed in Cayre, Canoll and Goldman, 2009). GBM cells use pre-existent brain structures as routes for invasion, namely: the brain parenchyma, the perivascular space, the white matter axonal tracts, and the leptomeningeal space (Scherer, 1938). These routes of invasion were first described, in 1938, by a German neuropathologist, Hans Joachim Scherer and, for that reason, they are commonly referred to as the "Scherer's structures" (Figure 1.3). Whether GBM cells use one route preferentially over the other, or whether the cells utilise additional routes, is not well understood.

Nevertheless, each route of invasion presents a different advantage or challenge to the invading cells. The subarachnoid space is filled with cerebrospinal fluid and contains the large blood vessels that supply the brain and spinal cord. The white matter tracts are made up of myelinated axons that the GBM cells physiologically use to move along. It is of particular interest to mention that the corpus callosum is the largest white matter tract, and it allows GBM cells to travel for a long distance. As such, it is often used as a highway to invade the opposite brain hemisphere (Pedersen *et al.*, 1995). The brain parenchyma accommodates densely packed neurons and glial

cells in a soft matrix; thereby making the extracellular space narrow for GBM cells to get through. (Scherer, 1938). The perivascular space, found around all blood vessels, comprises more rigid matrix components but provides lower physical resistance from cells than the brain parenchyma (de Gooijer *et al.*, 2018).

Independently from the invasion route, GBM cells invade as individual cells. This is also another feature that they share with NSCs (Reviewed in both Claes, Idema and Wesseling, 2007 and Cayre, Canoll and Goldman, 2009). In contrast, systemic malignant tumours that metastasise to the brain, invade as groups of cells rather than as single cells and have more defined and delineated margins compared to GBMs (Reviewed in Friedl and Wolf, 2003).

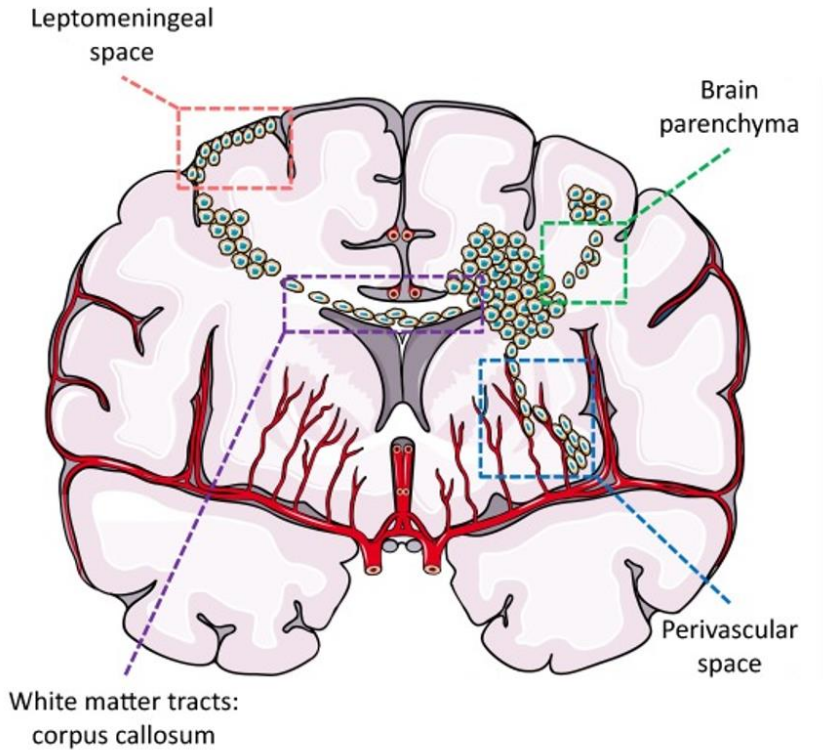


Figure 1.3: Routes of GBM cell invasion within the brain. *GBM cells can invade the brain using four structures known as the "Scherer's structures" namely: the brain parenchyma, the perivascular space, the white matter axonal tracts, and the leptomeningeal space. Modified from (de Gooijer et al., 2018)*

1.2.5 Modification of the brain ECM by GBM cells

The ECM comprises about 15-20% of normal brain volume. The brain ECM is composed of *hyaluronan*, the major component of the ECM within the brain, proteoglycans (versican, neurocan, aggrecan), glycosaminoglycans, thrombospondin-1 and tenascin-C. These proteins give the brain ECM its unique gelatinous consistency, not found elsewhere in the body (Reviewed in Zimmermann and Dours-Zimmermann, 2008).

Unlike other organs, the brain ECM lacks rigidity due to the absence of fibrillar protein, such as collagen and laminin (Reviewed in G. Gritsenko, Ilina and Friedl, 2012). GBM cells can, however, increase the rigidity of the ECM by modifying its composition. The ECM that has been modified by GBM cells is referred to as the "tumour ECM".

Hyaluronan is upregulated four-times more in the tumour ECM, reaching comparable levels to those present during the central nervous system (CNS) embryonic development (Delpech *et al.*, 1993). *GBM cells also upregulate their expression of the two transmembrane hyaluronan-binding* proteins, cluster differentiation 44 (*CD44*) and receptor for hyaluronan mediated motility (*RHMMR*) (Turley *et al.*, 1993). *CD44* expression has been shown to be higher in GBMs compared to low-grade gliomas (Yoshida *et al.*, 2012). The inhibition of both CD44 and RHMMR by monoclonal antibodies reduced GBM cells migration and invasion *in vitro* (Merzak, Koocheckpour and Pilkington, 1994; Akiyama *et al.*, 2001). Other ECM components identified within the tumour ECM include vitronectin, osteopontin, and brain enriched hyaluronic acid-binding protein (BEHAB). These modifications to the ECM are thought to facilitate tumour growth, proliferation and invasion, although specific

interactions and exact mechanisms are not well understood (de Gooijer *et al.*, 2018).

1.2.6 Modification of the perivascular ECM by GBM cells

Conversely, fibrillar proteins are widely present within the ECM of other organs, such as collagen (type IV, V), fibronectin, vitronectin, heparin sulfate, entactin and laminin, are only restricted to the perivascular space within the brain (Gladson, 1999). Nevertheless, GBM cells alter the composition of the ECM in the perivascular space to further promote cell invasion. GBM cells secrete tenascin-C, thrombospondin-1, and secreted protein acidic and rich in cysteine (SPARC) which bind and activate growth factors in the perivascular ECM as explained below.

Tenascin-C, which is usually upregulated during embryogenesis, is expressed at high levels by GBM cells and is particularly associated with the perivascular ECM (Brösicke *et al.*, 2013).

Moreover, the intensity of *tenascin-C* expression is shown to correlate with glioma grade (Leins *et al.*, 2003). Tenascin-C has been shown to interact with MMP12 while the knockdown of MMP12 has resulted in the attenuation of the tenascin-C–

stimulated GBM cell invasion *in vitro* three-dimensional matrix assay (Shi *et al.*, 2010). *Thrombospondin-1* also has been shown to be expressed at high levels by GBM cells and to be negatively correlated with patient prognosis (Daubon *et al.*, 2019). Thrombospondin-1 can bind and activate the growth factor, TGFβ1 (transforming growth factor beta 1), by releasing it from Latent Activating Protein (LAP) (Schultz-Cherry, Lawler and Murphy-Ullrich, 1994). This interaction results in the formation of a complex that involves conformational changes in TGFβ1, thereby making it accessible to its receptor to promote its pro-invasive downstream signalling (Schultz-Cherry *et al.*, 1995). The knockdown of thrombospondin-1 decreased GBM cell invasion in *in vitro* spheroids invasion assay in collagen type I, as well as in animals xenograft, which has significantly improved animals survival (Daubon *et al.*, 2019). SPARC is highly expressed in GBM cells, and cells with SPARC high expression show enhanced invasion *in vitro* (Pannuru *et al.*, 2014) While SPARC increases tumour invasion, it concomitantly decreases tumour growth (Kunigal *et al.*, 2006). The negative effects of SPARC on cell proliferation could be brought about by its ability to inhibit the activation of the Vascular endothelial growth factor (VEGF) (Brekken and Sage, 2001) which would

otherwise be negatively regulating tumour cell invasion (Lu *et al.*, 2012).

In addition, GBMs express bradykinin receptor 2 at high levels to promote cell invasion along with the perivascular space by binding to the bradykinins secreted by the vascular endothelial cells. The inhibition of bradykinin receptor 2 has been shown to decrease the number of GBM cells associated with blood vessels (Montana and Sontheimer, 2011).

Another form of modulating perivascular ECM to promote GBM cell invasion is by disturbing the BBB in order to create new routes for the invasion as discussed below. Vascular endothelial cells form the BBB though creating tight junctions between each other, to trap the blood serum and cells within the vascular lumen. The vascular wall is covered by one or two basement membranes anchoring endothelial cells around large blood vessels and capillaries, respectively. In the healthy brain, astrocyte endfeet cover around 99% of the vascular surface (Mathiisen *et al.*, 2010). The astrocyte endfeet, by anchoring into the basement membrane, serve to protect the endothelial tight junctions and release vasoactive molecules that regulate vascular diameter (Mathiisen *et al.*, 2010).

GBM cells travelling along the blood vessels, cause a localised disruption of the BBB by displacing the astrocyte endfeet, degrading the basement membrane and downregulating the expression of and degrading the endothelial tight junction proteins (Ishihara *et al.*, 2008; Watkins *et al.*, 2014) (Figure 1.4). In turn, serum components leak into the surrounding parenchyma. The displacement of the astrocyte endfeet also causes the loss of functional regulation of vascular diameter by astrocytes (Ishihara *et al.*, 2008). This gives GBM cell the advantage of easy access to oxygen and nutrients from the bloodstream, but it may also present an opportunity for targeted delivery of chemotherapeutics which are thought to be prevented from reaching the brain by the BBB (Reviewed in Cuddapah *et al.*, 2014).

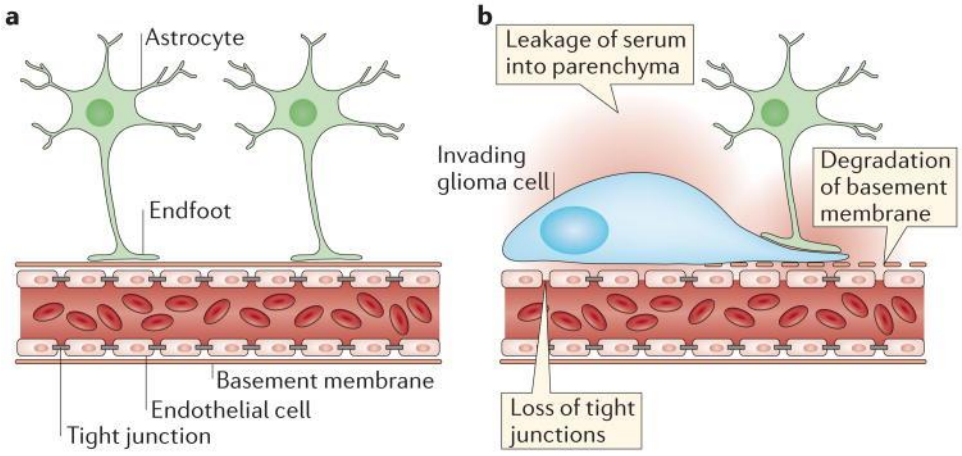


Figure 1.4: GBM-displacing astrocyte endfeet.
(a) In the healthy brain, astrocyte endfeet protect vascular endothelial cells tight junctions. (b) Invading GBM cells displace astrocyte endfeet and cause degradation of tight junctions

between endothelial cells and breakdown of the basement membrane surrounding blood vessels. Taken from (Cuddapah et al., 2014 Review Paper).

1.2.7 Clinical targeting of GBM cell invasion

The molecular mechanisms of GBM invasion have been exploited therapeutically. Drugs against several of the aforementioned targets along with the standard first-line GBM drugs have been taken to clinical trials in primary newly diagnosed GBMs.

In particular, the MMP2, MMP3 and MMP9 inhibitor (Prinomastat) reached phase II clinical trials in 2002 to be tested in combination with TMZ following radiotherapy and surgery in patients diagnosed with GBM. The results showed that survival did not differ significantly between the Prinomastat-treated and placebo-treated groups, and that Prinomastat efficacy is not enhanced over TMZ alone (Levin *et al.*, 2002).

Another inhibitor of MMPs, the Food and Drug Administration (FDA) approved Marimastat, has been used on GBM patients who had undergone surgery and radiotherapy in a phase I clinical trial in 2006. Marimastat, however, did not improve survival when compared to placebo (Levin *et al.*, 2006).

Targeting integrins is another promising strategy for inhibiting cell invasion. Cilengitide which targets αvβ3 and αvβ5 was in phase I/II trials in 2010, in combination with TMZ/radiotherapy for GBM patients with a methylated MGMT status. The trial showed that patient survival improved after the addition of cilengitide (Stupp *et al.*, 2010). However, in the follow-up phase III trial in 2014, the survival was not significantly improved with the addition of cilengitide as an adjuvant (Stupp *et al.*, 2014). The low degree of success might be due to acquired drug resistance and/or upregulation of compensatory pathways or due to poor drug penetration into the CNS (Stupp *et al.*, 2014).

1.2.8 *In vitro* assays to study GBM invasion

1.2.8.1 Two-Dimensional (2D) Assays

2D *in vitro* assays are the simplest method in which the behaviour of GBM cells can be studied. The most widely used technique is the 'monolayer wound-healing assay' or scratch assay. GBM cells are grown as 2D monolayers on a flat surface which could be coated with ECM components to trigger integrin signalling and mesenchymal cell movement.

After a scratch is made, the time that the cells require to migrate and fill the gap is measured. This gives an estimation

of the migratory capacity of these cells. However, a major drawback is that the estimate can be easily varied by the width of the scratch, which can change the migration velocity of the cells and reduces the comparability between the different experimental reports (Valster *et al.*, 2005; Justus *et al.*, 2014). Although they can breakdown the ECM components coating the surface they are plated on, cells are free to move into the open space. Therefore, scratch assays might be more suited to study migration as opposed to invasion, which involves changing cell shape to get through narrow spaces.

In addition, 2D assays cannot recapitulate the complexity of the tumour, e.g. the different cell types, and the interaction with the brain microenvironment, e.g. the biochemical gradient of different chemoattractant molecules present through the brain (Rao *et al.*, 2014).

1.2.8.2 Three-Dimensional (3D) Assays

Several studies have shown important discrepancies between 2D and 3D invasion studies, most likely due to the influence of physical cell-cell and/or cell-matrix interaction on invasion (Friedl *et al.*, 2012; Levin *et al.*, 2012). Many 3D assays have been developed to capture more complex

mechanistic aspects and recapitulate different microenvironmental features affecting GBM invasion.

The most popular of these techniques is the Boyden chamber assay, also known as filter membrane assay, chemotaxis assay, or transwell assay, which was originally introduced by Boyden to study leukocyte chemotaxis (Boyden, 1962). Cells are seeded on top of a porous insert, and the number of cells that move into the bottom compartment is quantified over time. The insert can be coated with ECM components to assay cell invasion. The ECM components added to the insert is, however, static; thus, the addition of serum or chemoattractants in the lower compartment is often required to trigger cell movement, which may not be physiologically relevant (Rao *et al.*, 2014). Although the seeded cells are in 2D cell cultures, their movement is the 3D space across a gradient of chemoattractants. Moreover, the chemoattractants are also static; thus, it is not possible to study the effect of the interstitial fluid pressure using this assay. Furthermore, this assay is not suitable to allow the investigation of the role of hypoxic gradients.

As a general limitation, transwell assays are only relevant for the study of perivascular invasion route as collagen and laminin are the most commonly used ECM components for coating the surface on which GBM cells are plated (Reviewed in G. Gritsenko, Ilina and Friedl, 2012).

Bioengineered scaffolds, such as hyaluronan-based hydrogels, are another type of 3D assays used to assay GBM invasion. In particular, they are designed to understand the influence of physical matrix properties such as elasticity, density, or stiffness on GBM invasion (Thomas and DiMilla, 2000; David *et al.*, 2004; Ulrich, de Juan Pardo and Kumar, 2009; Y. Yang *et al.*, 2011; S. S. Rao *et al.*, 2013). Cells are often embedded within a scaffold, the scaffold is cross-sectioned, and the cells are stained and visualised. Nevertheless, such an assay is unable to include multiple cell types surrounding the tumour in its natural brain microenvironment (Coniglio and Segall, 2013; L. Wang *et al.*, 2013).

To resolve this limitation, a microfluidic co-culture platform has been developed to be used as a 3D invasion assay. It consists of a gel scaffold flanked by two parallel channels in which different types of cells, grown in 2D, can be seeded (Gao *et al.*,

2011; Fernandes *et al.*, 2016; Chonan *et al.*, 2017). Using this platform, it is possible to also dynamically assess the invasive hierarchy of the tumour cells, in which more invasive cells led the way and followed by the relatively less invasive ones (Chonan *et al.*, 2017).

1.2.9 *In Vivo* Models to Study GBM Invasion

In vivo models, orthotopic xenograft invasion models, have the advantage of the presence of the native microenvironment of the brain. As such, the different invasion routes, as well as the effect of blood flow and immune response on invasion, can be studied. In these models, cultured cells are injected into a mouse brain. Invasion is then assessed using histology or live imaging techniques (Zhang *et al.*, 2011; Jensen *et al.*, 2016). In contrast to histological analysis which can only be taken at the one timepoint when the animal is sacrificed, live imaging can provide spatiotemporal data per animal to give a dynamic insight into the behaviour of tumour cells and their interaction with brain structures (Mitchison, 2011; Ricard and Debarbieux, 2014). However, the image resolution is often limited by the depth of tissue penetration. In general, the degree of invasion is measured as the distance between satellite cells and the main tumour mass. Yet, there are currently no standardised methods

which allow robust comparisons between studies, although algorithms that discriminate invasive cells from stationary cells are being developed to robustly quantify invasion in the future (Sampetrean *et al.*, 2011).

Because *in vivo* studies are expensive and time-consuming with associated ethical concerns, it is difficult to scale up experiments. In addition, inter-animal variability adds to the cost to use more animals to obtain a conclusive finding.

1.2.10 Ex Vivo Models to Study GBM Invasion

Brain slice invasion assay, also known as organotypic brain slice cultures, combine the relevant *in vivo* brain environment with the throughput of *in vitro* models (Ohnishi *et al.*, no date; Jung *et al.*, 2001, 2002; Yoshida *et al.*, 2002; Nakada *et al.*, 2005; Valster *et al.*, 2005). In this setup, thin slices are cut from post-mortem mouse brain and cultured on transwell inserts. Tumour cells are seeded on the slice, invaded cells are imaged, and the distance and penetration depth into the brain slice is used as a measure of quantifying cell invasion. Brain slices allow imaging at a higher resolution than in living *in vivo* models (Reviewed in Yamada and Cukierman, 2007). When brain slice invasion assay was compared to *in vivo* models, it was shown that it

recapitulated the *in vivo* invasion patterns very well (Jensen *et al.*, 2016). It also requires fewer animals than *in vivo* studies, since multiple slices can be generated from one brain. As well as allowing different invasion routes to be investigated within the physiological brain microenvironment, this assay enables in-depth studies of tumour–stroma–ECM interactions (Farin *et al.*, 2006). Deterioration of tissue viability, lasts up to 7 to 14 days, is the main limitation of *ex vivo* models (Jung *et al.*, 2002; Pencheva *et al.*, 2017). Another important limitation is the lack of blood supply, although capillaries have been reported to survive and secrete various molecules (Moser *et al.*, 2003; Hutter-Schmid, Kniewallner and Humpel, 2015).

In summary, our understanding of GBM invasion has been advanced through *in vivo* and *in vitro*, as well as *ex vivo* models. GBM invades as single cells and adopts a mesenchymal mode of movement. The molecular mechanism underlying GBM invasion has been exploited as therapeutic targets with some clinical trials being conducted. However, successful clinical trials await to be seen. Maybe there is a need to target other pathways in which GBM has vulnerability, along with targeting invasion.

1.3 Cancer cell metabolic reprogramming

Metabolic reprogramming has recently been recognised as one of the 10 hallmarks of cancer (Hanahan and Weinberg, 2011). Metabolic reprogramming refers to the process in which the catabolism and/or the anabolism of cellular metabolites, such as glucose, amino acids and lipids, in cancer cells is altered relative to their non-transformed counterparts as a consequence of oncogenic mutations and/or adaptation to the tumour microenvironment (Phan, Yeung and Lee, 2014).

Reprogramming cellular metabolism provides cancer cells with many advantages including i) augmented biosynthetic activity; ii) enhanced bioenergetic activity; iii) reduced oxidative stress; iv) acquired apoptotic resistance; and v) enhanced invasive potential, each of which will be discussed in the following section.

1.3.1 Advantages of metabolic reprogramming to cancer cells

1.3.1.1 Fuelling biosynthetic/anabolic pathways

Glycolysis occurs in response to hypoxia in non-neoplastic cells, but Otto Warburg in the 1920s observed that glycolysis occurs in neoplastic cells in the presence of oxygen, a process termed

"aerobic glycolysis" (Warburg, 1956). Aerobic glycolysis primarily provides metabolic intermediates for macromolecular biosynthesis, such as fatty acids (FAs) biosynthesis and nucleotide biosynthesis, through the pentose phosphate pathway (PPP) (Reviewed in both Vander Heiden, Cantley and Thompson, 2009 and Lunt and Vander Heiden, 2011). Through the PPP, about 90% of ribose 5-phosphate used for nucleotide biosynthesis is generated from glycolytic intermediates (Ramos-Montoya *et al.*, 2006).

Moreover, the nicotinamide adenine dinucleotide (NADH) molecules, generated in the process of aerobic glycolysis, are reduced into nicotinamide adenine dinucleotide phosphate (NADPH) when carbon is diverted from glycolysis into the oxidative arm of the PPP. NADPH is essential for FAs biosynthesis (Lazo, 1981). Moreover, the glycolytic enzyme pyruvate kinase type *M2 (PKM2)*, often found to be overexpressed in cancer, periodically suppresses lactate formation to facilitate the accumulation of metabolites that act as precursors for amino acid and FA biosynthesis (Eigenbrodt *et al.*, 1992).

Likewise, tricarboxylic acid (TCA) cycle provides NADH and metabolic intermediates for macromolecule biosynthesis; however, metabolic intermediates pool must be replenished in the TCA cycle by a process called anaplerosis (Reviewed in Oliver E. Owen, Kalhan and Hanson, 2002). Two activities that provide anaplerotic fluxes in cancer cells are glutaminolysis, which produces α-KG from glutamine, and pyruvate carboxylation, which produces oxaloacetate (OAA) from pyruvate, the end product of aerobic glycolysis. As such, increased glutaminolysis and accelerated aerobic glycolysis in cancer provide a constant supply of anaplerotic flux required by proliferating cells.

1.3.1.2 Enhancing bioenergetics/catabolic pathways

While ATP can still be generated through oxidative phosphorylation (OXPHOS) in glycolytic tumour cells, generating ATP via aerobic glycolysis is more favourable for the continuous and fast production of ATP per molecule of glucose. The production of ATP via glycolysis limits the yield of ATP per molecule of glucose consumed. This, in turn, prevents the accumulation of ATP, which would otherwise allosterically inhibit phosphofructokinase (PFK) that acts in the third step of

glycolysis to convert fructose-6-phosphate to fructose-1,6-diphosphate (Zheng, 2012; Yang *et al.*, 2016). Cancer cells also catabolises FAs by the process of fatty acid oxidation (FAO), also known as the β-oxidation pathway, to support ATP production via oxidative phosphorylation. Compared to the oxidation of one glucose molecule containing six carbons which only generate 36-38 ATP molecules, oxidation of one fatty acid containing 16 carbons (such as palmitate) generates 129 ATP molecules (Carracedo, Cantley and Pandolfi, 2013).

1.3.1.3 Fortification of redox homeostatic system and the evasion of apoptosis

Cancer cells show increased tolerance for oxidative stress, whereby moderate ROS levels promote proliferation and differentiation. However, excessive ROS levels cause oxidative damage and induce apoptosis, also known as programmed cell death (L. Jin *et al.*, 2015; Rinaldi *et al.*, 2016). Yet, cancer cells acquire the ability to evade apoptosis and recalibrate the redox balance.

Although cells acquire their glycolytic phenotype under normoxic conditions, the hypoxic tumour microenvironment,

created by an overgrowth of cells with limited oxygen supply, exert further adaptive pressure on tumour cells and causes more alterations in their metabolic programme (Gatenby and Gillies, 2004; Masson and Ratcliffe, 2014). Fluctuating oxygen levels can also result from an altered degree of vascularity (Gatenby and Gillies, 2004), as well as following the detachment of metastatic cells from the ECM (Schafer *et al.*, 2009). Under low oxygen conditions, the downregulation of OXPHOS decreases oxygen consumption which protects cells from genomic damage caused by the resultant reactive oxygen species (ROS) (Kondoh *et al.*, 2007). However, the enhancement of the antioxidant capacity of tumour cells can restore ATP generation through oxidative metabolism (Schafer *et al.*, 2009). Antioxidant capacity is enhanced through the upregulation of glutathione metabolism, and increasing the production of other antioxidants, such as NDAPH which act a ROS scavenger (Ahmad *et al.*, 2005).

Finally, cell apoptosis is evaded by inducing resistance to mitochondrial membrane permeability (Bonora and Pinton, 2014). Tumour cells employing aerobic glycolysis suppress membrane permeability by the action of the glycolytic enzyme, hexokinase II (HK II), which directly attach to the voltage-

dependent anion channel (VDAC), which is a mitochondrial inter-membrane transporter (Colombini; Mathupala, Ko and Pedersen, 2006). This, in turn, prevents the pro-apoptotic protein, Bax, from associating with VDAC by forming a mitochondrial permeability transition pore (PTP), across the mitochondrial membrane, through which cytochrome-c is released (Shimizu, Narita and Tsujimoto, 1999) (Gottlob *et al.*, 2001; Majewski *et al.*, 2004). Without the release of cytochrome-c, cellular cytotoxicity, and thus apoptosis, will be evaded (Cai, Yang and Jones, 1998).

1.3.1.4 Promoting cancer cell invasion

Apart from providing the energy to fuel invasion and the macromolecular for the remodelling of the lipid membrane, cancer metabolic reprogramming can further promote cancer cell invasion via changing the composition of the tumour microenvironment (Han *et al.*, 2013). Invasion is stimulated by acidic microenvironment created by the excessive secretion of the glycolytic by-product, lactate (Kato *et al.*, 2013). This augments cathepsin B release and promotes a pH-dependent activation of MMPs in the ECM (Swietach, Vaughan-Jones and Harris, 2007) (Victor *et al.*, 2011).

1.3.2 Reprogrammed metabolic pathways in cancer, with a specific focus on GBM Lipid metabolism

1.3.2.1 *De novo* FA synthesis

While normal cells rely on exogenous FAs from dietary sources, cancer cells upregulate *de novo* FA synthesis independently of dietary intake (Khandekar, Cohen and Spiegelman, 2011; Ross and Davis, 2014). In cancer cells, glucose metabolism feeds into *de novo* FA synthesis at the point of citrate (Figure 1.5).

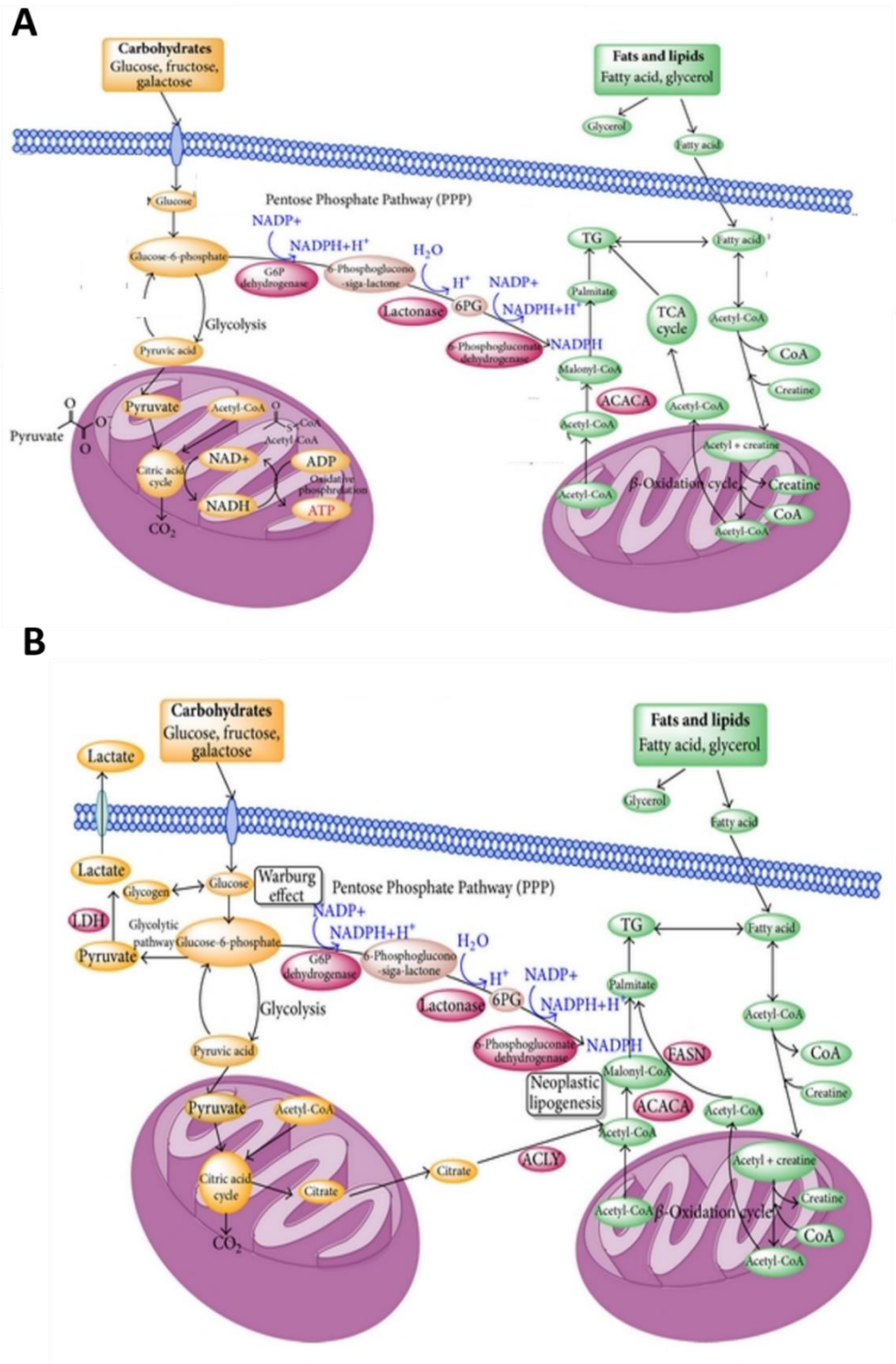


Figure 1.5: Glucose and Lipid metabolism in (A) normal and (B) cancer cells.

While normal cell use citrate in the TCA cycle, cancer cell divert citrate away from the TCA cycle into the fatty-acid synthesis pathway. Modified from (Cheng, Wang and Chen, 2014 Review Paper).

In normal cells, pyruvate, generated from glycolysis, is transported into mitochondria and converted into acetyl-CoA by pyruvate dehydrogenase (PDH). Citrate is then synthesised from the condensation of acetyl-CoA with OAA by citrate synthase, in the first step of the TCA cycle (Wiegand and Remington, 1986). Normal cells then shuttle citrate through the rest of the TCA cycle and generate NADHs, which are used by the electron transport chain to generate ATP.

In tumour cells, the citric acid cycle is truncated due to an inhibition of the enzyme aconitase, which converts citrate to isocitrate, as a result of the accumulation of high levels of ROS (Gardner *et al.*, 1995; Kim *et al.*, 2001). Citrate is, instead, used to make acetyl-CoA for the synthesis of FAs. When citrate is transported out of the mitochondria to the cytosol by the action of translocases; citrate is converted into acetyl-CoA by ATP-citrate lyase (ACL). It was found that the depletion of *ACL*, which is expressed at high levels, can result in impair cancer cell growth as seen, for example, in GBM (Beckner *et al.*, 2009). Acetyl-CoA carboxylase (ACC) then irreversibly carboxylates acetyl-CoA to form malonyl-CoA. *ACC* expression is also elevated in many cancers, including GBM, and its inhibition

result in reduced cell proliferation (Jones *et al.*, 2017). Both malonyl-CoA and acetyl-CoA are then converted by fatty acid synthase (FASN) into long-chain FAs, primarily palmitate (Currie et al., 2013). *FASN* is highly expressed in many cancers, including gliomas, where its expression positively correlates with glioma grade, with the highest expression being seen in GBM (Tao et al., 2013). Indeed, the inhibition of FASN inhibits growth and/or induces apoptosis in several cancers (Yan *et al.*, 2014; C.-S. Yang *et al.*, 2015).

Palmitate, as well as exogenous FAs, are then elongated to very-long-chain in four steps: condensation, reduction, dehydration, and reduction, occurring in the endoplasmic reticulum. In the first step, ELOngation of Very Long-FAs (ELOVL1–ELOVL7) enzymes catalyse the condensation of malonyl-CoA with a fatty acyl-CoA precursor. Tumours, such as breast cancer, show aberrant expression of *ELOVL* genes (Yamashita *et al.*, 2017). In the second step, a 3-ketoacyl-CoA reductase (KAR) reduces the resulting 3-ketoacyl-CoA to 3-hydroxyacyl-CoA using NADPH as a cofactor (Moon and Horton, 2003). The third step involves the dehydration of 3-hydroxyacyl-CoA to trans-2-enoyl-CoA by 3-hydroxyacyl-CoA dehydratases (HACD1-4) (Ikeda *et al.*, 2008). In the final step,

the product of the third step is reduced by trans-2,3-enoyl-CoA reductase (TER), in a NADPH-dependent manner to generate a FA with two more carbon units than the original FA (Moon and Horton, 2003).

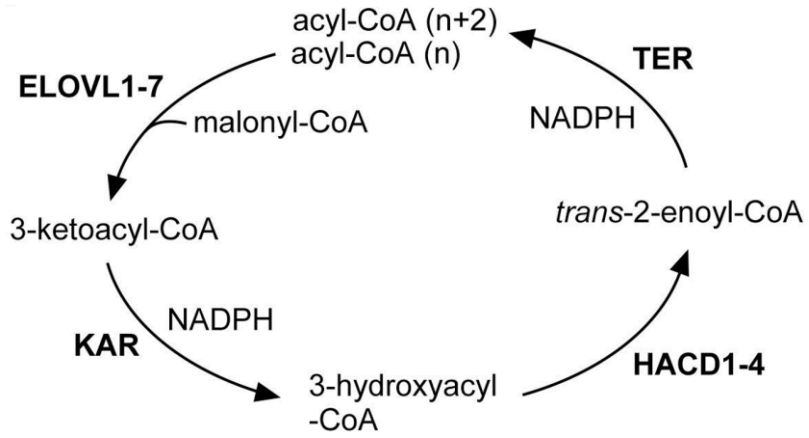


Figure 1.6: The process of fatty acid elongation.
Modified from (Naganuma and Kihara, 2014 Review Paper).

Subsequently, unsaturation can be introduced to FAs to create monounsaturated, polyunsaturated, and highly-unsaturated FAs by the desaturase enzymes: stearoyl-CoA desaturase and fatty acid desaturases 1 and 2 (SCD1 and SCD2). FAs can be esterified with glycerol to generate triglycerides (TGs) which are shuttled into lipid droplets upon exposure to hypoxia in order to fuel cellular bioenergetics via FAO upon re-oxygenation (Bensaad et al., 2014). As such, FA synthesis has been shown to continue in cancer cells even under low-oxygen conditions (Lewis et al., 2015).

1.3.2.2 The role of lipid droplets in cancer lipid metabolism.

Lipid droplets, also referred to as lipid bodies, oil bodies or adiposomes, are lipid-rich cellular organelles formed within the double-membrane leaflet of the endoplasmic reticulum (Figure 1.7). The biogenesis of LDs is initiated by the deposition of excess neutral lipids, mainly TGs and cholesterol esters, between the leaflets of the endoplasmic reticulum followed by the emergence of a lens-shaped structure. The lens-shaped structure protrudes towards the outer leaflet of the endoplasmic reticulum into the cytosol and eventually detach from the endoplasmic reticulum membrane to form a mature lipid droplet Reviewed in (Shyu *et al.*, 2018).

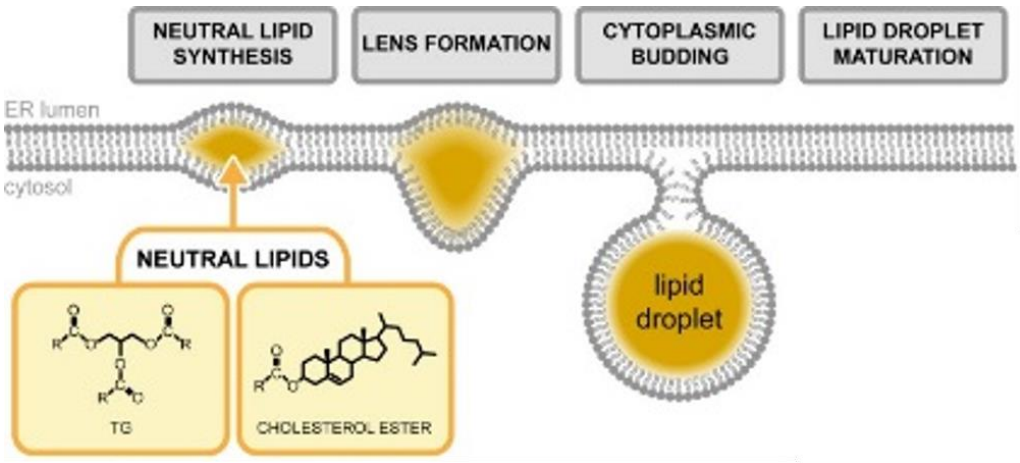


Figure 1.7: Synthesis of lipid droplets in the endoplasmic reticulum.
The neutral lipids, triglycerides (TG) and cholesterol esters, are synthesised by endoplasmic reticulum (ER) membrane proteins. Neutral lipid then merge to form the core of a lens-

shaped structure that protrudes towards the cytosol. The budding LD detach from the ER membrane to form the mature cytoplasmic organelle. Modified from (Shyu *et al.*, 2018)

Moreover, the single phospholipid of LDs selectively houses a subset of cytosol-derived or ER-derived proteins (Tan *et al.*, 2014), regulated in response to nutrient availability. These proteins are divided into three classes: (1) structural proteins, (2) membrane-trafficking proteins, and (3) enzymes implicated in lipid synthesis, such as DGAT2, and catabolism, such as ATGL (Brasaemle *et al.*, 2004; Tirinato *et al.*, 2017). The structural proteins are particularly used to visualise the presence of lipid droplets in the cell. They belong to the PAT family of proteins which include five members: perilipin 1 (PLIN1) (Grahn *et al.*, 2013), perilipin 2 (PLIN2/ADRP/adipophilin) (Brasaemle, 2007), perilipin 3 (PLIN3/TIP47) (Wolins, Rubin and Brasaemle, 2001), perilipin 4 (PLIN4/S3–12) (Wolins, Rubin and Brasaemle, 2001), and perilipin 5 (PLIN5/OXPAT) (Bickel, Tansey and Welte, 2009; Granneman *et al.*, 2011). PLIN1 and PLIN2 are constitutively lipid droplet-localised proteins, hence, they are the ones that are used to stain lipid droplets in the lab, while PLIN4, PLIN5 and PLIN6 are regarded as exchangeable proteins that respond to lipogenic or lipolytic stimuli (Wolins, Brasaemle and Bickel, 2006).

It is becoming clear that aberrant lipid droplets biogenesis in cancer is a consequence of intracellular imbalances in energy metabolism and redox homeostasis caused by nutrient overload (Sztalryd and Kimmel, 2014), complete or partial nutrient or oxygen deprivation (Brasaemle *et al.*, 2004; Olofsson *et al.*, 2009), mitochondrial dysfunction and the induction of apoptotic cell death (Boren and Brindle, 2012), and treatments with chemotherapeutic agents (Cotte *et al.*, 2018).

Thus, lipid droplets plays different roles to help cancer cells adapt to these imbalances. First, lipid droplets provide cells with a storage depot to prevent cellular dysfunction (due to lipotoxicity) by sequestering excess lipids or breaking them down through lipophagy, a lipid droplet-selective form of autophagy (Singh *et al.*, 2009; Jarc *et al.*, 2018). Second, lipid droplets establish membrane contact sites with other cellular organelles, including the mitochondria, to coordinate the consumption of lipids and cholesterols for energy production, by enabling optimal transfer of FAs to mitochondria (Herms *et al.*, 2015; Rambold, Cohen and Lippincott-Schwartz, 2015), for the maintenance of redox homeostasis, by stimulating NADPH synthesis (Bensaad *et al.*, 2014), and for membrane biogenesis during rapid cell growth (Barbosa *et al.*, 2015). Third, while

autophagy drives lipid droplet biogenesis by providing lipids recycled from membranous organelles, lipid droplets degradation promotes autophagy by providing lipids for the formation of autophagosomal membranes (ʀeviewed in (Li, Zong and Ding, 2017) and (Garcia, Vevea and Pon, 2018). Finally, the degradation of lipid droplets provides lipids that act as signalling molecules by themselves (Reviewed in (Garcia, Vevea and Pon, 2018)).

Although aberrant lipid droplets homeostasis has been well characterised in cancer, the question remains whether lipid droplets biogenesis is an adaptive response or a contributor to the disrupted cellular homeostasis. Yet, the function and regulation of lipid droplet in cancer cells remains to be poorly understood.

1.3.2.3 Degradation of FA

Because FAs provide twice as much ATP as glucose relative to their dry mass, cancer cells mainly use FAs to as energy sources compared to normal cells (Carracedo, Cantley and Pandolfi, 2013). FAO starts by the conjugation of free long-chain FAs with COA in the cytosol (Figure 1.8). The acyl groups of acyl-CoA are then transferred from CoA to carnitine, and shuttled across the outer mitochondrial membrane, by palmitoyl-CoA transferase 1

(CPT1) - also known as carnitine acyltransferase 1 (van der Leij *et al.*, 2000; Bonnefont *et al.*, 2004). Acyl-carnitines is then converted back to acyl-CoAs, and shuttle across the inner mitochondrial membrane, by palmitoyl-CoA transferase 2 (CPT2). Acyl-CoAs, inside the mitochondria, enters a cycle of four reactions, the catalysing enzymes of which were all found to be upregulated in GBM (Lin *et al.*, 2017), which results in the release of an acetyl-CoA unit, a molecule of FADH2 and a molecule of NADH (Figure 1.8).

Acetyl-CoA is then either used for *de novo* FA synthesis or it is fed into the Tricarboxylic acid cycle (TCA cycle), where additional FADH2 and NADH are generated (Teoh and Lunt, 2018). NADH and FADH2 that are generated by both FAO and the TCA cycle are then used by the electron transport chain to produce ATP.

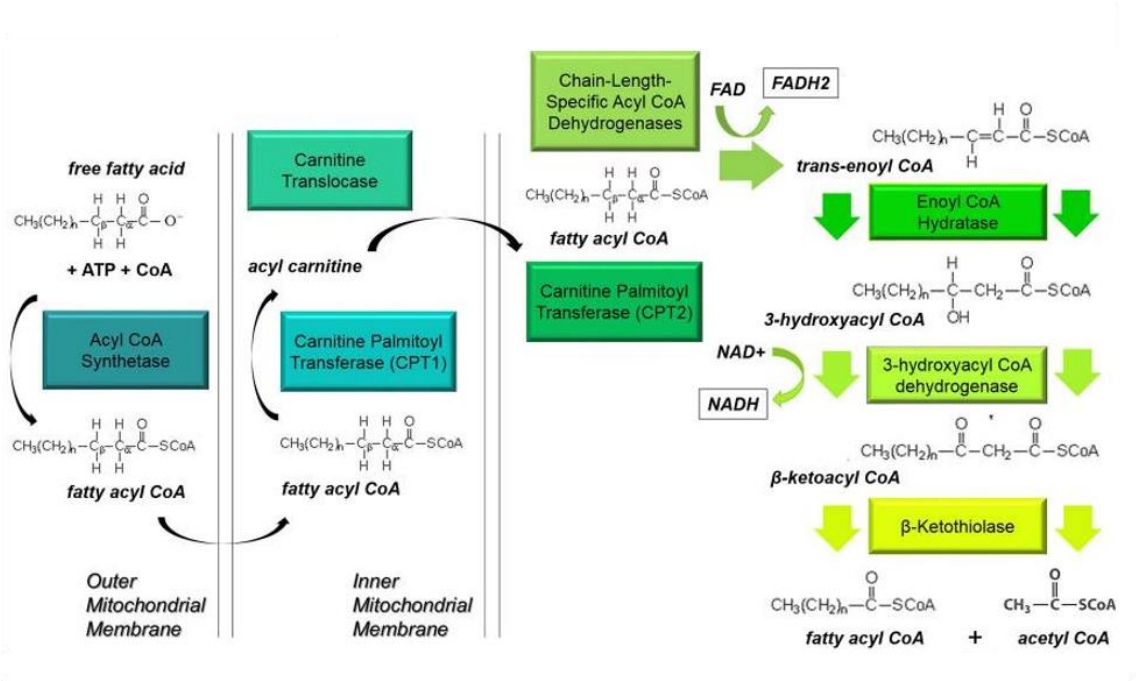


Figure 1.8: Fatty acid oxidation (FAO) cycle.
The acyl groups of acyl-CoA are transferred from CoA to carnitine, shuttled across the outer mitochondrial membrane, and then converted into acylcarnitine, to be transferred across the inner mitochondrial membrane, for further degradation. Taken from (Izquierdo-Garcia et al., 2015)

1.3.2.4 Cholesterol metabolism

Cholesterol plays an important structural role in cell membrane (Krause and Regen, 2014). Cells can either synthesise cholesterol or import it into the cell from exogenous sources. *De novo* cholesterol synthesis occurs via the mevalonate pathway. In this pathway, acetyl-CoA is converted into 3-hydroxy-3-methylglutaryl (HMG)-CoA by the action of HMG-CoA synthase 1 (HMGCS1). *HMGCS1* has been found to be amplified in various cancers (Pandyra *et al.*, 2015). HMG-CoA is then converted into mevalonate by HMG-CoA reductase

(HMGCR) which is the rate-limiting step in the pathway. Subsequent enzyme-catalysed reactions generate several fundamental end-products, including cholesterol and isoprenoids (Goldstein and Brown, 1990). *HMGCR* has also been reported to have either deficient feedback control or to be highly expressed or active in a number of cancers (Larsson, 1996).

To reduce energy expenditure on *de novo* biosynthesis of cholesterol, exogenous cholesterol is taken up by the cell. Circulating low-density lipoproteins (LDLs) are incorporated into cells via the Low-density lipoprotein receptor (LDLR) family (Brown and Goldstein, 1986). In normal cells, cholesterol homeostasis is maintained through sterol regulatory element-binding protein (SREBP) pathway, which suppresses *HMGCR* and *LDLR* expression (Brown and Goldstein, 1999; Goldstein and Brown, 2009). In GBM cells, *LDLR* is expressed at a higher level compared to normal brain, while *HMGCS1* and *HMGCR* expression is found to be relatively lower, which indicates that lipoprotein uptake is the main mechanism employed by GBM cells to meet their cholesterol requirements (Villa *et al.*, 2016).

To prevent the toxic accumulation of cholesterol, cells activate sterol O-acyltransferase (SOAT), to store excess free cholesterol in an esterified form within LDs. Indeed, the

inhibition of SOAT1 was found to suppress tumour growth and prolongs survival in xenograft models (Geng *et al.*, 2016). Excess cholesterol is also exported out of the cell through the ATP-binding cassette (ABC) superfamily of transporters (Tarling, de Aguiar Vallim and Edwards, 2013). ABC transporters shuttle cholesterol to apolipoprotein A (ApoA) which leads to the formation of high-density lipoprotein particles which are ultimately returned to the liver for excretion as bile (Vedhachalam *et al.*, 2007).

1.3.2.5 Electron transport chain

In the electron transport chain, electrons are transferred from electron donors, NADHs, to electron acceptors, oxygen molecules, through a series of enzymes, complexes I through to IV, within the inner mitochondrial membrane in order to generate ATP from ADP.

Normal cells employ complete oxidation of glucose in the TCA cycle to generate FADH2 and NADH to be used by the electron transport chain. In contrast, cancer cells mainly use FAO, which feeds into the TCA cycle, and the generated FADH2 and NADH from both can then be used by the electron transport chain. In light of this, several studies, although with somewhat conflicting

findings, attempted to investigate the possibility of the impairment of the electron transport chain in GBM. In 2014, Feichtinger et al. reported that Complex I-IV have lower activity in GBMs compared with the normal brain in cell dissociated from fresh-frozen human tissue samples (Feichtinger et al., 2014). Moreover, the expression of some Complex I subunits were shown to be downregulated in GBM (Deighton et al., 2014). Yet, some other subunits of Complex I, such as ND46, were previously shown to exhibit mutations that promote the stabilisation of the whole enzyme (DeHaan et al., 2004). Therefore, it may potentially be that there are differences in the degree of reliance upon the electron transport chain among the different cell population within the GBM tumour.

1.3.2.6 Aerobic glycolysis

Although normal cells use glycolysis under hypoxia, some cancer cells heavily rely upon, or sometimes completely switch to, aerobic glycolysis to generate ATP for the cell (Yu *et al.*, 2017). Glycolysis represents a ten-step pathway starting with the conversion of glucose to glucose-6-phosphate (G6P). This is catalysed by hexokinases (HK). In cancer, and particularly GBM, the Hexokinase 2 (*HK2*) isoform is strongly expressed (Wolf, Agnihotri, Munoz, *et al.*, 2011). The step that is

considered to be the rate-limiting step in glycolysis is where phosphoglucose isomerase (PGI) converts G6P to fructose-6-phosphate (F6P). The phosphorylation of F6P into fructose-1,6-biphosphate (F16BP) by phosphofructokinase 1 (PFK1). *PFK1* is highly expressed in many cancers, and its knockdown and pharmacological inhibition in GBM mouse models led to a significant increase in survival (G. Wang *et al.*, 2013; Sanzey *et al.*, 2015).

From F16BP, the consecutive catalytic activities of aldolase A (ALDOA), glyceraldehyde 3-phosphate dehydrogenase (GAPDH) and phosphoglycerate kinase 1 (PGK1) result in the production of 3-phosphoglycerate (3PG). Next, phosphoglycerate mutase 1 (PGAM1) isomerises 3PG to 2-phosphoglycerate (2PG). *PGAM1* shows high expression in gliomas, which positively correlates with glioma grade (H. Gao *et al.*, 2013). Enolases then convert 2PG to phosphoenolpyruvate (PEP). Amongst the three enolase isoforms (*ENO 1* through to *3*), only *ENO1* and *ENO2* are expressed in the brain, and *ENO1* is the major isoform in GBM, accounting for 75–90% of total enolase activity in the cell (Muller *et al.*, 2012). The terminal glucose enzyme is pyruvate kinase (PK) catalyses the conversion of PEP to pyruvate

(Noguchi, Inoue and Tanaka, 1986). As mentioned before, the M2 isoform of pyruvate kinase, PKM2, has a relatively decreased enzymatic activity than other PK isoforms which leads to the accumulation of upstream glucose intermediates, that can be channelled into different biosynthetic pathways (Christofk *et al.*, 2008a). *PKM2* is highly expressed in cancer cells, including in GBM cells where it is selectively expressed at low levels while being completely absent in normal brain (Christofk *et al.*, 2008b). Finally, pyruvate dehydrogenase kinase (PDK), which is upregulated in GBM (Velpula *et al.*, 2013), inhibits pyruvate dehydrogenase, thereby preventing the entry of pyruvate into the TCA cycle. PDK inhibition also improves survival in *in vivo* GBM models (Sanzey *et al.*, 2015). Pyruvate is then converted to lactate by lactate dehydrogenase-A (LDHA) (Feng *et al.*, 2018). *LDHA* expression has a significant positive correlation with glioma grade, and its knockdown in GBM cells inhibited cell growth (Di *et al.*, 2018).

1.3.2.7 Nucleotide synthesis through the pentose phosphate pathway (PPP)

The PPP is parallel to and branched from the first rate-limiting step of glucose metabolism. Under high demand for nucleotide, G6P is diverted from the glycolysis into the PPP. While normal cells frequently rely on the oxidative arm of PPP, cancer cells use both oxidative and non-oxidative arms (Boros *et al.*, 2000; Cascante *et al.*, 2000; Langbein *et al.*, 2006).

In the oxidative arm of PPP, G6P is converted into 6-phosphogluconolactone, which is converted 6-phosphogluconate, then into ribulose 5-phosphate in three consecutive steps mediated by G6P dehydrogenase, 6-phosphogluconolactonase, ribulose-5-phosphate, respectively.

In this process, two molecules of NADP are reduced to two molecules of NADPH to be used as reducing equivalent for several reactions, including FA synthesis as well as glutathione synthesis, to maintain redox homeostasis. In the non-oxidative arm of PPP, ribulose 5-phosphate isomerase converts ribulose 5-phosphate into ribose 5-phosphate to be used for nucleotide biosynthesis. The non-oxidative arm of PPP also plays a key role in anaplerosis in tumour cells, based on higher expression and

activity of transketolases in some cancers, including GBMs (Langbein *et al.*, 2006; Völker *et al.*, 2008).

1.3.2.8 Glutaminolysis

To compensate for the removal of citrate and other metabolites from the TCA cycle that are used as precursors for biosynthetic reactions, tumour cells use anaplerotic reactions to refill the pool of TCA cycle intermediates. This is largely achieved through upregulating the uptake of the non-essential amino acid, glutamine, as well as upregulating its breakdown through glutaminolysis (DeBerardinis et al., 2007; Pavlova and Thompson, 2016).

In GBM and other cancer cell lines, glutamine is taken up from the cell culture media was found to contribute up to 90% to the OAA pool (DeBerardinis *et al.*, 2007). When glutamine is not supplied with the media, OAA is made from the carboxylation of pyruvate by pyruvate carboxylase as described by Cheng et al. who investigated the growth of glutamine deprived GBM cells (Cheng *et al.*, 2011). In the plasma, glutamine is the most abundant amino acid. Glutamine is transported into the cell by SLC1A5, which is often upregulated in numerous cancer cells (Bhutia *et al.*, 2015). This phenomenon leads to glutamine

addiction in cancers, including myeloma and glioma (Bolzoni et al., 2016; Márquez et al., 2017).

Glutamine is converted into glutamate by glutaminase (GLS), which is upregulated in cancer. Upon the knockdown of *GLS* in GBM cells, cell growth was inhibited, and apoptosis was induced (Campos-Sandoval et al. 2015). In contrast to normal cells with intact TCA cycle that generate α-KG from the oxidative decarboxylation of isocitrate by IDH2, cancer cells, with truncated TCA cycles, rely on glutamate to create α-KG through the action of glutamate dehydrogenase (GDH) (Yang, Venneti and Nagrath, 2017). α-KG can fuel the anaplerotic process via, the TCA cycle-independent, reductive carboxylation reaction of αKG to isocitrate, which takes place in the cytosol and is mediated by IDH1 (Metallo et al. 2012). Isocitrate is converted to citrate, then to acetyl-CoA, which supports lipid synthesis, as well as to OAA and other TCA intermediates (as seen in Figure 1.9) (Mullen et al., 2011).

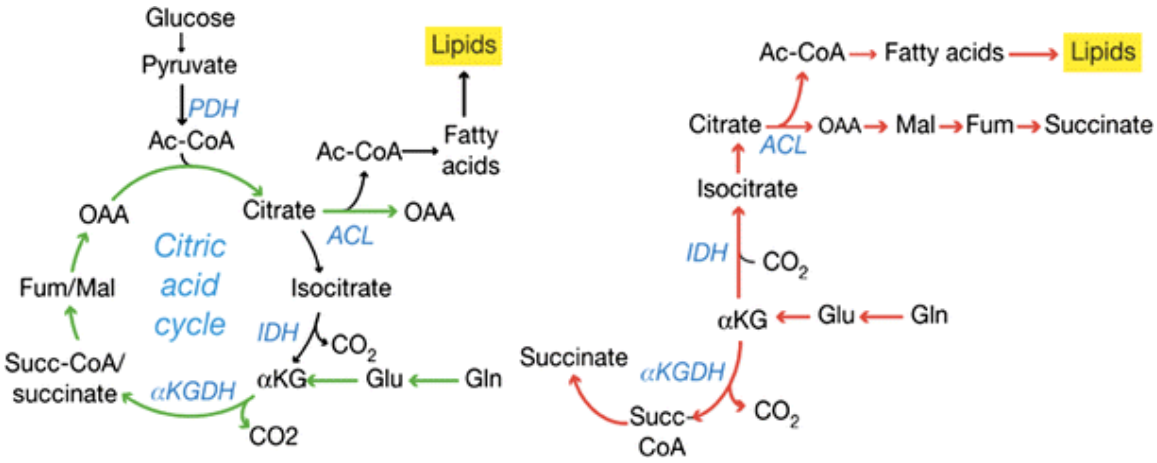


Figure 1.9: TCA cycle in normal cells (green) and cancer (red).
When the TCA cycle is truncated in cancer cells, IDH-dependent reductive carboxylation sustains the formation of metabolic intermediates for the TCA cycle and fatty acid synthesis. Taken from Mullen et al. (2012).

α-KG can be converted back to glutamate (Figure 1.10) by branched-chain amino acid transaminase 1 (BCAT1) (Tönjes et al. 2013). Moreover, the Knockdown of *BCAT1* reduces GBM cell growth as well as invasion, possibly due to the reduced influx of acetyl-CoA and succinyl-CoA into the TCA cycle. Interestingly, IDH-mut GBMs intrinsically have low *BCAT1* expression grow slower than IDH wild-type GBMs (Tönjes et al., 2013).

Moreover, in IDH-mut GBMs, mutated IDH1 does not convert αKG to isocitrate, but instead mediate the conversion of αKG into 2-HG (Figure 1.10). 2-HG directly binds and inhibits ATP synthase (Reuss *et al.*, 2015). Thus, GBM harbouring *IDH1*

mutation show energy potential, correlating with their reduced aggression (Fack *et al.*, 2017).

While NADPH is generated by both oxidative decarboxylation (of isocitrate to αKG) and reductive carboxylation (of αKG to isocitrate) reactions mediated by wild type IDH enzymes, the conversion of αKG into 2-HG consumes NADPH to generate NADP+ which limits the available NADPH for *de novo* FA synthesis as observed fibrosarcoma cells, although not yet shown in gliomas (Badur *et al.*, 2018).

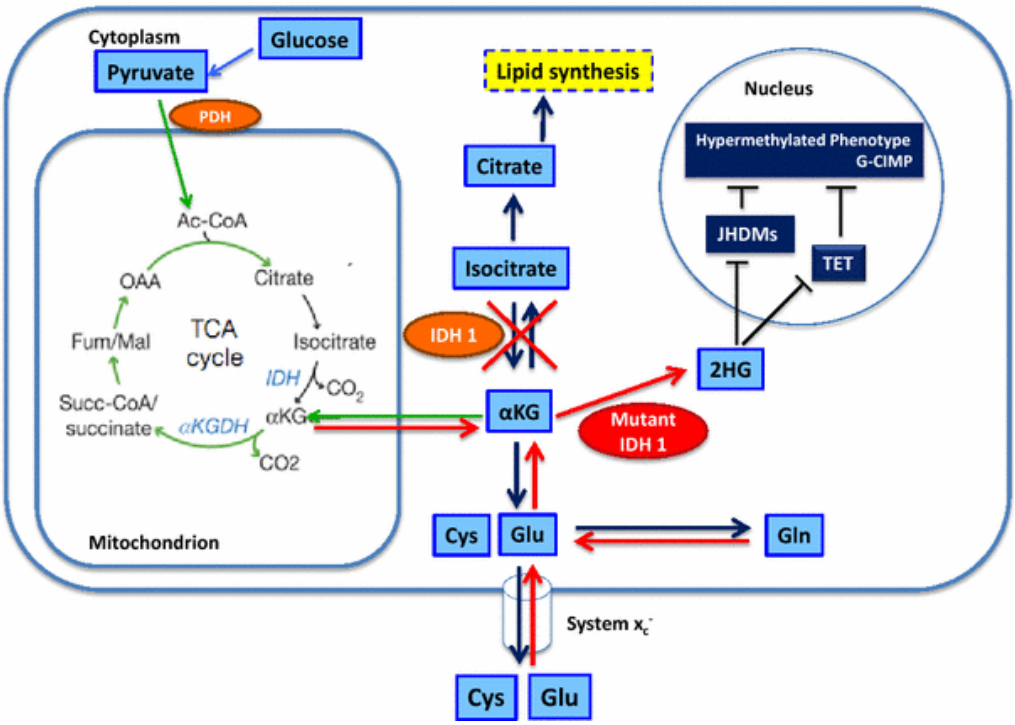


Figure 1.10: Overview of the change in glutamate metabolism in IDH mutant cells
In a normal cell (green arrows), αKG is used in the TCA cycle. In a cancer cell (blue arrows), αKG is used to generate isocitrate and other TCA cycle intermediates. αKG can also be converted back to glutamate (Glu) to be secreted in exchange for cytosine (Cys). When IDH is mutated in cancer cells (red arrows), αKG is converted into 2HG and glutamate is taken up in exchange for cytosine.Taken from (Maus and Peters, 2017).

As well as contributing to anaplerosis, glutaminolysis also contributes to catabolic processes in the cell. Glutamate can serve as a substrate for glutamate OAA transaminase or glutamate pyruvate transaminase to synthesise aspartate and alanine, respectively; which are converted into OAA and pyruvate, respectively, to feed into the TCA cycle (Reviewed in Oliver E. Owen, Kalhan and Hanson, 2002). Furthermore, aspartate can be converted into asparagine by asparagine synthetase (AS). It has been reported that the knockdown of

AS led to apoptosis, while the exogenous addition of asparagine completely restored survival in GBM cells (Zhang et al. 2014). Similar findings were also reported in sarcoma (Hettmer et al. 2015), melanoma and epidermoid carcinoma cells (Li et al. 2015).

1.3.2.9 Glutathione synthesis

Glutathione is a tripeptide (γ-glutamylcysteinylglycine) comprised of cysteine, glutamate, and glycine. Glutamate contributes directly to redox balancing by functioning as a precursor to the antioxidant, glutathione. The inhibition of glutamate conversion from glutamine by glutaminase reduced tumour cell proliferation (Ulanet *et al.*, 2014) and invasion (Wang, 1989), and decreased glutathione production.

Although glutamate is a major component to glutathione, when intracellular glutamate levels rise, excessive glutamate is exported out of the cell via the glutamine/cysteine antiporter system in exchange for cysteine (C.-S. Shin *et al.*, 2017). Indeed, cysteine deprivation has been shown to decrease GBM cell proliferation (Liu et al. 2015).

Cancer cells take up exogenous serine for conversion into glycine, by mitochondrial serine hydroxymethyltransferase

(SHMT2) (Labuschagne et al., 2014). *De novo* synthesis of serine can also take place by diverting 3PG from glycolysis to make 3-phosphohydroxypyruvate (3-PHP), a reaction that is catalysed by Phosphoglycerate dehydrogenase (PHGDH). PHGDH is found to be amplified in breast cancer and melanoma (Mullarky *et al.*, 2011; Possemato *et al.*, 2011). Moreover, PHGDH expression increases with the increase in glioma grade, with the highest expression being observed in GBM tumours (J. Liu *et al.*, 2013). Following the conversion of 3-PHP is into 3-phosphoserine (3-PS) by phosphoserine aminotransferase (PSAT), 3-PS is converted into serine by phosphoserine phosphatase (PSPH) (Possemato et al., 2011).

Cells make glutathione in two ATP-dependent steps. First, glutamate-cysteine ligase (GCL) synthesises γ-glutamylcysteine from glutamate and cysteine. This step is the rate-limiting step in glutathione synthesis. Second, glutathione synthetase catalyses the addition of glycine to the C-terminal of γ-glutamylcysteine to make glutathione (GSH) as an end product (Lu, 2009).

GSH protects cells from ROS-induced oxidative stress by neutralising (reducing) ROS. It does this by serving as

an electron donor. In this process, glutathione is converted to its oxidised form glutathione disulfide (GSSG). Oxidised glutathione (GSSG) is recycled back by glutathione reductase, which converts the oxidised glutathione back into its reduced form, glutathione, using NADPH as an electron donor (White *et al.*, 2003).

Despite the decrease in cysteine uptake in IDH-mut GBMs (Maus and Peters, 2017), GSH synthesis is still maintained via the transsulfuration pathway which supplies cysteine from the methionine cycle (Fack *et al.*, 2017), as detailed in the next section.

1.3.2.10 Creatine, methionine and folate biosynthesis

As well as feeding into the synthesis of GSH, the conversion of serine to glycine can feed into the synthesis of creatine. Creatine serves as a cellular energy reserve, because when it is converted into phosphocreatine by creatine kinase, it donates its phosphate group to convert ADP to ATP (Guimarães-Ferreira, 2014). Creatine is made from the glycine and arginine which are used as substrates for L-arginine:glycine amidinotransferase (AGAT) to produces guanidinoacetate acid (GAA). Methionine is then used to methylate GAA to produce

creatine, through the action of guanidinoacetate methyltransferase (GAMT) (da Silva *et al.*, 2009).

The conversion of serine to glycine releases one-carbon unit to be used in the one-carbon metabolism which consists of the folate and methionine cycles (Figure 1.11). Intermediates generated from the methionine cycle are fed into the transsulfuration pathway while the folate cycle supplies intermediates for purine biosynthesis.

In the methionine cycle, methionine, which is obtained from exogenous sources, is converted into SAMe (S−Adenosyl Methionine), which is a methyl donor for numerous reactions. SAMe becomes SAH (S−Adenosyl Homocysteine) when it loses its methyl group. SAH is converted to homocysteine, which subsequently enters the transsulfuration pathway to produce cysteine (Ducker and Rabinowitz, 2017). Cysteine can then be used to generate either GSH, as mentioned above, or it can be used to produce taurine (Figure 1.11) (Stipanuk and Ueki, 2011). Taurine has a potential role as an antioxidant, by ensuring an efficient flux of reducing equivalents through the electron transport chain in order to prevent the diversion of electrons to the acceptor oxygen and the generation of ROS (Jong, Azuma and Schaffer, 2012).

If homocysteine does not enter the transsulfuration pathway, it gets converted into cystathionine and ultimately to succinyl-CoA. By the action of succinyl coenzyme A synthetase (SCS), succinyl-CoA is then converted into succinate to be used in the TCA cycle (Tymoczko and Stryer, 2002).

Alternatively, homocysteine is converted back to methionine by the addition of a methyl group by one of two pathways (Figure 1.11). In one pathway, a methyl group is transferred from methylated folate (folic acid - methylenetetrahydrofolate, MTHF) to homocysteine, by methionine synthases and assisted by folate (vitamin B12). In another pathway, choline is oxidised to betaine which acts as the source of the methyl group transferred to homocysteine (Ueland, 2011).

MTHF is converted into tetrahydrofolate (THF). THF in turn is converted into 5,10-methylene-THF (5,10-meTHF) by hydroxymethyl transferase 2 (SHMT2) (Fowler, 2001). Next, 5,10-meTHF enters the mitochondria to be converted into 10-formyl-THF by methylenetetrahydrofolate dehydrogenase enzymes, MTHFD2. Both 5,10-meTHF, and 10-formyl-THF are used for purine synthesis; the newly synthesized pyrimidines

and purines are used to maintain cell proliferation (Mejia and MacKenzie, 1988; Yang and MacKenzie, 1993; Di Pietro *et al.*, 2002).

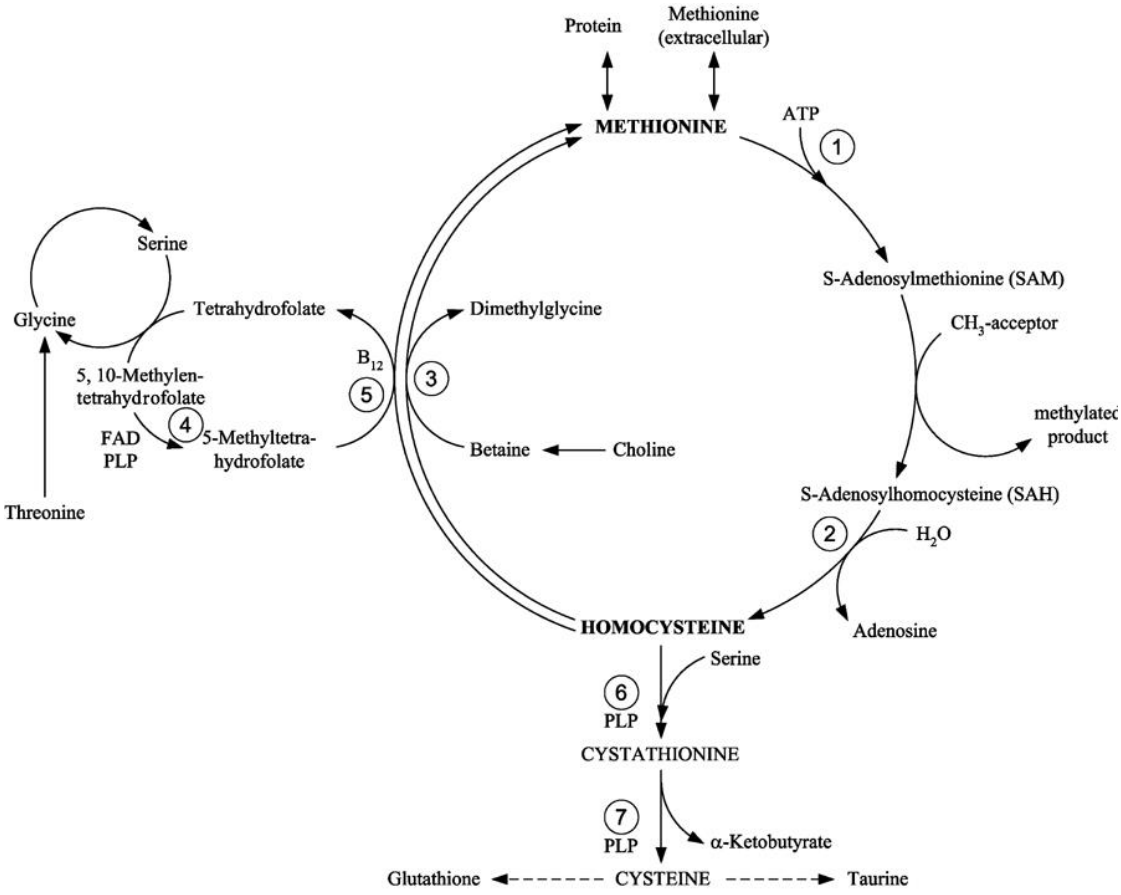


Figure 1.11: One-carbon metabolism - folate and methionine cycles.
Methionine is converted into homocysteine, which subsequently enters the transsulfuration pathway to produce cysteine. Cysteine is used to produce either glutathione or taurine.*Taken from* https://www.benbest.com/health/Meth.html.

1.3.3 Analytical profiling platforms to study cancer metabolism

Metabolic profiling is the measurement of the relative abundance of the entire metabolite collection within the cells

(Nicholson, Lindon and Holmes, 1999; Lindon *et al.*, 2003). The measurement of metabolite profiles from a biological sample, such as tissue/cells or biofluid, have provided many opportunities to understand the dynamic response to external stimuli, like an ectopic genetic modification or drug treatment, and inherent biological variations, for example - pathophysiological or developmental stimuli.

The terms metabonomics and metabolomics are historically used to describe this field based on the principal platform developed to detect metabolites. As such, metabonomics is based on the use of proton nuclear magnetic resonance spectroscopy, whereas metabolomics is based on employing mass spectrometry as an analytical platform.

1.3.3.1 Analytical profiling using mass spectrometry (MS)

Since many of the metabolites within the tumour associated metabolic pathways, such as glycolysis, glutaminolysis, and one-carbon metabolism, have hydrophilic chemical properties, analytical platforms that can measure these "water-soluble metabolites" are critical to understanding the changes in cancer cell metabolism.

MS-based approaches are the most powerful techniques employed to determine the metabolic profiles of hydrophilic metabolites. A chromatographic separation step coupled to MS is necessary in order to separate isomers, which have the same mass and will otherwise not be resolved by an MS.

There are two types of chromatographic techniques that are used for these purposes, namely gas chromatography (GC) and liquid chromatography (LC), and they will be compared and contrasted in the following section.

For LC-based metabolite separation, using either hydrophilic interaction liquid chromatography (HILIC) or reversed-phase ion-pair chromatography allows the separation of hydrophilic metabolites (Bajad *et al.*, 2006; Lu *et al.*, 2010). During HILIC-based separation, hydrophilic metabolites are dissolved in a solvent (mobile phase), such as acetonitrile. Then the sample is injected into a column packed with the hydrophilic stationary phase, such as –NH2 column (Rabinowitz and Kimball, 2007). As the mobile phase passes through the column, the metabolites separate by adsorbing onto the stationary phase

based on their relative affinity. The higher the affinity, the longer the metabolite takes to travel to the end of the column. Alternatively, during reversed-phase ion-pair chromatography-based separation, an ion-pairing reagent that consists of both hydrophilic and hydrophobic residues in a single molecule is applied. As such, hydrophilic metabolites interact with the hydrophilic part of the regent while the hydrophobic part interacts with the hydrophobic stationary phase of the column, such as –C18 column (Bajad *et al.*, 2006).

In contrast, in GC-based metabolite separation, hydrophilic residues undergo derivatisation (e.g., trimethylsilylation) where the hydrophilic group in a molecule is chemically converted to a hydrophobic group in order to make the molecule volatile (DeHaven *et al.*, 2010). Then, a chemically inert carrier gas, such as Helium, is used as a mobile phase to carry the metabolites across a column containing a hydrophobic stationary phase (DeHaven *et al.*, 2010).

Metabolites separated by LC are eluted from the column by applying a mobile phase gradient to release metabolites from the column based on their affinity. Mobile phase gradient is established by increasing the percentage of solvent in a time-

dependent way. Thus, the optimisation of the mobile phase gradient can improve metabolite separation.

Metabolites separated by GC are eluted by increasing the column temperature in a time-dependent fashion. Thus, separation may be optimised by changing the temperature gradient.

The eluted metabolites, separated on the basis of their retention time on the column, are sprayed one-by-one into atmospheric pressure ion source, where they are converted into ions. Electrospray ionisation (ESI) is applied for liquid chromatography-mass spectroscopy (LC-MS) while electron impact (EI) is used for GC-MS-based analysis. In contrast to ESI, which only adds a charge to the metabolites, EI fragments the metabolite into multiple ions. On the other hand, the LC process itself fragments and ionises the metabolites through the loss of H+ ions.

The ions enter into the mass analyser compartment which sorts chemically similar metabolites according to their mass to charge (m/z) ratio (Lu *et al.*, 2010; Yuan *et al.*, 2012). The mass detector then counts the ions emerging from the mass analyser and generate a mass spectrum, which shows the intensity of

the ion signal (metabolites abundance) plotted as a function of the m/z ratio.

Because of their hydrophobic chemical properties, specialised MS techniques have been optimised for analysing the profiles of lipids (lipidomics), such as tandem MS (or MS/MS) (Yang and Han, 2016). Both LC-MS and GC–MS-based platforms have been employed to profile lipid metabolism in cancer (Sánchez-Ávila *et al.*, 2009; Kamphorst *et al.*, 2011). Moreover, while many metabolites, such as amino acids, can be detected by both LC–MS-based and GC–MS-based platforms, some metabolites can only be detected by one specific platform. Metabolites involved in bioenergetics processes, such as CoA, ATP or NADPH, as well as larger and non-volatile molecules, such as complex peptides, can only be detected by LC-MS. In contrast, GC–MS is required for adequately separating metabolites, such as sugar alcohols and very short chain FAs. Thus, the use of both platforms could increase the coverage of a wider range of metabolite, though LC-MS is a more popular technique due to its wider metabolite coverage (Lu *et al.*, 2017).

1.3.3.2 Analytical profiling using proton nuclear magnetic resonance (1H-NMR) spectroscopy

1H-MRSI is a non-invasive technique used in routine clinical practice to quantify local metabolites in tissue samples. This technique is less sensitive than MS and is based on the detection of resonance frequency signals generated by a spinning hydrogen-1 nucleus. These signals are generated when the nucleus changes the orientation of its rotational axis to align itself with an external magnetic field. 1H is commonly used in this technique due to its presence in almost all molecules in the human body. 1H in different molecules resonates at a slightly different frequency. Each molecule exhibits a characteristic chemical shift in resonance frequency due to the differences in the local electron cloud that may shield the nucleus from the main magnetic field. The chemical shift for each molecule is detected, and an NMR spectrum is generated. The spectrum displays peaks–representing a proton in a different resonance state—and a peak area, which is directly proportional to the concentration of the molecule detected. Stable structures such as aromatic compounds appear earlier on the of the spectrum, and more flexible structures such as

aliphatic methyl groups appear towards the end of the spectrum, while other nonaromatic ring structures, such as sugars, appear in the middle of the spectra.

Despite the advantage of being a non-destructive process, NMR is especially good for providing structural information, which enables the identification of novel compounds. The main advantages that MS has over NMR are the higher detection sensitivity, which allows more coverage of the metabolome. MS detect concentrations around 10^{-12} M; while NMR has a detection limit of 10^{-5} M. However, NMR has a faster run time compared to LC-MS. NMR generates a spectrum from a biological sample within about 10 minutes, whereas LC-MS takes 20-30 min per sample).

1.3.4 Clinical targeting of cancer cell metabolism

Recent advances in the field of GBM metabolism have revealed exciting new therapeutic targets. Several drugs targeting GBM metabolism are now entering clinical trials holding a great promise for such an approach (Seliger and Hau, 2018).

1.3.4.1 Statins

Statins inhibit the 3-hydroxy-3-methylglutaryl coenzyme-A reductases (HMGCR), the enzyme responsible for catalysing the rate-limiting step for cholesterol synthesis (Endo, Kuroda and Tanzawa, 1976). Statins can also negatively affect the RAS-RAF-MEK-ERK (Afshordel *et al.*, 2015) or AKT (Yanae *et al.*, 2011) signalling pathways.

So far, there are no significant association of statins with the risk of glioma or survival of glioma patients. The long-term use of statins has shown no significant reduction in the risk of GBM (Seliger, Meier, *et al.*, 2016); neither did it show a significant effect on progression-free survival of GBM patients (Bhavsar *et al.*, 2016).

Despite that clinical trials testing statins in combination with standard therapies have mostly failed to show survival benefits in other cancers (Eberhart *et al.*, 2009; Lim *et al.*, 2015; Lee *et al.*, 2017; Seckl *et al.*, 2017), there is currently one clinical trial (phase II) that is investigating the use of atorvastatin in combination with standard therapy (radiotherapy and TMZ) in patients with primary GBM (ClinicalTrials.gov Identifier:

NCT02029573). The median overall survival results from the trial have not yet been reached to date (Altwairgi *et al.*, 2016).

1.3.4.2 Ritonavir

Ritonavir is a human immunodeficiency virus (HIV) protease inhibitor, which interferes with the reproductive cycle of HIV. Ritonavir was found to inhibit GLUT4 in multiple myeloma cells (Adekola *et al.*, 2015). In GBM cells, ritonavir inhibits multiple glucose transporters, including GLUT4 and GLUT1, and decreases glucose uptake and cell proliferation (Azzalin *et al.*, 2017).

A clinical trial (phase II) in 2011 was conducted in recurrent GBM patients (ClinicalTrials.gov Identifier: NCT01095094) showed no survival benefit of ritonavir which was combined with another HIV protease inhibitor, lopinavir (Ahluwalia *et al.*, 2011).

However, a recent *in vitro* study of a suite of drugs called the CUSP9 drugs, namely: aprepitant, artesunate, auranofin, captopril, celecoxib, disulfiram, itraconazole, sertraline, and ritonavir have shown cytotoxic effects on GBM cells resulting from blocking key metabolic and oncogenic signalling pathways

including AKT, aldehyde dehydrogenase, angiotensin-converting enzyme (ALDH2), carbonic anhydrase -2,- 9, -12 (CA2, CA9, CA12), cyclooxygenase-1 and -2 (COX1 and COX2), cathepsin B, Hedgehog, interleukin-6 (IL6), 5-lipoxygenase (5-LO), MMP2, MMP9, mTOR, neurokinin-1 (NK1), p-glycoprotein (p-gp) efflux pump, thioredoxin reductase (TrxR), tissue factor, 20 kDa translationally controlled tumor protein (TCTP), and vascular endothelial growth factor (VEGF) (Kast, Karpel-Massler and Halatsch, 2014). As such, a clinical trial (phase I) combining the CUSP9 drugs and continuous low dose TMZ for the treatment of patients with recurrent GBM is currently being conducted and is expected to be completed in 2020 (ClinicalTrials.gov Identifier: NCT02770378).

1.3.4.3 Disulfiram

Disulfiram is an inhibitor of the aldehyde dehydrogenase (ALDH1A1); which converts aldehyde to carboxylic acid and produces NADH as a by-product to be used as an energy source for ATP production (Skinner *et al.*, 2014). Disulfiram is a member of the CUSP-9 drug suite, is also being tested in several clinical trials in combination with standard GBM therapy.

A phase I clinical trial (ClinicalTrials.gov Identifier: NCT01907165) demonstrated the safety, tolerability and efficacy of disulfiram in combination with adjuvant TMZ after radiotherapy in patients with primary GBM and reported pro-apoptotic effect through inhibiting proteasomal degradation of proteins for cellular recycling of amino acid (Huang *et al.*, 2016). Subsequently, a phase II clinical trial (ClinicalTrials.gov Identifier: NCT03034135) was recently completed (July 2018) also investigated the safety, tolerability and efficacy of disulfiram and Copper Gluconate, used to treat copper deficiency, in recurrent GBM. Copper forms complexes with disulfiram, which enhances the disulfiram-mediated inhibition of proteasomes (Zhang *et al.*, 2017). The results of the trial have not yet been published. Nevertheless, a phase II clinical trial of the same (ClinicalTrials.gov Identifier: NCT02678975) is currently being performed and expected to be completed by September 2023.

This was followed by three-phase II clinical trials testing disulfiram as an adjunctive and concurrent TMZ in the treatment of patients with primary GBM, including a trial expected by January 2020 (ClinicalTrials.gov Identifier: NCT01777919), and a trial examining dose-escalation expected

by April 2021 (ClinicalTrials.gov Identifier: NCT02715609), and finally a trial in GBM patient with MGMT promoter methylation expected by March 2021 (ClinicalTrials.gov Identifier: NCT03363659).

1.3.4.4 Metformin

Metformin, originally developed for type 2 diabetes (Corcoran and Jacobs, 2019), is a direct inhibitor of complex 1 of the electron transport chain with an effect on the activation of AMPK and the inhibition of mTOR (Birsoy, Sabatini and Possemato, 2012). The functional effects of metformin on glioma cells has been evaluated in many studies which suggested its inhibitory effects on cell growth (Isakovic *et al.*, 2007; Gritti *et al.*, 2014; Yu *et al.*, 2015; Seliger, Meyer, *et al.*, 2016), and invasion (L.-B. Gao *et al.*, 2013), and on the induction of apoptosis (Isakovic *et al.*, 2007; Gritti *et al.*, 2014; Yu *et al.*, 2015) or autophagy (Sesen *et al.*, 2015).

With relation to patients, metformin has been evaluated in terms of its association with the risk of developing glioma and for its suitability as a predictor for progression-free survival in diabetic glioma patients. Unfortunately, the use of metformin

was not significantly associated with a reduced risk of glioma (Seliger, Ricci, *et al.*, 2016).

Yet, it is plausible that metformin does not affect the development of glioma, and instead affect survival after glioma diagnosis. As such, a small study found that diabetic GBM patients on metformin have prolonged progression-free survival (Adeberg *et al.*, 2015). In another small study, metformin was found to serve as a good predictor for improved progression-free survival among diabetic patients with GBM (Welch and Grommes, 2013).

However, a larger study showed that the use of metformin was associated with improved overall and progression-free survival of diabetic patients with grade III glioma, but not with grade IV glioma. It was speculated that the higher prevalence of IDH mutations in grade III glioma patients compared to patients with grade IV glioma could render the tumours more sensitive to the effect metformin (Seliger *et al.*, 2019). Indeed, a different study showed that glioma patients with IDH mutations were more susceptible to metformin (Cuyàs *et al.*, 2015).

So far, there are no published results from clinical trials on metformin in glioma. However, several clinical trials are

currently being undertaken to evaluate metformin in combination with adjuvant treatment for GBM. Two clinical trials are performed for patients with recurrent GBM. In the first clinical trial (phase I), metformin is combined with radiotherapy as well as low-carbohydrate diet in order to selectively starve tumour cells while normal cells are capable of utilising ketone bodies during glucose restriction (ClinicalTrials.gov Identifier: NCT02149459). The trial was due to be completed in July 2018, but the results are still pending. In the second clinical trial (phase II), metformin is tested in combination with low dose TMZ and the trial is expected to be completed in December 2019 (ClinicalTrials.gov Identifier: NCT03243851). Another phase II clinical trial is evaluating the effect of combining metformin to with TMZ followed by concomitant TMZ and accelerated hypo-fractionated limited-margin radiotherapy and followed by adjuvant TMZ in patients with primary GBM. This trial is expected to be completed by December 2021 (ClinicalTrials.gov Identifier: NCT02780024). Furthermore, another clinical trial (phase I) in patients with primary GBM treated with TMZ and a combination of metformin and/or mefloquine and/or memantine after receiving radiotherapy is expected to completed by September 2019 (ClinicalTrials.gov Identifier: NCT01430351).

Encouraging effects of metformin on glioma cells both *in vitro* and *in vivo*, as well as some promising results from a clinical trial (phase II) in non-small cell lung cancer using carboplatin, paclitaxel, and bevacizumab with concurrent metformin for four to six cycles followed by maintenance therapy with bevacizumab ± metformin showing a significant survival benefit compared to when metformin was not used in the treatment regimen (Marrone *et al.*, 2018), provide a great hope for this therapeutic intervention in GBM.

1.3.4.5 Dichloroacetate (DCA)

DCA is a specific inhibitor of PDK (Kato *et al.*, 2007). *In vitro*, for example, DCA depolarised the mitochondria membrane, which led to increased permeability and induced ROS production and subsequent apoptotic cell death of GBM cells (Michelakis *et al.*, 2010). Another *in vitro* study showed that combing metformin, which also disrupts OXPHOS, with DCA enhances DCA-induced oxidative stress, and hence its cytotoxic effect (Ward *et al.*, 2017). Thus, the investigation of DCA and metformin in combination might have the potential to be used as a treatment for GBM patients. So far, one clinical trial (phase I) in 2014 (ClinicalTrials.gov Identifier:

NCT01111097) demonstrated both the safety and Efficacy of DCA in Recurrent GBM (Dunbar *et al.*, 2014).

1.3.4.6 Ketogenic diet

The ketogenic diet is a diet high in fat and low in carbohydrates that causes the body to undergo Ketosis. Ketosis is the process by which medium-chain TGs are broken down into ketones, which become the main source of energy for the cell. Currently, Phase 1 clinical trial of a 4-month Ketogenic Diet in Combination With Standard-of-care Radiation and TMZ for Patients With Newly/Recently Diagnosed Glioblastoma. The trial expected to complete by September 2020 (ClinicalTrials.gov Identifier: NCT03451799).

Mickel Jenkinson and his colleagues conducted a randomised pilot study to investigate the feasibility (assessed by retention and recruitment rates prior to starting chemoradiotherapy) of the ketogenic diet for GBM patients (Martin-McGill *et al.*, 2017). The initial results were reported at the 23rd Annual Meeting of the Society for Neuro-Oncology (SNO), in November 2018. They achieved a 29% recruitment rate, with 12 out of 42 eligible patients being recruited. In addition, retention was poor; only four patients completed the 3-months dietary trial and achieved

ketosis (1.65 – 1.3 mmol/L) while the median duration on the diet of the eight patients who discontinued before the end of 3-months was 36.5 days. The patient suggested that 3-month diet duration might be better shorten to 1.5-month to make it more attainable (ClinicalTrials.gov Identifier: NCT03075514).

Finally, also in SNO 2018 meeting, the early outcomes of another pilot study assessing the feasibility applying isocaloric ketogenic diet carried a 3:1 weight ratio of fat to the combined weight of carbohydrate and protein in addition to radiotherapy and TMZ for 6 weeks for a total of 9 GBM patients. Three patients (mean age 28 years), currently being monitored, so far show progression-free survival of 42, 26, and 24 months the other six patients (mean age 54 years) died between 9 and 25 months after diagnosis. As such, the ketogenic diet may serve as a good initial treatment of GBM, especially in younger patients, although a larger study is required to confirm this (Schwartz *et al.*, 2018).

1.3.5 Summary

Our understanding of cancer metabolism has been advanced through the use of profiling platforms. The overarching theme is that cancer cells reprogram their metabolism to provide a

selective advantage to proliferate, invade and avoid apoptotic cell death, through enhancing cellular bioenergetics, supporting anabolic demands, and maintaining redox balance. Some of these metabolic activities have been exploited as therapeutic targets. In some cases, these have been translated into clinical trials. Ultimately, effective metabolic therapy will take into account the stage of tumour progression as well as the regional heterogeneity in each pathway where it is best seen to provide its benefit to the cancer cell.

1.4 MicroRNAs

1.4.1 microRNAs biogenesis and function

microRNAs (miRNAs) are a class of small non-coding RNA of approximately 20-22 nucleotides in length that regulate gene expression at the post-transcriptional level. miRNAs are transcribed from miRNAs encoding sequences, present with introns of protein-coding genes (approximately 30% of all miRNAs) or within dedicated miRNA gene loci (70% of all miRNAs), by RNA polymerase II (pol II) (Lee *et al.*, 2004). Identical miRNAs encoding sequences with one or more nucleotides variants are annotated with an additional lower case letter (Ambros *et al.*, 2003). The primary transcripts of miRNA (pri-miRNA) can either produce a single miRNA or contain clusters of two or more miRNAs. Nonetheless, pri-miRNA are processed by a microprocessor, which includes DiGeorge syndrome critical region 8 (DGCR8) and Drosha, a nuclear ribonuclease III (RNAse III), to produce a 60-70 nucleotide hairpin-shaped precursor miRNAs (pre-miRNAs) (Lee *et al.*, 2003) (Figure 1.12). Pre-miRNAs are then exported out of the nucleus to the cytoplasm by exportin 5 (XPO5) (Yi *et al.*, 2003) for further processing by Dicer, a cytoplasmic RNAse III enzyme. Dicer performs an asymmetrical cleavage of the hairpin-shaped pre-miRNA close to the terminal loop sequence to produce ~20-

22 nucleotide mature miRNA duplex (Park *et al.*, 2011). Dicer binds to the transactivation-responsive RNA-binding proteins (TRBPs) which recruit the Argonaute proteins (AGO1, AGO2, AGO3 or AGO4) to initiate the assembly of the miRNA-induced silencing complex (miRISC) (Chendrimada *et al.*, 2005). One strand of the mature miRNA (the passenger strand) is degraded while the other strand (the guide strand) binds the Argonaute protein to be retained in the miRISC to guide it, together with members of the GW182 family of proteins, to target messenger RNAs (mRNAs) (Elkayam *et al.*, 2017) (Figure 1.12). The guide strand can be generated from the 5' or the 3' strand of the pre-miRNA, and it is annotated by the suffix -5p or -3p respectively (Griffiths-Jones *et al.*, 2006), although many miRNAs lack the 5p-strand/3p-strand feature annotations (Kuo *et al.*, 2015). Post-transcriptional gene silencing is arbitrated by complementary binding of the mature miRNA strand within miRISC to the target mRNA 3'-untranslated region (3'-UTR) (ʀeviwed in Meister, 2013).

Complete complementarity leads to mRNA cleavage, while partial complementarity, which is common in mammalian cells, leads to mRNA translational silencing or degradation (ʀeviwed in both Meister and Tuschl, 2004 and Huntzinger and Izaurralde,

2011). The post-transcriptional gene silencing occurs in processing bodies (P-bodies) (Figure 1.12), which are the cytoplasmic foci that are induced by, but are not necessarily for, miRNA-mediated gene silencing (Gregory *et al.*, 2005; Liu *et al.*, 2005; Eulalio *et al.*, 2007).

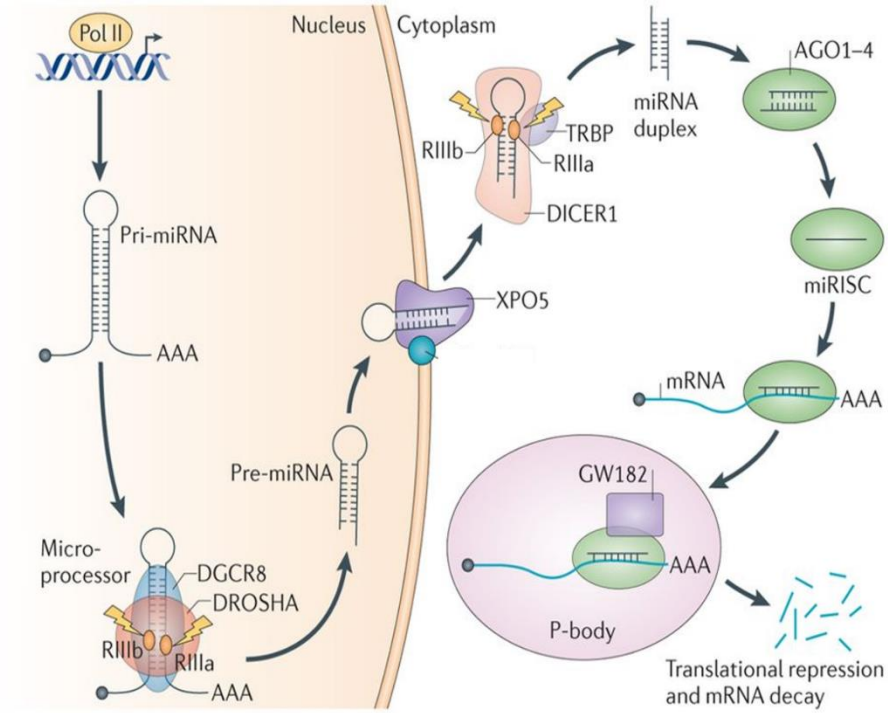


Figure 1.12: miRNA biogenesis.
Primary transcripts of miRNA (pri-miRNA) are processed by a microprocessor, which includes DiGeorge syndrome critical region 8 (DGCR8) and Drosha to produce precursor miRNAs (pre-miRNAs). Pre-miRNAs are exported to the cytoplasm by exportin 5 (XPO5) to be asymmetrical cleaved by Dicer to produce mature miRNA duplex. The guide strand associates with miRNA-induced silencing complex (miRISC) and binds to its target mRNA thereby causing translational repression.
Taken from (Lin and Gregory, 2015 review paper)

1.4.2 The role of miRNAs in cancer

In the context of cancer, miRNAs function as oncogenes (oncomiRs) or tumour suppressors. OncomiRs miRNAs downregulate tumour suppressors while tumour suppressor miRNAs target and suppress oncogenes. As such, oncomiRs and tumour suppressor miRNAs are found to be overexpressed and downregulated, respectively.

In GBM, besides acting as biomarkers (Hermansen and Kristensen, 2013), miRNAs regulate glucose metabolism by targeting mRNAs of genes encoding glycolytic transporters and enzymes and genes that regulate the glycolytic pathway.

miRNAs can simultaneously target multiple mRNAs. Conversely, the expression of one miRNA target is regulated by several other miRNAs. Eventually, the biological effect of miRNAs is determined by the relative abundance of the miRNA and its mRNA targets (Ebert and Sharp, 2012), which can change dynamically in response to the tumour microenvironment (Leung and Sharp, 2010a).

1.4.3 miRNA regulation of GBM biology

The regulation of RTK/RAS/PI3K pathway by miRNAs has been extensively studied in GBM. Some of these miRNAs have also been shown to target gene involved in regulating cell metabolism or to be associated with cell migration/invasion and/or chemotherapeutic-resistance in GBM as described below (Figure 1.13). Only studies that have validated direct mRNA-miRNA interaction via luciferase assay were included in this review. However, the mRNA-miRNA interaction was studied in un-stratified GBM patient cohort, where IDH status was not reported. Thus, it must be noted that IDH mutation status may confound many reported associations between expression of particular miRNAs and the malignancy grade and prognosis of gliomas. In addition, many prognostic associations for specific miRNAs discussed in this review are only based on retrospective analyses of patient cohorts of various size, in which the treatment regime might not have been according to the current standard of care which may limit the generalisation of such findings.

1.4.3.1 miRNA regulation of RTKs

c-Met is targeted by miR-144-3p, and miR-410, which are found to be downregulated in GBM compare to normal brain (Yunqing

Li *et al.*, 2009; Chen *et al.*, 2012; Lan *et al.*, 2015). Moreover, the overexpression of miR-410 reduced GBM cells invasion (Chen *et al.*, 2012). *c-Met* is also targeted by miR-34a, which is downregulated in GBM. *PDGFRA*, which is also targeted by miR-34a, exerts a negative effect on miR-34a expression in GBM in a negative feedback loop. The administration of Imatinib mesylate (Gleevec or Glivec), an inhibitor developed for *BCR-ABL* which can also inhibit *PDGFR, KIT and ARG* (Kantarjian *et al.*, 2002; Haberler *et al.*, 2006), reversed the negative effect of PDGFRA on miR-34a expression (Silber *et al.*, 2012). Moreover, miR-34a indirectly regulates EGFR expression by targeting its transcriptional activator Yin Yang-1 (YY1). miR-34a overexpression was also observed to decrease GBM cell migration (Yin et al., 2013). Another indirect regulation of EGFR by miRNAs is via the EGFR transcriptional activator Stat3 which is directly targeted by miR-21 (Zhou et al., 2010a),(Rehmsmeier et al., 2004; Löffler et al., 2007; Kung and Raab-Traub, 2008; Zhou et al., 2010b). miR-21 was the first miRNA reported as deregulated in GBMs (Chan, Krichevsky and Kosik, 2005). Its expression level positively correlates with glioma grade, with GBM expressing the highest levels of miR-21 (Hermansen et al., 2013; Piwecka et al., 2015). Moreover, the knockdown of miR-21 expression in GBM cells was

associated with increased chemo-sensitivity of GBM cells as shown by Wong et al. (Wong *et al.*, 2012) who developed TMZ-resistant GBM sub-clones and treated them with miR-21 inhibitors and TMZ or with TMZ alone. The knockdown of miR-21 suppressed the growth of the TMZ-resistant cells and, in the presence of TMZ treatment, cells treated with miR-21 inhibitors showed a further increase in their apoptotic rate compared to those that were not treated with miR-21 inhibitor (Wong *et al.*, 2012). Furthermore, miR-128, which is downregulated in GBM, directly targets EGFR and PDGFRA (Papagiannakopoulos *et al.*, 2012) (Skalsky and Cullen, 2011). miR128 was also found to target Rap1B, which mediates cytoskeletal remodelling and promotes cell invasion. The overexpression of miR-128 also enhanced the chemo-sensitivity of GBM cells to TMZ (She *et al.*, 2014). Similarly, miR-21 inhibition has been shown to increase sensitivity of GBM cells to paclitaxel (taxol, an anti-microtubule agent)(Lidar *et al.*, 2004), teniposide (VM-26, a topoisomerase II inhibitor)(Weller *et al.*, 2003), and 5-fluorouracil (a pyrimidine analogue)(Menei *et al.*, 2004), three chemotherapeutic agents which are being investigated for the treatment of GBM.(Yiming Li *et al.*, 2009; Ren, Kang, *et al.*, 2010; Ren, Zhou, *et al.*, 2010)

Additionally, *EGFR* is also directly targeted by miR-219-5p, which is downregulated in GBM (Rao, Santosh and Somasundaram, 2010; S. A. M. Rao *et al.*, 2013). However, the overexpression of EGFR mRNA lacking 3'-UTR in GBM cells overexpressing miR-219-5p reversed the inhibitory effects of miR-219-5p on *EGFR* expression (S. A. M. Rao *et al.*, 2013). Additionally, Kefas et al. (2008) and Webster et al. (2009) suggested that *EGFR* is targeted by miR-7, although Liu et al. (2014) proposed that *EGFR* is not a miR-7 target in GBM (Kefas *et al.*, 2008; Webster *et al.*, 2009; Liu *et al.*, 2014). miR-7 shows a tissue-specific expression in normal brain tissue and a relatively decreased expression in GBM tissue and cell lines. The overexpression of miR-7 has been shown to abolish GBM cells' migratory and invasive abilities (Lu *et al.*, 2011; Wu *et al.*, 2011).

1.4.3.2 miRNA regulation of the RAS and its antagonist, NF1

RAS, a downstream effector of RTKs, is antagonised by NF1 which is regulated by miR-9. miR-9, which targets *NF1*, is overexpressed in GBM compared to normal brain (Z. Wu *et al.*, 2013). The expression of miR-9 was also associated with chemotherapeutic resistance in GBM cells (Munoz *et al.*, 2015).

In addition, *N-RAS* is regulated by miR-340, which is downregulated in GBM (Huang *et al.*, 2015; Fiore *et al.*, 2016). *N-RAS* is also regulated by miR-143 (Wang *et al.*, 2014), which directly targets hexokinase II (*HK II*), that acts at the first step of glucose metabolism (Zhao, Liu, *et al.*, 2013a). miR-143 is downregulated in GBM compared to normal brain (Zhao, Liu, *et al.*, 2013a; Wang *et al.*, 2014), although was shown to be overexpressed in invasive GBM cell line sub-population (Koo *et al.*, 2012). Moreover, *K-RAS* is regulated by miR-134, which is also found to be downregulated in GBM compared to normal brain (Zhang *et al.*, 2014). let-7a, which targets *K-RAS* (X.-R. Wang *et al.*, 2013), also regulates the expression PKM2. The expression levels of let-7a are lower in GBM relative to normal brain (X.-R. Wang *et al.*, 2013; Luan *et al.*, 2015).

1.4.3.3 miRNA regulation of RTK/RAS/PI3K and the PI3K antagonist, PTEN

miR-7, mentioned above to regulate *EGFR*, also targets *PI3K*. The ectopic expression of miR-7 was shown to downregulate *PI3K* expression in a dose-dependent fashion (Liu *et al.*, 2014). miR-542-3p, which directly targets *AKT* (specifically *AKT1*), is also downregulated in GBM. The overexpression of miR-542-3p

repressed *AKT1* expression and its downstream signalling (Cai *et al.*, 2015). PTEN antagonises the effect of AKT on PI3K. *PTEN* is regulated by the above-mentioned miR-21 (Zhou *et al.*, 2010a). *PTEN* is also targeted by miR-26a, which is upregulated by c-Myc (Guo *et al.*, 2013). miR-26a is also overexpressed in GBM (Ciafrè *et al.*, 2005; Huse *et al.*, 2009; Kim *et al.*, 2010). miR-1908 is another suppressor of *PTEN* expression that is overexpressed in GBM relative to normal brain (Xia *et al.*, 2015). The expression of *PTEN* is also repressed by miR-494-3p and miR-10a/10b, which are upregulated in GBM (Liu, Sun and Lan, 2013; X.-T. Li *et al.*, 2015). Moreover, the knockdown of miR-10a/10b was shown to decrease GBM cell migration and invasion (Liu, Sun and Lan, 2013). Furthermore, *PTEN* is indirectly downregulated by miR-128, which is upregulated in GBM compared to normal brain. *Bmi-1*, a miR-128 target, directly associates with the *PTEN* locus to downregulate *PTEN* transcription (Song *et al.*, 2009). *PTEN* is also downregulated by miR-221/-222 cluster which is found to be overexpressed in GBM (Ciafrè *et al.*, 2005; Conti *et al.*, 2009). The knockdown of miR-221/-222 upregulated the expression of *PTEN* and activated PI3K. Moreover, the ectopic expression of PTEN mRNA lacking 3‘UTR or administrating the PI3K inhibitor, wortmannin,

had the same effect on GBM cells as knocking down miRNA-221/-222 (Xie *et al.*, 2014).

1.4.3.4 miRNA regulation of AMPK/mTOR

mTORC1, a positive regulator of *c-Myc*, is negatively regulated by *AMPK,* which is targeted by miR-451. The expression of miR-451 is found to be elevated in GBM patient samples (Godlewski *et al.*, 2010). miR-451 directly targets CAB39, which encodes the binding partner for the protein kinase LKB1, which phosphorylates and activates AMPK (Godlewski *et al.*, 2010).

Moreover, miR-451 was reported to cooperatively suppress GBM neurosphere formation when administered in combination with imatinib (Gal *et al.*, 2008). The downstream effectors of AMPK, mTORC1 and mTORC2, are directly targeted by miR-199a-3p, which is downregulated in GBM samples in comparison to normal brain tissues. The overexpression of miR-199a-3p in GBM cells suppressed proliferation while miR-199a-3p overexpression in GBM cells treated with an mTOR inhibitor had no significant effect on proliferation (Shen *et al.*, 2015). Moreover, the mTORC2 binding partner, *Rictor*, is targeted by the above-mentioned miR-34a (Hresko and Mueckler, 2005;

Rathod *et al.*, 2014). Interestingly, the forced overexpression of miR-34a mimicked the effect of the knock-down of Rictor in GBM cells (Rathod *et al.*, 2014).

1.4.3.5 miRNA regulation of FoxO3a/c-Myc

mTORC2 positively regulates *c-Myc* expression by suppressing FoxO3a activity. FoxO3a enhances the expression of miR-34c, which directly targets *c-Myc*. mTORC2 inhibits the phosphorylation of class IIa histone deacetylases (HDACs) rendering them inactive. This leads to the acetylation of FoxO3a. The acetylated FoxO3a is inactive (Mihaylova *et al.*, 2011; Masui *et al.*, 2013). Therefore, the inactivation of FoxO3a relieves the miR-34c-mediated suppression on *c-Myc* (Masui *et al.*, 2013). In addition to its suppression by mTORC2, the expression of *FoxO3a* is suppressed by miR-mediated mechanisms in GBM. *FoxO3a* expression is negatively regulated by miR-27a, which is highly expressed in GBM relative to normal brain. miR-27a also targets *BTG2* which suppresses cell migration. As such, the knockdown of miR-27a in GMB cells reduced their migration (K. Wang *et al.*, 2015; W.-Q. Li *et al.*, 2015). miR-155 is another negative regulator of *FOXO3a* expression, which is overexpressed in GBM tissue and cell lines

relative to normal brain tissue and astrocytes (Ling *et al.*, 2013). The knockdown of miR-155 enhanced the anticancer effect of TMZ and reduced migration and invasion of GBM cells (Ling *et al.*, 2013; Liu *et al.*, 2015). *FoxO3a* is also targeted by miR-184 which is expressed at higher levels in GBM tissue and cell lines compared to normal brain tissue and astrocytes (Cui *et al.*, 2014), although controversial (Cheng *et al.*, 2015; Emdad *et al.*, 2015) (Malzkorn *et al.*, 2010). miR-184 expression is associated with GBM cells chemo-resistance (Emdad *et al.*, 2015). Similar to the other *FoxO3a* negative regulators, miR-184 knockdown reduced GBM cells' migration and invasion potentials (Cui *et al.*, 2014) (Figure 1.13).

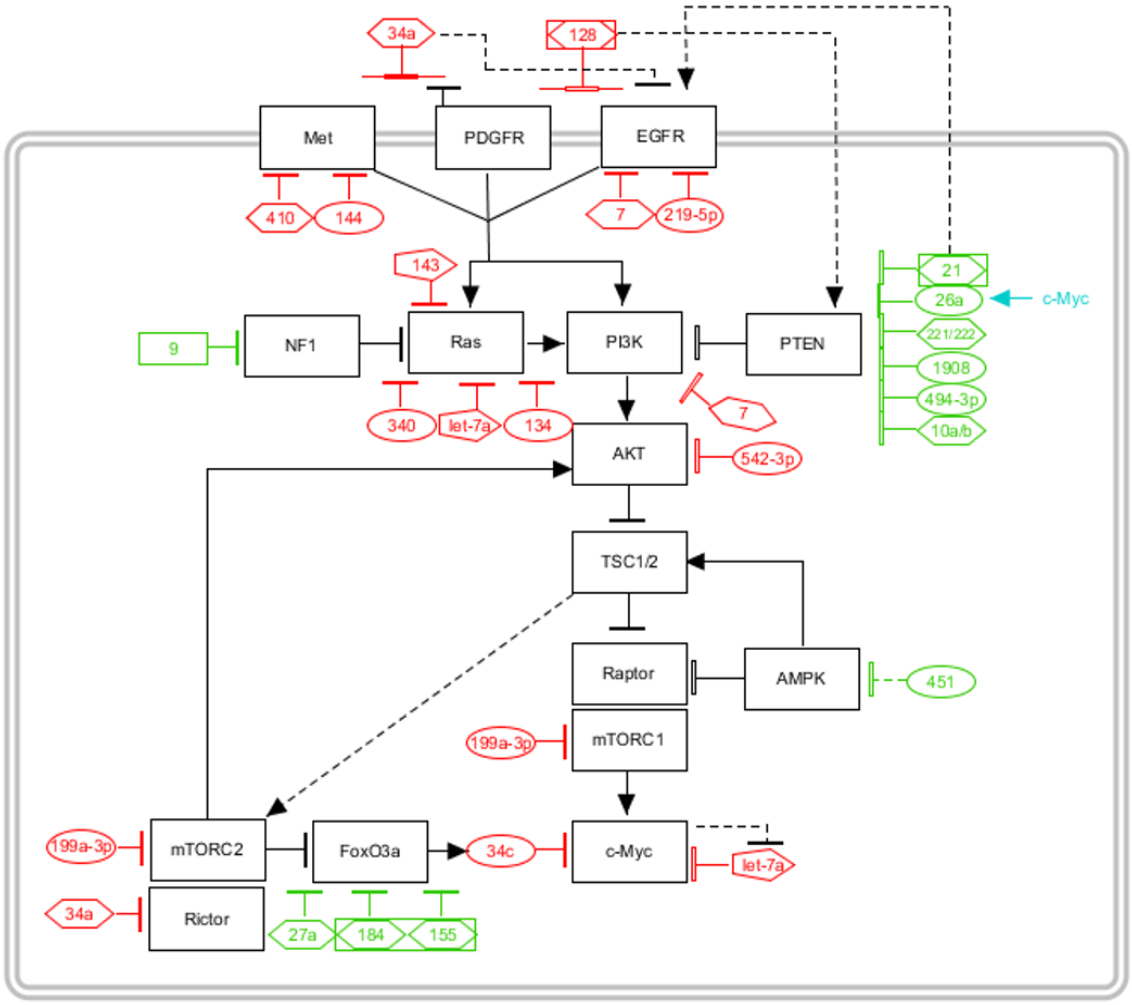


Figure 1.13: miRNA regulation of GBM biology

miRNAs regulating PI3K/AKT/mTOR signalling pathway in GBM are shown in ovals with green showing miRNAs that are upregulated and red showing those which are downregulated. miRNAs which, in addition to regulating PI3K/AKT/mTOR signalling, regulate invasion/migration, glucose metabolism or are associated with chemotherapeutic-resistance are shown in hexagons, pentagons or rectangles, respectively. miRNAs in hexagons with a rectangle around are involved in the regulation of both invasion/migration and chemotherapeutic-resistance. Arrowheads designate positive regulation. Blunt heads designate negative regulation. Dashed lines indicate indirect effects.

1.4.4 miRNA Regulation of Glycolytic Transporters and Enzymes in GBM

To date, four miRNAs have been reported to directly modulate the expression of glycolytic transporters and enzymes in GBM (Figure 1.14). The expression of GLUT3 is downregulated by miR-106a (Dai *et al.*, 2013) However, miR-106a is found to be downregulated in GBM compared to normal brain.(Dai *et al.*, 2013) The low miR-106a expression is associated with shorter-term survival of GBM patients.(G. Yang *et al.*, 2011; Dai *et al.*, 2013; Zhao, Yang, *et al.*, 2013) Moreover, the expression of miR-106a in high-grade glioma is lower than that in low-grade glioma, an expression pattern that is opposite to GLUT3 (Boado, Black and Pardridge, 1994; Liu *et al.*, 2009; Dai *et al.*, 2013). Thus, miR-106a downregulation promotes glycolysis and enhance glucose flux by releasing the suppression of GLUT3.

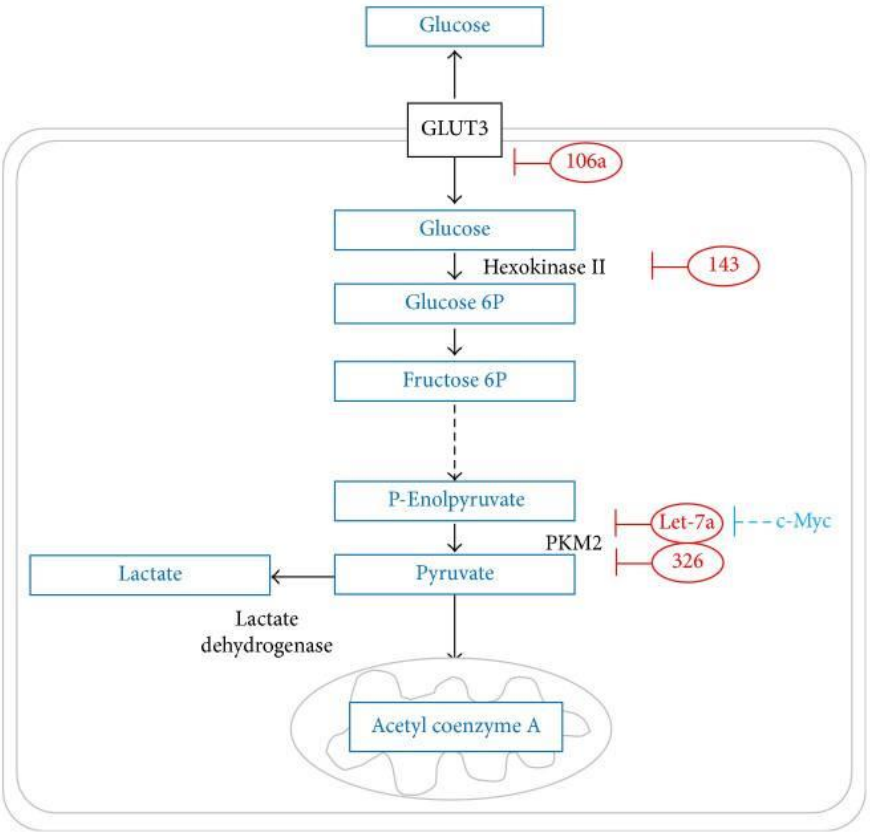


Figure 1.14: miRNA regulation of glycolytic transporters and enzymes in GBM
Red ovals represent downregulated miRNAs, and blunt ends designate negative regulation. c-Myc (downstream effector of RTKs signalling pathways) upregulates glycolysis by negatively regulating let-7a which targets PKM2: pyruvate kinase type M2. Dashed black lines indicate that several steps have been omitted. Mitochondria represent the entry into the citric acid cycle. P: phosphate. P-: phospho-.

Furthermore, the glycolytic enzyme HKII is also targeted by miR-143 (Zhao, Liu, *et al.*, 2013b). miR-143 is found to be downregulated in GBM compared to low-grade glioma and normal brain(Zhao, Liu, *et al.*, 2013b; Wang *et al.*, 2014). miR-143 expression is negatively correlated with HKII levels (Zhao, Liu, *et al.*, 2013b), which is associated with poor prognosis (Wolf, Agnihotri, Micallef, *et al.*, 2011). Furthermore, miR-143

has been identified as a direct regulator of *HKII* in head and neck squamous cell carcinoma and in colon and lung cancers. Like in GBM, miR-143 expression is downregulated in these tumours (Fang *et al.*, 2012; Gregersen *et al.*, 2012; Peschiaroli *et al.*, 2013).

Another glycolytic enzyme, PKM2, is regulated by the miRNA, let-7a (Luan *et al.*, 2015). c-Myc, which is also targeted by let-7a, upregulates the expression of the heterogeneous nuclear ribonucleoprotein A1 (hnRNPA1) splicing factor which, in turn, downregulates let-7a in a positive feedback loop (Luan *et al.*, 2015). hnRNPA1 binds to the pri-let-7a and blocks its processing by Drosha (Michlewski and Cáceres, 2010). In addition, hnRNPA1 mediates the splicing of PK into the PKM2 isoform as well as that of the Myc-interacting partner Max into the Delta Max isoform. Delta Max forms a complex with c-Myc to drive the transcription of the c-Myc target genes, including hnRNPA1 (Mäkelä *et al.*, 1992; Chen, Zhang and Manley, 2010; David *et al.*, 2010; Babic *et al.*, 2013). As such, let-7a/c-Myc/hnRNPA1/PKM2 regulatory loop ensures the downregulation of let-7a in order for PKM2 to be expressed in GBM.

Another miRNA which targets PKM2, miR-326, is downregulated in GBM compared to normal brain as a result of the decreased transcription of its host gene, β-arrestin1 (Kefas *et al.*, 2009, 2010). In GBM cells, the overexpression of miR-326 or the knock-down of its target, PKM2, reduced cellular proliferation, metabolic activity and ATP levels (Kefas *et al.*, 2010). Such a decrease in ATP levels was, however, rescued by transfecting GBM cells with PKM2 mRNA lacking the 3'-UTR which renders them insensitive to miR-326 (Kefas *et al.*, 2010). Therefore, miR-326 mediates its effects on tumour metabolism by repressing PKM2 expression.

1.4.5 miRNA Regulation of Glutamine Transporters in GBM

Only one miRNA has been reported to directly modulate the expression of enzymes within the glutamine metabolism pathway in GBM. miR-153, which is downregulated in GBM compared to normal brain tissue, has been found to directly target glutaminase (GLS) (Liu *et al.*, 2017). The downregulation of miR-153 is attributed to the increased methylation levels (hypermethylation) in the upstream region of miR-153 in GBM tissues compared to normal brain tissues. Indeed, treating GBM cells with the demethylation agent, 5-aza-dC, led to the

reduction of miR-153 methylation level and the subsequent re-expression of miR-153 (Ghasemi, Fallah and Ansari, 2016).

In GBM tissue, the relative expression of miR-153 and its target showed a reverse correlation (Liu *et al.*, 2017). Moreover, the level of the miR-153 expression was also found to be downregulated in GBM cell lines compared to normal human astrocyte (NHA) cell line. The overexpression of miR-153 in GBM cells caused a reduction in glutamate production, decreased cellular proliferation, and an increased rate of apoptosis. On the other hand, the overexpression of GLS abrogated the inhibitory of miR-153 on glutamate production. These findings suggest that miR-153 regulates glutamine metabolism through targeting GLS (Liu *et al.*, 2017).

1.4.6 miRNA regulation of one-carbon metabolism in GBM

There are two miRNAs that are known to directly regulate the expression of a gene within the one-carbon metabolism pathway. MTHFD2 in the folate metabolism pathway was found to be a direct target of miR-940 (Xu *et al.*, 2019). miR-940 is downregulated in GBM tissue and cell lines compared to normal brain and NHA cells, respectively, and its expression negatively correlates with glioma grade (Xu *et al.*, 2019). Furthermore, the

overexpression of miR-940 in GBM cells significantly their proliferation and induced apoptosis. miR-940 also reduced GBM cell invasion as determined by the transwell assay. MTHFD2 suppression caused by miR-940 overexpression or small interfering RNA (siRNA) treatment reduced GBM cell invasion. However, transfecting cells overexpressing miR-940 with an expression vector containing MTHFD2 reversed the negative effect of MTHFD2 suppression on cell invasion (Xu *et al.*, 2019). Notably, MTHFD2 has been shown to upregulate the expression of vimentin and promotes cell migration and invasion in breast cancer (Nilsson *et al.*, 2014).

Another target in the folate metabolism pathway, FLOT2 is directly targeted by miR-449a (Huang *et al.*, 2019).

miR-449a was found to be downregulated in GBM compared to normal brain.

Moreover, miR-449a expression in high-grade glioma has also been shown to be lower than that in low-grade glioma (Yao *et al.*, 2015). In contrast, FLOT2 is found to be upregulated in GBM tissues and cell lines, and its expression is positively associated with tumour grade and poorer patients' survival (Huang *et al.*, 2019). The overexpression of miR-449a mediated the

suppression of FLOT2 and reduced viability, migration and transwell invasion of GBM cells (Huang *et al.*, 2019).

1.4.7 miRNA regulation of lipid metabolism in GBM

So far, two miRNA, namely miR-132 and miR-29, have been reported to regulate lipid metabolism in GBM. miR-132 expression was found to be decreased in GBM compared to normal brain (Zhou *et al.*, 2015). The expression of miR-132 decreases with the increase in glioma grade, with the lowest expression being seen in GBM (Zhou *et al.*, 2015). miR-132 directly targets SIRT1, the key factor that regulates lipid and cholesterol biosynthesis (Y. Li *et al.*, 2016). The overexpression of miR-132 led to a significant decrease in intra-cellular FAs and cholesterol while the knockdown of the endogenous miR-132 levels in increased the expression of SIRT1, and subsequently the levels of FAs and cholesterol in GBM cells (Y. Li *et al.*, 2016).Furthermore, miR-132 overexpression in GBM cells was shown to reduce cell clonogenicity, migration and invasion while its knockdown was shown to have the opposite effect (Y. Li *et al.*, 2016).

The three members of the miR-29 family, miR-29a, -29b and -29c (miR-29a/b/c) were found to be downregulated GBM

compared to normal brain tissue (J. Shin *et al.*, 2017; Liu, Duan and Duan, 2018; Shi *et al.*, 2018). Moreover, the expression of miR-29a/b/c negatively correlated with the histopathological grade in glioma tissues (Liu, Duan and Duan, 2018). Furthermore, the decrease in miR-29a/b/c expression is associated with poor prognosis in patients (Shi *et al.*, 2018). The overexpression of miR-29a/b/c in GBM cells suppressed cell proliferation, migration and invasion (Liu, Duan and Duan, 2018; Shi *et al.*, 2018). miR-29a/b/c were all found to target SCAP and SREBP-1 in GBM, directly. As such, the overexpression of miR-29a/b/c in GBM suppressed FA biosynthesis, which led to a reduction in FA and TG levels in the cell and subsequent suppression of cell growth. This was rescued by the addition of exogenous FAs or by the overexpression of SREBP-1, which upregulated the expression of its downstream targets, ACC, FASN and SCD1 (Ru *et al.*, 2016).

Interestingly, SREBP-1 was found to regulate miR-29a/b/c expression in a negative feedback loop. As such, the overexpression of SREBP-1 significantly promoted the expression of miR-29a/b/c. Similarly, the treatment of GBM cells with the liver X receptor (LXR) agonist GW3965

upregulated SREBP-1 expression (Guo *et al.*, 2011) and consequently upregulated miR-29a/b/c expression (Ru *et al.*, 2016).

1.4.8 miRNA regulation of GBM cell invasion

Many miRNAs acting as negative regulators of invasion are found to be downregulated in GBM tumours. These miRNA, namely miR-218, miR-419-5p, miR-146b-5p, miR-133b, and miR-221, directly target MMPs or their upstream regulators as described below. In all studies presented, miRNA binding to its target mRNA was confirmed by luciferase assay.

miR-218 is expressed at high levels within the normal brain, while its expression levels have been found to be low in GBM tumours (Song *et al.*, 2010; Liu *et al.*, 2012; Gao and Jin, 2014). Moreover, miR-218 expression shows an inverse correlation with glioma grade, with GBM showing the lowest expression levels (Peng *et al.*, 2014). miR-218 indirectly regulate the expression of MMP9 via targeting the transcription factor Lymphoid Enhancer Binding Factor 1 (Lef1) that drives its expression (Liu *et al.*, 2012). As such, the overexpression of miR-218 in U87 and U251 cells caused a significant decrease in MMP9 levels and cell invasion in the *in vitro* transwell assay (Liu *et al.*, 2012). Another mechanism through which miR-218

target transcription factors to negatively regulate MMP9 is by targeting nuclear factor kappa-light-chain-enhancer of activated B cells (NF-κB) as well as its activator IκB kinase α (IKKα) (Song *et al.*, 2010). Target genes for NF-κB include MMP-9; thus, NF-κB suppression by miR-218 results in a reduction of MMP9 mRNA and protein levels (Song *et al.*, 2010). MMP9 has also been shown to be a direct target of miR-491-5p in GBM (Yan *et al.*, 2011). miR-491-5p is downregulated in GBM tumours compared to normal brain (X. Li *et al.*, 2015). Furthermore, the overexpression of miR-491-5p in GBM cells inhibited their *in vitro* transwell invasion (Yan *et al.*, 2011). Another miRNA, miR-211, which is downregulated in GBM tumours, was found to directly target MMP9 (Asuthkar *et al.*, 2012). miR-211has a highly significant inverse correlation observed between miR-211 expression and MMP-9 protein levels in GBM tumours (Asuthkar *et al.*, 2012). Moreover, the overexpression of miR-211 in U87 cells had an inhibitory effect on the transwell invasion ability of the cells (Asuthkar *et al.*, 2012).

Another miRNA that directly regulates MMPs expression is miR-132. miR-132 plays a role in regulating GBM metabolism, as shown above, and has been reported to promote invasion in

GBM by directly targeting MMP16 (Zhou *et al.*, 2015). As such, the overexpression of miR-132 inhibited migration and invasion in GBM cells (Zhou *et al.*, 2015). MMP16 is also targeted by miR-146b-5p (Xia *et al.*, 2009; Li *et al.*, 2013). miR-146b-5p was found to be downregulated in GBM, which was strongly correlated with chromosome 10q loss, according to Li *et al.* (2013). Moreover, miR-146b overexpression significantly reduced *in vitro* cell invasion in transwell assays. Conversely, miR-146b inhibition resulted in an enhanced MMP16 expression at the mRNA and protein level, as well as in a significant increase in transwell invasion of GBM cells (Xia *et al.*, 2009).

Another MMP that is regulated by miRNAs is MMP14. MMP14 has been shown to be a direct target of miR-133b (Chang *et al.*, 2015). miR-133b is expressed at lower levels in GBM tumours than in normal brain (Chang *et al.*, 2015; C. Li *et al.*, 2016). The overexpression of miR-133b in GBM cells resulted in a significant decrease in cell invasion in the *in vitro* transwell invasion assay (Chang *et al.*, 2015).

Other miRNAs are upregulated in GBM due to their ability to target suppressors of MMPs function, thereby promoting invasion of GBM cell. These miRNAs are miR-125b and miR-21, as discussed below.

The expression level of miR-125b was found to upregulated in GBM, displaying a positive correlation with the malignant grade of glioma (N. Wu *et al.*, 2013). miR-125b indirectly targets MMP2 and MMP9 by targeting, PIAS3,the protein inhibitor of activated STAT 3 (Shi *et al.*, 2014). PIAS3 binds and negatively regulates the transcriptional activity of STAT3 transcription factor (Suman *et al.*, 2012). MMP2 and MMP 9 are well known downstream targets of STAT3 signalling as determined in other cancer types, including melanoma (Xie *et al.*, 2004), breast cancer (Zhang *et al.*, 2015), and ovarian cancer (Jia *et al.*, 2017). Thus, the inhibition of miR-125b in GBM cells led to the downregulation of both MMP2 and MMP9 and, subsequently, to the suppression of *in vitro* cell invasion in transwell assays (Shi *et al.*, 2010).

miR-21 was also shown to promote invasion in GBM by targeting the MMP inhibitors, *RECK* and *TIMP3* (Gabriely *et al.*, 2008). As such, the downregulation of MMP inhibitor by miR-21 enhances the expression of MMPs. On the other hand, the inhibition of miR-21 led to elevated levels of TIMP3 and therefore reduces MMPs mRNA and protein expression and the invasive abilities of GBM cells in the *in vitro* transwell assays

(Gabriely *et al.*, 2008). Finally, another MMP inhibitor, TIMP2, was found to be a direct target of miR-20a (Z. Wang *et al.*, 2015) in GBM. Indeed, miR-20a is expressed at higher levels in GBMs tissue than in normal brain tissue; thereby promoting the upregulation of MMPs in GBM (Liao, Chen and Wang, 2019). Similarly, miR-221/222, which is downregulated in GBM and directly targets PTEN as discussed above, promotes GBM cell invasion by targeting TIMP2 (F. Yang et al., 2015).

1.4.9 miRNAs targeting as a therapeutic approach for GBM.

Targeting glycolytic metabolism by directly inhibiting metabolic enzymes has shown promising results in GBM clinical trials as described in the previous section. However, a concern has been raised regarding the possibility that other healthy cells might have similar metabolic programming as cancer cells (Altman and Dang, 2012). For that reason, molecular approaches, are used to target the specific genetic alteration driving the abnormal tumour metabolism without affecting normal cells. Recently developed targeted molecular therapies, however, are already facing the challenge of acquired resistance attributed mostly to the redundancy and complexity of signalling pathways (recently reviewed in (H. Wang *et al.*, 2015)). Nevertheless, the development of miRNA-based therapy, which can

simultaneously target multiple pathways, has the potential to overcome the limitations in current GBM therapies (Purow, 2011; Hatziapostolou, Polytarchou and Iliopoulos, 2013). In fact, the modulation of microRNA expression has been shown to be able to change the clinical behaviour of GBM cells. Several miRNAs have been shown to not only improve the effectiveness of targeted therapeutically by inhibiting/activating multiple targets, but also to help alleviate the chemo-radio-therapeutic resistance obstacle by sensitising GBM cells to chemo and/or radiotherapy.

Despite the potential of miRNA-based therapy, there are several challenges to be addressed before reaching the clinic. First, the consequences of the off-target effects of miRNAs must be critically evaluated. This is a challenge for both siRNAs arising from non-specific binding to complementary sequences designed to selectively target specific pathway components, and for miRNAs which simultaneously target multiple genes within a pathway. Moreover, it could be speculated that endogenous miRNAs (Patton *et al.*, 2015) or endogenous non-coding RNAs (Kartha and Subramanian, 2014), would compete with the target mRNAs for miRNA binding; this would likely

modulate the effect of miRNA-based therapy, although this has never been reported in the literature.

A second issue relates to the low stability and short half-life of miRNAs *in vivo*, owing to degradation by ribonucleases (RNase) (Czauderna *et al.*, 2003). Various chemical modifications can, nevertheless, augment miRNA stability and protect from RNases. Most modifications are made to the 2′ position of the ribose sugar backbone. These include: 2′-O-methyl (Yoo *et al.*, 2004), 2′-O-methoxyethyl (Sazani, Astriab-Fischer and Kole, 2003), and 2′-fluoro (Pallan *et al.*, 2011) substitutions. Moreover, chemical medication have extend to generate RNA analogues such as locked nucleic acid (LNA) in which the "locked confirmation" of the sugar-backbone is achieved by the introduction of a 2'-O,4'-C methylene bridge (Grünweller and Hartmann, 2007; Stenvang *et al.*, 2008) and peptide nucleic acids (PNA) in which the sugar backbone is entirely replaced by N-(2-aminoethyl)-glycine units linked by peptide bonds (Hyrup and Nielsen, 1996; Fabbri *et al.*, 2011). These modifications have been shown to improve target binding affinities and increase resistance to RNases.

A third key issue is regarding the lack of efficient systems to deliver miRNA-based therapeutics to GBM tumours, especially across the BBB. Intracellular delivery systems using viral vectors or polymer/lipid-based nanoparticles have been conjugated to agents that can either disrupt or allow the transfer across the BBB (Zhang, Wang and Gemeinhart, 2013) (Black and Ningaraj; Kumar *et al.*, 2007; Mathupala, 2009; Liu *et al.*, 2010). Such agents are mostly administered locally due to the diffuse/infiltrative growth and rare metastasis of GBM cells. The most promising local delivery technique is the convection-enhanced delivery (CED) technique which replaces the brain interstitial fluid with low-pressure infusions via a catheter therapy, thereby reaching large areas of the brain (Allard, Passirani and Benoit, 2009; Bidros, Liu and Vogelbaum, 2010). However, one must be conscious that, even with the local delivery, there would be a likelihood of an off-target-tissue effect whereby therapeutic miRNAs modulate gene expression in the surrounding non-cancerous tissues.

A fourth challenge concerns the *in vivo* assessment of miRNA-targeted therapy. So far, murine models that have been used *in vivo* studies were established by the subcutaneous or the intracranial injection of human GBM cells. As such, miRNA-

based therapeutics must be pre-administered to the GBM cells *ex vivo* or locally injected into GBM xenografts *in vivo*; both of which approaches would fail to reflect the true therapeutic response of human GBM in a real patient (Jacobs *et al.*, 2011; Huszthy *et al.*, 2012). Moreover, most of these studies have used immunodeficient rodents, which would probably limit the opportunity to evaluate the immunogenicity of miRNA-targeted therapy *in vivo*, which is yet remained to be examined.

Finally, it is possible that acquired resistance may become an issue for miRNA-based therapies in the future. However, targeting families of miRNA and/or using cocktails of either miRNA can potentially reduce the likelihood of resistance. It is worth noting, nevertheless, that using a combinatorial approach can overload the miRNA processing machinery (Purow, 2011), as shown previously (Grimm *et al.*, 2006).

In spite of the major challenges, a few miRNAs that regulate gliomagenesis and GBM cell metabolism, which were discussed above, have demonstrated their therapeutic potential in pre-clinical models. Therapeutic targeting of miRNAs may be accomplished by the inhibition of the overexpressed miRNAs (oncomiRs) or the replacement of the downregulated miRNAs

(tumour suppressor miRNAs), as described below. In the first strategy, miRNA antagonists (antagomiRs or anti-miRs) are used to inhibit miRNA function. Anti-miRs are used in miRNA-based therapy as antisense oligonucleotides that bind to the mature miRNAs in order to prevent its interaction with the miRISC complex. Corsten et al. (Corsten *et al.*, 2007) transfected GBM cell lines with LNA-anti-miR-21, implanted them into mice intracranially, and monitored their growth over 6 days. The knockdown of miR-21 resulted in a remarkable reduction in tumour volume. Another group demonstrated *in vitro* transfection of LNA-anti-miR-21 conjugated to lipid nano-capsules to not only decrease cell viability but also increase GBM cell sensitivity to radiotherapy with an 80% decrease in cell viability induced by the knockdown of miR-21 (Griveau *et al.*, 2013). Another *in vitro* study also showed that cells transfected with poly[lactic-co-glycolic]acid nanoparticles encapsulating anti-miR-21 prior to TMZ treatment had an increased TMZ-induced cell death compared to cells treated with TMZ alone (Ananta, Paulmurugan and Massoud, 2015).

A different method to suppress miRNA in GBM cells is via the use of small-molecule inhibitors that interfere with miRNA transcription and processing or with its interaction with miRISC

or its target mRNA (for a detailed explanation, see review (Li and Rana, 2014)). A proof-of-principle experiment for this approach used luciferase reporter constructs to screen for small molecule inhibitors of miR-21 (Gumireddy *et al.*, 2008). The luciferase reporter constructs carried complementary sequences of miR-21 and were transfected into cells endogenously expressing high miR-21 levels. This resulted in low luciferase activity due to the hybridisation of the complementary sequences. Following the screening of >1000 small molecule compounds, azobenzene 2, which showed the most significate increase in the intensity of the luciferase signal compared to the untreated cells, was characterised as a specific and efficient inhibitor of miR-21 transcription (Gumireddy *et al.*, 2008).

In another study to identify a small-molecule inhibitor of miR-21, Shi et al. (Shi *et al.*, 2013) developed a high-throughput docking-based virtual screening method that selects candidate small-molecule inhibitors which potentially dock to the computationally predicted Dicer binding sites on the 3D model of pre-miR-21. Shi et al. identified AC1MMYR2 as a small-molecule inhibitor that specifically blocks Dicer processing of pre-miR-21 to mature miR-21-5p. Furthermore, the

intraperitoneal administration of AC1MMYR2 to intracranial tumour models resulted in reduced tumour growth and increased animal survival compared to control-treated group (Shi *et al.*, 2013).

Another strategy to sequester miRNAs from their target mRNAs is using miRNA sponges, which are transgenic expression constructs encoding RNA molecules harbouring multiple binding sites for the miRNA of interest. Such RNA molecule will "soak up"/decoy/attract endogenous miRNAs, thereby preventing their binding native target transcript (Ebert and Sharp, 2010). A major downside of miRNA sponges is the limited control over the induction of their transcription leading to heterogeneity in the expression levels of the miRNA sponges (Zhang, Wang and Gemeinhart, 2013). In GBM, this approach has been shown to successfully knockdown miR-146a in astrocytes and increase the expression of the miR-146a target genes (Mei, Bachoo and Zhang, 2011).

The alternative concept in miRNA-based therapy, miRNA replacement, aims to restore the expression of downregulated miRNA via introducing vectors expressing pri-miRNA from an RNA Pol II promoter or pre-miRNA mimetics which are short,

double-stranded RNAs containing a guide strand identical to the mature miRNA and a complementary passenger strand (Bader, Brown and Winkler, 2010). For instance, miR-7–expressing vectors encapsulated in liposome and systemically administered to GBM xenografts resulted in decreased tumour growth (W. Wang *et al.*, 2013). Another study by Liu et al. (X. Liu *et al.*, 2013) used an alternative polymer-based delivery system with relatively higher transfection efficiency. GBM cells pre-transfected with miR-7 oligonucleotide encapsulated in poly(amidoamine) prior to transplantation into mouse brain showed a more significant reduction in their growth compared to those pre-treated with liposome-encapsulated miR-7 (X. Liu *et al.*, 2013). In another study, U87 cells were pre-transfected with miR-940 then injected subcutaneously into the bilateral axillary lymph nodes of nude mice on the left side, while U87 cells transfected with non-targeting control were injected on the right side to compare tumour growth in the same animal (Xu *et al.*, 2019). By day 17 after injection, tumour growth was inhibited in cells that overexpressed miR-940, and a significant difference in size was seen between tumours expressing miR-940 and tumours expressing non-targeting control (Xu *et al.*, 2019).

A different therapeutic approach which relies on indirect delivery of miRNAs into GBM cells through non-target cells has been evaluated in GBM. Katakowski et al. (Katakowski *et al.*, 2013) transfected miR-146b expression vectors into rat mesenchymal stem cells (MSCs). MSCs expressed and packaged miR-146b into exosomes that they secreted into their growth medium. Subsequently, the miR-146b-containing exosomes were isolated from the medium and intratumorally injected into intracranially inoculated rats with GBM cells. The tumour volume was significantly reduced in rats treated with miR-146b-containing exosomes compared to those receiving the control treatment (Katakowski *et al.*, 2013). In another study, MSCs transfected with fluorescently labelled miR-124 mimetics were shown to be transferred to the co-cultured GBM cells via gap junction–dependent and independent mechanisms (H. K. Lee *et al.*, 2013). *In vivo*, MSCs were administered intracranially to deliver fluorescently labelled miR-124 mimetics into green fluorescent protein (GFP)-labelled GBM cells implanted within the mouse brain. GFP-labelled GBM cells were re-isolated, and the delivery of the fluorescently labelled miR-124 by the MSCs was verified by fluorescence microscopy (H. K. Lee *et al.*, 2013). An analogous study used the same approached to deliver anti-miRs. The study showed that the co-

culturing of GBM cells with anti-miR-9 transfected MSC or with MSC-derived exosomes carrying anti-miR-9 resulted in significant downregulation of miR-9, although these GBM cells were shown to be originally resistant to treatment with anti-miR-9 (Munoz *et al.*, 2013). The downregulation of miR-9 in such cells has also rendered GBM cells more susceptible to TMZ (Munoz *et al.*, 2013).

Another indirect miRNA-based technique uses a lentiviral vector that contains a cell suicide gene, such as the herpes simplex virus thymidine kinase (HSV-TK) gene, with an artificial 3'-UTR harbouring miRNA binding sites for an endogenous brain-enriched miRNA, such as miR-128, which is downregulated in GBM (Skalsky and Cullen, 2011). GBM cells transduced with miR128-regulated HSV-TK vector were selectively killed when cultured in the presence of the deoxy-guanosine mimic, ganciclovir (GCV) (Fillat *et al.*, 2003) which, upon its phosphorylation by HSV-TK, incorporates into DNA leading to DNA synthesis inhibition. In contrast, neuronally differentiated SH-SY5Y cells expressing miR128-regulated HSV-TK vector, the highly expressed miR-128 suppressed HSV-TK expression (Skalsky and Cullen, 2011). Moreover, one can speculate that even if normal brain cells failed to suppress all suicide gene

transcripts, such cells with lower proliferation rates than to GBM cells will be less affected by DNA synthesis inhibition induced by phosphorylated GCV. Though, it was shown that phosphorylated GCV can still damage the mitochondrial DNA of non-dividing cells (Laberge *et al.*, 2013).

A similar study was done in mice intracranially inoculated with GBM cells and intratumorally injected with an insect baculovirus-based vector expressing HSV-TK under the regulation of miR-31, miR-127, and miR-143 which are downregulated in GBM, followed by daily injection of GCV (Wu *et al.*, 2009). Although the vector did not show significant therapeutic effect compared to control HSV-TK vector lacking miRNA binding sites, possibly due to the variable expression of the three selected miRNAs, the vector expression was shown to be suppressed in astrocytes which such miRNAs at high levels (Wu *et al.*, 2009).

Combinatorial approaches of miRNA-based therapeutics have been proposed using *in vivo* systemic administration of liposomes carrying both anti-miR21 and miR34a mimetics. The treatment with anti-miR21 and miR34a combination significantly increased apoptosis and senescence compared to

treatment with either anti-miR21 or miR34a alone (Ornell *et al.*, 2015).

Clinical translation of miRNA-based therapy in GBM is emerging with the first clinical trial currently recruiting participants (clinicaltrials.gov, identifier NCT01849952). This clinical trial aims to evaluate the therapeutic effect of the anti-mir-10b after it was demonstrated in pre-clinical studies to diminish tumour growth and release targets repression (Teplyuk *et al.*, 2016).

In conclusion, targeting miRNAs, which can simultaneously target multiple genetic pathways, has demonstrated great potential as a therapeutic strategy for GBM. However, the potential of off-target effects, low stability and short half-life in plasma of miRNAs(Singh, Narang and Mahato, 2011) as well as the lack of efficient delivery systems for miRNA-based therapy(Yang, 2015), present major challenges that would need to be solved before miRNA-based therapies can widely be used for the treatment of GBM patients.

1.5 Intra-tumour heterogeneity in cancer

1.5.1 Sources of intra-tumour heterogeneity

The clonal evolution model of cancer progression suggests that individual cells acquire sequential random genetic or epigenetic mutations (Nowell, 1976). The accumulation of multiple mutations cause genetic instability in these cells (Nowell, 1976; Shen, 2011). As such, mutations that provide a selective growth advantage would arise by chance in some cells (Nowell, 1976). Such cells would then expand following the linear or the branched clonal expansion models (Greaves and Maley, 2012). In the branched model, heterogeneous sub-clones will emerge simultaneously and independently. The linear model, on the other hand, involves the sequential acquisition of advantageous mutations which give rise to fitter sub-clones that outcompete the ancestral clones, a process known as clonal sweep. However, heterogeneity within the cell population occur due to the presence of the remaining sub-clones. Extrinsic micro-environmental factors, such as varying levels of oxygen, nutrients and pH, exert selective pressure on the sub-clones to favour those which can expand efficiently under that particular micro-environmental condition (Cahill *et al.*, 1999). In addition, following chemo- or radiotherapy, resistant sub-clones, that give rise to recurrent tumours, emerge *de novo* or from pre-

existing clones that previously acquired mutations that would rendered them resistant to therapy. These sub-clones are the main cause of therapeutic failure and tumour recurrence after treatment (Burrell and Swanton, 2014).

1.5.2 Genetic and phenotypic intra-tumour heterogeneity in GBM

Core pathways altered in GBM have been largely determined based on the genetic characterisation of tumour samples isolated from a single tumour mass (Cancer Genome Atlas Research Network, 2008). However, the infiltrative growth of GBM creates heterogeneous micro-environmental niches that define distinct tumour regions. The cellular adaptation to within the different tumour regions is reflected in the gene expression profile of each region (Pistollato *et al.*, 2010; Charles *et al.*, 2011). Regional heterogeneity in gene expression was comprehensively characterised by Sottoriva et al. who employed fluorescence-guided multiple sampling facilitated by 5-aminolevulinic acid (5-ALA) administration (Stummer *et al.*, 2006; Piccirillo *et al.*, 2012) to collect spatially distinct (superficial and deep) tumour fragments (Sottoriva *et al.*, 2013). Genome-wide transcriptional profiling revealed that single tumours contained at least two different GBM subtypes

(according to Verhaak classifier). Moreover, differentially expressed genes within each tumour were mainly involved in angiogenesis, proliferation and cell migration and invasion, which suggested that differential phenotypic profiles may exist within the same tumour (Sottoriva *et al.*, 2013). Indeed, Stieber et al. later showed that xenografts of genetically distinct GBM clones derived from different tumour fractions (36 samples) displayed differential infiltrative growth and tumorigenic potential *in vivo* while maintaining the same genetic profile as their parental patient tumours (Stieber *et al.*, 2014). Transcriptional profiling of isolated single cells from image-guided surgically resected core and invasive edge tumours also showed that the two regions displayed angiogenesis- or motility-related gene signatures, respectively (Hoelzinger *et al.*, 2005).

More recently, single-cell RNA sequencing of 430 cells from five GBM tumours showed that individual cells within the same tumour classified into different Verhaak's GBM subtypes (A. P. Patel *et al.*, 2014). Phenotypic heterogeneity was then demonstrated *in vitro* using 44 single cell-derived clones from four GBM patients. Under the same culture conditions, each clone exhibited differential proliferation potential (Meyer *et al.*,

2015). Moreover, clones derived from recurrent GBMs were TMZ-resistant. Interestingly, some of the clones derived from primary GBMs that were never exposed to TMZ also displayed resistance to TMZ which shows that TMZ-resistance can pre-exist in untreated tumours (Meyer *et al.*, 2015). Furthermore, intra-tumour heterogeneity in *MGMT* status was also observed, as reported in another study (Parkinson *et al.*, 2008), however, the response to TMZ did not correlate with *MGMT* status in these clones. As such, intra-tumour heterogeneity may limit the usefulness of prognostic biomarkers. Nevertheless, subsequent transcriptional analysis showed that TMZ-resistant clones (which expressed high levels of migration/invasion-markers) predominately displayed mesenchymal GBM subtype while TMZ-sensitive clones mainly exhibited proneural and classical subtypes, suggesting that intra-tumour transcriptional heterogeneity could be driving the functional heterogeneity in response to TMZ (Meyer *et al.*, 2015). The parallel evolution of multiple clones carrying resistance-conferring mutations within the same tumour might allow the positive selection of the fittest clone during chemotherapeutic treatment thereby leading to treatment failure (Inda, Bonavia and Seoane, 2014).

1.5.3 Intra-tumour heterogeneity of cell metabolism in GBM and other cancers

Intra-tumour gradients of micro-environmental conditions, such as hypoxia, orchestrates a corresponding metabolic adaptation in the different regions of the tumour (Pistollato *et al.*, 2010).

To date, intra-tumour global metabolic heterogeneity has only been recently described in kidney cancer. Okegawa et al., 2017 characterised the metabolic profiles of spatially distinct regions within the kidney tumour using targeted analysis of combined data generated by three platforms: GC-MS-MS, IP-LC-MS-MS, and lipidomics; in order to cover a wide range of hydrophilic and hydrophobic metabolites. They analysed 2-4 regions harvested from nephrectomy specimens of eight kidney cancer patients and found increased levels of metabolites in the pyruvate metabolism pathway in the tumour regions situated more centrally within the tumour. However, they found no notable difference in the lipidomics profiles across the different regions. Okegawa et al., 2017 used another approach to validate their findings from the metabolomics study that kidney cancer is dependent on pyruvate metabolism. They incubated tissue slices obtained from 7-8 regions from two patient tumours with

a stable isotopic-tracer 13C 6-glucose for 24h. Fractional enrichment of pyruvate was measured by incorporating 13C into pyruvate. The expected product when 13C6glucose-derived pyruvate has been converted to citrate by PDH was found to be higher in some tumour regions and lower in others (without apparent correlation to the location within the tumour) compared to normal tissue. While the expected product if 13C6glucose-derived pyruvate has been converted to citrate by PC was found to be lower than or the same as in the normal tissue in some parts of the tumour. Such finding suggested that PDH and PC activities vary at different sites within a single tumour. While metabolomics results indicated changes in pathway activity, these changes were not associated with genetic variation by microarray.

They finally explored the possibility of inhibiting pyruvate transport as a therapeutic approach for kidney cancers. They treated patient-derived xenograft (PDX) tumours with a mitochondrial pyruvate carrier inhibitor (UK-5099) and observed reduced growth of PDX tumours in mice without severe loss of animal bodyweight (Okegawa *et al.*, 2017).

It is worth mentioning, however, that Okegawa et al. limitation lack failed to multi-sampling technique was not standardised across the tumour specimens and regions were not uniformly collected from a different site, and no account of the location within the tumour was made. Moreover, in their analysis, they grouped all eight patient tumours and compared the metabolic profiles of an unequal number of regions from each tumour. This may reduce the reliability of their results.

In GBM, there has been only one study devoted to exploring the regional heterogeneity in GBM metabolism. Intra-tumour heterogeneity in glucose metabolism in GBM was demonstrated by Santandreu et al. using six GBM samples surgically removed in one block then freshly sectioned to isolate central and peripheral regions (Santandreu *et al.*, 2008). They revealed that isolated mitochondria from peripheral regions showed higher oxidative activity than those isolated from the central regions (Santandreu *et al.*, 2008). Since the mitochondrial abundance (measured by mitochondria DNA content) was invariant between the two regions, this finding was explained as a regional adaptation to the hypoxic gradient (Santandreu *et al.*, 2008).

1.5.4 Intra-tumour heterogeneity in GBM invasion

Aggressive invasiveness remains a common feature of malignant GBMs, despite high levels of intra-tumour heterogeneity. For example, an *in vitro* study comparing cells taken from the tumour core and periphery showed that the peripheral cells are less proliferative but more invasive than their central counterparts (Molina *et al.*, 2010). As such, intra-tumour heterogeneity can be seen in the secreted ECM components, as well as in the expression of integrins and their Rho GTPase effectors, and in the expression of matrix proteases.

1.5.5 Intra-tumour heterogeneity in ECM remodelling by GBM cells

Tenascin-C has been has recently been reported to be expressed by cells of tumour margin relative at higher levels than those within the tumour core (Xia *et al.*, 2016). Xie et al also showed that the knockdown of Tenascin-C in GBM cells reduces tumour invasion *in vivo* while it increases tumour proliferation. Conversely, the overexpression of Tenascin-C increases invasion but decreases proliferation of GBM tumour *in vivo*. This suggests that Tenascin-C regulates the "go-or-grow" phenotypic switch of GBM cells (Xia *et al.*, 2016). Furthermore, a human PDX model was used to microdissect central and

peripheral tumour areas and RNA sequencing showed that thrombospondin-1 expression was the highest in the peripheral tumour areas (Daubon *et al.*, 2019).

Vitronectin is preferentially expressed at the periphery of the GBM tumour *in vivo*. Vitronectin has been shown to induce the expression of Bcl-2 and Bcl-X antiapoptotic proteins in these GBM cells at the tumour periphery. As such, it is thought that vitronectin confers a survival advantage to these cells that may, in part, underlie their potential to cause tumour recurrence (Uhm *et al.*, 1999).

1.5.6 Intra-tumour heterogeneity in the expression of molecular regulators of GBM invasion

Along with their increased expression, integrins and proteases demonstrate a crosstalk that promotes GBM cell invasion. In this regard, Western blot, IHC, and immunofluorescence, by use of two monoclonal antibodies able to recognise the functional integrin heterodimer showed that αvβ3 colocalises with MMP-2 to a bigger extent in the GBM tumour periphery than in the centre (Uhm *et al.*, 1999). On the cellular level, Cdc42 and Rac1 activate p21-activated kinase 4 (Manser *et al.*, 1994). PAK in turn forms a complex with αvβ3 and MMP-2 which further

highlights the functional cooperativity between these proteins (Kesanakurti *et al.*, 2012). Furthermore, enhanced activity of CDC42 and RAC-1 have been reported in infiltrating GBM cells (Hirata *et al.*, 2012).

With regards to adhesion receptors, Brown et al showed that in GBM xenografts, the proportion of cells expressing CD44+ at high levels had low expression of proliferation markers and shown enhanced invasion potential *in vitro*. This was in agreement with their previous report that CD44 expressing cells were enriched in the mesenchymal GBM subtype (Brown *et al.*, 2015, 2017).

Furthermore, cadherins show a differential expression pattern in invasive versus proliferative GBM cells. Although GBM is of neuroepithelial origin, a number of studies have shown that invasive GBM cell shares common molecular features with cells undergoing EMT-like processes (Iwadate, 2016). In epithelial cancers, the loss of the epithelial E-cadherin and the increase in the neuronal N-cadherin is considered to be a hallmark of EMT and tumour cell infiltration (Lamouille, Xu and Derynck, 2014).

However, in GBM tissue, microarray analysis showed that the mRNA expression of N-cadherin is upregulated compared to normal brain tissue (Asano *et al.*, 2004). However, western blot analysis showed that N-cadherin levels, although still variable, were generally lower in high-grade gliomas than in normal brain samples (Camand *et al.*, 2011). Nevertheless, the immunohistochemical (IHC) staining of N-cadherin was strongly positive in glioma cells that showed high Ki-67 labelling indices, which is an indicator of high proliferation (Utsuki *et al.*, 2002). This could imply that N-cadherin is highly expressed in the proliferative cell population of the tumour; but might be downregulated in the invasive cells.

Indeed, it has been suggested that loss of N-cadherin could contribute to the invasive capacity of GBM cells (Asano *et al.*, 2004; Camand *et al.*, 2011). The re-introduction of N-cadherin expression to GBM cells reduced their motility (Camand *et al.*, 2011). Furthermore, the overexpression of N-cadherin resulted in a slight decrease in cell adhesion to type IV collagen, fibronectin, and laminin, but a significant decrease in adhesion to type I collagen (Asano *et al.*, 2004). N-cadherin overexpression also correlated with decreased GBM cell invasive *in vitro* (Asano *et al.*, 2004). *In vivo*, N-cadherin

expression is inversely correlated with invasion into surrounding tissues, irregular margins, and extracranial invasion (Asano *et al.*, 2004).

Finally, matrix proteases also show increased expression in invasive GBM cells compared to the rest of cells the tumour bulk. Cathepsin B has been shown to upregulated in GBM compared to low-grade glioma and normal brain, with increased mRNA correlating with increased activity in GBM (Rempel *et al.*, 1994). Moreover, GBM *in vitro* and *in vivo* invasion was found to be impaired upon the knockdown of cathepsin B (Sanjeeva Mohanam *et al.*, 2001). In addition, uPA is predominantly expressed at the tumour invasive margin. Its role in invasion is evidenced by uPA-knockdown studies which resulted in a loss of *in vitro* invasive capacity of GBM cells (S Mohanam *et al.*, 2001). Furthermore, increased expression uPAR is correlated with increased expression of mesenchymal biomarkers; thereby might be supporting the mesenchymal mode of invasion (Gilder *et al.*, 2018).

In summary, the localised upregulation of ECM components, adhesion molecules and modulators of cytoskeleton remodelling

supports the notion that pro-invasive phenotypes are prevalent at the advancing tumour margin of GBM.

1.5.7 Clinical implications of GBM intra-tumour heterogeneity

The existence of intra-tumour heterogeneity has been demonstrated by comparative analyses of different subsections of GBM tumours since the late 1990s, and it is becoming increasingly recognised that heterogeneity at the molecular level is one of the primary reasons underlying treatment failure and recurrence. It is only through recent advances in next-generation sequencing and single-cell analysis that we have begun to uncover the possible mechanisms which explain why this molecular heterogeneity is as problematic as it is.

Heterogeneous tumours are made up of multiple subclones. Selection pressures from treatments such as chemo and radiotherapy may cause subclones with either intrinsic or acquired resistance to be selected for, and thus become dominant in a given tumour mass. As such, treatments may actually serve to drive disease progression (Engelman and Settleman, 2008; Misale *et al.*, 2012). This phenomenon has been observed in several tumour types, including, among

others, lung (Kosaka *et al.*, 2006; Turke *et al.*, 2010), colorectal (Diaz Jr *et al.*, 2012), gastrointestinal (Liegl *et al.*, 2008), and brain (Johnson *et al.*, 2014) tumours, as well as chronic myeloid leukemia (Shah *et al.*, 2002).

According to Burrell & Swanton (2014), the mechanisms by which a tumour develops resistance may involve multiple somatic events affecting distinct signal transduction pathways, thereby resulting in multiple distinct drug resistance events within the same tumour(Burrell and Swanton, 2014). Naturally, this raises considerable challenges for the design and selection of effective drug combinations. However, there is evidence for phenotypic convergence within and across tumour types (Gerlinger *et al.*, 2012, 2014; Fisher, Pusztai and Swanton, 2013; K. Patel *et al.*, 2014; Lohr *et al.*, 2014; Swanton, 2014; E, 2016). This suggests that genetic events driving resistance and disease progression may lie within a specific set of signalling pathways. If these particular pathways are therapeutically targetable, opportunities may arise for therapeutic intervention.

To overcome the challenges posed by clonal heterogeneity, Gatenby et al. have proposed adaptive therapy. Adaptive

therapy is where cancer treatment is continuously adapted in order to maintain a fixed population of drug-sensitive cells. The presence of these cells can suppress the growth of drug-resistant cells, and therefore allow the overall tumour to remain stable (Gatenby *et al.*, 2009). Early detection of low-frequency resistant subclones may allow for the use of combined therapeutic regimens that target mechanisms of resistance.

Evidence for the parallel evolution of subclones during tumour evolution suggests that there are constraints on tumour growth. Again, these may be exploitable. With more knowledge of how tumour progression unfolds, perhaps it will be possible at any given point to predict the likely next step of the tumour's development and apply preventative measures to delay the onset of cancer progression (Swanton, 2014).

Hypotheses, Aims and Objectives

Hypotheses

It is recognised that studies using tissue samples obtained from one tumour region fail to characterise the heterogeneous genomic landscape of GBM. Thus, extensive effort has been directed toward characterising the intra-tumour heterogeneity of transcriptomic profiles in GBM. However, intra-tumour heterogeneity in the expression profiles of miRNA, which regulate mRNA expression, has not been examined in a similar fashion to studies conducted on gene expression.

I hypothesise that:

(1) There will be changes in the expression levels of several miRNAs within the different regions of the same tumour.

(2) These changes will correlate with regional differences in the expression of miRNA target genes.

(3) Differences in miRNA target gene expression underlie phenotypic differences observed in GBM cell metabolism.

(4) These metabolic differences contribute to the differential invasion abilities of the cells.

Aim 1

To characterise, comprehensively, the regional differences in miRNA expression profiles within GBM tumours.

Objectives:

i) Isolate total RNA from spatially distinct regions (core, rim and invasive margin) of GBM tumours and patient-derived cell lines.

ii) Assess the quality of the RNA samples in order to shortlist a cohort of RNA samples to be sent to a commercial company who will perform miRNA microarray.

iii) Analyse miRNA expression data using R/Bioconductor to (1) identify miRNA expression heterogeneity between different tumour regions, and to (2) identify miRNA expression differences between region-derived cell lines.

iv) Validate miRNA expression levels in GBM tissue and cell lines, using an analytical technique other than a microarray; namely, qRT-PCR.

v) Based on the endogenous miRNA expression levels in that cell line, select the most appropriate cell line model for studying the function of the miRNAs of interest.

Aim 2

To investigate whether the expression levels of the miRNAs, and those of their respective mRNA and protein targets, will be inversely correlated.

Objectives:

i) Computationally predict miRNA gene targets.

ii) Perform pathway analysis on relevant miRNA gene targets.

iii) Overexpress or knockdown miRNA expression to study the effect of a given miRNA on the expression of its target genes.

iv) Validate the expression of miRNA target genes in transfected cells using qRT-PCR and Western blot.

v) Validate mRNA-miRNA interaction using luciferase assay.

vi) Validate miRNA target expression in GBM tissue using qRT-PCR and immunohistochemistry.

Aim 3

The miRNA gene targets were found to be involved in the regulation of lipid metabolism, which is a pathway known to be dysregulated in GBM. Therefore, I aimed to characterise the global metabolomics profiles of GBM cells.

Objectives:

i) Extract polar and non-polar metabolites from GBM cells transfected with miRNA.

ii) Perform liquid chromatographic separation of metabolites and identify their abundance levels using a mass spectrometry detector.

iii) Analyse the mass spectrometry data using Progenesis QI and Lipid Search softwares to elevate whether differential expression of miRNAs will result in differences in metabolites abundance.

iv) Validate the abundance of metabolites of interest in cells transfected with miRNA, using a different analytical method, namely Nile-Red staining.

v) Validate metabolites abundance in patient samples using immunohistochemistry to evaluate regional metabolic differences.

Aim 4

The most clinically-relevant region to treat is the invasive margin of the GBM tumour, as the cells in that region remain behind after surgery and could cause tumour recurrence. Thus, I aimed to evaluate whether the differential expression of miRNAs, or of their target genes, affects GBM cell invasion.

Objectives:

i) Perform transwell assays after miRNA transfection to identify the effect of miRNA expression on cell invasion.

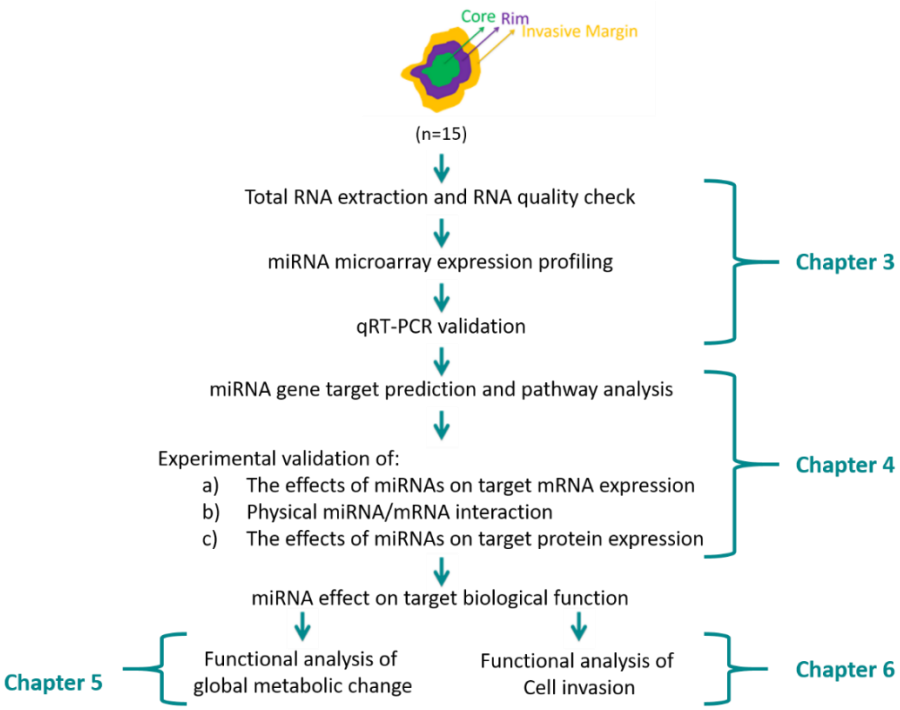
ii) Perform transwell assays after siRNA transfection to knockdown miRNA gene target to identify the effect of miRNA gene targets on cell invasion.

iii) Perform transwell assays after the treatment with pharmacological inhibitors of miRNA gene/pathway targets to identify the effect of the miRNA gene/pathway targets on cell invasion.

iv) Evaluate the changes in metabolite levels in response to inhibiting miRNA gene/pathway targets with siRNA or pharmacological agents.

Overall, the identification of miRNA expression signatures—and of their identified gene targets—may underlie the metabolic heterogeneity within the GBM tumour. This, in turn, may affect the invasive behaviour of the cells. Understanding this relationship more fully could potentially open up a route to the development therapeutics that modulate miRNA expression, using either antisense oligonucleotides or precursor/mimic sequences. It could also provide the potential to re-purpose drugs that target miRNA target genes that regulate GBM cell metabolism. These drugs would aim to selectively disrupt dysregulated cellular processes in the invasive margin of GBM tumours across a widespread area of the brain, whilst sparing normal brain cells that employ normal functional pathways.

Summary of Aims:



Chapter 2:

Materials and Methods

2.1 Clinical Samples

2.1.1 Patient Tissue Collection

Patient recruitment was conducted within the Nottingham University Hospitals NHS Trust at Queens's Medical Centre, Nottingham UK, between 2013 and 2016 by Mr Stuart Smith. Written consent was obtained from all patients prior to surgery in accordance with The Human Tissue Authority (HTA) Codes of Practice for Research. Independent neuro-pathological review confirmed the diagnosis of GBM for each case. Ethics approval for the use of tissue samples in this research project has been obtained from the National Research Ethics Service (NRES) of the East Midlands Research Ethics Committee (Reference 11/EM/0076).

A multi-region sampling technique was adopted to collect tumour fragments from the core, proliferative rim and invasive margins of each tumour based on pre-operative MRI scans (Figure 2.1) and intra-operative views of 5-aminolevμlinic acid (5-ALA) (Stummer *et al.*, 2006; Piccirillo *et al.*, 2012) (Figure 2.2). The administration of 5-ALA allows the tumour to be visualised during the time of the surgery. This is because 5-ALA is converted into a fluorescent metabolite, protoporphyrin IX (PPIX) within tumour cells, but remains as a non-fluorescent compound in non-neoplastic cells (Figure 2.2).

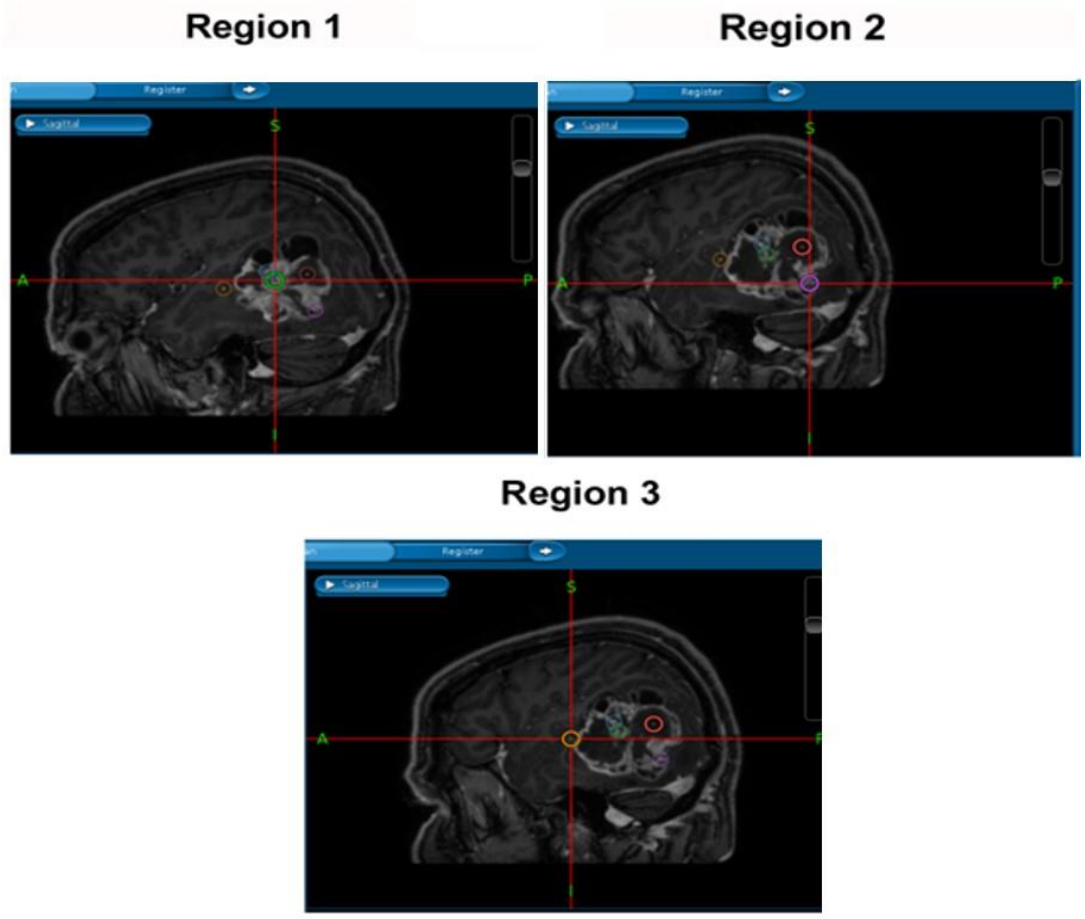


Figure 2.1: Pre-operative MRI scans of a GBM patient's brain allow the selection of different regions of the tumour.
Regions 1, 2 and 3 represent the core, rim and invasive margin, respectively. Scans were captured using the StealthStation™ surgical navigation system (Medtronic, Dublin, Ireland).

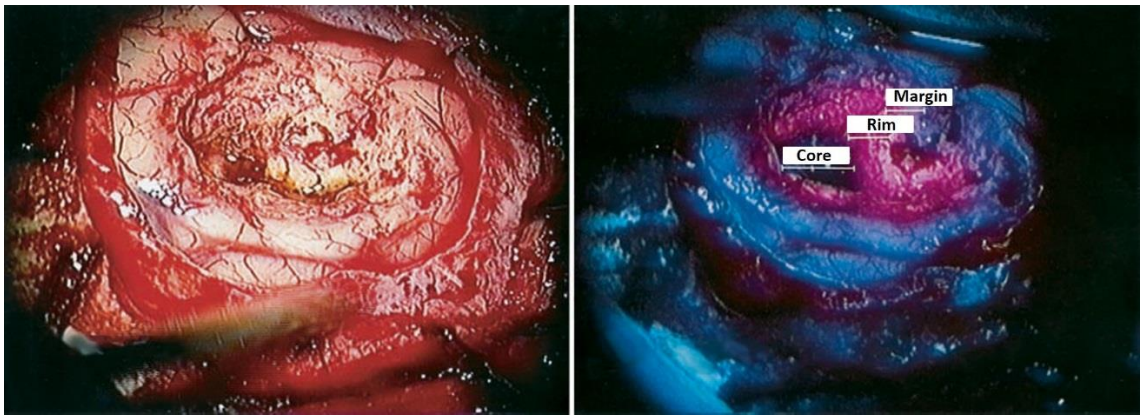


Figure 2.2: Intra-operative images of a GBM patient's tumour showing how 5-aminolevμlinic acid (5-ALA) can aid the surgery.
Tumour viewed conventional white light (left) and violet-blue illumination (right). Different regions can be selected based on the intensity of the fluorescence. Tumour core can be necrotic and appears non-florescent. The tumour rim is enhanced while the tumour margin (invasive regions) displays a low degree of fluorescence as the number of tumour cells is lower.

Fresh surgical specimens from each tumour region were processed by either dissociating fresh tissue into single cells (to derive primary cell line), formalin-fixed paraffin-embedded or fresh-frozen and stored in liquid nitrogen. For each of these purposes, patient samples were archived pseudo-anonymously in-house according to the HTA ethical standards. The clinicopathological characteristics of GBM patients were recorded and maintained in a local database (See Appendix 1).

2.1.2 Patient Cohort for Fluorescence-Activated Cell Sorting (FACS) Analysis

A limited number (n=6) of patient tumours were FACS analysed to estimate the percentage of fluorescent cells (5-ALA positive or 5-ALA/+) relative to non-fluorescent cells (5-ALA negative or 5-ALA/-) in each region (see chapter 3 for patient's details). Following the dissociation of fresh tumour samples from each region, cells were sorted using the MoFlo XPD sorter (Beckman Coulter) with excitation at 405 nm, and emission detection at 605 – 625 nm, to detect the presence of 5-ALA derived fluorescence.

The 5-ALA/+ and 5-ALA/- sorted cells were centrifuged in a microcentrifuge (Prism; Labnet) at 180 ×g for 5 minutes at room temperature, and cell pellets were snap-frozen in liquid nitrogen then stored at -80°C.

2.2 Cell Culture

2.2.1 Cell lines

The commercial GBM cell lines U251 (U.S. National Cancer Institute (NCI)-60) and U87 (American Type Culture Collection; ATCC) were obtained from Dr. Anna Grabowska at the Cancer Biology Unit, The University of Nottingham. Primary cell lines (GIN8, GIN28 and GIN31) and the recurrent cell line (GIN3R) were derived from

invasive margin tissue (from patient 8, 3 (recurrent), 28 and 31; Table 1) that has been dissociated into single cells. Primary cell lines (GCE28 and GCE31) were derived from the tumour core of GBM patients 28 and 31. The clinicopathological characteristics of GBM patients from whom these cell lines were derived are shown in Appendix 8.1. The short tandem repeats (STRs) genotyping data for the cell lines has been included in the Appendix 8.2.

Table 2.1: Medium recipes for commercial and primary GBM cell lines.

Cell line (Splitting ratio)		**Source**	**Tissue from which the cell line was derived**	**Medium recipe**
U87	**1:5**	Commercial	Standard	Dulbecco's Modified Eagle Medium (DMEM; GibcoTM) supplemented with 10% foetal bovine serum (FBS; HyCloneTM), 1% L-Glutamine (L-Glu; Sigma-Aldrich) and 1% Penicillin/Streptomycin (Pen/Strep; Sigma-Aldrich) DMEM supplemented with 15% FBS,1% L-Glu and 1% Pen/Strep
U251	**1:10**			
GIN	**1:2**	Derived in-house	Invasive margin	
GCE			Tumour core	

2.2.2 Sub-culturing monolayer cells

All cells were grown in 75cm^2 flasks (T75) at 37°C, 5% CO_2, humidified atmosphere using in medium as shown in Table 2. After cells reached 70-80% confluency, they were sub-cultured to maintain the exponential growth. Cell sub-culture began with aspirating cell culture medium and washing with 4ml of Hanks'

Balanced Salt Solution (HBSS; GibcoTM) to remove any remaining medium. This was done because cell culture medium supplemented with FBS contains protease inhibitors (particularly α1-antitrypsin), which inhibits trypsin activity. After aspirating the HBSS, 3ml of pre-warmed 1X trypsin – EDTA (Sigma-Aldrich) was then used to detach cells. Trypsin was then deactivated after 5min with 4ml of growth medium. Next, the cell suspension was centrifuged (Sigma 3-16 Centrifuge) at 123 x g for 5min. The cell pellet was re-suspended in pre-warmed cell culture medium and cells were seeded in a total volume of 12ml per T75 flask. Cells were sub-cultured every 3-4 days. If cells have not reached confluency, they were fed by replacing 6ml of medium with 6ml of fresh medium (half-medium change, for primary cell lines) or performing a full media change for established cell lines.

2.2.3 Cell Counting

Cells were detached from 70-80% confluent T75 flasks and routinely counted using a haemocytometer. The haemocytometer (Hawksley) was examined under an inverted light microscope (Brunel Microscopes Ltd) to assess cell numbers. The number of viable cells was counted in four squares and a mean number of cells per square generated. The initial concentration (Ci) of cells was calculated by

multiplying the average count by the haemocytometer square area of 10^4. Hence Ci = cell count x10^4.

2.2.4 Snap Freezing Cell Pellets

Cells were detached from 70-80% confluent T75 flasks, and the cell pellet was re-suspended in 1ml HBSS to wash the cells. The cell suspension was then transferred into a 1.5ml sterile Eppendorf tube which was centrifuged at 200xg for 5min. The supernatant was carefully removed, and the Eppendorf with the pellet was snapped frozen by submerging it into a canister containing liquid nitrogen (—210°C). Then it was stored at —80°C.

2.2.5 Cryopreservation of Cells in Liquid Nitrogen Storage

Cells were detached from 70-80% confluent T75 flasks, and cell pellets were re-suspended in 1ml of freezing medium [10% Dimethyl Sulfoxide (DMSO; Sigma-Aldrich) + 90% FBS] and pipetted into a cryovial DMSO was added to prevent the formation of ice crystals during the freezing process. For slow cooling of stocks, the cryovials were then placed in a Nalgene TM Mr Frosty container (Thermo Scientific) and stored at -80°C for at least 3h Cryovials were subsequently transferred into liquid nitrogen tank for long-term storage.

2.2.6 Recovering cells from liquid nitrogen storage

A cryovial of frozen cells was briefly thawed in a 37°C water bath (ThermoFisher Scientific). The thawed cell suspension was then transferred to a T75 flask with 11ml of pre-warmed medium. A half-medium change was performed after 24h.

2.3 Gene-based Assays

2.3.1 Total RNA isolation

RNA was extracted either from frozen tissue samples or from fresh or frozen cell pellets of $4x10^6$ cells. The protocol for the Ambion® mirVana™ miRNA isolation kit (Life Technologies) was followed.

2.3.1.1 RNA Extraction from Cultured Cells

The cell pellets that were previously stored at -80°C were re-suspended in 300µl of Lysis Buffer and mixed by pipetting until the pellet was fully broken. Next, 30µl of miRNA homogenate additive solution were added, and the lysate mixture was vortexed (WhirlMixer; ThermoFisher Scientific) to obtain a uniform homogenate. The lysate mixture was then incubated on ice for 10min. Following this, 300µl of Acid-Phenol:Chloroform (5:1 ratio; Ambion) was added, the mixture was vortexed and then centrifuged at 10,000 x g for 5min. After centrifugation, two distinct phases were formed, with an interphase in between. Phenol formed the lower organic

phase, containing non-polar lipids and proteins, while Chloroform which was immiscible with, and less dense than Phenol, formed the upper aqueous phase containing nucleic acids which were polar because of their negatively charged phosphate backbone. Proteins that have two charges would form the interphase with their hydrophilic part touch the aqueous phase and their hydrophobic interacting with phenol (KIRBY, 1956; Sambrook and Russell, 2006). The aqueous upper phase was collected, and 1.25 x volumes of 100% ethanol (Fisher Chemicals) were then added. The lysate/ethanol mixture was passed through a filter column at 10,000 x g for 1min in the microfuge. The addition of ethanol neutralises the negative charge of the RNA molecules with positive ions, decreases their solubility and thus allows their adsorption onto a filter membrane. However, residuals, such as proteins and salts, will pass through the filter membrane; and therefore, the flow-through was discarded. Any other residuals that have bound to the filter membrane were subsequently washed with 700µl of miRNA wash solution 1, then washed twice with 500µl of miRNA wash solution 2/3. The washes were performed by centrifugation of the columns at 10,000 x g for 1min. In order to remove residual fluid from the filter, the empty column was centrifuged at 10,000 x g for another 1min. 50µl of pre-heated (95°C) nuclease-free water (NFW; Applied Biosystems) was applied to the filter, incubated for 3min at RT to

rehydrate the filter membrane. The use of NFW helps avoid RNA degradation by nucleases. Water would break the ionic bonds between the RNA phosphate groups and the positive ions and solubilise the RNA molecules. Subsequently, the column was centrifuged at 10,000 x g for 1min to elute the RNA from the filter. RNA was immediately placed on ice or stored at -80°C.

2.3.1.2 RNA Extraction from Tissue Samples

2.3.1.2.1 miRNA Microarray Patient Cohort

All fresh surgical specimens from each tumour region were directly placed in cryovials (Alpha Laboratories) and snap-frozen in liquid nitrogen then stored at -80°C. Total RNA was extracted (see2.3.1 section 2.3.1.1) from 20 of the frozen fresh tumour samples and was used for miRNA microarray expression analysis (See Appendix 1 for patients' details).

2.3.1.2.2 RNA Extraction Procedure

20-30mg was cut from each tumour sample using a sterile scalpel on dry ice and under sterile conditions. Immediately, 500µl of lysis buffer was added. The tissue was pulse-homogenised using the Stuart SHM1 handheld homogeniser (Bibby Scientific) for 2-3 seconds each time until no visible clumps were observed. The

homogeniser was sequentially washed in disinfectant (Chemgene; Medimark Scientific), 70% ethanol and distilled water in between different tissue samples. Next, 50µl of miRNA homogenate additive solution was added, and the lysate mixture was incubated on ice for 10min. Subsequently, the RNA extraction procedure from the lysate mixture was carried out as outlined above (section 2.3.1.1).

2.3.2 Spectrophotometric Analysis

Spectrophotometric analysis is essential for determining biomolecules concentration. The concentration of RNA and DNA was quantified using the NanoDrop 2000 (ThermoFisher Scientific). Prior to its use, the instrument was calibrated with sterile NFW to clear any previous sample spectrum and provide a blank reading. The NanoDrop 2000 (version 3.7) was used as the analytical software for this instrument.

The NanoDrop works by shining Ultraviolet (UV) light through the sample and measuring the amount of UV light absorbed at 260 nm (A260) in order to quantify the amount of nucleic acid in the sample. The NanoDrop also measures the absorbance of protein and phenol at 280 and 230 nm, respectively (A280 and A230). The A260/A280 and A260/A230 ratio was then used to determine nucleic acid purity. For the 260/280nm absorbance ratio, a value of 1.8 was considered good quality for DNA and a value of around 2.0 was considered good

quality for RNA. For the 260/230nm absorbance ratio, values from 1.8 to 2.2 were accepted.

2.3.3 miRNA Expression Analysis by microarray

2.3.3.1 Bioanalyser measurements

The quality of the RNA samples extracted from patient tissue (as per section 2.3.1) was further analysed using the Agilent 2100 bioanalyser (Agilent Technologies) in order to ensure that the quality of the samples is suitable for microarray analysis. The bioanalyser uses capillary electrophoresis and a fluorescence assay to separate RNA molecules according to their molecular weight and measures the amount of fluorescence as the RNA sample was pulsed through the separation channel. The results were visualised as an electropherogram with an accompanying gel image to show the amount of measured fluorescence and the size of the RNA.

Here, reagents were used from the Agilent RNA 6000 Nano kit (Agilent Technologies). 1µl of the RNA 6000 Nano dye was added to 50µl of RNA 6000 Nano gel matrix then vortexed and centrifuged at 13000 x g for 10min to precipitate the undissolved gel. 9µl of the gel-dye mix was loaded into one well on the RNA NanoChip (Figure 2.3) and dispensed using an air-filled syringe. Next, two more wells were filled with 9µl of the gel-dye mix. 5µl of the RNA 6000 Nano marker was then loaded into each well on the chip. Up to 12 RNA

samples were denatured at 70°C for 2min to minimise RNA secondary structure. 1µl of the RNA ladder was added to the ladder well, and 1µl of each sample was loaded into the samples' wells or 1µl of the RNA 6000 Nano marker was added to the unused sample wells. The chip was vortexed horizontally (IKA vortex mixer) for 60sec. The chip was then read in the Agilent 2100 bioanalyser using the Agilent 2100 expert software (Revision B.02.02).

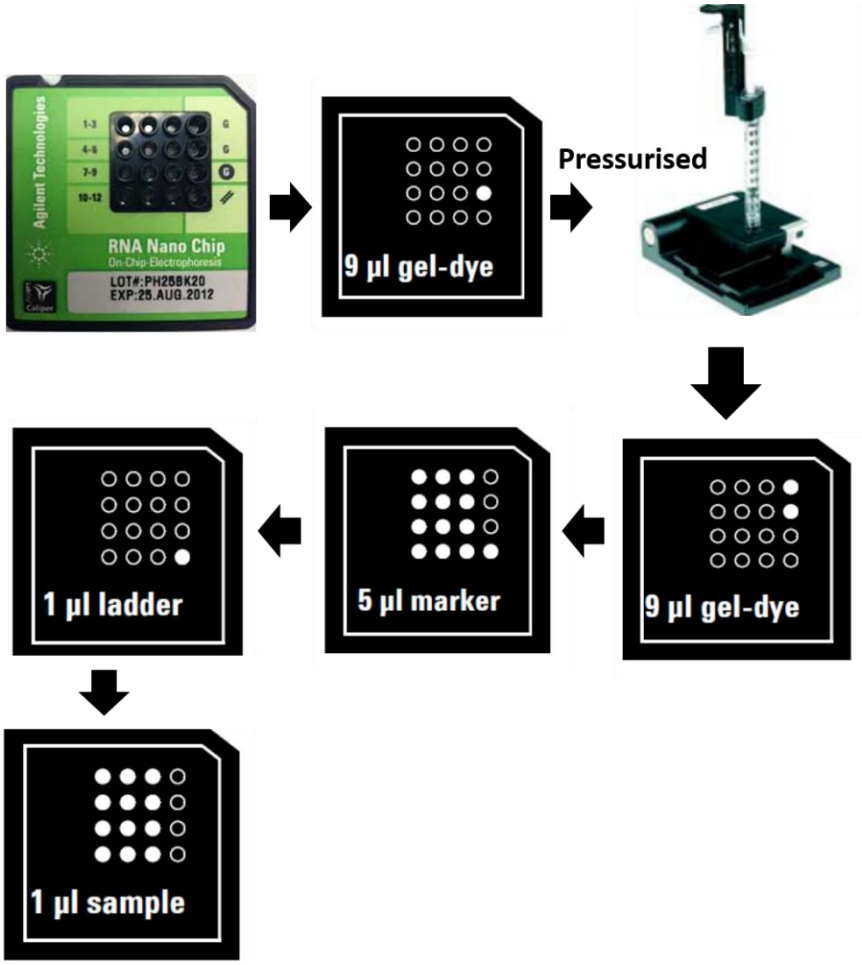


Figure 2.3: Preparation of the Agilent RNA NanoChip
Following the direction of the arrows, the gel was first loaded and pressurised then the ladder, marker, gel-dye and RNA samples were loaded.

2.3.3.2 miRNA microarray experiment

Total RNA samples were sent to Aros Applied Biotechnology (Eurofins Genomics, Aarhus, Denmark) to perform miRNA microarray. The technique they use consisted of i) labelling RNA using the Affymetrix FlashTag Biotin HSR kit (Affymetrix); ii) mixing the biotin-labelled RNA with hybridisation cocktail supplied in the Affymetrix GeneTitan® Hyb, ISH and Stain Kit (Affymetrix) and control oligonucleotides supplied in the 3' IVT Express Kit (Affymetrix); iii) denaturing and applying the mixture onto GeneChip® Affymetrix miRNA Array (version 4.1; see Table 2.2 for array content description for human probe sets); and iv) in situ hybridisation (ISH), staining and scanning the arrays on the GeneTitan® instrument (Affymetrix) according to the Affymetrix GeneTitan® Hyb, ISH and Stain Kit protocol. The scanned images' features were converted into numerical values of the probe intensity signals and stored as a 'CEL-file' data using GeneTitan® software (version 4.0). The array data were analysed in-house.

Table 2.2: GeneChip® Affymetrix miRNA Array (version 4.1) human probe sets content.

Probe sets	Number of probe sets	Database source
Human mature miRNA	2,578	miRBase (version 20)
Human pre-miRNA	2,025	
Human snoRNA and scaRNA	1,996	snoRNAbase (Version 3)

2.3.3.3 miRNA microarray data analysis

2.3.3.3.1 Quality control (QC)

Using the Affymetrix® Expression Console™ Software (freeware, version 1.4.1.46), the array images were visually inspected, and CHP-files were generated in order to detect any array readings outside the range of the scanner. CEL-files were pre-processed using the in-built Robust Multi-Array Average (RMA) method, as discussed below. To ensure that all the samples were comparable, the overall distribution of data before and after pre-processing was visualised using boxplots.

2.3.3.3.2 Data pre-processing in R

CEL-files were read in R-Studio (version 0.99.902; RStudio, Inc. Boston, MA) using the "ReadAffy" function in the R package Affy (Gautier *et al.*, 2004) which is part of the Bioconductor project (http://www.bioconductor.org) (Gentleman *et al.*, 2004). The "RMA" function of the Affy package was used for the pre-processing

of the CEL-files. RMA pre-processing method was used because it has been shown to have a negligible effect on the downstream analysis (McCall and Almudevar, 2012). Based on the signal intensity values of the control probes, RMA calculates the background-corrected intensity values for each perfect-match probe (PMP) in the array (Irizarry *et al.*, 2003) and performs a log-transformation (to the base-2 logarithm). PMP has an exact complementary sequence to the particular miRNA. These background-corrected and log-transformed PMP intensity values (BC-Log- intensity) from each array were normalised to eliminate the array-specific technical variations. RMA uses quantile normalisation (Bolstad *et al.*, 2003) to equalise the distribution of BC-Log- intensity between arrays by repeatedly averaging the highest BC-Log- intensity from each array and replacing the original values with the average value. RMA then fits an additive linear model to the normalised data to obtain an estimate of log-scale expression measure associated with each probe on each array. Tukey's median polish was then used to obtain an expression estimate of each probe set on each array by averaging the four identical probes per miRNA on each array. The expression estimates were saved as an expression set using the function "exprs" from Biobase package (Huber *et al.*, 2015).

2.3.3.3.3 Unsupervised clustering in R

Expression set data were clustered using K-means clustering using the "kmeans" and "Clusplot" functions in R. K-means is an unsupervised machine learning algorithm that groups a dataset into a (k) number of clusters with the nearest mean in order to minimise the within-cluster variance. The clusters are partitioned into "Voronoi cells". Voronoi cells are regions which are segregated based on the distance to individual points of a subset in planes of geometry called components. The optimum number of clusters was estimated using the Elbow method performed in R. The Elbow method performs K-mean clustering for a range of values of "k" and calculates the Sum of Squared Errors (SSE) between each data point and the centre of its cluster. The SSE for each value of "k" was then plotted as a line chart which resembles the shape of an arm with an elbow at the point where the SSE drops for a value for k. This value of k was considered the optimal number of clusters to explain the variance in the data.

2.3.3.3.4 Supervised clustering in Partek

Principal Component Analysis (PCA) was carried out as a supervised clustering technique in Partek® Genomics Suite® software (version 6.6; Copyright © 2016; Partek Inc., St. Louis, MO, USA). PCA takes into account n number of features which were not independent (i.e.,

regions of the tumour) in a dataset in order to classify the observations (i.e., miRNA expression profiles) based on these features. PCA first finds a set of coordinates to give one axis/dimension called "principal component" that explains the variance in the data. As such, the first principal component accounts for as much of the variability in the data as possible. Then, each succeeding component, which was orthogonal to the preceding component, would therefore account for lower amount of variability. Differential expression analysis was performed using ANOVA with tumour region as a factor. Then, BH was performed as a post-hoc test to carry out pair comparisons (core-rim, core-invasive and rim-invasive regions) in order to specifically determine, where the significant difference lies. Volcano-plots were generated to visualise the outcome of each comparison.

2.3.3.3.5 Differential expression analysis in R

This part of the analysis was done in collaboration with Dr. Anabrasu Loardsamy. miRNA expression datasets were filtered into human mature miRNA and pre-miRNAs (total n=4,603). The differential expression was then determined using limma, a regularly performed method in the literature (e.g. in (Bo *et al.*, 2015). Limma stands for Linear Models for Microarray Data (Smyth, 2004; Ritchie *et al.*, 2015) and is available as a package within the R environment. The

"model.matrix" function was first used to construct a design matrix to include details of the tumour region as a single factor with three levels (core, rim and invasive regions). Next, the "lmFit" function was used to fit the pre-processed data onto the linear model. A contrast matrix was then constructed using the "makecontrasts" function in order to compare the miRNA/pre-miRNA expression changes between the core and the rim, the core and the invasive and the rim and the invasive tumour regions.

The Benjamini-Hochberg (BH) multiple testing correction method was then used to control the false discovery rate (FDR), which was the proportion of p-values that were likely to have been identified by chance as statistically significant, which cause a false rejection of the null hypothesis (Type I error), due to the large number of tests performed. BH sorts the p-values in an ascending order then multiplies each p-value by the total number of probes and divide it by its rank. BH correction was performed as an argument within the "topTable" function which provides a list of the FDR-corrected p-values (at 0.05 threshold) for each compression. Finally, the log fold-change was converted into fold-change using the "logratio2foldchange" function from the gtools package (Gregory R. Warnes, 2015).

2.3.3.4 miRNA target gene prediction analysis

Computational algorithms have been developed to predict the Watson-Crick base pairing between the seed region of the miRNA and the miRNA recognition elements (MRE) in the target gene. However, due to the presence of miss-matches/incomplete complementarity, such algorithms often yield a large number of false positives (Watanabe, Tomita and Kanai, 2007; Bartel, 2009). Thus, computational algorithms incorporate additional parameters to minimise false positives when calculating the probability of the existence of an MRE within the mRNA of the target gene. Combining results from multiple prediction algorithms is also as common approaches to minimise false positives. For that purpose, miRWalk 2.0 (available from: http://zmf.umm.uni-heidelberg.de/apps/zmf/mirwalk2/index.html) (Dweep and Gretz, 2015) was used which adopts different algorithms, with each algorithm incorporating different sets of parameters to calculate a prediction score (Table 2.3). Based on the literature, cut-off for the prediction scores calculated by the different algorithms (Table 2.3) were used to filter the lists of the predicted miRNA target genes generated. Next, consensually predicted miRNA target genes from all four algorithms were integrated using V-lookup function in Microsoft Excel (Microsoft Office version 2013).

Table 2.3: Target prediction algorithms features.

Target prediction algorithm	Prediction score cut-off	Parameters contributing to the prediction score	Ref
TargetScan (Release 7.1)	< -0.2 (Jin et al., 2012; Jacobsen et al., 2013; Boele et al., 2014)	1) The detection of perfect seed sequence matches and the thermodynamic stability of miRNA-mRNA duplex. 2) Evolutionary conservation of miRNA target sites among orthologues 3'UTRs. 3) Secondary structures of 3' UTRs based on their AU content.	(Agarwal et al., 2015)
DIANA-microT-CDS (Version 5.0)	> 0.7 (Li et al., 2014; Salajegheh et al., 2015; Salvo et al., 2015)	1) The minimum binding energy of incomplete complementary compared with that of 100% complementary. 2) Conservation of target sites. 3) Whether the distance of the target site from the nearest 3'-UTR end allows for the formation of the secondary structure at the target site.	(Reczko et al., 2012; Paraskevopoulou et al., 2013)
mirDB	> 60 http://mirdb.org/miRDB/faq.html	1) Conservation is considered but not as a requirement. 2) Position of pairing at 3' UTR and composition of the regions next to the pairing.	(Wong and Wang, 2015)

mirMap	> 90 (Desjardin et al., 2014; Sharbati et al., 2015)	Conservation and AU content of target sites, the position of pairing at 3’ UTR and thermodynamic stability of miRNA:mRNA interaction.	(Vejnar and Zdobnov, 2012)

2.3.3.5 miRNA target gene pathway enrichment analysis

Pathway enrichment analysis of predicted miRNA target genes was carried out using KEGG2016 database in Enricher (available from http://amp.pharm.mssm.edu/Enrichr/) (Kuleshov et al., 2016). P-values for each matched pathway was calculated from the z-score test (threshold was set to 0.05 following FDR correction).

2.3.4 Expression analysis of miRNAs by quantitative real-time polymerase chain reaction (qRT-PCR)

Global change in expression reported by microarrays should be validated by an independent method to eliminate technical variability. qRT-PCR is commonly used to validate results obtained from microarray analysis due to its high detection sensitivity, sequence specificity, and reproducibility.

2.3.4.1 Patient cohort for qRT-PCR analysis of miRNAs

Total RNA was extracted from 6 frozen tumour samples to be used for PCR analysis (three tumours were, and three were not analysed by miRNA microarray). For all six tumours, total RNA was extracted (see section 2.3.1) from FACS-analysed invasive margin samples

sorted based on the presence of 5-ALA to determine miRNA and gene expression in the 5-ALA/+ and 5-ALA/- cell populations.

2.3.4.2 cDNA synthesis

Quantification using TaqMan® Advanced miRNA Assays (Thermofisher Scientific) requires the modification of mature miRNAs by the addition of a poly(A) tail at the 3’ end and an adaptor at the 5’ in order to synthesise cDNAs from miRNAs by a reverse transcription (RT) reaction followed by a universal amplification of cDNA step which enhances the detection sensitivity by PCR. TaqMan™ Advance miRNA cDNA synthesis kit (Thermofisher Scientific) was used for these purposes (Figure 2.4).

An exogenous/spike-in control (the C. elegans miRNA, cel-miR-54-3p), which is a synthetic miRNA with a target sequence that is not present in human, was used in the cDNA synthesis to monitor RT and amplification efficiencies.

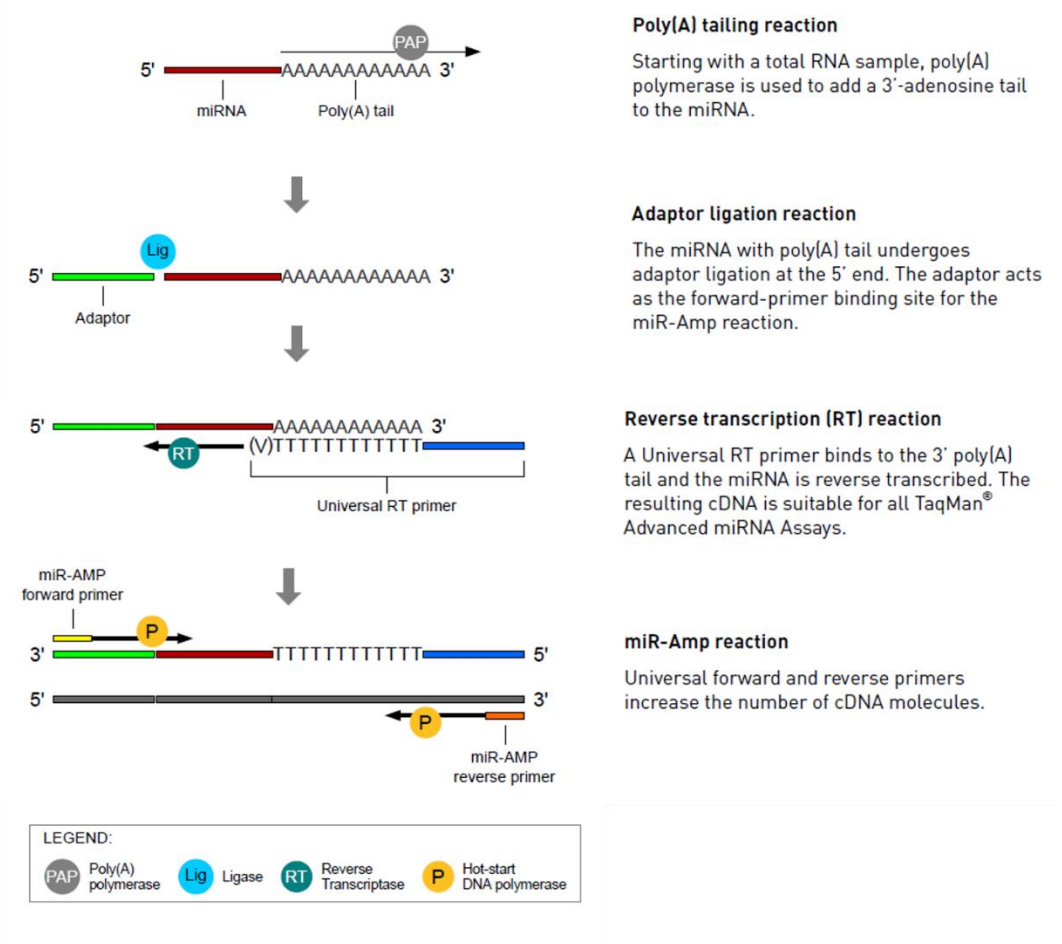


Figure 2.4: The four reactions employed in the TaqMan™ Advance miRNA cDNA synthesis kit.

2.3.4.3 Polyadenylation Tailing Reaction

First, in a 0.2µl Eppendorf tube, 2µl of RNA (5ng/µl) was pipetted into 3µl of Poly(A) reaction mix for the required number of reactions, see Table 2.4. The reaction was incubated in a thermocycler (Prime thermocycler).

Table 2.4: TaqMan™ Advanced miRNA polyadenylation tailing reaction mixture composition and cycling conditions.

Reaction Mixture	
Components per reaction	Volume (µl)
Spike-In Control (0.1875nM)	1.45
10X Poly(A) Buffer (ThermoFisher Scientific)	0.5
ATP (ThermoFisher Scientific)	0.5
RNase Inhibitor (ThermoFisher Scientific)	0.25
Poly(A) Enzyme (ThermoFisher Scientific)	0.3
Total reaction volume (after adding 2µl of RNA)	5
Cycling conditions	
Step	Temperature and duration
Polyadenylation	37°C for 45min
Stop reaction	65°C for 10min
Hold	4°C (infinite)

2.3.4.4 Adaptor Ligation

Next, the adaptor ligation reaction mix was prepared as in Table 2.5, and 10µl was transferred into the 5µl of poly(A) tailing reaction. The tube was vortex and spun down. The reaction is incubated in a thermal cycler for 60min.

Table 2.5: TaqMan™ Advanced miRNA adaptor ligation mixture composition and cycling conditions.

Reaction Mixture	
Components per reaction	Volume (µl)
NFW	0.4
5X DNA ligase Buffer (ThermoFisher Scientific)	3
50% PEG 8000 (ThermoFisher Scientific)	4.5
25X Ligation Adaptor (ThermoFisher Scientific)	0.6
RNA Ligase (ThermoFisher Scientific)	1.5
Total reaction volume	10
Cycling conditions	
Step	Temperature and duration
Ligation	16°C for 60min
Hold	4°C (infinite)

Following the incubation, the tube was removed from the thermal cycler and 15µl of the RT reaction mix (prepared as per Table 2.6) was added into the reaction then placed again in the thermal cycler for 20min.

Table 2.6: TaqMan™ Advanced miRNA RT reaction mixture composition and cycling conditions.

Reaction Mixture	
Components per reaction	Volume (µl)
NFW	3.3
5X RT Buffer (ThermoFisher Scientific)	6
dNTP mix (25mM each; ThermoFisher Scientific)	1.2
20X Universal RT primer (ThermoFisher Scientific)	1.5
10X RT Enzyme Mix (ThermoFisher Scientific)	3
Total reaction volume	15
Cycling conditions	
Step	Temperature and duration
Reverse transcription	42°C for 15min
Stop reaction	85°C for 5min
Hold	4°C (infinite)

Subsequently, the cDNA can be amplified. From each RT reaction, 6 miR-Amp reactions can be prepared. The miR-Amp reaction mix is made as in Table 2.7, and 45µl of the miR-Amp reaction mix is transferred into a new 0.2µl. 5µl of the RT reaction is then added into each respective tube, then vortex and spun down.

Table 2.7: TaqMan™ Advanced miRNA miR-Amp reaction mixture composition and cycling conditions.

Reaction Mixture	
Components per reaction	Volume (µl)
NFW	17.5
2X miR-Amp Master Mix	25

(ThermoFisher Scientific)		
20X miR-Amp Primer Mix (ThermoFisher Scientific)		2.5
Total reaction volume (after adding 5µl of the miR-Amp reaction)		50
Cycling conditions		
Cycle		Temperature and duration
Enzyme activation		95°C for 5min
Denaturation	14 cycles	95°C for 30sec
Annealing		60°C for 1min
Stop reaction		99°C for 10min
Hold		4°C (infinite)

2.3.4.5 TaqMan™ Advanced miRNA qRT-PCR Assay

miRNA expression analysis was performed using the TaqMan™ Advanced miRNA qRT-PCR Assay kit (Thermofisher Scientific).

Specific probes (primers) are designed for this assay to reporter dye (i.e. FAM™) at the 5′ end and a non-fluorescent quencher (NFQ) dye and a minor groove binder (MGB) at the of the probe.The probes anneal specifically to a sequence between the forward and reverse primer sites (

Figure 2.5). When the probe is intact, the proximity of the reporter dye and quencher dye suppresses the reporter fluorescence (

Figure 2.5). During polymerization, however, when the DNA polymerase cleaves probes that are hybridised to the target sequence, the reporter dye separates from the probe. The

separation of the reporter dye from the quencher dye results in increased fluorescence by the reporter dye (

Figure 2.5). Consequently, non-specific amplification is not detected as the 3' end of the probe is blocked by the MGB, which prevents probe extension. Therefore, the experimental setup did not include a no-RT control.

Probes for endogenous miRNAs (hsa-miR-191-5p and hsa-miR-361-5p), which have relatively constant and moderately abundant expression across all tissue samples, were used to eliminates differences due to variation in the amount of starting material and sample quality.

All probes were previously tested to have 100% efficiency. The corresponding miRNA sequences for each probe is shown in Table 2.8.

Table 2.8: TaqMan™ Advanced miRNA Assay Probes.

Assay Name	**Assay ID (Thermofisher Scientific)**	**Mature miRNA Sequence**
hsa-miR-619-5p	479103_mir	GCUGGGAUUACAGGCAUGAGCC
hsa-miR-4793-3p	480053_mir	UCUGCACUGUGAGUUGGCUGGCU
hsa-miR-330-5p	478830_mir	UCUCUGGGCCUGUGUCUUAGGC
hsa-miR-215-3p	478769_mir	UCUGUCAUUUCUUUAGGCCAAUA

hsa-miR-4440	479809_mir	UGUCGUGGGGCUUG CUGGCUUG
hsa-miR-191-5p	477952_mir	CAACGGAAUCCCAAA AGCAGCUG
hsa-miR-361-5p	478056_mir	UUAUCAGAAUCUCCA GGGGUAC

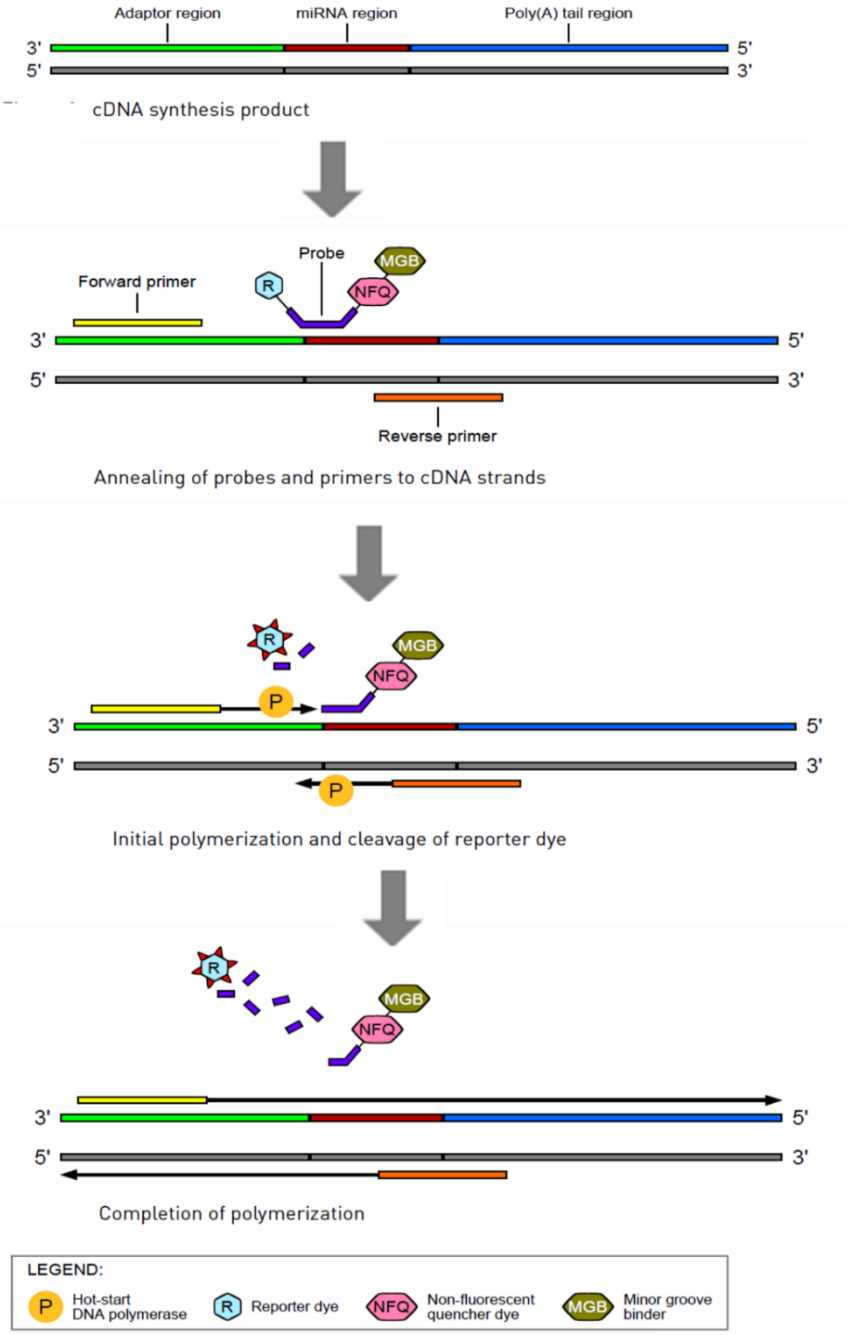


Figure 2.5: The three chemical reactions employed in the TaqMan™ Advanced miRNA qRT-PCR Assay.

The probes anneal specifically to a complementary sequence between the forward and reverse primer. DNA polymerase cleaves the probes during polymerisation. This leads to an increased

fluorescence by the reporter as it separates from the quencher dye (

Figure 2.5*).*

The qRT-PCR reaction started with the preparation of cDNA. 1:10 of the cDNA from the miR-Amp reaction was diluted in NFW, and 5µl was transferred per well into a Multiplate™ 96-Well unskirted PCR plates (Bio-Rad). NFW control wells were included; however, this can only identify contamination from spillage of another cDNA sample into the fresh well/reaction mix. Other contaminants will be identified as the assay only detects tagged cDNA converted from miRNA sequences.

A master mix was prepared for each TaqMan™ miRNA Advanced Assay probe, as shown in Table 2.9. The amount of master mix prepared was determined by the number of wells used (plus 1.5 extra to account for pipetting errors). The master mix was vortexed, briefly centrifuged, protected from light and kept on ice. 15µl of the master mix was then transferred into the appropriate well to make up a total reaction volume of 20µl/well. The plate was sealed and spun in a vertical plate spinner to ensure the mix was all in the base of the well. The PCR plate was read by CFX-96 Real-Time

System with a C100 Thermocycler and analysed by Bio-Rad CFX manager for Taqman dye. PCR cycling conditions (40 cycles) are described in Table 2.9.

Table 2.9: TaqMan™ Advanced miRNA qRT-PCR Assay reaction mixture composition and cycling conditions.

Reaction Mixture		
Components per reaction		Volume (µl)
2X TaqMan Fast Advance Master Mix (Thermofisher Scientific)		10
20X TaqMan Advance miRNA assay (Thermofisher Scientific)		1
NFW		4
Total reaction volume (after adding 5µl cDNA, no-RT or NFW)		20
Cycling conditions		
Cycle		Temperature and duration
Enzyme activation		95°C for 10min
Denature	40 cycles	95°C for 1sec
Annealing		60°C for 20sec
Hold		4°C (infinite)

2.3.4.6 Quantification of miRNA expression levels

Normalised expression (NE) values were calculated as in (Marabita *et al.*, 2016). The average expression values of two house-keeping miRNAs (hsa-miR-361-5p and hsa-miR-191-5p) were used as endogenous controls (Peltier and Latham, 2008), with a *C. elegans* miRNA, cel-miR-54-3p, as an exogenous spike-in control (as in Kuhlmann et al., 2014).

$$R = \frac{2^{-(Ct\ (miR\ of\ interest) - Ct\ (Spike-in\ control)}}{2^{-(Ct\ (average\ of\ endogenous\ controls) - Ct\ (Spike-in\ control)}}$$

Statistical analysis was carried out using one-way ANOVA significance test ($p<0.05$) followed by a Bonferroni multiple comparisons test in GraphPad Prism.

2.3.5 Gene expression analysis in cell line samples

In order to reduce genomic DNA contamination, the RNA samples were treated with DNAse. 1µg of total RNA was treated with 1µl of DNase I (1U/µl; ThermoFisher Scientific) mixed with 1µl of 10x DNase I buffer. The reaction volume was topped up to 10µl with NFW. The reaction was incubated in a 37°C for 30min. The DNAse was inactivated by adding 1µl of the stop buffer containing EDTA (ThermoFisher Scientific). EDTA is a synthetic amino acid that chelates the divalent metal cations (such as Ca2+ and Mg2+) in the reaction buffer that were needed for DNase I activity. The mixture was further incubated at 65°C for 10min.

2.3.5.1 cDNA synthesis

Complementary single-stranded DNA (cDNA) was generated from RNA templates by reverse transcriptase II (RT) that uses a short primer (Oligo-dT) complementary to the 3' poly-A tail of the RNA. For each sample, the 10µl DNase-treated RNA (approximately 1µg) was mixed with 1µl of Oligo-dT, 4µl of 5X reaction buffer, 2µl of

10mM dNTP, 1.5µl of NFW and 0.5µl of RiboLock RNase Inhibitor (40 U/µl; ThermoFisher Scientific) which was added to prevent RNA degradation by RNase during the reaction. Finally, 1µl of RevertAid RT (200U/µl; ThermoFisher Scientific) was added to the reaction. A separate reaction containing all reagents except the RevertAid RT (no-RT control) was made in parallel. This control assesses the amount of DNA contamination present in an RNA preparation. For the no-RT reaction, 1µl of NFW was added instead of RevertAid RT. Both the RT and the no-RT reactions were incubated at 42°C for 1h and then at 70°C for 10min, and then stored at -20°C until used. Finally, cDNA concentration was measured using the Nanodrop (see section 2.3.2).

2.3.5.2 SYBR Green Quantitative RT-PCR (qRT-PCR)

PCR relies on DNA Polymerase I to use primer sequences to synthesise double-stranded DNA (dsDNA). The fluorescent dye (SYBR green) binds to the minor groove of the dsDNA and serves as an indicator of DNA synthesis.

To each well in a 96-well PCR plate (Bio-Rad), 5µl of cDNA made from RNA of various GBM cell line was added. Alternatively, 5µl of no-RT was used to detect genomic DNA contamination that might

still be present in the cDNA sample) or 5µl of NFW was used to identify any contamination in the PCR reaction mixture.

For each gene of interest, a master mix was prepared using the appropriate primer pair, as shown in Table 2.10. The amount of master mix prepared was determined by the number of wells used (plus 1.5 extra to account for pipetting errors). The master mix was vortexed, briefly centrifuged and kept on ice. 20µl of the master mix was then transferred into the appropriate well to make up a total reaction volume of 25µl/well. The plate was sealed and spun in a vertical plate spinner to ensure the mix was all in the base of the well. The PCR plate was read by CFX-96 Real-Time System with a C100 Thermocycler (Bio-Rad) and analysed by Bio-Rad CFX Manager (version 3.0) with excitation at 494 nm and emission at 521 nm for SYBR Green.

PCR cycling conditions (40 cycles) are described in Table 2.10. The denaturation step involves heating up to 95°C the sample to separate the dsDNA into single strands. Next, the annealing step involves a reduction in temperature to 60°C to allow forward and reverse primer to attach the single-stranded DNA. Finally, in the elongation step, DNA polymerase synthesises the complementary DNA strand at 72°C. The amount of PCR product synthesised can be

estimated by the Ct value, which represents the number of cycles at which the reaction fluorescence exceeds the threshold of background fluorescence threshold.

Table 2.10: SYBR Green qRT-PCR reaction mixture composition and cycling conditions.

Reaction Mixture		
Components per reaction		Volume (µl)
iQ SYBR Master Mix (which contained DNA polymerase and dNTPs, SYBR green dye and Mg2+; Bio-Rad)		12.5
NFW		5.5
Forward and Reverse Primers		1 (each)
Total reaction volume (after adding 5µl of either cDNA, no-RT or NFW)		25
Cycling conditions		
Cycle		Temperature and duration
Enzyme activation		95°C for 5min
Denaturation	40 cycles	95°C for 30sec
Annealing		60°C for 1min
Elongation		72°C for 1min
Melting curve		Increments of 0.5°C every 5sec
Hold		4°C (infinite)

2.3.5.3 Primer design and PCR standard Curve

Forward and reverse primer pairs were designed for each target gene using the NCI Primer-BLAST tool (available from: www.ncbi.nlm.nih.gov/tools/primer-blast/). PCR product and primer size were set to a 50-150 bp and 18-25 bp, respectively. The annealing temperature was set to 58-60°C. Intron inclusion option was selected in order to obtain a primer set that would disable gDNA

from being amplified due to the template being too long to amplify in 40 cycles.

Primers were ordered as custom DNA oligos from (Eurofins Genomics), and the appropriate amount of NFW was added to reconstitute each primer to the final concentration of 100pmol/µl. Primers were diluted in NFW to unequal forward and reverse primer concentrations (Figure 2.6) to prevent the primer dimerisation. PCR reaction was carried out (as described above, see Table 2.10) using cDNA from U87 cell line which express the genes of interest at high levels as determined from the Human Protein Atlas (available from: www.proteinatlas.org).

(a)

	1	2	3	4	5	6	7	8	9
A	1:10F + 1:10R	1:10F + 1:20R	1:10F + 1:40R	1:20F + 1:10R	1:20F + 1:20R	1:20F + 1:40R	1:40F + 1:10R	1:40F + 1:20R	1:40F + 1:40R
B	1:10F + 1:10R	1:10F + 1:20R	1:10F + 1:40R	1:20F + 1:10R	1:20F + 1:20R	1:20F + 1:40R	1:40F + 1:10R	1:40F + 1:20R	1:40F + 1:40R
C	1:10F + 1:10R	1:10F + 1:20R	1:10F + 1:40R	1:20F + 1:10R	1:20F + 1:20R	1:20F + 1:40R	1:40F + 1:10R	1:40F + 1:20R	1:40F + 1:40R
D	1:10F + 1:10R	1:10F + 1:20R	1:10F + 1:40R	1:20F + 1:10R	1:20F + 1:20R	1:20F + 1:40R	1:40F + 1:10R	1:40F + 1:20R	1:40F + 1:40R
E	1:10F + 1:10R	1:10F + 1:20R	1:10F + 1:40R	1:20F + 1:10R	1:20F + 1:20R	1:20F + 1:40R	1:40F + 1:10R	1:40F + 1:20R	1:40F + 1:40R
F	1:10F + 1:10R	1:10F + 1:20R	1:10F + 1:40R	1:20F + 1:10R	1:20F + 1:20R	1:20F + 1:40R	1:40F + 1:10R	1:40F + 1:20R	1:40F + 1:40R
G	1:10F + 1:10R	1:10F + 1:20R	1:10F + 1:40R	1:20F + 1:10R	1:20F + 1:20R	1:20F + 1:40R	1:40F + 1:10R	1:40F + 1:20R	1:40F + 1:40R
H	1:10F + 1:10R	1:10F + 1:20R	1:10F + 1:40R	1:20F + 1:10R	1:20F + 1:20R	1:20F + 1:40R	1:40F + 1:10R	1:40F + 1:20R	1:40F + 1:40R

(b)

	1	2	3	4	5	6	7	8	9
A	1:40F + 1:40R	1:40F + 1:70R	1:40F + 1:100R	1:70F + 1:40R	1:70F + 1:70R	1:70F + 1:100R	1:100F + 1:40R	1:100F + 1:70R	1:100F + 1:100R
B	1:40F + 1:40R	1:40F + 1:70R	1:40F + 1:100R	1:70F + 1:40R	1:70F + 1:70R	1:70F + 1:100R	1:100F + 1:40R	1:100F + 1:70R	1:100F + 1:100R
C	1:40F + 1:40R	1:40F + 1:70R	1:40F + 1:100R	1:70F + 1:40R	1:70F + 1:70R	1:70F + 1:100R	1:100F + 1:40R	1:100F + 1:70R	1:100F + 1:100R
D	1:40F + 1:40R	1:40F + 1:70R	1:40F + 1:100R	1:70F + 1:40R	1:70F + 1:70R	1:70F + 1:100R	1:100F + 1:40R	1:100F + 1:70R	1:100F + 1:100R
E	1:40F + 1:40R	1:40F + 1:70R	1:40F + 1:100R	1:70F + 1:40R	1:70F + 1:70R	1:70F + 1:100R	1:100F + 1:40R	1:100F + 1:70R	1:100F + 1:100R
F	1:40F + 1:40R	1:40F + 1:70R	1:40F + 1:100R	1:70F + 1:40R	1:70F + 1:70R	1:70F + 1:100R	1:100F + 1:40R	1:100F + 1:70R	1:100F + 1:100R
G	1:40F + 1:40R	1:40F + 1:70R	1:40F + 1:100R	1:70F + 1:40R	1:70F + 1:70R	1:70F + 1:100R	1:100F + 1:40R	1:100F + 1:70R	1:100F + 1:100R
H	1:40F + 1:40R	1:40F + 1:70R	1:40F + 1:100R	1:70F + 1:40R	1:70F + 1:70R	1:70F + 1:100R	1:100F + 1:40R	1:100F + 1:70R	1:100F + 1:100R

Figure 2.6: Primer Optimisation PCR Plates Layout.
Forward (F) and reverse (R) primers are mixed at different ratios and tested on cDNA samples (Blue), no-template control samples (Pink) and nuclease-free water (Green).

Ratios of forward and reverse primers that produced the least amount of or no primer dimers were selected. The different ratios were tested in order to optimise the PCR amplification efficiency, which is defined as the rate at which a PCR product is generated. An efficiency of 100% indicates that the quantity of PCR product doubles with each PCR cycle. Efficiency values between 90 and 110% were considered satisfactory. The efficiency of the reaction using each primer pair was identified (Table 2.11).

The efficiency of the PCR reaction using each primer pair was determined from a PCR standard curve. A PCR standard curve is graphically represented as a semi-log regression line plot of CT value (y-axis) and log cDNA concentration (x-axis) (Figure 2.7). A 1:5 serial dilution of cDNA concentration was prepared in NFW using 100ng as a starting point and then diluted in series of 20ng, 4ng, 0.8ng, and 0.16ng. 5µl of each cDNA dilution (or of the no-RT or the no-template control) was added to a well in the 96-well PCR plate. PCR master mix was added to each well as the reaction proceeded as described above.

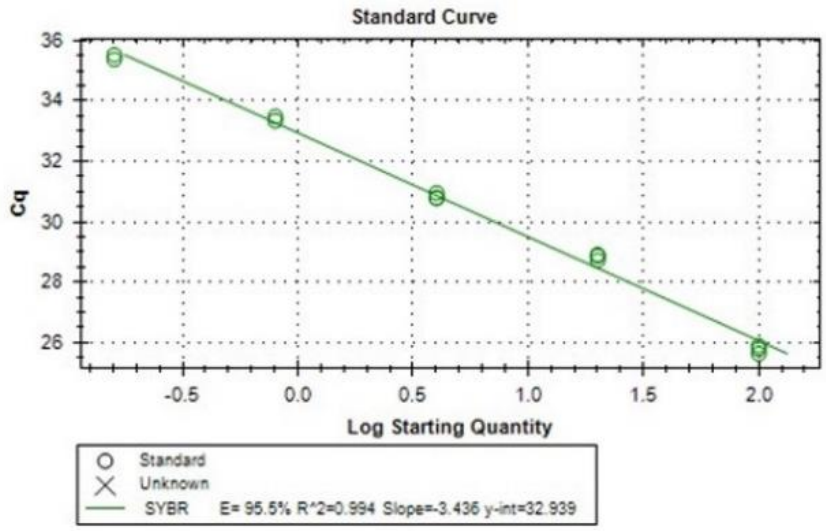


Figure 2.7: Scatter plot of mean Ct values for the HILPDA primer pair at serially diluted concentrations of DNA template.

The log of DNA concentration is plotted against the Ct values. Efficiency (E) was 95.5%, the slope was -3.538 and the goodness of fit measure (R2) was 0.994.

The efficiency of the PCR reaction can be assessed based on the slope of the standard curve using the formula E = (10(−1/slope) − 1) x 100 (Svec *et al.*, 2015). A 100% efficient reaction will yield a 10-fold increase in PCR product every 3.32 cycles during the exponential phase of amplification (log2 10 = 3.3219). Hence, a standard curve slope of –3.32 indicates a PCR reaction with 100% efficiency. R2 is then used as a goodness-of-fit measure for linear regression models. An R2 value of ≥ 0.90 indicates a strong correlation.

Table 2.11: Primers sequences and efficiencies for SYBR Green qRT-PCR

Gene	Forward Primer (5'-3')	Reverse Primer (5'-3')	Efficiency (%)	R2	Slope (-)
CPT2	ATGGGATTGGAAAAGAACTGCA	TCAAACCAGGGTCCCGAAAT	95.1	0.99	3.44
GK5	ATCCGCTGCCACGTCTAT	GTGTTGAAATGCCAAGACCAAC	103.2	0.93	3.25
ACOX1	GGATCTTCACTTGGGCATGTTC	CCAAGCCTCGAAGGTGAGTT	90.6	0.94	3.57
LDLR	AGGCTGTGGGCTCCATCGCCTA	AGTCAGTCCAGTACATGAAGCCA	95.1	0.98	3.44
PLIN3	AGCTGTCGCAGGTCCTAAG	TCTGGCTTGGGCGGC	93.1	0.92	3.50
ELOVL6	AGCCATTAGTGCTCTGGTCT	CCTGGTCACAAACTGACTGC	90.1	0.99	3.59
DGKH	TTGCTAAATCCGGCTCAGGT	TTCCATCGCCTCCACAAACA	103.8	0.91	3.23
ALDH1B1	AACCCAAGCGTGATCCTGAA	CCTGCCCTGGAGGCTAAG	90.4	0.99	3.58
HILPDA	AAGCATGTGTTGAACCTCTACC	GATGGAGAGTAGGGTCAGTACC	95.5	0.99	3.44
ALDH9A1	AAGGAGCAGGGTGCTAAAGT	CACACAGGTCATGTCGTCTC	91	0.99	3.56
MALAT1	AGGCGTTGTGCGTAGAGGA	GGATTTTTACCAACCACTCGC	100.6	0.99	3.31
GPD2	CATGAAGTTGGATATTGAGCA	AGGCAATGGAGCTGATAAATG	104.2	0.97	3.23
B-Actin	ATTGGCAATGAGCGGTTC	GGATGCCACAGGACTCCA	92	0.98	3.53

Optimisation involved testing different ratios of forward and reverse primers and running a standard curve for the optimal ratio where no primer dimers products are seen in amplification and melting curves (Figure 2.8).

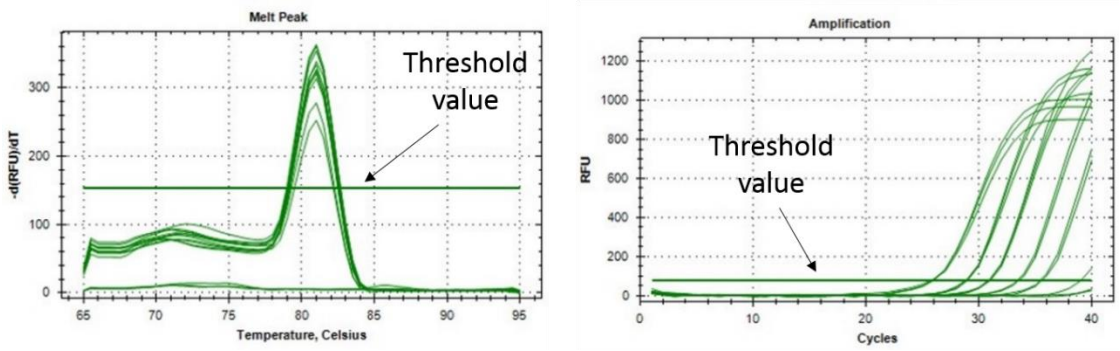


Figure 2.8: Amplification curve (left) and melting curve (right) for HILPDA from a serial dilution of control cDNA. *Amplification curve represents the amount of SBYR green fluorescence produced per PCR cycle from each DNA concentration. The melting curve is produced as a result of a reduction in the fluorescent signal of SYBR Green as the temperature is gradually increased. The ideal melting temperature curve is indicated by asymmetrical curve of product peaks with short temperature range (here, ~79 °C) which indicates a single specific amplicon. The cycle threshold (Ct) value for each reaction was the cycle value at which the reaction fluorescence exceeded the fluorescence threshold value. RFU= relative fluorescence units.*

2.3.5.4 Quantification of target gene expression levels in cell lines

The relative level of target gene expression (R) was calculated using the Pfaffl equation in Microsoft Excel by using the equation below.

$$R = \frac{(\text{Efficiency of GOI})^{\Delta\text{CT GOI (CT GOI in reference sample} - \text{ CT GOI in experimental sample)}}}{(\text{Efficiency of HKG})^{\Delta\text{CT HKG (CT HKG in reference sample} - \text{ CT HKG in experimental sample)}}}$$

R is the ratio of the difference in CT values of the target gene of interest (GOI) between the reference sample and the experimental sample of interest and the difference in CT values of the housekeeping gene (HKG) between the reference sample and the experimental sample. If R equals one, then there is no quantifiable difference between the two samples. R values were entered in Graphpad Prism to produce bar charts showing mean along with standard errors.

2.3.6 Gene Expression Analysis in Tissue Samples

Gene expression analysis in tissue sample was performed using TaqMan™ RNA-to-CT™ 1-Step Kit (Thermofisher Scientific), which performs reverse transcription and real-time PCR in a single reaction tube.

2.3.6.1 TaqMan™ RNA-to-CT™ 1-Step qRT-PCR

The TaqMan® RNA-to-CT™ 1-Step Kit provides high detection sensitivity at low target concentration, which is especially relevant in the case of limited tissue sample availability.

Approximately 5-10ng of RNA (in a total volume of 5µl) was added per well in a 96-well PCR plate. NFW control wells were included in the plate to detect potential contamination in the reaction mixture.

TaqMan™ RNA-to-CT™ 1-Step Kit is compatible with TaqMan™ Gene Expression Assay Probes which serve as primers for the gene of interest.

For each probe, a master mix was prepared, as shown in Table 2.12. The amount of master mix prepared was determined by the number of wells used (plus 1.5 extra to account for pipetting errors). The master mix was vortexed, briefly centrifuged and kept on ice. 15µl of the master mix was then transferred into the appropriate well to make up a total reaction volume of 20µl/well. The plate was sealed and spun in a vertical plate spinner to ensure the mix was all in the base of the well. The PCR plate was read by CFX-96 Real-Time System with a C100 Thermocycler and analysed by Bio-Rad CFX manager for Taqman dye. PCR cycling conditions (40 cycles) are described in Table 2.12.

The TaqMan™ RT-PCR Mix reagent contains AmpliTaq Gold® DNA Polymerase, which is only activated for hot-start PCR to prevent amplification during reaction setup. It also contains an ArrayScript™ UP reverse transcriptase, a dNTP blend including dUTP, for post-PCR amplicon degradation with uracil-DNA glycosylase (UDG) to minimise carryover contamination in subsequent PCR reactions, an RNase inhibitor to prevent degradation of the RNA template, and a

buffer optimised to improve sensitivity across a broad range of targets.

Table 2.12: TaqMan™ RNA-to-CT™ 1-Step qRT-PCR reaction mixture composition and cycling conditions.

Reaction Mixture		
Components per reaction		Volume (µl)
2X TaqMan™ RT-PCR Mix (Thermofisher Scientific)		10
20X TaqMan™ Gene Expression Assay Probe (Thermofisher Scientific)		1
40X TaqMan™ RT Enzyme Mix (Thermofisher Scientific)		0.5
NFW		3.5
Total reaction volume (after adding 5µl of RNA)		20
Cycling conditions		
Cycle		Temperature and duration
Reverse Transcription		48°C for 15min
Activation of AmpliTaq Gold DNA Polymerase UP (Ultra Pure)		95°C for 10min
Denature	40 cycles	95°C for 15sec
Anneal/ Extend		60°C for 1min
Hold		4°C (infinite)

2.3.6.2 TaqMan® Gene Expression Assay Probe Testing

For each probe, a standard curve was constructed using a 1:5 serial dilution (100ng-0.16ng) of RNA (instead of cDNA) from U87 cells. Information about the probes and reaction efficiencies are shown in Table 2.13.

Table 2.13: TaqMan™ Gene Expression Assay Probes and qRT-PCR Reaction Efficiencies.

Gene	Assay ID (Thermofisher Scientific)	Efficiency (%)	R2	Slope (-)
LDLR	Hs01092524_m1	96.4	0.99	3.41
CPT2	Hs00988962_m1	100.1	0.97	3.32
ACOX1	Hs01074241_m1	92.9	0.99	3.51
BA	Hs01060665_g1	92.9	0.99	3.50

2.3.6.3 Quantification of gene expression levels in the tissue sample

The relative level of target gene expression (R) was calculated the same way as in the quantification of gene expression in cell lines using the Pfaffl equation below where GOI is the target gene of interest and HKG is the housekeeping gene.

$$R = \frac{(\text{Efficiency of GOI})^{\Delta\text{CT GOI (CT GOI in reference sample} - \text{CT GOI in experimental sample)}}}{(\text{Efficiency of HKG})^{\Delta\text{CT HKG (CT HKG in reference sample} - \text{CT HKG in experimental sample)}}}$$

2.4 Cell-based Assays

2.4.1 PrestoBlue Viability Assay

PrestoBlue® cell viability reagent (ThermoFisher Scientific) was used to determine the cytotoxicity of different reagents used throughout the project. The assay is based on the metabolism of resazurin into resorufin by viable cells. The amount of resorufin present in the cell media is proportional to the number of the viable/metabolically active cells and, therefore, can be measured quantitatively.

The cell culture medium was removed, adherent monolayer cells were washed with HBSS, and 1ml of the 1:10 Presto blue solution was added to each well in a 6-well cell culture plates (ThermoFisher Scientific). The plates were protected from light and incubated at 37°C in a 5% CO2 humidified atmosphere for 30min.

After incubation, 100µl from each well was transferred into a black 96-well plate in triplicate. A medium-only control was also included to correct for background fluorescence. Fluorescence was read at 544-excitation and 590-emission settings on the FLUOstar Omega microplate reader (BMG LABTECH). The remaining Presto blue solution was removed from cells, and the cells were washed with HBSS ready for the downstream applications or further incubation in fresh media.

2.4.2 Transfection of GBM Cells with Small RNAs

There are three methods for the transfection of small RNA: standard (forward), Reverse Transfection Format (RTF) plates from Thermo Scientific, and reverse transfection. They differ in the order and timing of the addition of the three necessary components of transfection: the small RNA, the transfection reagent and the cells. In forward transfection, RNA and transfection reagent are complexed then added to pre-plated cells (Figure 2.9). In RTF transfection, pre-plated dried siRNA are rehydrated and complexed with the

transfection reagent; thereafter, the cells are added on top (Figure 2.9). In reverse transfection, all three components are added to the wells at the same time (Figure 2.9). In this project, reverse transfection was used because it does not only reduce the hands-on time for transfection from two days to only one, but it also gives the flexibility of testing different concentration of RNA.

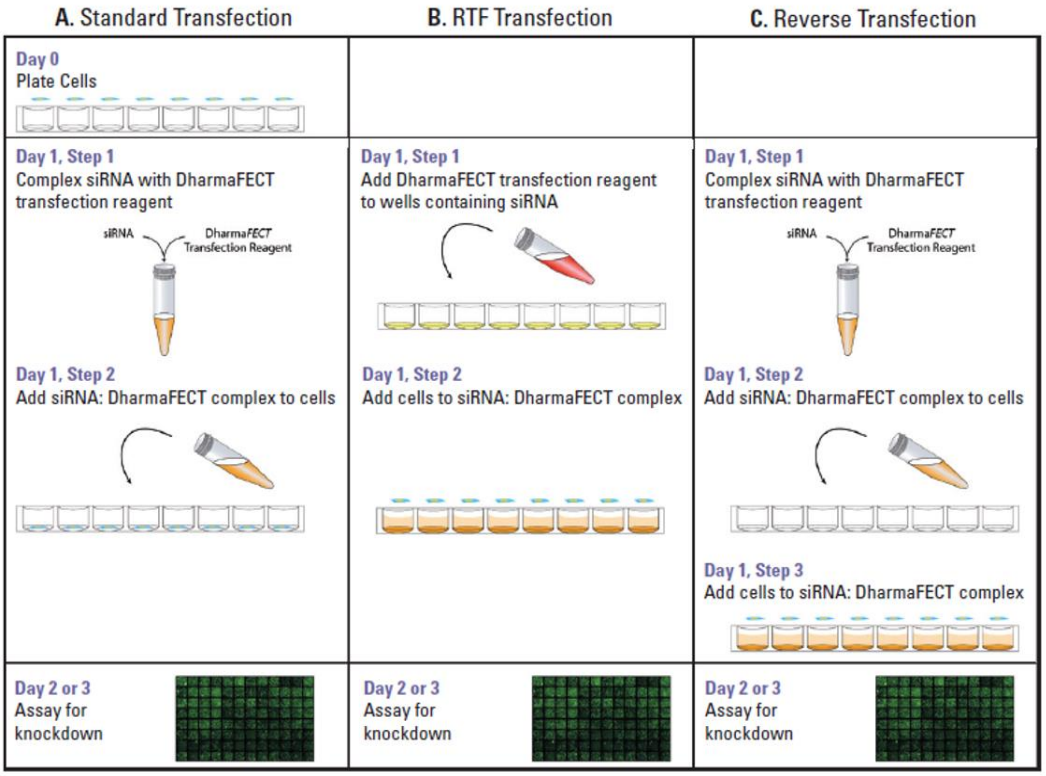


Figure 2.9: Methods of small RNA transfection.
Small interfering RNA (siRNA) was used as an example to illustrate the three different transfection methods.

Small RNAs are short nucleotides (20–25 in length). In this project, four types of small RNAs were used, namely: siGlo Green Transfection Indicator Control, miRNA mimics, miRNA hairpin inhibitors, and small interfering RNA (siRNA).

siGlo Green is a fluorescent non-RISC engaging oligonucleotide duplex that acts as a transfection indicator by localising to the nucleus. The detection of siGlo Green fluorescent nuclei under the fluorescence microscope (Nikon Eclipse Ti; analysed by NIS Element Software v3.21.03) at 488-507 wavelength indicates efficient uptake of RNA into the cells of interest. Information about siGlo Green used in this project is described in Table 2.14.

Table 2.14: siGlo Green sequence information.

Gene	Full Product Name	Product Code (Horizon Discovery)
siGlo Green	siGLO Transfection Indicator Control	D-001630-01-05

An siRNA is a synthetic RNA duplex designed to specifically target a particular mRNA for degradation. siRNAs are used to assess the individual contributions of genes to a particular cellular phenotype. Non-targeting controls are also used as a chemically-matched negative control for siRNA experiments help to separate sequence-specific effects from the effects of experimental conditions on cellular response. Information about siRNA used in this project is described in Table 2.15.

Table 2.15: siRNA sequence information.

Gene	Full Product Name	Product Code (Horizon Discovery)
CPT2	SMARTpool ON-TARGETplus CPT2 siRNA	L-008574-00-0005
Non-targeting siRNA Control	ON-TARGETplus Non-targeting Pool	D-001810-10-05

miRNA mimics are double-stranded RNAs chemically enhanced to preferentially load RISC, and they were therefore used to overexpress miRNAs in the cells (Table 2.16).

miRNA hairpin inhibitors are single-strand RNAs designed to bind and to sequester the complimentary the mature miR strand, and thus, they were used to knock down the levels of miRNAs in the cells (Table 2.16).

Universal non-targeting mimic/inhibitor negative controls are identically designed and modified mature sequences based on Cel-miR-67, which has minimal sequence identity with miRNAs targets in human. Non-targeting mimic/inhibitor controls were used to distinguish mimicry/inhibitory effect from background effect (Table 2.16).

Table 2.16: miRIDIAN miRNA mimics and hairpin inhibitors information.

miRNA	Product Name	Product Code (Horizon Discovery)	Mature miRNA Sequence
hsa-miR-619-5p	Mimic	C-303062-00-0005	GCUGGGAUUACAGGCAUGAGCC
	Hairpin Inhibitor	IH-303062-01-0005	
hsa-miR-4793-3p	Mimic	C-302420-00-0005	UCUGCACUGUGAGUUGGCUGGCU
	Hairpin Inhibitor	IH-302420-01-0005	
Cel-miR-67	Non-targeting Mimic Control	CN-001000-01-05	UCACAACCUCCUAGAAAGAGUAGA

	Non-targeting Inhibitor Control	IN-001005-01-05	

2.4.2.1 Testing the cytotoxicity of the transfection reagent

The DharmaFECT™ 1 Transfection Reagent (GE Healthcare) is a lipid-based transfection reagent designed for effective transfection of small RNAs at low concentrations and with low cytotoxicity. The optimal range of concentrations of the transfection reagent was recommended by the manufacturer. Three concentration from that range were assessed for their cytotoxicity on GBM cells by measuring cell viability using PrestoBlue after 24h of incubating the cells with the transfection reagent.

In a 96 well-plate, 80µl of pre-warmed (37°C) cell culture media (DMEM supplemented with 10% FBS) containing 3.125×10^4 cells/ml (previously optimised to give reaches cells 70% confluent in 24h) was added to each well containing a different concentration of the DharmaFECT™ 1 Transfection Reagent.

Prior to adding the cells, each well-contained 0.1µl of DharmaFECT™ 1 Transfection Reagent was added to 9.9µl of serum-free cell culture medium and incubated for 5min at room temperature. 10µl of fresh

cell culture medium was mixed and incubated for 20min and 20µl was transferred to each well.

The transfection medium was replaced by PresoBlue after 24h and incubated at 37°C, 5% CO2, humidified atmosphere for 30min then cell viability was quantified as described above.

2.4.2.2 Reverse transfection of GBM Cells with Small RNAs

Cell transfection for both patient-derived primary and commercial GBM cell lines was done using the same protocol. The transfection was performed either in 6-well plates or T75 flasks (Table 2.17). Accordingly, the appropriate amount of DharmaFECT™ 1 Transfection Reagent was added to serum-free cell culture medium and incubated for 5min at room temperature (Tube 1). In parallel, the appropriate concentration of small RNAs was prepared in serum-free cell culture medium for a final concentration of either 25nM or 50nM (Tube 2). Subsequently, Tube 1 was mixed with Tube 2 at 1:1 ratio (Tube 3) and incubated for 20min at room temperature. This allows the transfection reagent to encapsulate the small RNAs. After 20min, the content of Tube 3 (transfection reagent + small RNA) was transferred into a well in a 6-well plate or into a T75 flask (see Table 2.17). The transfection medium was prepared for the amount of wells/flasks needed (plus 1.5 to account for pipetting errors).

Transfection experiments for the targeting miRNA/siRNA were set up at the same time as those for a non-targeting control.

Finally, the appropriate amount of pre-warmed (37°C) cell culture media containing 3.125 x 10^4 cells/ml (Tube 4) was added on top of the transfection reagent/small RNA complex in the well or the flask. The cells were then incubated at 37°C in a 5% CO2 humidified atmosphere for 24h.

Table 2.17: Transfection mixture based on cell culture vessel format.

		In a well of a 6-Well Plate (µl)	**In T75 Flask (µl)**
Tube 1	miRNA/siRNA (5 or 10 µM stock)	10	75
	Serum-free media	190	1425
Tube 2	DharmaFECT™ 1 Transfection Reagent	2	15
	Serum-free media	198	1485
Tube 3	Tube 1	200	1,500
	Tube 2	200	1,500
Tube 4	Cells in serum-supplemented culture media	1,600	12,000
	Total Volume of transfection media	2,000	15,000

For siGlo Green, the transfection medium was replaced by phosphate-buffered saline (PBS; Sigma-Aldrich) after the 24h of incubation. PBS as used to avoid background signal noise from the

cell culture medium when imaging fluorescent nuclei under the fluorescence microscope (Leica Microsystems). The images were analysed using ImageJ to count the number of fluorescent nuclei. The percentage of florescent give the transfection efficiency at different siGlo Green concentrations.

For siRNAs and miRNA mimics/hairpin inhibitors, the transfection medium with fresh cell culture medium after 24h to continue incubation at 37°C in a 5% CO2 humidified atmosphere for up to 72h.

2.4.3 Luciferase Assay

The Luciferase reporter system. The putative 3′ UTR target of miRNA is cloned downstream of the Renilla luciferase gene (RenSP) under the control of a constitutive promoter. The expression of luciferase, as detected by bioluminescence, will be reduced upon the binding of a miRNA mimic to the 3′UTR of its target.

2.4.3.1 Forward co-transfection of luciferase reporter vector with miRNA mimic or non-targeting control.

The 3′UTRs of the genes of interest were designed using TargetScan to obtain the miRNA recognition element in the 3′UTR and the Ensemble tool (available from www.ensembl.org) to obtain the

3’UTR sequences (Table 2.18). The cloning of the designed 3’UTRs downstream of the RenSP reporter gene in the pLightSwitch_3UTR vector (Figure 2.10) was performed externally by SwitchGear Genomics custom cloning service. For some genes, the cloned 3‘UTRs sequences were purchased “off-the-shelf” from SwitchGear Genomics (Table 2.18).

An empty vector, which is the parental luciferase construct that contains no 3`UTR cloned into it, was used in order to assess background signal noise in the experiment. In addition, a reporter vector that contains a random genomic fragment and a report that contains the 3’UTR of a housekeeping gene (β-Actin) were included for the purposes of normalisation against non-specific binding (Table 2.18).

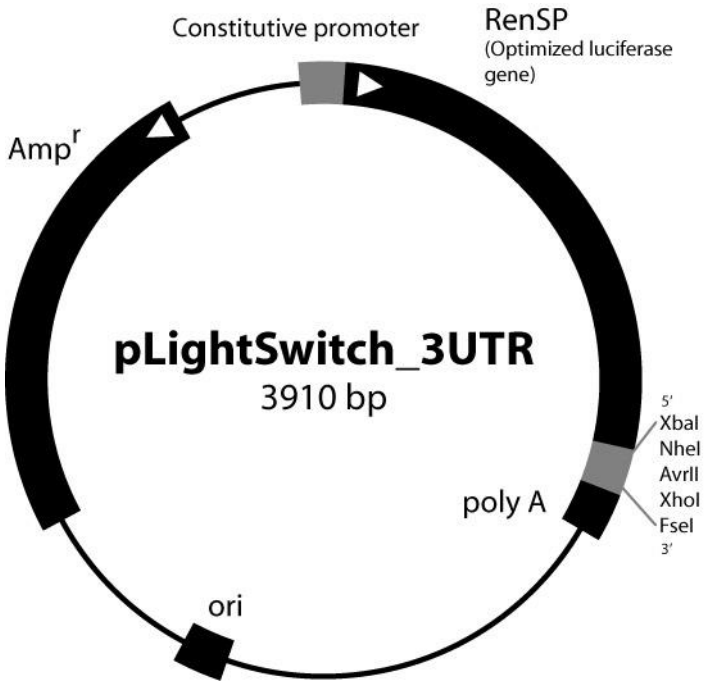


Figure 2.10: Schematic of pLightSwitch_3UTR vector.
3' untranslated regions (3'UTRs) of the genes of interest are inserted between the restriction sites NHE1 and XHO1 downstream of the RenSP reporter gene.

Table 2.18: The sequences of 3'UTRs cloned into the pLightSwitch_3UTR vector.

3'UTR Type	Product Code (Active Motif)	Insert Length	3'UTR Sequence
ACTB (β-Actin)	S804753	680	GGATCAGCAAGCAGGAGTATGACGAGTCCGGCCCCTCCATCGTCCACCGCAAATGCTTCT AGGCGGACTATGACTTAGTTGCGTTACACCCTTTCTTGACAAAACCTAACTTGCGCAGAA AACAAGATGAGATTGGCATGGCTTTATTTGTTTTTTTTGTTTTGTTTTGGTTTTTTTTTT TTTTTTGGCTTGACTCAGGATTTAAAAACTGGAACGGTGAAGGTGACAGCAGTCGGTTGG AGCGAGCATCCCCCAAAGTTCACAATGTGGCCGAGGACTTTGATTGCACATTGTTGTTTT TTTAATAGTCATTCCAAATATGAGATGCGTTGTTACAGGAAGTCCCTTGCCATCCTAAAA GCCACCCCACTTCTCTCTAAGGAGAATGGCCCAGTCCTCTCCCAAGTCCACACAGGGGAG GTGATAGCATTGCTTTCGTGTAAATTATGTAATGCAAAATTTTTTTAATCTTCGCCTTAA TACTTTTTTATTTTGTTTTATTTTGAATGATGAGCCTTCGTGCCCCCCCTTCCCCCTTTT TTGTCCCCCAACTTGAGATGTATGAAGGCTTTTGGTCTCCCTGGGAGTGGGTGGAGGCAG CCAGGGCTTACCTGTACACTGACTTGAGACCAGTTGAATAAAAGTGCACACCTTAAAAAT GAGGCCAAGTGTGACTTTGT
Random Genomic Fragment	S890003	781	GTTTTCCTGTTTCCAGCACTTCATGTGCCATGAGACTTTCCTTCTATCTTGAAATGAAACCA GGGAAGCCCACTCAGCACTTTCACAGCTTTGAAATATATGCCAGAATTATTCTTCTGACAA C CCCCATTACCTAAAACCAAGGCATTCAAACAAATGTGACATAAATGCAGTTACACTTCTCA C TACCACCATCCGCCATACTCACAAATATAAATGTTATCTGGAATATTAGCATCCTAAAGGA G

			GCAGTGTTTTACATGATATTTTCAGGACTTCGCCATCTGGGTCAACAGTATACTTTCTAAA G AATTTTTAAGATGACATCATAAAGAACTGATATAATTGAACTTTTATATTAAAACTTCAATA CTGACATGAAATCACTATTTGGATATATATTTAAGCCAAGAAAATGCCTCATGTAGTTATGC TGTAACATTGTATAAAAGAAGACTTTAAAACATGAATTTTACTGCAAAATGTCATGTTCACT CTGCAGGCATCTTGCTAAGATGATCAACTGAATTCAAGGGATGTCTCTAGGATATCTTCAG A TAGAAACCATTTACCACATTTGAGTTCTTGGTGAAAATTCAGAGACATAACACAATATTTAT CAAAAATACTATTGGTAGAGATCATGCCATAAAAATTTGCTAAAATTAAACAGACTAATTAC CTTGGTAATTAACATCAATAGACATGAGGCCATCTAGATTATTCATAATAAAGTGAATACTG AAATTGTACACCACTCAGATTGATAAGGAAAACTGAT
CPT2	S805462	700	GCCTTAGAAGGCAAATCCATCAAAAGTTAACTTCTGGGCAGATGAAAAGCTACCATCACT TCCTCATCATGAAAACTGGGAGGCCGGGCATGGTGGCTCATGCCTGTAATCCCAGCATTT TGAGAGGCTGAGGCGGGTGGATCACTTGAGGTCAGGAGTTTGAGACCAACCTGGCCAAC A TGGTGAAACCTTGTCTCTACTAAAAATACAAAAATTAGCTGGGTGTGGTGGCATGTGCCT ATAATCCCAGCTACTTGGGAGGTTGAAGCAGAATTGCTTGAACCCAGGAGGTGGAGGTTG CAGTGAGCTGAGATCACACCACTGCACTCCGGCCTGGGCGACAGAGCGAGACTGTCTCA A AAAAACAAAAAAGAAAAAAAAACTGGGGCCTGTGTAGCCAGTGGGTGCTATTCTGTGAAA CTAATCATAAGCTGCCTAGGCAGCCAGCTACAGGCTTGAGCTTTAAATTCATGGTTTTAA AGCTAAACGTAATTTCCACTTGGGACTAGATCACAACTGAAGATAACAAGAGATTTAAGT TTTAAGGGCATTTAATCAGGAGGAAAGGTTTGGAAAACTAACTCAGGTGTATTTATTGTT TAAGCAGAAATAAAGTTTAATTTTTGCTTGAAGATGGTTCTTAATTTCTTTTAACCTAAT TCCTAATCCTCACAAAGATCTTTCCAACAGCAAGTTCAGT
LDLR	S811473	2585	 TACCATTTGTTGGCAGAGACAGATGGTCAGTCTGGAGGATGACGTGGCGTGAACATCTGC CTGGAGTCCCGTCCCTGCCCAGAACCCTTCCTGAGACCTCGCCGGCCTTGTTTTATTCAA AGACAGAGAAGACCAAAGCATTGCCTGCCAGAGCTTTGTTTTATATATTTATTCATCTGG

			GAGGCAGAACAGGCTTCGGACAGTGCCCATGCAATGGCTTGGGTTGGGATTTTGGTTTCT TCCTTTCCTCGTGAAGGATAAGAGAAACAGGCCCGGGGGGACCAGGATGACACCTCCATT TCTCTCCAGGAAGTTTTGAGTTTCTCTCCACCGTGACACAATCCTCAAACATGGAAGATG AAAGGGGAGGGGATGTCAGGCCCAGAGAAGCAAGTGGCTTTCAACACACAACAGCAGAT G GCACCAACGGGACCCCCTGGCCCTGCCTCATCCACCAATCTCTAAGCCAAACCCCTAAAC TCAGGAGTCAACGTGTTTACCTCTTCTATGCAAGCCTTGCTAGACAGCCAGGTTAGCCTT TGCCCTGTCACCCCCGAATCATGACCCACCCAGTGTCTTTCGAGGTGGGTTTGTACCTTC CTTAAGCCAGGAAAGGGATTCATGGCGTCGGAAATGATCTGGCTGAATCCGTGGTGGCAC CGAGACCAAACTCATTCACCAAATGATGCCACTTCCCAGAGGCAGAGCCTGAGTCACTGG TCACCCTTAATATTTATTAAGTGCCTGAGACACCCGGTTACCTTGGCCGTGAGGACACGT GGCCTGCACCCAGGTGTGGCTGTCAGGACACCAGCCTGGTGCCCATCCTCCCGACCCCT A CCCACTTCCATTCCCGTGGTCTCCTTGCACTTTCTCAGTTCAGAGTTGTACACTGTGTAC ATTTGGCATTTGTGTTATTATTTTGCACTGTTTTCTGTCGTGTGTGTTGGGATGGGATCC CAGGCCAGGGAAAGCCCGTGTCAATGAATGCCGGGGACAGAGAGGGGCAGGTTGACCG GG ACTTCAAAGCCGTGATCGTGAATATCGAGAACTGCCATTGTCGTCTTTATGTCCGCCCAC CTAGTGCTTCCACTTCTATGCAAATGCCTCCAAGCCATTCACTTCCCCAATCTTGTCGTT GATGGGTATGTGTTTAAAACATGCACGGTGAGGCCGGGCGCAGTGGCTCACGCCTGTAA T CCCAGCACTTTGGGAGGCCGAGGCGGGTGGATCATGAGGTCAGGAGATCGAGACCATCC T GGCTAACACGTGAAACCCCGTCTCTACTAAAAATACAAAAAATTAGCCGGGCGTGGTGGC GGGCACCTGTAGTCCCAGCTACTCGGGAGGCTGAGGCAGGAGAATGGTGTGAACCCGGG A AGCGGAGCTTGCAGTGAGCCGAGATTGCGCCACTGCAGTCCGCAGTCTGGCCTGGGCGA C AGAGCGAGACTCCGTCTCAAAAAAAAAAAACAAAAAAAAACCATGCATGGTGCATCAGCA GCCCATGGCCTCTGGCCAGGCATGGCGAGGCTGAGGTGGGAGGATGGTTTGAGCTCAGG

			C ATTTGAGGCTGTCGTGAGCTATGATTATGCCACTGCTTTCCAGCCTGGGCAACATAGTAA GACCCCATCTCTTAAAAAATGAATTTGGCCAGACACAGGTGCCTCACGCCTGTAATCCCA GCACTTTGGGAGGCTGAGCTGGATCACTTGAGTTCAGGAGTTGGAGACCAGGCCTGAGC A ACAAAGCGAGATCCCATCTCTACAAAAACCAAAAAGTTAAAAATCAGCTGGGTACGGTGG CACGTGCCTGTGATCCCAGCTACTTGGGAGGCTGAGGCAGGAGGATCGCCTGAGCCCAG G AGGTGGAGGTTGCAGTGAGCCATGATCGAGCCACTGCACTCCAGCCTGGGCAACAGATG A AGACCCTATTTCAGAAATACAACTATAAAAAAATAAATAAATCCTCCAGTCTGGATCGTT TGACGGGACTTCAGGTTCTTTCTGAAATCGCCGTGTTACTGTTGCACTGATGTCCGGAGA GACAGTGACAGCCTCCGTCAGACTCCCGCGTGAAGATGTCACAAGGGATTGGCAATTGTC CCCAGGGACAAAACACTGTGTCCCCCCCAGTGCAGGGAACCGTGATAAGCCTTTCTGGTT TCGGAGCACGTAAATGCGTCCCTGTACAGATAGTGGGGATTTTTTGTTATGTTTGCACTT TGTATATTGGTTGAAACTGTTATCACTTATATATATATATATACACACATATATATAAAA TCTATTTATTTTTGCAAACCCTGGTTGCTGTATTTGTTCAGTGACTATTCTCGGGGCCCT GTGTAGGGGGTTATTGCCTCTGAAATGCCTCTTCTTTATGTACAAAGATTATTTGCACGA ACTGGACTGTGTGCAACGCTTTTTGGGAGAATGATGTCCCCGTTGTATGTATGAGTGGCT TCTGGGAGATGGGTGTCACTTTTTAAACCACTGTATAGAAGGTTTTTGTAGCCTGAATGT CTTACTGTGATCAATTAAATTTCTTAAATGAACCAATTTGTCTAAACTCGATGCACGTTC TTCTG
ACOX1	Custom cloning	1099	GGTCCACGAATCTTACAAGCACCTGAAGTCACTGCAGTCCAAGCTCTGAAGTGTCACAAG GACAAGTTTAATCTGCTTCAGAAAGCGCCTGTGTGCAACTCAAATTTTGTGGAATCTTTTT CGAATTCAAATAGCTATAGAGCAAATGATAAATTGACCCCTTTTTATAAATGGAGGGAAAA AATGAACAGATTTCAGAGATTAAATGAAAAAAAGCAGATGTTTTAAGTGCAATTAACACTG AAAGAGACCTGTTAAACCATTCAGAAAAAGCTTAAGAAATGCGATATGACTTCCTTTTGTA ATGCTGCTGATCCCAGTAGACTATGACTTTTGATAATTAGCAGAATTTAACTACTGAGTAG TTGATTATTTTCACATTTTAATTGCTAATCACTGGCTATATAAGTGTTTTTAAGCAAAGGTAT TTTTGAAGTGGTGTAGAACCCTTCCAAGCTTTCCTGCTCAGTGTTCTACCAGACTTACCCT

			GGGGCCTGGCTTAAAAGCAGGATTGAAGAAAAGGGACTGGGGGAAGGAAACTTATTGGA AAACTTGATGCGAATGAGTTTCTGCTTGGCACAGTCTCTGCCTGCTTGCTCTCCTTTGCTG ATGGATTGCATTTATCAAACTATTCATGCTAGCATTTTTCCAACGAGGGAACTTATTCCGCA CGGGCCTACTGTAGGACCATTGTCTCGTGTAATTAGGAATTTTCCATTTGAAGGATTGCTA AATTGTCACAGTAGTAGGAAGTATAGGGAAACCTCTCAGCTGTGGCACTGTTGTAGCTTT GGAGTGCAGAGTGTAACTCTGGGACAATCAGATTTCACATATTCTGTCATCTTGGCATAAG CCATTAAAAGCTTGGAGATTACTGTATTTGGCATTAAAAAAAAATGTCACTTAGGTCAGCA CTCCCAGACGTAGCACAGAAAAACCCTTTGACACAAACCATGTGTTCTGATTTTTGGTTCA GAAAATATTGAAACTGTGAGTTGTTTTTTTTTTAACAACTGGGAAAAAACAAAAACAAAAAA CTATAGTTAGAAAAATGGAAGTTCCATAGGTTCTATTTCTTACTCTATGTATGGCTTTGTTT
miR-619-5p synthetic sequence repeats	Custom cloning	50	GGCTCATGCCTGTAATCCCAGCACTGACGGCTCATGCCTGTAATCCCAGC
miR-4793-3p synthetic sequence repeats	Custom cloning	50	AGCCAGCCAACTCACAGTGCAGAATCGAGCCAGCCAACTCACAGTGCAGA

A 3'UTR bearing reporter vector (100ng final concentration) was mixed with the appropriate miRNA mimic or non-targeting control (50nM final concentration) in serum-free media (Tube1; Table 2.19). Empty vectors (lacking the 3'UTR) were used as negative controls. The transfection reagent was prepared in a separate tube for the required number of transfections. Transfections were performed in replicates. The DharmaFECT DUO™ Transfection Regent (Horizon Discovery) was mixed in serum-free media (Tube 2). After 5min of incubation at room temperature, 10µl from Tube 2 was added to each prepared Tube 1 of vector plus miRNA mimic or non-targeting control for a total volume of 20µl per transfection.

Table 2.19: Co-transfection mixture per replicate

		Volume (µl)
Tube 1	GoClone reporter vector (30ng stock)	3.33
	miRNA mimic or non-targeting mimic control (2µM stock)	5
	Serum-free media	1.67
Tube 2	DharmaFECT DUO™ Transfection Reagent	0.15
	Serum-free media	9.85

Each mixture was incubated for 20min at room temperature. After 20 minutes, 80µl of pre-warmed (37°C), serum-supplied cell culture media per transfection was added to each tube for a total of 100µl per transfection.

The transfection media was added on top of confluent U87 cells seeded into a 96-well solid bottom white cell culture plates (Avantor) 24h before transfection. Each well was seeded with 100µl of 3.125 x 10^4 cells/ml of U87 cells to yield ≥80% confluency at the time of transfection.

The seeded plate was removed from the incubator, and the media was aspirated off from each well. Subsequently, 100µl of the transfection mixture was added to each well, and the plate was incubated for 48h.

The plate was then removed from the incubator and covered with Foil Plate Sealing Tape (E&K Scientific) to protect from light and placed in the -80°C freezer. The plate was frozen for at least 6h in order to increase cell lysis and subsequently luciferase signal.

2.4.3.2 Reading Luciferase Assay Signal

LightSwitch™ Luciferase Assay Kit (Active Motif) was used to assess miRNA binding to its putative 3'UTR. The frozen plates were thawed at room temperature 30min before assaying. To each well, 100µl of the LightSwitch Assay Solution (made as in Table 2.20) was directly added (without aspirating the media) using a multi-channel pipettor.

Table 2.20: LightSwitch Assay Solution mixture.

Reagent	Volume per well (µl)
100X Substrate **Contains; protected from light; kept on ice**	1
Assay Buffer	99
Total volume	100

The plate was covered to protect from light and incubate for 30min at room temperature. Luminescence was read with an emission filter gain of 3600 and a measurement interval time of 2 sec in the FLUOstar Omega microplate luminometer.

2.4.3.3 Quantification of Luciferase expression

The knockdown of luciferase expression was calculated as the ratio of the signal of the specific miRNA mimic over the non-targeting control. This ratio was calculated as (luminescence form a 3'UTR vector= specific miRNA mimic/non-targeting control). The data was normalised to the housekeeping, random, and empty constructs in order to control for non-3'UTR specific treatment effects.

2.4.4 Pharmacological CPT2 Inhibitors Treatment

Cells to be treated were seeded at 3.125 x 10^4 cell/ml in a 6-well plate and allowed to attach overnight at 37°C, 5% CO2, humidified atmosphere. The next day, the medium was replaced with medium containing the appropriate concentration of the CPT2 inhibitor (see

Table 2.21 for inhibitors details). Vehicle controls were prepared using solvent only to account for solvent cytotoxicity.

Table 2.21: Pharmacological CPT2 inhibitors information.

Drug (CPT1/2 inhibitor)	**Full Name**	**Solvent used for reconstitution (stock concentration)**	**Product Code (Sigma-Aldrich)**	**Universal Chemical Abstracts Service (CAS) Number**
Perhexiline maleate salt	2-(2,2-dicyclohexylethyl)piperidine	DMSO (5 mg/ml)	SML0120	6724-53-4
Etomoxir sodium salt hydrate	R(+)-2-[6-(4-Chlorophenoxy)hexyl]-oxirane-2-carboxylic acid sodium salt hydrate	Water (1 mg/ml)	E1905	828934-41-4

The cells were incubated with the drug at 37°C, 5% CO2, humidified atmosphere for 72h before performing cell viability assay using PrestoBlue as described in section 2.4.1. Alternatively, cells were harvested to either stain their lipid droplets content using Nile Red (section 2.4.9) or assess their invasive property using Transwell Assay (section 2.4.10).

2.4.5 Nile Red

Nile Red (9-diethylamino-5H-benzo[alpha]phenoxazine-5-one) is a strongly fluorescent dye, but only in the presence of a hydrophobic environment. Thus, Nile Red is used to selectively stain lipid droplets within the cells.

Cells were seeded in a 6-well plate containing glass coverslips and the wells were stained with 4µg/ml Nile red in cell culture medium (made from 1mg/ml Nile Red stock solution in acetone (Sigma-Aldrich, product code 72485) for 15min at 37°C, 5% CO2, humidified atmosphere. After the removal of the staining solution, the cells were washed with PBS then fixed in 0.4% paraformaldehyde (PFA) for 30min at room temperature. The coverslip was then removed from the well and stained for DAPI with a drop of 10µl anti-quenching mounting medium (Vector Laboratories Inc). The coverslip was

immediately mounted onto a glass slide and the edges were sealed with nail varnish.

The slides were kept at 4°C until imaged. Imaging was performed on a Leica TCS SPE confocal laser scanning DMI6000 inverted microscope (Leica Microsystems) using a 40× objective coupled to a Hamamatsu camera) at 485-695 wavelengths. The number of lipid droplets was counted in ImageJ.

2.4.6 Transwell assay

Transwell assay is commonly used to assess GBM cell invasion. The cells are placed on the upper surface of a polycarbonate membrane containing randomly distributed pores through which the cell invade into the lower surface of the membrane in response to a chemoattractant. The membrane is often coated with an ECM component (such as collagen) to mimic the basement membrane.

Cells were harvested following transfection or drug treatment and re-suspend in cell culture medium containing only 1%FBS. In a 24-well cell culture plate, 200µl of cell suspension was seeded into the upper surface of a ThinCert™ cell culture insert (8 μm pore size; Corning). The insert was pre-coated with 100µl of 0.5 mg/ml Collagen IV (Cultrex) and incubated overnight at 37°C in a dry incubator. To the bottom of the well, underneath the insert, 600µl of cell culture media (supplemented with 10% FBS) was added as a

chemoattractant. The plate was then incubated at 37°C, 5% CO2, humidified atmosphere.

After 24h of incubation, the non-invading cells along with collagen IV were removed from the upper surface of the membrane by scrubbing with cotton buds. The cells on the lower surface of the membrane were fixed for 30min with ice-cold 100% methanol (VWR Chemicals). Subsequently, the cells were stained for 5min with 0.5% crystal violet (Sigma-Aldrich). The number of invaded cells was counted from three pre-selected microscopic fields at 40x magnifications using an inverted light microscope.

2.5 Protein-based assays

2.5.1 Western Blotting

2.5.1.1 Protein extraction

Cell pellets were lysed with protease cocktail. Cell lysis buffer was made by dissolving 1 tablet of protease cocktail tablets (Complete Mini EDTA-Free; Roche Diagnostics) in water and diluting 1:50 in protease cocktail buffer [150 mM NaCl, 1% Triton X-100, 0.5% sodium deoxycholate, 0.1% sodium dodecyl sulfate (SDS), and 50 mM Trizma Base (Tris; Sigma-Aldrich) in water and the solution was adjusted to pH 8.0]. 25µl of cell lysis buffer was used to resuspend the cell pellet and was left to incubate on ice for 20min. At the end of the incubation period, cell lysates were centrifuged at 14,000 x g

for 30min with the centrifuge (Sigma 3-18K Centrifuge) set to 4^0 C. The supernatant containing protein was transferred into a fresh Eppendorf tube for storage at -80^0 C.

2.5.1.2 Protein quantification

The traditional method for calculating protein concentration of an unknown sample is to use a standard curve that is generated from known protein standards such as bovine serum albumin (BSA). A series of standard dilutions between 0 to 500 µg/ml was prepared from a 1 mg/mL BSA stock solution dissolved in water. Bradford assay was then used to quantify protein concentrations. 200µl of the Protein assay dye reagent (Bio-Rad), diluted at 1:4 ratio in water, was added to each standard. 200µl of the diluted protein assay dye reagent was also added to 2µl of protein extracts. The 200µl of the Bio-Rad protein assay plus the standards or protein extracts were transferred to a 96-well plate and absorbance was measured at 595nm using the FLUOstar Omega microplate reader. Standard curves were constructed in Microsoft Excel using the linear equation (y= mx+c) with the absorbance values on y-axis and the BSA concentrations x-axis. The protein extract concentrations were determined from the standard curve.

2.5.1.3 Gel preparation and electrophoresis

Gels were prepared using the Mini-PROTEAN Tetra cell (Bio-Rad) in order to separate proteins according to their molecular weight. Lower (resolving) gel was prepared with 15% acrylamide (Sigma-Aldrich), 0.6% of 10% aqueous ammonium persulfate (APS; Sigma-Aldrich), and 0.08% tetramethylethylenediamine (TEMED; Sigma-Aldrich) in lower gel buffer [1.5 M Tris and 0.4% sodium dodecyl sulphate (SDS; MP Biomedicals),dissolved in water, and solution was adjusted to pH 8.8].

The lower gel was cast into a casting frame and left to polymerise for 1h at room temperature. A layer of 70% ethanol was added on top of the gel to exclude air bubbles and prevent evaporation during gel polymerisation. Ethanol was fully discarded, and the upper gel was added and left to polymerise for 30min at room temperature.
Upper (stacking) gel was prepared with 4% acrylamide, 0.5% of 10% APS and 0.1% TEMED in upper gel buffer [0.5 M Tris and 0.4% SDS, dissolved in water, and the solution was adjusted to pH 6.7]. A 15 lane 1.5 mm comb was inserted into the upper gel to form wells upon polymerisation. Gels were placed into a tank filled with electrode buffer [25 mM Tris and 193 mM glycine (Sigma-Aldrich), dissolved in water, with a 1% final concentration of SDS].

Combs were removed from the upper gel, and the sample was loaded in each well. SDS sample buffer (Laemmli, Sigma-Aldrich) was added at 20% of the appropriate volume of protein samples, and samples were boiled at 95^0 C for 3 min to denature protein structures. Amersham ECL Rainbow Marker (GE Healthcare) was loaded onto the SDS gel next to samples. The gel was run at 140V (100mA) for 1h at room temperature.

2.5.1.4 Protein transfer

After separating proteins on SDS gel, the upper gel was excised and discarded while the lower gel was placed into contact with Amersham Hybond P membrane (GE Healthcare). The membrane was activated in 100% methanol for 10 sec and hydrated in water and transfer buffer [25 mM Tris and 193 mM glycine dissolved in water with 20% final concentration of 100% methanol and 1% final concentration of SDS] for 5min and 10 min, respectively. The gel and the membrane were sandwiched between two pieces of filter paper and two sponges pre-soaked in transfer buffer, on each side. A roller was used to ensure the removal of any air bubbles that would impede protein transfer. The assembly clipped into a cassette and placed in tanks filled with transfer buffer. The transfer process was run at 25V overnight at 4°C.

2.5.1.5 Antibody probing

At the end of the transfer process, the membrane was the assembly and blocked for 1h with 5% milk dissolved in buffered saline-Tween 20 (TBS-T) buffer [2 mM Tris, 13.5 and 0.1% Tween-20 (Sigma-Aldrich) adjusted to pH 7.6]. Subsequently, the membrane was washed twice in TBS-T incubated with primary antibodies diluted in either 5% milk T. The primary antibodies used are shown in

Table 2.22.

Table 2.22: Primary antibodies used in this project.

Gene	Product Code (Abcam)	Species	Clonality	Dilution	Protein Size (kDa)	Incubation time	Exposure Time (min)
CPT2	ab181114	Rabbit	monoclonal	1:200	72	Overnight at 4°C	30min
LDLR	ab52818	Rabbit	monoclonal	1:1000	140	1h at RT	5min
ACOX1	ab184032	Rabbit	monoclonal	1:500	74	1h at RT	2min
GAPDH	ab8245	Mouse	monoclonal	1:1000	37	1h at RT	2min

The membrane was washed twice with 5% milk-TBS-T for 10 min each followed by two washes in TBS-T for 5min each. The membrane was then incubated for 1h at room temperature with the appropriate horseradish peroxidase-linked (HRP)-conjugated secondary anti-rabbit (7074S; Cell Signalling Technology) or anti-mouse antibody (97166S; Cell Signalling Technology) diluted 1:2000 in 5% milk. Antibody binding was assessed through chemiluminescent measurement.

2.5.1.6 Enhanced chemiluminescence (ECL) detection

Luminol and enhancer solutions (ECL kit; GE Healthcare) were mixed at 1:1 ratio. The mixture was spread across the membrane and incubated for 5min at room temperature. Protein bands were detected using photographic film (Kodak biomax) in a dark room.

2.5.1.7 Membrane Stripping

Membranes were stored over a short time period in TBST at 4°C. Re-probing of the same membrane was conducted by first stripping previously applied antibodies. The membrane was washed for 10min twice with stripping buffer [15 g glycine 1 g

SDS 10 ml Tween20 Adjust pH to 2.2 Bring volume up to 1 L with water]. Next, the membrane was washed for 10min twice with TBST. Then for 5min twice in PBS. The Western blotting procedure was performed on the striped membrane, starting from the blocking stage as outlined above.

2.5.2 Immunohistochemical Analysis

2.5.2.1 Tissue Microarray Patient Cohort

Formalin-fixed paraffin-embedded (FFPE) blocks were made for individual regions of the GBM tumours from each fresh patient sample following surgical resection.

Cores of 0.6mm in diameter were taken in triplicates from each FFPE sample and built into an empty FFPE block following a map (Figure 2.11) to create a tissue microarray (TMA). TMAs allow the study of a larger number of samples in a more cost-effective manner.

For some tumour regions, however, only 1-2 cores were included due to the limited tissue availability. A non-neoplastic brain tissue sample from the temporal lobe of an epileptic patient was included in the TMA as a normal brain control and to orientate the sample on the slide. Four TMAs were used for

immunostaining in this project; which incorporated a total of 36 patient tumours (See Appendix 1 for patients' details). Each TMA block was sequentially cut at a thickness of 4µm and mounted onto slides pre-coated with 3-Aminopropyltriethoxysilane (APES) for immunohistochemical (IHC) analysis (Figure 2.11).

GBM1.2a	GBM1.2b	GBM1.2c	GBM1.3a	GBM1.3b	GBM1.3c	GBM1.5a	GBM1.5b	GBM1.5c	
GBM2.1a	GBM2.1b	GBM2.1c	GBM2.2a	GBM2.2b	GBM2.2c	GBM2.4a	GBM2.4b	GBM2.4c	
GBM3.2a	GBM3.2b	GBM3.2c	GBM3.1a	GBM3.1b	GBM3.1c	GBM3.4a	GBM3.4b	GBM3.4c	
GBM5.2a	GBM5.2b	GBM5.2c	GBM5.1a	GBM5.1b	GBM5.1c	GBM5.5a	GBM5.5b	GBM5.5c	
GBM6.2a	GBM6.2b	GBM6.2c	GBM6.1a	GBM6.1b	GBM6.1c	GBM6.4a	GBM6.4b	GBM6.4c	
GBM7.1a	GBM7.1b	GBM7.1c	GBM7.2a	GBM7.2b	GBM7.2c	GBM7.4a	GBM7.4b	GBM7.4c	
GBM8.2a	GBM8.2b	GBM8.2c	GBM8.1a	GBM8.1b	GBM8.1c	GBM8.4a	GBM8.4b	GBM8.4c	
GBM9.2a	GBM9.2b	GBM9.2c	GBM9.1a	GBM9.1b	GBM9.1c	GBM9.5a	GBM9.5b	GBM9.5c	
GBM10.3a	GBM10.3b	GBM10.3c	GBM10.2a	GBM10.2b	GBM10.2c	GBM10.5a	GBM10.5b	GBM10.5c	Temporal lobe
	CORE			RIM			INVASIVE		

Figure 2.11: Typical tissue microarray layout.
Three cores from each region are shown for each patient tumour sample, and the orientation core (temporal lobe) at the bottom right could also be used as normal brain control.

2.5.2.2 Immunohistochemistry procedure

Immunohistochemistry (IHC) is a method for visualising the presence and the localisation of proteins in cells of FFPE tissue

sections. In this project, the cytoplasmic proteins PLIN2 and CPT2 were stained.

2.5.2.2.1 Tissue Deparaffinisation and Hydration

Because formalin fixation can mask antigens by forming protein cross-links with them, which prevents staining or weakens its intensity, FFBE tissue sections (prepared as described in the previous section) were warmed at 60°C overnight then deparaffinised in xylene (Fisher Chemicals) for 15min. Tissue sections were then rehydrated in 100% then in 95% ethanol (Sigma-Aldrich) for 10min each.

2.5.2.2.2 Antigen Retrieval

Tissue sections were then washed in water before heat-induced epitope retrieval was performed in citrate buffer [10.5g of citric acid monohydrate (ThermoFisher scientific) in 5L of water and adjusted to pH 6 with ~65ml of 2M NaOH). The tissue sections immersed in citrate buffer were placed in a pressure cooker at full pressure (121°C) for 1min for PLIN2 or with a steamer at 98°C for 40min. The sections were incubated for further 20min in citrate buffer following removal from heat. Slides were then washed with PBS in a Coplin jar for 5 minutes and placed in a

humidified chamber (lidded container lined with wet paper towels)

Tissue sections were encircled with a hydrophobic barrier PAP Pen (Vector Laboratories) and blocked with 20% normal goat serum (NGS) for 20min at room temperature. Sections were washed in PBS for 5min then incubated with hydrogen peroxidase blocking solution (Dako) for 5min at room temperature. This was done in order to prevent non-specific background signal from endogenous peroxide that is present at high levels in brain tissue.

2.5.2.2.3 Antibody probing

Tissue sections were washed in PBS for 5min then incubated in primary antibodies: CPT2 same as used for Western blotting, and PLIN2 mouse monoclonal antibody purchased from Progen (product code 610102S). The primary antibodies were prepared in antibody diluent (Dako) at a dilution of 1:50 for PLIN2 (as published in Kohe et al., 2017) and the dilutions of 1:100 and 1:200 were tested for CPT2. A positive control tissue section was also probed with primary antibody (also used for antibody concentration optimisation). Liver was used as a control tissue for both CPT2 and PLIN2 as it is known to express the genes of interest at high levels according to the Human Protein Atlas. A

negative control issue section was prepared by adding only the antibody diluent and omitting the primary antibody. Tissue sections were then incubated with secondary antibody (Dako EnVision Reagent A) for 30min at room temperature and then washed in PBS for 5min.

2.5.2.2.4 Detection and counterstaining

Antibody detection was carried out using 3-3'-diaminobenzidine (DAB) chromogen diluted 1:50 in Dako REAL substrate buffer (Dako EnVision kit). The tissue sections were dried with tissue paper to eliminate excess PBS then incubated with DAB for 5min. Sections were then washed with water and counterstained with Haematoxylin (TCS Bioscientific) for 10 seconds and lithium carbonate for 5-10 seconds until nuclei turned blue. Subsequently, the tissue sections were washed under running water to remove residual reagent and dehydrated in ethanol (95% followed by 100%) then xylene for 10min each. Finally, the tissue sections were mounted with a coverslip using Distyrene, Plasticiser, and Xylene (DPX) mounting medium (Sigma-Aldrich). The slides were dried on a hotplate (Raymond A Lamb Hotplate).

Expression was then analysed in ImageJ to count cells. Statistical differences were assessed using Fisher's exact test in GraphPad Prism.

2.6 Metabolomics and Lipidomics Analysis

2.6.1 Cells growth curve

To ensure a comparable cell number between the different transfection conditions, a growth curve was constructed by counting cells after 24h, 48h and 72h and inputting the initial concentration at each time point into a sigmoid function using GraphPad Prism version 7.00 for Windows (GraphPad Software).

The equation ViCi=VfCf was used to obtain the required initial volume (Vi) of cells at the required final concentration (Cf) and the required final volume (Vf) The equation was rearranged as Vi = (VfCf)/Ci. The initial volume of cells was topped up with medium to bring it to final volume.

2.6.2 Metabolites Extraction

Three-phase methanol-water-chloroform (at 1:1:3 ratio) extraction method was used to extract metabolites and lipids from cells. Cell culture medium was removed from a T75 flask and cells were washed with 4ml of pre-warmed (37^0 C) PBS.

Cellular metabolism was then quenched by the addition of 400µl of ice-cold high-performance liquid chromatography (HPLC)-grade methanol. The flask was placed on ice and cells were scraped off the surface and transferred into pre-cooled Eppendorf tubes. Extracts were shaken (Thermomixer Comfort; Eppendorf) at 4°C for 30min to facilitate cell lysis. Subsequently, 1200µl of ice-cold HPLC-grade chloroform (Sigma-Aldrich) and 400µl of ice-cold HPLC-grade water was added to the cell lysates. Next, the mixture was vortexed well and centrifuged at maximum speed for 10min at 4°C to separate the different phases. The upper phase (containing polar metabolites) and the lower phase (containing the non-polar metabolites) were then transferred into fresh pre-cooled Eppendorf tubes. The middle phase contained protein sediments and was not disrupted.

2.6.3 Sample Preparation for LC-MS

In order to concentrate the metabolites, methanol/chloroform solvents were evaporated using a vacuum evaporator (SpeedVac; ThermoFisher Scientific) set to room temperature and with pulsed ventilation. The dried metabolites were then reconstituted in 70µl of methanol (for polar metabolites) or 100µl isopropanol (for non-polar metabolites). Samples were then centrifuged for 10min at 13,000 x g at a temperature of

4^0 C. Supernatants were carefully removed and transferred into MS vials, and quality controls (QCs) were prepared by pooling 5µl from each sample.

2.6.4 LC-MS profiling of polar and non-polar metabolites

The LC-MS metabolomic analysis of extracted non-polar metabolites was conducted by Dr Salah Abdelrazig (University of Nottingham).

Chromatographic separation was performed using Accela UHPLC system (ThermoFisher Scientific) on a ZIC-pHILIC column (4.6 × 150 mm, 5µm particle size; Merck Sequant). The column was maintained at 45 °C and a flow rate of 300 µL/min in a ThermoFisher Dionex UltiMate 3000 LC system (ThermoFisher Scientific). Mobile phases used were: (A) 20 mM ammonium carbonate in 18.2 MΩ water (Elga Maxima; Elga LabWater) and (B) 100% acetonitrile. Linear LC gradient was performed from 80% (B) decreasing to 5% (B) and 20% (A) and increasing to 95% (A) over 15min then the compositions of A and B were returned to their initial conditions in 2min and the column was left to re-equilibrate for 7 min (24min total run time).

MS was performed using an Exactive Orbitrap (ThermoFisher Scientific) and controlled by Xcalibur 3.0.63 software (ThermoScientific). The Exactive Orbitrap was operated in a polarity switching mode. For positive ionisation mode (ESI+), spray voltage was 4.5 kV, and the capillary voltage was 20 V. For negative ionisation mode (ESI-), spray voltage was -3.5 kV and capillary voltage was -15 V. Sheath, auxiliary and sweep gas flow rates were: 40, 5 and 1 (arbitrary unit), respectively, for both modes. Capillary and heater temperatures were maintained at 275°C and 150°C, respectively. The sample injection volume was set to 10µl and samples were maintained at 4°C during the analysis. Mass calibration was performed before each batch of samples using pooled QC samples. Data were acquired in full scan mode with resolution 50,000 and a mass range of m/z 70-1400 with 4 Hz scan rate.

2.6.5 LC-MS profiling of non-polar metabolites

The LC- LC-tandem MS/MS lipidomics analysis of extracted non-polar metabolites was conducted Dr Catherine Ortori (University of Nottingham).

Chromatographic separation was performed using a reverse-phase ACE Excel 2 C18 column (50 x 2.1 mm), and the column temperature was maintained at 50°C in a ThermoFisher Dionex UHPLC UltiMate 3000 system (ThermoFisher Scientific).

The mobile phase consisted of (A) 60% or (B) 10% of 0.1% MS-grade ammonium acetate in 18.2 MΩ water with 40% (in the case of A) or 10% (in the case of B) of acetonitrile and 80% isopropanol (in the case of B). Both mobile phases were modified with 0.1% ammonium acetate and the gradient adopted is displayed in Table 2.23.

Table 2.23: Mobile phase gradient setting.

Time (min)	**% B**	**Flow mL/min**
0	30	0.4
1	35	0.4
7.5	100	0.4
10	100	0.4
11	100	0.5
12	20	0.5
15	20	0.5

MS was performed using a Q-Exactive Plus Orbital ion-trap mass spectrometer (ThermoFisher Scientific) and controlled by Xcalibur 3.0.63 software (ThermoScientific). The mass spectrometric readings were taken simultaneously in full scan

ion mode (m/z 150-1500 with a resolution of 70,000) in both positive and negative ionisation modes. The settings for positive/negative ionisation modes were as follows: spray voltage, 3.5/-3.5 kV. The flow rates of sheath gas, desolvation gas and sweep gas were 47.5, 11.25 and 2.25 units, respectively. The capillary and desolvation heater temperatures were set to 225^0 C and 400^0 C, respectively. The automatic gain control (AGC) target for MS acquisitions was set to 3 x 10^6 ions with a maximum ion injection time of 100ms. Tandem MS/MS spectra were produced on the most intense 5 per MS scan (with a dynamic exclusion of 10sec) with an AGC target of 2 x 10^5 ions with a maximum ion injection time of 50ms and a resolution of 17,500.

The injection volume was set to 10µl, with samples maintained at 4^0 C. The samples were randomly injected independent of cell type to eliminate systematic bias. A series of 6 pooled QC samples were used for system equilibration at the beginning of the sequence and subsequently every 6 injections.

2.6.6 Pre-processing of LC-MS data

The acquired LC-MS raw data files were imported into Progenesis QI software (Nonlinear Dynamics). The ionisation mode for each analysis was specified, either positive or negative,

which determines the appropriate possible adduct ions for each chromatographic peak of a compound ion detected in that mode. Quality check for each sample run started with inspecting the total ion chromatogram (TIC) which displays all the chromatographic peaks of mass ions detected in that run. Each chromatographic peak area detected in a sample run was then normalised to the total chromatographic peak area of all mass ions in that run.

The run that is the least different from all the other sample runs was selected as a normalising reference run. This run was used to calculate the normalisation factor. The normalisation factor was calculated by finding the mean of the log abundance ratios of the mass ions that fall within the robust estimated limits (REL). Any compound found outside the REL was considered as an outlier and was not included in the calculation of the normalisation factor. The log of the abundance ratio for a compound ion was determined as (compound ion abundance in the sample run divided by the abundance in the normalising reference run).

Next, the pooled QC samples were set as alignment reference candidates because they display the largest set of common

compound ions. The most suitable run from the alignment reference candidates was automatically selected. Subsequently, the peaks of mass ions in each sample run were aligned to the peaks present in the alignment reference run. The thresholds for the detection of peaks of mass ions across all of the aligned runs were adjusted by applying a minimum peak width in minutes (0.15min).

2.6.7 Statistical Analysis of LC-MS data

In the Progenesis QI software, the experiment design was set up by defining biological repeats and experimental groups, and univariate analysis (UVA) was performed using one-way ANOVA. The variances were not assumed to be equal between groups, and the p-value cut-off threshold was set 0.05 following correction for multiple comparison based on false discovery rate (FDR). A two-sample t-test comparison was then performed to select differentially abundant mass ions.

2.6.8 Clustering of LC-MS data

The heights of the peaks of mass ions are also known as mass/charge (m/z) values. The peak areas represent the abundance levels, and the peak widths represent the retention time.

A data matrix consisting of the normalised pre-processed data (m/z values, abundance levels and retention times) was constructed in Microsoft Excel. The data matrix was then imported into the SIMCA-P 14.0 software package (Umetrics AB) for multivariate analysis (MVA) including unsupervised principal component analysis (PCA) and orthogonal partial least-squares discriminant analysis (OPLS-DA). The unsupervised PCA was used to observe the natural cluster trend of the biological repeats within each experimental group in order to determine outliers and ensure that the QC samples are representative of all experimental group. The OPLS-DA, on the other hand, was applied to explore differences in each comparison between two or more experimental groups. The data were Pareto-scaled to reduce instrumental and chemical noise before MVA.

2.6.9 Metabolites identification and pathway analysis

LipidSearch™ Software (Thermo Fisher Scientific) and the Human Metabolome Database (HMDB) (available from http://www.hmdb.ca/spectra/ms/search) were used to identify mass ions detected as differentially abundant from the LC-MS

analysis of non-polar and polar metabolites based on the possible adduct ions.

The heat map of the relative abundance levels of each identified metabolite was constructed using heatmapper (available from http://www.heatmapper.ca/expression/). The average linkage hierarchical clustering was also performed in heatmapper, and is defined as the average distance between each point in one cluster to every point in the other cluster. Pearson's correlation coefficient was then calculated as a statistical measure of the strength of a linear relationship between paired data.

The affected metabolic pathways by the identified differential metabolites were analysed in MetaboAnalyst 3.0 (available from http://www.MetaboAnalyst.ca/) based on the Homo sapiens (human) pathway library.

Chapter 3:

Evaluation of Intra-Tumour Heterogeneity of miRNA Expression in GBM

3.1 Introduction

The infiltrative growth of GBM creates physiological intra-tumour heterogeneity that defines distinct tumour regions. Most importantly, a population of cells at the invasive margin of the tumour diffusely disseminate into the brain such that they cannot be isolated with surgical resection. These cells remain behind and cause tumour recurrence, which often occurs within 2 cm of the surgical resection margin (Gaspar *et al.*, 1992; Silbergeld and Chicoine, 1997; Berens and Giese, 1999). However, little is known about the molecular features that distinguish these invasive margin cells from cells in the tumour bulk. Genome-wide transcriptional profiling revealed that invasive margin cells have distinct transcriptomic signatures (See Introduction Section 1.1.5). Given that intra-tumour heterogeneity exists in GBM at the transcriptomic level, it would be logical to assume that this may also apply to miRNAs. This chapter of the thesis is, therefore, focused on characterising the intra-tumour heterogeneity in the expression profiles of miRNA, in a similar fashion to studies conducted on gene expression, comparing spatially distinct regions of the GBM tumour.

To date, intra-tumour heterogeneity in miRNA expression has only been described in breast cancer, colorectal cancer and in hepatocellular carcinoma. Raychaudhuri et al., 2012 investigated the intra-tumour expression heterogeneity of two pro-metastatic miRNAs (miR-10b and miR-210) and two anti-metastatic miRNAs (miR-31 and miR-335) in 16 primary breast tumour specimens by qRT-PCR (Raychaudhuri *et al.*, 2012). Each tumour was dissected into three regions (central, intermediate, and peripheral region), and each region was further cut into 2-3 samples with 5 mm distance between each sample. They showed that despite the slight miRNA expression variation between the samples within each region, considerable miRNAs expression heterogeneity existed between defined tumour regions for all four miRNAs.

Similarly, using qRT-PCR, Jepsen et al., 2015 assessed the intra-tumour variation in the expression of three miRNAs which are often used for colorectal cancer classification (miRNAs: miR-375, miR-424 and miR-92a) (Jepsen *et al.*, 2016). They analysed five regions (two luminal, one central and two from invasive border zone) from nine tumour specimens and found significant expression difference in all three miRNAs between the invasive and luminal parts of the tumour. The expression of

these miRNAs was then further assessed in three normal mucosa samples. The expression of miR-375 was found to be lower, and the expression of miR-92a and miR-424 were found to be higher in tumour tissue compared to normal mucosa. A more recent study by Eriksen et al., 2017 compared the expression of five disease-stage related and chemo-radiotherapy responsive miRNAs (miR-21, miRNA-31, miRNA-125b, miRNA-145, and miR-630) between three different compartments of rectal adenocarcinoma using two technical approaches, qRT-PCR and *in situ* hybridisation (Eriksen *et al.*, 2016). They analysed 27 patient samples and found that the expression of only three miRNAs (miRNA-125b, miRNA-145, and miRNA-630) varied between tumour compartments. The only large-scale profiling study looking at miRNA intra-tumour heterogeneity was performed by Peveling-Oberhag et al. (2014), using microarray technology (Peveling-Oberhag *et al.*, 2014). They identified over 50 miRNAs, involved in the regulation of oncogenic signalling and extracellular matrix signalling, to be differentially expressed between four histological compartments of six hepatocellular carcinoma samples. They then used previous data from miRNA expression profiles of healthy livers to confirm no dysregulation of the 50 miRNAs in normal samples. Their results from microarray were

then validated in an independent cohort of patients using qRT-PCR.

Of note, all of these studies that were mentioned above have used total RNA extracted from formalin-fixed, paraffin-embedded (FFPE) tumour tissue samples which were micro-dissected into different histological localisations based on a pathological assessment of hematoxylin and eosin (H&E) staining. However, previous work in our labs disagrees with the argument that FFPE conserves the stability of small RNAs and successfully shows that FFPE tissue exhibit substantial differences in miRNA profiles compared to fresh/frozen tumour tissue. Even the significant difference in the expression of well-recognised oncomirs, such as miR-21, is found to be lost in FFPE samples when compared to normal brain (Stuart Smith PhD Thesis 2014). Thus, this current PhD project will utilise fresh/frozen tumour samples for miRNA expression studies.

The current study used surgical multi-sampling scheme facilitated by administration of 5-aminolevulinic acid (5-ALA), which is metabolised into a fluorescent compound in tumour tissue, to isolate three spatially-distinct tumour fragments (tumour core, proliferative rim and invasive margin regions) from 15 adult (age 30-60 years old) GBM patients. Total RNA

was extracted from fresh/frozen samples, and miRNA intra-tumour heterogeneity was investigated using microarray technology to compare miRNA profiles of the three tumour regions. GBM cell lines derived from the core and the invasive margin of the same tumour from a limited number of patients were included in the microarray. Microarray findings were validated by an independent technique, qRT-PCR..

Hypothesis: There is a regional difference in miRNA expression profiles within GBM tumours.

3.2 Results

3.2.1 RNA yield and quality

RNA was initially extracted from 68 primary GBM specimens from 21 patient (three spatially distinct samples were taken from each patient (Table 3.1; See also appendix 1 for clinicopathological details of each patient). However, only two samples (core and rim) were available from one of the patients (patient 6).

Table 3.1: Summary of Clinicopathological characteristics of adult GBM cases

	Variable	Number of patients (% of total)
Age	Age: <50	8 (21.1)

	Age: 50-65	17 (44.7)
	Age: >65	13 (34.2)
Gender	Male	19 (50)
	Female	19 (50)
Location	Tumour location: Supratentorial	38 (100)
Treatment Received	Treatment: Radiotherapy	4 (10.5)
	Treatment: Chemotherapy	0 (0)
	Treatment: Chemo + Radio	25 (65.8)
	Treatment: None - BSC	3 (7.9)
	Treatment: None – N/A	6 (15.8)
Survival	Survival time: <6 months	7 (18.4)
	Survival time: <12 months	18 (47.4)

RNA was also extracted from two samples (temporal white, and grey matter of the temporal lobe) from an epileptic patient. In addition, RNA was extracted from nine patient-derived primary cell lines (Table 3.2) and two commercial cell lines (U87 and U251).

RNA was also extracted from four recurrent GBM tissues and two patient-derived recurrent cell lines to be included in the microarray in order to use the data for another potential study by the research group (See appendix 1 for initial analysis of microarray profiles from recurrent samples).

Table 3.2: Patient-derived cell lines

Patient Number	Cell Line	Region
8	GIN8	Invasive
21	GIN21	Invasive
17	GIN17	Invasive
3	GIN3R	Invasive (recurrent tumour)
5	GIN5	Invasive

22	GIN22R	Invasive (recurrent tumour)
28	GIN28	Invasive
28	GCE28	Core
31	GCE31	Core

Total RNA was assessed for RNA purity by the A260/A280 and A260/230 ratios where ratios close to 1.8 (Glasel, 1995; Manchester, 1995) were interpreted as an indicator of the absence of major contaminants absorbing at A280 and A230, respectively (Table 3.3). The quality of RNA was assessed using RNA integrity number (RIN), which was based on the ratio of the quantities of the ribosomal RNA (rRNA) molecules (Schroeder *et al.*, 2006).

rRNA are reliable housekeeping RNA used for assessing total *RNA quality because they are: i) the most abundant (>80%) constituent of total RNA sample* (O'Neil, Glowatz and Schlumpberger, 2013) *and ii)* transcribed by RNA polymerase I (except for 5S rRNA species, which is transcribed by RNA polymerase, independently from other RNA polymerase II-transcribed loci (Paule and White, 2000). RIN values range from 1-10 with values close to 1 indicating degraded RNA samples and values close to 10 indicating completely intact RNA.

Table 3.3: Quality and quantity of total RNA samples.
Patient number and region are indicated after "GBM". For example, GBM2.1 refers to patient "2", region "1". "rec" indicated recurrence. "GCE" and "GIN" refer to primary cells derived from the core and invasive edge, respectively. N/A values indicate that the bioanalyser was unable to calculate a RNA integrity number (RIN) for a given sample. RNA concentration (conc.) re-represented as an average between nanodrop and bioanalyser readings.

Sample	Region	Average RNA conc. (ng/µl)	260/ 230 ratio	260/ 280 ratio	RIN
Adult brain Temporal lobe (Grey Matter)	Healthy	523.1	2.1	1.8	5.3
Adult brain Temporal lobe (White Matter)	Healthy	433.9	2.1	1.7	5.8
GBM2.1	Core	240.7	1.9	1.9	N/A
GBM2.2	Rim	290.2	2.1	1.3	6.2
GBM2.4	Invasive	164.1	2.0	0.7	3.3
GBM3.2	Core	222.3	2.0	1.4	6.6
GBM3.1	Rim	290.4	2.0	2.1	8.4
GBM3.4	Invasive	103.0	1.9	1.6	3.3
GBM 3.5 rec	Invasive	4876.1	2.1	2.1	5.1
GBM5.2	Core	1057.0	2.0	2.0	6.6
GBM5.1	Rim	419.4	2.0	2.0	8.7
GBM5.5	Invasive	405.1	2.0	1.2	7.3
GBM5.7 rec	Core	424.8	2.1	1.8	6.9
GBM5.6 rec	Rim	504.6	2.1	2.1	6.3
GBM5.10 rec	Invasive	308.3	2.8	0.1	5.9
GBM6.2	Core	367.0	2.0	1.7	5.1
GBM6.3	Rim	870.9	2.0	2.1	8.4
GBM7.2	Core	61.7	2.0	1.9	3.9
GBM7.1	Rim	132.9	2.0	2.1	7.1
GBM7.4	Invasive	42.5	1.9	1.4	2.9
GBM8.2	Core	400.8	1.9	0.6	2.3
GBM8.1	Rim	201.4	2.0	2.0	7.6
GBM8.4	Invasive	154.3	2.0	2.0	N/A
GBM9.2	Core	2033.4	2.1	2.1	5.7
GBM9.1	Rim	553.9	2.0	2.0	5.0
GBM9.5	Invasive	1081.4	2.1	2.1	5.2

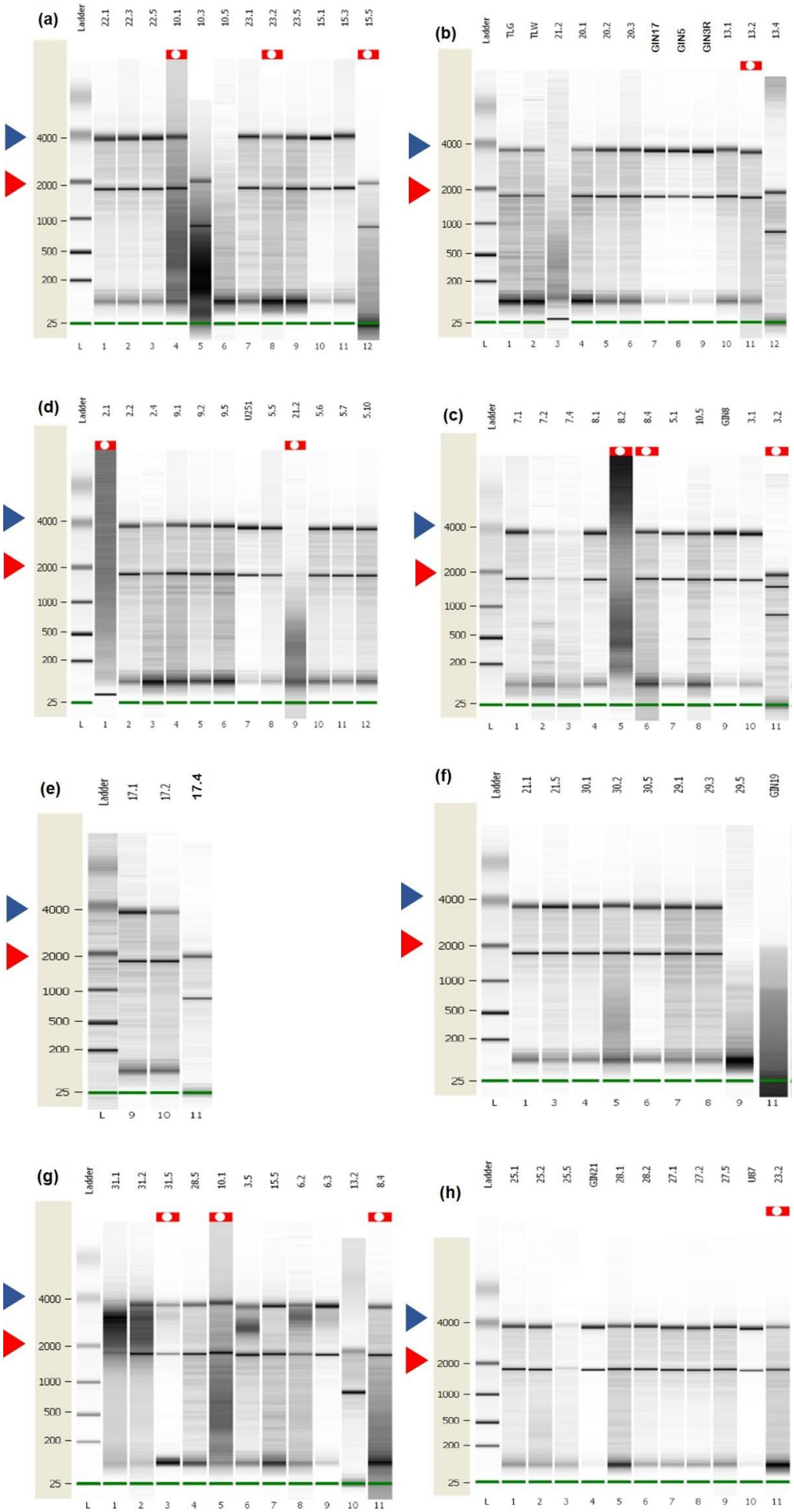
GBM10.3	Core	842.6	1.9	2.1	2.7
GBM10.1	Rim	1039.4	2.0	1.9	4.3
GBM10.5	Invasive	109.0	2.0	1.9	5.5
GBM13.2	Core	1117.6	2.0	2.0	7.2
GBM13.1	Rim	586.2	2.1	1.1	6.6
GBM13.4	Invasive	147.1	2.0	0.6	5.6
GBM15.3	Core	1030.8	2.1	2.1	7.6
GBM15.1	Rim	315.9	2.0	0.7	8.2
GBM15.5	Invasive	777.9	2.0	1.8	6.1
GBM17.2	Core	1130.0	2.0	1.9	5.3
GBM17.1	Rim	478.0	2.0	1.9	6.0
GBM17.4	Invasive	267.0	2.0	2.0	7.0
GBM20.2	Core	284.7	2.1	1.9	6.0
GBM20.1	Rim	367.7	2.1	1.6	4.0
GBM20.5	Invasive	198.9	2.1	1.6	5.4
GBM21.2	Core	54.2	1.9	1.3	2.0
GBM21.1	Rim	373.0	2.0	1.7	7.2
GBM21.5	Invasive	115.0	2.0	1.6	6.5
GBM22.3	Core	579.4	2.0	1.7	6.8
GBM22.1	Rim	1046.3	2.1	2.0	6.5
GBM22.5	Invasive	4778.5	2.1	2.1	6.6
GBM23.2	Core	255.4	2.0	1.5	N/A
GBM23.1	Rim	209.8	2.0	1.4	6.0
GBM23.5	Invasive	415.7	2.1	1.9	5.2
GBM25.2	Core	347.9	2.0	1.9	6.4
GBM25.1	Rim	276.6	2.0	1.8	6.9
GBM25.5	Invasive	78.8	2.0	1.1	4.1
GBM27.2	Core	893.0	2.1	1.9	7.2
GBM27.1	Rim	1736.7	2.1	2.1	7.4
GBM27.5	Invasive	362.9	2.1	1.8	7.0
GBM28.2	Core	304.6	2.0	1.8	7.2
GBM28.1	Rim	322.9	2.1	1.7	5.8
GBM28.5	Invasive	818.2	2.0	1.8	5.5
GBM29.3	Core	678.0	2.0	2.0	5.8
GBM29.1	Rim	648.8	2.0	1.8	5.6
GBM29.5	Invasive	80.0	2.0	1.8	5.3
GBM30.2	Core	466.6	2.0	1.7	5.0
GBM30.1	Rim	487.6	2.0	1.4	7.0
GBM30.5	Invasive	2225.7	2.1	1.8	8.2
GBM31.2	Core	375.0	2.0	1.4	5.3
GBM31.1	Rim	390.5	2.0	2.0	N/A

GBM31.5	Invasive	304.7	2.0	1.6	N/A
U87	Cell line	585.5	2.0	1.6	10.0
U251	Cell line	1725.8	2.1	1.9	9.3
GIN8	Cell line	902.0	2.1	2.0	8.7
GIN21	Cell line	380.3	2.0	1.5	9.3
GIN17	Cell line	825.1	2.1	2.1	9.2
GIN3R	Cell line	1607.9	2.1	2.1	9.3
GIN5	Cell line	478.6	2.1	1.4	9.6
GIN22R	Cell line	375.3	2.1	2.0	9.4
GIN28	Cell line	1107.6	2.1	2.0	9.3
GCE28	Cell line	911.7	2.1	2.0	9.2
GCE31	Cell line	485.8	2.1	1.7	7.9

Because RNA degradation interferes with the labelling and hybridisation of RNA, which results in poor microarray performance, the minimum RIN number for RNA samples to be included in the microarray experiment was RIN > 5. There were six samples with RIN < 5 (namely 2.4, 3.2, 3.4, 10.1, 10.3 and 25.5 samples) and another seven samples for which the bioanalyser has not calculated a RIN number (2.1, 8.4, 10.1, 15.5, 23.2, 21.1 and 31.5). However, before excluding any samples on base on the RIN number, the gel images for all RNA samples were visually inspected. Good quality RNA samples showed two distinct bands corresponding to the 28S (at 4000nt) and 18S (at 2000nt) rRNA species, components of the 60S large and 40S small ribosomal subunits, respectively, which are assumed to be reflective of unspecific damage to the RNA population in the total RNA sample.

Nevertheless, some RNA samples were flagged by the scanner (or have been recognised by visual inspection of the gel images) to have issues. In particular, three issues were identified: faint bands, progressively shifted bands, and *smearing of bands*. First, faint bands (3.4, 7.2, 7.4, 25.5 and 29.5 samples) were indicative of low concentrations of RNA (Table 3.3). Low concentration RNA samples (< 70 ng) were only included in the RNA sample cohort for miRNA microarray if their RIN > 5 (Table 3.3). Thus, 7.2 and 7.4 samples were excluded.

As a result, sample 7.1 was also excluded as it cannot be included without the other regions. Secondly, poor mixing of reagents during vortexing (especially as these samples were loaded onto wells positioned at the corners of the chip; 10.3, 13.2, 13.4, 15.5, 17.4 samples) may have disrupted the scanner reading causing the detection of the marker to be delayed. As such, marker baseline adjustment caused all bands to shift; however, these samples had distinct S18/S28 bands on the gel. Finally, smearing of bands (2.1, 3.2, 8.2, 10.1, 10.3, 10.5, 21.2, 29.5, 31.1, 31.2, GIN19 samples) was indicative of the presence of degraded RNA products which was confirmed from the electropherogram results (Table 3.4).


(a)
Ladder
22.1
22.3
22.5
10.1
10.3
10.5
23.1
23.2
23.5
15.1
15.3
15.5
4000
2000
1000
500
200
25
L 1 2 3 4 5 6 7 8 9 10 11 12
(b)
Ladder
TLG
TLW
21.2
20.1
20.2
20.3
GIN17
GIN5
GIN3R
13.1
13.2
13.4
4000
2000
1000
500
200
25
L 1 2 3 4 5 6 7 8 9 10 11 12
(d)
Ladder
2.1
2.2
2.4
9.1
9.2
9.5
U251
5.5
21.2
5.6
5.7
5.10
4000
2000
1000
500
200
25
L 1 2 3 4 5 6 7 8 9 10 11 12
(c)
Ladder
7.1
7.2
7.4
8.1
8.2
8.4
5.1
10.5
GIN8
3.1
3.2
4000
2000
1000
500
200
25
L 1 2 3 4 5 6 7 8 9 10 11
(e)
Ladder
17.1
17.2
17.4
4000
2000
1000
500
200
25
L 9 10 11
(f)
Ladder
21.1
21.5
30.1
30.2
30.5
29.1
29.3
29.5
GIN19
4000
2000
1000
500
200
25
L 1 3 4 5 6 7 8 9 11
(g)
Ladder
31.1
31.2
31.5
28.5
10.1
3.5
15.5
6.2
6.3
13.2
8.4
4000
2000
1000
500
200
25
L 1 2 3 4 5 6 7 8 9 10 11
(h)
Ladder
25.1
25.2
25.5
GIN21
28.1
28.2
27.1
27.2
27.5
U87
23.2
4000
2000
1000
500
200
25
L 1 2 3 4 5 6 7 8 9 10 11

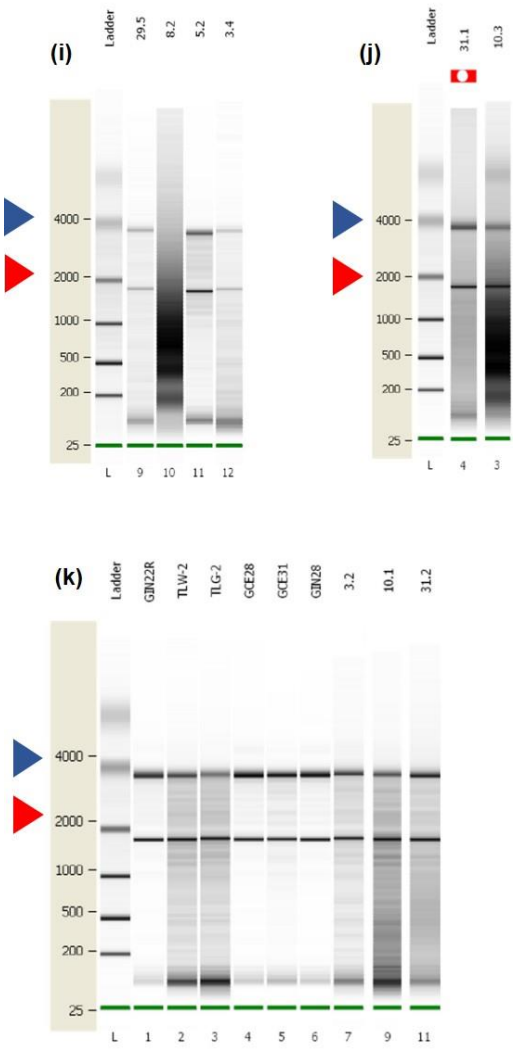


Figure 3.1: Bioanalyser gel images of total RNA samples.

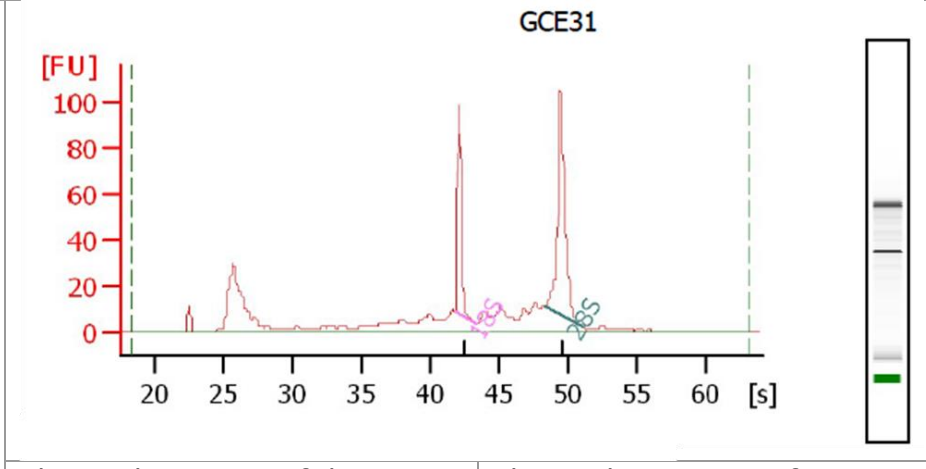
Gel images were labelled a-k to represent the order at which the gels were run. Tissue samples were represented as numbers without the prefix GBM. Samples numbers are as shown in Table 3.3. Primary GBM cells derived from the core and invasive margin were represented with the prefixes GIN and GCE, and commercial cell lines with prefix U. Numbers annotate patient from whom the cell line was derived Ladder represents the length of nucleotides (nt). The marker shows a band (green) at 25nt. The two sharp bands at 4000nt (blue arrow) and 2000nt (red arrow) represent S28 and S18 rRNAs, respectively. See text for sample quality interpretation. TLW; Temporal lobe (White matter). TLG; Temporal lobe (Grey matter).

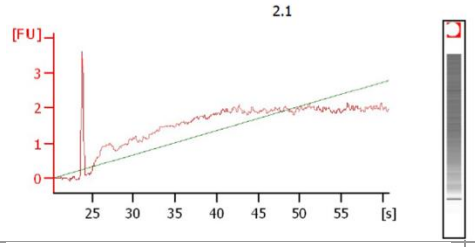
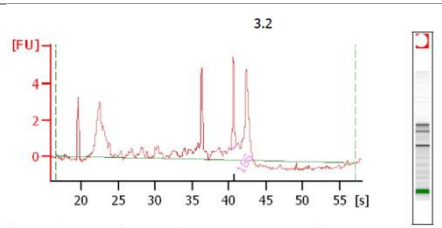
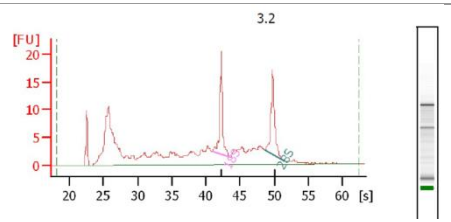
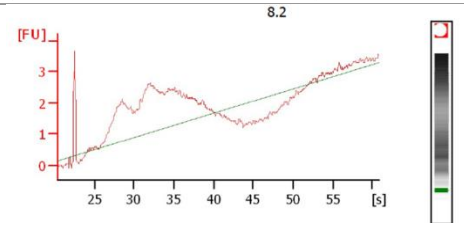
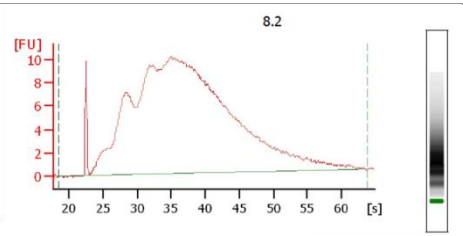
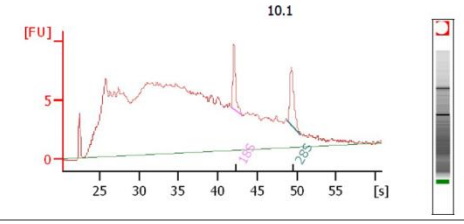
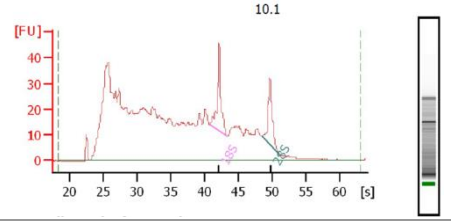
Because smaller molecules take a shorter time to travel through the separation channel, their fluorescence is detected first, and they appear on the left side of the electropherogram. A good-quality RNA sample (GCE31 sample; Table 2) shows two sharp/narrow 28S and 18S rRNA peaks with 28S:18S rRNA ratios close to 2 *(based on the molecular weight)*. The ratio can be inferred by comparing areas under the peaks. The area of the 28S rRNA peak decreases with the degradation of the 28S rRNA, which degrades more quickly than the 18S rRNA due to its larger molecular size. This leads to a progressive increase in the baseline area below the 18S rRNA, which becomes wider as the 28S rRNA fragments become smaller.

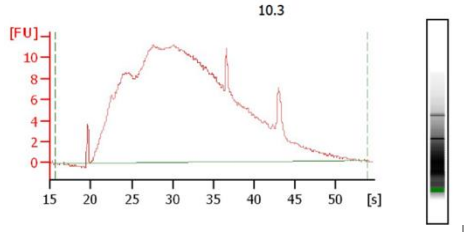
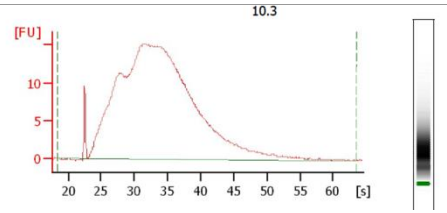
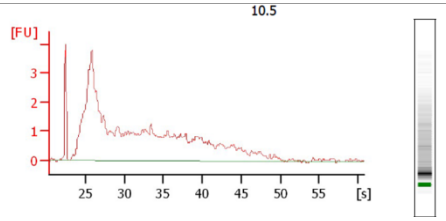
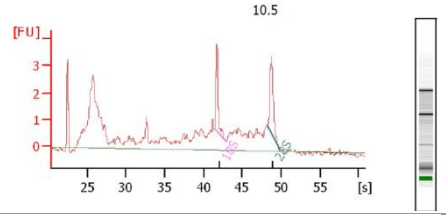
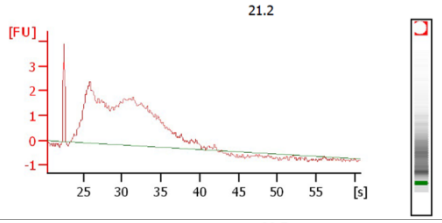
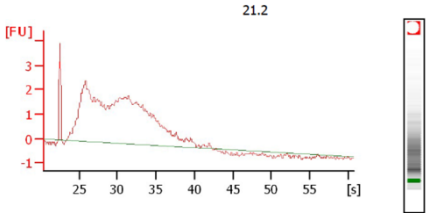
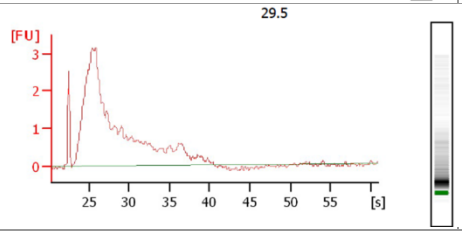
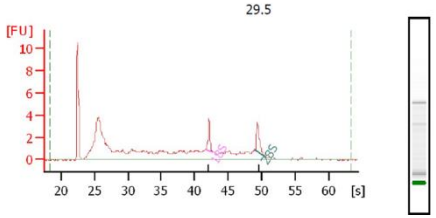
RNA degradation was confirmed by the presence of spikes between 18S/28S peaks or by the absence of low molecular weight species at 24-29 seconds which corresponds to the 5S rRNA species (*a* component of the 60S large ribosomal subunit; 1.2kb was the size). Total RNA was re-isolated, were possible, if RNA samples were degraded. Total RNA was also re-isolated from TLG, TLW, 15.5 and 3.4 samples to obtain higher RIN number (Table 3.3). The re-isolated RNA samples were then re-analysed (Table 3.3 and Table 3.4 and Figure 3.1), and samples 2.1, 8.2, 10.3, 21.2 and GIN19 were excluded from the RNA

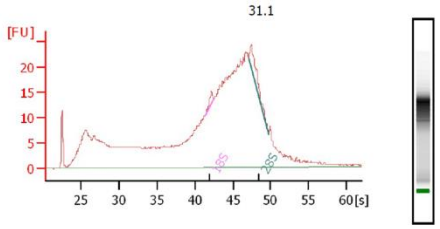
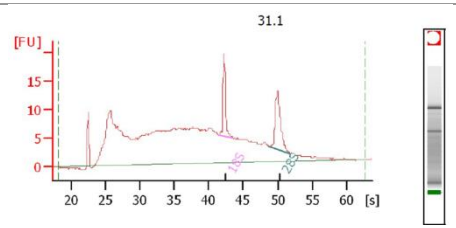
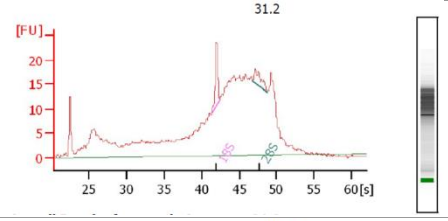
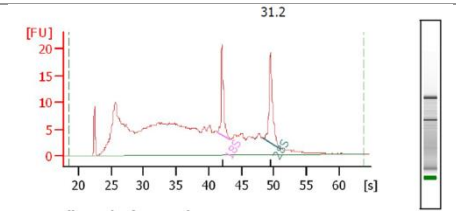
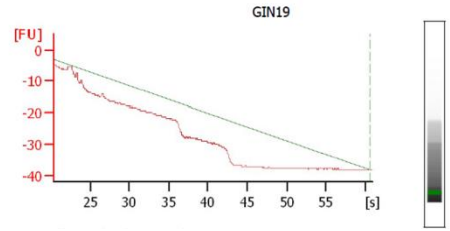
sample cohort for miRNA microarray accordingly (Table 3.4). Fortunately, there was no major DNA contamination in my total RNA samples as this would appear as a spike past the S28 peak in the electropherogram.

Table 3.4: Electropherogram results for total RNA samples that showed RNA degradation.
The y-axis represents fluorescence in fluorescence units (FU), and the x-axis represents time in seconds (s). Fluorescence baseline is shown in green. The molecular size marker is shown as a peak at 20-23 s. Peaks for S18 and S28 rRNA were detected around 40 and 50 seconds, respectively. RNA samples that were excluded from the RNA sample cohort for microarray were denoted with an asterisk (*).Tissue samples were represented as numbers without the prefix GBM. GIN19 and GCE31 are primary GBM cell lines. Samples numbers are as shown in Table 3.3.

Status	Sample	Electropherogram	
Good-quality RNA	GCE31		
		Electropherogram of the problematic sample	Electropherogram after RNA re-isolation

Degraded RNA	2.1 *		Tissue sample was depleted
	3.2		
	8.2 *		
	10.1		

	10.3 *		
	10.5		
	21.2 *		
	29.5		

	31.1		
	31.2		
	GIN19*		The cell line was not growing well in culture

3.2.2 miRNA microarray analysis

3.2.2.1 Data pre-possessing and quality control (QC)

Based on their quality, 61 (out of 68; See previous section for details) tissue RNA samples (normal brain tissue=2, core=16, rim=20, invasive margin=19 and recurrent tumours=4) were suitable to run on Affymetrix microarray (see methods section 2.3.3.2 about the details of the microarray experiment), along with 11 RNA samples from tumour-derived cells, commercial cell lines and a commercial astrocyte RNA samples as a control. The generated microarray data were pre-processed, and boxplots of the raw and pre-processed data were constructed to assess if median values after pre-processing were similar across arrays, which indicates that the normalisation method applied have been appropriate, and to identify problematic arrays. The normalisation method has succeeded to equalise the distribution of probe intensities between arrays, and the array GIN-22R (A3276_64; Figure 3.2) has been identified as a potential outlier.

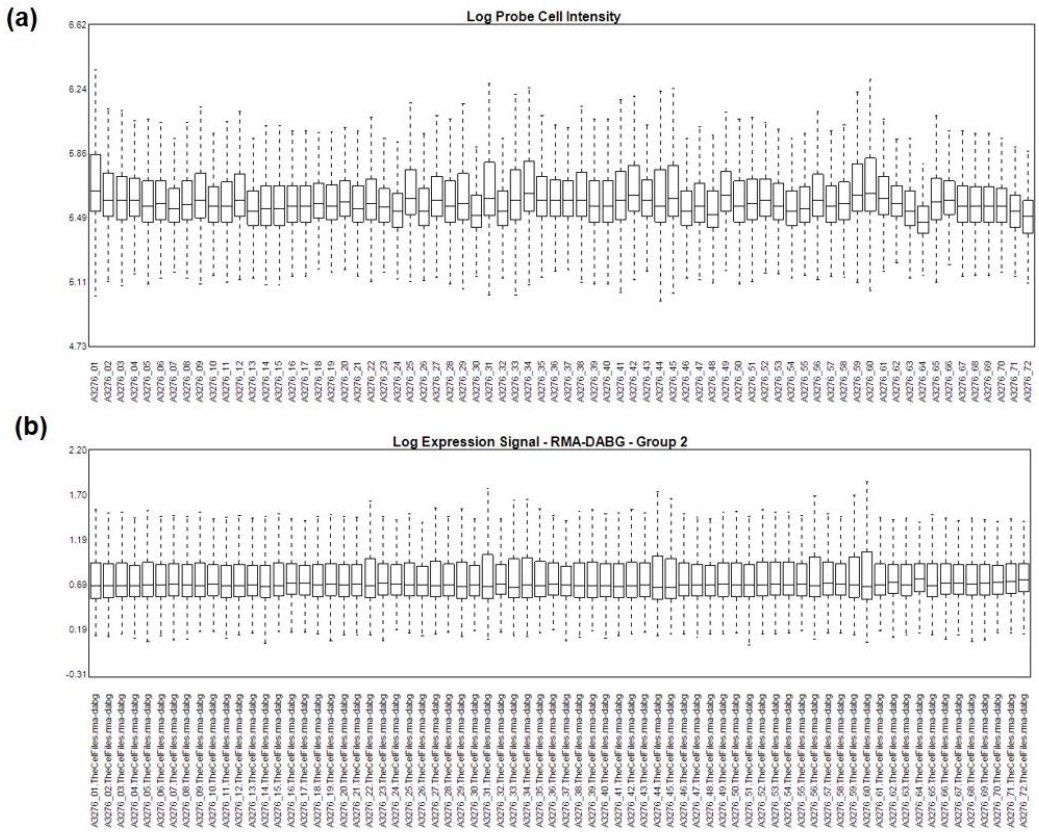


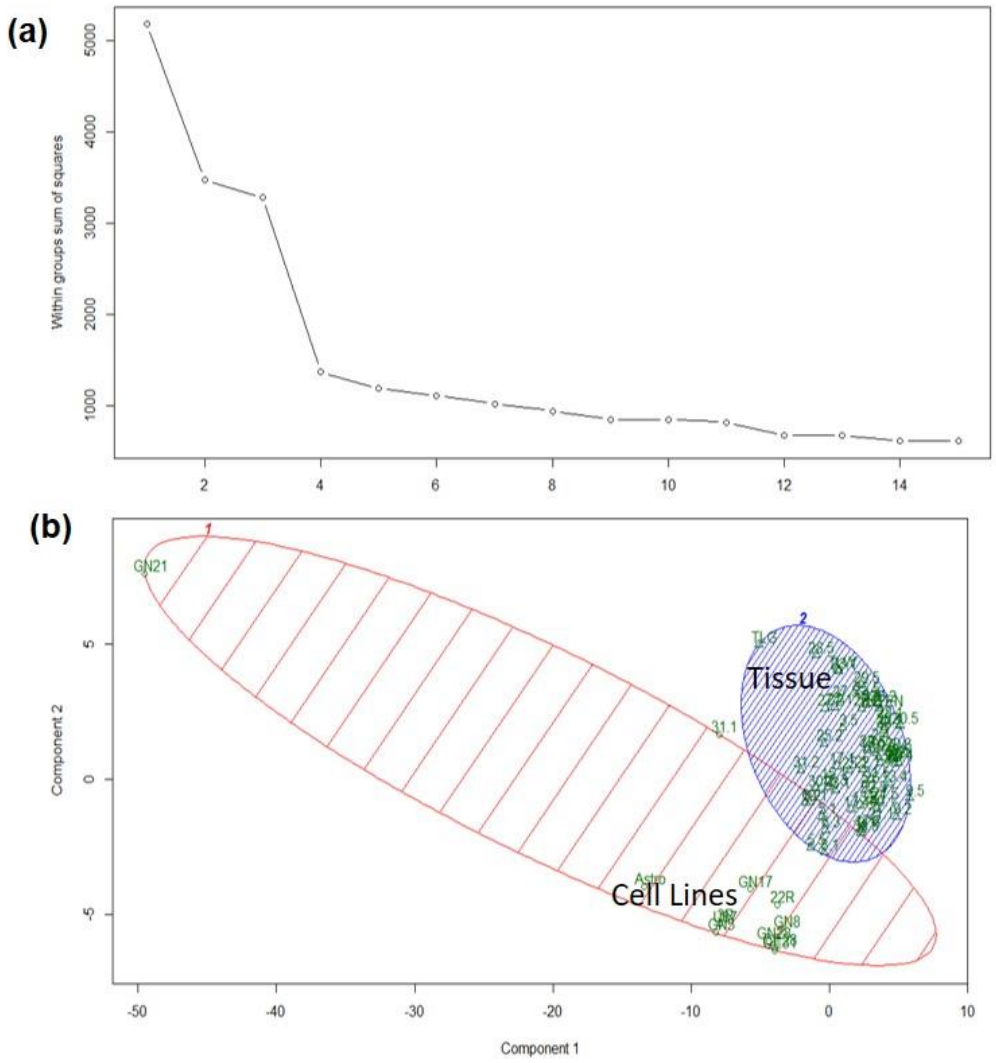
Figure 3.2: Boxplot of probe intensities distributions (n=72).

Boxplot of microarray data (a) before and (b) after pre-processing. Sample names are unimportant for this figure. The figure shows similar median values of probe intensities across all arrays.

3.2.2.2 Unsupervised clustering of miRNA expression profiles

Given that each single microarray can survey the expression of 2,578 mature miRNAs to generate an expression profile for a given sample, it was possible to investigate the similarities in the expressions of each miRNA across the samples using a clustering approach. The unsupervised k-means clustering method was used and samples were grouped into k clusters

based on the similarities of their miRNA expression profile (i.e. the average expression for every miRNAs across all samples). The optimal number of clusters (the value of k) was estimated to be either 2 or 4 using the Elbow method (Figure 3.3).



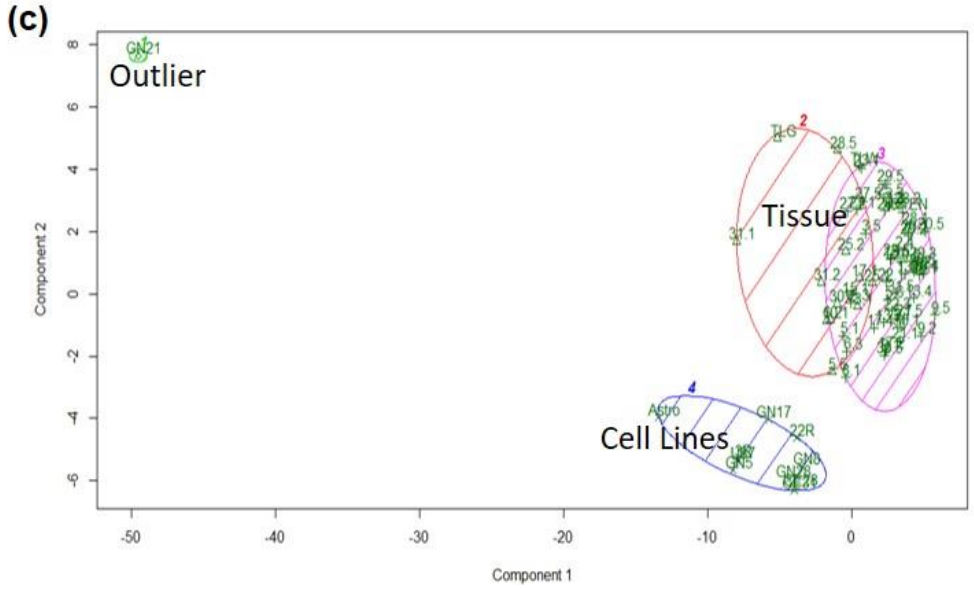


Figure 3.3: K-means clustering (n=72 arrays).
The similarities in the miRNA expression profiles across the samples was analysed using k-means clustering approach. (a) The elbow method of finding the optimal number (x-axis) of clusters as (b) 2 clusters or (c) 4 clusters. Corresponding samples have been grouped into either cell lines or tissue clusters.

Whether the data were clustered into 2 or 4 clusters, cell lines and tissue microarray data have clustered separately while the cell line GIN-21R seemed not to cluster with the bulk of the data (an outlier; Figure 3.3c). Moreover, investigations of the CHP-files indicated that signals from the GIN-21R array were outside the reading range of the scanner. K-means clustering and the elbow method for k estimation were repeated following the exclusion of the GIN-21R array (Figure 3.4). The number of clusters was estimated to be 2, which corresponded to the cell lines and tissue clusters.

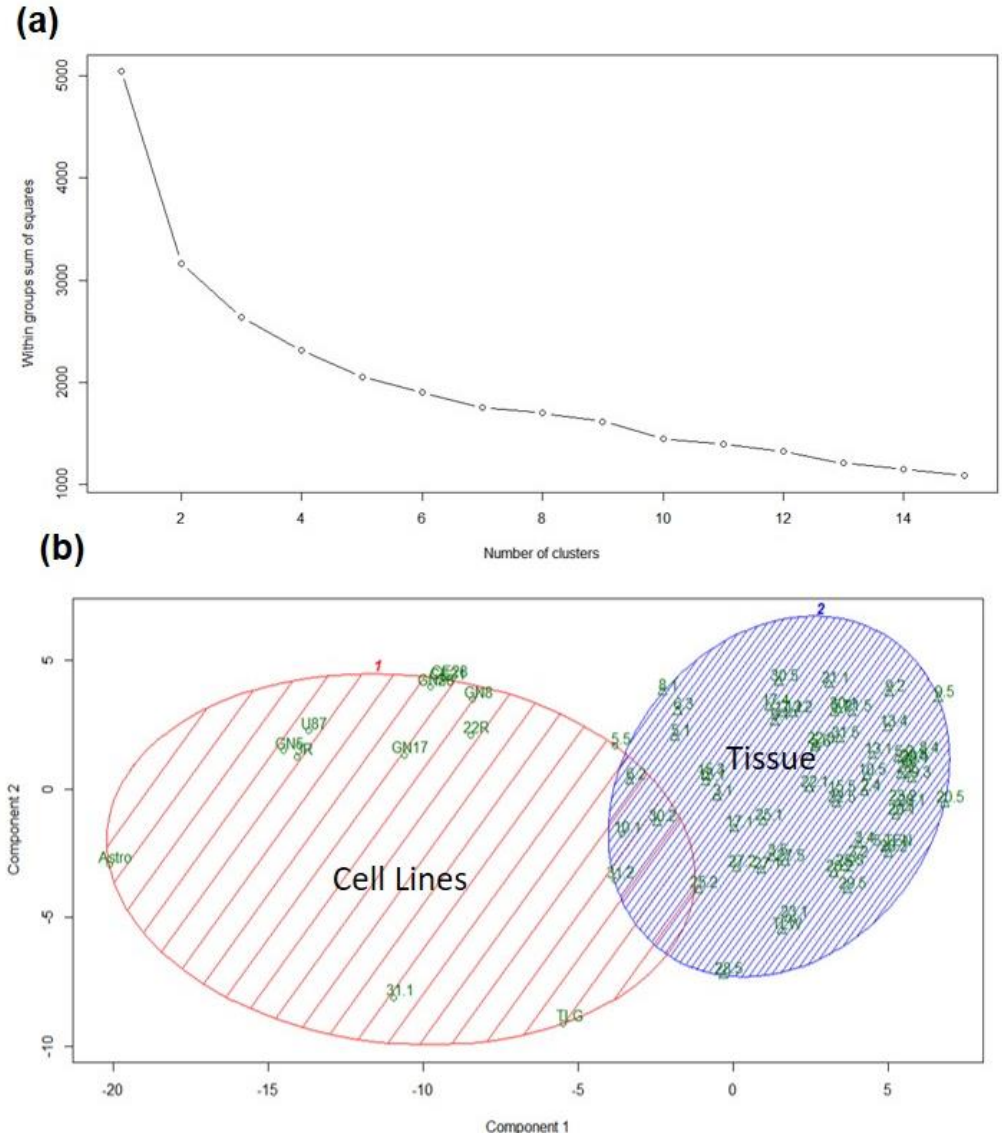


Figure 3.4: K-means clustering (n=71 arrays).
The similarities in the miRNA expression profiles across the samples was analysed using k-means clustering approach. (a) The elbow method of finding the optimal number of clusters, (b) K-means clustering using 2 clusters. Corresponding samples have been grouped into either cell lines or tissue clusters.

3.2.2.3 Comparison of miRNA expression profiles between core, rim and invasive margin tissue samples

Next, a supervised clustering method, PCA, was used to investigate the similarities in the miRNA expression profiles between tumour regions using Partek software (Figure 3.5; see also methods section 2.3.3.3). The core and the rim had almost identical miRNA expression profiles. Although overlaps with the other two regions, due to the similarities within regions of each patient tumour, the invasive margin had a somewhat distinct miRNA expression profiles. This suggests that some miRNAs in the invasive region were differentially expressed.

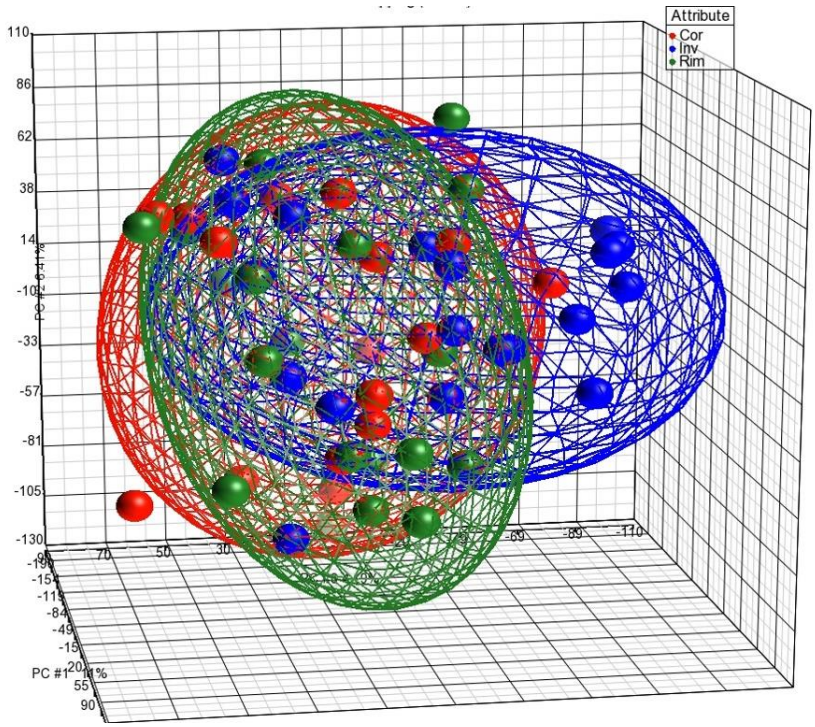


Figure 3.5: PCA of miRNA expression profiles based on GBM tumour regions.
The invasive margin (Inv) cluster was more distinct than the core (Cor) and the rim clusters; although all clusters overlapped due to the similarities between the different regions taken from the same patient tumour.

3.2.2.4 Identification of differentially expressed miRNAs between core, rim and invasive margin

In order to identify the particular miRNAs whose expression between tumour regions is significantly different, a pair-wise statistical comparison of the expression profiles was performed using the limma method (see methods section 2.3.3.3.4). There were no publicly available datasets for normal human brain compatible with the most up-to-date version of the microarray I used, which has the 5p-strand/3p-strand feature annotations. I also had an insufficient number of samples to obtain a representative measure of miRNA expression in the normal brain from the microarray. Therefore, because of these two reasons, I could not normalise the tumour expression profiles (n=45) to the normal brain (n=2) at that stage. Only patients who had data available from all three regions were included in my differential expression analysis; there were only 15 patients with three tumour regions, thus, only 45 miRNA expression

profiles were used to carry out the pair-wise analysis of the three regions.

There were only five miRNAs that showed differential expression within the GBM tumour following FDR-correction. Two of these miRNAs were found to be significantly upregulated in the invasive margin (miR-330-5p and miR-215-3p) while three of the miRNAs were downregulated in the invasive margin (miR-619-5p, miR-4440, and miR-4793-3p) compared to the rim and the core (Figure 3.6; large error bars resulted from inter-patient variation; See also appendix 1 for expression values from each patient). Moreover, miR-330-5p, miR-4793-3p and miR-4440 show relatively high differential fold changes between the invasive margin and the other two tumour regions, whereas miR-215-3p and miR-619-5p show low differential fold changes Table 3.5.

Table 3.5: Relative expression levels of differentially expressed miRNAs within the GBM tumour.
miRNA expression for paired samples from 15 patients. Negative log2 transformed fold change (FC) values represent lower expression levels in the region written first. FDR = False discovery rate.

	Core vs Rim			**Rim vs invasive edge**			**Core vs invasive edge**		
miRNA ID	Log(FC)	p-value	FDR	Log(FC)	p-value	FDR	Log(FC)	p-value	FDR
hsa-miR-215-3p	0.00	0.88	0.99	-0.06	0.00	0.08	-0.06	0.00	0.07
hsa-miR-4793-3p	0.66	0.39	0.99	2.65	0.00	0.35	3.32	0.00	0.07
hsa-miR-4440	0.99	0.15	0.99	1.68	0.02	0.56	2.67	0.00	0.18
hsa-miR-330-5p	0.19	0.70	0.99	-2.04	0.00	0.10	-1.85	0.00	0.23
hsa-miR-619-5p	0.46	0.07	0.99	0.46	0.07	0.68	0.92	0.00	0.23

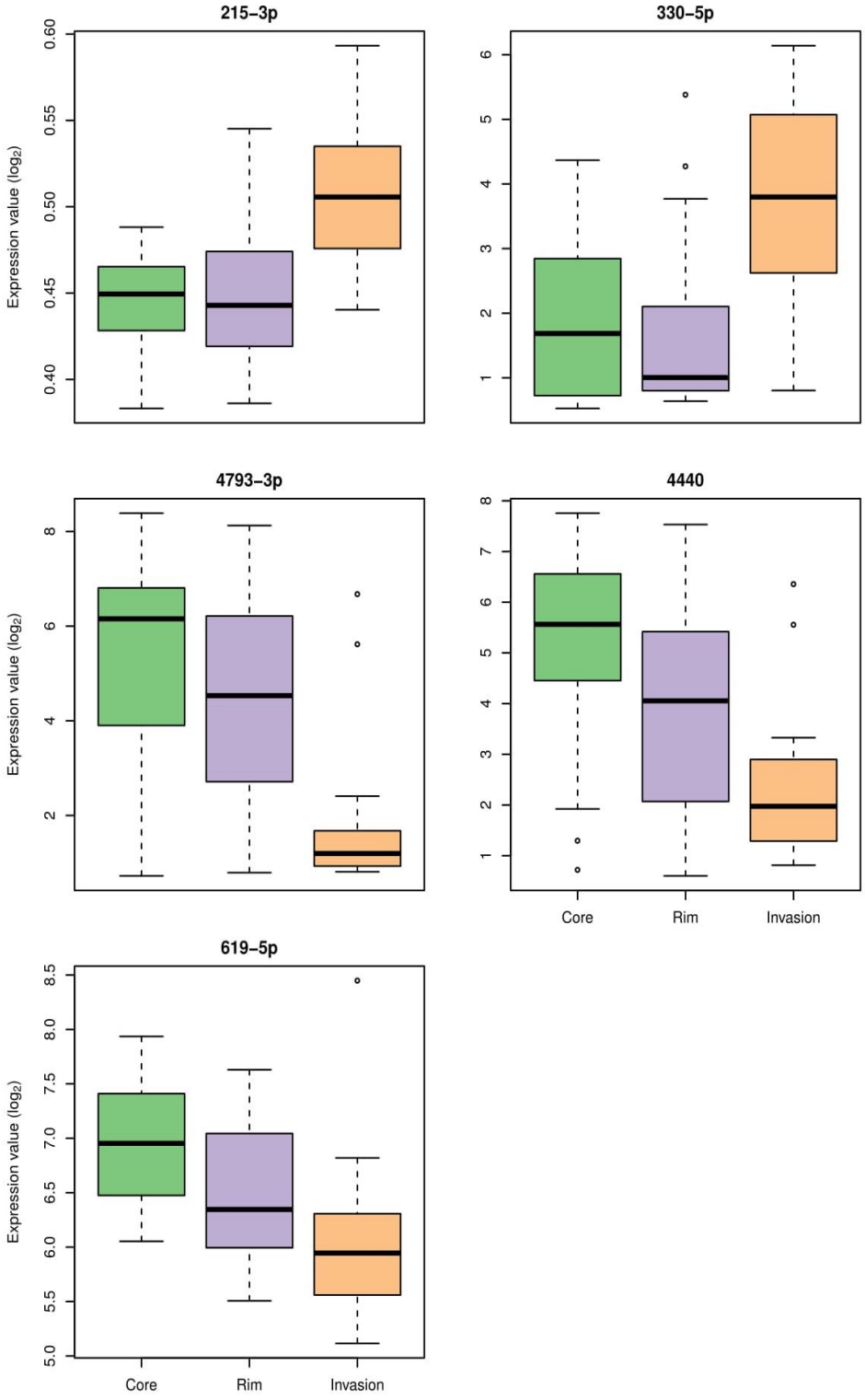


Figure 3.6: Boxplot of differentially expressed miRNAs between the different GBM tumour regions.
miRNA expression values are shown for 15 patient tumours multi-sampled from the core (green), purple (rim), and invasive margin (orange) regions.

3.2.3 Molecular validation of GBM intra-tumour heterogeneity through qRT-PCR

3.2.3.1 Expression analysis of miRNA by qRT-PCR

miRNA expression reported by my microarray was validated by an independent method to eliminate technical variability. qRT-PCR—a gold-standard method for RNA quantification which is often used for microarray data validation (Git *et al.*, 2010)—was used to validate the results obtained from microarray analysis due to its high detection sensitivity, sequence specificity, and reproducibility (See methods section). qRT-PCR was performed against the five selected miRNAs (miR-330-5p, miR-215-3p, miR-619-5p, miR-4440, and miR-4793-3p) with a *C. elegans* miRNA, cel-miR-54-3p, as an exogenous spike-in control (as in Kuhlmann et al., 2014) and hsa-miR-191-5p and hsa-miR-361-5p as endogenous controls ("housekeeping" miRNAs) in order to generated normalised expression values. Endogenous controls were selected based on literature (Peltier and Latham, 2008), the qRT-PCR manufacture recommendations and on the relatively constant and moderately abundant expression of these two miRNAs across all tissue samples according to the microarray data (Figure 3.7).

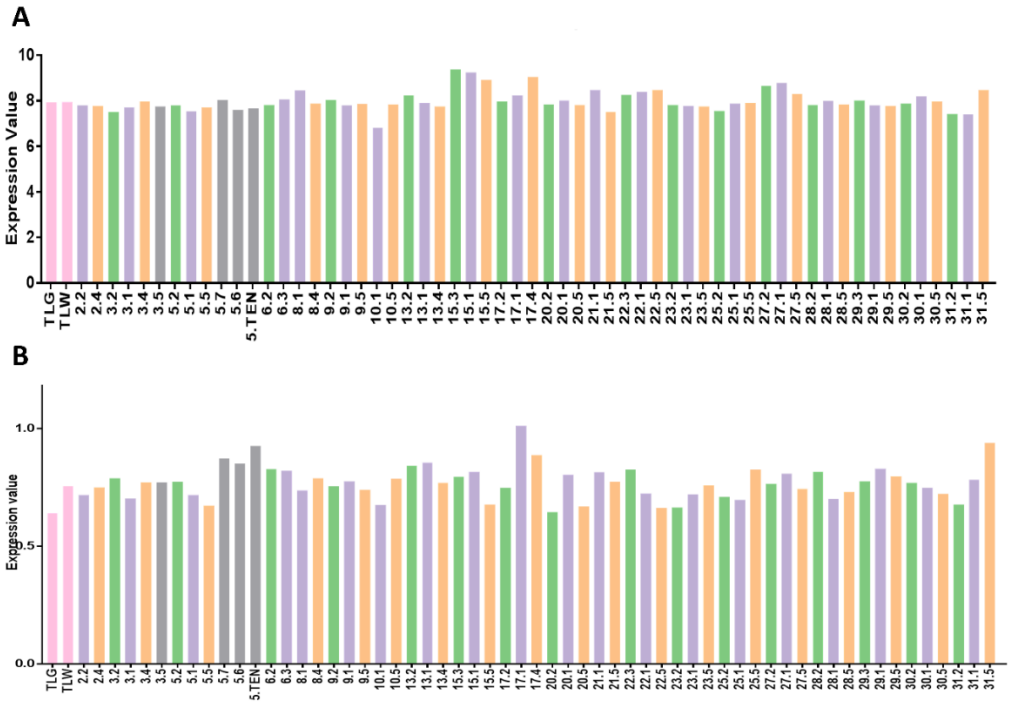


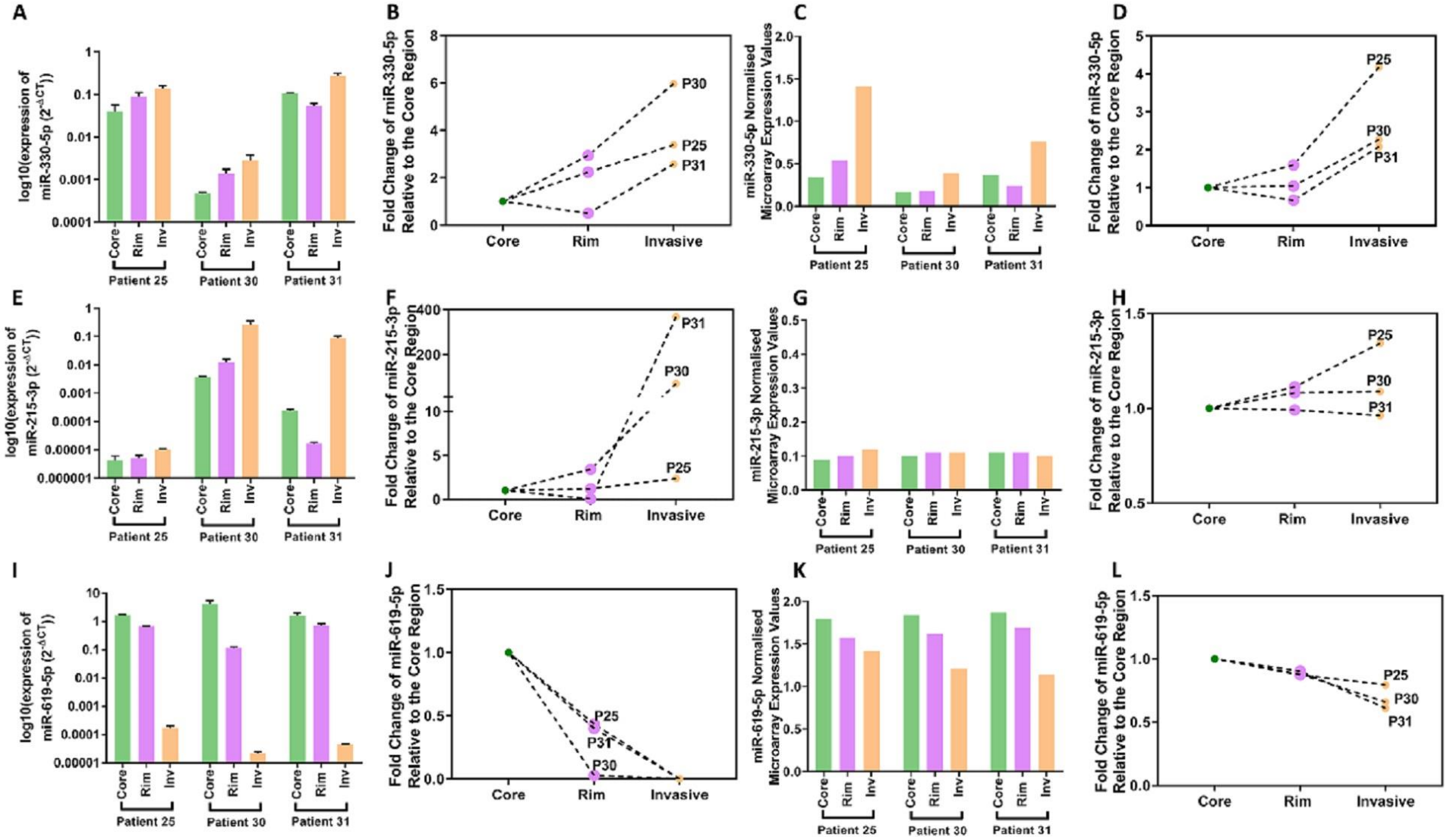
Figure 3.7: Expression of housekeeping miRNAs.
Each bar represents one expression value (A) hsa-miR-361-5p and (B) hsa-miR-191-5p across brain and tumour tissue samples (n=1). Pink bars correspond to normal temporal lobe samples. Green, purple and yellow bars correspond to the core, rim and invasive margin tumour samples, respectively. Grey bars correspond to recurrent samples.

3.2.3.2 qRT-PCR validation of miRNA expression in tumour samples

qRT-PCR was performed on three regions from three patient samples that were used in the microarray and also had the invasive margin region sorted into 5-ALA/+ and 5-ALA/- cell populations (as seen in section 3.3.2.4). The reason I only used three patients was because of the limited availability of the biomaterial from the invasive region. All of the qRT-PCR miRNA expression patterns for the three patients were found to be

consistent with those seen from the microarray (Figure 3.8). In particular, miR-619-5p, miR-4793-3p and miR-4440 were downregulated in the invasive margin compared to the rim and the core regions while miR-330-5p and miR-215-3p were upregulated in the invasive margin; except in the cases of patient 31 (whose microarray data showed no differential expression of miR-215-3p between the tumour regions) and patient 30 (whose microarray data showed the same expression levels of miR-215-3p in the invasive margin as in the rim region). Yet, the qRT-PCR data for both patients 30 and 31 showed that miR-215-3p is expressed at higher levels in the invasive margin than in the rim region. Moreover, the relative levels in the core and rim provided by the qRT-PCR and microarray methods were variable. In qRT-PCR data, the levels in the core may be reported higher than the rim, while in microarray data, the rim may be reported higher than the core. The differences in the magnitude of regional miRNA expression between the microarray and qRT-PCR results could be due to multiple factors. One factor may be the lack of overlap in the location of PCR primers and microarray probes, which may lead to identifying fewer or more sequences. Another reason for such differences in the magnitude of miRNA expression is the intrinsic technical difference in detection sensitivity of the

measurements of miRNA expression between the two molecular techniques (global change in the expression of thousands of miRNAs simultaneously versus absolute quantification of specific miRNAs)


A
log10(expression of miR-330-5p ($2^{-\Delta CT}$))
1
0.1
0.01
0.001
0.0001
Core
Rim
Inv
Patient 25
Patient 30
Patient 31
B
Fold Change of miR-330-5p Relative to the Core Region
8
6
4
2
0
P30
P25
P31
Core
Rim
Invasive
C
miR-330-5p Normalised Microarray Expression Values
2.0
1.5
1.0
0.5
0.0
Core
Rim
Inv
Patient 25
Patient 30
Patient 31
D
Fold Change of miR-330-5p Relative to the Core Region
5
4
3
2
1
0
P25
P30
P31
Core
Rim
Invasive
E
log10(expression of miR-215-3p ($2^{-\Delta CT}$))
1
0.1
0.01
0.001
0.0001
0.00001
0.000001
Core
Rim
Inv
Patient 25
Patient 30
Patient 31
F
Fold Change of miR-215-3p Relative to the Core Region
400
200
10
5
0
P31
P30
P25
Core
Rim
Invasive
G
miR-215-3p Normalised Microarray Expression Values
0.5
0.4
0.3
0.2
0.1
0.0
Core
Rim
Inv
Patient 25
Patient 30
Patient 31
H
Fold Change of miR-215-3p Relative to the Core Region
1.5
1.0
0.5
P25
P30
P31
Core
Rim
Invasive
I
log10(expression of miR-619-5p ($2^{-\Delta CT}$))
10
1
0.1
0.01
0.001
0.0001
0.00001
Core
Rim
Inv
Patient 25
Patient 30
Patient 31
J
Fold Change of miR-619-5p Relative to the Core Region
1.5
1.0
0.5
0.0
P25
P31
P30
Core
Rim
Invasive
K
miR-619-5p Normalised Microarray Expression Values
2.0
1.5
1.0
0.5
0.0
Core
Rim
Inv
Patient 25
Patient 30
Patient 31
L
Fold Change of miR-619-5p Relative to the Core Region
1.5
1.0
0.5
0.0
P25
P30
P31
Core
Rim
Invasive

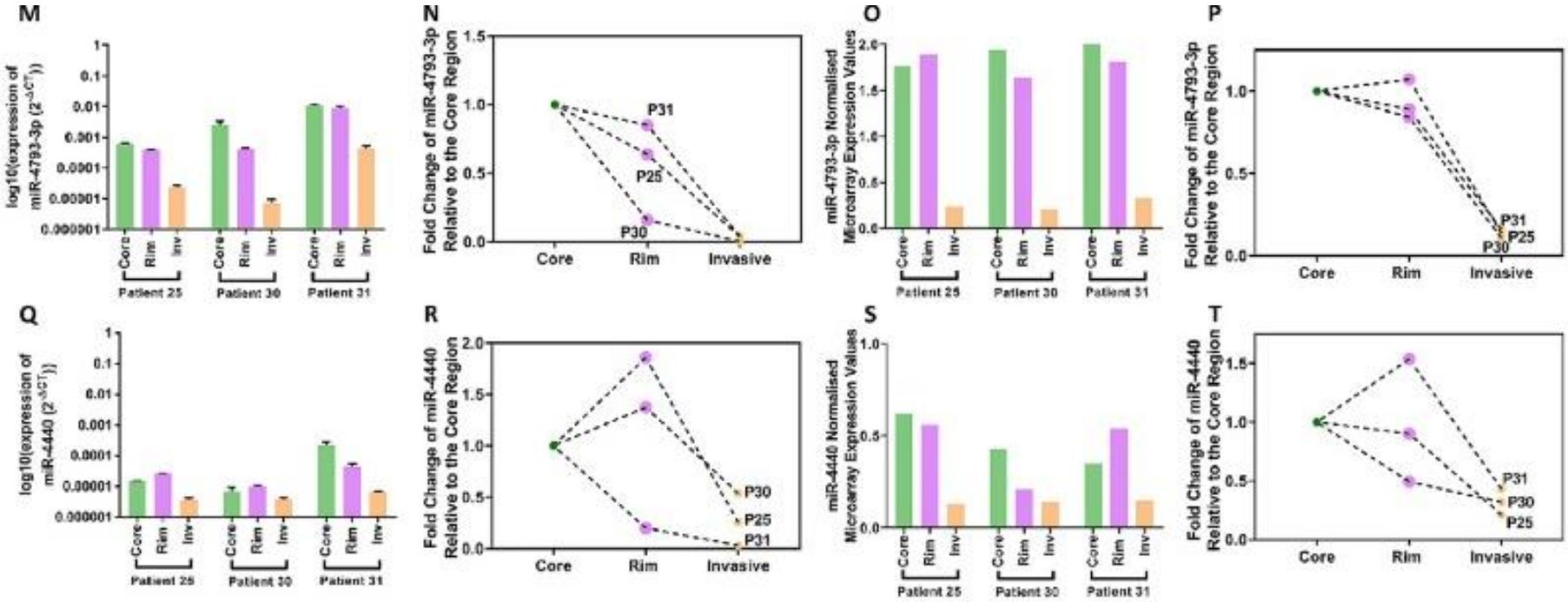

M
log10(expression of miR-4793-3p (2^-ΔCT))
Core
Rim
Inv
Patient 25
Patient 30
Patient 31
N
Fold Change of miR-4793-3p Relative to the Core Region
P31
P25
P30
Core
Rim
Invasive
O
miR-4793-3p Normalised Microarray Expression Values
P
Fold Change of miR-4793-3p Relative to the Core Region
Q
log10(expression of miR-4440 (2^-ΔCT))
R
Fold Change of miR-4440 Relative to the Core Region
S
miR-4440 Normalised Microarray Expression Values
T
Fold Change of miR-4440 Relative to the Core Region

Figure 3.8: qRT-PCR validation of miRNA expression reported by microarray in the same patient cohort used for the microarray.

Log of expression values for each tumour regions (left panel) and the fold change of the expression value in each region relative to the core region (right panel) are shown for (A,B) miR-330-5p, (C,D) miR-215-3p, (E,F) miR-619-5p, (G,H) miR-4794-3p, and (I,J) miR-4440. The numbers 25, 30, and 31 label the different patients. Error bars represent standard error of three technical repeats.

Next, in order to draw a more general conclusion about intra-tumour heterogeneity of miRNA expression, I PCR to validate the microarray findings on a cohort of different to, and independent from, the one used in the microarray (

Figure 3.9). Except in the case of miR-215-3p, where no differential expression between the tumour regions was seen in patient 32 (

Figure 3.9), the results of the qRT-PCR on the independent cohort were in line with the expected pattern of miRNA expressions from the microarray findings.

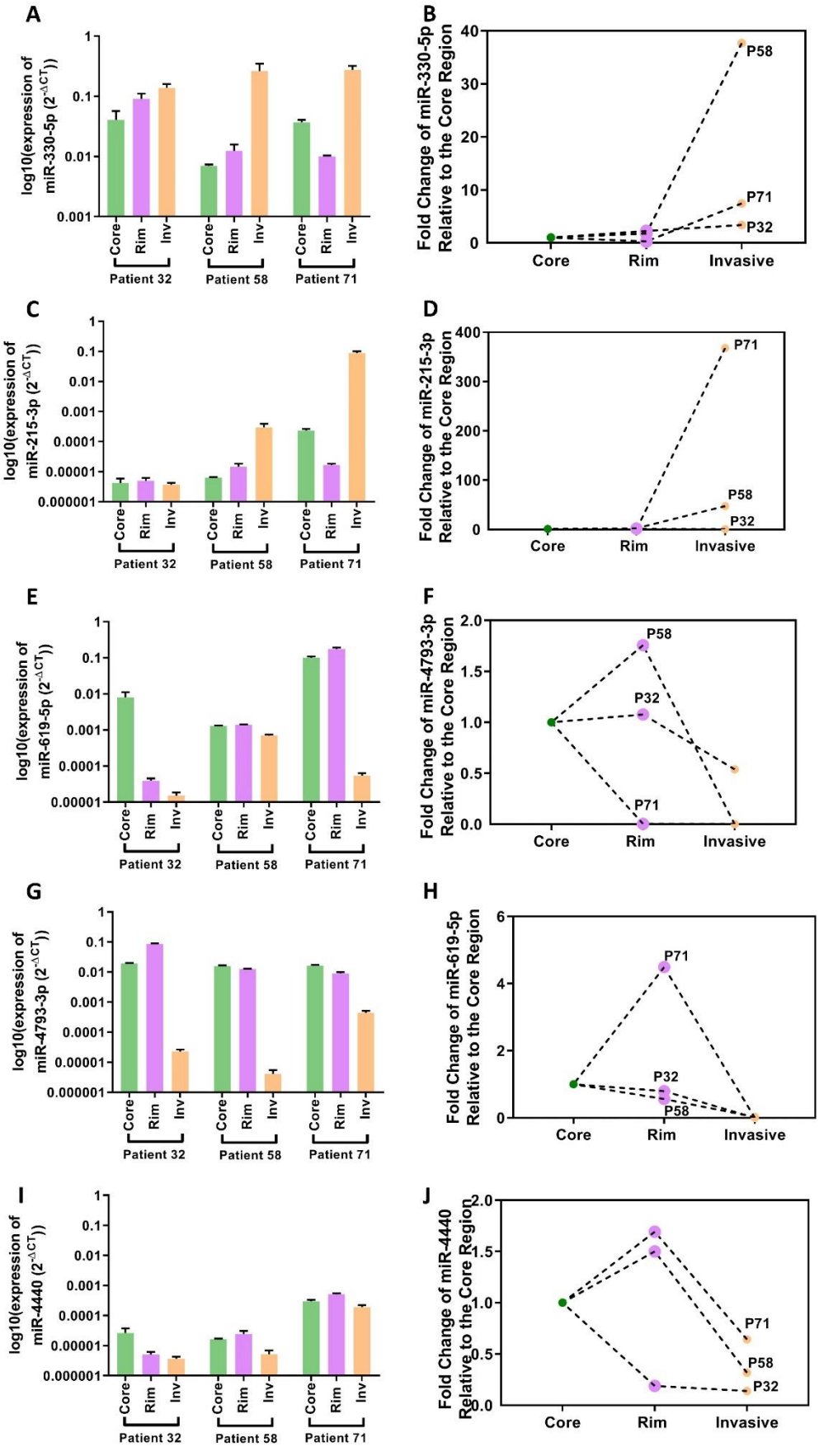

A
log10(expression of miR-330-5p (2^-ΔCT))
Core
Rim
Inv
Patient 32
Patient 58
Patient 71
B
Fold Change of miR-330-5p Relative to the Core Region
P58
P71
P32
Core
Rim
Invasive
C
log10(expression of miR-215-3p (2^-ΔCT))
D
Fold Change of miR-215-3p Relative to the Core Region
E
log10(expression of miR-619-5p (2^-ΔCT))
F
Fold Change of miR-4793-3p Relative to the Core Region
G
log10(expression of miR-4793-3p (2^-ΔCT))
H
Fold Change of miR-619-5p Relative to the Core Region
I
log10(expression of miR-4440 (2^-ΔCT))
J
Fold Change of miR-4440 Relative to the Core Region

Figure 3.9: qRT-PCR validation of miRNA expression reported by microarray in an independent GBM patient cohort.

Log of expression values for each tumour regions (left panel) and the fold change of the expression value in each region relative to the core region (right panel) are shown for (A,B) miR-330-5p, (C,D) miR-215-3p, (E,F) miR-619-5p, (G,H) miR-4794-3p, and (I,J) miR-4440. The numbers 32, 58, and 71 label the different patients. Error bars represent standard error of three technical repeats.

3.2.3.3 miRNA expression in the 5-ALA sorted invasive margin samples

While the percentage of tumour in the core and rim samples is 99-100% (based on pathological assessment of H & E stains), the invasive margin samples contain, on average, 97-95% normal (non-GBM) tissue, and only 3-5% tumour (based on FACS analysis estimations). To verify that the observed expression signals from the invasive margin samples were produced by the tumour residues and not the normal tissue, qRT-PCR was performed on FACS-analysed invasive margin samples: 5-ALA positive tumour cells (5-ALA/+) and 5-ALA negative (5-ALA/-) non-neoplastic cells from adjacent to

tumour. Three samples were from the patients cohort that was used in the microarray (
Figure 3.10), and three samples were from an independent patient cohort (Figure 3.11). From both cohorts, miR-619-5p and miR-4793-3p seem to have higher expression in the 5-ALA/+ than in the 5-ALA/- cell population. miR-215-3p and miR-330-3p, however, were predominantly expressed in the 5-ALA/- cell population. This was true in all patients except for patient 31, who showed particularly high expression of miR-215-3p in the 5-ALA/+ cell population. miR-4440 showed inconsistent results, but four out of the six patients showed higher levels in the 5-ALA/- cell population, when compared with the 5-ALA/+ cells (
Figure 3.10 and Figure 3.11).

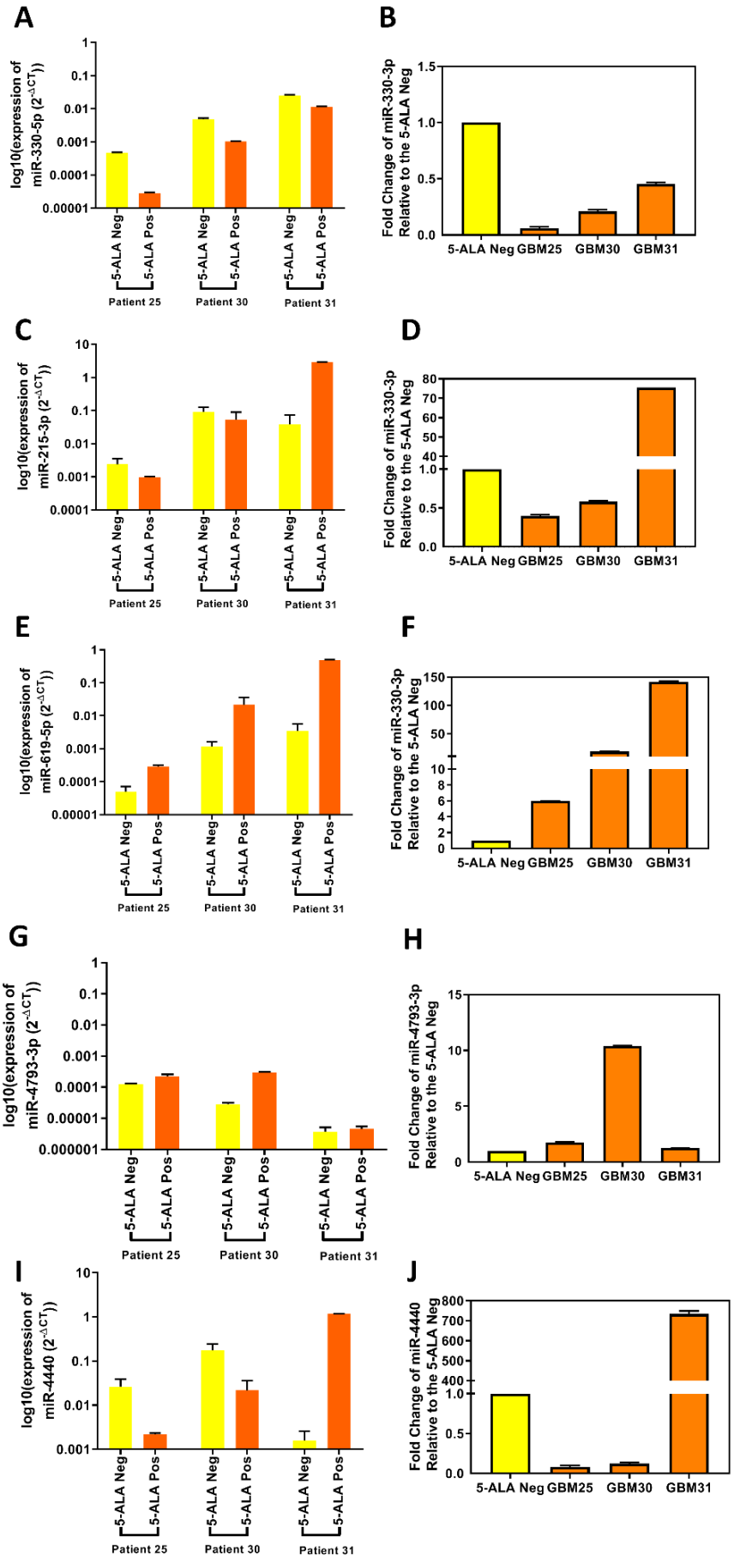

A
log10(expression of miR-330-5p ($2^{-\Delta CT}$))
1
0.1
0.01
0.001
0.0001
0.00001
5-ALA Neg
5-ALA Pos
Patient 25
Patient 30
Patient 31
B
Fold Change of miR-330-3p Relative to the 5-ALA Neg
1.5
1.0
0.5
0.0
5-ALA Neg
GBM25
GBM30
GBM31
C
log10(expression of miR-215-3p ($2^{-\Delta CT}$))
10
1
0.1
0.01
0.001
0.0001
D
Fold Change of miR-330-3p Relative to the 5-ALA Neg
80
70
60
50
40
1.0
0.5
0.0
E
log10(expression of miR-619-5p ($2^{-\Delta CT}$))
0.00001
F
Fold Change of miR-330-3p Relative to the 5-ALA Neg
150
100
50
10
8
6
4
2
0
G
log10(expression of miR-4793-3p ($2^{-\Delta CT}$))
0.000001
H
Fold Change of miR-4793-3p Relative to the 5-ALA Neg
15
10
5
0
I
log10(expression of miR-4440 ($2^{-\Delta CT}$))
0.001
J
Fold Change of miR-4440 Relative to the 5-ALA Neg
800
700
600
500
400

Figure 3.10: qRT-PCR validation of miRNA expression reported by microarray in the FACS analysed samples.
FACS (+ve) and (-ve) correspond to 5-ALA/+ and 5-ALA/- cells. The numbers 25, 30, and 31 label the different patients. Log of expression values for invasive margin region, sorted into 5-ALA/+ and 5-ALA/- cell regions (left panel) and the fold change of the expression value in 5-ALA/+ relative to 5-ALA/- cell population are shown for (A,B) miR-330-5p, (C,D) miR-215-3p, (E,F) miR-619-5p, (G,H) miR-4794-3p, and (I,J) miR-4440. The numbers 25, 30, and 31 label the different patients. Error bars represent standard error of three technical repeats.

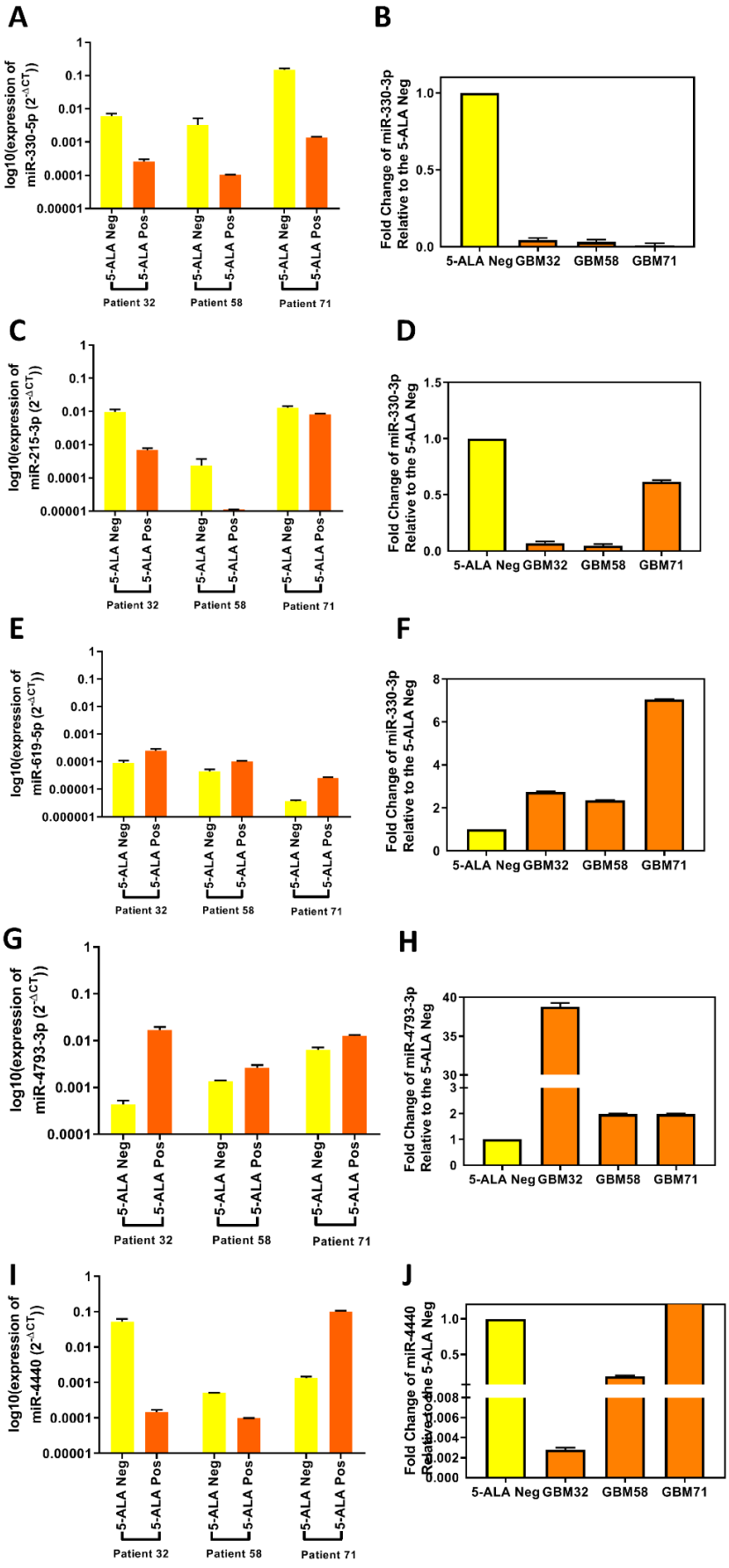

A
log10(expression of miR-330-5p (2-ΔCT))
1
0.1
0.01
0.001
0.0001
0.00001
5-ALA Neg
5-ALA Pos
Patient 32
Patient 58
Patient 71
B
Fold Change of miR-330-3p Relative to the 5-ALA Neg
1.0
0.5
0.0
5-ALA Neg
GBM32
GBM58
GBM71
C
log10(expression of miR-215-3p (2-ΔCT))
D
Fold Change of miR-330-3p Relative to the 5-ALA Neg
1.5
1.0
0.5
0.0
E
log10(expression of miR-619-5p (2-ΔCT))
0.000001
F
Fold Change of miR-330-3p Relative to the 5-ALA Neg
8
6
4
2
0
G
log10(expression of miR-4793-3p (2-ΔCT))
H
Fold Change of miR-4793-3p Relative to the 5-ALA Neg
40
35
30
3
2
1
0
I
log10(expression of miR-4440 (2-ΔCT))
J
Fold Change of miR-4440 Relative to the 5-ALA Neg
1.0
0.5
0.008
0.006
0.004
0.002
0.000

Figure 3.11: qRT-PCR validation of miRNA expression reported by microarray in an independent GBM patient cohort in the FACS analysed invasive margin samples.
FACS (+ve) and (-ve) correspond to 5-ALA/+ and 5-ALA/- cells. The numbers 32, 58, and 71 label the different patients. Log of expression values for invasive margin region, sorted into 5-ALA/+ and 5-ALA/- cell regions (left panel) and the fold change of the expression value in 5-ALA/+ relative to 5-ALA/- cell population (right panel) are shown for (A,B) miR-330-5p, (C,D) miR-215-3p, (E,F) miR-619-5p, (G,H) miR-4794-3p, and (I,J) miR-4440. Error bars represent standard error of three technical repeats.

3.2.3.4 Comparison of miRNA expression in 5-ALA sorted invasive margin samples and unsorted tumour regions

Because each patient sample was ran on the same PCR plate for all the regions and the 5-ALA/+ and 5-ALA/- cell populations of the invasive edge, it is possible to compare the 5-ALA sorted cell populations from the invasive margin with their corresponding unsorted core, rim and invasive margin regions (Figure 3.12). The comparison showed that the expression pattern of miR-330-5p, where it is higher in the invasive edge than in the core and rim regions, has been lost when the invasive edge sample was sorted into 5-ALA/+ and 5-ALA/- cell populations. As such, the 5-ALA/+ cell population showed lower expression of miR-330-5p than the core and rim regions while

the expression of miR-330-5p was higher in the 5-ALA/- cell population when compared to the 5-ALA/+ cell population.

On the other hand, miR-215-3p maintained its expression patten after the sorting of the invasive margin. Except for patient 58, the 5-ALA/+ cell population had higher expression than in the core and the rim. However, for all patients except patient 31, miR-215-3p had low expression in the 5-ALA/- than in the 5-ALA/+ cell population. In the case of the three miRNAs that were expressed at higher levels in the core and the rim than the unsorted invasive edge, only miR-619-5p and miR-4793-3p preserved their expression pattern after invasive edge sorting.

Although still low in the unsorted invasive margin and the 5-ALA/+ cell population compared to the core and the rim, miR-619-5p expression was higher in the 5-ALA/+ cell population than in the unsorted invasive margin region for all patients except for patients 58 and 71. Nevertheless, miR-619-5p was expressed at higher levels in the 5-ALA/+ cell population than in the 5-ALA/- cell population.

In the case of miR-4793-3p, both 5-ALA/+ and 5-ALA/- cell populations express it at higher levels than the unsorted invasive margin except for patient 31; yet, the expression of miR-4793-3p is still lower in the 5-ALA/+ cell population than in the core and rim regions. In all cases, 5-ALA/+ shows higher expression of miR-4793-3p than 5-ALA/- cell population.

miR-4440 is no longer down-regulated in the invasive margin, and is expressed more in the 5-ALA/+ (and 5-ALA/-) cell populations than it is in the core and the rim regions.

In summary, the sorting of the invasive margin shows miRNA expression in the 5-ALA enriched (5-ALA/+) cell population which is representative of the infiltrating tumour cell population in the invasive margin; although the sorting approach has many limitations as discussed in the general discussion section. I found that the microarray expression pattern for all miRNA were validated by qRT-PCR in the unsorted regions. However, after sorting the invasive margin region based on 5-ALA, only miR-619-5p and miR-4793-3p were expressed in 5-ALA/+ cell population and that expression levels was lower than their expression in the rim and core regions. miR-330-5p, on the other hand, was expressed higher in the core and rim regions

than in the 5-ALA/+ cell population; a pattern that is opposite to that seen from the unsorted invasive margin region. Although miR-215-3p was expressed higher in the 5-ALA/+ cell population than in the core and rim regions as expected from looking at the unsorted invasive margin, its expression was higher in the 5-ALA/- than in te 5-ALA/+ cell population. Moreover, based on the microarray data of the unsorted regions, miR-215-3p expression was indifferent between the tumour regions in three out of six patients. Finally, the expression of miR-4440 is somewhat inconsistent in the 5-ALA/+ and 5-ALA/- cell populations. Four out of six patients showed that miR-4440 is expressed higher in the 5-ALA/- than in the 5-ALA/+ population; nevertheless, all patients showed higher miR-4440 expression in the 5-ALA/+ cells than in the rim and core region; which is an expression pattern that is opposite to than seen from comparing the unsorted regions.

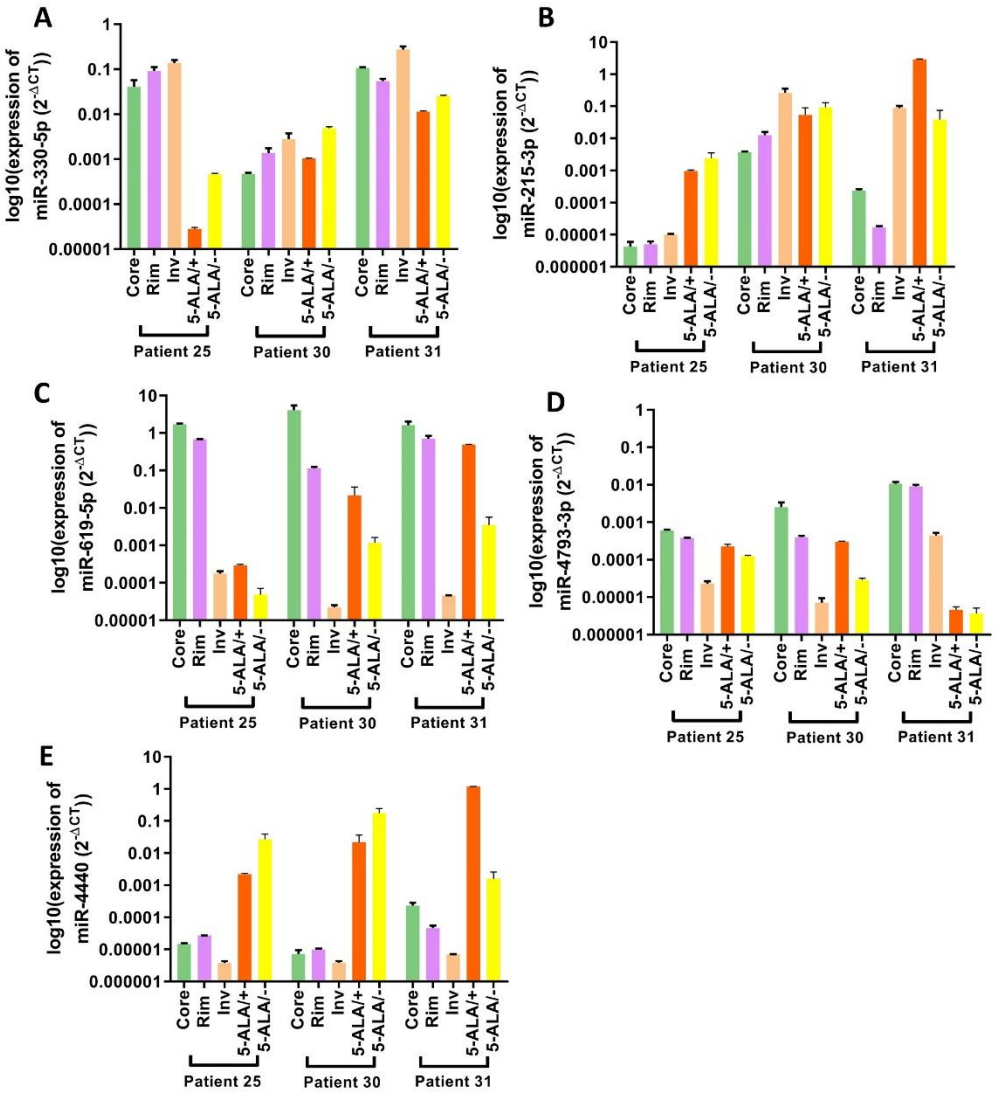


Figure 3.12: 5-ALA cell population compared to tumour core and rim for patients 25, 30, and 31.

Log of expression values for each tumour regions (left panel) and the fold change of the expression value in each region relative to the core region (right panel) are shown for (A,B) miR-330-5p, (C,D) miR-215-3p, (E,F) miR-619-5p, (G,H) miR-4794-3p, and (I,J) miR-4440. The numbers 25, 30, and 31 label the different patients. Error bars represent standard error of three technical repeats.

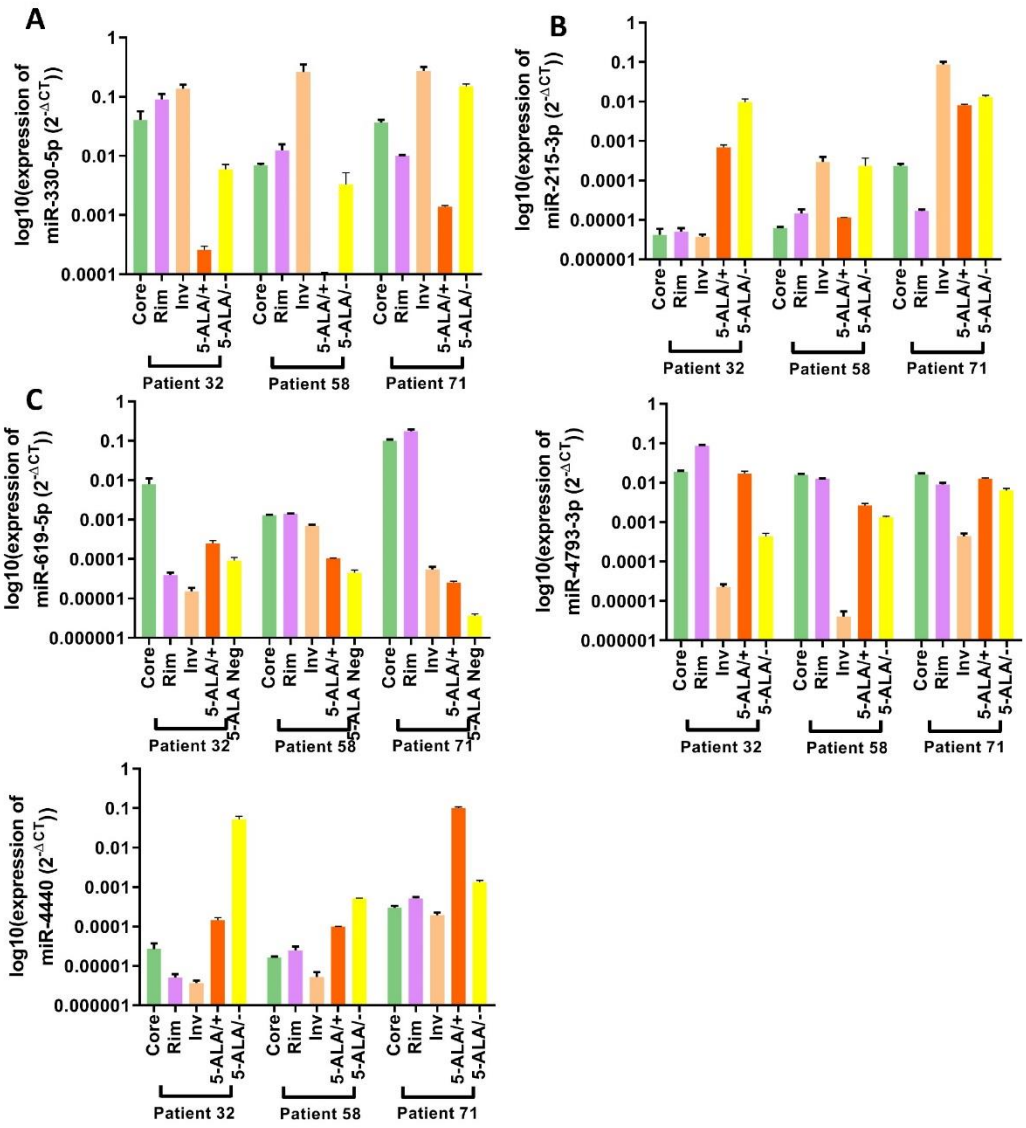


Figure 3.13: 5-ALA cell population compared to tumour core and rim for patients 32, 58, and 71

Log of expression values for each tumour regions (left panel) and the fold change of the expression value in each region relative to the core region (right panel) are shown for (A,B) miR-330-5p, (C,D) miR-215-3p, (E,F) miR-619-5p, (G,H) miR-4794-3p, and (I,J) miR-4440. The numbers 25, 30, and 31 label the different patients. Error bars represent standard error of three technical repeats.

3.2.4 Selection of miRNAs to be taken forward for functional analysis

Since this project aims to understand the features that distinguish the invasive margin cells from the tumour bulk (core and rim regions), only miRNAs that are predominantly expressed in the 5-ALA/+ tumour cell population, as opposed to the 5-ALA/- non-neoplastic cells population, of the invasive margin region will be taken forward for functional analysis.

Although the analysis of the microarray data from 15 patients identified five miRNAs to be significantly differentially expressed between the different regions of the GBM tumour, the qRT-PCR data from six patients showed that the expression signals of only miR-619-5p and miR-4793-3p were predominantly present in the 5-ALA/+ tumour cells when compared to the ALA/- non-neoplastic cells. Moreover, when 5-ALA/+ samples from each patient were compared to their corresponding core and rim samples, miR-619-5p and miR-4793-5p were consistently observed to be downregulated in the 5-ALA/+ tumour cells relative to the core and rim.

It is important to note that inter-patient heterogeneity introduces variability in the magnitude of fold change in miRNA

expression between regions, which obscured statistical significance when comparing the average miRNA expression in each regions with one another. Therefore, I relied on the individual miRNA expression values for each region from each patient sample to determine the overall pattern of miRNA expression change. Both miR-619-5p and miR-4793-3p were found to be expressed at lower levels in the invasive margin relative to the tumour core/rim regions, which matches the pattern seen from comparing 5-ALA/+ samples to core and rim samples.

Thus, I decided to take miR-619-5p and miR-4793-3p forward for functional analysis.

3.2.5 miRNA expression in primary and commercial cell lines, according to microarray and qRT-PCR.

Since GBM cells will be used as *in vitro* tumour models for miRNA functional analysis, it was crucial to assess the expression levels of miR-619-5p and miR-4793-3p in commercial GBM cell lines and in primary cells derived from different tumour regions to identify the most suitable cell model. I used the same house-keeping miRNAs (miR-361-5p and miR-191-5p) as endogenous controls (Figure 3.14).

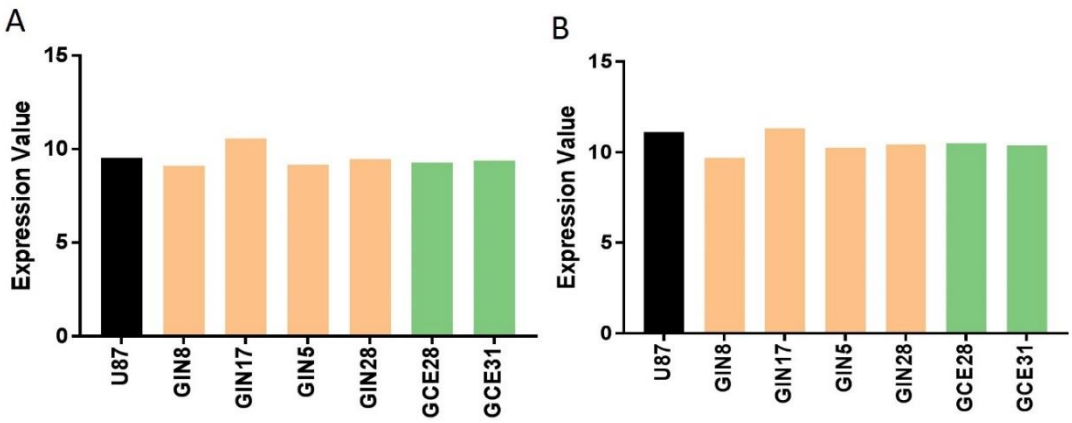


Figure 3.14: Expression of housekeeping miRNAs: (A) hsa-miR-361-5p and (B) hsa-miR-191-5p across GBM cell lines.
The absence of error bars is due to the fact that each sample was run once only on the microarray, and thus, each bar represents one expression value. Black bar corresponds to U87 (commercial cell line). Green and yellow bars correspond to primary cells derived from the core (GCE) and invasive margin (GIN) tumour regions, respectively.

I focused my analysis on the only paired cell line that I had available at this point in the project, GCE28 and GIN28. These cell lines were derived from the core and the invasive margin regions from the same patient (patient 28). From the microarray (Figure 3.15), the expression levels of all five miRNAs seem to be similar between cell lines, even for primary cell lines derived from two different regions (core-derived and invasive edge-derived cell lines). In line with the microarray expression data, qRT-PCR results also showed that almost all miRNAs, except miR-4440, showed indistinguishable expression

levels between all cell lines, including GCE28 and GIN28 (Figure 3.15).

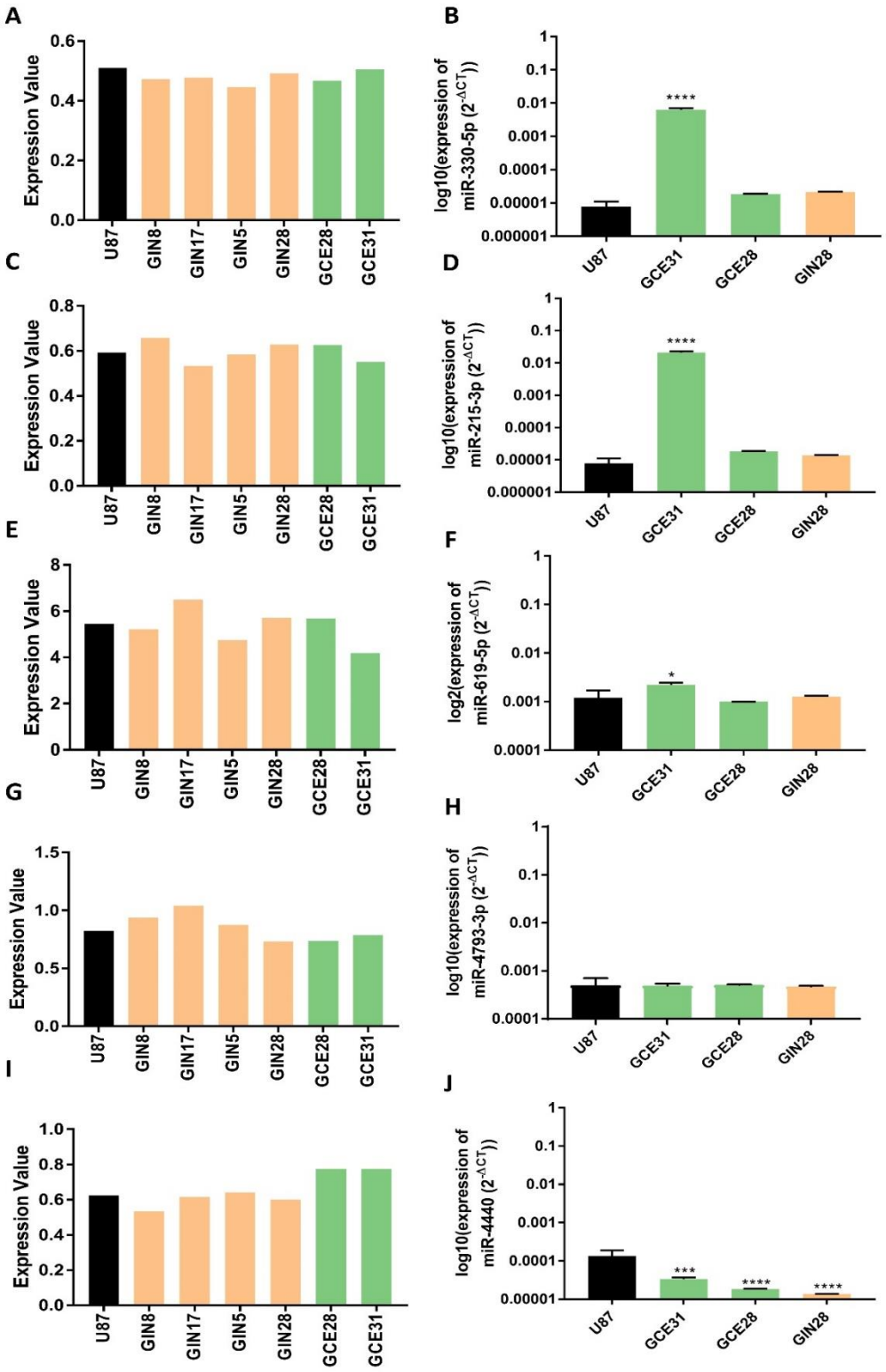


Figure 3.15: Expression of miRNAs in GBM cell lines by microarray (left panel) and by qRT-PCR (right panel). *The absence of error bars is due to the fact that each sample was run once only on the microarray, and thus, each bar*

*represents one expression value. Data are shown for (A,B) miR-330-5p, (C,D) miR-215-3p, (E,F) miR-619-5p, (G,H) miR-4794-3p, and (I,J) miR-4440. Black bar corresponds to U87 (commercial cell line). Green and yellow bars correspond to primary cells derived from the core (GCE) and invasive margin (GIN) tumour regions, respectively. Numbers annotate the patient from whom the cell line was derived. Black bars correspond to a commercial GBM cell line. One-way ANOVA was performed followed by Bonferroni post-hoc test; P<0.05 = *, P<0.001 = ***, and P< 0.0001 = ****.*

3.3 Discussion

As far as I am aware, this is the first study reporting profiles of miRNA expression in different regions of the GBM tumour. The two identified and validated differentially expressed miRNAs between the core, rim and invasive margin regions (miR-619-5p and miR-4793-3p) have not been previously recognised as having a role in GBM. miR-619-5p encoding sequence is located within the intragenic region of the slingshot homolog 1 (SSH1) gene (Niwa *et al.*, 2002). High serum miR-619-5p levels have been demonstrated to serve as potential biomarkers for autism spectrum disorder (ASD) (Kichukova *et al.*, 2017). High plasma miR-619-5p also serves as a possible biomarker for prostatic cancer growth and dissemination beyond the prostatic capsule (Knyazev *et al.*, 2016; Shkurnikov *et al.*, 2017). In support of notation of the probable role of miR-619-5p in promoting cancer cell motility, the literature on validated target genes regulated by miR-619-5p has shown the nuclear long non-coding RNA,

metastasis-associated lung adenocarcinoma transcript 1 (MALAT1) to be a target of miR-619-5p in colorectal carcinoma (CC) (Qiu *et al.*, 2016). Moreover, several studies showed that MALAT1, which is upregulated in CC, promotes CC cell proliferation, migration and invasion and is associated with chemoresistance and poor prognosis (Ji *et al.*, 2013, 2014; M.-H. Yang *et al.*, 2015; Li *et al.*, 2017).

miR-4793-3p, on the other hand, is encoded by exon 26 of the cadherin EGF LAG seven-pass G-type receptor 3 (CELSR3) gene. CELSR3 is an adhesion G protein-coupled receptor (GPCR) that is differentially downregulated in mesenchymal GBM compared to the other subtypes, thereby presenting itself as a potential inhibitor of mesenchymal differentiation (Moreno *et al.*, 2017). Again, miR-4793-3p is upregulated in my GBM tumour core samples relative to the rim and invasive margin samples which could be a result of the high expression of its host gene, and this is explored in the forthcoming chapter. miR-4793-3p targets, however, are not well-documented in the literature, with only one study reporting Toll-like receptor 4 (TLR4) as a putative target of the upregulated miR-4793-3p in small bowel tissues of infants with necrotising enterocolitis (NEC) (Ng *et al.*, 2015).

Interestingly, however, both miR-4793-3p and TLR4 were significantly upregulated relative to the control tissues. Yet, their expression was inversely correlated within each of the NEC samples. This alerts us to the possibility that miR-4793-3p alone might not be adequate to regulate its putative targets in GBM, and it may perhaps need a synergic effect of another miRNA. In my case, this miRNA would be miR-619-5p, as both miR-619-5p and miR-4793-3p are expressed at higher levels in the core compared to the tumour periphery.

An intrinsic limitation of the study design to be highlighted was the difficulty in acquiring a sufficient number of control normal brain samples to be included in my microarray. That meant that pair-wise differential expression analysis was carried out on microarray data comparing the difference in the expression profiles of the core, rim and the invasive margin regions, without normalising to the expression levels in the normal brain.

This, however, is not major a disadvantage as it has been previously shown that different expression values and fold changes can be observed in miRNA profiles of GBM depending

on which reference non-neoplastic brain control it has been compared to (Visani *et al.*, 2013).

Another inherent limitation of this study is that invasive margin samples contain a high percentage of non-neoplastic tissue from adjacent to the tumour. Therefore, I carried out FACS analysis in order to separate 5-ALA/+ from 5-ALA/-. I then compared 5-ALA/+ to the core and the rim regions. I would argue that data from samples that have been FACS analysed can be compared to data from samples that have not been FACS analysed. This is based on unpublished data from Dr Rahman's group, who have compared unsorted rim and core regions to FACS sorted invasive edge regions and identified the same set of differentially expressed RNAs as those identified from comparing FACS sorted rim and core to FACS sorted invasive edge; thereby indicating that comparing sorted and unsorted samples is a sound approach that can yield meaningful results (manuscript in press). However, a key limitation of their approach was that they did not compare the RNA expression difference between each FACS sorted invasive edge sample and its unsorted counterpart to identify significant changes to each sample as a results of the FACS analysis process.

When 5-ALA/+ and 5-ALA/- samples were compared, miR-619-5p and miR-4793-3p were predominantly expressed in the 5-ALA/+ cell population. This suggests that these miRNAs are specific to tumour cells. It is worth noting, however, that the 5-ALA/- population is not particularly representative of normal brain. Instead, 5-ALA/- tissue contains a mixture of cell types, such as reactive astrocytes, microglia and T lymphocytes, which could have been somewhat transformed by the influence by the surrounding neoplastic cells (Charles *et al.*, 2011). In addition, there is a likelihood that some 5-ALA/+ leaked through the FACS gating process and contaminated the 5-ALA/- population as a consequence of the constraints on the accuracy of the technique and the efficiency of the protocol. This also explains why there was detectable low levels of miRNA expression in the 5-ALA/- cells.

It was surprising that my patient-derived primary cell lines had the same miRNA expression levels as the commercial U87 cell line. The similarity in expression levels could perhaps be due to fundamental cellular adaptation to culture conditions, evidenced by the distinct miRNA expression profiles of cultured cells from tissue samples. Nevertheless, the results would mean that miRNAs would need to be overexpressed or downregulated

relative to the baseline level to model the miRNA expression pattern in the different regions of the tumour.

3.4 Future work

An interesting area of future work is that which explores the mechanisms that drive the higher expression of miR-619-5p and miR-4793-3p in the core/rim regions of the tumour relative the invasive margin regions. Such mechanisms could include hypoxia and/or higher rate of transcription of the miRNA host genes.

3.5 Chapter Summary

- From the analysis of microarray from 15 patients, two miRNAs were found to be significantly upregulated in the invasive margin (miR-330-5p and miR-215-3p) while three miRNAs were significantly downregulated in the invasive margin (miR-619-5p, miR-4440, and miR-4793-3p) compared to the rim and the core regions.
- Following the validation of microarray results by qRT-PCR using six patients (three from the microarray cohort and three from an independent patient cohort), miRNA

expression patterns for the three patients were found to be fairly consistent with those seen from the microarray.

- However, the analysis of miRNA expression in the 5-ALA/+ enriched cell population of the invasive margin region, which could represent the infiltrating tumour cell population, showed that miR-215-3p and miR-330-3p were predominantly expressed in the 5-ALA/- cell population while miR-619-5p and miR-4793-3p were predominantly expressed in the 5-ALA/+ cell population.
- miR-4440 showed inconsistent results, but four out of the six patients showed higher levels in the 5-ALA/- cell population, when compared with the 5-ALA/+ cells.
- When 5-ALA/+ samples from each patient were compared to their corresponding core and rim samples, only miR-619-5p and miR-4793-5p were consistently observed to be downregulated in the 5-ALA/+ cells relative to the core and rim, which is in agreement with the initial microarray analysis.
- miR-330-5p and miR-4440 had expression patterns that were opposite to the expression patterns seen from the microarray analysis of the 5-ALA unsorted invasive margin region.

- Although showed higher expression in the 5-ALA/+ cell population relative to the core and rim regions, miR-215-3p was expressed at lower levels in 5-ALA/+ than in 5-ALA/- cell populations.
- As such, only miRNAs that have predominantly localised expression to the 5-ALA/+ cell population of the invasive margin region are selected for further functional analysis.

Chapter 4:
Evaluation of miR-619-5p and miR4793-3p gene targets in GBM

4.1 Introduction

Identification of miRNA target genes has been a challenge. The most common approach is to use computational algorithms to predict elements within the 3'-UTR of gene transcripts that are complementary to a seed sequence of the miRNA. Because seed pairing may not be sufficient to cause mRNA-miRNA interaction (Didiano and Hobert, 2006), predicted miRNA targets need to be verified experimentally.

There are two major experimental strategies (indirect and direct strategies) for miRNA target validation, to complement the computational miRNA target prediction approach.

The indirect experimental strategy starts with an exogenous expression of a miRNA (gain-of-function) or inhibition of an endogenous miRNA function (loss-of-function). miRNA can be over-expressed by the stable introduction of a miRNA expression construct, typically with a lentiviral vector, or by transient transfection of a given miRNA mimic into a cell type known to express the putative gene target. On the other hand, specific miRNA function can be inhibited by anti-miR oligonucleotides in cells that express the mature miRNA at high levels (Stenvang *et al.*, 2012).

Following the modulation of the expression of the miRNA of interest, either gene-specific or high-throughput techniques are often employed to identify its targets. The gene-specific technique investigates the effect of the ectopically expressed miRNA on the mRNA level by qRT-PCR or Northern blot and on the protein level by Western blot, ELISA or immunocytochemistry. However, if antibodies are not available for a particular protein target, then functional assays such as enzymatic assays can be employed.

The high-throughput technique provides a large-scale identification of the effect of the miRNA on regulating a complex gene network. It explores the effect of manipulating the expression of a single miRNA on gene and protein expression profile by microarray or RAN-Seq and proteomic analysis, respectively. Proteomic analysis identifies and quantifies the relative mass of proteins by mass spectrometry following either stable isotope labelling with amino acids in cell culture (SILAC), where samples are labelled with different isotopes, or two-dimensional differentiation in-gel electrophoresis (2D-DIGE), where two samples labelled with different fluorescent dyes are run on a single gel. Proteomic analysis is limited in its depth of

coverage compared to gene expression analysis, but this should become less problematic as the resolution of the technology improves (Chen, Hou and Liu., 2015).

Although it may assist in describing predominate genes and pathways affected by a miRNA, the indirect experimental strategy cannot distinguish between direct and secondary miRNA targets. Secondary miRNA targets are often affected indirectly by the change in the expression of the direct miRNA target.

The direct experimental strategy, on the other hand, confirms the existence of a miRNA–mRNA binding through one of two techniques.

The first technique is to isolate the miRNA–mRNA duplexes and identify the target genes either by microarray or RNA-seq. There are four methods that are widely used for the isolation of miRNA–mRNA duplexes: (1) to transfect cells with biotinylated miRNA duplexes and use streptavidin beads to pull down mRNAs bound to that specific miRNA; however, (the effect of biotin tag on miRNA binding is unclear (Ørom and Lund, 2007), (2) to ectopically express epitope-tagged Argonaute (AGO2 or

AGO1) together with the miRNA mimic, then use an antibody against the epitope tag to pull down the AGO proteins and its associated miRNA–mRNA duplexes (Karginov *et al.*, 2007); however, the interaction between the miRNA–mRNA and the

AGO proteins must be stable enough to survive the immunoprecipitation process (Mili and Steitz, 2004), (3) to use UV irradiation is used to crosslink miRNA–mRNA duplexes to AGO proteins prior to immunoprecipitation (aka cross-linking immunoprecipitation or CLIP); however the efficiency of UV crosslinking is low (Chi *et al.*, 2009), (4) to incubate cells with a photoactivatable nucleoside, such as 4-thiouridine, which gets incorporated into the RNA of the cells and causes thymidine (T) to cytidine (C) transitions at the site of crosslinking near the centre of the AGO–miRNA–mRNA complex (aka photoactivatable-ribonucleoside-enhanced crosslinking and immunoprecipitation - PAR-CLIP) (Hafner *et al.*, 2010).

The second technique is to use luciferase reporter system to evaluate the effect of miRNA binding to the 3'UTR of its putative target (Jin *et al.*, 2013).

First, the entire sequence of the 3'UTR of the target gene of interest is cloned immediately downstream of the open reading

frame sequence of the luciferase reporter gene contained in a plasmid vector (Figure 4.1). The reporter vector is then transiently co-transfected with a miRNA mimic, or a non-targeting control, into a host cell that does not endogenously express that particular miRNA. Alternatively, for cells that endogenously express high levels of the miRNA, just the reporter vector is transfected, along with a control experiment whereby a vector containing a mutant version of the 3'UTR is transfected. The binding of miRNA to the wild-type 3'UTR will repress the reporter protein expression; thereby reducing the activity (bioluminescence) that can be measured (usually after 48hrs) and compared to the control (Jin *et al.*, 2013). However, often the transcription from the promoter contained in the vector is too strong, resulting in the endogenous miRNA is not being able to mediate detectable repression. Therefore, miRNA mimics are commonly used in the luciferase reporter assay.

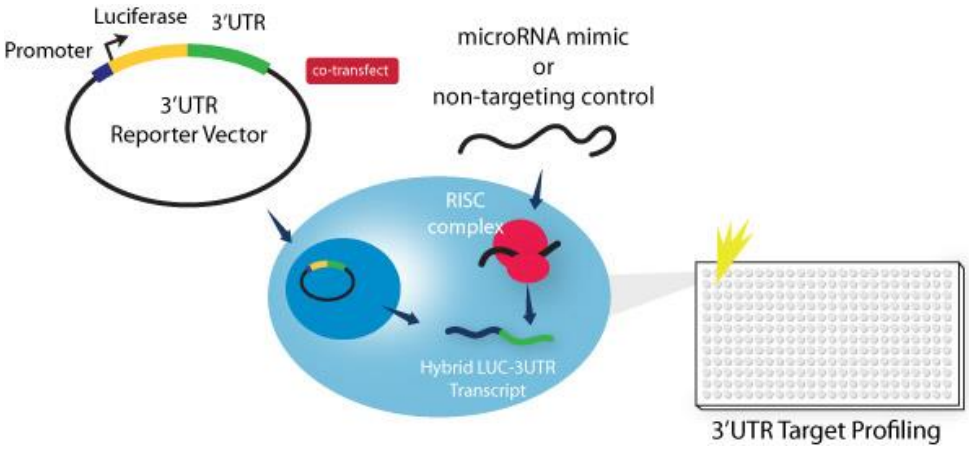


Figure 4.1. Luciferase reporter system.
The putative 3' UTR of a gene target is cloned downstream of the luciferase gene under the control of a constitutive promoter. Figure was taken from SwtichGear Genomics.

Although the ability of miRNAs to repress translation of the reporter gene confirms the physical interaction with the target 3'UTR, the transfection of supra-physiological concentrations of a miRNA may force the two molecules with complementary surfaces to engage in non-physiological interactions. As such, evaluating the effects of miRNAs on their putative target expression in the relevant tissue will provide physiologically relevant information.

In this chapter, gene targets for miR-619-5p and miR4793-3p will be predicted using computational prediction algorithms. Next, these targets will be validated experimentally, following the overexpression of miRNAs using synthetic mimic (a double-stranded RNA oligonucleotide chemically enhanced to

preferentially load RISC) and knockdown using a hairpin inhibitor (a single-strand RNA oligonucleotide designed to bind and to sequester the complimentary the mature miRNA strand).

In addition, universal non-targeting mimic/inhibitor negative controls (an identically designed and modified mature sequences based on Cel-miR-67 which have minimal sequence identity with miRNAs targets in human) will be used to distinguish mimicry/inhibitory effect from background effect. I will then evaluate the mRNA expression (by PCR which requires low amounts of starting material and is quick and relatively cheap) and the protein expression (by Western blot which is readily available) of some putative targets for mir-619-5p and miR4793-3p. I will also validate the physical interaction between miRNA and mRNA by luciferase assay. Finally, I will evaluate the mRNA and protein expression of the validated targets in multi-regional tumour patient samples.

Hypothesis: *Gene targets for miR-619-5p and miR4793-3p will have an opposite expression to miR-619-5p and miR4793-3p expression, and thus will be downregulated in the core (or upon miR-619-5p/miR4793-3p overexpression) and upregulated in*

the invasive margin and 5-LAL/+ (or following miR-619-5p/miR4793-3p knockdown).

4.2 Results

4.2.1 Optimisation of miRNA transient transfection conditions in a commercial GBM cell line

Although potentially clinically relevant miRNAs were selected based on findings from patient samples, the functional work must first be carried out in a model cell line before it is validated in patient samples.

Since the baseline expression difference for my miRNAs of interest between commercial and primary cell lines was insignificant, I decided to select the commercial cell, U87, to be used as an initial model due to the ease of handling and the availability of literature on its biological behaviours U87 (> 3000 citations in PubMed). Subsequently, the work optimised in U87 was replicated in a primary low passage cell line, GIN28, in order to validate the findings in a cost-efficient manner.

4.2.1.1 Optimisation of transfection reagent cytotoxicity

The manufacturers' protocol for transfecting U87 cell line using DharmaFECT ™ – a standard transfection reagent used for miRNA – was tested to determine whether re-optimisation is required. First, PrestoBlue cell viability assay was used to assess the potential cytotoxicity of the transfection reagent. The fluorescence signal of PrestoBlue is proportional to the level of metabolic activity in the cell and is often used as a relative measure for cell number or viability.

As per the manufacturers' recommendation for the U87 cell line, the transfection reagent should be used as 1:100 dilution of the transfection mixture's volume (which itself is 1:10 of the final volume) with a cell concentration of 3.125×10^4 cells/ml.

Here, I tested the 1:100 dilution (0.1µl in 10µl transfection mixture's volume) and two additional dilutions 1:67 and 1:50 (0.15µl and 0.2µl in 10µl transfection mixture's volume) of the transfection reagents with 3.125×10^4 cells/ml (2.5×10^3 cells per well) seeded in 96-well plate for 24h. Control wells were prepared in parallel where cells were not treated with the transfection reagent (untreated control).

The minimal cytotoxicity was seen with the 1:100 dilution of the transfection reagent, where the viability of the treated cells was comparable to the untreated control (Figure 4.2). Thus, it was concluded that the manufacturers' recommended regent volume of 0.1µl is the least cytotoxic.

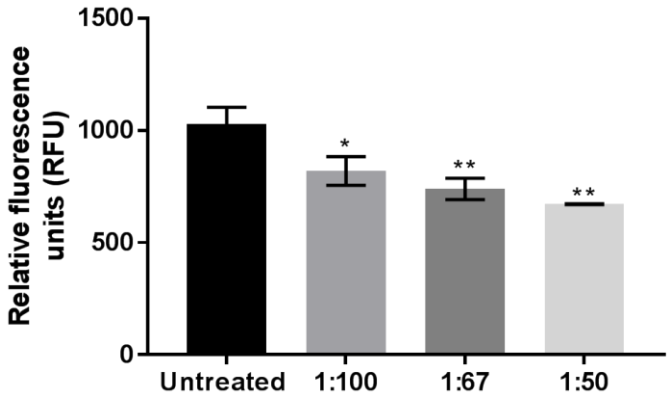


Figure 4.2. Comparison of U87 cell viability using PrestoBlue to assess the cytotoxicity of different dilutions of the DharmaFECT ™ transfection reagent after 24h.
Comparison between the conditions was performed by post-hoc analysis using Bonferroni's multiple comparisons test following the one-way ANOVA test; (*) p-value < 0.01; (**) p-value < 0.001. Each condition was done in three biological repeats (mean ± SEM).

4.2.1.2 Optimisation of transfection efficiency

Second, siGLO Green transfection indicator, a fluorescent oligonucleotide duplex that localises to the nucleus and displays a green fluorescence, was transfected into U87 cells to visually

assess the efficiency of transfection under the fluorescent microscope.

The manufacturer recommended using 25-100nM as a final concentration of miRNA mimic/inhibitors. Here, four siGLO Green final concentrations 12.5nM, 25nM, 50nM and 100nM were tested with 3.125 x 10^4 cells/ml (5 x 10^4 cells/well) seeded in 6-well plate for 24h using the 1:100 dilution of the DharmaFECT ™ transfection reagent. Mock-transfection control wells were prepared in parallel where cells were only treated with the transfection reagent containing no siGLO Green (untransfected control).

Two out of the four concentrations had a transfection efficiency of about >80% after 24h (Figure 4.3 and Figure 4.4). These two concentrations (50nM and 100nM) were taken forward to be used for evaluating the optimal functional concentration of miRNA mimics and inhibitors.

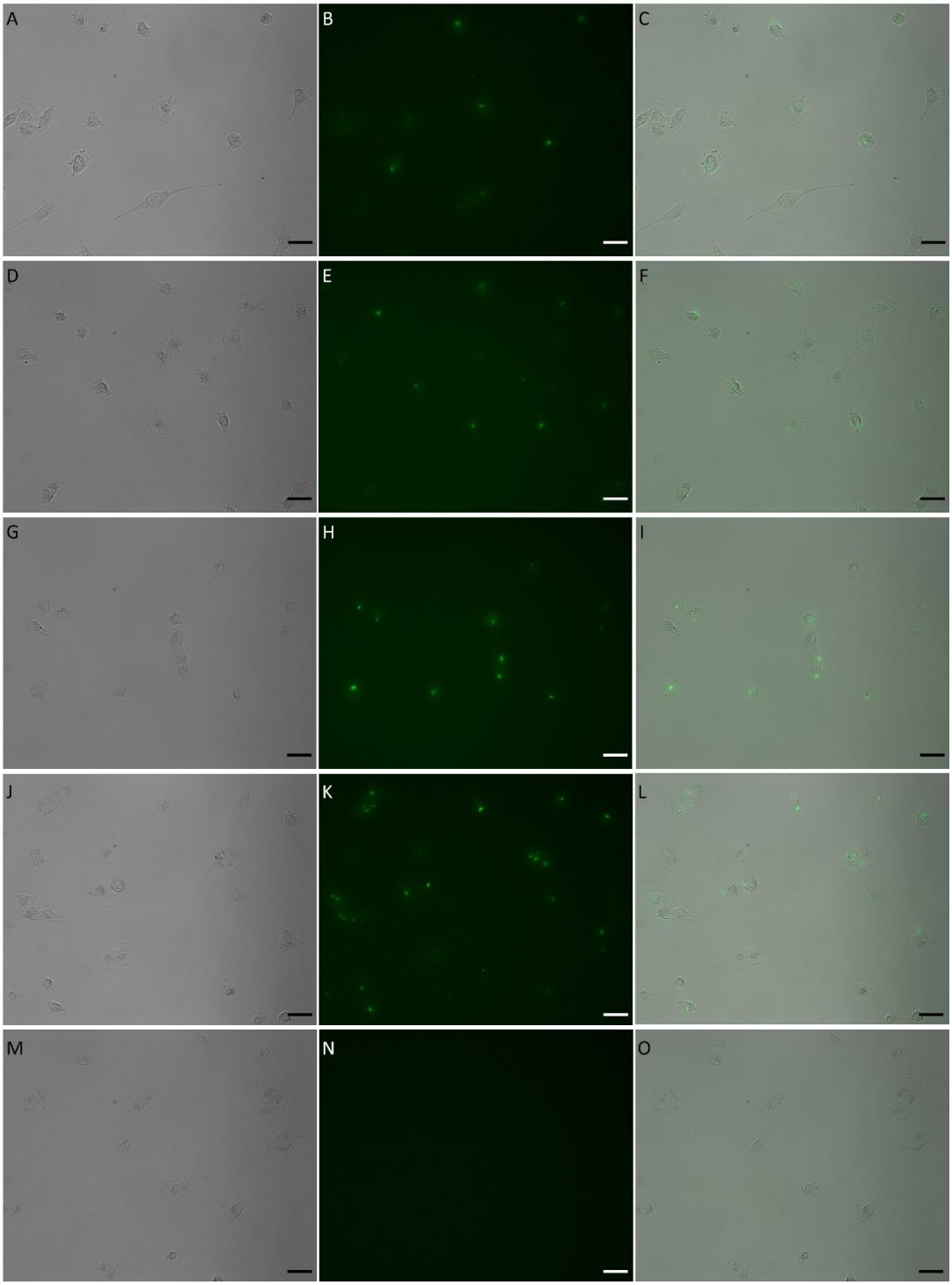


Figure 4.3. U87 cells transfected with siGLO Green for 24h. *Graphs from left-to-right show bright field, FITC, and overlaid images for siGLO Green transfection at (A-C) 12.5nM, (D-F) 25nM, (G-I) 50nM, and (J-L) 100nM. Graphs (M-O) show untransfected control. Images were taken with x20 magnification. The red scale bar at the bottom left indicates a length of 50 μm.*

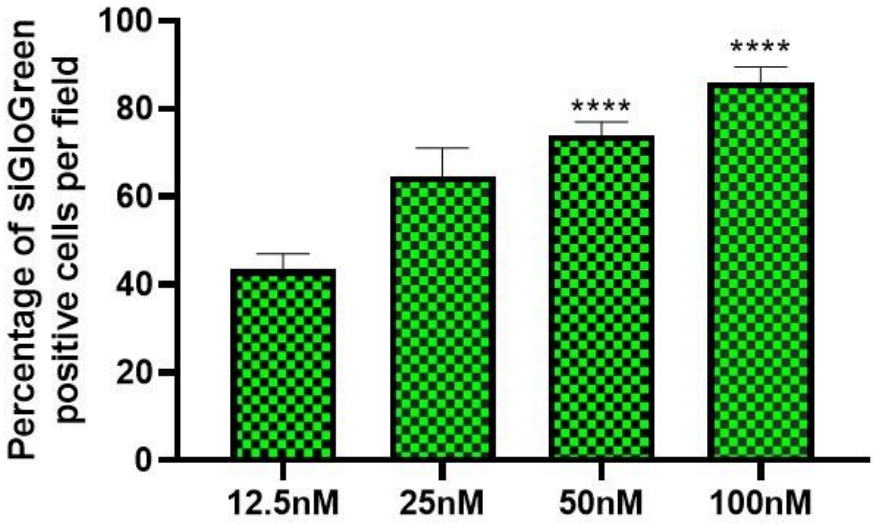


Figure 4.4. Transfection efficiency assessed by counting siGlo Green positive U87 cells.
Statistical testing was performed using one-way ANOVA (P<0.0001) followed by Bonferroni's multiple-comparison test comparing each concentration to the minimum concentration of 12.5nM; (****) p-value < 0.0001. Each transfection was done in three biological repeats (mean ± SEM).

4.2.1.3 Optimisation of functional concentration of miRNA mimics and inhibitors

Finally, qRT-PCR was used to evaluate the expression of the miRNAs after the transfection of mimic or inhibitor. Non-targeting mimic (NT) or inhibitor (Inh-NT) controls were used to account for the effect of transfection on the endogenous miRNA expression.

For miRNA knock-in, miR-619-5p and miR-4793-3p mimics were transfected at the lowest optimal functional concentration of 50nM as determined from siGlo Green transfection for 24h.

qRT-PCR was performed to evaluate the success of the knock-in (Figure 4.5). I achieved comparable knock-in levels in both transfections. Thus, I performed a miR-619-5p and miR-4793-3p mimic co-transfection with 1:1 ratio of each miRNA (50nM of miR-619-5p and 50nM of miR-4793-3p). The co-transfection was performed to account for the possibility that one miRNA alone might not be adequate to downregulate its putative targets, and it may perhaps need a synergic effect of another miRNA. qRT-PCR also showed comparable knock-in levels in the co-transfection.

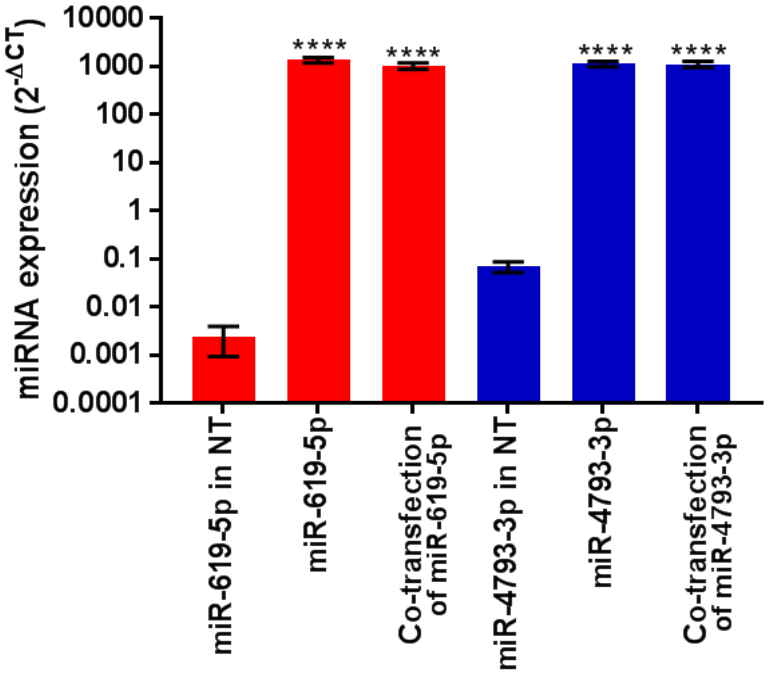


Figure 4.5. miRNA knock-in transfection in U87.
50nM of miR-619-5p or miR-4793-3p mimics were transfected into U87 at, and the expression levels of miR-619-5p or miR-4793-3p were measured by qRT-PCR after 24hrs. The expression level of (red bars) miR-619-5p and (blue bars) miR-4793-3p in U87 transfected with either: non-targeting negative control (NT), miR-619-5p mimic (miR-619-5p), miR-4793-3p

mimic (miR-4793-3p) or co-transfected with both miR-619-5p and miR-4793-3p at 1:1 ratio where 50nM of each miRNA was simultaneously transfected. Co-transfection of miR-619-5p is shown in Red and co-transfection of miR-4793-3p is shown in blue. Each transfection was done in three biological repeats (mean ± SEM). Statistical differences were calculated using one-way ANOVA (P<0.0001) followed by Bonferroni's multiple-comparison test comparing the expression levels of miR-619-5p and miR-4793-3p transfected samples relative to NT; (****) p-value < 0.0001.

For miRNA knock-down, miR-619-5p and miR-4793-3p inhibitors were transfected in the optimal concentration of 50nM, again, as determined from siGLO Green transfection for 24h. However, the inhibitory effect of the miRNA inhibitors was not detectable by qRT-PCR; the CT values were below 38 or gave no readings. In other words, the reading was at the absolute minimum possible value the machine could detect, before the inhibitor was applied. After the inhibitor, the value was too small to be detected by the machine, resulting in null values for all readings. While these null values could be construed as successful inhibition, because the pre-inhibitor values were already so small, I couldn’t calculate the efficiency of knockdown and, therefore, couldn’t be sure that the inhibitor actually worked, and that what I was observing wasn’t simply due to noise in the readings. Thus, I decided not to include a knockdown condition in future experiments. Instead, the relatively low expression of miR-619-5p and miR-4793-3p in

U87s when compared to the mimic treatment will serve as a model for the low expression in the invasive edge cells compared to the tumour core and rim.

4.2.2 Evaluation of miRNA transient transfection conditions in a patient-derived primary GBM cell line.

The optimised transfection conditions were re-tested in a primary GBM cell line. GIN28 was chosen because it: (1) is an invasive margin derived cell line where the expression of both miR-619-5p and miR-4793-3p is inherently low, (2) represents the tumour region of interest for therapeutic targeting, and (3) has practically the same size as U87 and grows stably in cell culture with a comparable growth rate to U87 cells.

The level of miR-619-5p and miR-4793-3p knock-in at 50nM was equivalent to that seen in U87 cells (Figure 4.6). Moreover, I achieved comparable levels of knock-in for each miRNA transfected individually or co-transfected at the ratio of 1:1.

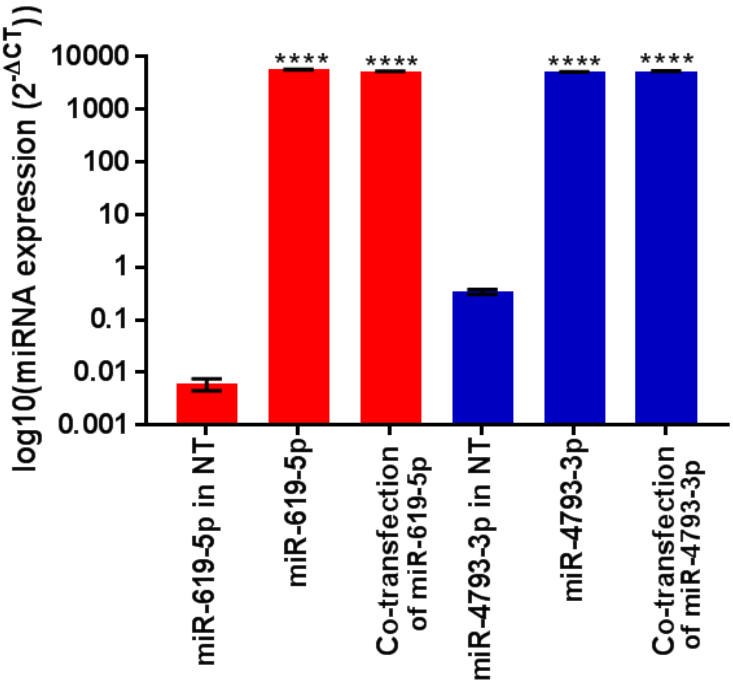


Figure 4.6. miRNA knock-in transfection in GIN28.
50nM of miR-619-5p or miR-4793-3p mimics were transfected into U87 at, and the expression levels of miR-619-5p or miR-4793-3p were measured by qRT-PCR after 24hrs. The expression level of (red bars) miR-619-5p and (blue bars) miR-4793-3p in GIN28 transfected with either: non-targeting negative control (NT), miR-619-5p mimic (miR-619-5p), miR-4793-3p mimic (miR-4793-3p) or co-transfected with both miR-619-5p and miR-4793-3p at 1:1 ratio where 50nM of each miRNA was simultaneously transfected. Co-transfection of miR-619-5p is shown in Red and co-transfection of miR-4793-3p is shown in blue. Each transfection was done in three biological repeats (mean ± SEM). Statistical differences were calculated using one-way ANOVA (P<0.0001) followed by Bonferroni's multiple-comparison test comparing the expression levels of target genes in miR-619-5p or miR-4793-3p transfected samples relative to NT; (****) p-value < 0.0001.

4.2.3 Computational target prediction and pathway analysis

I followed the recommended guidelines for the miRNA target prediction by (Kuhn *et al.*, 2008) and (Ritchie, Flamant and

Rasko, 2009) to short-list predicted targets that are worth validating experimentally. There were five stages for miRNA target prediction according to (Kuhn *et al.*, 2008). First (stage 1), I utilised multiple algorithms since different algorithms often predict distinct miRNA binding sites. Next (stage 2), I ensured that at least two algorithms predicted the same miRNA binding site(s). This is because algorithms often yield a large number of false positives due to the differences in parameters used by each algorithm (Ekimler and Sahin, 2014). Thus, combining results from multiple prediction algorithms is a common approach to minimise false positives. I then (in stage 3), identified instances of multi-targeting where genes are targeted by both miRNAs at the same time. Consequently (stage 4), I compared each overlap with a dataset of experimentally validated targets for each miRNA; however, I am aware that the validated dataset is not very large this step may omit many true targets yet to be validated. Finally (stage 5), I opted to identify groups of genes targeted by the same miRNAs that share a biological function which would help to understand the potential role of these miRNAs.

Thus, computational predictions of miR-619-5p and miR-4793-3p targets were performed using miRWalk 2.0 http://zmf.umm.uni-

heidelberg.de/apps/zmf/mirwalk2/index.html (Dweep and Gretz, 2015), which relies on multiple algorithms to predict the binding of the miRNA seed region and the miRNA recognition elements (mRE) within its target 3'UTR. Each algorithm in miRWalk 2.0 incorporates a set of parameters to calculate a prediction score which is used to shortlist the predicted targets for each miRNA (See Table 2.3 in Chapter 2: Materials and Methods). Targets that were not predicted by at least two algorithms were eliminated. Finally, mutually predicted targets for both miRNAs that are also experimentally validated targets for at least one miRNA were selected (156 targets) (Figure 4.7). Only 18 of these genes were predicted and experimentally validated as targets for both of the miRNAs.

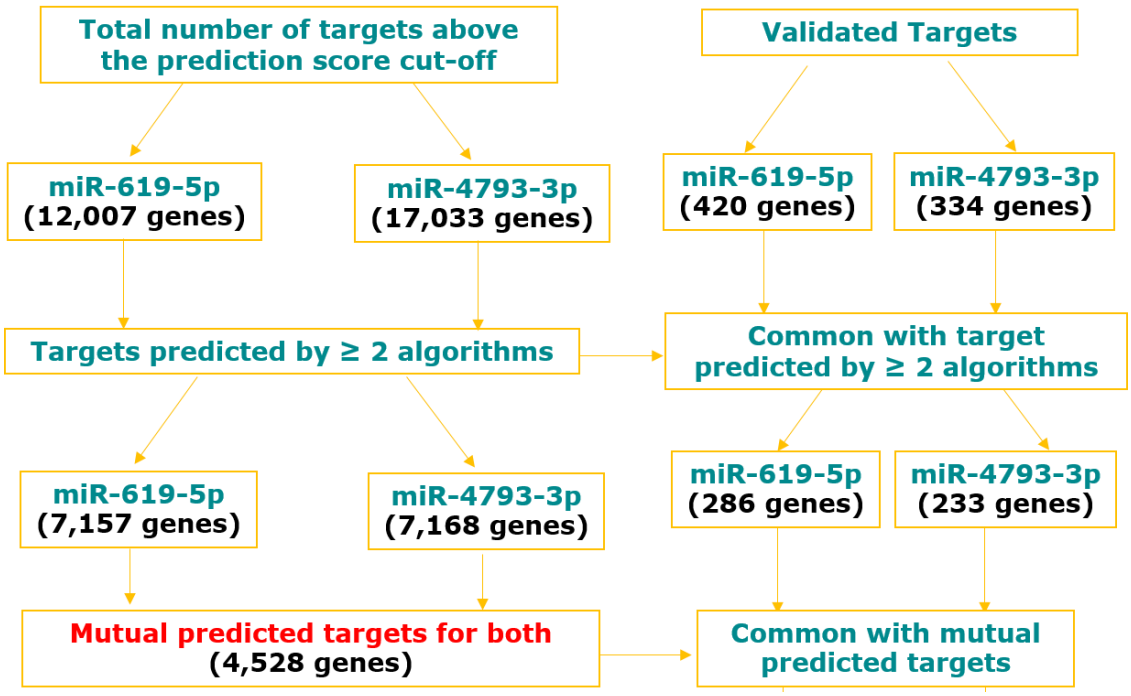


Figure 4.7. Target prediction filtering scheme.
Validated targets of either miR-619-5p or miR-7493-3p that overlapped with mutually predicted targets (156 genes) were taken forward for pathway analysis — targets obtained from miRWalk 2.0.

Because individual miRNAs can simultaneously regulate multiple genes often within the same pathway, pathway enrichment analysis was carried out on the short-listed targets using KEGG2016 database in Enricher (available from: http://amp.pharm.mssm.edu/Enrichr/)(Kuleshov *et al.*, 2016). FA degradation and metabolism and glycerolipid were the most significantly enriched (Figure 4.8 and **Error! Reference source not found.**); therefore, they will be taken forward for further analysis.

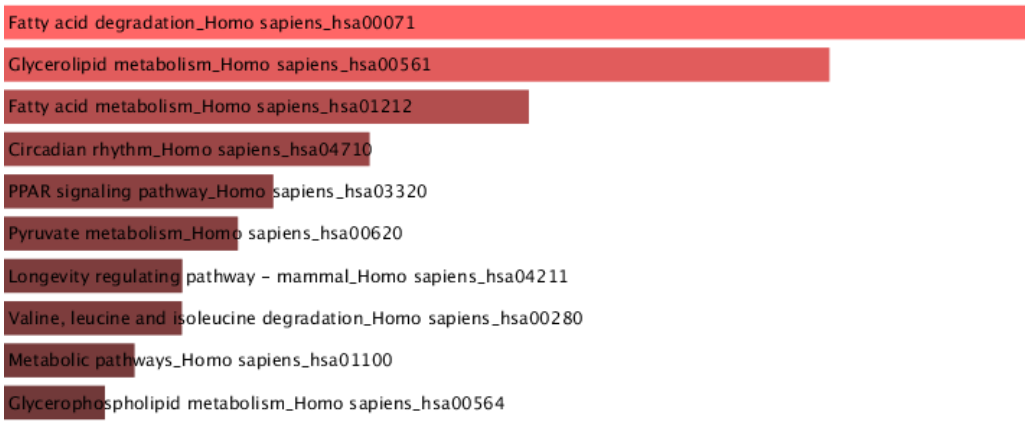


Figure 4.8. Graphical representation of significantly enriched pathways for miR-619-5p and miR-4793-3p targets.

P-values for each matched pathway was calculated from the z-score test (threshold was set to 0.05 following FDR correction). The colour shades from pink to black denotes different levels of statistical significance where pink is highly significant.

Table 4.1 Pathway enriched for the significantly changed metabolites following miRNA transfection.

Fisher's exact test was applied for the over-representation analysis, and Degree Centrality was chosen for the topology analysis. p-values were corrected for multiple comparisons using the false discovery rate (FDR). Abbreviations of significantly enriched genes: DGKH: diacylglycerol Kinase Eta GPD2: glycerol phosphate dehydrogenase 2; ALDH1B1: aldehyde dehydrogenase 1; ALDH9A1: aldehyde dehydrogenase 9; ACOX1: acyl-CoA oxidase 1; CPT2: carnitine palmitoyltransferase 2; LDLR: low density lipoprotein receptor; HILPDA: hypoxia-inducible lipid droplet-associated; GK5: glycerol kinase 5 (putative); ELOVL6: fatty acid elongase 6; ACSBG1: acyl-CoA synthetase bubblegum family member 1; PLIN3: perilipin 3.

	Total pathway gene count	**Hits**	**Raw p value**	**FDR**	**Z-score**	**Combined score**	**Genes**
Fatty acid degradation_hsa00071	44	5	0.00003	0.0042	-1.93	20.2	ALDH1B1;CPT2;ACOX1;ACSBG1;ALDH9A1
Glycerolipid metabolism_hsa00561	59	5	0.00012	0.0087	-1.93	17.4	GK5;HILPDA; DGKH; GDP2; PLIN3
Fatty acid metabolism_hsa01212	48	4	0.00063	0.0307	-1.79	13.2	CPT2;ACOX1;ELOVL6;LDLR
Circadian rhythm_Homo sapiens_hsa04710	30	3	0.00184	0.0675	-1.74	10.9	CREB1;CRY2;CSNK1E

PPAR signaling pathway_hsa03320	69	4	0.00244	0.0716	-1.59	9.6	CPT2;GK;ACOX1;ACSBG1
Pyruvate metabolism _hsa00620	40	3	0.00421	0.1019	-1.66	9.1	ALDH1B1;ACACB; ALDH9A1
Longevity regulating pathway_hsa04211	94	4	0.00735	0.1052	-1.69	8.3	CREB1;FOXO3;EIF4E; ADIPOR2
Valine, leucine and isoleucine degradation_ _hsa00280	48	3	0.00703	0.1052	-1.67	8.3	ACAD8;ALDH1B1; ALDH9A1
Metabolic pathways_ hsa01100	1239	18	0.01238	0.1517	-1.74	7.6	ACAD8;FAHD1;ALG9;GK;AK2;EPT1; MBOAT1;ADO;ACACB;AGMAT;DHODH;ALDH1B1;ACOX1;CYCS;ACSBG1;A4GALT;ALDH9A1;DGKH
Glycerophospholipid metabolism_hsa00564	95	4	0.00762	0.1052	-1.48	7.2	GPD2;EPT1; MBOAT1;DGKH

4.2.4 Validation of putative miR-619-5p and miR-4793-3p targets in U87 cells.

The target genes within the most significantly enriched pathway were validated by qRT-PCR. The expression of these genes was evaluated following the overexpression of miR-619-5p and miR-4793-3p or the co-transfection of both of them, at the ratio of 1:1, because the physiological ratio of the two miRNAs in the core and the rim regions were approximately 1:1 (core was 1.6:1, and rim was 1.2:1).

In addition, I evaluated the expression of MALAT1, which is the only published target of miR-619-5p (see Chapter 3). Although not a gene target (it is a non-coding RNA), the expression of MALAT1 was investigated to see if it would act as a positive control for genuine miR-619-5p targets.

Based on the literature, ectopically transfected miRNAs act after 48h to exert their effect on the mRNA of their target gene, for example (Ru *et al.*, 2016). Thus, I assessed mRNA expression 48h post-transfection.

The mRNA levels of ACOX1 and LDLR genes were repressed by the overexpression of either miR-619-5p and/or miR-4793-3p

mimics in U87 cells, but mRNA levels of ACOX1 were not significantly changed in co-transfection compared to NT (Figure 4.9). Although was repressed upon the overexpression of miR-619-5p, CPT2 was upregulated upon miR-4793-3p overexpression. In the co-transfection, however, CPT2 levels were repressed.

As a general note, miR-619-5p transfected and co-transfected U87 cells showed a similar pattern of gene expression change for most of the putative targets; whereas, only three of the 12 candidate genes showed significant change at the mRNA level in response to the overexpression of miR-4793-3p (Figure 4.9).

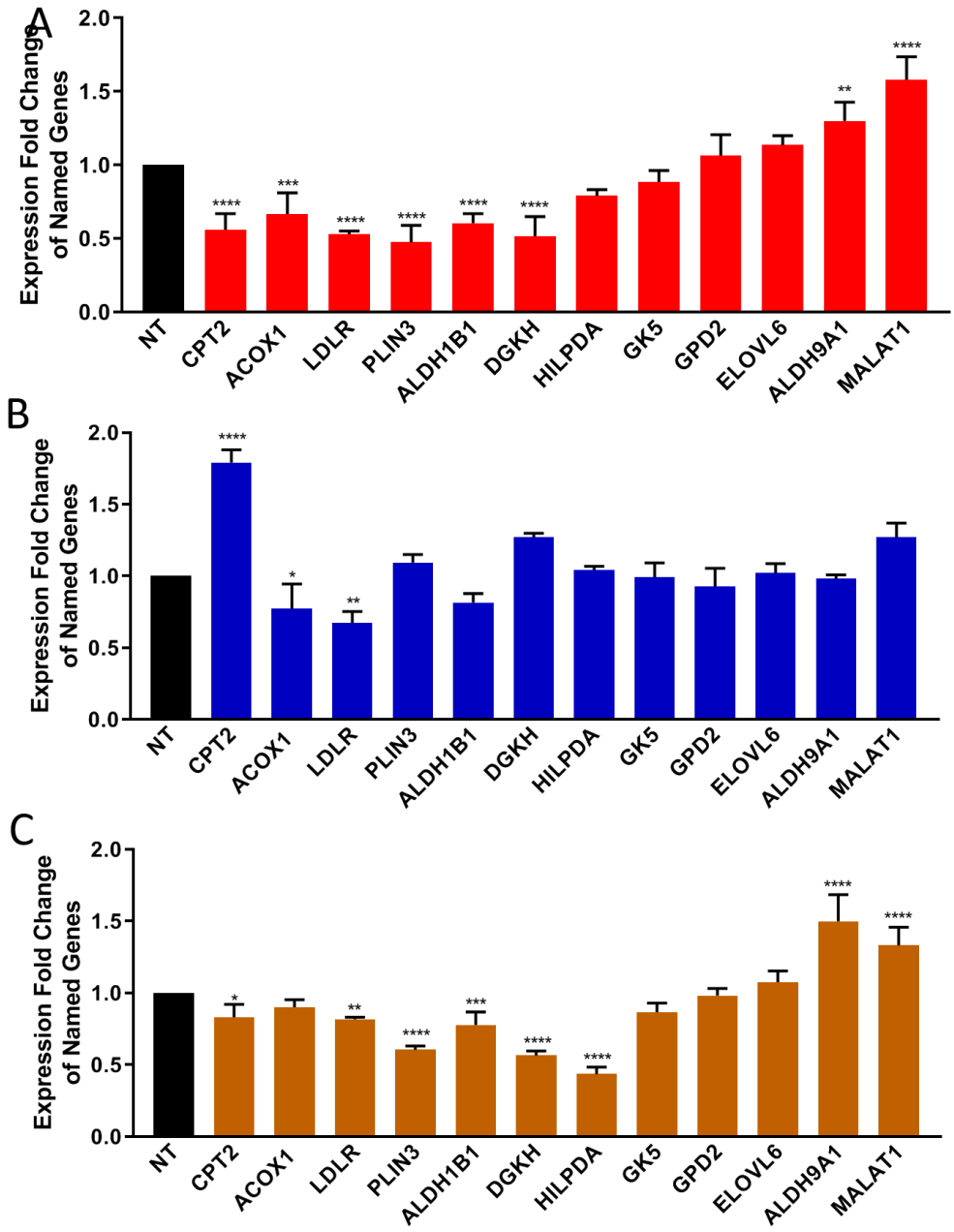


Figure 4.9. mRNA expression of predicted gene targets 48h following miR-619-5p and miR-4793-3p overexpression in U87 cells.

The expression of each genes in the y-axis in U87 cells transfected with 50nM of (A) miR-619-5p, (B) miR-4793-3p or (C) both miR-619-5p and miR-4793-3p at 1:1 ratio is represented as fold change relative to its expression in U87 cells transfected with non-targeting mimic control (NT). Each gene was evaluated in technical triplicates and in three biological

repeats (mean ± SEM). Statistical analysis was performed by post-hoc analysis using Bonferroni's multiple comparisons test following the one-way ANOVA test; (*) p-value < 0.05; (**) p-value < 0.01; (***) p-value < 0.001; (****) p-value < 0.0001; non-significant values were not indicated on the graph.

4.2.5 Selection of a subset of target genes for further analysis

Three genes, CPT2, ACOX1, and LDLR, from the qRT-PCR study, were selected because their expression change was highly significant following miR-619-5p and miR-4793-3p overexpression. Moreover, these genes can act as clinically relevant targets due to their potential drugability by pharmacological inhibitors, such as those that were described in the literature (Burns-Cox *et al.*, 1971; Schmidt-Schweda and Holubarsch, 2000; Holubarsch *et al.*, 2007).

4.2.6 Validation of three putative miR-619-5p and miR-4793-3p targets in GIN28 cells.

The expression of the three selected target genes was assessed in GIN28 following the overexpression of miR-619-5p and miR-4793-3p. qRT-PCR showed that the levels of mRNA for CPT2, ACOX1 and LDLR were significantly repressed miR-619-5p transfected and co-transfected (Figure 4.10). However, miR-4793-3p overexpression in GIN28 cells reduced LDLR but

increased CPT2 transcript levels while no significant change was observed for ACOX1 expression.

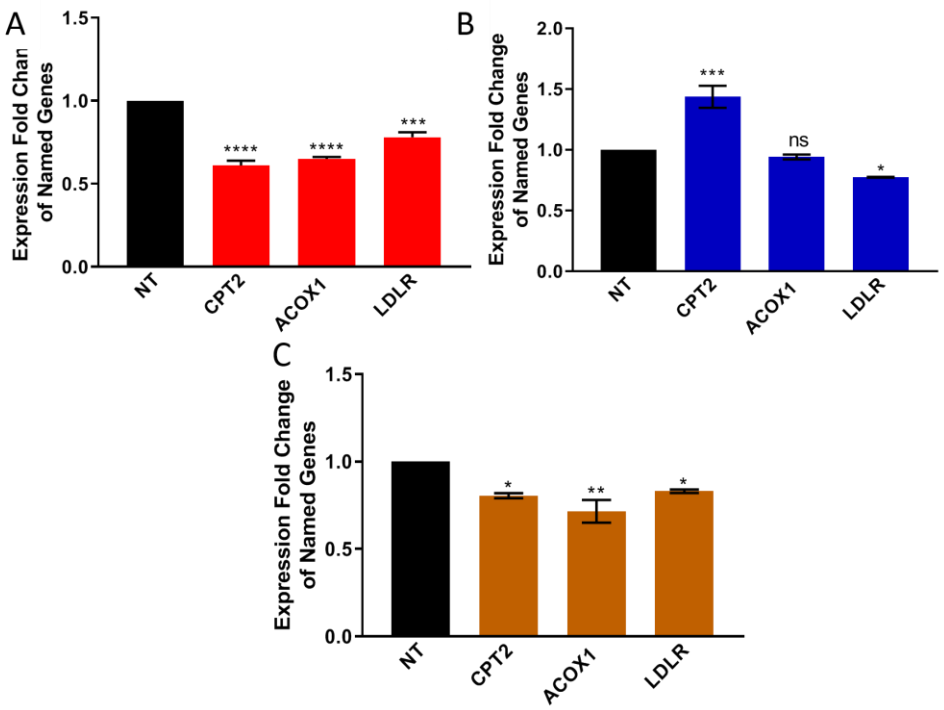


Figure 4.10. mRNA expression of predicted gene targets 48h following miR-619-5p and miR-4793-3p overexpression in GIN28 patient-derived cells.
The expression of each genes in the y-axis in GIN28 cells transfected with 50nM of (A) miR-619-5p, (B) miR-4793-3p or (C) both miR-619-5p and miR-4793-3p at 1:1 ratio is represented as fold change relative to its expression in GIN28 cells transfected with non-targeting mimic control (NT). Each gene was evaluated in technical triplicates and in three biological repeats (mean ± SEM). Statistical differences were calculated using one-way ANOVA followed by Bonferroni's multiple-comparison test comparing the expression levels of miR-619-5p and miR-4793-3p transfected samples relative to NT; (*) p-value < 0.05; (**) p-value < 0.01; (***) p-value < 0.001; (****) p-value < 0.0001; ns: not significant.

4.2.7 Confirming direct physical mRNA-miRNA interaction

I next searched for miR-619-5p and miR-4793-3p target sites in the 3'UTRs of CPT2, ACOX1 and LDLR using TargetScan. LDLR and ACOX1 have conserved miR-619-5p and miR-4793-3p target sites, whereas CPT2 only have conserved miR-619-5p target sites in their 3' UTRs (Figure 4.11).

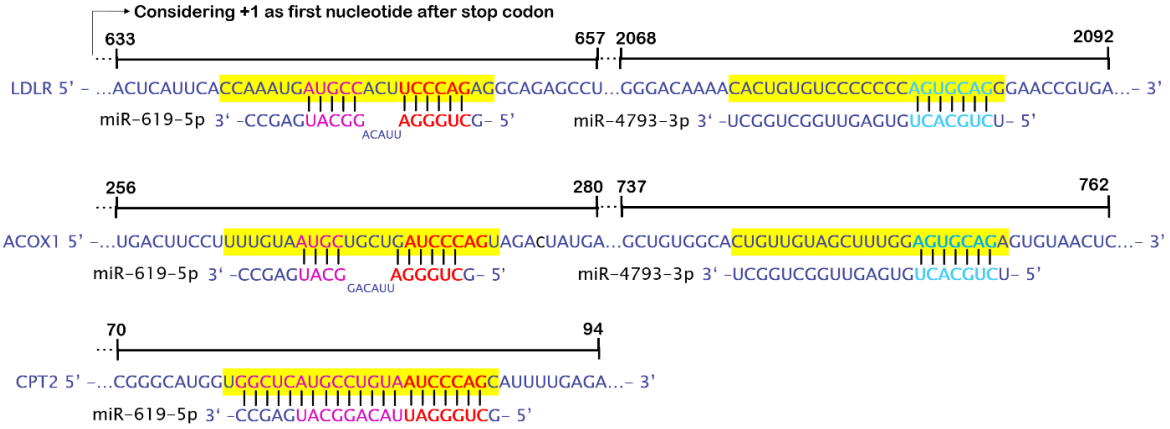


Figure 4.11. Sequence alignment between miR-619-5p or miR-4793-3p and the 3'UTR of CPT2, ACOX1 and LDLR in human from TargetScan.
Solid line: seed match region; Red/Blue: seed region and miRNA recognition element in the 3'UTR for miR-619-5p or miR-4793-3p, respectively; Purple: other bindings between miRNA and the 3'UTR; Dashed lines: omitted nucleotides; nucleotides in small letters in the miRNA sequence are not interacting with the 3'UTR due to secondary structure configuration.

The direct physical mRNA-miRNA interaction was confirmed with luciferase reporter assay. The full-length 3`UTRs of miRNA targets (LDLR, ACOX1 and CPT2) have been cloned into

luciferase reporter vectors. U87 cells were co-transfected with miR-619-5p mimic, miR-4793-3p mimic or NT and either:

1) Target gene reporter vector containing the full human 3'UTR for that target gene.
2) Positive control reporter vector containing synthetic sequence repeats that are fully complementary to miRNA sequence. This was used in order to optimise the efficiency of the co-transfection of the reporter vector with miRNA mimics.
3) One of the negative control vectors:
    I. An empty vector which is the parental luciferase construct that contains no 3`UTR cloned into the luciferase reporter. This was used in order to assess background signal noise in the experiment.
    II. A scrambled negative control reporter vector that contains a random 3' UTR sequence.
    III. A housekeeping control reporter vector contaning the 3'UTR of β-Actin. This was used for normalisation against non-specific binding.

Luciferase activities were measured 48h post-transfection as per manufacturer recommendation. Co-transfection of cells with either empty vector, β-actin 3'UTR vector or scrambled

3’UTRs vector plus the miR-619-5p mimic did not change the expression of the luciferase reporter. Same was seen in co-transfection with miR-4793-3p mimic (Figure 4.12).

I found that miR-619-5p mimic significantly decreased the luciferase activity when co-transfected with the 3’UTRs of CPT2 and ACOX1 while miR-4793-3p showed a strong inhibitory effect only on ACOX1 3-UTR-luciferase activity. Co-transfection with NT had no effect on luciferase activity in 3’UTRs.

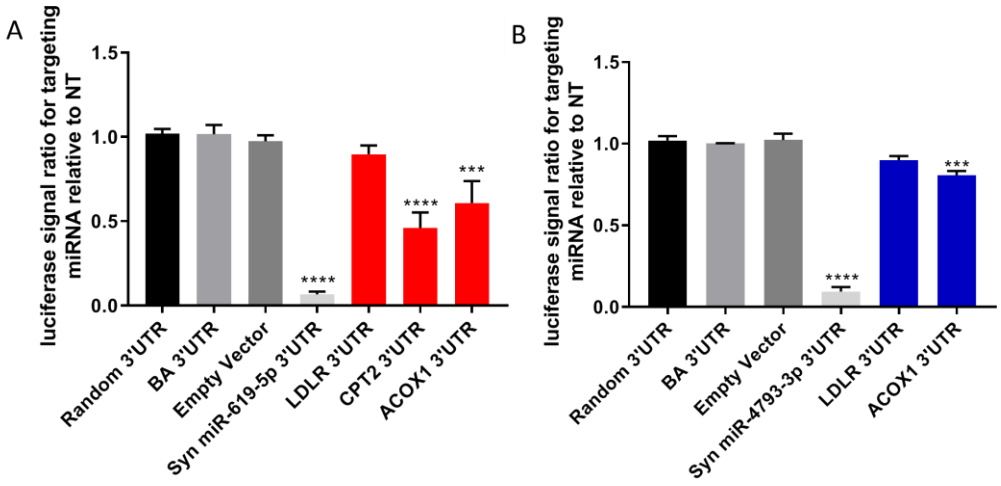


Figure 4.12. Luciferase activity in U87 cells.
Cells were co-transfected with a mimic for (A) miR-619-5p or (B) miR-4793-3p and a luciferase reporter vector in y-axis. Luciferase activity in each transfection was normalised to the non-targeting control (NT). Luciferase signal is presented relative to the scramble 3’UTR sequence (Random 3’UTR). Each transfection was done in triplicate, and the experiment was repeated three times (mean ± SEM). Statistical significance was evaluated using Student’s t-test following one-way ANOVA; (***) p-value <0.001; (****) p-value <0.0001. Abbreviations BA 3’UTR: reporter vector containing the 3’UTR of β-Actin*; Syn miR-619-5p 3’UTR and Syn miR-4793-3p 3’UTR: reporter vector containing synthetic sequence repeats that are fully complementary to the given miRNA sequence. Empty vector:*

the parental luciferase construct that contains no 3`UTR cloned into the luciferase reporter.

4.2.8 Protein expression of putative miR-619-5p and miR-4793-3p targets

In addition to mRNA levels, the protein levels of the putative miR-619-5p and miR-4793-3p were assessed using Western blot. Based on the literature, 72h is sufficient to see a miRNA-mediated inhibitory effect on the translation of its mRNA target. Thus, protein expression was evaluated 72h post-transfection in U87 (Figure .4.13) and GIN28 (Figure 4.14) cells. Expression of NT had no effect on protein expression in both cell lines.

LDLR protein levels were markedly reduced upon the transfection of miR-619-5p or miR-4793-3p in both cell lines.

Protein levels of CPT2 were only clearly and consistently reduced in miR-619-5p–overexpressing cells.

Interestingly, overexpression of miR-619-5p or miR-4793-3p did not result in a significant reduction of ACOX1 protein expression. Moreover, in all of the co-transfection samples, I found no expression change in any of the targets.

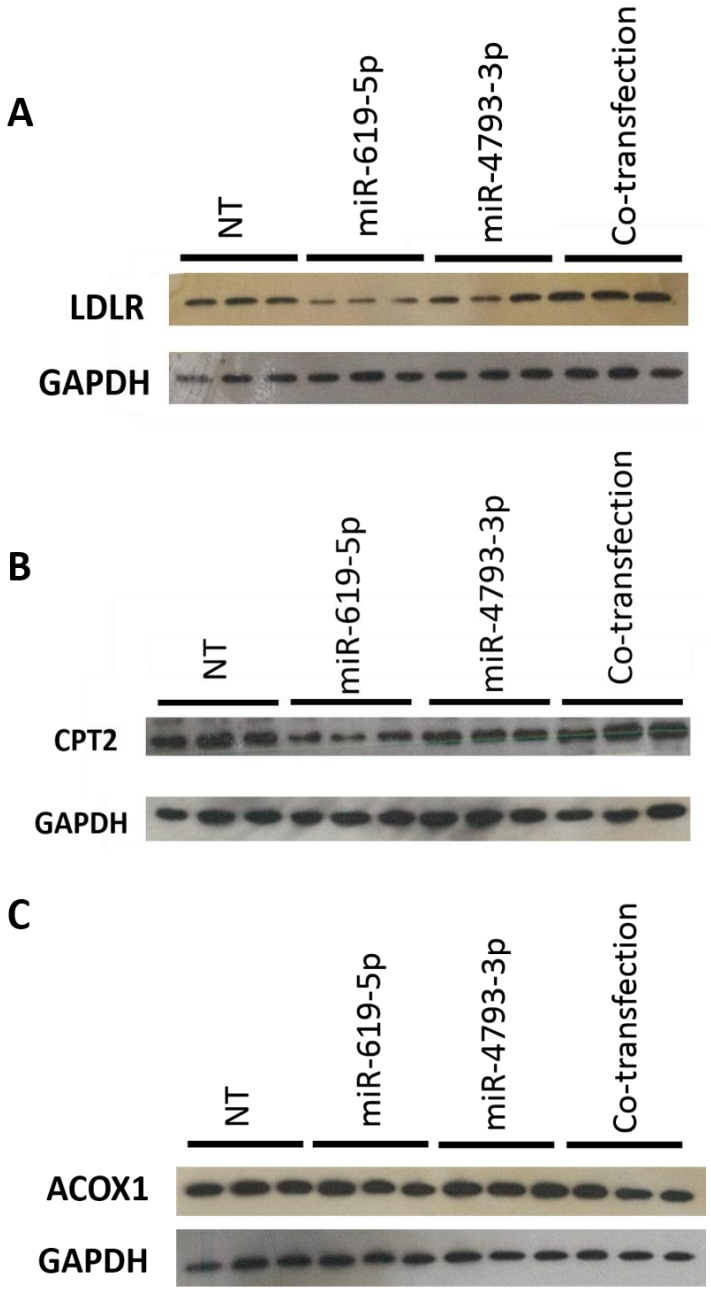


Figure .4.13. Immunoblot of miR-619-5p and miR-4793-3p targets in U87 cells.

(A) LDLR (120 kDa), (B) CPT2 (72 kDa), and (C) ACOX1 (74kDa). Blotting of GAPDH (37 kDa) was performed to serve as a loading control. NT: non-targeting mimic control. Data are represented as three biological repeats for each transfection condition.

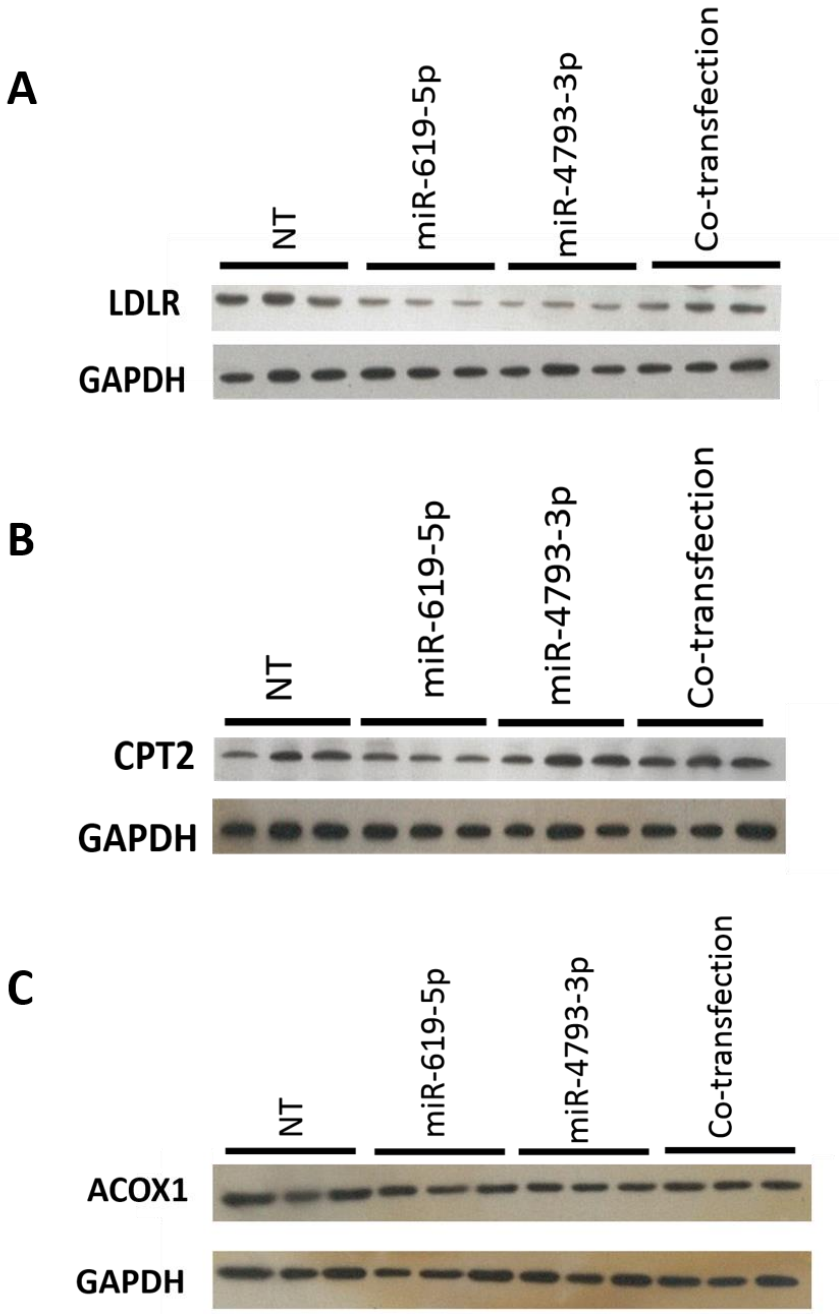


Figure 4.14. Immunoblot of miR-619-5p and miR-4793-3p targets in GIN28 cells.

(A) LDLR (120 kDa), (B) CPT2 (72 kDa), and (C) ACOX1 (74kDa). Blotting of GAPDH (37 kDa) was performed to serve as a loading control NT: non-targeting mimic control. Data are represented as three biological repeats for each transfection condition.

4.2.9 mRNA expression of putative miR-619-5p and miR-4793-3p targets in patient samples

As described in chapter 3, both miR-619-5p and miR-4793-3p were found to be upregulated in the tumour core and rim relative to the invasive margin region. Thus, the expression of the putative targets of these two miRNAs was expected to be downregulated in the tumour core/rim relative to the invasive margin, because miRNAs would downregulate the expression of their target genes.

The mRNA levels of LDLR, CPT2 and ACOX1 (the three putative target genes from above) were quantified, by qRT-PCR, in the core, rim and invasive margin samples from three IDH-wt adult GBM patients (Figure 4.15). I examined the mRNA expression pattern in each patient sample and I found that the expression of LDLR, CPT2 and ACOX1 is generally highest in the invasive margin, followed by the rim than the core regions. However, due the inter-patient variation in the magnitude of the fold change in gene expression between each tumour region, statistical significance was not achieved when comparing the average gene expression value from the three patients in each region to that in another region.

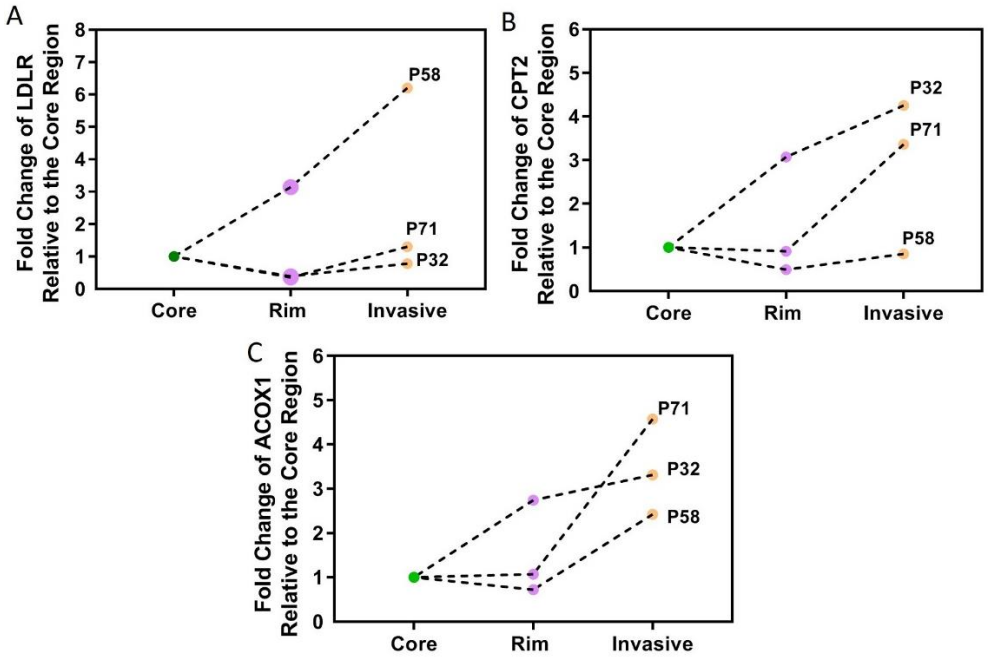


Figure 4.15. mRNA expression in different regions of the GBM tumour.
*T*he *expression of* (A) LDLR, (*B*) CPT2 and (*C*) ACOX1 *in each tumour region is represented as fold change relative to its expression in the corresponding core region. Data is shown for individual patients. No statistical analysis was performed due to the limited sample size.*

To evaluate that miRNA target genes are expressed in the tumour enriched 5-ALA/+ cell population of the invasive margin region, mRNA levels were measured in both 5-ALA/+ and 5-ALA/- cell populations (Figure 4.16). I found that the expression of LDLR, CPT2 and ACOX1 was lower in the 5-ALA/+ population relative to the 5-ALA/- population.

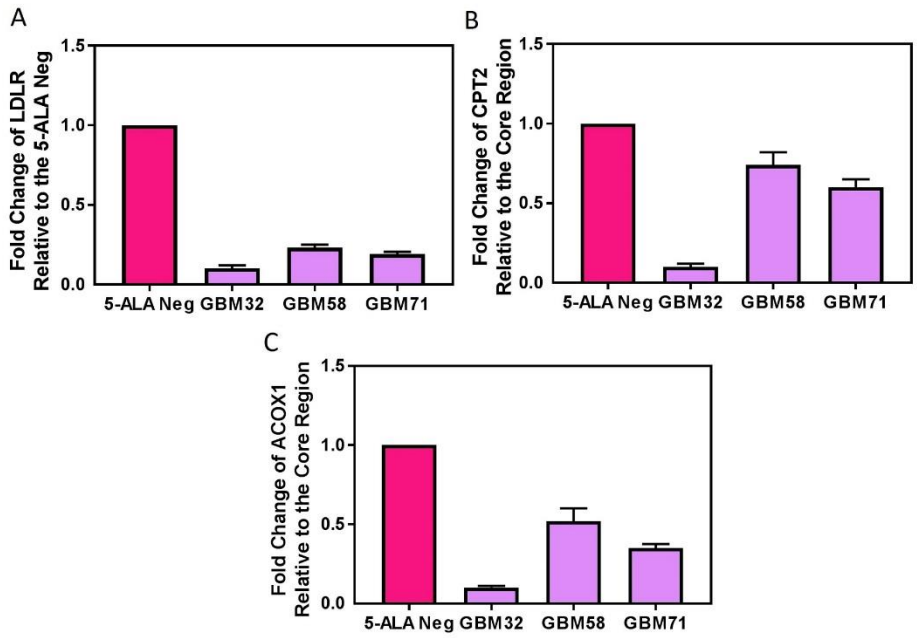


Figure 4.16. mRNA expression in 5-ALA sorted invasive margin samples.
The expression of (A) LDLR, (B) CPT2 and (C) ACOX1 in 5-ALA/+ cell population (5-ALA Pos, purple) in individual patient is represented as fold change relative to its expression in the corresponding 5-ALA/- cell population (5-ALA Neg, pink). No statistical analysis was performed due to the limited sample size.

4.2.10 Protein expression of putative miR-619-5p and miR-4793-3p targets in patient samples

Due to the limited availability of TMA section, it was necessary to choose one target for the evaluation of the intra-tumour protein expression heterogeneity. I have chosen CPT2 due to its clinical relevance as a potential therapeutic target with a known pharmacological agent available to be re-purposed for the treatment of GBM, as detailed in this chapter's upcoming discussion section.

4.2.10.1 Optimisation of CPT2 antibody dilution

From the TGCA database, a positive control tissue sample that expresses CPT2 at high levels was identified, in this case it was healthy liver tissue. CPT2 antibody was tested on healthy liver tissue at two different dilutions (1:00 to 1:200), and incubated for 1 hour at room temperature. I found that antibody concentration with the least amount non-specific background staining but with clear specific staining was used for subsequent experiments, in this case, 1:200 (Figure 4.17).

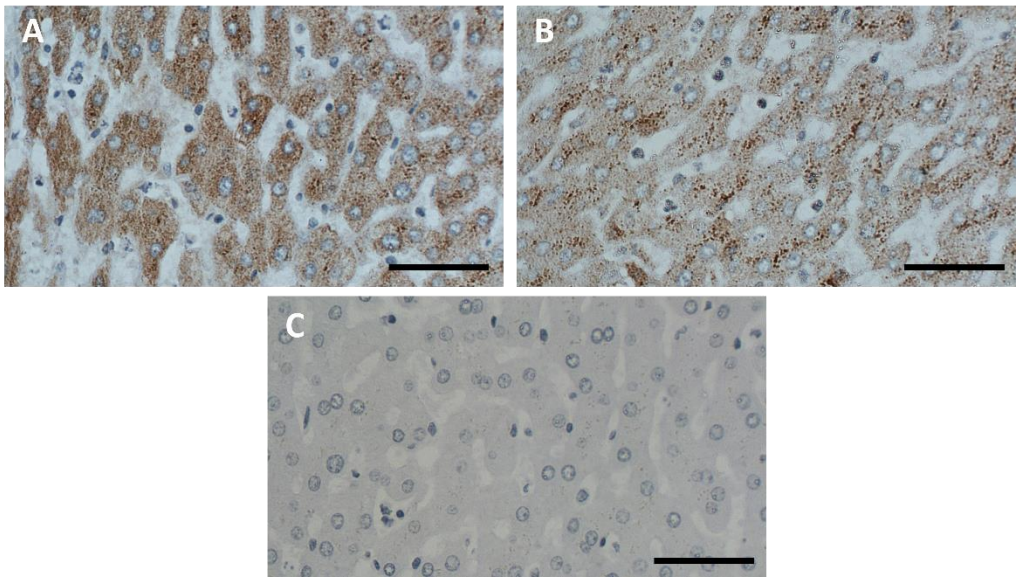
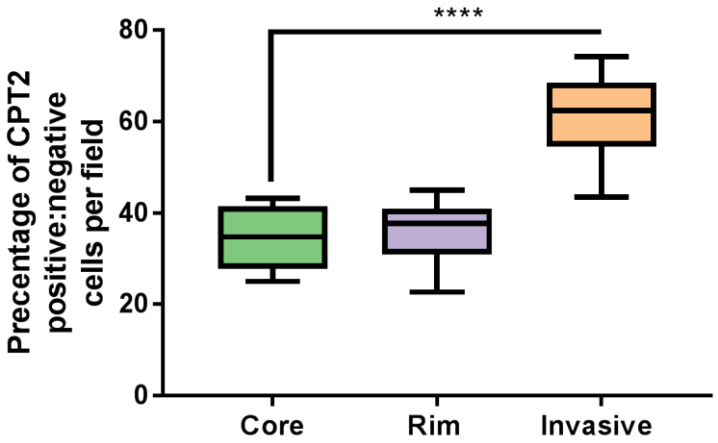


Figure 4.17. Optimisation results of primary anti-CPT2 antibody on normal liver tissue.
All images were captured at 40x magnification, scale bar: 50μm. Anti-CPT2 antibodies at (A) 1:100 dilution; (B, 1:200 dilution; and (C) negative control.

4.2.10.2 CPT2 protein expression in GBM

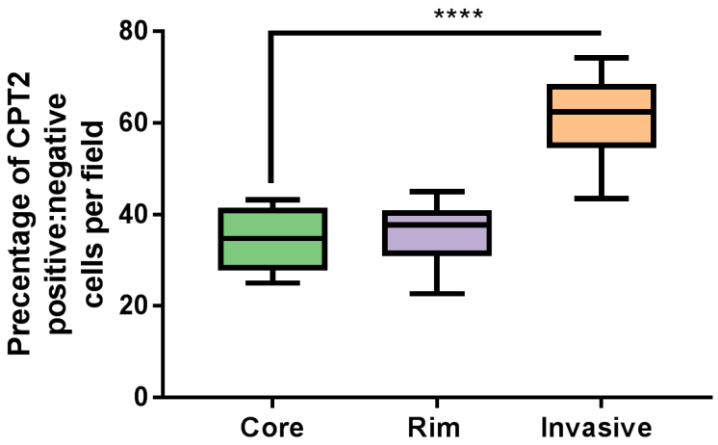
Immunohistochemical staining of CPT2 showed that CPT2 was very weakly expressed within the normal brain, suggesting that CPT2 is present at low levels in normal brain tissue



(

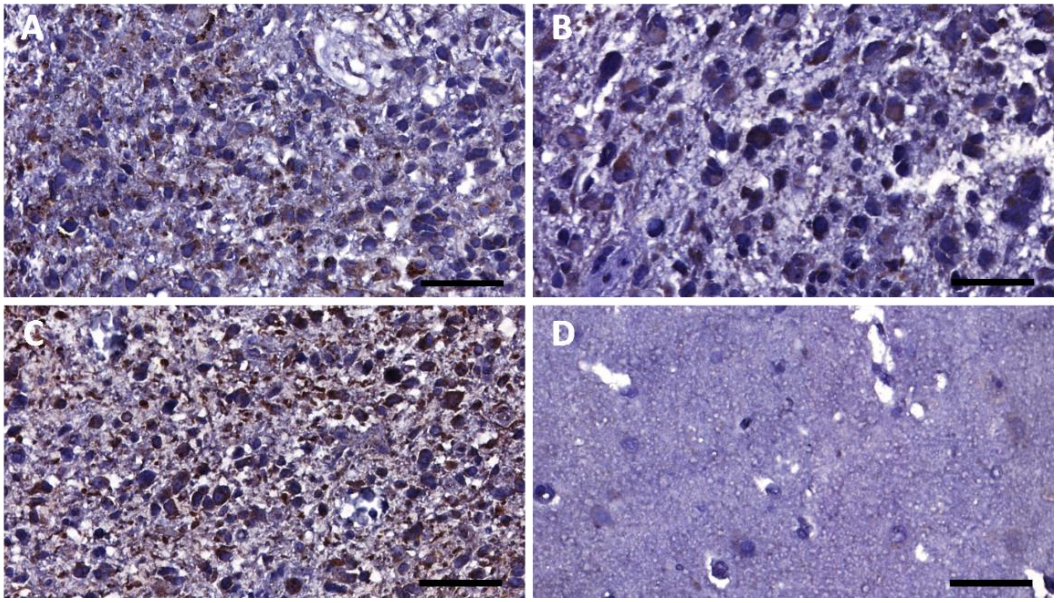
Figure 4.18).

Staining of TMAs showed that CPT2 expression is higher in the invasive edge relative to the tumour core and rim regions



(

Figure 4.18). Subsequently, in each tumour regions, the percentage of cells containing CPT2-positive cytoplasmic staining per field of view was calculated in order to determine statistical significance (Figure 4.18).



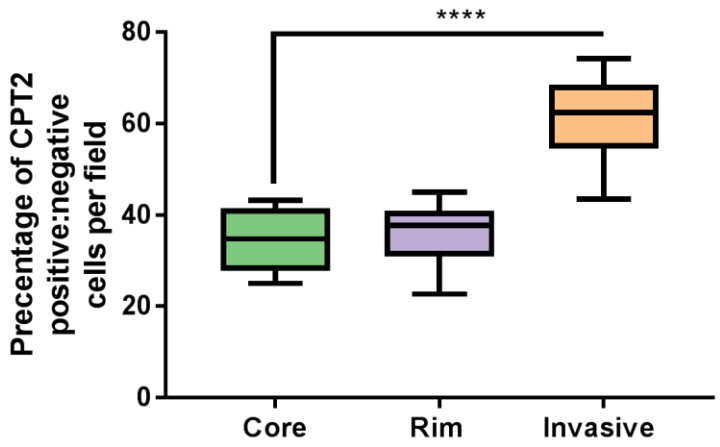


Figure 4.18: Immunohistochemical staining pattern of CPT2 in GBM tumours.
Immunohistochemical analysis of adult GBM tissue microarrays (TMA) at 1:200 anti-CPT2 dilution are shown as representative images of each region; tumour (A) core (B) rim (C) invasive

margin and a (D) normal brain control are shown. All images were captured at 40x magnification; scale bars correspond to 50 μm.
*The box blot shows, per tumour region, the number of cells containing CPT2-positive cytoplasmic staining represented a percentage of the total number of cells counted on each high-powered microscope fields of view (captured at 40x magnification) taken from a TMA tissue core. Statistical analysis was conducted using ANOVA (P>0.05) followed by Bonferroni's multiple-comparison test comparing each region to the core; ****p-value < 0.0001. Only the invasive margin region was significantly different from the core.*

4.3 Discussion

As far are I am aware, there are currently no experimentally validated targets for miR-619-5p and miR-4793-3p in GBM. As a novel contribution, the work of this chapter identifies and validates new targets for these two miRNAs.

Pathway enrichment analysis identified 12 of the mutual putative targets for miR-619-5p and miR-4793-3p to be within the lipid metabolism pathway. Based on the initial qRT-PCR screening of all 12 targets in U87 cells, only three targets (ACOX1, LDLR, CPT2) were affected by both miRNAs. Based on the subsequent series of experiments to validate all three targets, only CPT2 was supported by a consistent line of evidence (qRT-PCR, luciferase, Western blot and IHC) as a genuine target; even then, it was only a genuine target for miR-619-5p.

First, the qRT-PCR analysis showed that elevated miR-619-5p levels were accompanied by marked reductions of CPT2 mRNA expression in both U87 and GIN28 cells. Second, miR-619-5p overexpression led to a significant decrease in CPT2 protein levels in both U87 and GIN28 cells. Third, the luciferase reporter assay subsequently confirmed the direct binding of miR-619-5p to the 3'UTR of CPT2. Fourth, qRT-PCR data obtained from three patient samples showed that reduced miR-619-5p levels in the invasive margin of the GBM tumour were accompanied by marked elevation of CPT2 mRNA expression in the same tissue sample. Likewise, a significant increase in CPT2 protein levels in the invasive margin was demonstrated by IHC.

The rate-limiting step for FAO, a key bioenergetic process for GBM cells, is the transport of the long-chain fatty acylcarnitine into the mitochondrial matrix by the CPT1/2 (Melone *et al.*, 2018). This enzymatic complex is made up of two distinct proteins which are CPT1, that is located in the outer, and CPT2 that is located in the inner mitochondrial membrane (McGarry and Brown, 1997). While CPT1 has tissue-specific expression through the so-called "liver", "muscle", and "brain" isoforms (Britton *et al.*, 1995; Yamazaki *et al.*, 1996; Price *et al.*, 2002); CPT2, however, is ubiquitously expressed in all cell types

(Demaugre *et al.*, 1990), Therefore, I viewed CPT2 as a valuable target to follow up on in later chapters.

The role of CPT2 has not been reported in relation to GBM. In fact, little is known about CPT2 deregulation in cancer. Park et al., (2016) showed that the knockdown of CPT2 in triple-negative breast cancer (TNBC) cells significantly inhibited the transwell migration potential of TNBC cells (Park *et al.*, 2016). This indeed has led me to consider the potential role of CPT2 in GBM cell invasion in Chapter 6.

There are several findings with regards to CPT2, ACOX1, and LDLR from the current work that need to be explained. As an initial assessment, sequence alignment showed that more bases from CPT2 3'UTR are involved in the interaction with miR-619-5p (21 bases) as opposed to LDLR and ACOX3 5-ALA (10 bases). On the other hand, only 7 bases from both LDLR and ACOX1 3'UTR of were involved in the interaction with miR-4793-3p, while there was no interaction with CPT2 3'UTR.

Although CPT2 was initially predicted as a target for miR-4793-3p, I could not identify a binding site for miR-4793-3p in the 3'UTR of CPT2 to perform luciferase assay. False-positive predictions such as these could be attributed to the source of

3’UTR sequences. For example, Targetscan uses the Ensembl database (Flicek *et al.*, 2008), whereas miRanda uses the University of California Santa Cruz (UCSC) database (Bina, 2008) to predict the boundaries of the 3’UTR region. When Thomson et al. applied the Targetscan algorithm to the UCSC database, only a 47% overlap of predicted targets was observed. Similarly, when they applied the miRanda algorithm to the Ensembl database, only a 65% overlap was observed (Thomson, Bracken and Goodall, 2011). Thus, the boundaries of a 3’UTR region might be different and predicted miRNA seed sequence alignment by different algorithms might lie outside the true boundaries of the 3’UTR of the putative target (Ritchie and Rasko, 2014; Breda *et al.*, 2015). In fact, I obtained the 3’UTR sequences for luciferase assay from SwitchGear Genomics who rely on their in-house database of predicted 3’UTR regions. This database might predict different boundaries for the 3’UTR to those from the databases used by my prediction algorithms.

Although I confirmed that both miR-619-5p and miR-4793-3p directly target the 3’UTR of the ACOX1 transcripts and reduce its mRNA levels, ACOX1 expression was not reduced at the protein level. This discrepancy between qRT-PCR and Western blot analysis might be because miRNAs do not impede the

process of transcription, and therefore, as mRNAs are being degraded, more copies of mRNAs are also being transcribed as a compensatory mechanism by the cell (Dori-Bachash, Shema and Tirosh, 2011). In addition, it is often observed in the literature that the number of targets affected at the protein levels is far less than those initially identified by gene expression analysis (Lim *et al.*, 2005). Nevertheless, the magnitude of reduction in ACOX1 mRNA levels following individual miR-619-5p and miR-4793-3p transfections (although was statistically significant) was not very large, especially when compared to the magnitude of reduction in the expression of the other genes. In fact, ACOX1 lost statistically significant in miR-4793-3p-overexpressing GIN28 cells. Therefore, it was reasonably expected to see little change in expression (if any) at the protein level.

The mRNA expression value of CPT2 in the co-transfected samples was an average of the values from miR-619-5p and miR-4793-3p samples. The overall mRNA levels of CPT2 were decreased in the co-transfected samples. However, despite the overall decrease in mRNA levels, the protein levels of CPT2 were not affected in the co-transfected samples. In fact, I observed no change in the protein levels of all three targets in the co-

transfected samples. A plausible explanation for why the effect seen with a single miRNA transfection is lost in the case when both miRNAs were co-transfected is that co-transfection has higher miRNA concentration (I transfected 50μM of miR-619-5p and 50μM miR-4793-3p), which could saturate the RISC complexes and prevent other endogenous miRNAs from binding (Janas et al., 2012). This, in turn, alters the expression of many miRNA target genes, including transcription factors, which would then affect the expression of downstream target proteins such as those that were originally affected by single miRNA transfections(Lei *et al.*, 2016).

The mRNA and protein expression of LDLR was reduced following miR-619-5p and miR-4793-3p overexpression; however, luciferase assay did not confirm the direct binding of either miRNA to the 3'UTR of LDLR. This is because miRNA overexpression suffers from the knock-on effect where the miRNA of interest directly targets a gene that in-turn regulates the expression of multiple other genes that do not contain miRNA binding site (Ritchie *et al.*, 2009). Similarly, I observed an increase in CPT2 mRNA expression in U87 and GIN28 cells upon the overexpression of miR-4793-3p. In such case, miR-4793-3p may potentially be targeting transcriptional repressors

of CPT2, and the overexpression of miR-4793-3p would lead to an increase in the mRNA levels of CPT2 in the cell.

There are findings with regards to other targets identified from the present study that need to be discussed.

I have found that ACSBG1 levels to be undetectable by qRT-PCR in U87 cells, even after using multiple different primers. As such, although it was predicted, I could not validate ACSBG1 as a target. This is because, although not taken into account by prediction algorithms, miRNA and its target must be co-expressed in order for the miRNA to repress the target expression.

Since it was the only reported target in the literature (Qiu *et al.*, 2016), I have evaluated whether MALAT1, a long non-coding RNA, is a target for miR-619-5p in U87. However, MALAT1 was not present in the list of the predicted targets (because the algorithm only predict mRNA targets). Qiu et al. concluded that MALAT1 is a target for miR-619-5p in colon cancer from the observation that the expression of miR-619-5p and MALAT1 were inversely correlated in the same tissue (Qiu *et al.*, 2016). Since I found MALAT1 to be increased upon miR-619-5p

overexpression, I concluded that MALAT1 is not repressed by miR-619-5p in GBM cells.

I also expected genes within the glycerolipid or glycerophospholipid biosynthesis pathways to emerge as targets; however, I only studied the expression of the top enriched genes, and from that subset, I couldn't identify valid targets. Other genes that fell below the prediction score cut-off threshold could be valid targets and could be attempted to be validated in the future.

There are several limitations to this study. First, I observed differences in CPT2 protein expression between tissue samples, which had both miRNA upregulated, and cell lines, which I ectopically transfected with both miRNAs (co-transfected samples). I explain this observation in two ways. On one hand, the biological effect of miRNAs is eventually determined by the relative abundance of the miRNA and each of its mRNA targets (Ebert and Sharp, 2012). This also varies in response to the dynamic tumour microenvironment (Leung and Sharp, 2010b), which is not present in the case of cell lines, including tissue-derived cell lines. An important observation from my miRNA microarray analysis in Chapter 3 was the loss of region-specific

miRNA expression signature in the tissue-derived cell lines. On the other hand, it is important to highlight that studies based on the supra-physiological increase in miRNA levels achieved by overexpression of a given miRNA must be interpreted with caution (H. Y. Jin *et al.*, 2015). miRNA overexpression has the potential to generate off-target effects where a miRNA targets genes that would otherwise not be affected in a physiologic context leading to even low-affinity target sites to appear functionally important. In addition, although miRNA mimic duplexes are typically designed with the aim of activation of only one miRNA strand, the passenger strand might not necessarily be equivalent to the natural miRNA* form. As such, there is a possibility that the passenger strand is incorporated into RISC to mediate off-target effects.

A key limitation was that although the mRNA expression of CPT2 in tissue sample has demonstrated a pattern of increase moving from the tumour core to the rim to the invasive margin, some rim samples had lower expression than that in the core. This is because the rim region is subjected to sampling errors during surgery. The tumour mass resembles a loose ball which makes it hard to know if the sample was taken too deep into the tumour core or sampled correctly as the middle proliferative rim.

This will affect the pattern of gene expression and might make what I call the rim to seem to behave like another core.

Furthermore, I found that the 5-ALA/- cell population within the invasive margin—which was enriched for the non-tumour cell population (see chapter 3)—showed higher expression of CPT2, and other two targets, than the 5-ALA/+ cell population. This is consistent with my expectations that in the 5-ALA/+ cells, where both miRNAs are upregulated, the expression of the target, CPT2, will be low. Inversely, I expected that in the 5-ALA/- cells, where both miRNAs are downregulated, the expression of CPT2, will be high.

Another limitation exists in the interpretation of IHC results. The high expression levels of CPT2 in the tumour's invasive margin that I observed by IHC might only be a reflection of the low tumour fraction (1-3% tumour) within the invasive margin. Indeed, it is difficult to distinguish non-neoplastic brain tissue from the infiltrated tumour cells in the invasive margin of GBM due to the lack of a universal histological GBM-specific marker that would allow tumour cells to be distinguished from the surrounding brain tissue. Perhaps mutated proteins that are specific to some GBMs can be used as markers; however, many

of these events are clonal within the tumour or specific to the molecular profile of the patient. For example, secondary glioblastoma could be identified by IDH1/IDH2 or some GBMs can be distinguished by their EGFR mutation status but such markers cannot be widely used for all GBMs (K. S. Lee *et al.*, 2013). There are markers which most gliomas may express, but they are to be also expressed in some of the normal brain tissue, such as GFAP (Goyal *et al.*, 2015) and OLIG2 (Ligon *et al.*, 2004). In addition, stem cell markers have also been used to stain GBM tumour cells, such as OCT4, Nanog, KLF4 and SOX2 (Hattermann *et al.*, 2016) or Nestin and CD133 (Zhang *et al.*, 2008); however, not all cells in the tumour express these markers and no one 'master-marker' could define the complete glioma stem cell subset.

Finally, because anti-miR oligonucleotides may sequester endogenous miRNAs without aiding their decay, it is difficult to measure a decrease in miRNA levels following miRNA inhibition. This makes it challenging to determine the silencing efficiency by qRT-PCR. Both of my miRNAs were already very low expressed in U87 and GIN28, and I could not measure their levels when I attempted to downregulate them further.

4.4 Future work

There are a few areas of future work that would enhance the work presented in this chapter. First, because current methods of predicting patients' survival rely on gene expression values obtained from the main tumour mass, it would be interesting to explore whether the survival analysis carried out using gene expression data from the invasive margin would serve as a better predictor of survival. This is because the residual tumour cells found within the invasive margin are more likely to affect the survival of the patient.

Furthermore, in order to determine the protein expression in tumour cells within the invasive margin region, it might be possible to stain the tumour with antibodies against the protein of interest prior to FACS analysis to sort the sample based on 5-ALA presence. As such, double-positive cells for both 5ALA/+ and the gene of interest can be identified, although antibody incubation time might affect 5-ALA fluorescence.

4.5 Chapter Summary

- The overexpression of miR-619-5p and miR-4793-3p in U87 and GIN28 cells was successfully optimised.
- It was not possible to further inhibit the already downregulated miR-619-5p and miR-4793-3p in U87 and GIN28 cells.

- Target prediction algorithms predicted 12 genes within the fatty acid degradation/metabolisms and the glycerolipid/glycerophospholipid metabolism pathways to be mutual targets of both miR-619-5p and miR-4793-3p.
- Subsequent to the transient overexpression of miR-619-5p and miR-4793-3p, the mRNA and protein expression of their putative targets was evaluated by qRT-PCR and Western blot, respectively.
- qRT-PCR analysis showed that the mRNA levels of CPT2, ACOX1 and LDLR were significantly reduced 48h following the overexpression of miR-619-5p in both U87 and GIN28 cells.
- However, miR-4793-3p overexpression in both cell lines reduced LDLR and increased CPT2 but in GIN28 cells, miR-4793-3p overexpression had no significant change on ACOX1 expression.

- Western blot analysis showed a significant decrease in LDLR but not ACOX1 protein levels 72h following the overexpression of miR-619-5p or miR-4793-3p while CPT2 levels were only reduced after miR-619-5p overexpression in both U87 and GIN28 cells.

- The luciferase reporter assay confirmed the direct binding of miR-619-5p to the 3'UTR of CPT2 and ACOX1 but not to LDLR. The luciferase reporter assay confirmed miR-4793-3p binding to the 3'UTR of ACOX1 but not to LDLR.
- qRT-PCR analysis of patient samples showed that expression of LDLR, CPT2 and ACOX1 is generally highest in the invasive margin, where both miR-619-5p and miR-4793-3p are upregulated, followed by the rim then the core regions.
- The qRT-PCR analysis also showed that the expression of LDLR, CPT2 and ACOX1 was lower in the 5-ALA/+ relative to the 5-ALA/- cell populations.
- IHC analysis of patient samples showed that CPT2 protein levels were downregulated in the invasive margin.

Chapter 5:
Evaluation of Global Metabolic Alterations Following miR-619-5p and miR-4793-3p Overexpression in GBM Cells

5.1 Introduction

The past decade has witnessed remarkable progress in elucidating the miRNA-mediated regulation of gene expression in GBM. However, no work has been done to discover metabolites that are associated with miRNA expression changes in GBM cells. In chapter 4, I found that miR-619-5p and miR-4793-3p target and downregulate multiple genes within the fatty acid catabolism pathway. This chapter is, therefore, focused on characterising the metabolome and the lipidome of GBM cells following miR-619-5p and miR-4793-3p overexpression.

Several studies have investigated the alteration in the cell metabolome following a stable or transient transfection of miRNAs (Bi *et al.*, 2014; Chemello *et al.*, 2018; Lai *et al.*, 2018). For example, Wang et al., 2016 used lentiviral transfection to introduce an encoding gene for miR-143/145 or a negative control vector into endothelial cells. After 72h, an untargeted metabolomics study was carried out using liquid chromatography coupled to time-of-flight mass spectrometry (TOF-MS). A total of 738 metabolites were detected in both the overexpression and control groups. However, only 25 metabolites showed differential abundance, with fold changes ranging from 2 to 8, between the two groups

(Wang *et al.*, 2016). It is important to note that only a small percentage of metabolites (3.52% of the total metabolites detected) have changed significantly as a result of changing miRNA expression in the cell. Moreover, these changes were not intense in magnitude. This is consistent with the notion that miRNAs regulate the function of a pathway by 'fine-tuning' the production of multiple components within the pathway (Bartel, 2009). Nevertheless, the significant metabolites identified as a consequence of miR-143/145 overexpression in endothelial cells may provide interesting insights into the changes caused by miR-143/145 released from smooth muscle cells to regulate the function of their neighbouring endothelial cells (Wang *et al.*, 2016).

In another study, Ramirez et al., 2013 transiently transfected hepatic (HepG2) cells with miR-33b mimic or a non-targeting control for 48h. They found that miR-33 targets key regulatory enzymes of hepatic gluconeogenesis, namely carboxykinase (PCK1) and glucose-6-phosphatase (G6PC). Next, they assessed the global metabolomics profile using two analytical techniques: ultrahigh performance liquid chromatography-mass spectrometry (UHPLC-MS) optimised for acidic species and gas chromatography coupled to mass spectrometry

(GC/MS) in order to cover a wider range of metabolites with different chemical properties. miR-33 overexpression resulted in altered intracellular concentrations of 271 metabolites, only 28 of which were significantly changed between the overexpression and control groups. Despite this small change in the metabolic profile, the metabolic differences caused by the overexpression of miR-33 supported their hypothesis that miR-33 may regulate glucose metabolism in hepatic cells (Ramírez *et al.*, 2013).

In summary, these studies demonstrate that miRNAs exert their effect in regulating metabolic pathways through relatively subtle modulation of numerous targets, rather than through dramatic regulation of single targets (Bartel, 2009; Liu and Olson, 2010; Small and Olson, 2011). Nonetheless, a metabolomics approach can be used to bridge the gap between gene expression changes caused by miRNA-mediated mechanisms and global change in cellular metabolic phenotype.

In this study, I prepared—in six biological replicates—a dual extraction of the polar metabolites (i.e. water-soluble) and non-polar metabolites (i.e. water-insoluble such as lipids) obtained from U87 cells 72h following the transfection with miR-619-5p

mimic, miR-4793-3p mimic, co-transfection or non-targeting control (NT). I performed an untargeted analysis using LC-MS and LC-tandem MS/MS to compare the global metabolomics and lipidomics profiles of the four transfection conditions. Furthermore, I validated some of my findings by examining the abundance levels of lipid droplets in GBM cells and tissue.

Hypothesis: *Metabolites associated with glycerophospholipid metabolism will be downregulated following miR-619-5p and miR-4793-3p overexpression.*

5.2 Results

5.2.1 Growth Curve of U87 and GIN28 following miRNA transfection for metabolomics analysis.

To ensure robustness in the experiment, the commercial glioma cell line, U87, was chosen to study the effect of miR-619-5p and miR-4793-3p overexpression on the GBM metabolome and lipidome. In order to ensure a sufficient number of cells to generate a strong LC-MS signal for metabolomics and lipidomics analysis, U87 cells were grown in T75 flasks seeded at a density of 375,000 for optimal transfection efficiency (See chapter 4; Figure 4.3). This seeding density was just above the minimum

recommended number of cells (350,000 cells) to generate a signal that falls within the instrument detection range.

Based on findings from chapter 4, a 72h time point was chosen for the metabolomics and lipidomics analyses. This is because significant changes in target protein expression were manifested at this time point following miRNA transfection.

However, in order to ensure comparability between the experimental conditions, I sought to examine the number of cells at the 72h time point. I constructed a growth curve using the standard cell concentration (3.125×10^4 cells/ml) optimised for miRNA transfection. Cells were counted, and the cell concentration was calculated every 24h (Figure 5.1).

No cell division was observed during incubation in the transfection media (24h), which synchronised cell growth in all four conditions. In addition, the cell numbers after 72h in all four transfection conditions were within an average of 8% of each other. It is accepted that up to 15% change in cell number will not affect the readings of the mass analyser due to the limited instrument sensitivity (Personal Communications with Dr Hyun Dong). This would, therefore, remove the need for an

extensive normalisation procedure to account for differing cell numbers that might be caused by miRNA transfection.

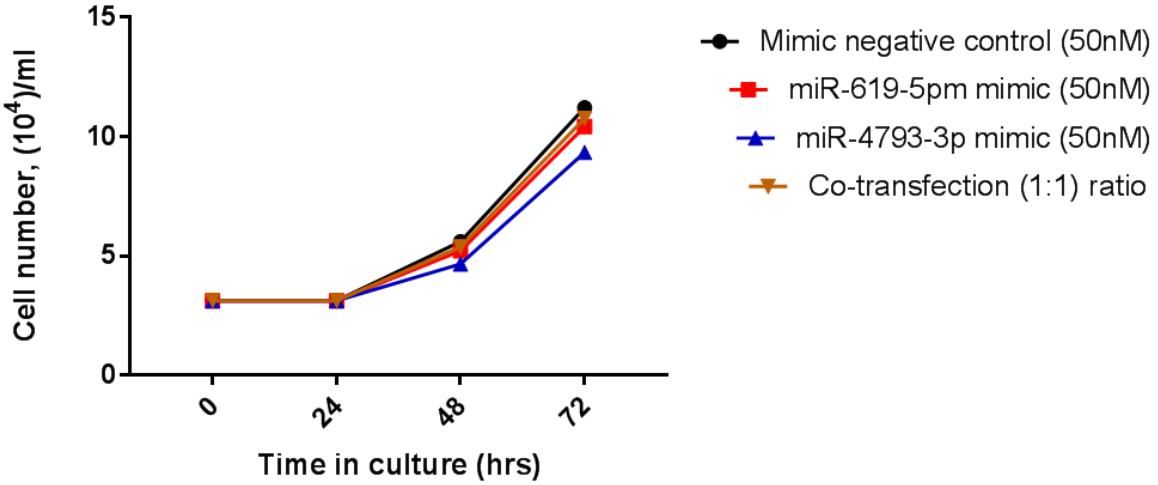


Figure 5.1: Growth curve of U87 cells.
Cells were plated at 3.125 x 104 cells/ml, and the number of cells was counted using a haemocytometer. The concentration of cells was calculated every 24h.

5.2.2 Metabolomics analysis of intra-cellular polar metabolites with LC-MS

5.2.2.1 Assessment of the quality of the samples and the stability of the LC-MS run

Quality control samples (QCs) samples are often used to monitor the stability of the LC-MS run and to ensure that the quality of the samples is not compromised as a result of the

relatively long time spent from sample preparation until the completion of the LC-MS data acquisition. 24 polar cell extracts (six biological repeats for each of the four transfection conditions) were analysed in this run. The QC sample was collected from pooled polar cell extracts of all 24 samples and injected at seven different time points throughout the LC-MS run. At the end of the run, a total of 3632 and 3148 peaks were detected in the positive and negative ionisation modes, respectively. Each peak represented a mass to charge ratio (m/z value) for each mass ion, which has an area or intensity and a retention time at which the ion was detected. Peaks were aligned to a reference QC run according to their retention time (Figure 5.2).

After an accurate alignment, every run will have readings for all compound ions. Hence, for every run, a ratio can be taken for the value of the compound ion abundance in that run to the value in the reference QC run (Figure 5.3). This corrects for factors that result in technical variation when running samples, such as sample loading. The effect of these systematic errors can be modelled by calculating a unique normalisation factor for each sample. The normalisation factor is represented by a

scalar multiplier that is applied to each ion abundance measurement (Table 5.1).

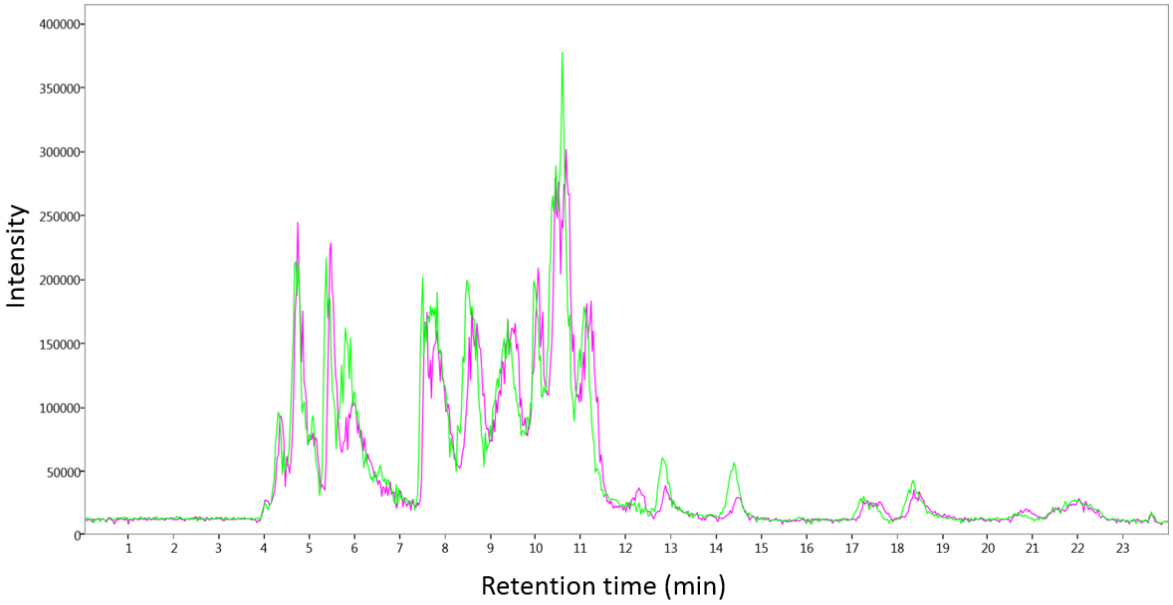


Figure 5.2: Representative peak alignment.
A selected quality control rn was set as an alignment reference run because they display the largest set of common compound ions The metabolic profile of a non-targeting control run (in green) is aligned to the reference run (in pink) according to the retention time of the compound ions. After an accurate alignment, the non-targeting control run will have readings for all compound ions.

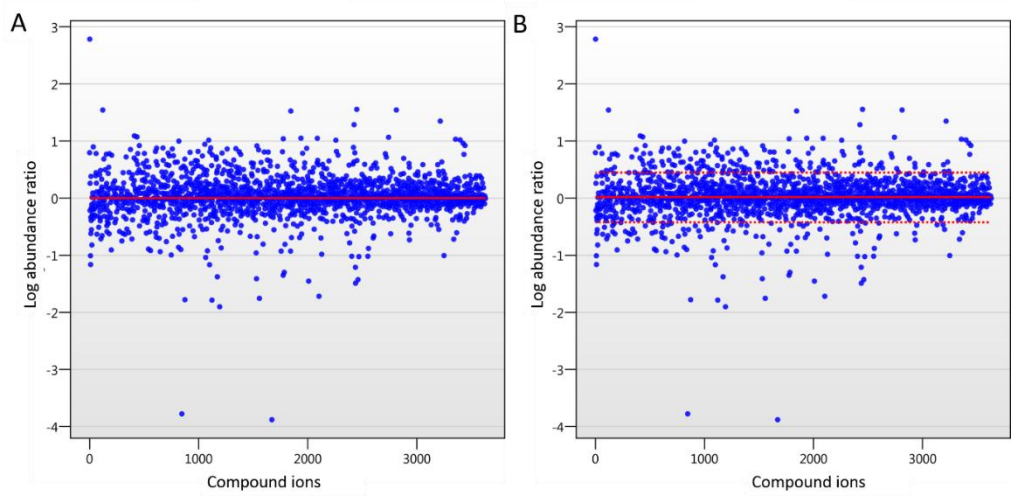


Figure 5.3: Representative normalisation.
The metabolic profile of a miR-4793-3p mimic transfection run (A) before and (B) after normalisation factor calculations. A quality control run was selected as a normalising reference run to calculate the normalisation factor. The normalisation factor was calculated by finding the mean of the log abundance ratios of the mass ions that fall within the robust estimated limits (dashed red lines) and compounds found outside of this would be considered as an outliers so they were not included in the calculation of the normalisation factor. The log of the abundance ratio for a compound ion was determined as (compound ion abundance in the sample run divided by the abundance in the normalising reference run).

Table 5.1: Normalisation factor multiplier that is applied to the abundance measurement of each ion in the sample.

	Normalisation factor for each biological repeat per transfection condition					
	R1	R2	R3	R4	R5	R6
NT	0.91	0.95	0.88	0.94	1.02	0.99
Co-transfection	0.90	0.99	0.88	1.10	1.04	0.91
miR-619-5p	1.02	0.91	0.98	1.03	0.92	0.92
miR-4793-3p	0.92	0.92	1.04	1.11	0.90	1.16
QC	0.92	0.93	1.05	1.01	0.85	1.17

The data sets were then combined (positive and negative ionisation modes) and imported into SIMCA-P for a multivariate

analysis (MVA) of metabolic profiles. A PCA was initially performed to obtain the natural clustering trend for the four transfection conditions (Figure 5.4). The PCA score plot shows that all samples were situated within 95% confidence tolerance ellipse based on Hotelling's T-squared test; thus, no outliers were detected. In addition, the QC samples are located within the centre of the plot. This indicates that the quality of the QC samples is reflective of the quality of each sample in the run, thereby indicating that the LC-MS run was stable and that the samples' quality remained intact. Hence, it could be said that the samples are comparable. However, the presence of the QC samples in the plot obscured the differences between the conditions. Thus, OPLS-DA score plot was subsequently applied to find differences in the metabolome profiles (Figure 5.4).

OPLS-DA showed a clear separation between the four transfection conditions. Moreover, OPLS-DA showed apparent clustering of the 6 biological repeats from each condition and hence confirmed the reproducibility of the repeats (See Appendix 1 for total ion count for each repeat). As such, it can be assumed that any observed differences are derived from the biological differences between the conditions instead of technical errors.

For each of the PCA and OPLS-DA models, t1 and t2 score vectors are the model components that best summarise the X-variables. The score t1 (first component) explains the largest variation in X dimension, followed by t2 (second component). Thus, the scatter plot of t1 vs t2 display how the X observations are situated with respect to each other.

The quality of the model is described by R2 and Q2 values. R2 is a measure of how well the model fits the training data, while Q2 is a measure of how well the model predicts new data. My OPLS-DA model had R2=0.909 and Q2=0.536, which were close to the optimal value of 1 and 0.5 for R2 and Q2, respectively. My PCA had R2=0.700 and Q2=0.442. Therefore, both of my models had good fitness and good predictive ability.

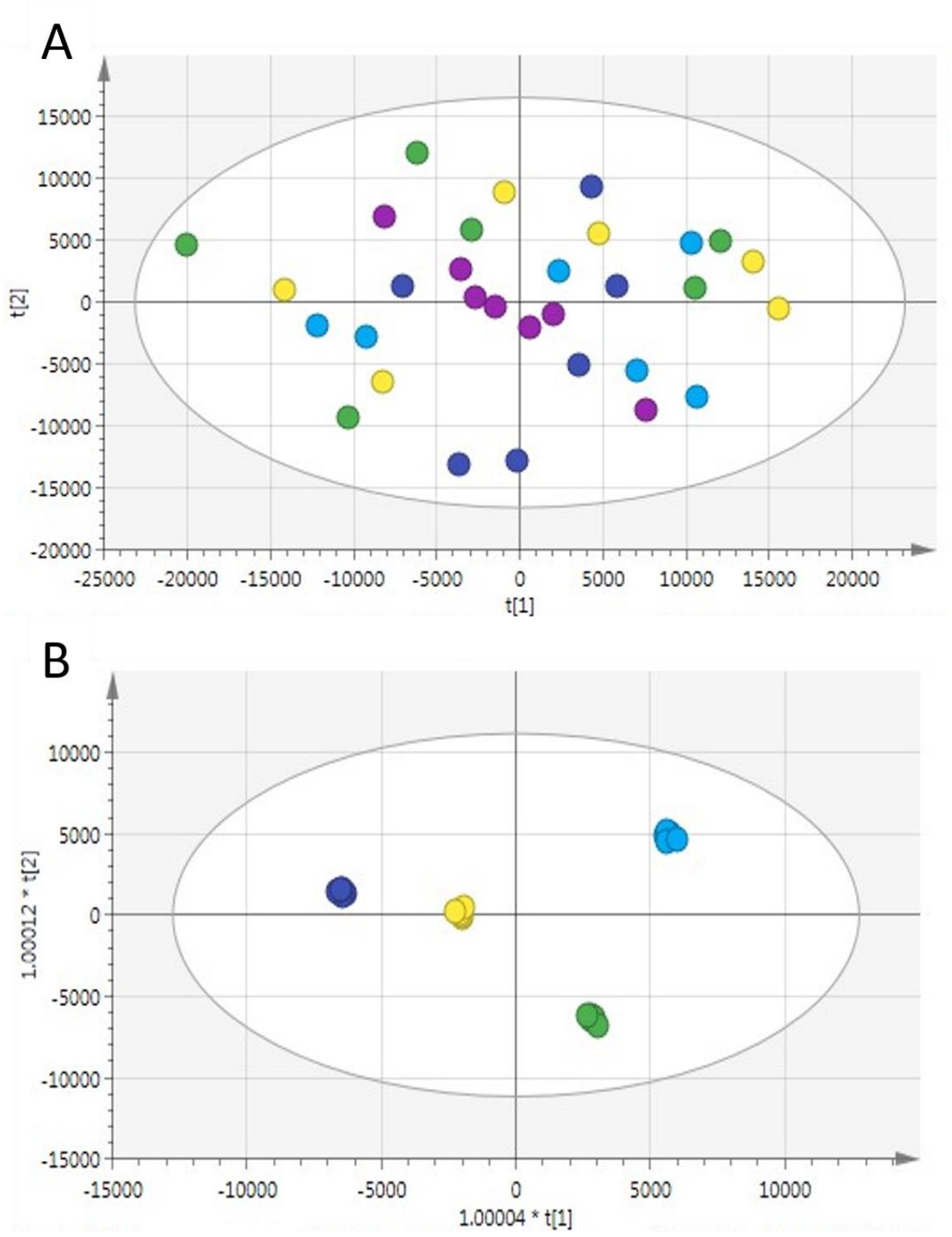


Figure 5.4: Multivariate analysis for the U87 cell metabolome following miRNA transfection.
(A) shows the Principal Component Analysis (PCA) score plot and (B) the OPLS-DA score plots based on the combined LC-(+) ESI-MS and LC-(-) ESI-MS data sets. For each of the PCA and OPLS-DA models, t1 and t2 score vectors are the model components that best summarise the X-variables. PCR score plots show that the quality of the QC samples reflects the quality of each sample in the LC-MS run. The OPLS-DA score

plots showed marked discrimination of the metabolic profiles of the different sample groups. The colours indicate the sample group; purple for quality control (QC) samples, light blue for non-targeting control, dark blue for miR-619-5p, green for miR-4793-3p, and yellow for co-transfection of miR-619-5p and miR-4793-3p at 1:1 ratio.

5.2.2.2 Comparison of metabolic profiles between miRNA transfection conditions

Differential analysis was carried out in Progenesis QI to find metabolites that show a difference in abundance between NT and miR-619-5p, NT and miR-4793-3p or NT and co-transfection.

Initially, in the positive ionisation mode, I found 166, 98 and 75 compound ions to be differentially abundant between NT and miR-619-5p, NT and miR-4793-3p and NT and co-transfection, respectively.

Furthermore, in the negative ionisation mode, I found 141, 99 and 86 compound ions to be differentially abundant between NT and miR-619-5p, NT and miR-4793-3p and NT and co-transfection, respectively.

However, following false discovery rate (FDR) correction, I found twelve significantly changed differential metabolites (Bonferroni adjusted $p < 0.05$) in the positive ionisation mode (nine were identifiable) and 28 in negative ionisation mode (three were identifiable).

25 of the metabolites in the negative ionisation mode were differentially expressed between NT and co-transfection with two mutual metabolites between NT and miR-4793-3p. One and two metabolites in the negative ionisation mode were uniquely differentially expressed between NT and miR-619-5p and NT and miR-4793-3p, respectively.

Of the metabolites in the positive ionisation mode, five were uniquely differentially expressed between NT and co-transfection and seven were uniquely differentially expressed between NT and miR-619-5p.

A hierarchical cluster analysis of all differentially abundant metabolites is shown in Figure 5.5. Two significant hierarchical clustering groups were observed. Cluster 1 shows metabolites that were predominately decreased in NT compared to the other transfection conditions and cluster 2 shows metabolites that

were increased in NT compared to co-transfection and miR-619-5p.

Differentially abundant metabolites were then identified based on the HMDB and Progenesis MetaScope with a mass error threshold of 5 parts per million (5 ppm) (as described in chapter 2). Five metabolites were identified from Cluster 1, and seven were identified from Cluster 2 (Figure 5.5). Such metabolites showed an average fold change of 2 between the transfection conditions. Each peak had a unique identification except for glycerophosphocholine, which had two corresponding peaks in Cluster 2. Additionally, taurine was the only identifiable overlapping metabolite that contributed to the distinctions between NT and miR-4793-3p and between NT and miR-619-5p/miR-4793-3p co-transfections.

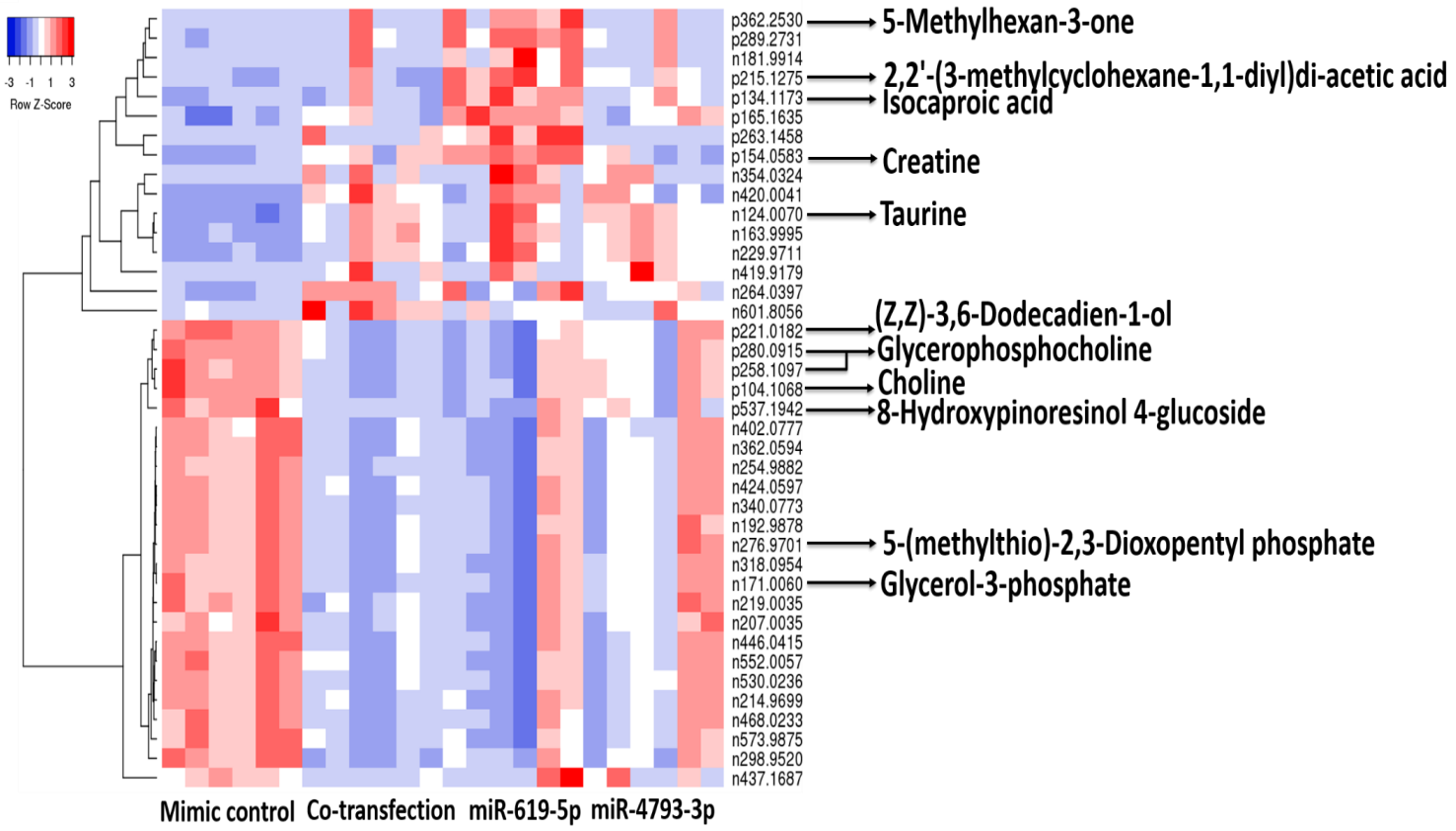


Figure 5.5: Hierarchical cluster analysis of differential metabolites in miR-619-5p, miR-4793-3p or miR-619-5p/ miR-4793-3p co-transfections relative to non-targeting control (NT). *Shades of blue and red represent a decreased or increased abundance, respectively. Average linkage was applied as a clustering method, and the Spearman rank correlation was used as a distance measurement method.*

Table 5.2: Fold change differences for identified differentially abundant metabolites.
Blue and red arrows represent significantly reduced or elevated metabolite levels relative to the non-targeting control (NT). Only Statistically significant fold changes are shown in bold. Statistical analysis was performed using a t-test, and p-values were corrected for multiple comparisons using the false discovery rate (FDR).

	Cluster 1									
Metabolite	m/z value	Polarity	Adduct	Chemical formula	Significant fold change in miR-619-5p relative to NC	Significant fold change in miR-4793-3p relative to NC	Significant fold change in co-transfection relative to NC	Identification score	Confidence score	FDR corrected p-value
Taurine	124.0071	ESI-	M-H	C2H7NO3S	2.1	↑ **2.2**		1	37.8	0.0112
							↑ **2.1**			0.0302
5-Methylhexan-3-one	362.2531	ESI+	M+NH4	C9H16O3	↑ - **Not present in NC**	↑ - Not present in NC	↑ - Not present in NC	1	34.7	0.0112
2,2'-(3-methylcyclohexane-1,1-diyl)di-acetic acid	215.1275	ESI+	M+H	C11H18O4	↑ **1.9**	↑ 1.3	↑ 1.2	3	37.6	0.0216
Isocaproic acid	134.1174	ESI+	M+Na	C6H12O2	↑ **2.3**	↑ 1.4	↑ 1.2	20	39.4	0.0120
Creatine	154.0584	ESI+	M+Na	C4H9N3O2	↑ **2.1**	↑ 1.3	↑ 1.5	1	39.1	0.00189
	Cluster 2									
Glycerol-3-phosphate	171.006	ESI-	M-H	C3H9O6P	↓ 1.6	↓ 1.3	↓ **1.7**	2	38.6	0.0267
5-(methylthio)-2,3-Dioxopentyl phosphate	276.9702	ESI-	M+Cl	C6H9O6PS-2	↓ 1.7	↓ 1.3	↓ **1.9**	1	35.4	0.0267
Choline	104.1068	ESI+	M+H	C5H14NO	↓ 1.5	↓ 1.3	↓ **1.7**	12	39.2	0.0186
Glycerophosphocholine	280.0915	ESI+	M+Na	C8H20NO6P	↓ 1.5	↓ 1.3	↓ **1.6**	1	37.7	0.0186
	258.1097		M+H		↓ 1.5	↓ 1.2	↓ **1.6**	9	39.4	0.0195
(Z,Z)-3,6-Dodecadien-1-ol	221.0182	ESI+	M-H2O+H	C12H22O	↓ 1.7	↓ 1.3	↓ **1.7**	2	35	0.0195
8-Hydroxypinoresinol 4-glucoside	537.1943	ESI+	M+H	C26H32O12	↓ 2.2	↓ 1.7	↓ **2.8**	3	34.7	0.0377

5.2.2.3 Metabolic pathway enrichment analysis

Based on the analysis from MetaboAnalyst 3.0, the altered metabolites were mapped to nine key metabolic pathways (Table 5.3, Figure 5.6). Glycerophospholipid was the only significantly enriched pathway for choline, glycerophosphocholine and glycerol-3-phosphate.

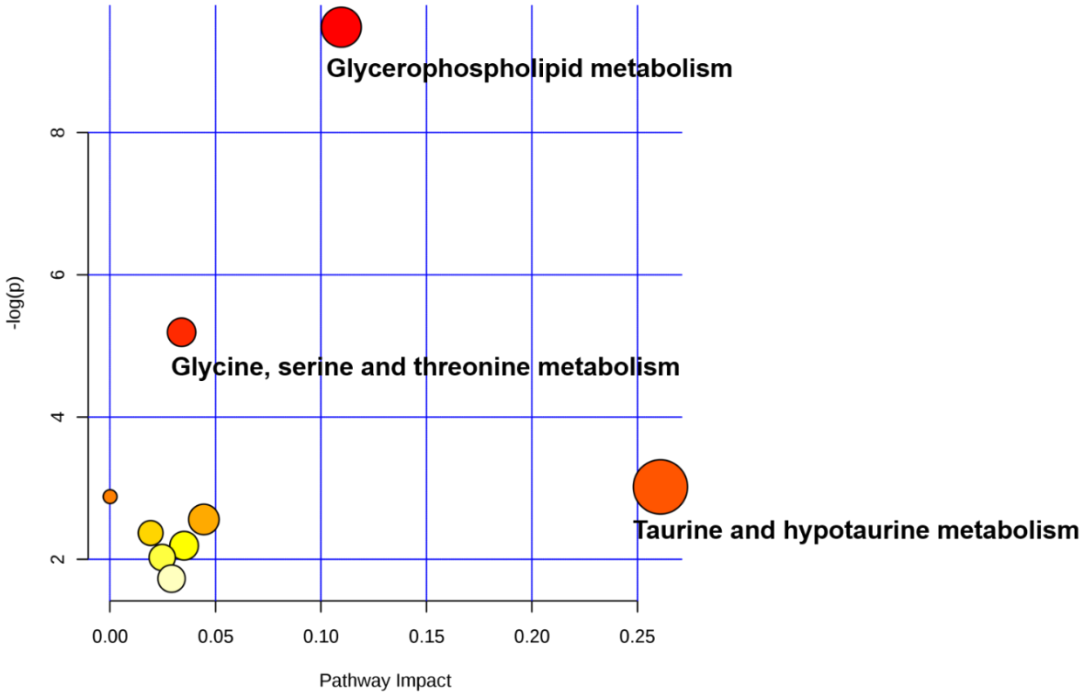


Figure 5.6: Graphical representation of significantly altered pathways following miR-619-5p and miR-4793-3p individual or co-transfection.
P-values for each matched pathway was calculated from the pathway enrichment analysis (threshold was set to 0.05 following FDR correction), and the impact-value was calculated from the pathway topology analysis (threshold was set to 0.10). The colour shades from red to yellow denote different levels of significance where red is highly significant.

Table 5.3: Metabolic pathway enriched for the significantly changed metabolites following miRNA transfection. *Fisher's exact test was applied for the over-representation analysis, and Degree Centrality was chosen for the topology analysis, p-values were corrected for multiple comparisons using the false discovery rate (FDR).*

Pathway	Total	Hits	Names of metabolites	Raw p value	- Log(p)	FDR	Impact
Glycerophospholipid metabolism	39	3	Choline, glycerophosphocholine and Glycerol-3-phosphate	7.6E-05	9.483	0.006	0.110
Glycine, serine and threonine metabolism	48	2	creatine and choline	5.6E-03	5.194	0.222	0.034
Taurine and hypotaurine metabolism	20	1	Taurine	4.9E-02	3.018	1.000	0.261
Ether lipid metabolism	23	1	glycerophosphocholine	5.6E-02	2.882	1.000	0.000
Glycerolipid metabolism	32	1	Glycerol-3-phosphate	7.7E-02	2.561	1.000	0.044
Nitrogen metabolism	39	1	Taurine	9.3E-02	2.370	1.000	0.019
Primary bile acid biosynthesis	47	1	Taurine	1.1E-01	2.192	1.000	0.035
Cysteine and methionine metabolism	56	1	2,3-Diketo-5-methylthiopentyl-1-phosphate	1.3E-01	2.026	1.000	0.025
Arginine and proline metabolism	77	1	creatine	1.8E-01	1.729	1.000	0.029

5.2.3 Lipidomics analysis of intra-cellular polar metabolites with LC-tandem MS/MS

A total of 6201 and 3577 peaks were detected in the positive and negative ionisation modes, respectively. Despite the detection of thousands of compound ions, only a total of 382 lipid species were putatively identified using LipidSearch due to the inherent complexity of lipid structures.

Different grades of identification were obtained for lipid species based on the confidence of lipid class and fatty acid structure. The lipidomic profiles of miR-619-5p and miR-4793-3p or co-transfection were then compared to that of NT. Lipids with grade C identification and an average fold change of >1.6 or <0.7 were grouped into lipid classes to demonstrate the pattern of how major lipid species were altered following miR-619-5p and miR-4793-3p overexpression (Table 5.4).

Initially, I found 27, 84 and 24 lipid species to be differentially abundant between NT and miR-619-5p, NT and miR-4793-3p and NT and co-transfection, respectively. Then, only four lipids species were identified as significantly altered following FDR correction (Figure 5.7). The contents of the triglyceride species [TG (18:0/18:1/18:1)] were 1.4 fold lower in GBM cells

overexpressing miR-619-5p compared to the control cells while triglyceride species [TG (18:1/18:2/20:3)] were 1.3 folds higher in GBM cells overexpressing miR-4793-3p compared to the control cells.

The phosphatidylcholine [PC (18:1/20:4)] was 1.4 folds lower in miR-4793-3p than in NT. Finally, the sphingomyelin [SM (d20:0/14:0)] exhibited 1.6 times higher levels in miR-619-5p relative to NT. No significant change in lipid species was observed when comparing NT and co-transfection.

Table 5.4: Lipid classes of significantly altered lipid species before FDR correction in cells overexpressing miR-619-5p and miR-4793-3p.
Lipid classes are shown within their lipid category: pink for glycerolipids, yellow glycerophospholipids and light blue for sphingolipids. The number of each lipid species increased or decreased in abundance compared to non-targeting control (NT) is indicated under each class. Zero indicates no relative difference in abundance above the threshold for statistical significance (t-test < 0.05, before FDR correction), grade (C or above) and the average fold change (<1.6 or >0.7) when compared to NT. Abbreviations: TG - triglyceride; DG - diacylglycerol; PC - phosphatidylcholine; LPC - lysophosphatidylcholine; PE - phosphatidyl-ethanolamine; LPE - lysophosphatidylethanolamine; PG - phosphatidylglycerol; PS - phosphatidyl-serine; PI - Phosphatidylinositol; SM - sphingomyelin; Cer - ceramide.

	TG	DG	PC	LPC	PE	LPE	PG	PS	PI	SM	Cer
	miR-619-5p										
Up	0	0	0	0	0	0	3	0	0	3	1
Down	15	2	0	0	0	0	0	0	1	1	1
	miR-4793-3p										
Up	9	0	0	0	0	0	0	0	0	0	0
Down	0	7	28	1	14	1	2	2	1	18	1
	Co-transfection										
Up	3	0	1	0	2	0	0	0	0	0	0
Down	0	6	2	0	0	0	0	0	1	9	0

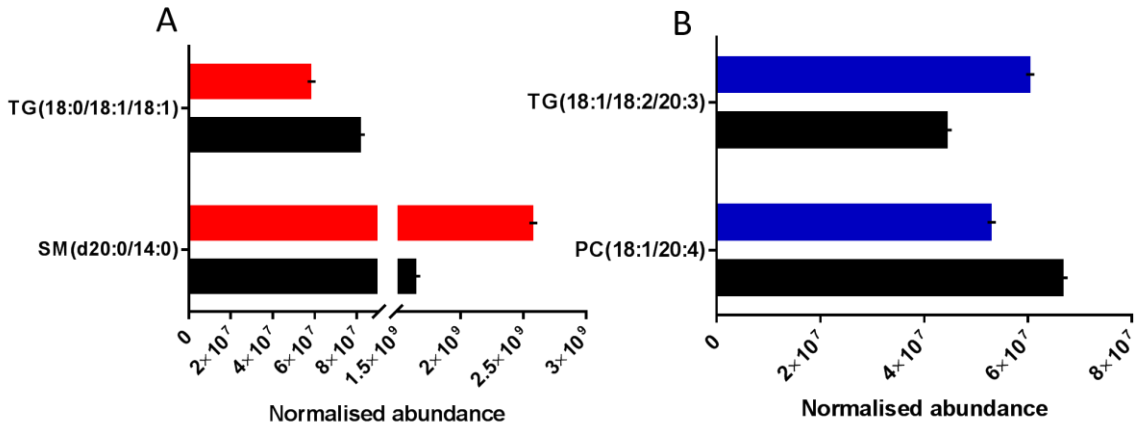


Figure 5.7: Abundance levels of significantly altered non-polar metabolites following (A) miR-619-5p and (B) miR-4793-3p transfections.
Values are shown as mean ± standard error. *Abbreviations: PC - phosphatidylcholine; SM - sphingomyelin; TG - triglyceride.*

5.2.4 Lipid droplets (LD) analysis in U87 cells

From my lipidomics study, I found an interesting pattern within the glycerolipids pathway (Table 5.4). The levels of triglyceride species were downregulated in miR-619-5p but upregulated in miR-4794-3p and NT. However, the levels of diacylglycerol species were downregulated in all the samples. Thus, I used Nile Red to perform an in situ staining of triglyceride (Figure 5.8).

I found that the stained triglyceride, which is localised to the LD and thus is indicative of the number of LDs in the cell, was significantly reduced in miR-619-5p compared to NT. In the co-transfected sample, triglyceride was also reduced but to a lesser extent than that in miR-619-5p (Figure 5.9).

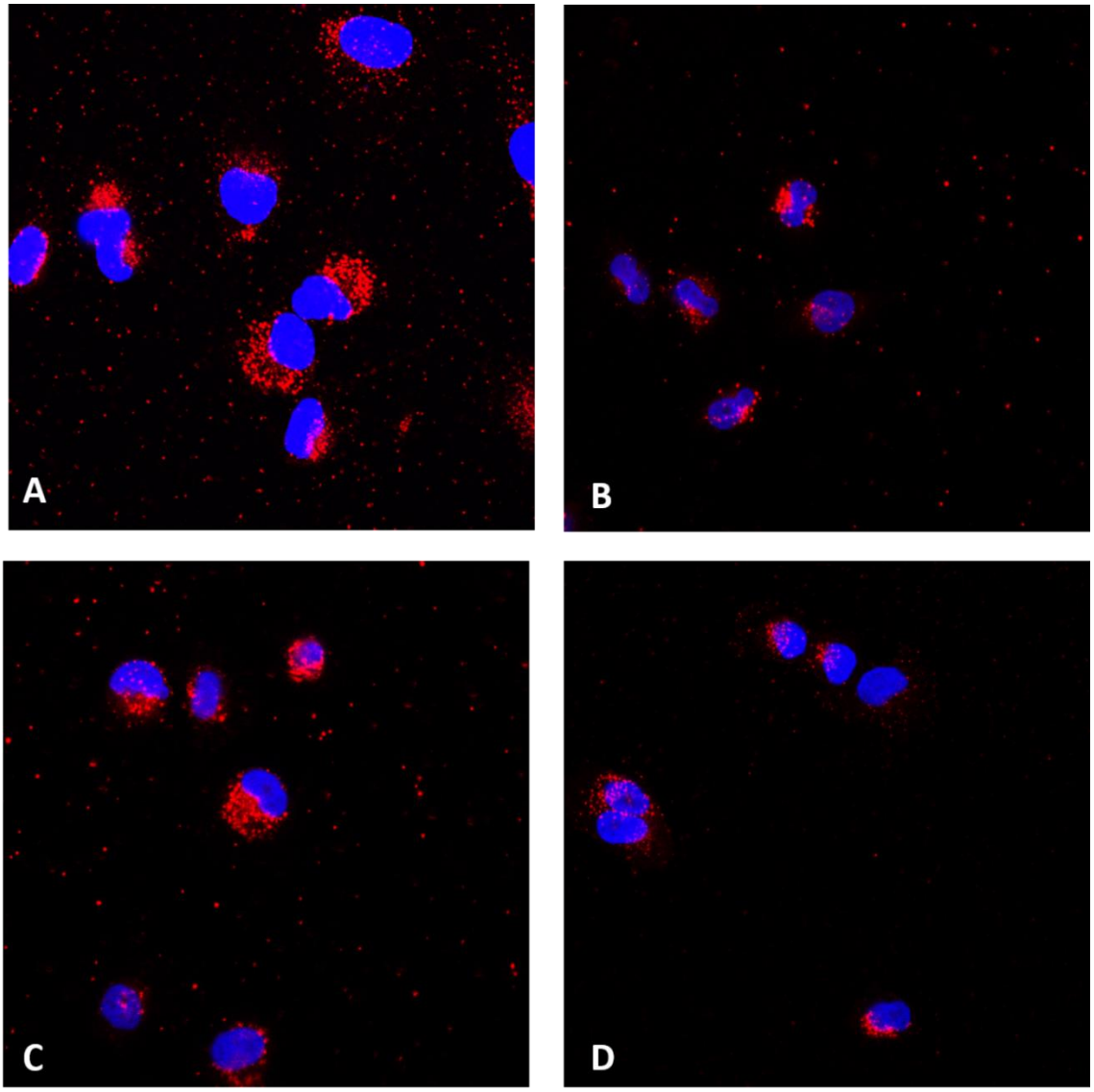


Figure 5.8: Confocal analysis of lipid droplets in U87 cells following miR-619-5p and miR-4793-3p individual or co-transfection.

U87 cells stained with Nile Red (1mg/ml) after 72h of (A) non-targeting control transfection, (B) miR-619-5p, (C) miR-4793-3p, and (D) co-transfection of both miRNAs at 1:1 ratio. Nile red (red) stains triacylglycerol content of lipid droplets while DAPI (blue) stains the nucleus.

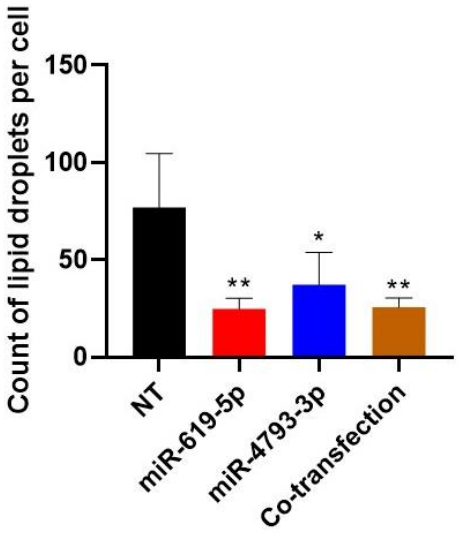


Figure 5.9: Count of lipid droplets per cell in U87 cells following miR-619-5p and miR-4793-3p individual or co-transfection.
*Data is shown as mean ± standard error. Statistical analysis using ANOVA (P<0.01 = **) followed by Bonferroni's multiple-comparison test comparing each transfection condition to NT; ** p-value < 0.01; * p-value < 0.05.*

5.2.5 LDs analysis in GBM patient samples

Since the work of this chapter has been conducted using the U87 cell line, I found it valuable to evaluate the levels of lipids and metabolites in actual patient GBM tissue. A different project in our laboratory is conducting global metabolomics and lipidomics studies on multi-regional tumour samples from 3 GBM patients. Therefore, instead of repeating the same work, I focused on LDs in multi-regional tumour samples to follow up on my work in the GBM cell cultures.

Because PLIN2 is the first lipid droplet surface protein to be identified, it has been considered as the marker protein of LD (Straub *et al.*, 2013). I first optimised the antibody concentration for anti-PLIN2 antibodies using breast carcinoma tissue sections, which are known to exhibit positive staining for PLIN2 (according to the TGCA database). Two concentration were tested, 1:50 and 1:100 as recommended by Kohe et al., 2017 (Kohe *et al.*, 2017). The concentration, 1:50, showed sharp and localised staining with minimal background staining, while lowering the concentration to 1:100 resulted in faded staining. Thus, 1:100 was not used for subsequent experiment, and 1:50 was used instead.

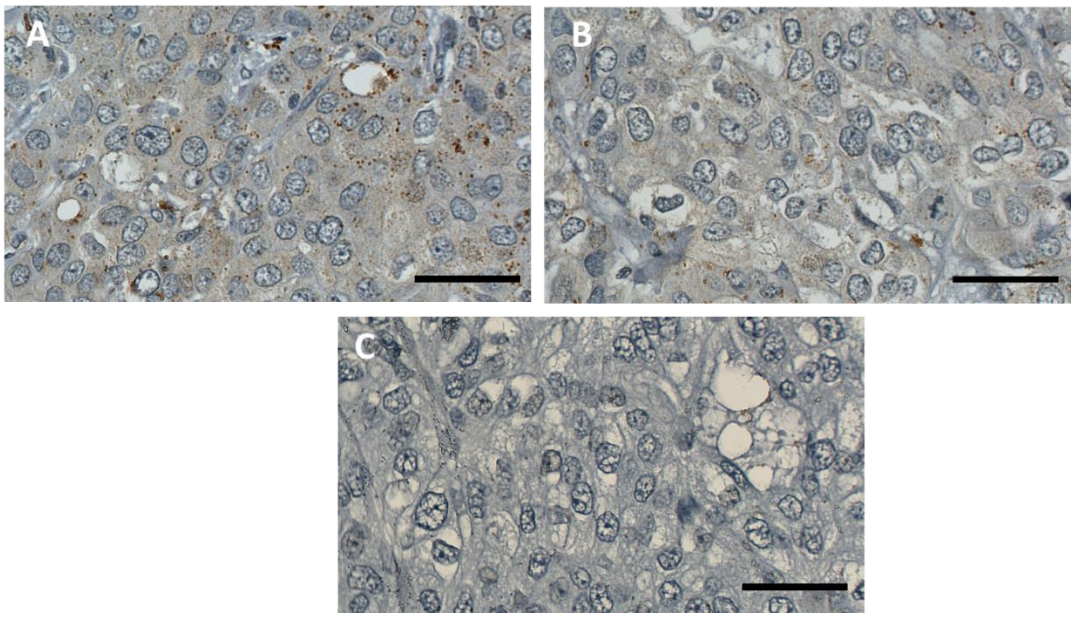


Figure 5.10: Optimisation results of primary anti-PLIN2 antibody on breast carcinoma tissue.
All images were captured at 40x magnification, scale bar: 50μm. (A) 1:50 dilution; (B) 1:100 dilution; and (C) negative control.

Using 1:50 as the optimal dilution, I stained tissue microarrays containing triplicate samples of each of the three regions (core, rim and invasive margin) of the GBM tumour from 36 patients with PLIN2 (**Error! Reference source not found.**). Next, quantification of the percentage of tumour cells containing cytoplasmic positivity for PLIN2-stained lipid droplets was performed (**Error! Reference source not found.**). I observed no significant change in PLIN2 expression between the different regions of the tumour. No strong PLIN2 positivity was detected within the normal brain, suggesting that lipid droplets might be present only at low levels in normal brain tissue.

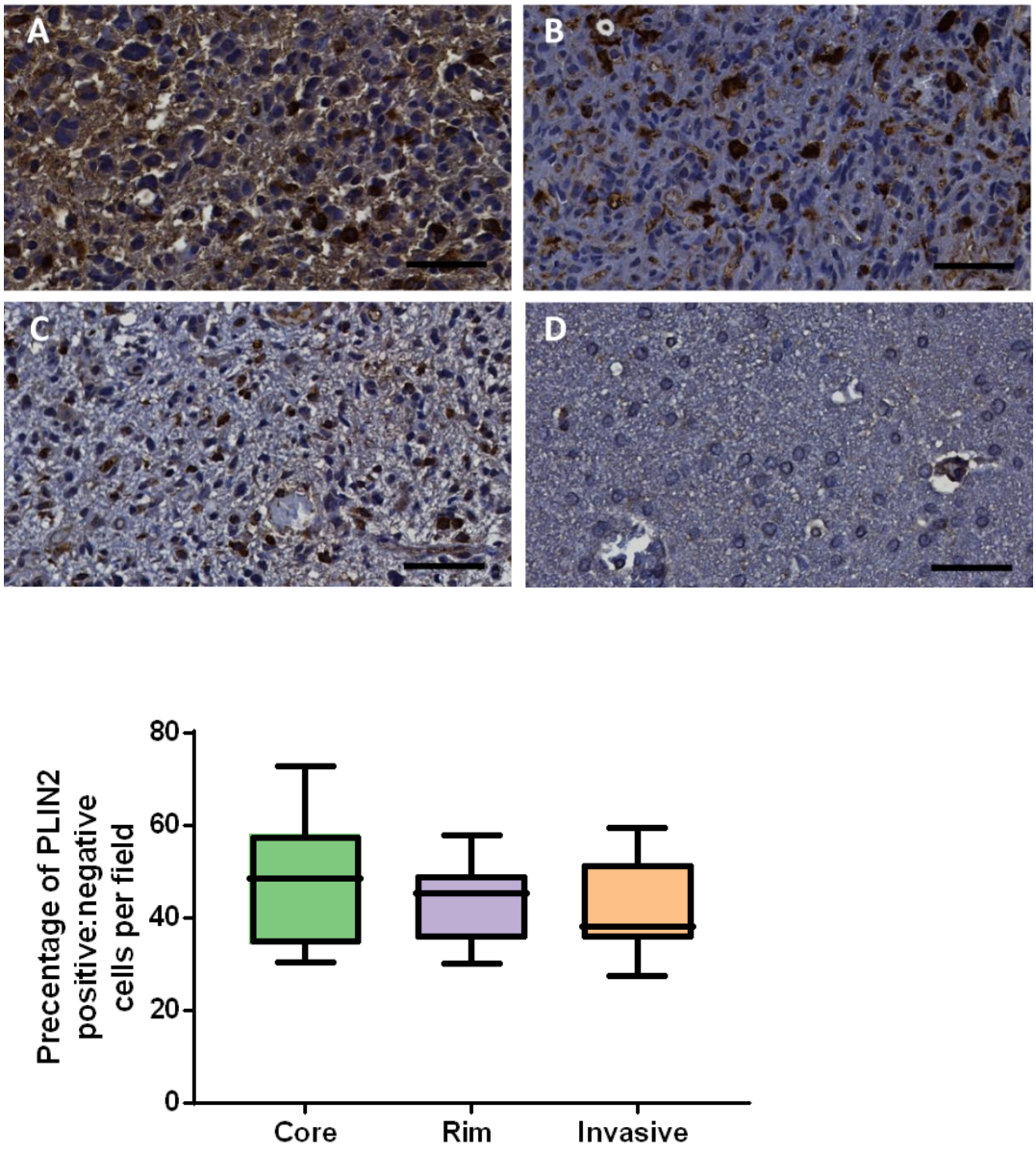


Figure 5.11 Immunohistochemical staining pattern of PLIN2 in GBM tumours.

Immunohistochemical analysis of adult GBM tissue microarrays at 1:100 anti-PLIN2 dilution *are shown as representative images of each region; tumour (A) core (B) rim (C) invasive margin and a (D) normal brain control are shown. All images were captured at 40x magnification; scale bars correspond to 50 μm.*

The box blot shows, per tumour region, the number of cells containing PLIN2-positive cytoplasmic staining represented a percentage of the total number of cells counted on each high-powered microscope fields of view (captured at 40x magnification) taken from a TMA tissue core. Statistical analysis

using ANOVA (P>0.05) sowed no significant difference between the regions.

5.3 Discussion

Based on miRNA target prediction analysis, both miR-619-5p and miR-4793-3p regulate genes within the FAO and glycerophospholipid biosynthesis pathways. In chapter 4, I showed that miR-619-5p and miR-4793-3p regulate genes in the FAO pathway. In this chapter, I demonstrate that miR-619-5p and miR-4793-3p regulate the levels of multiple metabolites within the glycerophospholipid biosynthesis pathway.

The work of this chapter described 40 significantly-changed metabolites from the polar metabolites pool; however, only 12 were identified using the Human Metabolome Database (HMDB). This is a key limitation of the untargeted metabolomics approach in general, where a large amount of mass ion peaks are detected but only a small subset correspond to a match in metabolite databases (Patti, Yanes and Siuzdak, 2012).

Moreover, the pathway analysis will only accept metabolites that have been identified. There are two potential sources of bias here: the small number of metabolites I put through pathway analysis, and limited capability of the database to

identify metabolites across a broad range of pathways. On the one hand, the reason I had a small number of metabolites to put through the pathway analysis was because I eliminated non-significantly changed metabolites by conducting an FDR-correction step; my intention was to only take significantly-changed metabolites forward for pathway analysis. If anything, this reduces bias. On the other hand, because the identified metabolites were mapped to nine different pathways and not just to lipid-related pathway, I can be confident that there won't be any bias in the types of pathways found to be differentially regulated because of the contents of the database which includes metabolites from a wide variety of pathways, not only those based on lipids.

That said, the glycerophospholipid biosynthesis pathway did have the highest number of metabolites mapped to it. Although this does not neglect the importance of pathways, it does give reason to further investigate the potential relevance of glycerophospholipid pathways in particular, if only one option was to be chosen.

I will now discuss each of the identified metabolites, in turn. Phosphatidylcholine is a major glycerophospholipid component

of the phospholipid monolayer of the cell membrane, mitochondrial membrane and LDs. Various research groups have shown using 1H-MRS that phosphatidylcholine is significantly higher in GBM compared with normal brain tissues (Tugnoli *et al.*, 2001; Srivastava *et al.*, 2009). In my lipidomics study, I found phosphatidylcholine levels to be downregulated in U87 cells overexpressing miR-4793-3p compared with un-transfected cells. The same pattern, although not statistically significant, was also seen for cells co-transfected with both miR-4793-3p and miR-619-5p; which may suggest that miR-4793-3p is the main effector miRNA or that miR-619-5p requires miR-4793-3p to exert its effect.

To explain this observation, I considered the levels of the upstream component of the phosphatidylcholine biosynthesis pathway generated from my metabolomics study. The CDP-choline pathway produces the majority of phosphatidylcholine in the cell (Fagone and Jackowski, 2013). Therefore, I hypothesised that low levels of precursor metabolites in the CDP-choline pathway might result in low levels of the end product, phosphatidylcholine.

Studies showed that elevated total cellular levels of choline-containing metabolites detected by 1H-MRS, primarily choline - the initial substrate for the CDP-choline pathway, can serve as a diagnostic biomarker for GBM tumours (Reviewed in Horská & Barker, 2010). However, I found that choline levels were reduced after the miR-619-5p and miR-4793-3p individual or co-transfections. Based on the literature, I can speculate two possible causes for detecting low levels of choline in the cell.

The first cause may be the low amount of choline supplied to the cells. Mammalian cells are unable to synthesise choline *de novo* and instead rely on exogenous dietary sources. During choline deficiency, the intracellular concentrations of choline were shown to decrease rapidly in hepatic cells (Zeisel *et al.*, 1989). In my experiment, the amount of choline supplied in the cell culture medium was identical across all of the experimental conditions; thus, differences in intra-cellar choline could not be due to variations in the exogenous choline levels.

The second cause may be the low amount of choline transported into the cells. Choline is taken up into cells via facilitative transport; as such, it could be hypothesised that differences in choline transporters expression could alter the amount of

choline present in the cell. The uptake of choline is accomplished predominantly by intermediate-affinity transporters, such as choline transporter-like protein 1 (CTL1), which is specifically proposed to regulate choline supply for the synthesis of phosphatidylcholine (Michel *et al.*, 2006). CTL1 has been shown to be upregulated in multiple cancers; which facilitates an increased choline uptake (Machová *et al.*, 2009; Inazu *et al.*, 2013). Interestingly, I identified CTL1, encoding by SLC44A1 gene, as a putative target for both miR-4793-3p and miR-619-5p. Thus, it could be expected that CTL1 will be downregulated upon miR-4793-3p and miR-619-5p overexpression; therapy leading to decreased choline uptake. This hypothesis could be tested by evaluating the mRNA and protein levels of CTL1 as well as the rate of choline uptake by biochemical assays following 72h of miR-4793-3p and miR-619-5p overexpression and after the direct knockdown of CTL1 by siRNA in U87 cells.

Several studies showed that phosphatidylcholine biosynthesis is closely linked to the availability of choline (Li and Vance, 2008). A study in human leukemic monocyte-like U937 cells showed that Lidocaine, a local anaesthetic, inhibited the uptake of choline into the cells and reduced phosphatidylcholine levels by

limiting the availability of choline for the CDP-choline biosynthetic pathway (Chu and Lee, 1994). Another interesting study in human alveolar epithelia-derived A549 cells showed that the anticancer agent, gefitinib, reduces phosphatidylcholine biosynthesis by inhibiting cellular choline uptake by CTL1 (Ishiguro *et al.*, 2008).

This relationship makes it difficult to dissociate changes in choline transporter expression from secondary effects driven by other enzymes that affect the metabolic flux through the CDP-choline pathway. For example, facilitated uptake of choline is enhanced by its rapid phosphorylation by choline kinases, encoded by CHKA and CHKB genes. Interestingly, CHKA is predicted to be a putative target for both miR-4793-3p and miR-619-5p. Likewise, the rate-limiting step in CDP-choline pathway is catalysed by CTP:phosphocholine cytidylyltransferases (CCTs), encoded by PCYT1a and PCYT1b genes (Kalmar *et al.*, 1994; Lykidis, Murti and Jackowski, 1998), which were highlighted by the target prediction analysis as putative targets for both miR-619-5p and miR-4793-3p.

Thus, these targets need to validate, and the contribution of individual enzymes to altered choline metabolism in GBM cells

must be dissected using pharmacological or siRNA silencing methods. However, such experimental series is proven to be beyond the timeline time for this project and was left as an area of future work.

In the final step of the CDP-choline pathway, the choline head group is added onto a diacylglycerol (DAG) backbone to form phosphatidylcholine (see introduction chapter). DAG is made from glycerol 3-phosphate (G3P). I found DAG, although not statistically significant, to be downregulated after the miR-619-5p and miR-4793-3p individual or co-transfections. Likewise, I found the DAG precursor, G3P, to be indeed significantly downregulated in cells overexpressing either miR-619-5p or miR-4793-3p or in cells overexpressing both miRNAs together. As such, the availability of DAG and G3P could affect the levels of phosphatidylcholine.

Both G3P and choline are products of glycerophosphocholine (GPC) degradation by glycerophosphodiesterase (GDE); whereas GPC itself is a product of phosphatidylcholine degradation by phospholipase PLA1 and PLA2. Typically, astrocytomas have increased levels of GPC (Righi *et al.*, 2009). However, the levels of GPC were decreased following miR-619-

5p and miR-4793-3p individual or co-transfections. While GDE is not, PLA1 is a putative target for miR-619-5p and PLA2 is a putative target for both miR-619-5p and miR-4793-3p. Hence, a reduction of PLA1/2 expression may imply a reduction of phosphatidylcholine degradation into GPC; especially since the levels of phosphatidylcholine are already low in cells overexpressing miR-619-5p and miR-4793-3p. Furthermore, since GPC levels were low, both G3P and choline can be expected to be low; which is what I observed.

Levels of creatine are often reported to be reduced in GBM relative to normal brain tissue in 1H-MRS studies (Yerli *et al.*, 2007). In fact, a high ratio of choline-containing compounds (choline, phosphocholine, and GPC) to creatine became a distinct characteristic of GBM tumours (Castillo, 2013), although some exceptions were reported (Bowen, 2003). Like GBM tissue, U87 cell line is characterised by high choline to creatine ratio (Shao *et al.*, 2014). Consistent with this, my NT cells had a high choline to creatine ratio. However, comparison of the miR-619-5p and miR-4793-3p individual or co-transfection versus NT revealed a significant increase in creatine levels and a corresponding low choline/creatine ratio in

miR-619-5p cells and a similar pattern in miR-4793-3p and co-transfection conditions.

Creatine plays a key role in cellular energy buffering and transport. The mitochondrial creatine kinase (CK) converts (creatine and ATP) to (phosphocreatine and ADP) at sites of energy production (the mitochondria) in order to store the chemical energy in a more stable form. The cytosolic CK regenerates ATP via the anaerobic degradation of phosphocreatine to creatine and the re-phosphorylation of ADP to ATP at the ATP consuming sites (Bessman and Fonyo, 1966; Wallimann *et al.*, 1992). The mitochondrial isoform (CKMT1B) is a predicted putative target for miR-619-5p. This may suggest, if proven, that the transphosphorylation of creatine by ATP, which is catalysed by CKMT1B, might be compromised by the low expression of CKMT1B; thereby leading to creatine accumulation following miR-619-5p overexpression.

Since the mitochondrial membrane is composed of phosphatidylcholine, choline deficiency has been associated with mitochondrial dysfunction, the loss of membrane potential and the generation of high levels of ROS in hepatocytes (Vrablic *et al.*, 2001; Guo *et al.*, 2005). Therefore, although I have not

directly measured ROS levels, I can speculate that the low levels of choline might have resulted in an increase in the levels of ROS in the cell. With this assumption in mind, significantly high taurine levels observed in miR-4793-3p and co-transfection conditions (a similar pattern was observed in miR-619-5p) can be explained as a mean of protection from ROS. This is because taurine is a well-known neuroprotective antioxidant (reviewed in Menzie, Prentice, & Wu, 2013). In support of this notion, 5-(methylthio)-2,3-Dioxopentyl phosphate which is used for the synthesis of methionine, a precursor for taurine, is downregulated in cells transfected with miR-619-5p and miR-4793-3p; thereby suggesting that 5-(methylthio)-2,3-Dioxopentyl phosphate has been used up in the cell in order to make more taurine.

Sphingomyelin (SM), another class of phospholipid that are abundant in cell membranes (Slotte and Ramstedt, 2007), is made from phosphatidylcholine by SM synthases (SMS). Despite the augmented levels of phosphatidylcholine, GBM tumours maintain low levels of sphingomyelin SM (Abdel Hadi *et al.*, 2015). As such, GBM tumour cells seem to conserve the phosphatidylcholine pool instead of converting it into SM.

However, upon overexpressing miR-619-5p, while the levels of the phosphatidylcholine were decreased, the levels of SM were significantly increased compared to NT; likely reflecting changes to membrane structure due to aberrant biosynthetic reactions. This might suggest that phosphatidylcholine is converted into SM in miR-619-5p overexpressing cells. Although miR-619-5p is not predicted to target SMS, it could target a negative regulator of SMS, thereby exerting an activator effect on SMS function. For example, the SMS activator, 2-hydroxyoleic acid (2-HOA), a potent antitumor compound, strongly increased SM levels while causing a depletion in phosphatidylcholine levels and suppressing tumour growth (Barcelo-Coblijn *et al.*, 2011). As such, investigating the regulatory network of SMS and how miR-619-5p might control it would be an interesting future work area.

Although I predicted that miR-619-5p and miR-4793-3p regulate both FAO and glycerophospholipid biosynthesis pathways, it is possible that with the current limitation in metabolites identification, FAO-related metabolites were detected as mass ion peaks with no corresponding match in the HMDB. In addition, FDR correction can often result in rigorous elimination of significant findings (Noble, 2009). This could also

lead to excluding peak ions that corresponded to FAO associated metabolites. Indeed, I found that 3-hydroxyoctanoyl carnitine (m/z = 321.2394) was downregulated by 2.9, 1.7 and 1.5 folds following miR-619-5p, miR-4793-3p and co-transfection, respectively (FDR-corrected p-value = 0.19, 0.9 and 0.9).

Other identified metabolites that were not significant in my pathway analysis were not discussed here primarily because these metabolites have no reported significance in cell function and cancer biology.

Furthermore, the low fold change observed for the significantly abundant metabolites supports the notion that changes in miRNA expression induce subtle changes in the cell because of the multi-targeting property of miRNAs. In fact, PCA did not show clear separation for the four transfection conditions; possibly because differences, although significant, were not dramatic.

I was able to validate my findings from the lipidomics study that miR-619-5p transfected cells exhibit low levels of triacylglycerol, which was visualised in LDs. This could be attributed to the

possibility that miR-619-5p is targeting different genes that are involved in the synthesis of LDs.

According to my lipidomics analysis, triacylglycerol levels were increased in the miR-4793-3p and co-transfection conditions which is consistent with the recent proposal that in the absence of phosphatidylcholine synthesis, excess FAs could be re-directed into triacylglycerol biosynthesis (Barbosa and Siniossoglou, 2017). According to my Nile Red staining, however, I found that the co-transfected samples exhibited reduced levels of triacylglycerols, although miR-4793-3p had the expected high triacylglycerol abundance. This is perhaps due to the action of miR-619-5p not miR-4793-3p in the co-transfected samples.

It is worth noting that differences in triacylglycerol levels were not detected in the lipidomics analysis of co-transfection. This could be due to the rigorous FDR correction procedure required for large datasets generated from a global analysis of multiple lipid species. On the other hand, the analysis for Nile Red staining, which was focused on one lipid species, and this might allow a difference of such size to be detected.

The results of the staining of the LD associated protein, PLIN2, in GBM patient samples were not in agreement with my findings from Nile red staining. I found that PLIN2 expression was not significantly different between the tumour regions. This could be attributed to the technical difference in the type of experiment employed to label LD. Moreover, discrepancies between cells and tissue are often reported in the literature often due to the absence of the influence of the tumour microenvironment.

5.4 Future work

Although a decrease in LDs numbers correlated with the reduction in TGs levels in cells overexpressing miR-619-5p, I can not make the assertion that the TGs molecules solely belong to LDs. As such, a future study would directly isolate LDs from the cell so that LDs contents can be investigated separately by lipidomic analysis. Furthermore, in my patent tissue samples, I have visualised LDs in the cell by staining for PLIN2, which is a universal marker used for staining LDs. However, it might be interesting to stain for PLIN3; because PLIN3 was identified as a target for miR-619-5p. Staining for PLIN3 could indeed elucidate a difference in LDs regulation in different regions of GBM where miR-619-5p is differentially expressed.

5.5 Chapter summary

- An untargeted metabolomics screening revealed that miR-619-5p and miR-4793-3p are potential regulators of the phosphatidylcholine biosynthesis pathway.
- miRNA transfection exerted subtle changes on the intracellular metabolic profile, with an average fold change values of 1.5 for the significantly abundant metabolites between the transfection conditions.
- I found that the levels of phosphatidylcholine and its precursor metabolites, including choline, glycerol-3-phosphate and glycerophosphocholine, were downregulated upon miR-619-5p and miR-4793-3p overexpression.
- I speculated that miR-619-5p and miR-4793-3p might directly target or indirectly affects the expression of enzymes that regulate the relative proportion of substrates and products in the phosphatidylcholine biosynthesis pathway.
- Creatine had relatively higher abundance in GBM cells overexpressing miR-619-5p and miR-4793-3p when compared to the control cells.
- As such, the choline/creatine ratio was low in miR-619-5p and miR-4793-3p overexpressing cells.

- Taurine levels were upregulated upon miR-619-5p and miR-4793-3p overexpression; perhaps to act as an antioxidant.
- Only in GBM cells overexpressing miR-619-5p; however, the levels of sphingomyelin were increased while triacylglycerol levels were decreased; this is likely due to aberrations in the biosynthetic pathway.

Chapter 6:

miR-619-5p and miR-4793-3p regulate GBM cell invasion by targeting lipid metabolism enzymes

6.1 Introduction

miR-619-5p and miR-4793-5p have been shown to play a role in regulating lipid metabolism. In this chapter, I will investigate the effect of inhibiting lipid metabolism pathways, FAO in particular, on the invasiveness of GBM cells. I will perform *in vitro* transwell assay following miR-619-5p and miR-4793-5p overexpression. Moreover, I will perform *in vitro* transwell assay following siRNA-mediated inhibition of the direct miR-619-5p target gene, CPT2. Next, I will assess invasion following the pharmacological inhibition of FAO through the re-purposing of perhexiline and etomoxir, which were initially developed to treat cardiovascular diseases (Burns-Cox *et al.*, 1971; Schmidt-Schweda and Holubarsch, 2000; Holubarsch *et al.*, 2007). I therefore endeavoured to characterise the therapeutic potential of targeting FAO as a way to attenuate GBM invasion.

GBM cells acquire the ability to invade into the surrounding brain parenchyma by breaking through ECM. Moreover, many of the invading cells move along perivascular spaces (Zagzag *et al.*, 2008). The close proximity of GBM cells to the blood vessels assures a constant supply of oxygen and nutrients essential for cell growth. The association with the vasculature also exposes GBM cells to various chemotactic factors, including growth

factors, chemokines, cytokines and kinins (Montana and Sontheimer, 2011).

The term chemotactic factor (or chemoattractant) refers to a molecule which stimulates the directional locomotion of cells across its gradient. The directional cell movement toward a chemotactic factor is known as chemotaxis.

I am aware of the different models for assessing the locomotion of cells *in vitro* - See Introduction Section 1.2 for the comparison between methods. Here, I use the Boyden chamber assay, also known as filter membrane assay, chemotaxis assay, or transwell assay, which was originally introduced by Boyden to study leukocyte chemotaxis (Boyden, 1962). The Boyden chamber assay has become one of the most commonly used assays to study cancer cell migration and invasion (Roussos, Condeelis and Patsialou, 2011).

The classical Boyden chamber consists of two medium-filled compartments. The compartments are separated by a microporous membrane which represents a physical barrier that cells placed in the upper compartment can overcome only by active migration through the pores into the lower compartment,

in which a chemotactic factor is present. The size of the pores used is smaller than the diameter of the cell, thereby preventing passive movement of cells through the pores. As such, the cells need to rearrange their cytoskeleton structure in order to extend their leading edge to get through the pores, moving in dimensional (3D) space.

The Boyden chamber can be adapted to study invasion by coating the microporous membrane with a variety of ECM proteins to create a barrier for cells to invade through (Figure 6.1). ECM proteins support cell attachment and promote invasiveness by exerting mechanical force and biochemical effects on the shape and the composition of the plasma membrane of the cell.

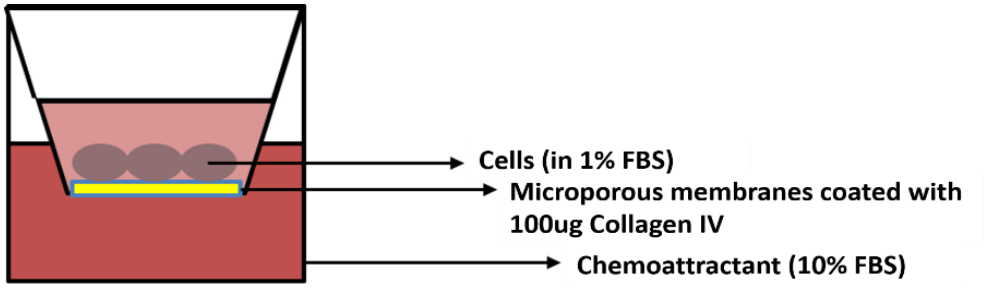


Figure 6.1: Graphical illustration of the transwell invasion assay.
Cells are seeded on a porous membrane coated with collagen IV. After an appropriate incubation time, the cells that have invaded through to the lower side of the membrane can be fixed and stained to be counted, or the presence of cells on lower-side of the membrane can be quantified by a colourimetric assay. Ultimately, the readout of the assay is the number of cells that

relocate from the upper to the lower compartment in response to the chemoattractant. FBS:foetal bovine serum.

I chose to employ Boyden chamber assay to understand the relative change in cell invasion, following manipulating the levels of miRNA or their target gene/pathway, for several reasons. First, it is the most convenient option, given the limited time-scale of the project at the point of conducting this work. Second, it is the most cost-efficient assay, given the number of conditions I wanted to test. Third, the Boyden chamber is the most commonly employed chemotaxis assay in GBM, making interpreting my results in the context of the literature more relevant.

Finally, the Boyden chamber assay is more suited to accommodate the time restriction placed on the assay by the sensitivity of the duration of miRNA transfection treatment prior to the assay. Throughout this project, I studied the effect of my miRNAs after 72h of transfection (including the 24h that the cells are in the transfection media). Thus, I have a time window of 48 hours post-transfection to conduct the invasion assay within. Compared to other 3D assays, such as spheroids, only the Boyden chamber assay can be measured within this time frame.

I selected the appropriate assay parameters for GBM cells. First, I determined that the most used pore size for GBM cells in the literature is 8.0 μm. Second, I coated the membrane with collagen IV. Finally, I choose to use the staining method for the quantification of invading cells because it takes morphologic features into account.

There are several reasons why I chose to use collagen IV over Matrigel, the best known commercially available ECM. Matrigel, a natural ECM extracted from the Engelbreth-Holm-Swarm (EHS) mouse sarcoma, has major disadvantages which can lead to difficulties with reproducibility of the assay. Firstly, the Matrigel's exact constituents are not clearly defined; it is composed of approximately 60% laminin, 30% collagen IV, and 8% entactin. This causes batch-to-batch variation, which unfavourably affects reproducibility. Secondly, Matrigel contains an unknown mixture of growth factors and enzymes that naturally occur in the EHS tumour, such as: Transforming growth factor beta 1, epidermal growth factor, insulin-like growth factor, fibroblast growth factor, tissue plasminogen activator, and residual matrix metalloproteinases (Hughes, Postovit and Lajoie, 2010). Even if a growth factor-reduced

matrigel was used, the presence of unknown amounts of growth factors in different batches may influence the reproducibility of the assay and/or interfere with the gradient of, and perhaps the response to, the chemotactic factor used in the assay.

To overcome this, a single matrix protein can be purified from the EHS mouse sarcoma. The ECM of GBM consists of collagen IV, laminin and fibronectin, which are mainly localised to the basement membrane of the blood vessels (Chintala *et al.*, 1996); and tenascin-C, vitronectin and hyaluronan, which surround the tumour (Bellail *et al.*, 2004; Zamecnik, 2005)
While low in the normal brain ECM, collagen IV levels are elevated in the ECM of the GBM and play a key role in driving tumour progression (Ogawa *et al.*, 1989). Thus, I chose to the coat Boyden chamber with the collagen IV component of the basement membrane that lines the blood vessels because blood is a source of chemotactic factors and the *in vitro* assay I am using is more suited for measuring chemotaxis. The Boyden chamber assay will thereafter be referred to as the transwell assay.

Because invasive edge cells cannot be eliminated with surgical resection or be completely targeted by conventional

radiotherapy (thereby leading to tumour recurrence), understanding more about the invasive property of GBM is of interest to this thesis project. In this chapter transwell invasion assay will be performed in U87 and the GIN28 primary GBM cell line 72h following miR-619-5p mimic transfection, miR-4793-3p mimic transfection, miR-619-5p/miR-4793-3p mimic co-transfection or non-targeting mimic negative control transfection in order to functionally validate the role of these miRNAs in GBM. Transwell invasion assay will also be performed in U87 and GIN28 cells 72h following siRNA transfection against CPT2 in order to establish whether the phenotypic effects of miRNA overexpression on invasion is due to its action on a gene target. Finally, a pharmacological inhibitor of CPT2 will be used to treat U87 and GIN28 cells for 72h before performing the transwell invasion assay in order to assess the therapeutic implication of the identified miRNA gene targets.

Hypothesis (1): miR-619-5p is upregulated in the tumour core where its target gene, CPT2, is downregulated – a pattern that is inverted in the tumour's invasive margin. Therefore, I hypothesise that the overexpression of miR-619-5p or the inhibition of CPT2 will reduce cell invasiveness.

Hypothesis (2): Since miRNAs exert their biological effect through suppressing the expression of their gene targets, I hypothesise that siRNA treatment against miRNA targets will give similar results to those obtained from miRNA overexpression, and hence will reduce cell invasiveness.

Hypothesis (3): The treatment of GBM cells with FAO inhibitors, perhexiline or etomoxir, will reduce cell invasiveness.

6.2 Results

6.2.1 Optimisation of the transwell invasion model to test the invasion of the U87 cells

Throughout this project, I used U87 cells to carry out optimisation work due to the similarity in cell size and growth rate between U87 and GIN28 cells. As such, U87 will be used to optimise the cell number for the transwell invasion assay, and the knowledge of the optimised cell number will be used to carry out the transwell invasion assay in GIN28 cells.

6.2.1.1 Optimisation of collagen coating consistency

I purchased Cultrex® Collagen IV Cell Invasion Assay, which recommends using 100µg (200µl) of collagen IV as the maximum invasion barrier for highly invasive cells, such as GBM cells. I initially left the collagen IV coat to air-dry overnight in the cell the culture hood. Once dried, collagen IV formed a thin white layer on top of the membrane; however, I noticed a non-homogenous distribution of the collagen IV coat across the insert. Thus, I instead dried the inserts in a non-humidified 37C incubator shaking overnight. As a result, I achieved uniform coating across the membrane, which was also consistent in all my inserts; thereby providing a reliable assay for future use.

6.2.1.2 Optimisation of cell seeding density

The seeding density of U87 cells was determined by testing three different seeding densities commonly reported in the literature. These seeding densities were 1×10^4 cells/well (An *et al.*, 2013), 2.5×10^4 cells/well (Chen *et al.*, 2018), and 5×10^4 cells/well (Zhou *et al.*, 2015). Although 24h is the standard length of the assay in the literature (such as in Xue *et al.*, 2016), the duration of the assay was optimised over three time-points:

at 12h, 24h,and at an intermediate time-point (16h) as I am the first to use Collagen IV in transwell assays for GBM cell invasion.

For each cell concentration at a given time-point, I tested three serum conditions:

For condition 1:

FBS gradient was applied across the two compartments of the transwell. Cells were seeded in 200µl of 1% FBS DMEM medium in the upper compartment while 400µl of 10% FBS DMEM medium was used as a chemotactic factor in the lower compartment.

Until now, this FBS gradient is the most frequently reported in the literature to be used with GBM cells (Lara-Velazquez *et al.*, 2019; Omar Zaki *et al.*, 2019). The volume of the DMEM medium in the lower compartment was chosen as the minimum amount of medium to be added in order to fill the compartment up to the point that touches the bottom of the upper compartment.

For condition 2:

- 1% FBS DMEM medium was added to both upper and lower compartments.

For condition 3:

- 10% FBS DMEM medium was added to both upper and lower compartments.

I found that the seeding density of 2×10^4 cells/well (Figure 6.3) demonstrated a clear difference in invasion towards the FBS gradient compared to the other seeding densities 1×10^4 cells/well (Figure 6.2) and 5×10^4 cells/well (Figure 6.4). Thus, 2×10^4 cells/well will be used as the optimal seeding density for the subsequent experiments.

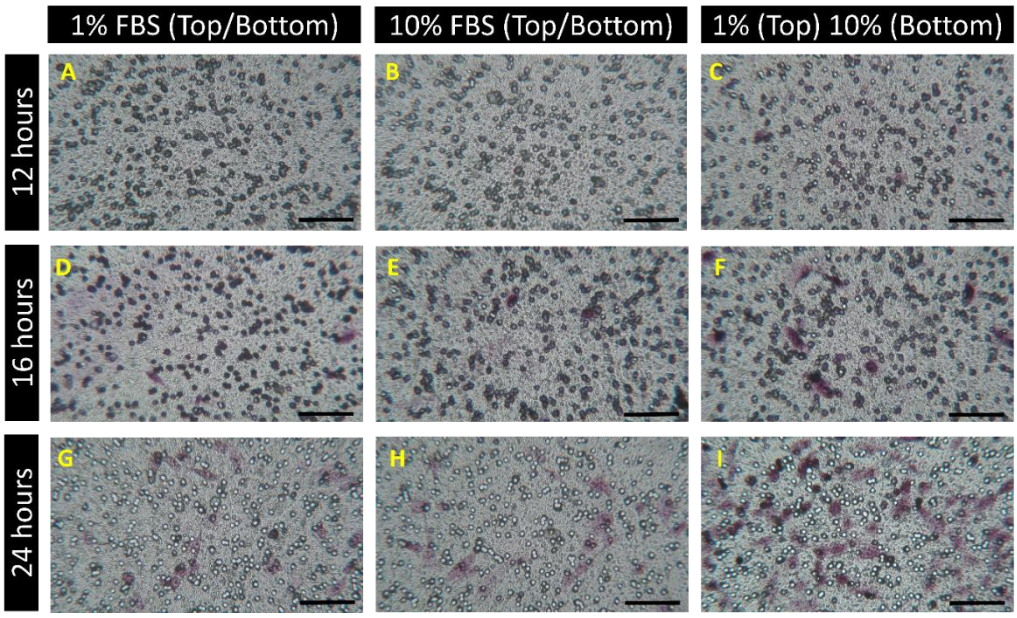


Figure 6.2 Optimisation of U87 cells invasion through collagen IV coated transwell inserts at a seeding density of 1×10^4 cells/well.
Plates were incubated at 37C at 5% CO2. Representative images of invasive cells at the bottom of the membrane, which was fixed with methanol and stained purple with 0.5% crystal violet. Images were captured at x40 magnification; scale bar corresponds to 100µm. Abbreviation: FBS -fetal bovine serum.

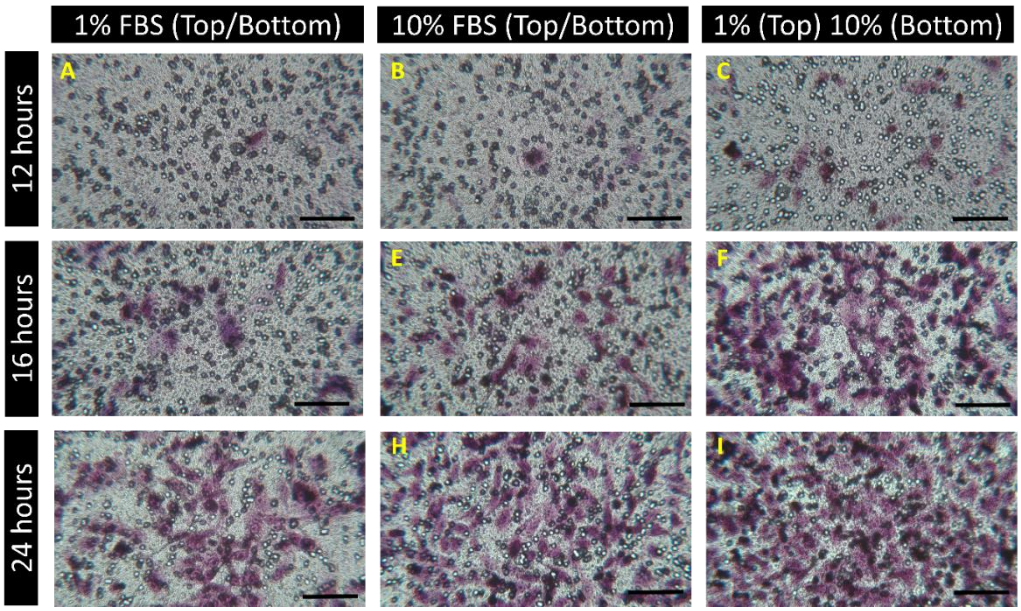


Figure 6.3 Optimisation of U87 cells invasion through collagen IV coated transwell inserts at a seeding density of 2 ×10⁴ cells/well.

Plates were incubated at 37C at 5% CO2. Representative images of invasive cells at the bottom of the membrane, which was fixed with methanol and stained purple with 0.5% crystal violet. Images were captured at x40 magnification; scale bar corresponds to 100µm. Abbreviation: FBS -fetal bovine serum.

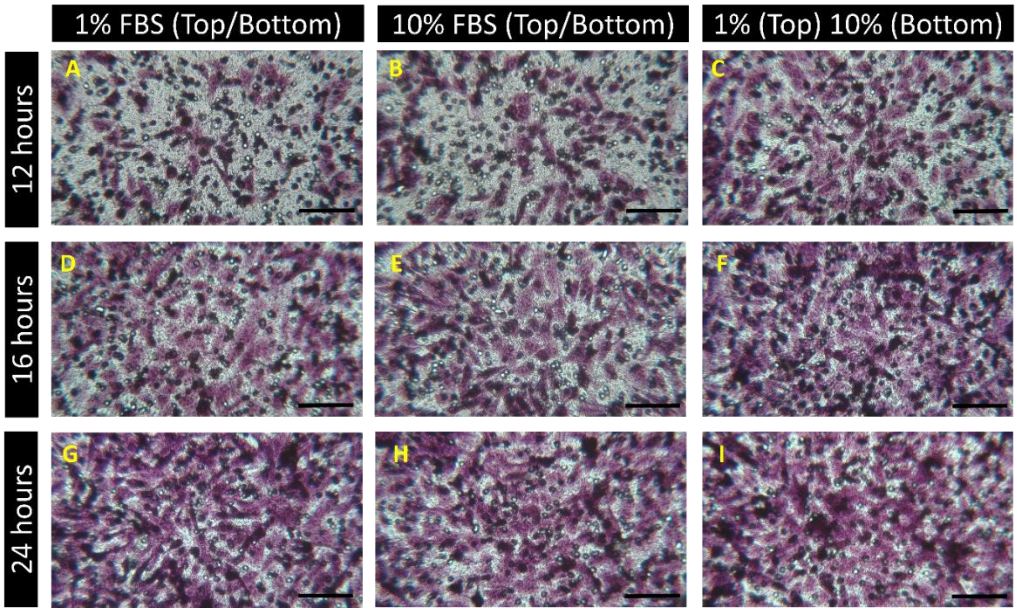


Figure 6.4 Optimisation of U87 cells invasion through collagen IV coated transwell inserts at a seeding density of 5×10^4 cells/well.
Plates were incubated at 37C at 5% CO2. Representative images of invasive cells at the bottom of the membrane, which was fixed with methanol and stained purple with 0.5% crystal violet. Images were captured at x40 magnification; scale bar corresponds to 100μm. Abbreviation: FBS -fetal bovine serum.

6.2.2 Transwell invasion assay following miR-619-5p and miR-4793-3p overexpression in U87 and GIN28 cells

To determine whether elevated levels of miR-619-5p and/or miR-4793-3p will influence the invasiveness of U87 cells, the transwell invasion assay was performed.

I observed a significant effect on miRNA protein target expression (Chapter 4) as well as on the cell metabolic profile (Chapter 5) after 72h of miRNA transfection. Therefore, I performed the transwell invasion assay after 72h of miR-6195p and miR-4793-3p of individual or co-transfections in U87 and GIN28 cells. Because the duration of the transwell invasion assay is 24h, I seeded the cells onto the transwell 48h following their transfection and let them spend the rest of the 72h in the transwell assay. This step was essential as I only understand the effect of my miRNAs after 72h and not 96h (which would be

the total number of hours post-transfection if I had seeded the cells after 72h and left them for another 24h in the transwell).

Based on the optimisation above, the number of cells seeded in the upper compartment containing 200µl of 1% FBS medium was 2×10^4 of cells. I found that in U87 cell, the overexpression of miR-619-5p resulted in reduced cell invasion by almost 72% compared to NT while co-transfection of both miR-619-5p and miR-4793-3p lead to an about 28% decrease in invasion relative to NT (Figure 6.5).

Similarly, in GIN28 cells, I observed a significant decrease in invasion following the transfection with miR-619-5p or the co-transfection with both miR-619-5p and miR-4793-3p. The magnitude of reduction in invasion compared to NT was 75% and 43%, respectively (Figure 6.6).

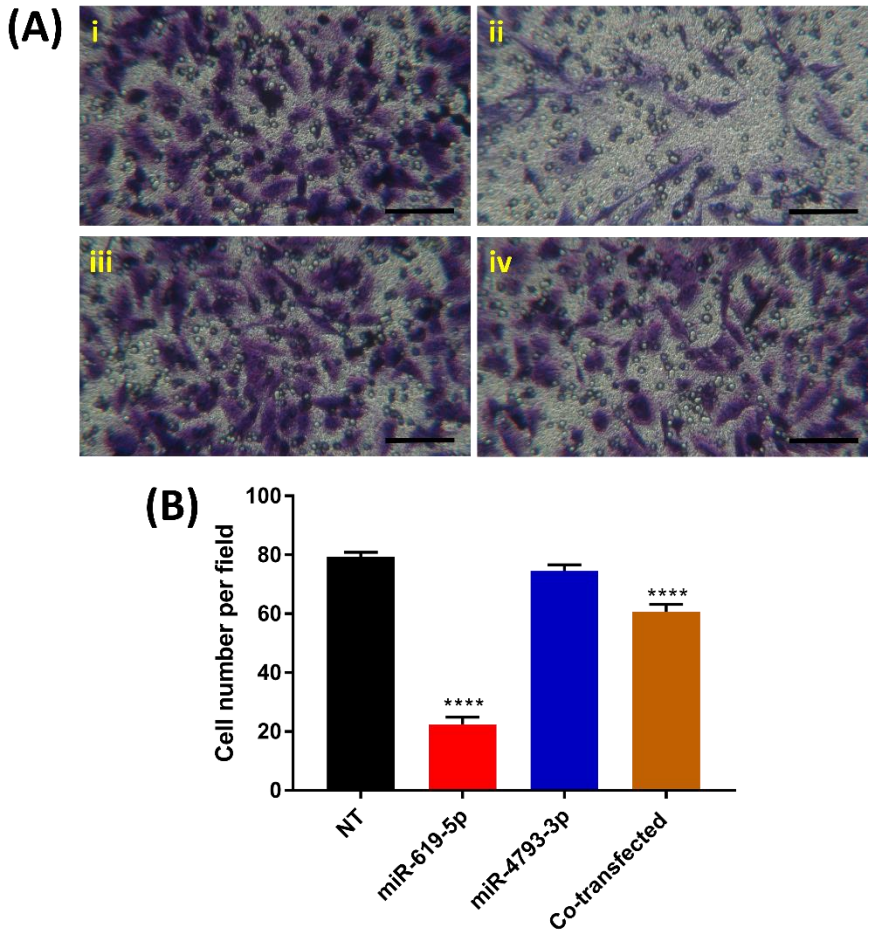


Figure 6.5 Transwell invasion assays of U87 cells overexpressing miR-619-5p and/or miR-4793-3p.
*(A) Representative images of stained invading cells from the lower surface of the transwell are shown 72h after transfection with 50nM of (i) non-targeting mimic (NT) control, (ii) miR-619-5p mimic, (iii) miR-4793-3p, and (iv) co-transfection of miR-619-5p and miR-4793-3p mimics at 1:1 ratio. All images were captured at 40x magnification; scale bars correspond to 100μm. (B) Quantitative analysis of invaded cells. Three high-powered microscope fields of view (captured at 40x magnification) were taken from the lower surface of each well, and the average cell count was calculated in ImageJ software. Results are presented as mean ± SEM of three independent experiments. Statistical analysis was performed using ANOVA ($p<0.0001$) followed by Bonferroni's multiple-comparison test comparing each transfection condition to NT; ****p-value < 0.0001.*

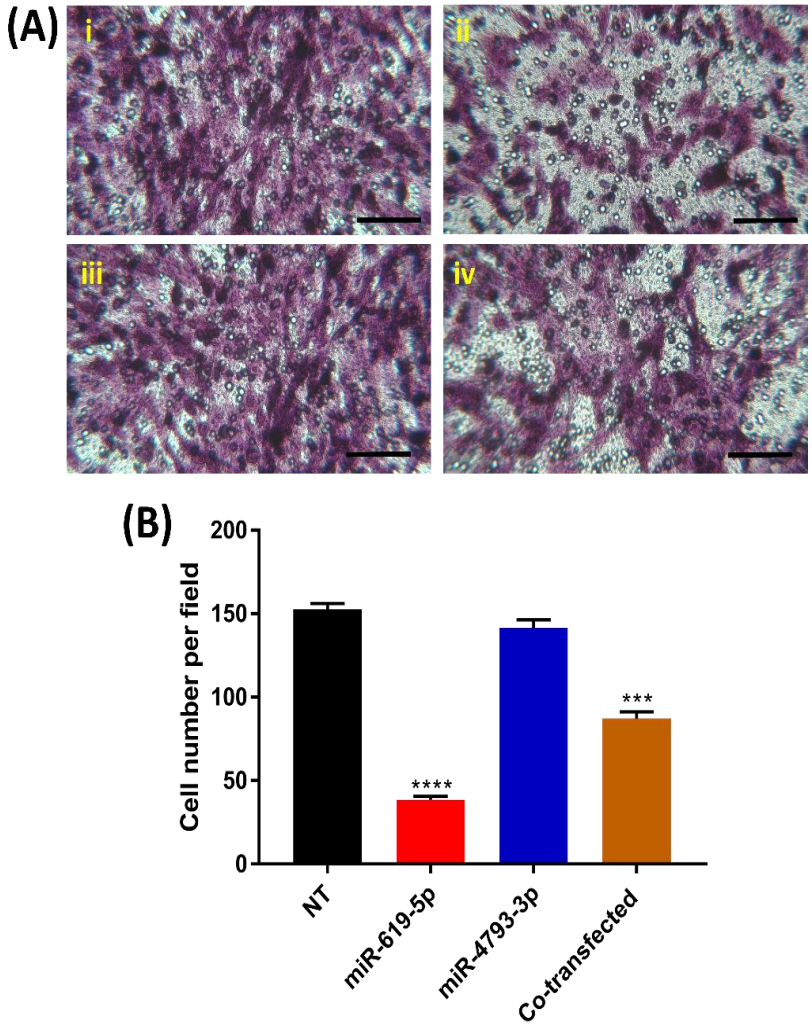


Figure 6.6 Transwell invasion assays of GIN28 cells overexpressing miR-619-5p and/or miR-4793-3p.

*(A) Representative images of stained invading cells from the lower surface of the transwell are shown 72h after transfection with 50nM of (i) non-targeting mimic (NT) control, (ii) miR-619-5p mimic, (iii) miR-4793-3p, and (iv) co-transfection of miR-619-5p and miR-4793-3p mimics at 1:1 ratio. All images were captured at 40x magnification; scale bars correspond to 100μm. (B) Quantitative analysis of invaded cells. Three high-powered microscope fields of view (captured at 40x magnification) were taken from the lower surface of each well, and the average cell count was calculated in ImageJ software. Results are presented as mean ± SEM of three independent experiments. Statistical analysis was performed using ANOVA ($p<0.0001$) followed by Bonferroni's multiple-comparison test comparing each transfection condition to NT; ****p-value < 0.0001; ***p-value < 0.001.*

6.2.3 Understanding the effect of CPT2 knockdown on GBM cell invasion

In order to select the optimal concentration of siRNA against CPT2 (siCPT2), I ran a series of optimisation experiments. As such, I first optimised the concentration of siCPT2 and knockdown efficiency in U87 cells and then re-tested the optimised siRNA concentration in GIN28 cells.

I hypothesised that siCPT2 treatment would have a similar effect on cell invasion to those from miR-619-5p overexpression.

6.2.3.1 Optimisation of siRNA concentration for CPT2 knockdown by qRT-PCR analysis

Two different siRNA concentrations were tested; 25nM and 50nM. qRT-PCR was performed to evaluate CPT2 expression in siRNA transfected cells after 48h as per manufactures recommendations (Figure 6.7). I found that the mRNA levels of CPT2 in U87 cells transfected with siCPT2 silenced were 76.9% and 98.9% of that in the control cells at 25nM and 50nM, respectively. As such, 50nM showed the maximal transfection efficiency and knockdown effect.

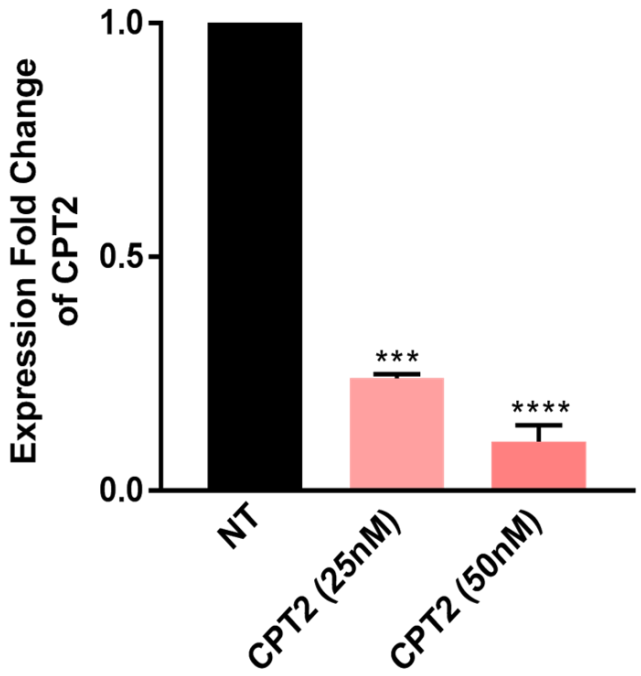


Figure 6.7 Transfection efficiency of siRNA against CPT2 in U87 cells.
*The expression of CPT2 in U87 cells transfected with 25nM or 50nM of miR-619-5p is represented as fold change relative to its expression in U87 cells transfected with non-targeting mimic control (NT). Data was generated from technical triplicates and in three biological repeats (mean ± SEM). Statistical analysis was performed using ANOVA (p-value < 0.0001) followed by Bonferroni test comparing each concentration to NT: non-targeting mimic control; ***p-value < 0.001; ****p-value < 0.0001.*

Next, I transfected GIN28 cells with 50nM of siCPT2. I found a comparable percentage of knockdown as seen in U87 cells. siCPT2 reduced CPT2 expression by 80% compared to the scrambled siRNA control (Figure 6.8).

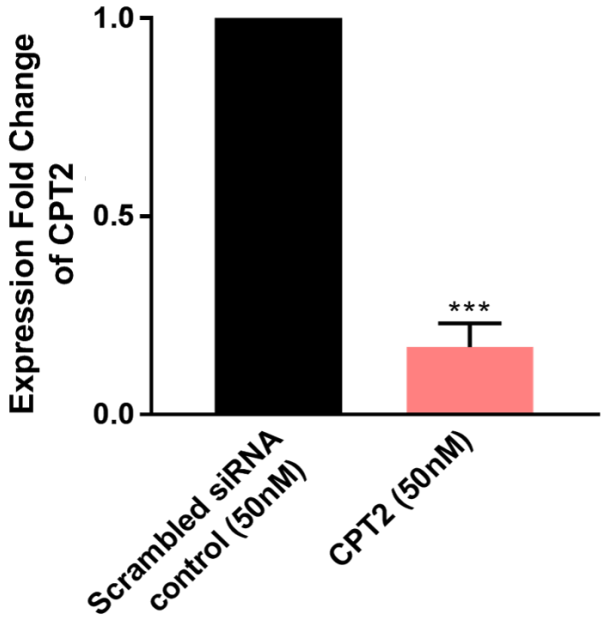


Figure 6.8 Transfection efficiency of siRNA against CPT2 in GIN28 cells.
*The expression of CPT2 in GIN28 cells transfected with 50nM of miR-619-5p is represented as fold change relative to its expression in U87 cells transfected with non-targeting mimic control (NT). Data are presented as SEM of three independent experiments conducted in triplicates. Statistical analysis was performed using ANOVA (p-value < 0.0001) followed by Bonferroni test comparing each concentration to NT: non-targeting mimic control; ***p-value < 0.001.*

6.2.3.2 Confirmation of CPT2 knockdown by Western blot analysis of CPT2 protein expression

The knockdown effect of 50nM of siCPT was then confirmed at the protein levels in both U87 and GN278 cells (Figure 6.9). It is worth mentioning that in U87, I stained for ACOX1 as part of

the same gel; hence, I see a faint band above CPT2 which corresponds to ACOX1 at 74kDa.

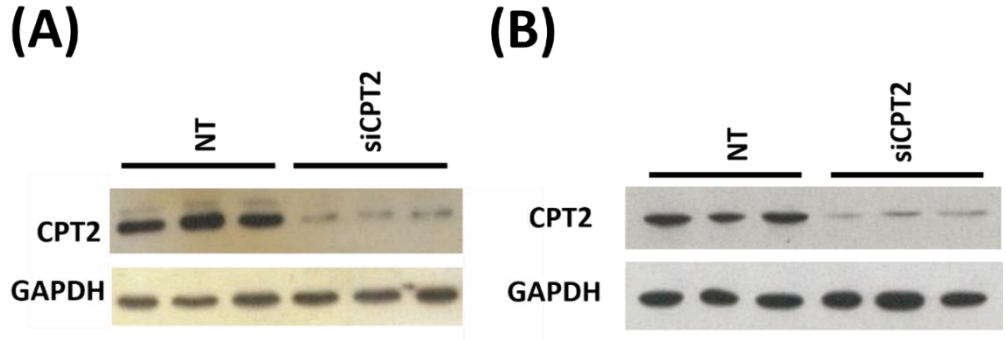


Figure 6.9 Immunoblot of CPT2 following siRNA knockdown in GBM cells.
Transfection of 50nM of siRNA against CPT2 (siCPT2) in (A) U87 cells and (B) GIN28 cells for 72h. CPT2 band is observed at 72kDa. GAPDH was used as a loading control (37kD). NT: non-targeting mimic control. Data are represented as three biological repeats for each transfection condition.

6.2.3.3 Assessing cell viability following CPT2 knockdown in U87 and GIN28 cells

In order to ensure comparability between the experimental conditions, I sought to examine the number of cells at the 72h time point. I constructed a growth curve using the standard cell concentration (3.125 x 10^4 cells/ml) as the 0h. Cells were counted, and the cell concentration was calculated every 24h (Figure 6.10).

No cell division was observed during incubation in the transfection media (24h), which synchronised cell growth in the two conditions (siCPT2 and scrambled siRNA control). The cell numbers after 72h in both transfection conditions were within an average of 2% of each other. This would, therefore, allows the direct comparison between the two conditions.

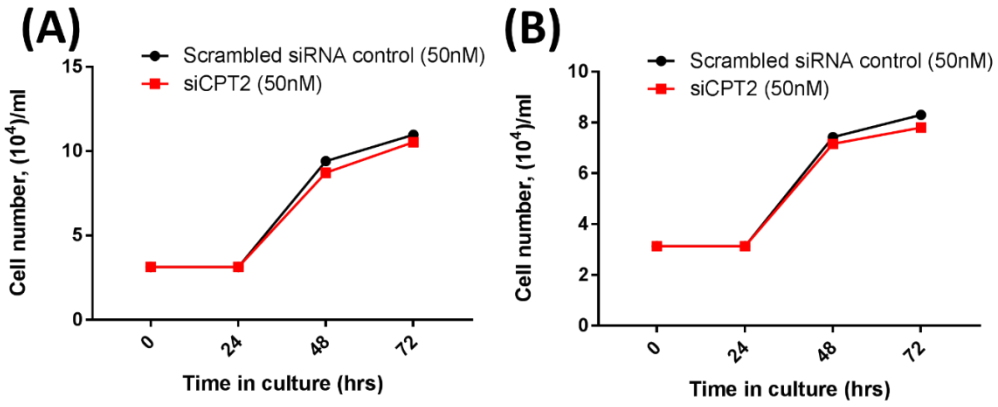


Figure 6.10 Growth curve of U87 and GIN28 cells following siRNA transfection.
(A) U87 and (B) GIN28 cells were plated at 3.125 x 104 cells/ml, cell number was counted using a haemocytometer, and the concentration of cells was calculated every 24h.

6.2.3.4 LD staining following CPT2 knockdown in U87 and GIN28 cells

To evaluate whether or not the FAO pathway was inhibited, I measured LD accumulation following knocking down CPT2 with siRNA (Figure 6.11). I found that LD abundance was

significantly increased after knocking down CPT2 compared to scrambled siRNA controls (Figure 6.12).

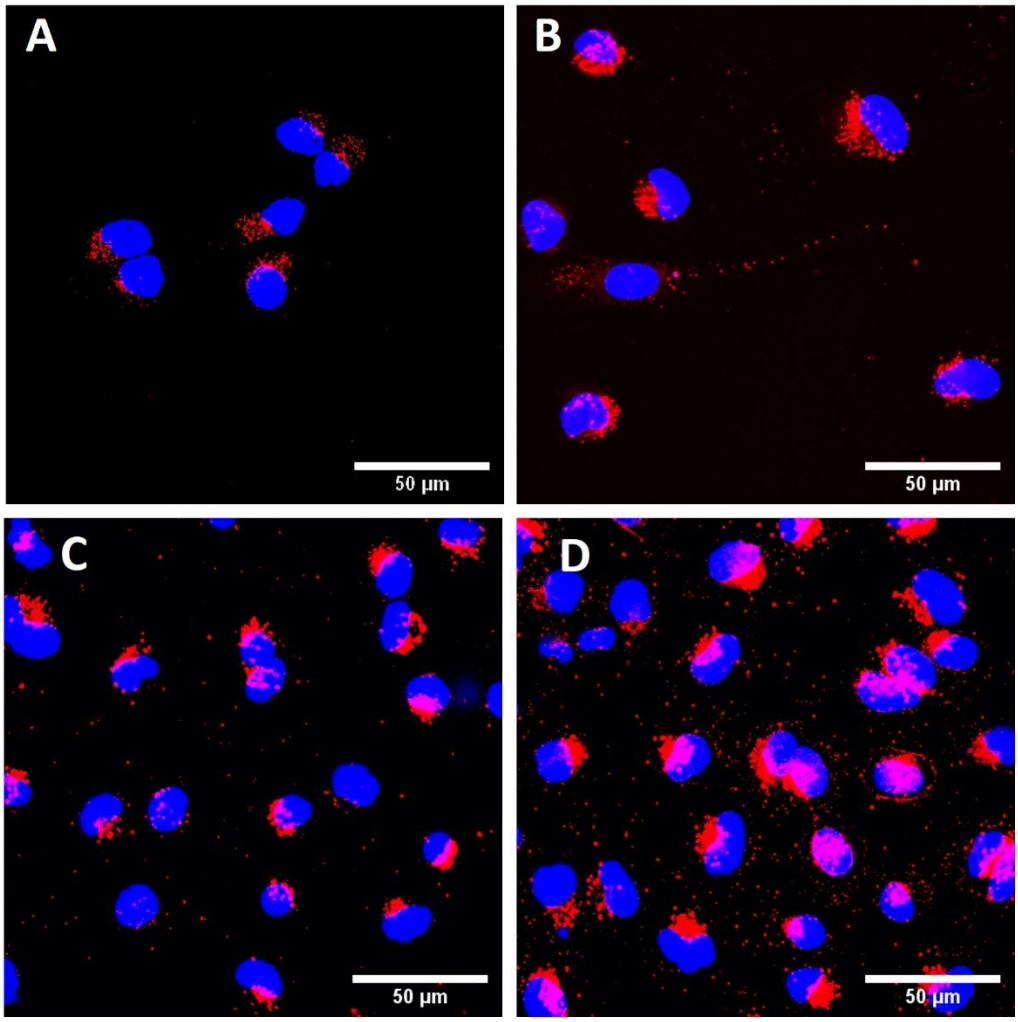


Figure 6.11: Confocal analysis of lipid droplets in U87 and GIN28 cells after siCPT2 treatment.
U87 (top panels) and GIN28 (bottom panels) cells stained with Nile Red (1mg/ml) after 72h of transfection with 50nM of (A,C) scrambled control or (B,D) siRNA against CPT2. Nile red (red) stains triacylglycerol content of lipid droplets while DAPI (blue) stains the nucleus.

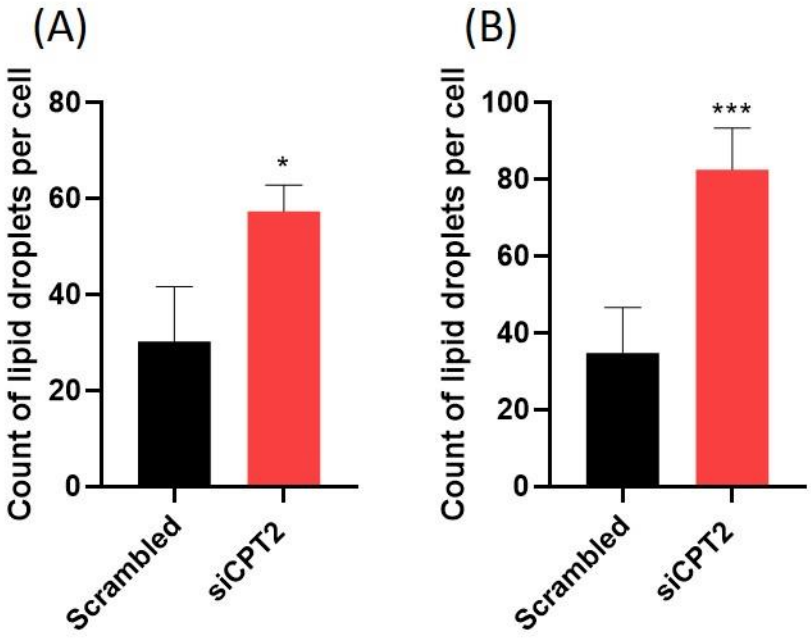


Figure 6.12: Lipid droplet count in (A) U87 and (B) GIN28 cells following CPT2 knockdown by siRNA (siCPT2).
*Count (mean ± standard error). Statistical analysis using t-test comparing siCPT2 condition to scrambled conditions; *** p-value < 0.001; * p-value < 0.05.*

6.2.3.5 Transwell invasion assay following CPT2 knockdown in U87 and GIN28 cells

Transwell invasion assay was also performed in U87 and GIN28 cells 72h following siRNA transfections against CPT2, in order to establish whether the phenotypic effects of miR-619-5p overexpression on invasion is due to the action of CPT2, one of its gene target. I found that CPT2 knockdown inhibited the

invasion of U87 by 24% and GIN28 by 40% compared to scrambled controls (Figure 6.13).

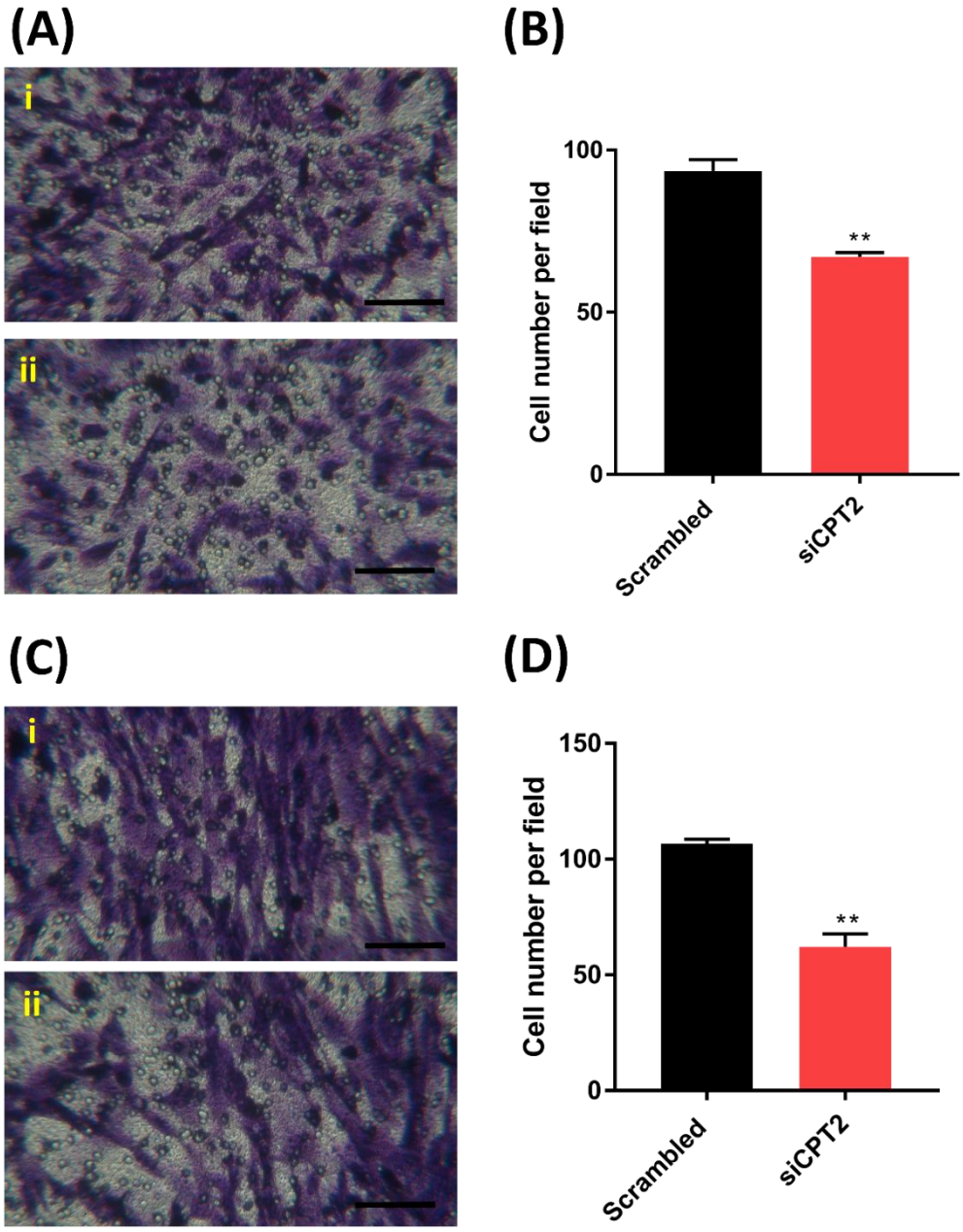


Figure 6.13 Effect of CPT2 knockdown on (A,B) U87 and (C,D) GIN28 cell invasion.
Representative images (left panels) of stained invading cells from the lower surface of the transwell are shown 72h after transfection with 50nM of (i) scrambled control, and (ii) siRNA against CPT2 (siCPT2). All images were captured at 40x magnification; scale bars correspond to 100μm. Quantitative analysis (right panels) of invaded cells. Three high-powered microscope fields of view (captured at 40x magnification) were

*taken from the lower surface of each well, and the average cell count was calculated in ImageJ software. Results are presented as mean ± SEM of three independent experiments. Statistical analysis was performed using t-test comparing siCPT2 to scrambled transfection condition to NT; **p-value < 0.01.*

6.2.4 Understanding the effect of the pharmacological inhibition of CPT2 on GBM cell invasion

Transwell invasion assay was also performed in U87 and GIN28 cells 72h following treatment with the FAO pharmacological inhibitors, perhexiline (CPT1 and CPT2 inhibitor) and etomoxir (CPT1 inhibitor), in order to establish whether the phenotypic effects of miR-619-5p overexpression on invasion is due to the action of its target pathway.

6.2.4.1 Optimisation of drug concentration for CPT2 pharmacological inhibitors, Perhexiline and Etomoxir, in U87 and GIN28 cells

In order to evaluate the potency of the CPT2 inhibitors, I constructed a dose-response curve (also known as a kill curve). 72h time-point was chosen based on the literature to assess cell viability after treating U87 and GN278 cells with a range of

concentrations of perhexiline and etomoxir (Park *et al.*, 2016; Vella *et al.*, 2016). Cell viability with respect to vehicle alone (either DMSO for perhexiline or water for etomoxir) was chosen as the response factor. The optimal concentration for each drug was chosen as the maximum concentration with the least cytotoxic effect was used to carry out the transwell assay.

Perhexiline treatment in U87 and GIN28 cells had an IC50 of 14.89 μM and 11.78 μM, respectively (Figure 6.14). Etomoxir had IC50 values of 675.4 μM and 451.6 μM for U87 and GIN28 cells, respectively (Figure 6.14). These results indicate that U87 cells are relatively less susceptible to the treatment of perhexiline and etomoxir compared to GIN28 cells. This could be due to the robustness of commercial cell lines grown in long-term cultures compared to recently derived primary cells.

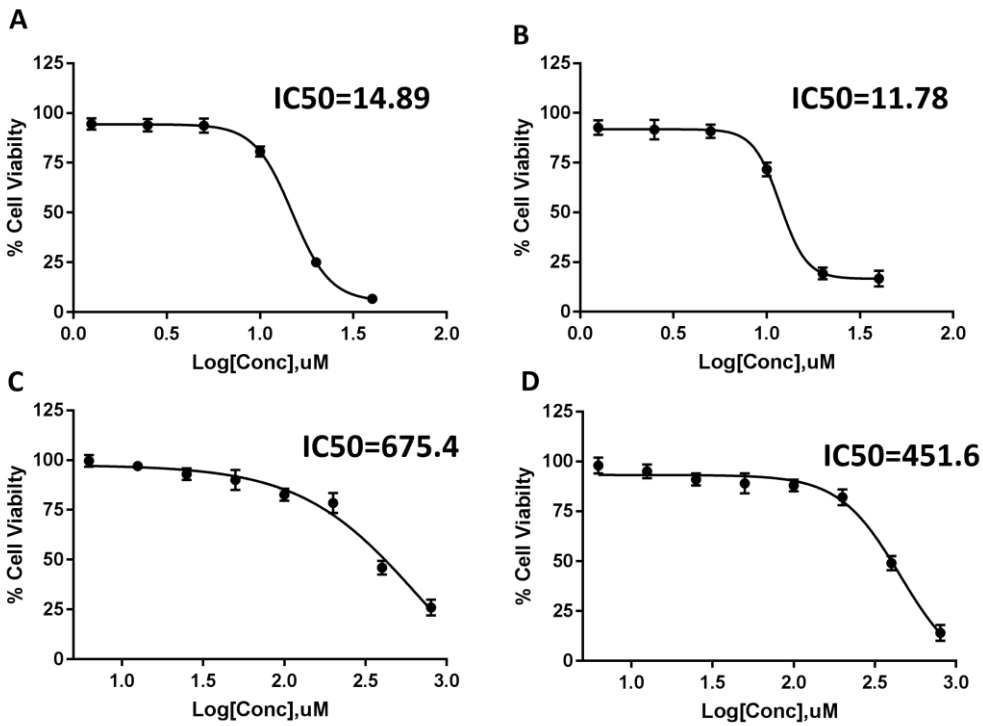


Figure 6.14 Determination of IC50 values for perhexiline and etomoxir in GBM cells.

Dose-response curves for (A) U87 and (B) GIN28 cells following exposure to perhexiline for 72h. Dose-response curves for (C) U87 and (D) GIN28 cells following exposure to etomoxir for 72h. Cell viability assessment was performed using the PrestoBlue assay. Curve obtained using a sigmoidal function. The concentration of the drug was log-transformed. Results are expressed as a percentage of the vehicle alone (either DMSO for perhexiline or water for etomoxir) control and presented as means ± SD of three independent biological repeats each conducted in triplicate.

6.2.4.2 LD staining following the treatment with CPT2 pharmacological inhibitor, Perhexiline, in U87 and GIN28 cells

I measured LD accumulation to confirm that the drug treatment leads to a successful inhibition of the FAO pathway.

I found that LD abundance was significantly increased after perhexiline treatment compared to controls in both U87 and GIN28 cell lines, as seen from confocal images (Figure 6.15) and LDs count (Figure 6.16).

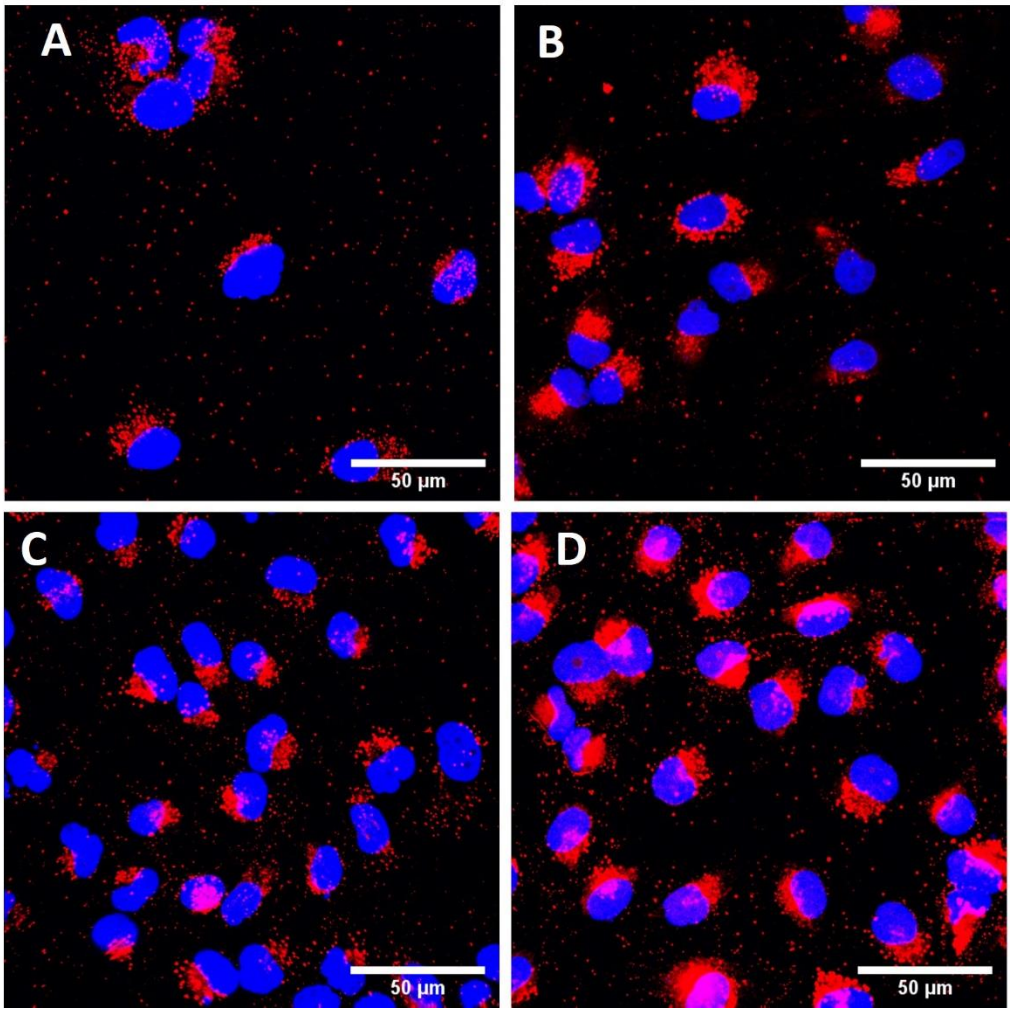


Figure 6.15: Confocal analysis of lipid droplets in U87 and GIN28 cells after 72h of perhexiline treatment.
U87 (top panels) and GIN28 (bottom panels) cells stained with Nile Red (1mg/ml) after 72h of treatment with 10 µM of (A,C) DMSO or (B,D) perhexiline. Nile red (red) stains triacylglycerol content of lipid droplets while DAPI (blue) stains the nucleus.

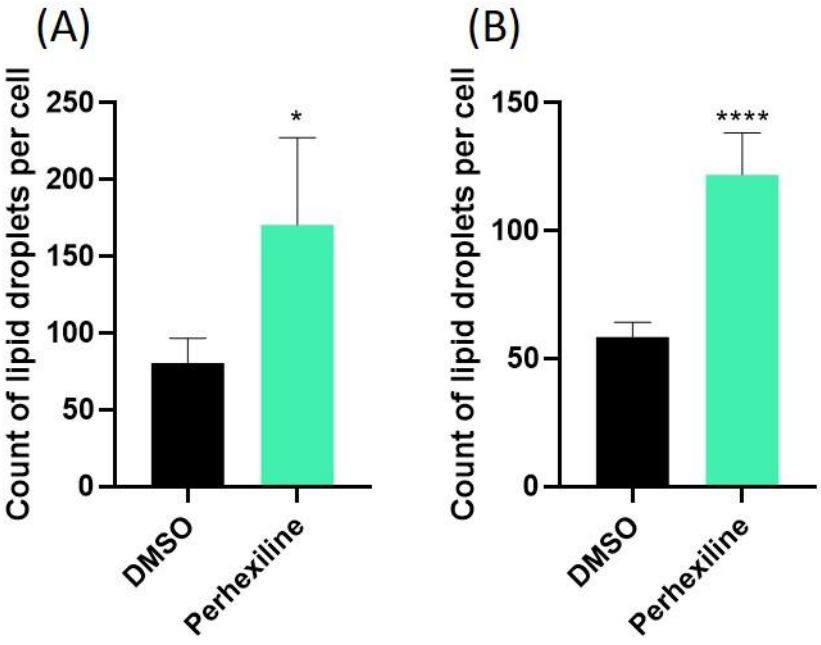


Figure 6.16: Lipid droplet count in (A) U87 and (B) GIN28 cells after perhexiline treatment.
*Count (mean ± standard error). Statistical analysis using t-test comparing perhexiline to DMSO; **** p-value < 0.0001; * p-value < 0.05.*

6.2.4.3 LD staining following the treatment with CPT2 pharmacological inhibitors, Etomoxir, in U87 and GIN28 cells

The treatment with Etomoxir resulted in a significant accumulation of LDs (Figure 6.17) and (Figure 6.18); thereby confirming that the successful inhibition of FAO in the cell.

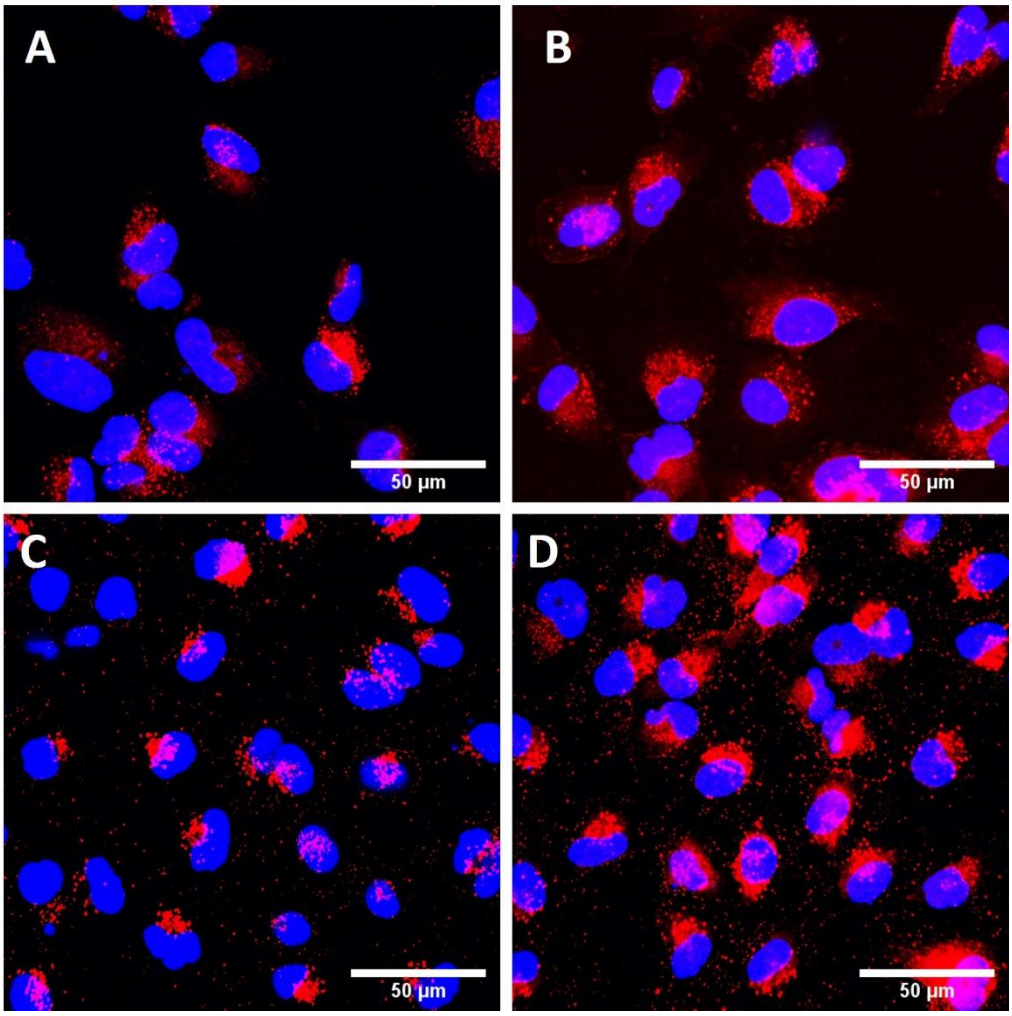


Figure 6.17: Confocal analysis of lipid droplets in U87 and GIN28 cells after 72h of Etomoxir treatment.
U87 (top panels) and GIN28 (bottom panels) cells stained with Nile Red (1mg/ml) after 72h of treatment with 400 µM of (A,C) water or (B,D) Etomoxir. Nile red (red) stains triacylglycerol content of lipid droplets while DAPI (blue) stains the nucleus.

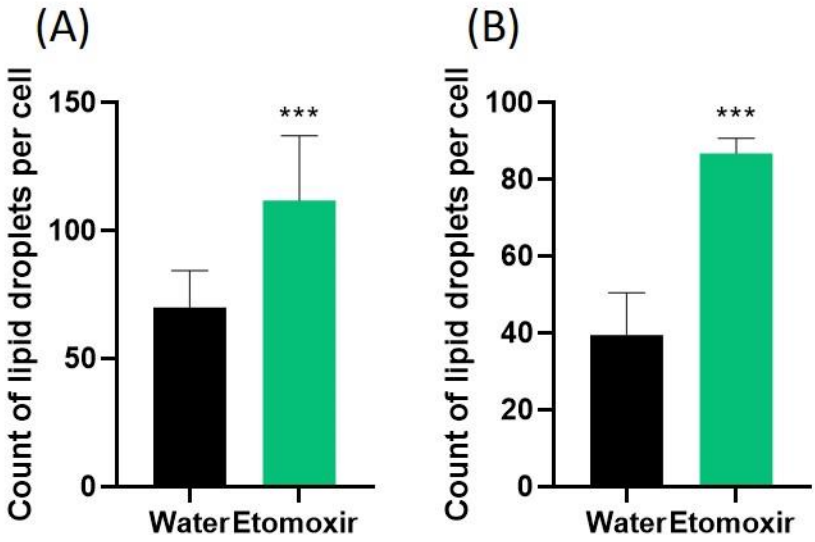


Figure 6.18: Lipid droplet count in (A) U87 and (B) GIN28 cells after Etomoxir treatment.
*Count (mean ± standard error). Statistical analysis using t-test comparing Etomoxir to water; *** p-value < 0.001.*

6.2.4.4 Transwell invasion assay following CPT2 inhibition with Perhexiline in U87 and GIN28 cells

Based on the dose-response curve, I chose 10μM as the optimal concentration of perhexiline with the least toxic effect as previously used with GBM cells (Harford-Wright, Bidère and Gavard, 2016).

The result showed that perhexiline treatment significantly reduced U87 and GIN28 cell invasion by 65% and 60% compared to vehicle alone controls (Figure 6.19).

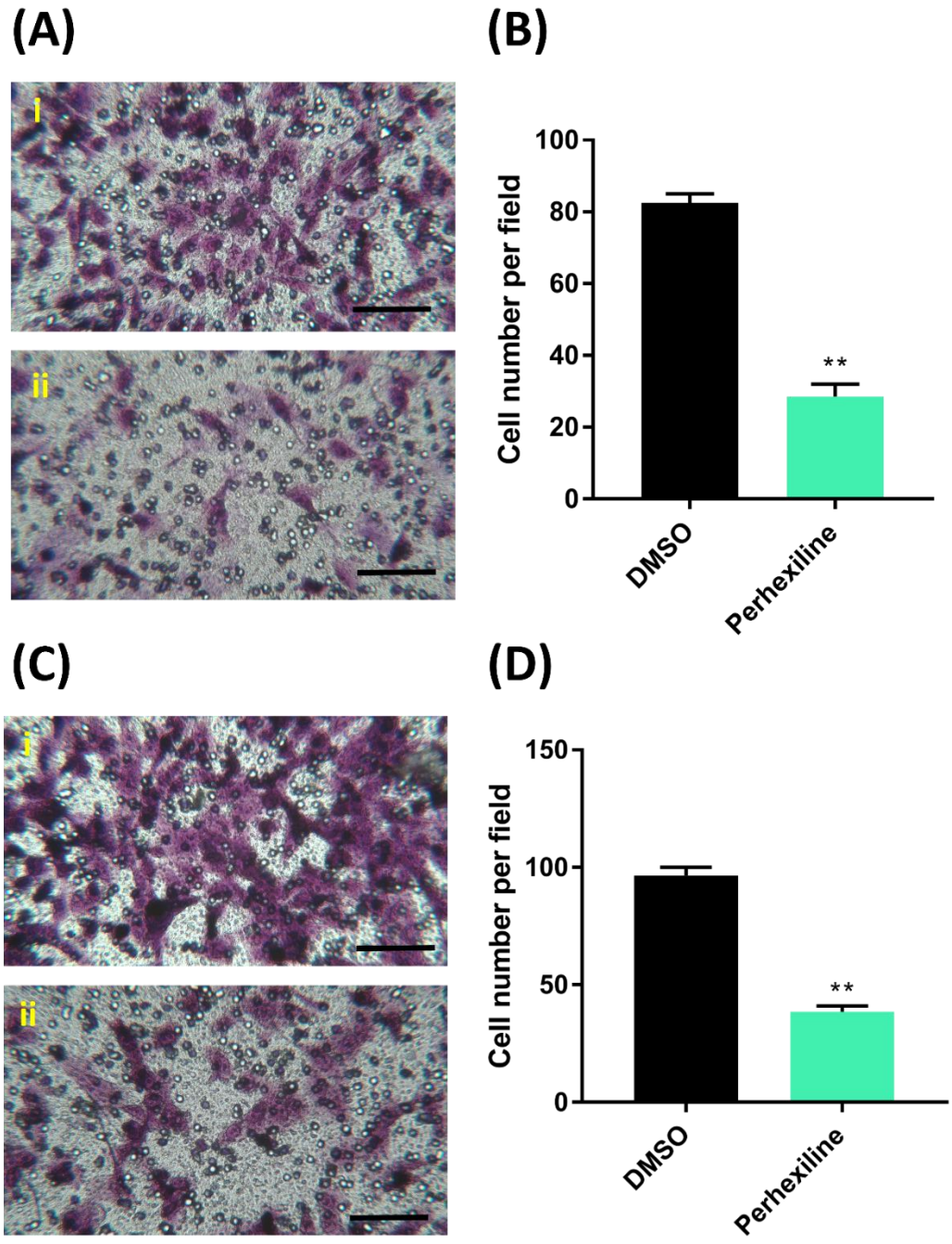


Figure 6.19 Effect of Perhexiline on the invasion of (A,B) U87 and (C,D) GIN28 cells.

Representative images (left panels) of stained invading cells from the lower surface of the transwell are shown 72h after transfection with 10μM of (i) vehicle alone (DMSO) control, and (ii) Perhexiline. All images were captured at 40x magnification; scale bars correspond to 100μm. Quantitative analysis (right panels) of invaded cells. Three high-powered microscope fields of view (captured at 40x magnification) were taken from the lower surface of each well, and the average cell count was

*calculated in ImageJ software. Results are presented as mean ± SEM of three independent experiments. Statistical analysis was performed t-test comparing Perhexiline to DMSO; **p-value < 0.01.*

6.2.4.5 Transwell invasion assay following FAO inhibition with Etomoxir in U87 and GIN28 cells

Since the inhibition of CPT2 leads to the inhibition of FAO, I tested the effect on invasion with a different FAO inhibitor, etomoxir, in order to validate my findings.

I initially used the maximum concentration with the least toxic effect (400μM) of etomoxir as determined from the dose-response curve with the aim to test a different concentration. However, I observed a significant effect; therefore, I repeated the experiment 2 more times.

The result showed that etomoxir treatment also significantly reduced U87 and GIN28 cell invasion by 64% and 56% compared to vehicle alone controls treated with water (Figure 6.20).

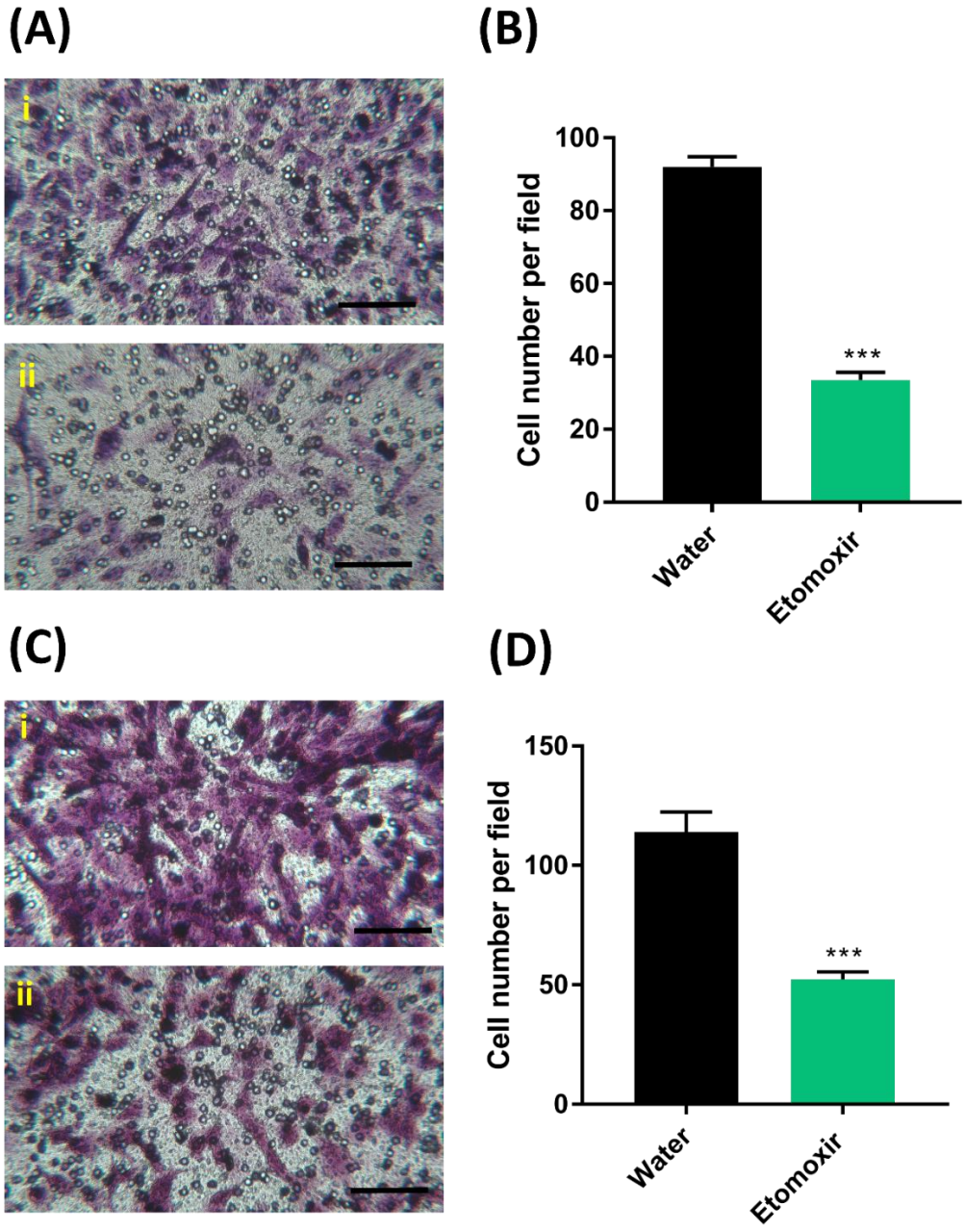


Figure 6.20 Effect of Etomoxir on the invasion of (A,B) U87 and (C,D) GIN28 cells.

Representative images (left panels) of stained invading cells from the lower surface of the transwell are shown 72h after transfection with 400μM of (i) vehicle alone (water) control, and (ii) Etomoxir. All images were captured at 40x magnification; scale bars correspond to 100μm. Quantitative analysis (right panels) of invaded cells. Three high-powered microscope fields of view (captured at 40x magnification) were taken from the lower surface of each well, and the average cell count was calculated in ImageJ software. Results are presented as mean ± SEM of three independent experiments. Statistical analysis

*was performed t-test comparing Etomoxir to water; ***p-value < 0.001.*

6.3 Discussion

6.3.1 FAO inhibition reduces GBM cell invasion

As far are I am aware, there are no reports on the role of miR-619-5p in regulating GBM invasion. As a novel contribution, the work of this chapter reveals a vulnerability of GBM in the FAO pathway (a target of miR-619-5p) which could serve as a potential therapeutic target to reduced cell invasion.

The role of lipid metabolism in cancer invasion has been explained in the introduction section of this thesis. Here, I will discuss the relevant findings of the use of perhexiline and etomoxir as a potential therapeutic agent for the treatment of GBM.

Perhexiline was originally developed as an anti-anginal drug in the 1970s (Burns-Cox *et al.*, 1971). Perhexiline reduces fatty acid (FA) metabolism through the simultaneous inhibition of CPT1 and CPT2 enzymes responsible for the mitochondrial uptake of long-chain FAs (Kennedy, Unger and Horowitz, 1996; Kennedy *et al.*, 2000). Although shown by Kennedy et al. to inhibit CPT2, only the exact mechanism of action of perhexiline

on CPT1 have been elucidated. Perhexiline is a competitive inhibitor of CPT1, which competes with the endogenous CPT1 inhibitor, malonyl CoA, for one of its two binding sites (the mitochondrial binding site). Unlike the cytoplasmic binding site, the mitochondrial binding site is protected and is not prone to alteration by proteolysis which renders the binding of perhexiline to CPT1 efficient (Kennedy, Unger and Horowitz, 1996; Kennedy *et al.*, 2000).

The anti-anginal efficacy of perhexiline lies in the ability to increase myocardial efficiency, which is defined as the work done per unit oxygen consumption. The inhibition of FAO shifts myocardial energy metabolism from principally FA toward greater carbohydrate metabolism. This, in turn, promotes the utilisation of glucose as an alternative energy source for myocardiocytes (Kennedy, Unger and Horowitz, 1996). Glycolysis is more oxygen-efficient because its increasing myocardial energy production at a lower oxygen cost then FAs, which consume more oxygen per unit ATP produced (Faadiel and Lionel, 2004). Moreover, perhexiline has been reported to have off-target effects, other than FAO inhibition, such as NADPH oxidase inhibition, weak blockade of voltage-gated L-type calcium channel and sodium channel, and inhibition of the

voltage-dependent potassium channel (Ashrafian, Horowitz and Frenneaux, 2007).

In 1985, perhexiline was, however, removed from the clinic in the UK due to its narrow therapeutic window and severe hepatotoxic or peripheral neuropathy in some patients, though it continues to be used clinically in other countries, especially in Australia and New Zealand, to patients who have little else in terms of treatment options. The challenges of utilising perhexiline in a clinical setting were the emerging of the 'poor-metabolisers'. Poor-metabolisers are patients who have altered activity of CYP2D6 (cytochrome P450 family 2 subfamily D member 6), which causes them hepatotoxic/neurotoxic side-effects when metabolising perhexiline (Sørensen *et al.*, 2003). To overcome this challenge, genetic tests are recommended to be performed prior to administrating the drug, while lowering the drug dosage can also be used to minimise the side-effects (Ashrafian, Horowitz and Frenneaux, 2007). Either way, an effective treatment for GBM would be licensed even if there was a risk of severe side effects given the current poor survival. Nevertheless, local drug delivery solutions that are currently being developed might be able negate concerns about

hepatotoxicity and neurotoxicity caused by systemic delivery (Nam *et al.*, 2018).

Used at low dosage, perhexiline can still inhibit CPT1/2 while it may confer gene expression changes as a direct consequence of its activity or as an indirect consequence of the induced metabolic stress. Other gene expression changes induced by perhexiline have recently been investigated in the effort to re-purpose this clinically approved compound for the treatment of cancer. In breast cancer (BC), the treatment with 2μM of perhexiline for 72h promotes the internalisation of the human epidermal growth factor receptor 3 (HER3). This, in turn, inhibits the subsequent signalling downstream of HER3 and reduces cell proliferation *in vitro* and tumour growth *in vivo*. In addition, the combination of 5μM perhexiline and 100nM of lapatinib, a tyrosine kinase inhibitor, for 36h prevented the reactivation of HER3 and downstream Akt signalling which suggests that perhexiline may be used to overcome the resistance to targeted therapies. Therefore, it was proposed that targeting HER3 with perhexiline, to remove HER3 from the cell membrane, may reduce tumour growth and improve survival in BC patients (Ren *et al.*, 2015). In GBM, perhexiline could be inhibiting cell invasion via the inhibition of FAO or via

other unknown mechanisms. Examination of transcriptomic profiles following perhexiline treatment might elucidate such mechanisms.

Another study reported that perhexiline is able to induce gene expression changes that enhance the effect of anti-cancer drugs. In neuroblastoma (NB), perhexiline was shown *in vitro* and *in vivo* to sensitise tumour cells to the chemotherapeutic agent, cisplatin. Perhexiline induces the expression of the non-coding RNA NDM29 (neuroblastoma differentiation marker 29), which promotes NB cell differentiation and reduces the expression of ABC transporters responsible for cisplatin resistance. As such, pharmacological induction of NDM29 the by a low dosage of perhexiline, as little as 0.1 μM for 24h, used with 100μM cisplatin, can significantly increase NB cells susceptibility to cisplatin (Vella *et al.*, 2016). These results allude to an opportunity of combinatorial treatment with low doses of perhexiline and TMZ in GBM to sensitise tumour cells to this chemotherapeutic agent, which could be explored in future studies.

Finally, in prostate cancer, the treatment with 5μM of perhexiline in combination with androgen deprivation therapy

(either Abiraterone or Enzalutamide) for 96h enhanced their effect on suppressing cell growth. In addition, exposure to 10μM of perhexiline for 24h was found to replicates the major consequences of the knockdown of the androgen receptor target, Enoyl-CoA delta isomerase 2 (ECI2) c ECI2 encodes an enzyme involved in lipid metabolism, and its knockdown led to the inhibition of FA degradation, as observed after perhexiline treatment. Either the treatment with perhexiline or the knockdown of ECI2 induced acute metabolic stress that led to the activation of incomplete autophagy (Itkonen *et al.*, 2017). This work highlights that blocking FAO can be achieved by knocking down Individual genes involved in FAO or by using pharmacological means to get the same effect thereby opening the opportunity for rapidly translating the use of such approach into the clinic.

My findings are not in conflict with the research showing that perhexiline caused incomplete autophagy in prostate cancer (Itkonen *et al.*, 2017). This is because incomplete autophagy might also occur in GBM, along with reduced invasion, at low concentrations of perhexiline. At high concentrations of perhexiline, I observed cell death, which is consistent with Itkonen et al. Thus, the activation of incomplete autophagy by

low doses of perhexiline, as measured by the prominent accumulation of the autophagy markers LC3 and adaptor protein p62, can be investigated in GBM in the future.

In GBM, the only report of the use of perhexiline was in the context of a viability screen to identify small molecules with cytotoxic activity in patient-derived glioblastoma-initiating cells (GIC). Perhexiline (used at 10μM for 48h) modestly affected the viability of GICs grown in 3D cultures (Harford-Wright, Bidère and Gavard, 2016). In agreement with this, 10μM was the concentration that I decided to use in my transwell assays based on the dose-response curve under my standard cell culture conditions.

I also used etomoxir, another CPT1 inhibitor, to further validate my findings that cell invasion is reduced upon the inhibition of FAO. Etomoxir was originally developed to treat type 2 diabetes mellitus (Ratheiser *et al.*, 1991). Etomoxir was then tested for the treatment of congestive heart failure (CHF), with phase I trial showing clinical improvement with 80 mg of etomoxir/day (Schmidt-Schweda and Holubarsch, 2000). Etomoxir progressed to phase II clinical trial, but the trial was terminated because 4 patients (of 226 taking the drug) developed severe

side-effects of high liver transaminase levels (Holubarsch *et al.*, 2007).

Unlike perhexiline, which is a competitive inhibitor, etomoxir binds irreversibly to CPT1 and reduces the mitochondrial uptake and thus, subsequent oxidation of FA (Spurway *et al.*, 1997). FAO inhibition in cancer studies cancer cells has mostly been driven by experimental findings related to CPT1 inhibition by etomoxir (Qu *et al.*, 2016). The specific effect of etomoxir on inhibiting tumour cell invasion/migration has been reported in other cancers, but not yet reported in GBM. Wright et al. showed that in metastatic triple-negative breast cancer (TNBC), which are characterised by high rates of FAO, the treatment with etomoxir inhibited FAO and reduced cell migration (Wright *et al.*, 2017).

Thus, it can be appreciate that the literature findings are in line with the finding in this chapter that etomoxir inhibits GBM cell invasion, very likely through inhibiting FAO. Nevertheless, as described above, we cannot exclude the possibility that other off-target effects of etomoxir, which may or may not be independent of FAO, caused the reduction in cell invasion. Yet, my observation that the knockdown of CPT2, which also inhibits

FAO, reduced the invasion of GBM cell, provides a stronger evidence for the role of FAO in GBM cell invasion. And since CPT2 is a genuine target of miR-619-5p, it can be concluded that miR-619-5p regulates invasion through its regulation of CPT2 and FAO pathway.

Furthermore, analogous to my approach in this chapter, Park et al. pharmacologically inhibited FAO in TNBC by 100μM of etomoxir or 10μM of perhexiline, or genetically by the knockdown of CPT genes. They found that etomoxir or perhexiline can abolish FAO-mediated activation of c-Src oncoprotein. Src stimulates FAO in a positive feedback loop. Thus, the inhibition of FAO and the subsequent Scr activation led to a significant reduction in the transwell migration potential of TNBC cells. Similarly, the inhibition of FAO through the knockdown of CPT1 or CPT2 by small hairpin RNA (shRNA) inhibited Src activation and reduced cell migration in transwell assays. Furthermore, treating TNBC cells with etomoxir with or knocking down CPT genes inhibited their wound healing potential. However, etomoxir-mediated inhibition of wound healing was significantly lower in CPT genes knockdown cells compared to control cells; thereby implying that etomoxir's

effect is redundant when either of CPT1 or CPT2 are knocked down (Jun Hyoung Park *et al.*, 2016).

The results of this chapter show that the magnitude of the decrease in GBM cell invasion was greater in etomoxir than in CPT2 knockdown conditions. The transwell invasion was reduced by 40% in etomoxir treated cells relative to the untreated controls, while CPT2 knockdown resulted in a 20% decrease in invasion compared to scrambled control. In support of this, Park et al. found that CPT1 and CPT2 lead to 60% and 70% decrease in transwell migration compared to the control while etomoxir decreased migration by 90% (Jun Hyoung Park *et al.*, 2016). In my case, the greatest effect was seen following miR-619-5p overexpression. This could be due to the multi-targeting effect of miRNAs to suppress invasion by simultaneously affecting more than one pathway. One reason why I observed the least effect on invasion following CPT2 knockdown could be potential off-target effects. I used ON-TARGET Plus technology to achieve a high percentage of knockdown while minimising possible off-target effects. Yet, siRNA transfection, just like miRNA transfection, can compete with the endogenous miRNAs for intracellular small RNA processing machinery; often leading to off-target effects that

include the upregulation of genes with sites for the highly expressed endogenous miRNAs (Khan *et al.*, 2009).

To confirm that my drug treatments and RNA transfections were successful in inhibiting FAO, I measured FA accumulation in cytoplasmic lipid droplets (LDs). I confirmed that perhexiline treatment leads to LD accumulation compared to DMSO control, similar findings to (Itkonen *et al.*, 2017). I also confirmed that etomoxir treatment caused LDs to accumulate in GBM cells. Consistent with my results, LD staining following etomoxir treatment suggested increased LD abundance in TNBC metastatic cells (Jun Hyoung Park *et al.*, 2016; Wright *et al.*, 2017). On the other hand, I have observed a reduction in LD abundance following miR-619-5p overexpression. Although Wright et al. showed that lower LD abundance correlates with invasiveness in 3D cultures of TNBC cells, it is merely a correlation. I therefore propose that a change in LD abundance is a consequence of the overall change in lipid metabolism homeostasis and not a cause of the effect I see of reduced invasion following miR-619-5p overexpression. The change on LDs abundance could be attributed to the multi-targeting property of miRNA whereby miR-619-5p could, in addition to inhibiting FAO via targeting enzymes such as CPT2 and ACOX1,

be promoting FA *de novo* biosynthesis via targeting other enzymes; but this is yet to be tested in the future.

FAO is thought to support cancer metabolism primarily in 2 ways: (1) to provide a source of ATP (Liu, 2006) and, (2) to indirectly provide NADPH to neutralise oxidative stress (Jeon, Chandel and Hay, 2012). When FAO is inhibited in the paediatric glioblastoma cell line, SF188, by the short exposure (25 mins) to 1 mM of etomoxir, NADPH levels and oxygen consumption rate have been shown to be decreased, thereby resulting in ATP depletion (Pike, Smift, Croteau, Ferrick, & Wu, 2011).

Lin et al., showed that longer exposure (24h) to 100μM of etomoxir reduced the proliferation of primary GBM cells, cultured in serum-free DMEM media (Lin *et al.*, 2017). In my experiment, however, the treatment with 100μM of etomoxir over 72h had no effect on the proliferation of primary or commercial GBM cell. The discrepancy between the two results may lie in the fact that I cultured my cells in 10% serum DMEM media, whereas Lin et al. used serum-free DMEM media. Culturing cells in serum is a common cell-culturing protocol that has been shown to cause genetic and phenotypic alterations to the primary cells (Pollard *et al.*, 2009). In addition, because

cells rely on lipid synthesis for aerobic respiration in serum-free conditions (Bailey *et al.*, 1972), inhibiting FAO in serum-free conditions cause a detrimental effect on cell viability.

Moreover, the genetic background varies between different primary cell lines derived in-house from different patients; Lin et al. used three primary lines and I used one primary line in my experiments which could very well be genetically distinct. In fact, my primary line was derived from the invasive margin of the tumour compared to tumour-bulk derived lines in the case of Lin et al., yet another factor contributing to the disparity in findings. In short, the number of samples, their patient origin and regional derivation, and the culture conditions are all differences between my work and that of Lin et al. Nevertheless, the mechanisms underlying this discrepancy are still unclear but may relate to the length of drug exposure (72h versus 24h), meaning that feedback regulation may increase CPT genes expression despite blocking FAO thereby increase resistance to drugs. This hypothesis can be tested by measuring CPT expression at different time-point of drug treatment.

Cellular viability assessment following 72h of drug exposure identified a dose-dependent response. IC50 values for both

drugs were lower in U87 cells compared to GIN28 cells. However, the mechanism underlying this increased susceptibility remains to be elucidated. Potential reasons include differential basal protein levels of CPT1 or CPT2 (which I observed), or differential expression levels of FA *de novo* biosynthesis genes (which I could be tested in future work).

In general, high concentrations of etomoxir, that is often used in cancer studies, leads to off-target effects. Etomoxir cause an inhibition of FA and cholesterol biosynthesis, depletion of cytoplasmic coenzyme A (CoA) (Agius, Meredith and Sherratt, 1991), inhibition of complex I of the electron transport chain (Yao *et al.*, 2018), and inhibition of the adenine nucleotide translocase (ANT) (Divakaruni *et al.*, 2018). These off-target effects suggest that general perturbations in lipid pathways and/or mitochondrial function could very well be responsible for the observed change in cell invasion.

In TNBC cells, the treatment with a range of concentrations (100-300μM) of etomoxir for 24h inhibited FAO and reduced oxygen consumption rate and ATP levels which is thought to cause a reduction in cell migration (Jun Hyoung Park *et al.*, 2016). Again in TNBC cells, 15min exposure to 40μM of

etomoxir inhibited FAO and the subsequent OXPHOS that depends on the products of FAO. This, in turn, can deprive cellular energy needed for migration and metastasis (Wright *et al.*, 2017).

Furthermore, slowing the rate of cell invasion has previously been shown to slow the overall progression of the tumour (Zhai *et al.*, 2011). My finding that blocking FAO shows promising results in slowing tumour progression through blocking cell invasion. In support of this, Lin et al., also showed that blocking FAO by treatment with 10 mg/kg/day etomoxir *in vivo* slowed tumour progression. At the final clinical endpoint, etomoxir-treated tumours eventually grew into similar-sized tumours to that of the untreated controls. However, until the end-point was reached, the treated tumours were smaller in size than the controls (Lin *et al.*, 2017). As such, I propose that FAO-inhibited cells are slower at invading/infiltrating and thus a tumour treated with FAO inhibitors will grow to their ultimate size at a slower rate.

In summary, etomoxir and perhexiline may have shown severe side-effects in a small proportion of patients with heart disease. Nonetheless, the treatment options and survival expectancy for

GBM patients is much direr. Thus, the potential benefit in regard to risk might provide promise for using etomoxir or perhexiline to slow cell invasion and tumour progression and hence as possible candidates for further evaluation *in vivo* and in clinical trials.

6.3.2 Technical considerations

The transwell techniques I used are similar to those published previously in GBM. In order to establish a chemotactic gradient, I used 1%FBS in the top compartment and 10% in the bottom compartment. I chose to form a gradient using FBS, which contains many chemotactic factors, including cytokines and growth factors, as opposed to using a single chemotactic factor. This is because a single chemotactic factor may be unreliable, given that the expression of the receptor responsible for responding to a given chemotactic factor may change as a result of drug treatment or miRNA transfection. Moreover, both my cell lines are cultured in the standard 10% FBS; thus, I can trust that they will respond to FBS.

I was unsure of optimal assay length, but I am aware that a large number of GBM publications employed a 24h time-point. However, the length of the assay may vary in response to the

concentration of chemotactic factors in the FBS. Thus, to ensure the optimal length of the assay (24h) remains consistent, I carried out the transwell assay for all my conditions (including optimisation, transfections, drug treatments, and biological repeats) from the same stock and aliquot of FBS in order to control for the variation in FBS composition.

I chose the optimal concentration of cells (20,000 cells) based on the ease in counting the invaded cells in the untreated condition and allowing for a differential effect on cell invasion to be clearly observed upon the introduction of treatment.

The reason I see background signals in negative control where a gradient is missing is because of chemokinetic (stimulated random locomotion) activity. In my optimisation, I had two negative controls (either 1% or 10% FBS in both compartments). This is because I wanted to control for the effect of the starvation condition (1% FBS) on cell movement verses the effect when the cells are in complete media supplemented with 10% FBS.

I consider a significant difference in chemotactic responses a reflection of real physiological significance where a strong

chemotactic response will efficiently move cells out of a tumour into surrounding tissues.

Cell synchronisation is often achieved by arresting cell cycle at the entrance to S-phase, and upon release from the block, they synchronously progress through S, G2 and M (Darzynkiewicz *et al.*, 2011). Because after adding the transfection media I achieved synchronous confluence, I did not see the need for using proliferation inhibitors, such as hydroxyurea, aphidicolin or thymidine, to prevent cell number changes that could potentially affect the outcome of the assay.

6.4 Future work

One of the key areas for future work would be to evaluate the dose-dependent effect of FAO inhibition on the global change gene expression profile of GBM cells as they change their invasive behaviour. A time-course experiment could also provide more information on the temporal effect of inhibiting FAO on cell invasion. These future investigations would allow us to better understand the mechanism by which FAO inhibition affect invasion.

6.5 Chapter Summary

- miR-619-5p overexpression inhibited *in vitro* cell invasion by 50% compared to NT control.
- The multi-targeting property of miRNAs could contribute to this significant effect seen on the invasion.
- The knockdown of CPT2, a rate-limiting FAO enzyme, by siRNA inhibited transwell invasion by 20% compared to scrambled control.
- Following the treatment with either etomoxir or perhexiline, the transwell invasion was reduced by about 40% relative to the untreated controls.
- Both the knockdown of CPT2 and the treatment with either etomoxir or perhexiline caused an increase in LDs content due to the inhibition of FAO.
- Thus, targeting FAO, perhaps in combination with other molecular targeted-drugs, may potentially reduce tumour cell invasion, but further *in vivo* work would be needed.

Chapter 7:
General Discussion, Final Conclusions, and Future Work

7.1 General Discussion

Previously, there has been a focus on using samples obtained from the tumour core region as the subject of research to develop targeted therapies for GBM. However, such therapies have failed to improve patient survival in clinical trials. One reason for this disparity between pre-clinical and clinical results may be the heterogeneous molecular profiles and clinical behaviour of the different regions of the GBM tumour, as discussed in section 1.1.6. The recent elucidation of intra-tumour heterogeneity (ITH) in the gene expression profiles of GBM tumours provided a clear rationale to investigate the hypothesis of regional differences in miRNA expression profiles.

In chapter 3 of this thesis, I profiled miRNA expression through microarray analysis of multi-region surgically-resected primary GBM tumour fragments. Although the approach of multi-region sampling has previously been employed to investigate genomic intra-tumour heterogeneity in GBM (Sottoriva *et al.*, 2013), this is the first attempt to use this approach to determine regional miRNA expression heterogeneity. The analyses of my microarray and qRT-PCR results (which are both limited by the number of patients used) suggested that two miRNAs (miR-619-5p and miR-4793-3p) are differentially upregulated in the

tumour core/rim regions compared to the invasive margin region of the GBM tumour. However, because of the high proportion non-neoplastic cells in the invasive margin region of the tumour, I sought to determine the miRNA expression specifically in 5-ALA enriched cell population which represent the infiltrating tumour cells. Although I found that miR-619-5p and miR-4793-3p were predominantly expressed in the 5-ALA/+ infiltrating tumour cells as opposed to the 5-ALA/- non-neoplastic cells, it is worth mentioning that 5-ALA-staining approach is limited in its accuracy; with more false-negative results being reported in the literature than false positives.

The false-negative results due to the lack of ALA-induced fluorescence in some tissue samples taken from the same GBM tumour may be attributed to the following (1) tumour necrosis (Ross *et al.*, 2017) (2) the presence of an intact BBB limiting 5-ALA from reaching tumour cells (Ennis *et al.*, 2003), (3) the prolonged exposure to light (>25 min of blue light or 87 min of standard white light) during surgery, or the prolonged period of time between when the samples were obtained until the cells are FACS analysed, can both cause fluorescent bleaching (the chemical degradation of a fluorophore) which leads to a decrease in fluorescence intensity (Lakowicz, 1988), and finally (4) the presence of different glioma molecular subtypes within

the tumour; for example, Bonnin et al., (2019) shown tumour cells which are 5-ALA/- resemble the gene expression profile of the neural subtype (Bonnin *et al.*, 2019). False-positive signals, on the other hand, have been reported to originate from gliosis and reactive astrocytes (Ando *et al.*, 2011). Non-neoplastic fluorescent signal accumulation can also occur from inflammatory cells such as microglia, neutrophils, macrophages, and lymphocytes (invading into the brain after an infection) (Omoto *et al.*, 2018). Further, extracellular fluorescence leaking from GBM cells, which actively export the metabolised product of 5-ALA (protoporphyrin 9) into the ECM (Utsuki *et al.*, 2007), can also generate false-positive signals. False-positive signals tend to also accumulate around blood vessels due to the high availability of 5-ALA (Ando *et al.*, 2011). Another source of false-positive results could be the FACS gating process; whereby lowing the fluorescence detection threshold to allow the inclusion of vague instead of only strong fluorescent signals may potentially result in 5-ALA/- cells ending up in the 5-ALA/+ fraction. With regards to my results, because 5-ALA fluorescence does not definitively indicate the presence of malignant tumour cells, I could never entirely conclude that the 5-ALA/+ cells are the same as the residual tumour cells left behind after surgical resection of the main tumour mass, but I

would argue that the analysis of these cells takes us close to that goal. Next, in order to exclude the possibility that the downregulation of miR-619-5p and miR-4794-3p in the invasive margin sample is due to the presence non-neoplastic cells in the sample, I compared their expression in the core and rim regions to that in the 5-ALA/+ enriched cell population of the invasive margin from the same patient. Indeed, I found that both miR-619-5p and miR-4794-3, which were downregulated in the unsorted invasive margin region, to be also expressed at lower levels in 5-ALA/+ cell population of the invasive margin compared to the core and the rim regions. An obvious limitation to this approach lies in the possibility that FACS-analysed invasive margin samples are not the same as their unsorted counterparts because the cell sorting process could have affected the cells' expression profiles.

Chapters 4, 5 and 6 were dedicated to studying the functional role of the newly identified miR-619-5p and miR-4793-3p in GBM. Their role was investigated via overexpressing them in two GBM cell lines, which intrinsically have low expression levels of such miRNAs. This approach has two potential limitations: (1) miRNA overexpression is prone to artefacts that might skew the function of miRNA beyond providing a subtle effect on a set

of genes (Martinez-Sanchez and Murphy, 2013); (2) my conclusion were based on using only two cell lines. My initial work was done using U87 cells, a well-characterised cell model with > 3000 citations in PubMed. However, U87 cells lack systematic clinical characterisation of the tumours from which they were derived, which makes it difficult to correlate the *in vitro* findings to patient parameters. But, I was also able to access and use a primary cell line particularly derived from the invasive margin, which is the most clinically relevant region, to validate the results that I obtained using U87 cells. Yet, a possible caveat is that *in vitro* culturing of primary cells selects for cells that grow like established cell lines which, although helpful in the optimisation experiments, might not have been representative of the growth rate of all of the cell population. However, this is a criticism that can be said about all cell culture experiments which naturally select for proliferative cell populations. The exact primary cell line I picked was a cell line derived from the invasive margin that had a pair derived from the tumour core region to facilitate future follow-up studies. However, I deemed it unnecessary to use the core derived cell line in my current project as it expressed my miRNAs of interest at the same levels as the invasive margin derived cell line; and thus would not be useful in studying the effect of the differential

expression of my miRNAs of interest. Nevertheless, the cells derived from the core region can serve as an isogenic control for the cells derived from the invasive margin region of the same tumour; a key point to be considered in future studies.

In chapter 4 of this thesis, I determined that miR-619-5p and miR-4793-3p target genes were enriched within the FAO and glycerophospholipid metabolic pathways. I found that the number of binding sites for miR-4793-3p, within the 3'UTR of FAO targets, was notably less than those for miR-619-5p; which supports my observation that the magnitude of reduction of luciferase activity – which measure the physical binding of miRNA:mRNA duplexes, was not as great in miR-4793-3p (~15%) as in miR-619-5p (~40-50%) for the same target. However, I must note that I only considered targets that contain miR-619-5p binding sites within their 3'UTRs; because miRNA binding sites within coding regions and 5' UTRs are less frequent and appear less effective than those in the 3'UTR (Farh et al., 2005; Lewis, Burge and Bartel, 2005; Lim et al., 2005). I have confirmed that miR-619-5p directly bind to the 3'UTR of CPT2 in two GBM cell lines using qRT-PCR, Western blots and luciferase assay. I then evaluated the protein expression of CPT2 in patients TMAs; however, due to the lack of a GBM

marker to co-stain with, it was not possible to conclude whether the observed protein CPT2 expression in the invasive margin is exclusively localised to the tumour cell population. As such, I could not make assertions regarding CPT2 protein expression in the infiltrating tumour cells in the invasive margin region compared to the tumour cells in the core/rim regions. Nevertheless, at the mRNA level, I found that the mRNA expression of its target, CPT2 was downregulated in the 5-ALA/+ cells, where miR-619-5p is upregulated.

Chapter 5 of this thesis aimed at validating the role of miR-619-5p and miR-4793-3p in regulating metabolites associated with FAO and glycerophospholipid metabolism pathways. I performed bi-phasic extraction of polar and non-polar metabolites and employed liquid chromatography-mass spectrometry (LC-MS) and tandem MS-MS techniques to profile the intracellular metabolome and lipidome of U87 cells from 6 biological repeats of U87 cells transfected with miR-619-5p mimic, miR-4793-3p mimic, miR-619-5p and miR-4793-3p mimic at 1:1 ratio, and non-targeting mimic negative control for 72h. I found that the overexpression of miR-619-5p and miR-4793-3p in U87 cells – which endogenously have very low expression of these miRNAs – downregulates the level of

metabolites associated with, amongst other pathways, glycerophospholipid metabolism pathway; which confirmed my findings from the miRNA target prediction and gene enrichment analysis conducted in Chapter 4.

However, because I showed that FAO-associated genes are targeted by both miR-4793-3p and miR-619-5p in Chapter 4, , I expected that the levels of metabolites associated with FAO would be affected; but this hypothesis was not confirmed from my metabolomics data. This could be due to the lack of reliable annotation for many ion peaks generated by MS-based methods. As such, FAO-associated metabolites could have been picked up by my analysis but I could not annotate them.

In Chapter 6 of this thesis, I investigated the potential role of miR-619-5p and its target genes/pathways in the regulation of the invasive behaviour of GBM. My results showed that the overexpression of miR-619-5p can specifically reduce the *in vitro* invasion of two GBM cell lines through collagen IV-coated transwells. I also observed the same results following the siRNA–mediated knockdown of CPT2 and the pharmacological inhibition of FAO. As such, FAO inhibitors can replicate the effect of CPT2 knock-down, which in itself, is a consequence of miR-

619-5p overexpression. Furthermore, Both CPT2 knockdown and pharmacological inhibition of FAO led to LDs accumulation, which alludes that LDs may have a role in regulating GBM invasion, as reported in other cancer types. However, miR-619-5p overexpression led to a reduction in LDs abundance, which would imply that changes in LDs abundance can just be a consequence of FAO inhibition. With regards to the reduction in LDs abundance upon miR-619-5p overexpression, one possibility is that LDs are reduced due to lipid deficiency in the cells caused by low PC enzymes, which I discuss in Chapter 5. Another possibility is the direct targeting of the LD-associated protein, PLIN3, and the indirect targeting of LDLR, by miR-619-5p; both of which will reduce the abundance of lipids available for storage in LDs; as I discuss this in Chapter 4.

In Chapter 6, I discuss that miR-4793-3p overexpression does not reduce GBM cell invasion, nor does it change LD abundance. Yet, Chapter 5 mentions that I observed that miR-4793-3p downregulates the abundance of the same lipid metabolites that miR-619-5p downregulates; although miR-4793-3p had lesser effect on metabolite abundance than in cells overexpressing miR-619-5p or cells co-transfected with both miRNAs. This can be due to differences in detection sensitivity of LD staining and

mass spectrometry techniques. Alternatively, it could be due to the presence of other targets than the ones I investigated in this thesis that slightly modulate lipid metabolism, without directly affecting cell invasion.

I used glucose-supplemented media to culture U87 and GIN28 cells for all of my experiments because I did not want to induce a metabolic stress response changing glucose levels in the cell culture media, as this may confound my ability to draw conclusions about miRNA function. For example, LDs are known to specifically deplete under glucose-deprived conditions (Hoang-Minh et al., 2018). Thus, by using glucose-supplemented media, I could ensure that the reduction in LDs I observed is due to the overexpression of miR-619-5p and not glucose-deprivation. Moreover, glucose can also help sustain cell viability when cells shift from lipid metabolism to glucose utilisation as a result of FAO inhibitor treatment (Ashrafian, Horowitz and Frenneaux, 2007). As such, invasion was reduced without affecting cell viability/proliferation which could suggest an independent mechanistic regulation of invasion by lipid metabolisms. However, although was not significantly affected, cell viability was more affected by miRNA transfection (8%) than by siRNA transfection (2%). This could be because of the

multi-targeting effect of miRNA versus the gene-specific siRNA targeting technology that I used. However, I am aware that the presence of serum changes both the genomics and transcriptomic profiles of GBM cells and may cause depletion of stem cell-like markers (Lee et al., 2006).

The metabolic profile of my control cells that expressed miR-619-5p at low levels (the cells of the invasive margin region) resembled that of the slow-cycling GBM cells (SCCs) described by Hoang-Minh et al. which preferentially use mitochondrial oxidative metabolism with FAO constituting the main source for mitochondrial energy production (Hoang-Minh et al., 2018). SCCs metabolic profile demonstrated elevated levels of lipid metabolite (MS-based methods) and high abundance of LDs (staining methods). Hoang-Minh et al. also showed that SCCs displayed enhanced migration (*in vitro* scratch assays) and produced invasive tumours *in vivo*. Then, they showed that the genetic or pharmacological inhibition of lipid metabolism in SCCs by targeting Fatty acid binding protein 7 (FABP7) leads to a decrease in *in vitro* migration and *in vivo* tumour invasion (Hoang-Minh et al., 2018). This might mean that the invasive margin cells arise from the SCCs subpopulation within the tumour mass. Alternatively, it could be implied that metabolic

profiles characterised by a high rate of lipid metabolism define SCCs-like phenotypic behaviours, such as augmented invasion potential. This further highlights that targeting lipid metabolism is a promising therapeutic strategy.

7.2 Final Conclusions

In this thesis, miRNA intra-tumour heterogeneity has been demonstrated. Analysis of miRNA microarray data from 15 patients identified five miRNAs that are significantly differentially-expressed within the GBM tumour. The expression of two of these miRNAs (miR-619-5p and miR-4793-3p) was validated by qRT-PCR to be downregulated in 5-ALA/+ cell population of the invasive margin region relative to the tumour core/rim, an expression pattern that is consistent with the microarray results from the unsorted tumour regions. However, I am not intending to show that the miRNAs that I have identified in this thesis constitute all of intra-tumour heterogeneity in miRNA expression in GBM. The results simply demonstrate the presence of *some* heterogeneity between different regions within the GBM tumour, at the miRNA level. Although the identified differentially expressed miRNAs in the invasive region may serve as potential therapeutic targets, determining the optimal miRNAs to target in treatments will

require comprehensively exploring all the miRNAs that are relevant to the invasive margin using a larger patient sample size as well as an improved accuracy of the 5-ALA method.
As such, my current work simply highlights the clinical relevance of miRNA heterogeneity and opens the opportunity to pursue a novel, and hopefully fruitful, avenue of research.

Moreover, the functions of miR-619-5p and miR-4793-3p have not been studied in GBM before, and my thesis is the first to comment on this. Both were found to play roles in regulating metabolic enzymes within the lipid metabolism pathways. There are many other miRNAs that are reported to regulate metabolic enzymes in GBM, and the overexpression of such miRNAs has also been reported to cause a reduction in metabolic activity. This reduction is often related to reductions in cell invasion and/or proliferation. My thesis shows that the artificial overexpression of miR-619-5p, in particular, reduced the expression of metabolic enzymes and the abundance of metabolic intermediates within the lipid metabolism pathways, and resulted in the reduction of GBM cell invasion.

Moreover, because my miRNAs are differentially expressed in the invasive margin and also affect tumour invasion, they are

particularly clinically relevant, out of all the possible miRNA targets identified in previous *in vitro* studies. This is because, if targeted correctly, they can provide a targeted means of controlling invasion and tumour recurrence stemming from the GBM tumour invasive edge, and thus may lead to increased GBM patient survival.

7.3 Future Projects

The miRNA gene targets introduced in this work were selected with the emphasis on exploring the potential therapeutic translation. Other gene targets will be elucidated in a future project where the data from a recently conducted RNA-Seq experiment will be integrated with my miRNA microarray data.

In addition, the metabolomics profiles of the different regions of the GBM tumour and the 5-ALA FACS-purified cells of the invasive margin region can be studied in the future using a Nano ultra-performance liquid chromatography-high resolution MS approach. This will allow an unbiased integrative approach, using miRNA, transcriptomics and metabolomics profiles, to build a map of clinically relevant pathways that are dysregulated in the invasive tumour margin. This work is the next logical step to elucidate the metabolites that are, yet such

study is limited by the availability of a sufficient number of 5-ALA/+ cells to carry out metabolites extraction and the accuracy of the 5-ALA staining and sorting method.

The FAO vulnerability of GBM cells can also be further exploited by testing more therapeutic agents alongside the standard therapies. Future studies might be conducted to assess the response to TMZ in combination with lipid metabolism modulators both *in vitro* and *in vivo*. In conclusion, designing effective therapy to prevent GBM cells from infiltrating further into the normal brain will require a detailed understanding of the regulatory process that drives cell invasion. Thus, it is hoped that the work outlined in the thesis can act as a step towards understanding the regulation of cell invasion via miRNAs (miR-619-5p) and their target genes/pathways (CPT2 in the FAO pathway) which are differentially expressed in the tumour cells in the invasive margin, as these cells may more closely resemble the residual cell population responsible for tumour recurrence.

Chapter 8: Appendices

8.1 Detailed information of patient samples used in the project

Table 8.1: Tissue samples information

GBM patients from which tissue were collected were given numbers following the prefix GBM. Abbreviations: PCV: Procarbazine, CCNU, and Vincristine; BSC: best supportive care; RT/CT: radiotherapy/chemotherapy; N/A: not applicable; WT: wild-type; R132H: point mutation changing arginine at 132 into histidine; TMZ: temozolomide

Tissue sample	Regions	Tumour Site (lobe)	Resection Status (%)	RT/CT	TMZ Response	Overall survival (months)	Age	Sex	IDH-1 status	ATRX status	MGMT status
GBM 1.2	Core	Right parietal	100	60	Did not tolerate	15.1	59	Male	WT	N/A	N/A
GBM 1.3	Rim										
GBM 1.5	invasive margin										
GBM 2.1	core	Right parietal	100	60/TMZ	Good	56.9	68	Female	WT	N/A	N/A
GBM 2.2	rim										
GBM 2.4	invasive margin										
GBM 3.1	rim	Right temporal	100	60/TMZ	Good	23.1	54	Female	WT	N/A	N/A
GBM 3.2	core										
GBM 3.4	Invasive margin										
GBM 3.5 (Recurrent)	Mixed	Right temporal	100								

GBM 5.1	rim	Left parietal, occipital	100	60/TMZ	Moderate	Alive	58	Female	WT	N/A	N/A
GBM 5.2	core										
GBM 5.5	invasive margin										
GBM 5.6 (Recurrent)	rim	Left parietal	95	PCV		Alive	59	Female	N/A	N/A	N/A
GBM 5.7 (Recurrent)	core										
GBM 5.10 (Recurrent)	invasive margin										
GBM 6.1	rim	Left occipital	100	60/TMZ		29.1	53	Male	WT	N/A	N/A
GBM 6.2	Core										
GBM 6.4	invasive margin										
GBM 7.1	core	Left parietal	100	60/TMZ		6.7	71	Male	WT	N/A	N/A
GBM 7.2	rim										
GBM 7.4	invasive margin										
GBM 8.1	rim	Left frontal	90	60/TMZ	Poor	5	54	Female	WT	N/A	N/A
GBM 8.2	core										
GBM 8.4	invasive margin										
GBM 9.1	rim		100			17.2	48	Male	WT	N/A	N/A

GBM 9.2 **GBM 9.5**	Core Invasive margin	Left frontal,		60/TMZ							
GBM 10.1 **GBM 10.3** **GBM 10.5**	rim core invasive margin	Right temporal	100	60/TMZ	Poor	4	64	Male	WT	N/A	N/A
GMB 12.1 **GMB 12.2** **GMB 12.4**	rim Core invasive margin	Left parietal	100	60/TMZ		6.9	46	Female	WT	N/A	Hypo
GBM 13.1 **GBM 13.2** **GBM 13.4**	rim core invasive margin	Right Parietal	100	60/TMZ	Good	9.7	26	Male	WT	N/A	N/A
GBM 15.1 **GBM 15.3** **GBM 15.5**	rim core invasive margin	Right temporal	100	60/TMZ	Good	25.7	33	Female	R132H	N/A	Interm ed
GBM 17.1 **GBM 17.2** **GBM 17.4**	rim core invasive margin	Left frontal	100	30		4.4	73	Female	WT	N/A	<10%
GBM 19.2 **GBM 19.3**	core rim	Left parietal	100	60/TMZ		14.7	68	Male	WT	N/A	0%

GBM 19.4	invasive margin										
GBM 20.1	rim	Right frontal	99	60/TMZ	Good	15.3	71	Male	WT	N/A	N/A
GBM 20.2	core										
GBM 20.5	invasive margin										
GBM 21.1	rim	Right temporal	90	60/TMZ	Good	32.5	67	Female	WT	N/A	75%
GBM 21.2	core										
GBM 21.5	invasive margin										
GBM 22.1	rim	Left temporal	95%			5.4	35	Female	R132H	N/A	N/A
GBM 22.3	core										
GBM 22.5	invasive margin										
GBM 23.1	rim	Left parietal	90%			6.2	53	Male	WT	N/A	N/A
GBM 23.2	core										
GBM 23.5	invasive margin										
GBM 25.1	rim	Left parietal	99%	60/TMZ		12.9	60	Female	WT	WT	0%
GBM 25.2	core										
GBM 25.5	invasive margin										
GBM 26.1	rim	Left temporal	100%	60/TMZ		6.8	56	Female	WT	WT	0%
GBM 26.2	core										
GBM 26.6	invasive margin										

GBM 27.1	rim	Right temporal	99%	60/TMZ		Alive	30	Female	WT	Mut	75%
GBM 27.2	core										
GBM 27.5	invasive margin										
GBM 28.1	rim	Right frontal	99%	BSC		3	71	Male	WT	WT	0%
GBM 28.2	core										
GBM 28.5	invasive margin										
GBM 29.1	rim	Left frontal	100			Alive	67	Female	WT	WT	0%
GBM 29.3	core										
GBM 29.5	invasive margin										
GBM 30.1	rim	Left frontal	100	BSC		9.3	53	Male	WT	WT	0%
GBM 30.2	core										
GBM 30.5	invasive margin										
GBM 31.1	rim	Right temporal	100	60/TMZ		16.1	57	Female	WT	WT	0%
GBM 31.2	core										
GBM 31.5	invasive margin										
GBM 32.3	core	Right parietal	100%	60/TMZ		17.7	54	Female	WT	WT	25%+
GBM 32.4	rim										
GBM 32.5	invasive margin										
GBM 33.2	core	Right parietal	100%			11.6	70	Male	WT	WT	0
GBM 33.3	rim										

GBM 33.5	invasive margin										
GBM 37.2	core	Right parietal	100%	60/TMZ		12	63	Female	WT	WT	0%
GBM 37.4	rim										
GBM 37.5	invasive margin										
GBM 38.1	rim	Right frontal	100%	60/TMZ		5.9	69	Male	WT	WT	0%
GBM 38.2	core										
GBM 38.5	invasive margin										
GBM 39.1	rim	Right frontal	100%	60/TMZ		14.6	58	Female	WT	WT	0%
GBM 39.3	core										
GBM 39.5	invasive margin										
GBM 40.3	rim	Right frontal	90%	30		7.2	44	Male	WT	WT	0%
GBM 40.4	core										
GBM 40.5	invasive margin										
GBM 41.1	rim	Left temporal	95%	BSC		2.8	55	Female	WT	WT	0%
GBM 41.4	core										
GBM 41.5	invasive margin										
GBM 42.1	invasive margin	Right temporal	100%			6.8	81	Male	WT	WT	10%
GBM 42.2	core										
GBM 42.3	rim										
GBM 44.2	core		100%			Alive	46		WT	WT	50%

GBM 44.4	rim	Right parietal		60/TMZ				Female			
GBM 44.5	invasive margin										
GBM 45.1	rim	Right parietal	100%	60/TMZ		Alive	66	Male	WT	WT	25%
GBM 45.2	core										
GBM 45.4	invasive margin										
GBM 46.1	rim	Right frontal	100%	60		11.5	60	Male	WT	WT	0%
GBM 46.2	core										
GBM 46.5	invasive margin										
GBM 47.2	core	Left temporal	100%			11.7	66	Male	WT	WT	0%
GBM 47.3	invasive margin										
GBM 47.4	rim										
GBM 52.1	rim	Right frontal	100	40/TMZ		Alive	59	Male	WT	WT	0
GBM 52.2	invasive margin										
GBM 52.4	core										

8.2 Short Tandem Repeats (STRs) genotyping results.

The prefix GIN and CCE refer to cells derived from the invasive margin and core regions, respectively.

DNA System	GIN-31 p11	GIN-31 p33	GIN-17 p11	GIN-17 p27	GIN-3R p8	GIN-3R p31	GIN-8 p11	GIN-8 p33	GIN-28 p11	GIN-28 p33	U-251MG p22
AM	X, X	X, X	X, X	X, X	X, X	X, X	X, X	X, X	X, Y	X, Y	X, Y
D3S1358	16, 18	16, 18	14, 15	14, 15	14, 15	14, 15	15, 16	15, 16	14, 17	14, 17	16, 16
D1S1656	12, 15	12, 15	14, 16.3	14, 16.3	13, 16	13, 13	12, 16	12, 16	12, 16	12, 16	16, 17.3
D6S1043	12, 18	12, 18	11, 12	11, 12	11, 16	11, 16	14, 18	14, 18	11, 13	11, 13	12, 12
D13S317	11, 13	11, 13	8, 8	8, 8	12, 13	12, 13	12, 12	12, 12	11, 12	11, 12	10, 11
Penta E	7, 12	7, 12	5, 10	5, 10	12, 12	12, 12	6, 9	6, 9	7, 17	7, 17	7, 10
D16S539	10, 11	10, 11	11, 13	11, 13	11, 13	11, 13	12, 12	12, 12	9, 12	9, 12	12, 12
D18S51	17, 18	16, 17, 18	12, 16	12, 16	14, 18	14, 18	16, 17	16, 17	14, 17	14, 17	13, 13
D2S1338	19, 25	11, 19, 25	17, 23	17, 23	17, 23	17, 23	17, 19	17, 19	19, 23	19, 23	22, 24
CSF1PO	11, 12	11, 12	11, 12	11, 12	11, 13	11, 13	11, 11	11, 11	11, 13	11, 13	11, 12
Penta D	11, 12	11, 12	13, 13	13, 13	10, 10	10, 10	12, 13	12, 13	12, 14	12, 14	10, 12
TH01	6, 9	6, 9	5, 9.3	5, 9.3	9.3, 9.3	9.3, 9.3	9, 9	9, 9	6, 9.3	6, 9.3	9.3, 9.3
vWA	14, 18	14, 15, 18, 21	16, 16	16, 16	16, 16	16, 16	17, ?	17, 17	14, 15	14, 15	16, 18
D21S11	29, 29	28, 29	28, 29	28, 29	28, 30	28, 30	30, 30	30, 30	27, 33	27, 33	29, 30
D7S820	7, 10	7, 10	9, 11	9, 11	8, 12	8, 12	9, 10	9, 10	8, 10	8, 10	10, 12
D5S818	11, 12	11.1, 12	10, 13	10, 13	11, 12	11, 12	12, 13	12, 13	11, 12	11, 12	11, 12
TPOX	9, 9	9, 9	9, 12	9, 12	8, 10	8, 10	8, 11	8, 11	8, 11	8, 11	8, 8
D8S1179	11, 13	11, 13, 14.1	11, 13	11, 13	12, 13	12, 13	10, 13	10, 13	10, 14	10, 14	13, 15
D12S391	17, 23	16, 17, 22.3, 23	18, 21	18, 21	19, 23	19, 23	18, 18	18, 18	20, 21	20, 21	17, 22
D19S433	12, 15	12, 13.1, 15	14, 14	14, 14	14, 14	14, 14	13, 13	13, 13	14, 14	14, 14	13, 15
FGA	22, 26	19.3, 22, 26	22, 25	22, 25	22, 24	22, 24	21, 22	21, 22	23, 25	23, 25	21, 25

Figure 8.1: Genotyping of GBM cell lines.

8.3 Raw microarray expression data of the five significantly expressed miRNAs between the three regions of the GBM tumour.

Each table below shows the readout (following normalisation to the internal control on the microarray) for a given miRNA obtained from the microarrays from three tumour regions (core, rim, invasive margin) of 15 patients. It aims to illustrate the difference in miRNA expression within the tumour regions each patient. Patients from which tissue were collected were given numbers following the prefix GBM. Regions are labelled as numbers following the patient number. 2 or 3 correspond to the core region, 1 corresponds to the rim region, and 4 or 5 correspond to the invasive margin region.

Table 8.2: hsa-miR-330-5p, ID: 20501275

Patient	**GBM 2**		**GBM 3**			**GBM 5**			**GBM 6**		**GBM 8**		**GBM 9**			**GBM 10**		**GBM 13**		
Region	2.2	2.4	3.2	3.1	3.4	5.2	5.1	5.5	6.2	6.3	8.1	8.4	9.2	9.1	9.5	10.1	10.5	13.2	13.1	13.4
REV	0.79	3.78	3.66	0.65	5.63	3.85	0.81	0.80	0.62	0.55	0.68	2.89	0.63	0.90	3.38	0.56	5.14	0.71	3.77	4.64
Patient	**GBM 15**			**GBM 17**			**GBM 20**			**GBM 21**		**GBM 22**			**GBM 23**			**GBM 25**		

Region	15.3	15.1	15.5	17.2	17.1	17.4	20.2	20.1	20.5	21.1	21.5	22.3	22.1	22.5	23.2	23.1	23.5	25.2	25.1	25.5
REV	0.53	0.92	3.80	0.62	0.70	1.81	1.69	1.90	4.92	0.72	5.38	1.94	1.44	3.09	4.37	4.27	5.21	1.39	2.31	6.14
Patient	**GBM 27**			**GBM 28**			**GBM 29**			**GBM 30**			**GBM 31**							
Region	27.2	27.1	27.5	28.2	28.1	28.5	29.3	29.1	29.5	30.2	30.1	30.5	31.2	31.1	31.5					
REV	2.03	0.64	2.15	4.04	5.38	4.93	2.00	1.31	5.61	0.74	0.80	1.69	1.48	1.00	3.57					

Table 8.3: hsa-miR-215-3p, ID: 20500474

Patient	GBM 2			GBM 3			GBM 5			GBM 6		GBM 8		GBM 9		GBM 10		GBM 13		
Region	2.2	2.4	3.2	3.1	3.4	5.2	5.1	5.5	6.2	6.3	8.1	8.4	9.2	9.1	9.5	10.1	10.5	13.2	13.1	13.4
REV	0.52	0.39	0.47	0.43	0.49	0.45	0.50	0.59	0.42	0.44	0.46	0.44	0.49	0.47	0.50	0.45	0.47	0.48	0.44	0.47
Patient	**GBM 15**			**GBM 17**			**GBM 20**			**GBM 21**		**GBM 22**			**GBM 23**			**GBM 25**		
Region	15.3	15.1	15.5	17.2	17.1	17.4	20.2	20.1	20.5	21.1	21.5	22.3	22.1	22.5	23.2	23.1	23.5	25.2	25.1	25.5
REV	0.43	0.41	0.51	0.48	0.39	0.54	0.44	0.55	0.54	0.47	0.46	0.43	0.39	0.45	0.43	0.46	0.59	0.38	0.44	0.54

Patient	**GBM 27**			**GBM 28**			**GBM 29**			**GBM 30**			**GBM 31**			
Region	27.2	27.1	27.5	28.2	28.1	28.5	29.3	29.1	29.5	30.2	30.1	30.5	31.2	31.1	31.5	
REV	0.46	0.40	0.51	0.45	0.47	0.53	0.47	0.47	0.44	0.42	0.47	0.46	0.43	0.43	0.48	

Table 8.4: hsa-miR-619-5p, ID: 20504364

Patient	GBM 2			GBM 3			GBM 5			GBM 6			GBM 8			GBM 9			GBM 10			GBM 13		
Region	2.2	2.4	3.2	3.1	3.4	5.2	5.1	5.5	6.2	6.3	8.1	8.4	9.2	9.1	9.5	10.1	10.5	13.2	13.1	13.4
REV	6.60	6.22	6.05	7.37	5.94	7.57	5.88	8.45	7.57	5.32	6.24	5.91	6.46	7.63	6.27	7.47	6.23	6.73	5.97	6.05
Patient	**GBM 15**			**GBM 17**			**GBM 20**			**GBM 21**			**GBM 22**			**GBM 23**			**GBM 25**					
Region	15.3	15.1	15.5	17.2	17.1	17.4	20.2	20.1	20.5	21.1	21.5	22.3	22.1	22.5	23.2	23.1	23.5	25.2	25.1	25.5
REV	7.22	5.86	6.36	6.68	6.35	6.34	7.23	7.19	6.82	6.24	6.48	6.46	6.02	5.70	6.48	6.17	5.66	7.40	6.73	6.21
Patient	**GBM 27**			**GBM 28**			**GBM 29**			**GBM 30**			**GBM 31**											
Region	27.2	27.1	27.5	28.2	28.1	28.5	29.3	29.1	29.5	30.2	30.1	30.5	31.2	31.1	31.5									

REV	6.23	5.51	5.58	6.95	6.27	5.11	7.42	6.50	5.54	7.93	7.23	5.26	7.57	6.90	5.36	

Table 8.5: hsa-mir-4440, ID: 20536693

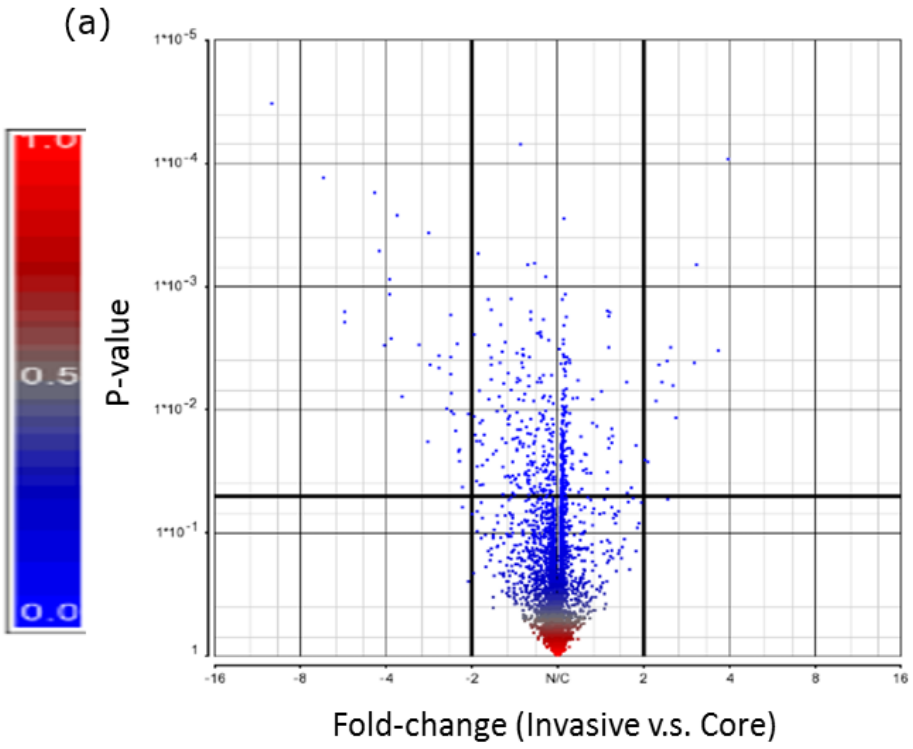
Patient	GBM 2			GBM 3			GBM 5			GBM 6		GBM 8		GBM 9		GBM 10		GBM 13		
Region	2.2	2.4	3.2	3.1	3.4	5.2	5.1	5.5	6.2	6.3	8.1	8.4	9.2	9.1	9.5	10.1	10.5	13.2	13.1	13.4
REV	0.59	0.65	0.68	0.84	0.61	0.76	0.56	1.09	0.87	0.60	0.62	0.58	0.65	1.06	0.61	1.17	0.68	0.64	0.64	0.74
Patient	**GBM 15**			**GBM 17**			**GBM 20**			**GBM 21**		**GBM 22**			**GBM 23**			**GBM 25**		
Region	15.3	15.1	15.5	17.2	17.1	17.4	20.2	20.1	20.5	21.1	21.5	22.3	22.1	22.5	23.2	23.1	23.5	25.2	25.1	25.5
REV	1.39	0.71	0.54	0.63	0.64	0.61	1.01	0.87	0.94	0.47	0.65	0.67	0.66	0.66	0.62	0.61	0.57	2.56	2.40	0.57
Patient	**GBM 27**			**GBM 28**			**GBM 29**			**GBM 30**			**GBM 31**							
Region	27.2	27.1	27.5	28.2	28.1	28.5	29.3	29.1	29.5	30.2	30.1	30.5	31.2	31.1	31.5					
REV	0.77	0.68	0.87	0.73	0.64	0.53	1.12	0.70	0.63	1.84	0.94	0.59	1.42	2.20	0.71					

Table 8.6: hsa-miR-4793-3p, ID: 20519689

Patient	GBM 2			GBM 3			GBM 5			GBM 6		GBM 8		GBM 9		GBM 10		GBM 13		
Region	2.2	2.4	3.2	3.1	3.4	5.2	5.1	5.5	6.2	6.3	8.1	8.4	9.2	9.1	9.5	10.1	10.5	13.2	13.1	13.4
REV	4.47	1.20	2.02	4.53	1.73	6.79	0.88	6.68	6.69	0.78	0.92	0.89	3.46	6.66	1.35	7.59	2.32	0.77	2.08	1.63
Patient	**GBM 15**			**GBM 17**			**GBM 20**			**GBM 21**		**GBM 22**			**GBM 23**			**GBM 25**		
Region	15.3	15.1	15.5	17.2	17.1	17.4	20.2	20.1	20.5	21.1	21.5	22.3	22.1	22.5	23.2	23.1	23.5	25.2	25.1	25.5
REV	6.73	3.35	0.94	5.40	5.51	1.20	6.57	5.77	5.61	2.75	2.11	4.34	4.24	2.41	4.66	1.85	0.81	7.28	8.12	1.04
Patient	**GBM 27**			**GBM 28**			**GBM 29**			**GBM 30**			**GBM 31**							
Region	27.2	27.1	27.5	28.2	28.1	28.5	29.3	29.1	29.5	30.2	30.1	30.5	31.2	31.1	31.5					
REV	0.72	4.36	0.86	6.16	0.79	0.93	6.82	5.61	0.97	8.39	7.31	0.91	8.22	7.38	1.54					

8.4 Alternative approach for differential expression analysis of miRNAs

Volcano plots generated in partek (Figure 8.2) can be used to visualise the outcome of comparing the core regions with the rim region, the core region with the invasive margin region and the rm region with the invasive margin region. These comparisons used p-values that were generated before the FDR-correction step. The miRNAs above the p-value threshold of 0.05 that showed more than 2 fold increase or decrease are seen in the far top right and the far top left quadrants of each plot, respectively. These data can be used in the future to explore the



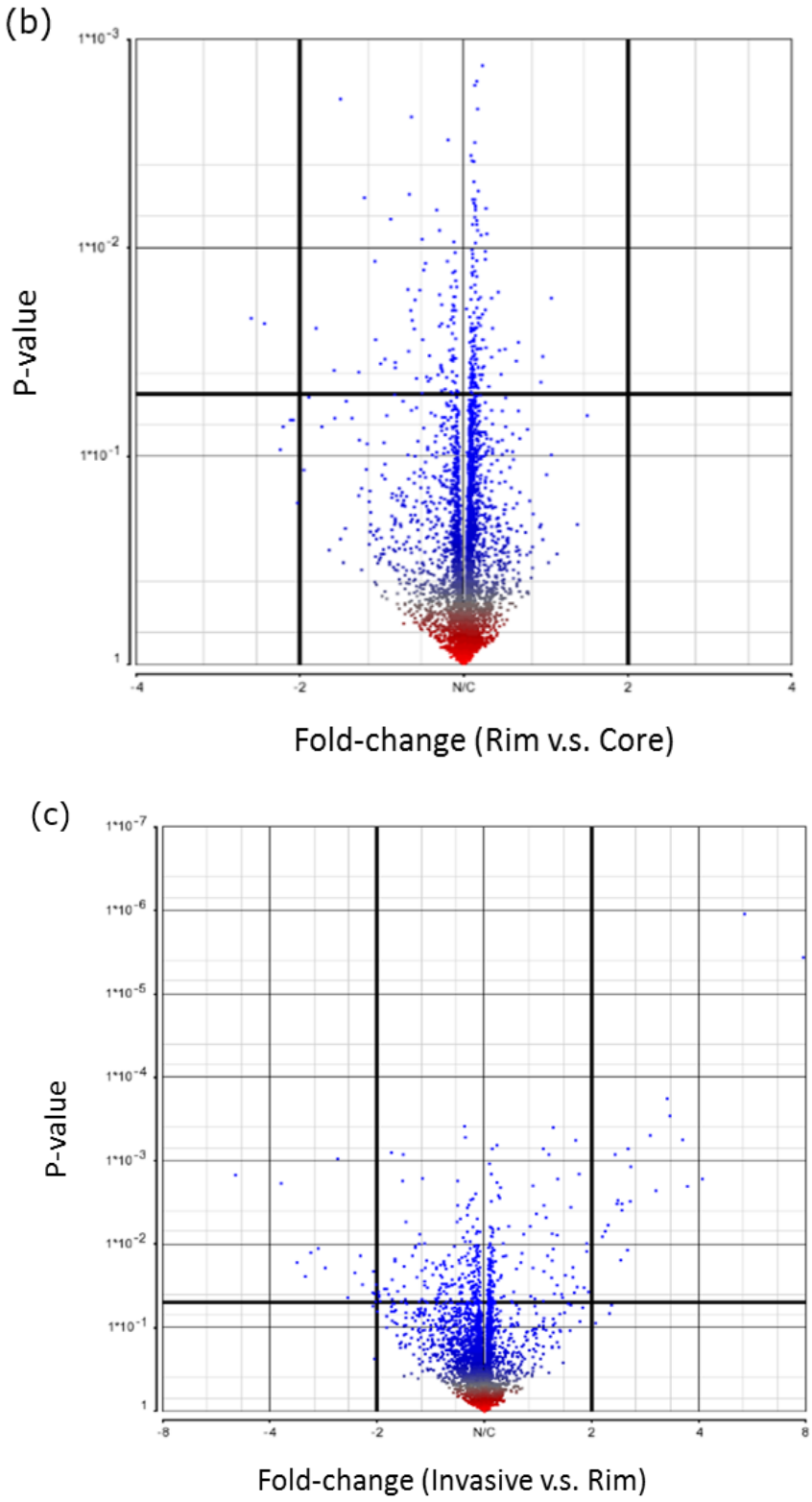


Figure 8.2: Volcano plots of miRNA expression profiles. *Thresholds indicate miRNAs with more than 2-fold change and FDR-uncorrected p-values of <0.05. Significantly upregulated or downregulated miRNAs are located in the upper-right or -left square of the plot.*

8.5 Full tissue microarray (TMA) images from 36 adult GBM patients.

Cores of 0.6mm in diameter were taken in triplicates from each FFPE blocks from different tumour regions. For some tumour regions, however, only 1-2 cores were included due to the limited tissue availability. Some tissue core were missing as a result of their position in the TMA block when the slides were sectioned. Moreover, some patients were included in the TMAs as their FFPE blocks were already used up by other projects.

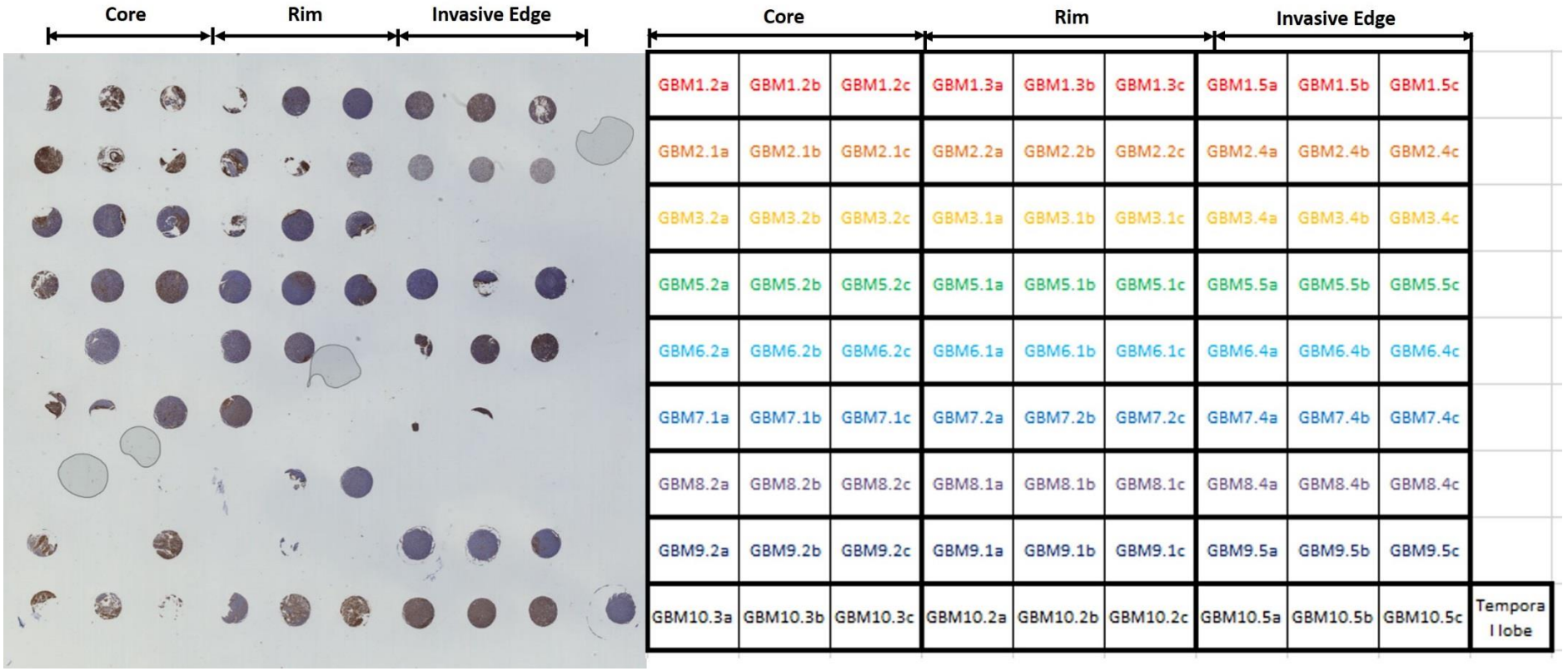


Figure 8.3: TMA containing three tumour regions from GBM patients number 1-3 and 5-10 (N=9).
A non-neoplastic brain tissue sample from the temporal lobe of an epileptic patient was included in the TMA as a normal brain control and to orientate the sample on the slide. Each tissue core of the microarray (left) has a corresponding position on the illustrative layout (right); for example, the top left tumour core in a given TMA corresponds to the top left square on its respective illustrative layout. Each row is coloured differently to represent one patient. GBM patients from which tissue were collected were given numbers following the prefix GBM. Tumour regions were given a number following patient number; for example, 4 or 5 is invasive margin. However, the

numbering is not consistent; therefore, the region is indicated above the rows. The suffixes a, b, and c following the patient number is were taken in triplicates from each region.

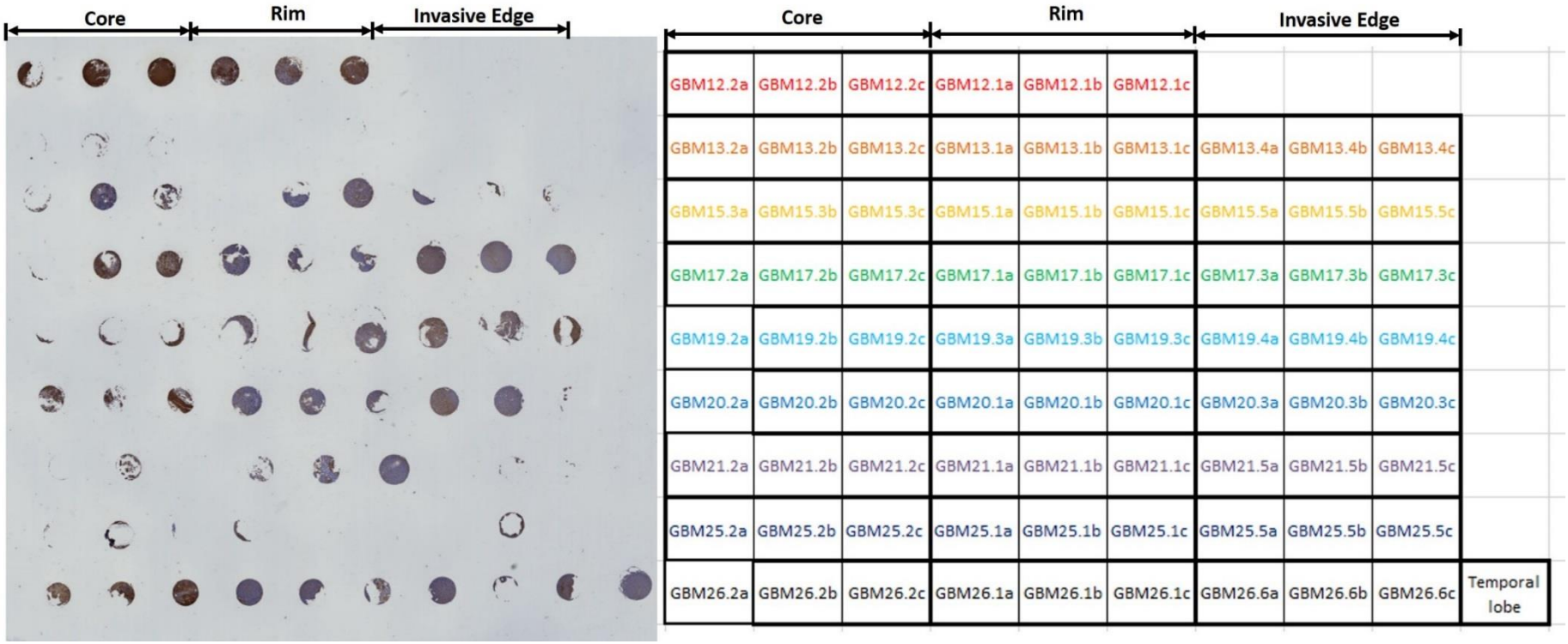
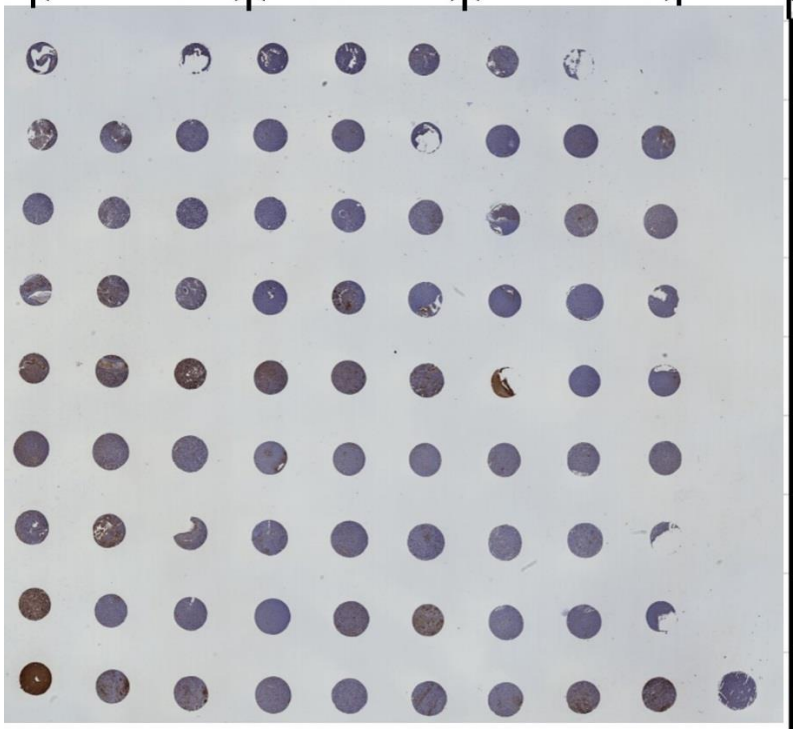


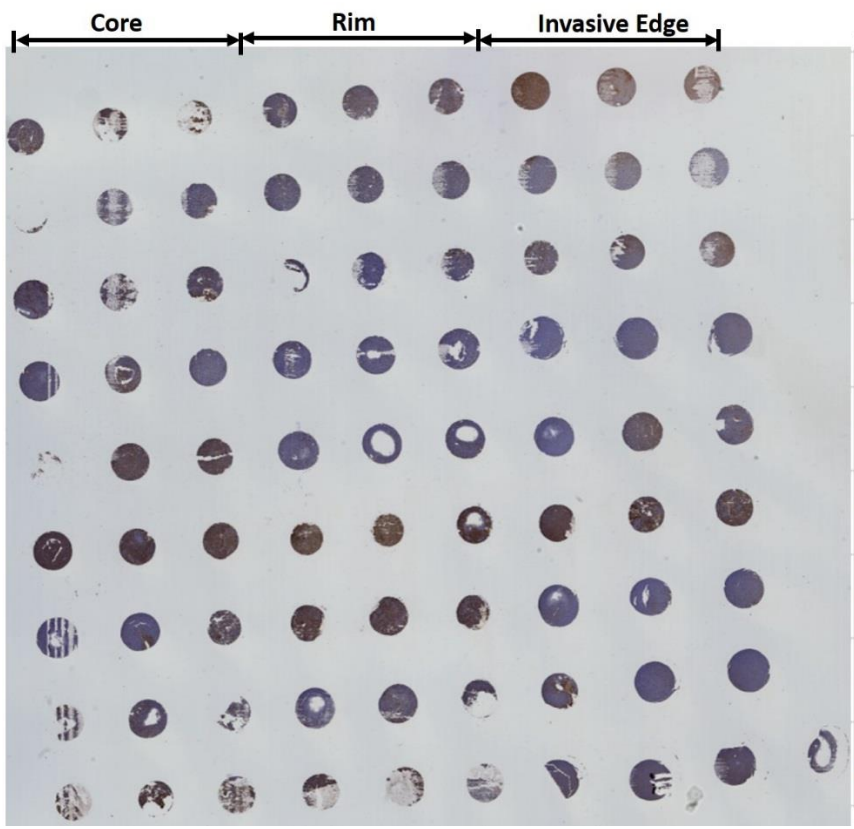
Figure 8.4: TMA containing three tumour regions from GBM patients 12, 13, 15, 17, 19, 20, 21, 25, and 26 (N=9).

For more information about how this figure is structured, please refer to Figure 8.3.



Core			Rim			Invasive Edge			
GBM27.2a	GBM27.2b	GBM27.2c	GBM27.1a	GBM27.1b	GBM27.1c	GBM27.5a	GBM27.5b	GBM27.5c	
GBM28.4a	GBM28.4b	GBM28.4c	GBM28.2a	GBM28.2b	GBM28.2c	GBM28.5a	GBM28.5b	GBM28.5c	
GBM29.3a	GBM29.3b	GBM29.3c	GBM29.2a	GBM29.2b	GBM29.2c	GBM29.5a	GBM29.5b	GBM29.5c	
GBM30.2a	GBM30.2b	GBM30.2c	GBM30.5a	GBM30.5b	GBM30.5c	GBM30.6a	GBM30.6b	GBM30.6c	
GBM31.2a	GBM31.2b	GBM31.2c	GBM31.4a	GBM31.4b	GBM31.4c	GBM31.5a	GBM31.5b	GBM31.5c	
GBM32.3a	GBM32.3b	GBM32.3c	GBM32.4a	GBM32.4b	GBM32.4c	GBM32.5a	GBM32.5b	GBM32.5c	
GBM33.2a	GBM33.2b	GBM33.2c	GBM33.3a	GBM33.3b	GBM33.3c	GBM33.5a	GBM33.5b	GBM33.5c	
GBM37.2a	GBM37.2b	GBM37.2c	GBM37.4a	GBM37.4b	GBM37.4c	GBM37.5a	GBM37.5b	GBM37.5c	
GBM38.2a	GBM38.2b	GBM38.2c	GBM38.1a	GBM38.1b	GBM38.1c	GBM38.5a	GBM38.5b	GBM38.5c	Temporal lobe

Figure 8.5: TMA of nine GBM patients 27-33, 37-38 (N=9).
For more information about how this figure is structured, please refer to Figure 8.3*.*



Core			Rim			Invasive Edge			
GBM39.3a	GBM39.3b	GBM39.3c	GBM39.1a	GBM39.1b	GBM39.1c	GBM39.5a	GBM39.5b	GBM39.5c	
GBM40.4a	GBM40.4b	GBM40.4c	GBM40.3a	GBM40.3b	GBM40.3c	GBM40.5a	GBM40.5b	GBM40.5c	
GBM41.4a	GBM41.4b	GBM41.4c	GBM41.1a	GBM41.1b	GBM41.1c	GBM41.5a	GBM41.5b	GBM41.5c	
GBM42.2a	GBM42.2b	GBM42.2c	GBM42.3a	GBM42.3b	GBM42.3c	GBM42.1a	GBM42.1b	GBM42.1c	
GBM44.2a	GBM44.2b	GBM44.2c	GBM44.4a	GBM44.4b	GBM44.4c	GBM44.5a	GBM44.5b	GBM44.5c	
GBM45.2a	GBM45.2b	GBM45.2c	GBM45.1a	GBM45.1b	GBM45.1c	GBM45.4a	GBM45.4b	GBM45.4c	
GBM46.2a	GBM46.2b	GBM46.2c	GBM46.1a	GBM46.1b	GBM46.1c	GBM46.5a	GBM46.5b	GBM46.5c	
GBM47.2a	GBM47.2b	GBM47.2c	GBM47.4a	GBM47.4b	GBM47.4c	GBM47.3a	GBM47.3b	GBM47.3c	
GBM52.4a	GBM52.4b	GBM52.4c	GBM52.1a	GBM52.1b	GBM52.1c	GBM52.2a	GBM52.2b	GBM52.2c	Temporal lobe

Figure 8.6: TMA containing three tumour regions from GBM patients 39-42, 44-47, and 52 (N=9).
For more information about how this figure is structured, please refer to Figure 8.3.

8.6 Metabolic profile of U87 cells

Data below show the MS readout for each of the six repeats per transfection condition. This illustrates that the data is comparable across experiments.

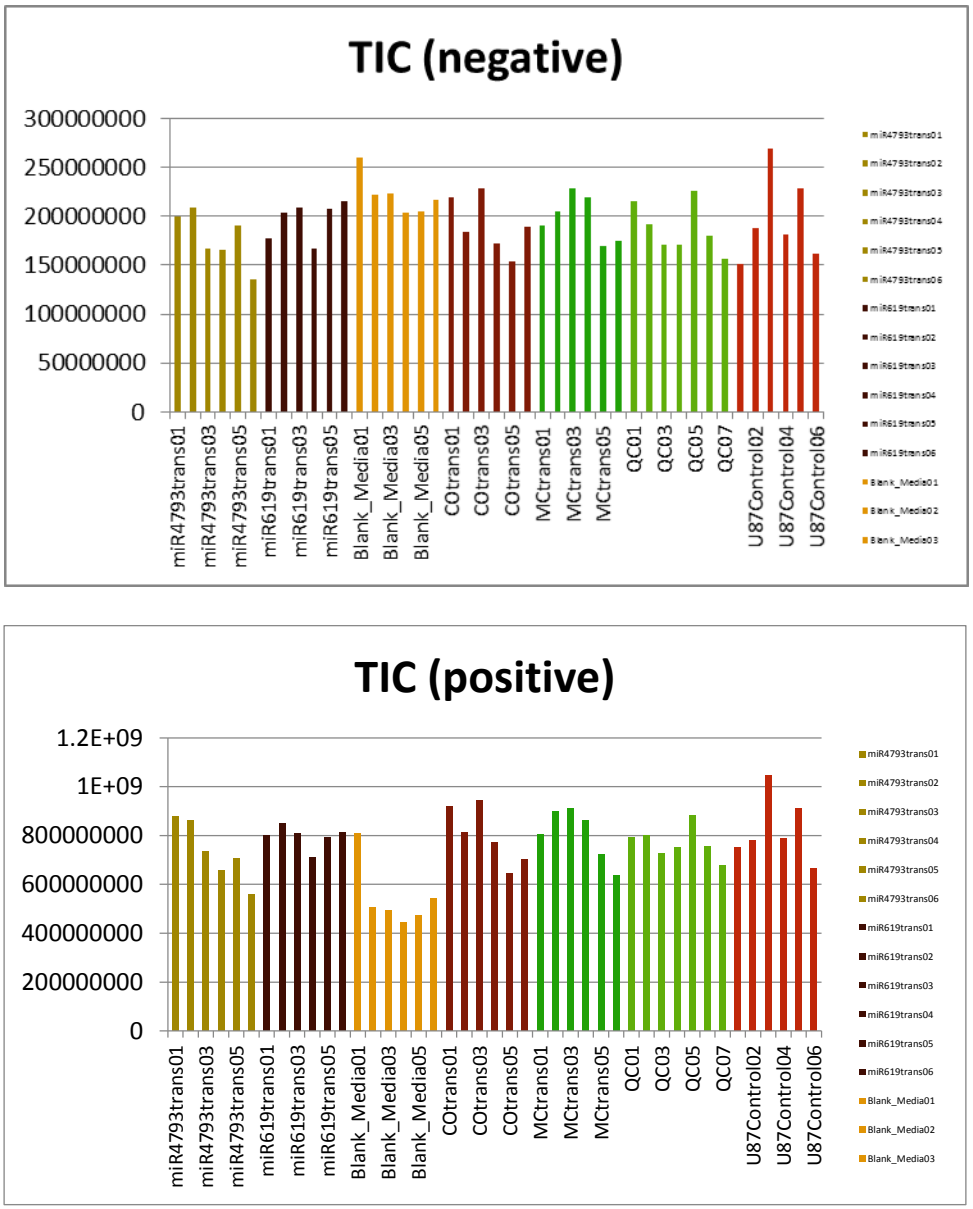


Figure 8.7: Total ion counts based on LC-MS metabolite analysis of U87 cells

Total ion counts represent positive and negative ionisation, and are displayed in top and bottom, respectively.

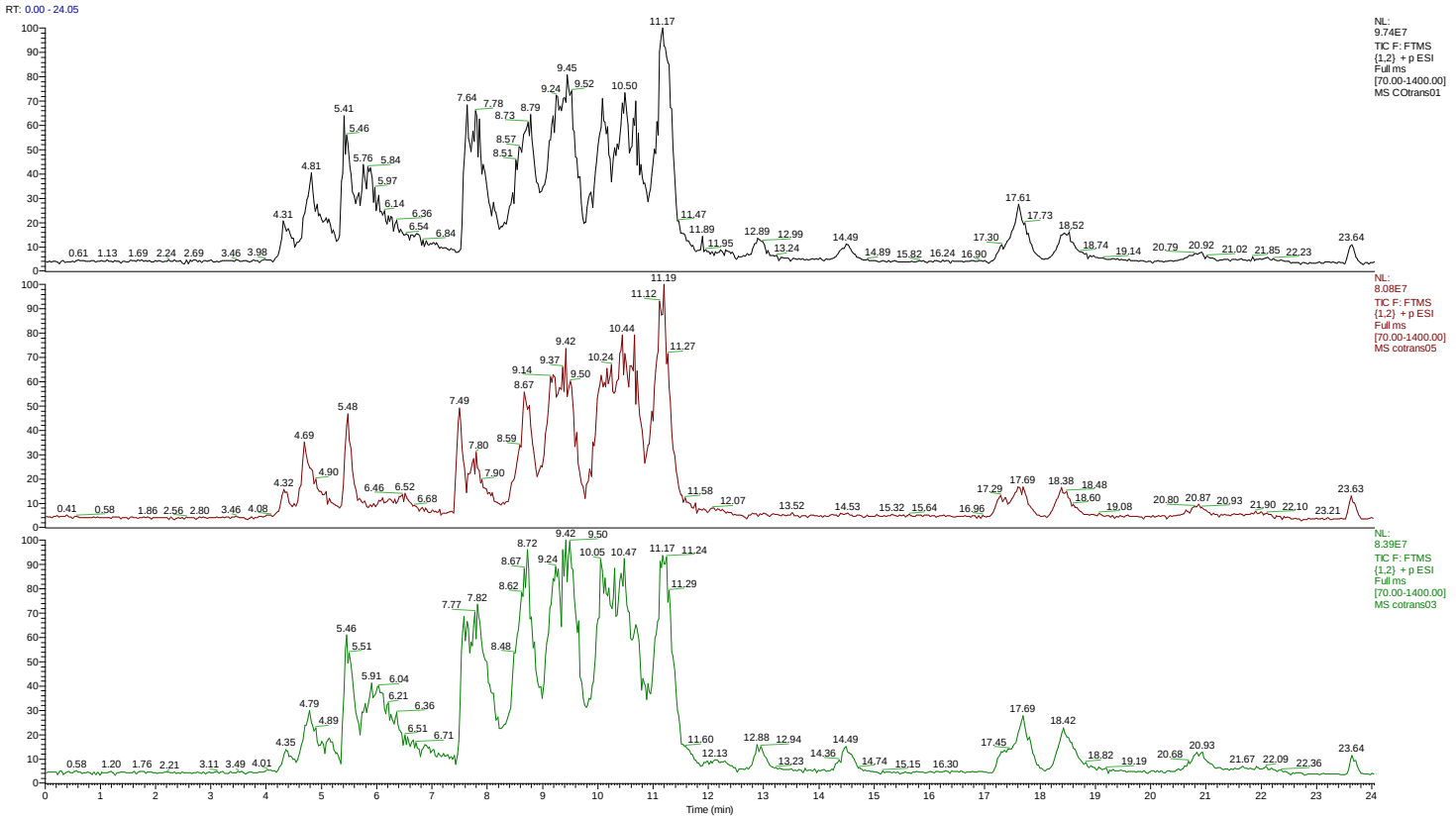


Figure 8.8: Ion chromatograms of U87 cells co-transfected with miR-619-5p and miR-4793-3p analysed by LC-MS.

Spectra in the positive ionisation modes are displayed. Two consistent biological repeats are shown on the top. One repeat, that is considered an outlier, is shown at the bottom. Maximum peak intensities are displayed at the top of each chromatogram.

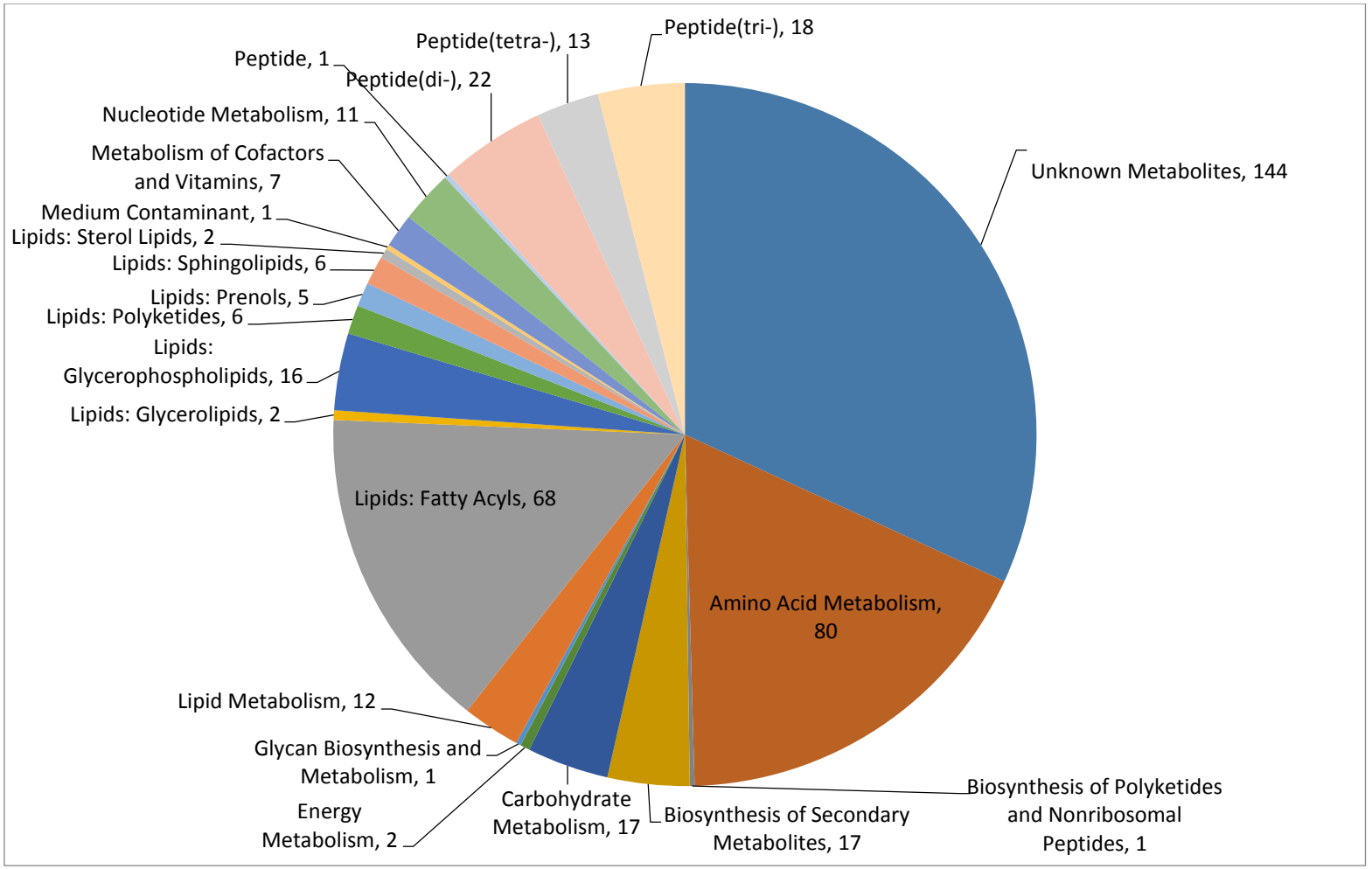


Figure 8.9: Pie Chart of Metabolites that changed abundance as a result of miR-619-5p, miR-4793-3p, and co-transfection of both miRNAs, relative to the non-targeting control.

Chapter 9: References

Abdel Hadi, L. *et al.* (2015) 'The Role and Function of Sphingolipids in Glioblastoma Multiforme', in *Bioactive Sphingolipids in Cancer Biology and Therapy*. Cham: Springer International Publishing, pp. 259–293. doi: 10.1007/978-3-319-20750-6_12.

Adeberg, S. *et al.* (2015) 'Metformin influences progression in diabetic glioblastoma patients', *Strahlentherapie und Onkologie*, 191(12), pp. 928–935. doi: 10.1007/s00066-015-0884-5.

Adekola, K. U. A. *et al.* (2015) 'Investigating and targeting chronic lymphocytic leukemia metabolism with the human immunodeficiency virus protease inhibitor ritonavir and metformin', *Leukemia & Lymphoma*, 56(2), pp. 450–459. doi: 10.3109/10428194.2014.922180.

Afshordel, S. *et al.* (2015) 'Lovastatin and perillyl alcohol inhibit glioma cell invasion, migration, and proliferation – Impact of Ras-/Rho-prenylation', *Pharmacological Research*, 91, pp. 69–77. doi: 10.1016/j.phrs.2014.11.006.

Agarwal, V. *et al.* (2015) 'Predicting effective microRNA target sites in mammalian mRNAs.', *eLife*. eLife Sciences Publications, Ltd, 4. doi: 10.7554/eLife.05005.

Agius, L., Meredith, E. J. and Sherratt, H. S. (1991) 'Stereospecificity of the inhibition by etomoxir of fatty acid and cholesterol synthesis in isolated rat hepatocytes.', *Biochemical pharmacology*, 42(9), pp. 1717–20. Available at: http://www.ncbi.nlm.nih.gov/pubmed/1930298 (Accessed: 30 March

2019).

Ahluwalia, M. S. *et al.* (2011) 'Phase II trial of ritonavir/lopinavir in patients with progressive or recurrent high-grade gliomas', *Journal of Neuro-Oncology*, 102(2), pp. 317–321. doi: 10.1007/s11060-010-0325-3.

Ahmad, I. M. *et al.* (2005) 'Mitochondrial O2*- and H2O2 mediate glucose deprivation-induced stress in human cancer cells.', *The Journal of biological chemistry*, 280(6), pp. 4254–63. doi: 10.1074/jbc.M411662200.

Akiyama, Y. *et al.* (2001) 'Hyaluronate receptors mediating glioma cell migration and proliferation.', *Journal of neuro-oncology*, 53(2), pp. 115–27. Available at: http://www.ncbi.nlm.nih.gov/pubmed/11716065 (Accessed: 13 May 2019).

Allard, E., Passirani, C. and Benoit, J.-P. (2009) 'Convection-enhanced delivery of nanocarriers for the treatment of brain tumors.', *Biomaterials*, 30(12), pp. 2302–18. doi: 10.1016/j.biomaterials.2009.01.003.

Allen, M. *et al.* (2016) 'Origin of the U87MG glioma cell line: Good news and bad news.', *Science translational medicine*. American Association for the Advancement of Science, 8(354), p. 354re3. doi: 10.1126/scitranslmed.aaf6853.

Altieri, R. *et al.* (2015) 'Glioma Surgery: Technological Advances to Achieve a Maximal Safe Resection.', *Surgical technology international*, 27, pp. 297–302. Available at: http://www.ncbi.nlm.nih.gov/pubmed/26680413 (Accessed: 20 July 2019).

Altman, B. J. and Dang, C. V (2012) 'Normal and cancer cell metabolism: lymphocytes and lymphoma.', *The FEBS journal*, 279(15), pp. 2598–609. doi: 10.1111/j.1742-4658.2012.08651.x.

Altwairgi, A. K. *et al.* (2016) 'Phase II study of atorvastatin in combination with radiotherapy and temozolomide In patients with glioblastoma (ART): interim analysis report', *Annals of Oncology*. Narnia, 27(suppl_6). doi: 10.1093/annonc/mdw367.32.

Ambros, V. *et al.* (2003) 'A uniform system for microRNA annotation.', *RNA (New York, N.Y.)*, 9(3), pp. 277–9. Available at: http://www.ncbi.nlm.nih.gov/pubmed/12592000 (Accessed: 7 June 2016).

An, L. *et al.* (2013) 'microRNA-124 inhibits migration and invasion by down-regulating ROCK1 in glioma.', *PloS one*. United States, 8(7), p. e69478. doi: 10.1371/journal.pone.0069478.

Ananta, J. S., Paulmurugan, R. and Massoud, T. F. (2015) 'Nanoparticle-Delivered Antisense MicroRNA-21 Enhances the Effects of Temozolomide on Glioblastoma Cells.', *Molecular pharmaceutics*. American Chemical Society, 12(12), pp. 4509–17. doi: 10.1021/acs.molpharmaceut.5b00694.

Ando, T. *et al.* (2011) 'Precise comparison of protoporphyrin IX fluorescence spectra with pathological results for brain tumor tissue identification.', *Brain tumor pathology*. Japan, 28(1), pp. 43–51. doi: 10.1007/s10014-010-0002-4.

Asano, K. *et al.* (2004) 'Correlation of N-cadherin expression in high grade

gliomas with tissue invasion.', *Journal of neuro-oncology*, 70(1), pp. 3–15. Available at: http://www.ncbi.nlm.nih.gov/pubmed/15527101 (Accessed: 12 May 2019).

Ashrafian, H., Horowitz, J. D. and Frenneaux, M. P. (2007) 'Perhexiline', *Cardiovascular Drug Reviews*. John Wiley & Sons, Ltd (10.1111), 25(1), pp. 76–97. doi: 10.1111/j.1527-3466.2007.00006.x.

Asuthkar, S. *et al.* (2012) 'Epigenetic regulation of miRNA-211 by MMP-9 governs glioma cell apoptosis, chemosensitivity and radiosensitivity.', *Oncotarget*. United States, 3(11), pp. 1439–1454.

Azzalin, A. *et al.* (2017) 'Inhibitors of GLUT/SLC2A Enhance the Action of BCNU and Temozolomide against High-Grade Gliomas.', *Neoplasia (New York, N.Y.)*. Neoplasia Press, 19(4), pp. 364–373. doi: 10.1016/j.neo.2017.02.009.

Babic, I. *et al.* (2013) 'EGFR mutation-induced alternative splicing of Max contributes to growth of glycolytic tumors in brain cancer.', *Cell metabolism*, 17(6), pp. 1000–8. doi: 10.1016/j.cmet.2013.04.013.

Bader, A. G., Brown, D. and Winkler, M. (2010) 'The promise of microRNA replacement therapy.', *Cancer research*, 70(18), pp. 7027–30. doi: 10.1158/0008-5472.CAN-10-2010.

Badur, M. G. *et al.* (2018) 'Oncogenic R132 IDH1 Mutations Limit NADPH for De Novo Lipogenesis through (D)2-Hydroxyglutarate Production in Fibrosarcoma Cells', *Cell Reports*. Cell Press, 25(4), pp. 1018-1026.e4. doi:

10.1016/J.CELREP.2018.09.074.

Bailey, J. M. *et al.* (1972) 'Control of lipid metabolism in cultured cells.', *Lipids*, 7(2), pp. 125–34. Available at: http://www.ncbi.nlm.nih.gov/pubmed/5066948 (Accessed: 30 March 2019).

Bajad, S. U. *et al.* (2006) 'Separation and quantitation of water soluble cellular metabolites by hydrophilic interaction chromatography-tandem mass spectrometry', *Journal of Chromatography A*, 1125(1), pp. 76–88. doi: 10.1016/j.chroma.2006.05.019.

Ballestrem, C. *et al.* (2001) 'Marching at the front and dragging behind', *The Journal of Cell Biology*, 155(7), pp. 1319–1332. doi: 10.1083/jcb.200107107.

Barbosa, A. D. *et al.* (2015) 'Lipid partitioning at the nuclear envelope controls membrane biogenesis', *Molecular biology of the cell*. Am Soc Cell Biol, 26(20), pp. 3641–3657.

Barbosa, A. D. and Siniossoglou, S. (2017) 'Function of lipid droplet-organelle interactions in lipid homeostasis', *Biochimica et Biophysica Acta (BBA) - Molecular Cell Research*. Elsevier, 1864(9), pp. 1459–1468. doi: 10.1016/J.BBAMCR.2017.04.001.

Barcelo-Coblijn, G. *et al.* (2011) 'Sphingomyelin and sphingomyelin synthase (SMS) in the malignant transformation of glioma cells and in 2-hydroxyoleic acid therapy', *Proceedings of the National Academy of*

Sciences, 108(49), pp. 19569–19574. doi: 10.1073/pnas.1115484108.

Bardella, C. *et al.* (2016) 'Expression of Idh1R132H in the Murine Subventricular Zone Stem Cell Niche Recapitulates Features of Early Gliomagenesis', *Cancer Cell*, 30(4), pp. 578–594. doi: 10.1016/j.ccell.2016.08.017.

Bartel, D. P. (2009) 'MicroRNAs: target recognition and regulatory functions.', *Cell*. NIH Public Access, 136(2), pp. 215–33. doi: 10.1016/j.cell.2009.01.002.

Barth, R. F. and Kaur, B. (2009) 'Rat brain tumor models in experimental neuro-oncology: the C6, 9L, T9, RG2, F98, BT4C, RT-2 and CNS-1 gliomas', *Journal of Neuro-Oncology*, 94(3), pp. 299–312. doi: 10.1007/s11060-009-9875-7.

Beauchesne, P. (2011) 'Extra-Neural Metastases of Malignant Gliomas: Myth or Reality?', *Cancers*, 3(1), pp. 461–477. doi: 10.3390/cancers3010461.

Beckner, M. E. *et al.* (2009) 'Identification of ATP citrate lyase as a positive regulator of glycolytic function in glioblastomas', *International Journal of Cancer*, 126(10), p. NA-NA. doi: 10.1002/ijc.24918.

Bell, C. D. and Waizbard, E. (1986) 'Variability of cell size in primary and metastatic human breast carcinoma.', *Invasion & metastasis*, 6(1), pp. 11–20. Available at: http://www.ncbi.nlm.nih.gov/pubmed/3941026 (Accessed: 22 July 2019).

Bellail, A. C. *et al.* (2004) 'Microregional extracellular matrix heterogeneity in brain modulates glioma cell invasion', *The International Journal of Biochemistry & Cell Biology*. Pergamon, 36(6), pp. 1046–1069. doi: 10.1016/J.BIOCEL.2004.01.013.

Bensaad, K. *et al.* (2014) 'Fatty acid uptake and lipid storage induced by HIF-1α contribute to cell growth and survival after hypoxia-reoxygenation', *Cell reports*. Elsevier, 9(1), pp. 349–365.

Berens, M. E. and Giese, A. (1999) '"...those left behind." Biology and oncology of invasive glioma cells.', *Neoplasia (New York, N.Y.)*. Neoplasia Press, 1(3), pp. 208–19. Available at: http://www.ncbi.nlm.nih.gov/pubmed/10935475 (Accessed: 6 August 2016).

Bernard-Arnoux, F. *et al.* (2016) 'The cost-effectiveness of tumor-treating fields therapy in patients with newly diagnosed glioblastoma.', *Neuro-oncology*, 18(8), pp. 1129–36. doi: 10.1093/neuonc/now102.

Bernstein, J. J. and Woodard, C. A. (1995) 'Glioblastoma Cells Do Not Intravasate into Blood Vessels', *Neurosurgery*, 36(1), pp. 124–132. doi: 10.1227/00006123-199501000-00016.

Bessman, S. P. and Fonyo, A. (1966) 'The possible role of the mitochondrial bound creatine kinase in regulation of mitochondrial respiration.', *Biochemical and biophysical research communications*, 22(5), pp. 597–602. Available at: http://www.ncbi.nlm.nih.gov/pubmed/5911090 (Accessed:

27 January 2019).

Beutler, A. S. *et al.* (1999) 'Tumor Gene Therapy Made Easy: Allogeneic Major Histocompatibility Complex in the C6 Rat Glioma Model', *Human Gene Therapy*, 10(1), pp. 95–101. doi: 10.1089/10430349950019228.

Bhavsar, S. *et al.* (2016) 'Preoperative statin use is not associated with improvement in survival after glioblastoma surgery', *Journal of Clinical Neuroscience*. Churchill Livingstone, 31, pp. 176–180. doi: 10.1016/J.JOCN.2016.03.010.

Bhutia, Y. D. *et al.* (2015) 'Amino Acid Transporters in Cancer and Their Relevance to "Glutamine Addiction": Novel Targets for the Design of a New Class of Anticancer Drugs', *Cancer Research*, 75(9), pp. 1782–1788. doi: 10.1158/0008-5472.CAN-14-3745.

Bi, H.-C. *et al.* (2014) 'N-methylnicotinamide and nicotinamide N-methyltransferase are associated with microRNA-1291-altered pancreatic carcinoma cell metabolome and suppressed tumorigenesis.', *Carcinogenesis*. Oxford University Press, 35(10), pp. 2264–72. doi: 10.1093/carcin/bgu174.

Bickel, P. E., Tansey, J. T. and Welte, M. A. (2009) 'PAT proteins, an ancient family of lipid droplet proteins that regulate cellular lipid stores', *Biochimica et Biophysica Acta (BBA)-Molecular and Cell Biology of Lipids*. Elsevier, 1791(6), pp. 419–440.

Bidros, D. S., Liu, J. K. and Vogelbaum, M. A. (2010) 'Future of convection-

enhanced delivery in the treatment of brain tumors.', *Future oncology (London, England)*, 6(1), pp. 117–25. doi: 10.2217/fon.09.135.

Bina, M. (2008) 'The Genome Browser at UCSC for Locating Genes, and Much More!', *Molecular Biotechnology*, 38(3), pp. 269–275. doi: 10.1007/s12033-007-9019-2.

Birsoy, K., Sabatini, D. M. and Possemato, R. (2012) 'Untuning the tumor metabolic machine: Targeting cancer metabolism: a bedside lesson', *Nature Medicine*, 18(7), pp. 1022–1023. doi: 10.1038/nm.2870.

Black, K. L. and Ningaraj, N. S. 'Modulation of brain tumor capillaries for enhanced drug delivery selectively to brain tumor.', *Cancer control : journal of the Moffitt Cancer Center*, 11(3), pp. 165–73. Available at: http://www.ncbi.nlm.nih.gov/pubmed/15153840 (Accessed: 30 May 2016).

Blanchoin, L. *et al.* (2000) 'Direct observation of dendritic actin filament networks nucleated by Arp2/3 complex and WASP/Scar proteins', *Nature*, 404(6781), pp. 1007–1011. doi: 10.1038/35010008.

Bo, L.-J. *et al.* (2015) 'Bioinformatics analysis of miRNA expression profile between primary and recurrent glioblastoma.', *European review for medical and pharmacological sciences*, 19(19), pp. 3579–86. Available at: http://www.ncbi.nlm.nih.gov/pubmed/26502847 (Accessed: 6 August 2016).

Boado, R. J., Black, K. L. and Pardridge, W. M. (1994) 'Gene expression of GLUT3 and GLUT1 glucose transporters in human brain tumors.', *Brain*

research. Molecular brain research, 27(1), pp. 51–7. Available at: http://www.ncbi.nlm.nih.gov/pubmed/7877454 (Accessed: 3 April 2016).

Boele, J. *et al.* (2014) 'PAPD5-mediated 3' adenylation and subsequent degradation of miR-21 is disrupted in proliferative disease.', *Proceedings of the National Academy of Sciences of the United States of America*, 111(31), pp. 11467–72. doi: 10.1073/pnas.1317751111.

Bolstad, B. M. *et al.* (2003) 'A comparison of normalization methods for high density oligonucleotide array data based on variance and bias', *Bioinformatics*, 19(2), pp. 185–193. doi: 10.1093/bioinformatics/19.2.185.

Bonnefont, J.-P. *et al.* (2004) 'Carnitine palmitoyltransferases 1 and 2: biochemical, molecular and medical aspects', *Molecular Aspects of Medicine*. Pergamon, 25(5–6), pp. 495–520. doi: 10.1016/J.MAM.2004.06.004.

Bonnin, D. A. A. *et al.* (2019) 'Characterizing the heterogeneity in 5-aminolevulinic acid–induced fluorescence in glioblastoma', *Journal of Neurosurgery JNS*. American Association of Neurological Surgeons.

Bonora, M. and Pinton, P. (2014) 'The mitochondrial permeability transition pore and cancer: molecular mechanisms involved in cell death.', *Frontiers in oncology*. Frontiers Media SA, 4, p. 302. doi: 10.3389/fonc.2014.00302.

Boren, J. and Brindle, K. M. (2012) 'Apoptosis-induced mitochondrial dysfunction causes cytoplasmic lipid droplet formation.', *Cell death and differentiation*. England, 19(9), pp. 1561–1570. doi: 10.1038/cdd.2012.34.

Boros, L. G. *et al.* (2000) 'Transforming growth factor beta2 promotes

glucose carbon incorporation into nucleic acid ribose through the nonoxidative pentose cycle in lung epithelial carcinoma cells.', *Cancer research*, 60(5), pp. 1183–5. Available at: http://www.ncbi.nlm.nih.gov/pubmed/10728670 (Accessed: 23 July 2019).

Bowen, B. C. (2003) 'Glial neoplasms without elevated choline-creatine ratios.', *AJNR. American journal of neuroradiology*. American Journal of Neuroradiology, 24(5), pp. 782–4. Available at: http://www.ncbi.nlm.nih.gov/pubmed/12748070 (Accessed: 16 January 2019).

Boyden, S. (1962) 'The chemotactic effect of mixtures of antibody and antigen on polymorphonuclear leucocytes.', *The Journal of experimental medicine*, 115, pp. 453–66. Available at: http://www.ncbi.nlm.nih.gov/pubmed/13872176 (Accessed: 30 March 2019).

Bralten, L. B. *et al.* (2011) 'Absence of common somatic alterations in genes on 1p and 19q in oligodendrogliomas.', *PloS one*. United States, 6(7), p. e22000. doi: 10.1371/journal.pone.0022000.

Brasaemle, D. L. *et al.* (2004) 'Proteomic analysis of proteins associated with lipid droplets of basal and lipolytically stimulated 3T3-L1 adipocytes', *Journal of Biological Chemistry*. ASBMB, 279(45), pp. 46835–46842.

Brasaemle, D. L. (2007) 'The perilipin family of structural lipid droplet proteins: stabilization of lipid droplets and control of lipolysis', *Journal of*

lipid research. ASBMB, 48(12), pp. 2547–2559.

Breda, J. *et al.* (2015) 'Quantifying the strength of miRNA–target interactions', *Methods*. Academic Press, 85, pp. 90–99. doi: 10.1016/J.YMETH.2015.04.012.

Brekken, R. A. and Sage, E. H. (2001) 'SPARC, a matricellular protein: at the crossroads of cell-matrix communication.', *Matrix biology : journal of the International Society for Matrix Biology*, 19(8), pp. 816–27. Available at: http://www.ncbi.nlm.nih.gov/pubmed/11223341 (Accessed: 23 July 2019).

Brennan, C. W. *et al.* (2013) 'The somatic genomic landscape of glioblastoma.', *Cell*, 155(2), pp. 462–77. Available at: http://www.sciencedirect.com/science/article/pii/S0092867413012087 (Accessed: 26 January 2016).

Bretscher, M. S. (1996) 'Getting membrane flow and the cytoskeleton to cooperate in moving cells.', *Cell*, 87(4), pp. 601–6. doi: 10.1016/s0092-8674(00)81380-x.

Britton, C. H. *et al.* (1995) 'Human liver mitochondrial carnitine palmitoyltransferase I: characterization of its cDNA and chromosomal localization and partial analysis of the gene.', *Proceedings of the National Academy of Sciences of the United States of America*. National Academy of Sciences, 92(6), pp. 1984–8. doi: 10.1073/PNAS.92.6.1984.

Brodbelt, A. *et al.* (2015) 'Glioblastoma in England: 2007-2011.', *European*

journal of cancer (Oxford, England : 1990), 51(4), pp. 533–42. doi: 10.1016/j.ejca.2014.12.014.

Brösicke, N. *et al.* (2013) 'Tenascin-C is expressed by human glioma in vivo and shows a strong association with tumor blood vessels', *Cell and Tissue Research*, 354(2), pp. 409–430. doi: 10.1007/s00441-013-1704-9.

Brown, D. V. *et al.* (2015) 'Coexpression analysis of CD133 and CD44 identifies Proneural and Mesenchymal subtypes of glioblastoma multiforme', *Oncotarget*, 6(8), pp. 6267–80. doi: 10.18632/oncotarget.3365.

Brown, D. V *et al.* (2017) 'Expression of CD133 and CD44 in glioblastoma stem cells correlates with cell proliferation, phenotype stability and intra-tumor heterogeneity.', *PloS one*. Public Library of Science, 12(2), p. e0172791. doi: 10.1371/journal.pone.0172791.

Brown, M. C. *et al.* (2008) 'Regulatory effect of nerve growth factor in α9β1 integrin–dependent progression of glioblastoma', *Neuro-Oncology*. Narnia, 10(6), pp. 968–980. doi: 10.1215/15228517-2008-0047.

Brown, M. and Goldstein, J. (1986) 'A receptor-mediated pathway for cholesterol homeostasis', *Science*, 232(4746), pp. 34–47. doi: 10.1126/science.3513311.

Brown, M. S. and Goldstein, J. L. (1999) 'A proteolytic pathway that controls the cholesterol content of membranes, cells, and blood.', *Proceedings of the National Academy of Sciences of the United States of America*. National Academy of Sciences, 96(20), pp. 11041–8. doi:

10.1073/pnas.96.20.11041.

Burns-Cox, C. J. *et al.* (1971) 'Clinical evaluation of perhexiline maleate in patients with angina pectoris.', *British medical journal*. British Medical Journal Publishing Group, 4(5787), pp. 586–8. doi: 10.1136/BMJ.4.5787.586.

Burrell, R. A. and Swanton, C. (2014) 'Tumour heterogeneity and the evolution of polyclonal drug resistance.', *Molecular oncology*, 8(6), pp. 1095–111. doi: 10.1016/j.molonc.2014.06.005.

Cahill, D. P. *et al.* (1999) 'Genetic instability and darwinian selection in tumours', *Trends in Genetics*, 15(12), pp. M57–M60. doi: 10.1016/S0168-9525(99)01874-0.

Cai, J. *et al.* (2015) 'MicroRNA-542-3p Suppresses Tumor Cell Invasion via Targeting AKT Pathway in Human Astrocytoma.', *The Journal of biological chemistry*, 290(41), pp. 24678–88. Available at: http://www.jbc.org/content/early/2015/08/18/jbc.M115.649004 (Accessed: 27 March 2016).

Cai, J., Yang, J. and Jones, D. (1998) 'Mitochondrial control of apoptosis: the role of cytochrome c', *Biochimica et Biophysica Acta (BBA) - Bioenergetics*, 1366(1–2), pp. 139–149. doi: 10.1016/S0005-2728(98)00109-1.

Camand, E. *et al.* (2011) 'N-cadherin expression level modulates integrin-mediated polarity and strongly impacts on the speed and directionality of

glial cell migration', *Journal of Cell Science*, 125, pp. 1–14. doi: 10.1242/jcs.087668.

Cancer Genome Atlas Research Network (2008) 'Comprehensive genomic characterization defines human glioblastoma genes and core pathways.', *Nature*, 455(7216), pp. 1061–8. doi: 10.1038/nature07385.

Capper, D. *et al.* (2018) 'DNA methylation-based classification of central nervous system tumours.', *Nature*. NIH Public Access, 555(7697), pp. 469–474. doi: 10.1038/nature26000.

Carracedo, A., Cantley, L. C. and Pandolfi, P. P. (2013) 'Cancer metabolism: fatty acid oxidation in the limelight.', *Nature reviews. Cancer*. NIH Public Access, 13(4), pp. 227–32. doi: 10.1038/nrc3483.

Carracedo, A. and Pandolfi, P. P. (2008) 'The PTEN-PI3K pathway: of feedbacks and cross-talks.', *Oncogene*. Macmillan Publishers Limited, 27(41), pp. 5527–41. Available at: http://dx.doi.org/10.1038/onc.2008.247 (Accessed: 15 March 2016).

Carragher, N. O. *et al.* (1999) 'Degraded Collagen Fragments Promote Rapid Disassembly of Smooth Muscle Focal Adhesions That Correlates with Cleavage of Pp125 ^{FAK} , Paxillin, and Talin', *The Journal of Cell Biology*, 147(3), pp. 619–630. doi: 10.1083/jcb.147.3.619.

Cascante, M. *et al.* (2000) 'Role of Thiamin (Vitamin B-1) and Transketolase in Tumor Cell Proliferation', *Nutrition and Cancer*, 36(2), pp. 150–154. doi: 10.1207/S15327914NC3602_2.

Castellano, E. and Downward, J. (2011) 'RAS Interaction with PI3K: More Than Just Another Effector Pathway.', *Genes & cancer*, 2(3), pp. 261–74. Available at: http://www.pubmedcentral.nih.gov/articlerender.fcgi?artid=3128635&tool=pmcentrez&rendertype=abstract (Accessed: 2 September 2014).

Castillo, M. (2013) 'Adult Brain Tumors: Clinical Applications of Magnetic Resonance Spectroscopy', *Neuroimaging Clinics of North America*. Elsevier, 23(3), pp. 527–555. doi: 10.1016/J.NIC.2013.03.002.

Cayre, M., Canoll, P. and Goldman, J. E. (2009) 'Cell migration in the normal and pathological postnatal mammalian brain', *Progress in Neurobiology*, 88(1), pp. 41–63. doi: 10.1016/j.pneurobio.2009.02.001.

Chakrabarti, I. *et al.* (2005) 'A population-based description of glioblastoma multiforme in Los Angeles County, 1974-1999.', *Cancer*, 104(12), pp. 2798–806. Available at: http://www.ncbi.nlm.nih.gov/pubmed/16288487 (Accessed: 5 March 2016).

Chan, J. A., Krichevsky, A. M. and Kosik, K. S. (2005) 'MicroRNA-21 is an antiapoptotic factor in human glioblastoma cells.', *Cancer research*. United States, 65(14), pp. 6029–6033. doi: 10.1158/0008-5472.CAN-05-0137.

Chang, L. *et al.* (2015) 'MicroRNA-133b inhibits cell migration and invasion by targeting matrix metalloproteinase 14 in glioblastoma', *Oncology Letters*. Spandidos Publications, 10(5), pp. 2781–2786.

Charles, N. A. *et al.* (2011) 'The brain tumor microenvironment.', *Glia*, 59(8), pp. 1169–80. doi: 10.1002/glia.21136.

Chemello, F. *et al.* (2018) 'Lipid utilization in skeletal muscle cells is modulated in vitro and in vivo by specific miRNAs', *bioRxiv*. Cold Spring Harbor Laboratory, p. 288035. doi: 10.1101/288035.

Chen, L.-P. *et al.* (2018) 'miR-103/miR-195/miR-15b Regulate SALL4 and Inhibit Proliferation and Migration in Glioma', *Molecules*. Multidisciplinary Digital Publishing Institute, 23(11), p. 2938. doi: 10.3390/molecules23112938.

Chen, L. *et al.* (2012) 'MiR-410 regulates MET to influence the proliferation and invasion of glioma.', *The international journal of biochemistry & cell biology*, 44(11), pp. 1711–7. Available at: http://www.sciencedirect.com/science/article/pii/S1357272512002269 (Accessed: 19 March 2016).

Chen, L., Hou, J. and Liu., L. (2015) 'High-Throughput Techniques for Identifying microRNA Target Genes', *Current Bioinformatics*, 10(4), pp. 370–376.

Chen, M., Zhang, J. and Manley, J. L. (2010) 'Turning on a fuel switch of cancer: hnRNP proteins regulate alternative splicing of pyruvate kinase mRNA.', *Cancer research*, 70(22), pp. 8977–80. doi: 10.1158/0008-5472.CAN-10-2513.

Chendrimada, T. P. *et al.* (2005) 'TRBP recruits the Dicer complex to Ago2

for microRNA processing and gene silencing', *Nature*, 436(7051), pp. 740–744. doi: 10.1038/nature03868.

Cheng, C.-S., Wang, Z. and Chen, J. (2014) 'Targeting FASN in Breast Cancer and the Discovery of Promising Inhibitors from Natural Products Derived from Traditional Chinese Medicine.', *Evidence-based complementary and alternative medicine : eCAM*. Hindawi, 2014, p. 232946. doi: 10.1155/2014/232946.

Cheng, T. *et al.* (2011) 'Pyruvate carboxylase is required for glutamine-independent growth of tumor cells', *Proceedings of the National Academy of Sciences*, 108(21), pp. 8674–8679. doi: 10.1073/pnas.1016627108.

Cheng, Z. *et al.* (2015) 'MicroRNA-184 inhibits cell proliferation and invasion, and specifically targets TNFAIP2 in Glioma.', *Journal of experimental & clinical cancer research : CR*, 34, p. 27. Available at: http://www.pubmedcentral.nih.gov/articlerender.fcgi?artid=4387599&tool=pmcentrez&rendertype=abstract (Accessed: 10 May 2016).

Cheung, K. J. *et al.* (2016) 'Polyclonal breast cancer metastases arise from collective dissemination of keratin 14-expressing tumor cell clusters.', *Proceedings of the National Academy of Sciences of the United States of America*. National Academy of Sciences, 113(7), pp. E854-63. doi: 10.1073/pnas.1508541113.

Chi, S. W. *et al.* (2009) 'Argonaute HITS-CLIP decodes microRNA–mRNA interaction maps', *Nature*, 460(7254), pp. 479–486. doi:

10.1038/nature08170.

Chintala, S. K. *et al.* (1996) 'Immunohistochemical localization of extracellular matrix proteins in human glioma, both in vivo and in vitro.', *Cancer letters*, 101(1), pp. 107–14. Available at: http://www.ncbi.nlm.nih.gov/pubmed/8625273 (Accessed: 30 March 2019).

Choe, G. *et al.* (2002) 'Active matrix metalloproteinase 9 expression is associated with primary glioblastoma subtype.', *Clinical cancer research : an official journal of the American Association for Cancer Research*, 8(9), pp. 2894–901. Available at: http://www.ncbi.nlm.nih.gov/pubmed/12231534 (Accessed: 12 May 2019).

Chonan, Y. *et al.* (2017) 'Endothelium-induced three-dimensional invasion of heterogeneous glioma initiating cells in a microfluidic coculture platform', *Integrative Biology*, 9(9), pp. 762–773. doi: 10.1039/C7IB00091J.

Christofk, H. R. *et al.* (2008a) 'The M2 splice isoform of pyruvate kinase is important for cancer metabolism and tumour growth.', *Nature*. Nature Publishing Group, 452(7184), pp. 230–3. Available at: http://dx.doi.org/10.1038/nature06734 (Accessed: 2 April 2016).

Christofk, H. R. *et al.* (2008b) 'The M2 splice isoform of pyruvate kinase is important for cancer metabolism and tumour growth.', *Nature*. Nature Publishing Group, 452(7184), pp. 230–3. doi: 10.1038/nature06734.

Chu, A. J. and Lee, J. M. (1994) 'Lidocaine inhibits choline uptake and

phosphatidylcholine biosynthesis in human leukemic monocyte-like U937 cells', *Cell Biochemistry and Function*, 12(2), pp. 89–98. doi: 10.1002/cbf.290120203.

Ciafrè, S. A. *et al.* (2005) 'Extensive modulation of a set of microRNAs in primary glioblastoma.', *Biochemical and biophysical research communications*, 334(4), pp. 1351–8. Available at: http://www.ncbi.nlm.nih.gov/pubmed/16039986 (Accessed: 4 March 2016).

Claes, A. *et al.* (2008) 'Phenotypic and Genotypic Characterization of Orthotopic Human Glioma Models and Its Relevance for the Study of Anti-glioma Therapy', *Brain Pathology*, 18(3), pp. 423–433. doi: 10.1111/j.1750-3639.2008.00141.x.

Claes, A., Idema, A. J. and Wesseling, P. (2007) 'Diffuse glioma growth: a guerilla war', *Acta Neuropathologica*. Springer-Verlag, 114(5), pp. 443–458. doi: 10.1007/s00401-007-0293-7.

Colombini, M. 'VDAC: the channel at the interface between mitochondria and the cytosol.', *Molecular and cellular biochemistry*, 256–257(1–2), pp. 107–15. Available at: http://www.ncbi.nlm.nih.gov/pubmed/14977174 (Accessed: 12 March 2016).

Coniglio, S. J. and Segall, J. E. (2013) 'Review: Molecular mechanism of microglia stimulated glioblastoma invasion', *Matrix Biology*, 32(7–8), pp. 372–380. doi: 10.1016/j.matbio.2013.07.008.

Conti, A. *et al.* (2009) 'miR-21 and 221 upregulation and miR-181b downregulation in human grade II-IV astrocytic tumors.', *Journal of neuro-oncology*, 93(3), pp. 325–32. Available at: http://www.ncbi.nlm.nih.gov/pubmed/19159078 (Accessed: 27 March 2016).

Corcoran, C. and Jacobs, T. F. (2019) *Metformin*, *StatPearls*. StatPearls Publishing. Available at: http://www.ncbi.nlm.nih.gov/pubmed/30085525 (Accessed: 19 July 2019).

Corsten, M. F. *et al.* (2007) 'MicroRNA-21 knockdown disrupts glioma growth in vivo and displays synergistic cytotoxicity with neural precursor cell delivered S-TRAIL in human gliomas.', *Cancer research*, 67(19), pp. 8994–9000. doi: 10.1158/0008-5472.CAN-07-1045.

Cotte, A. K. *et al.* (2018) 'Lysophosphatidylcholine acyltransferase 2-mediated lipid droplet production supports colorectal cancer chemoresistance.', *Nature communications*. England, 9(1), p. 322. doi: 10.1038/s41467-017-02732-5.

Cotteret, S. and Chernoff, J. (2002) 'The evolutionary history of effectors downstream of Cdc42 and Rac.', *Genome biology*, 3(2), p. REVIEWS0002. Available at: http://www.ncbi.nlm.nih.gov/pubmed/11864373 (Accessed: 19 May 2019).

Cuddapah, V. A. *et al.* (2014) 'A neurocentric perspective on glioma invasion.', *Nature reviews. Neuroscience*. NIH Public Access, 15(7), pp.

455–65. doi: 10.1038/nrn3765.

Cui, Q.-K. *et al.* (2014) 'MicroRNA-184 promotes proliferation ability of glioma cells by regulating FOXO3.', *Asian Pacific journal of tropical medicine*, 7(10), pp. 776–9. Available at: http://www.sciencedirect.com/science/article/pii/S1995764514601358 (Accessed: 27 March 2016).

Cuyàs, E. *et al.* (2015) 'Oncometabolic mutation IDH1 R132H confers a metformin-hypersensitive phenotype', *Oncotarget*, 6(14), pp. 12279–96. doi: 10.18632/oncotarget.3733.

Cvetkoivč-Dožič D, Skender-Gazibara M, D. S. (2004) 'Morphological and molecular features of diffuse infiltrating astrocytoma.', *Arch Oncol.*, 12, pp. 38–9.

Czauderna, F. *et al.* (2003) 'Structural variations and stabilising modifications of synthetic siRNAs in mammalian cells.', *Nucleic acids research*, 31(11), pp. 2705–16. Available at: http://www.pubmedcentral.nih.gov/articlerender.fcgi?artid=156727&tool=pmcentrez&rendertype=abstract (Accessed: 30 May 2016).

Dai, D.-W. *et al.* (2013) 'Decreased miR-106a inhibits glioma cell glucose uptake and proliferation by targeting SLC2A3 in GBM.', *BMC cancer*, 13, p. 478. doi: 10.1186/1471-2407-13-478.

Dang, L. *et al.* (2009) 'Cancer-associated IDH1 mutations produce 2-hydroxyglutarate.', *Nature*, 462(7274), pp. 739–44. doi:

10.1038/nature08617.

Darzynkiewicz, Z. *et al.* (2011) 'Cell synchronization by inhibitors of DNA replication induces replication stress and DNA damage response: analysis by flow cytometry.', *Methods in molecular biology (Clifton, N.J.)*. NIH Public Access, 761, pp. 85–96. doi: 10.1007/978-1-61779-182-6_6.

Dasgupta, B. *et al.* (2005) 'Glioma formation in neurofibromatosis 1 reflects preferential activation of K-RAS in astrocytes.', *Cancer research*, 65(1), pp. 236–45. Available at: http://www.ncbi.nlm.nih.gov/pubmed/15665300 (Accessed: 2 March 2016).

Daubon, T. *et al.* (2019) 'Deciphering the complex role of thrombospondin-1 in glioblastoma development', *Nature Communications*. Nature Publishing Group, 10(1), p. 1146. doi: 10.1038/s41467-019-08480-y.

David, C. J. *et al.* (2010) 'HnRNP proteins controlled by c-Myc deregulate pyruvate kinase mRNA splicing in cancer.', *Nature*. Macmillan Publishers Limited. All rights reserved, 463(7279), pp. 364–8. doi: 10.1038/nature08697.

David, L. *et al.* (2004) 'Reticulated hyaluronan hydrogels: a model for examining cancer cell invasion in 3D', *Matrix Biology*, 23(3), pp. 183–193. doi: 10.1016/j.matbio.2004.05.005.

DeBerardinis, R. J. *et al.* (2007) 'Beyond aerobic glycolysis: Transformed cells can engage in glutamine metabolism that exceeds the requirement for protein and nucleotide synthesis', *Proceedings of the National Academy of*

Sciences, 104(49), pp. 19345–19350. doi: 10.1073/pnas.0709747104.

DeHaven, C. D. *et al.* (2010) 'Organization of GC/MS and LC/MS metabolomics data into chemical libraries', *Journal of Cheminformatics*, 2(1), p. 9. doi: 10.1186/1758-2946-2-9.

Delpech, B. *et al.* (1993) 'Hyaluronan and hyaluronectin in the extracellular matrix of human brain tumour stroma', *European Journal of Cancer*. Pergamon, 29(7), pp. 1012–1017. doi: 10.1016/S0959-8049(05)80214-X.

DeMali, K. A., Barlow, C. A. and Burridge, K. (2002) 'Recruitment of the Arp2/3 complex to vinculin: coupling membrane protrusion to matrix adhesion', *The Journal of Cell Biology*, 159(5), pp. 881–891. doi: 10.1083/jcb.200206043.

Demaugre, F. *et al.* (1990) 'Immunoquantitative Analysis of Human Carnitine Palmitoyltransferase I and II Defects', *Pediatric Research*. Nature Publishing Group, 27(5), pp. 497–500. doi: 10.1203/00006450-199005000-00016.

Demuth, T. and Berens, M. E. (2004) 'Molecular Mechanisms of Glioma Cell Migration and Invasion', *Journal of Neuro-Oncology*, 70(2), pp. 217–228. doi: 10.1007/s11060-004-2751-6.

Desjardin, C. *et al.* (2014) 'Next-generation sequencing identifies equine cartilage and subchondral bone miRNAs and suggests their involvement in osteochondrosis physiopathology', *BMC Genomics*. BioMed Central, 15(1), p. 798. doi: 10.1186/1471-2164-15-798.

Devreotes, P. and Zigmond, S. (1988) 'Chemotaxis in Eukaryotic Cells: A Focus on Leukocytes and Dictyostelium', *Annual review of cell biology*. Available at: https://www.annualreviews.org/doi/pdf/10.1146/annurev.cb.04.110188.003245 (Accessed: 20 July 2019).

Di, H. *et al.* (2018) 'Silencing LDHA inhibits proliferation, induces apoptosis and increases chemosensitivity to temozolomide in glioma cells.', *Oncology letters*. Spandidos Publications, 15(4), pp. 5131–5136. doi: 10.3892/ol.2018.7932.

Diaz Jr, L. A. *et al.* (2012) 'The molecular evolution of acquired resistance to targeted EGFR blockade in colorectal cancers', *Nature*, 486(7404), pp. 537–540. doi: 10.1038/nature11219.

Didiano, D. and Hobert, O. (2006) 'Perfect seed pairing is not a generally reliable predictor for miRNA-target interactions.', *Nature structural & molecular biology*, 13(9), pp. 849–51. doi: 10.1038/nsmb1138.

Divakaruni, A. S. *et al.* (2018) 'Etomoxir Inhibits Macrophage Polarization by Disrupting CoA Homeostasis', *Cell Metabolism*. Cell Press, 28(3), pp. 490-503.e7. doi: 10.1016/J.CMET.2018.06.001.

Dori-Bachash, M., Shema, E. and Tirosh, I. (2011) 'Coupled Evolution of Transcription and mRNA Degradation', *PLoS Biology*. Edited by J. Bähler. Public Library of Science, 9(7), p. e1001106. doi: 10.1371/journal.pbio.1001106.

Ducker, G. S. and Rabinowitz, J. D. (2017) 'One-Carbon Metabolism in Health and Disease.', *Cell metabolism*. Elsevier, 25(1), pp. 27–42. doi: 10.1016/j.cmet.2016.08.009.

Dumin, J. A. *et al.* (2001) 'Pro-collagenase-1 (Matrix Metalloproteinase-1) Binds the α $_2$ β $_1$ Integrin upon Release from Keratinocytes Migrating on Type I Collagen', *Journal of Biological Chemistry*, 276(31), pp. 29368–29374. doi: 10.1074/jbc.M104179200.

Dunbar, E. M. *et al.* (2014) 'Phase 1 trial of dichloroacetate (DCA) in adults with recurrent malignant brain tumors.', *Investigational new drugs*. NIH Public Access, 32(3), pp. 452–64. doi: 10.1007/s10637-013-0047-4.

Dunn, J. *et al.* (2009) 'Extent of MGMT promoter methylation correlates with outcome in glioblastomas given temozolomide and radiotherapy', *British Journal of Cancer*. Nature Publishing Group, 101(1), pp. 124–131. doi: 10.1038/sj.bjc.6605127.

Dweep, H. and Gretz, N. (2015) 'miRWalk2.0: a comprehensive atlas of microRNA-target interactions', *Nature Methods*, 12(8), pp. 697–697. doi: 10.1038/nmeth.3485.

E, B. (2016) 'Mutational Analysis Reveals the Origin and Therapy-Driven Evolution of Recurrent Glioma', *science.sciencemag.org*. Available at: https://science.sciencemag.org/content/343/6167/189.short (Accessed: 27 July 2019).

Eberhart, K. *et al.* (2009) 'Low doses of 2-deoxy-glucose sensitize acute

lymphoblastic leukemia cells to glucocorticoid-induced apoptosis', *Leukemia*, 23(11), pp. 2167–2170. doi: 10.1038/leu.2009.154.

Ebert, M. S. and Sharp, P. A. (2010) 'MicroRNA sponges: Progress and possibilities', *RNA*, 16(11), pp. 2043–2050. doi: 10.1261/rna.2414110.

Ebert, M. S. and Sharp, P. A. (2012) 'Roles for microRNAs in conferring robustness to biological processes.', *Cell*, 149(3), pp. 515–24. doi: 10.1016/j.cell.2012.04.005.

Eigenbrodt, E. *et al.* (1992) 'Double role for pyruvate kinase type M2 in the expansion of phosphometabolite pools found in tumor cells.', *Critical reviews in oncogenesis*, 3(1–2), pp. 91–115. Available at: http://www.ncbi.nlm.nih.gov/pubmed/1532331 (Accessed: 12 March 2016).

Ekimler, S. and Sahin, K. (2014) 'Computational Methods for MicroRNA Target Prediction.', *Genes*. Multidisciplinary Digital Publishing Institute (MDPI), 5(3), pp. 671–83. doi: 10.3390/genes5030671.

Elkayam, E. *et al.* (2017) 'Multivalent Recruitment of Human Argonaute by GW182.', *Molecular cell*. Howard Hughes Medical Institute, 67(4), pp. 646-658.e3. doi: 10.1016/j.molcel.2017.07.007.

Emdad, L. *et al.* (2015) 'Suppression of miR-184 in malignant gliomas upregulates SND1 and promotes tumor aggressiveness.', *Neuro-oncology*, 17(3), pp. 419–29. Available at: http://www.pubmedcentral.nih.gov/articlerender.fcgi?artid=4483100&tool

=pmcentrez&rendertype=abstract (Accessed: 10 May 2016).

Endo, A., Kuroda, M. and Tanzawa, K. (1976) 'Competitive inhibition of 3-hydroxy-3-methylglutaryl coenzyme a reductase by ML-236A and ML-236B fungal metabolites, having hypocholesterolemic activity', *FEBS Letters*, 72(2), pp. 323–326. doi: 10.1016/0014-5793(76)80996-9.

Engelman, J. A., Luo, J. and Cantley, L. C. (2006) 'The evolution of phosphatidylinositol 3-kinases as regulators of growth and metabolism.', *Nature reviews. Genetics*, 7(8), pp. 606–19. Available at: http://www.ncbi.nlm.nih.gov/pubmed/16847462 (Accessed: 24 December 2015).

Engelman, J. A. and Settleman, J. (2008) 'Acquired resistance to tyrosine kinase inhibitors during cancer therapy', *Current Opinion in Genetics & Development*, 18(1), pp. 73–79. doi: 10.1016/j.gde.2008.01.004.

Ennis, S. R. *et al.* (2003) 'Transport of 5-aminolevulinic acid between blood and brain.', *Brain research*. Netherlands, 959(2), pp. 226–234. doi: 10.1016/s0006-8993(02)03749-6.

Entschladen, F. *et al.* (1997) 'Differential requirement of protein tyrosine kinases and protein kinase C in the regulation of T cell locomotion in three-dimensional collagen matrices.', *Journal of immunology (Baltimore, Md. : 1950)*, 159(7), pp. 3203–10. Available at: http://www.ncbi.nlm.nih.gov/pubmed/9317118 (Accessed: 20 July 2019).

Eriksen, A. H. M. *et al.* (2016) 'Intratumoral Heterogeneity of MicroRNA

Expression in Rectal Cancer', *PLOS ONE*. Edited by R. Dahiya. Public Library of Science, 11(6), p. e0156919. doi: 10.1371/journal.pone.0156919.

Eulalio, A. *et al.* (2007) 'P-Body Formation Is a Consequence, Not the Cause, of RNA-Mediated Gene Silencing', *Molecular and Cellular Biology*, 27(11), pp. 3970–3981. doi: 10.1128/MCB.00128-07.

Faadiel, E. and Lionel, O. (2004) 'Metabolic therapy for heart failure', *European Heart Journal*, 25(20), pp. 1765–1768. doi: 10.1016/j.ehj.2004.08.019.

Fabbri, E. *et al.* (2011) 'miRNA therapeutics: delivery and biological activity of peptide nucleic acids targeting miRNAs.', *Epigenomics*, 3(6), pp. 733–45. doi: 10.2217/epi.11.90.

Fack, F. *et al.* (2017) 'Altered metabolic landscape in IDH-mutant gliomas affects phospholipid, energy, and oxidative stress pathways.', *EMBO molecular medicine*. Wiley-Blackwell, 9(12), pp. 1681–1695. doi: 10.15252/emmm.201707729.

Fagone, P. and Jackowski, S. (2013) 'Phosphatidylcholine and the CDP–choline cycle', *Biochimica et Biophysica Acta (BBA) - Molecular and Cell Biology of Lipids*, 1831(3), pp. 523–532. doi: 10.1016/j.bbalip.2012.09.009.

Falcioni, R. *et al.* (1994) 'Expression of β1, β3, β4, and β5 Integrins by Human Lung Carcinoma Cells of Different Histotypes', *Experimental Cell Research*, 210(1), pp. 113–122. doi: 10.1006/excr.1994.1017.

Fang, R. *et al.* (2012) 'MicroRNA-143 (miR-143) regulates cancer glycolysis via targeting hexokinase 2 gene.', *The Journal of biological chemistry*. United States, 287(27), pp. 23227–23235. doi: 10.1074/jbc.M112.373084.

Fang, X. *et al.* (2011) 'The SOX2 response program in glioblastoma multiforme: an integrated ChIP-seq, expression microarray, and microRNA analysis.', *BMC genomics*. England, 12, p. 11. doi: 10.1186/1471-2164-12-11.

Farh, K. K.-H. *et al.* (2005) 'The widespread impact of mammalian MicroRNAs on mRNA repression and evolution.', *Science (New York, N.Y.)*. American Association for the Advancement of Science, 310(5755), pp. 1817–21. doi: 10.1126/science.1121158.

Farin, A. *et al.* (2006) 'Transplanted glioma cells migrate and proliferate on host brain vasculature: A dynamic analysis', *Glia*, 53(8), pp. 799–808. doi: 10.1002/glia.20334.

Feng, Y. *et al.* (2018) 'Lactate dehydrogenase A: A key player in carcinogenesis and potential target in cancer therapy', *Cancer Medicine*. Wiley-Blackwell, 7(12), pp. 6124–6136. doi: 10.1002/cam4.1820.

Fernandes, J. T. S. *et al.* (2016) 'A Novel Microfluidic Cell Co-culture Platform for the Study of the Molecular Mechanisms of Parkinson's Disease and Other Synucleinopathies', *Frontiers in Neuroscience*, 10. doi: 10.3389/fnins.2016.00511.

Fey, P. *et al.* (2002) 'SadA, a novel adhesion receptor in *Dictyostelium*',

The Journal of Cell Biology, 159(6), pp. 1109–1119. doi: 10.1083/jcb.200206067.

Fillat, C. *et al.* (2003) 'Suicide gene therapy mediated by the Herpes Simplex virus thymidine kinase gene/Ganciclovir system: fifteen years of application.', *Current gene therapy*, 3(1), pp. 13–26. Available at: http://www.ncbi.nlm.nih.gov/pubmed/12553532 (Accessed: 30 May 2016).

Fiore, D. *et al.* (2016) 'miR-340 predicts glioblastoma survival and modulates key cancer hallmarks through down-regulation of NRAS', *Oncotarget*. Impact Journals, pp. 19531–19547. Available at: http://www.impactjournals.com/oncotarget/index.php?journal=oncotarget&page=article&op=view&path%5B%5D=6968&path%5B%5D=19760 (Accessed: 4 June 2016).

Fisher, R., Pusztai, L. and Swanton, C. (2013) 'Cancer heterogeneity: implications for targeted therapeutics', *British Journal of Cancer*, 108(3), pp. 479–485. doi: 10.1038/bjc.2012.581.

Flicek, P. *et al.* (2008) 'Ensembl 2008.', *Nucleic acids research*. Oxford University Press, 36(Database issue), pp. D707-14. doi: 10.1093/nar/gkm988.

Fortin Ensign, S. P. *et al.* (2013) 'Implications of Rho GTPase Signaling in Glioma Cell Invasion and Tumor Progression.', *Frontiers in oncology*. Frontiers Media SA, 3, p. 241. doi: 10.3389/fonc.2013.00241.

Fowler, B. (2001) 'The folate cycle and disease in humans', *Kidney*

International. Elsevier, 59, pp. S221–S229. doi: 10.1046/J.1523-1755.2001.59780221.X.

Franke, T. F. *et al.* (1995) 'The protein kinase encoded by the Akt proto-oncogene is a target of the PDGF-activated phosphatidylinositol 3-kinase', *Cell*, 81(5), pp. 727–736. Available at: http://www.sciencedirect.com/science/article/pii/0092867495905340 (Accessed: 20 January 2016).

Frech, M. *et al.* (1997) 'High Affinity Binding of Inositol Phosphates and Phosphoinositides to the Pleckstrin Homology Domain of RAC/Protein Kinase B and Their Influence on Kinase Activity', *Journal of Biological Chemistry*, 272(13), pp. 8474–8481. Available at: http://www.jbc.org/content/272/13/8474 (Accessed: 3 April 2016).

Freedman, L. P. *et al.* (2015) 'Reproducibility: changing the policies and culture of cell line authentication', *Nature Methods*, 12(6), pp. 493–497. doi: 10.1038/nmeth.3403.

Friedl, P. *et al.* (1997) 'Migration of highly aggressive MV3 melanoma cells in 3-dimensional collagen lattices results in local matrix reorganization and shedding of alpha2 and beta1 integrins and CD44.', *Cancer research*, 57(10), pp. 2061–70. Available at: http://www.ncbi.nlm.nih.gov/pubmed/9158006 (Accessed: 20 July 2019).

Friedl, P. *et al.* (2012) 'New dimensions in cell migration', *Nature Reviews Molecular Cell Biology*, 13(11), pp. 743–747. doi: 10.1038/nrm3459.

Friedl, P., Borgmann, S. and Bröcker, E. B. (2001) 'Amoeboid leukocyte crawling through extracellular matrix: lessons from the Dictyostelium paradigm of cell movement.', *Journal of leukocyte biology*, 70(4), pp. 491–509. Available at: http://www.ncbi.nlm.nih.gov/pubmed/11590185 (Accessed: 20 July 2019).

Friedl, P. and Bröcker, E.-B. (2000) 'The biology of cell locomotion within three-dimensional extracellular matrix', *Cellular and Molecular Life Sciences (CMLS)*, 57(1), pp. 41–64. doi: 10.1007/s000180050498.

Friedl, P. and Wolf, K. (2003) 'Tumour-cell invasion and migration: diversity and escape mechanisms', *Nature Reviews Cancer*. Nature Publishing Group, 3(5), pp. 362–374. doi: 10.1038/nrc1075.

Friedl, P., Zänker, K. S. and Bröcker, E.-B. (1998) 'Cell migration strategies in 3-D extracellular matrix: Differences in morphology, cell matrix interactions, and integrin function', *Microscopy Research and Technique*. John Wiley & Sons, Ltd, 43(5), pp. 369–378. doi: 10.1002/(SICI)1097-0029(19981201)43:5<369::AID-JEMT3>3.0.CO;2-6.

Fukushima, Y. *et al.* (1998) 'Integrin α3β1-mediated interaction with laminin-5 stimulates adhesion, migration and invasion of malignant glioma cells', *International Journal of Cancer*. John Wiley & Sons, Ltd, 76(1), pp. 63–72. doi: 10.1002/(SICI)1097-0215(19980330)76:1<63::AID-IJC11>3.0.CO;2-H.

G. Gritsenko, P., Ilina, O. and Friedl, P. (2012) 'Interstitial guidance of

cancer invasion', *The Journal of Pathology*, 226(2), pp. 185–199. doi: 10.1002/path.3031.

Gabriely, G. *et al.* (2008) 'MicroRNA 21 promotes glioma invasion by targeting matrix metalloproteinase regulators.', *Molecular and cellular biology*. United States, 28(17), pp. 5369–5380. doi: 10.1128/MCB.00479-08.

Gal, H. *et al.* (2008) 'MIR-451 and Imatinib mesylate inhibit tumor growth of Glioblastoma stem cells.', *Biochemical and biophysical research communications*. United States, 376(1), pp. 86–90. doi: 10.1016/j.bbrc.2008.08.107.

Gao, H. *et al.* (2013) 'Correlation of expression levels of ANXA2, PGAM1, and CALR with glioma grade and prognosis', *Journal of Neurosurgery*, 118(4), pp. 846–853. doi: 10.3171/2012.9.JNS112134.

Gao, L.-B. *et al.* (2013) 'Metformin inhibits glioma cell U251 invasion by downregulation of fibulin-3', *NeuroReport*, 24(10), pp. 504–508. doi: 10.1097/WNR.0b013e32836277fb.

Gao, X. and Jin, W. (2014) 'The emerging role of tumor-suppressive microRNA-218 in targeting glioblastoma stemness.', *Cancer letters*. Ireland, 353(1), pp. 25–31. doi: 10.1016/j.canlet.2014.07.011.

Gao, Y. *et al.* (2011) 'A versatile valve-enabled microfluidic cell co-culture platform and demonstration of its applications to neurobiology and cancer biology', *Biomedical Microdevices*, 13(3), pp. 539–548. doi:

10.1007/s10544-011-9523-9.

Garcia, E. J., Vevea, J. D. and Pon, L. A. (2018) 'Lipid droplet autophagy during energy mobilization, lipid homeostasis and protein quality control.', *Frontiers in bioscience (Landmark edition)*, 23, pp. 1552–1563. doi: 10.2741/4660.

Gardner, P. R. *et al.* (1995) 'Superoxide radical and iron modulate aconitase activity in mammalian cells.', *The Journal of biological chemistry*. American Society for Biochemistry and Molecular Biology, 270(22), pp. 13399–405. doi: 10.1074/jbc.270.22.13399.

Gaspar, L. E. *et al.* (1992) 'Supratentorial malignant glioma: patterns of recurrence and implications for external beam local treatment.', *International journal of radiation oncology, biology, physics*. Elsevier, 24(1), pp. 55–7. doi: 10.1016/0360-3016(92)91021-e.

Gatenby, R. A. *et al.* (2009) 'Adaptive Therapy', *Cancer Research*, 69(11), pp. 4894–4903. doi: 10.1158/0008-5472.CAN-08-3658.

Gatenby, R. A. and Gillies, R. J. (2004) 'Why do cancers have high aerobic glycolysis?', *Nature reviews. Cancer*. Nature Publishing Group, 4(11), pp. 891–9. doi: 10.1038/nrc1478.

Gautier, L. *et al.* (2004) 'affy--analysis of Affymetrix GeneChip data at the probe level.', *Bioinformatics (Oxford, England)*, 20(3), pp. 307–15. doi: 10.1093/bioinformatics/btg405.

Geng, F. *et al.* (2016) 'Inhibition of SOAT1 Suppresses Glioblastoma Growth

via Blocking SREBP-1-Mediated Lipogenesis', *Clinical Cancer Research*, 22(21), pp. 5337–5348. doi: 10.1158/1078-0432.CCR-15-2973.

Gentleman, R. C. *et al.* (2004) 'Bioconductor: open software development for computational biology and bioinformatics.', *Genome biology*, 5(10), p. R80. doi: 10.1186/gb-2004-5-10-r80.

Georgescu, M.-M. (2010) 'PTEN Tumor Suppressor Network in PI3K-Akt Pathway Control.', *Genes & cancer*, 1(12), pp. 1170–7. Available at: http://www.pubmedcentral.nih.gov/articlerender.fcgi?artid=3092286&tool=pmcentrez&rendertype=abstract (Accessed: 3 April 2016).

Gerlinger, M. *et al.* (2012) 'Intratumor Heterogeneity and Branched Evolution Revealed by Multiregion Sequencing', *New England Journal of Medicine*, 366(10), pp. 883–892. doi: 10.1056/NEJMoa1113205.

Gerlinger, M. *et al.* (2014) 'Genomic architecture and evolution of clear cell renal cell carcinomas defined by multiregion sequencing', *Nature Genetics*, 46(3), pp. 225–233. doi: 10.1038/ng.2891.

Ghasemi, A., Fallah, S. and Ansari, M. (2016) 'MiR-153 as a Tumor Suppressor in Glioblastoma Multiforme is Downregulated by DNA Methylation.', *Clinical laboratory*, 62(4), pp. 573–80. Available at: http://www.ncbi.nlm.nih.gov/pubmed/27215075 (Accessed: 23 July 2019).

Gilder, A. S. *et al.* (2018) 'The Urokinase Receptor Induces a Mesenchymal Gene Expression Signature in Glioblastoma Cells and Promotes Tumor Cell Survival in Neurospheres', *Scientific Reports*. Nature Publishing Group, 8(1),

p. 2982. doi: 10.1038/s41598-018-21358-1.

Gingras, M. *et al.* (1995) 'Comparison of cell adhesion molecule expression between glioblastoma multiforme and autologous normal brain tissue', *Journal of Neuroimmunology*. Elsevier, 57(1–2), pp. 143–153. doi: 10.1016/0165-5728(94)00178-Q.

Git, A. *et al.* (2010) 'Systematic comparison of microarray profiling, real-time PCR, and next-generation sequencing technologies for measuring differential microRNA expression.', *RNA (New York, N.Y.)*. Cold Spring Harbor Laboratory Press, 16(5), pp. 991–1006. doi: 10.1261/rna.1947110.

Gladson, C. L. (1999) 'The Extracellular Matrix of Gliomas: Modulation of Cell Function', *Journal of Neuropathology & Experimental Neurology*. Narnia, 58(10), pp. 1029–1040. doi: 10.1097/00005072-199910000-00001.

Glasel, J. A. (1995) 'Validity of nucleic acid purities monitored by 260nm/280nm absorbance ratios.', *BioTechniques*, 18(1), pp. 62–3. Available at: http://www.ncbi.nlm.nih.gov/pubmed/7702855 (Accessed: 8 March 2016).

Godlewski, J. *et al.* (2010) 'MicroRNA-451 regulates LKB1/AMPK signaling and allows adaptation to metabolic stress in glioma cells.', *Molecular cell*, 37(5), pp. 620–32. Available at: http://www.pubmedcentral.nih.gov/articlerender.fcgi?artid=3125113&tool=pmcentrez&rendertype=abstract (Accessed: 9 May 2016).

Goldstein, J. L. and Brown, M. S. (2009) 'The LDL receptor.',

Arteriosclerosis, thrombosis, and vascular biology. Lippincott Williams & Wilkins, 29(4), pp. 431–8. doi: 10.1161/ATVBAHA.108.179564.

de Gooijer, M. C. *et al.* (2018) 'An Experimenter's Guide to Glioblastoma Invasion Pathways', *Trends in Molecular Medicine*. Elsevier Current Trends, 24(9), pp. 763–780. doi: 10.1016/J.MOLMED.2018.07.003.

Gottlob, K. *et al.* (2001) 'Inhibition of early apoptotic events by Akt/PKB is dependent on the first committed step of glycolysis and mitochondrial hexokinase.', *Genes & development*, 15(11), pp. 1406–18. doi: 10.1101/gad.889901.

Goyal, Rama *et al.* (2015) 'Immunohistochemical expression of glial fibrillary acidic protein and CAM5.2 in glial tumors and their role in differentiating glial tumors from metastatic tumors of central nervous system.', *Journal of neurosciences in rural practice*. Wolters Kluwer -- Medknow Publications, 6(4), pp. 499–503. doi: 10.4103/0976-3147.168426.

Grahn, T. H. M. *et al.* (2013) 'FSP27 and PLIN1 interaction promotes the formation of large lipid droplets in human adipocytes', *Biochemical and biophysical research communications*. Elsevier, 432(2), pp. 296–301.

Granneman, J. G. *et al.* (2011) 'Interactions of perilipin-5 (Plin5) with adipose triglyceride lipase', *Journal of Biological Chemistry*. ASBMB, 286(7), pp. 5126–5135.

Greaves, M. and Maley, C. C. (2012) 'Clonal evolution in cancer.', *Nature*.

NIH Public Access, 481(7381), pp. 306–13. doi: 10.1038/nature10762.

Gregersen, L. H. *et al.* (2012) 'MicroRNA-143 down-regulates Hexokinase 2 in colon cancer cells.', *BMC cancer*. England, 12, p. 232. doi: 10.1186/1471-2407-12-232.

Gregory, R. I. *et al.* (2005) 'Human RISC Couples MicroRNA Biogenesis and Posttranscriptional Gene Silencing', *Cell*, 123(4), pp. 631–640. doi: 10.1016/j.cell.2005.10.022.

Gregory R. Warnes, B. B. and T. L. (2015) 'gtools: Various R Programming Tools.', *R package version 3.5.0. https://CRAN.R-project.org/package=gtools*.

Griffiths-Jones, S. *et al.* (2006) 'miRBase: microRNA sequences, targets and gene nomenclature.', *Nucleic acids research*, 34(Database issue), pp. D140-4. doi: 10.1093/nar/gkj112.

Grimm, D. *et al.* (2006) 'Fatality in mice due to oversaturation of cellular microRNA/short hairpin RNA pathways.', *Nature*, 441(7092), pp. 537–41. doi: 10.1038/nature04791.

Gritti, M. *et al.* (2014) 'Metformin repositioning as antitumoral agent: selective antiproliferative effects in human glioblastoma stem cells, via inhibition of CLIC1-mediated ion current', *Oncotarget*, 5(22), pp. 11252–68. doi: 10.18632/oncotarget.2617.

Griveau, A. *et al.* (2013) 'Silencing of miR-21 by locked nucleic acid-lipid nanocapsule complexes sensitize human glioblastoma cells to radiation-

induced cell death.', *International journal of pharmaceutics*, 454(2), pp. 765–74. doi: 10.1016/j.ijpharm.2013.05.049.

Grünweller, A. and Hartmann, R. K. (2007) 'Locked nucleic acid oligonucleotides: the next generation of antisense agents?', *BioDrugs : clinical immunotherapeutics, biopharmaceuticals and gene therapy*, 21(4), pp. 235–43. Available at: http://www.ncbi.nlm.nih.gov/pubmed/17628121 (Accessed: 22 May 2016).

Guimarães-Ferreira, L. (2014) 'Role of the phosphocreatine system on energetic homeostasis in skeletal and cardiac muscles.', *Einstein (Sao Paulo, Brazil)*. Instituto de Ensino e Pesquisa Albert Einstein, 12(1), pp. 126–31. doi: 10.1590/S1679-45082014RB2741.

Gumireddy, K. *et al.* (2008) 'Small-molecule inhibitors of microrna miR-21 function.', *Angewandte Chemie (International ed. in English)*, 47(39), pp. 7482–4. doi: 10.1002/anie.200801555.

Guo, D. *et al.* (2011) 'An LXR Agonist Promotes Glioblastoma Cell Death through Inhibition of an EGFR/AKT/SREBP-1/LDLR-Dependent Pathway', *Cancer Discovery*, 1(5), pp. 442–456. doi: 10.1158/2159-8290.CD-11-0102.

Guo, P. *et al.* (2013) 'C-Myc negatively controls the tumor suppressor PTEN by upregulating miR-26a in glioblastoma multiforme cells.', *Biochemical and biophysical research communications*, 441(1), pp. 186–90. Available at: http://www.sciencedirect.com/science/article/pii/S0006291X13017063

(Accessed: 26 March 2016).

Guo, W.-X. *et al.* (2005) 'Mitochondrial dysfunction in choline deficiency-induced apoptosis in cultured rat hepatocytes', *Free Radical Biology and Medicine*, 39(5), pp. 641–650. doi: 10.1016/j.freeradbiomed.2005.04.013.

Gutenberg, A. *et al.* (2004) 'Expression of tyrosine kinases FAK and Pyk2 in 331 human astrocytomas', *Acta Neuropathologica*, 108(3), pp. 224–30. doi: 10.1007/s00401-004-0886-3.

Haberler, C. *et al.* (2006) 'Immunohistochemical analysis of platelet-derived growth factor receptor-alpha, -beta, c-kit, c-abl, and arg proteins in glioblastoma: possible implications for patient selection for imatinib mesylate therapy.', *Journal of neuro-oncology*, 76(2), pp. 105–9. doi: 10.1007/s11060-005-4570-9.

Hafner, M. *et al.* (2010) 'Transcriptome-wide Identification of RNA-Binding Protein and MicroRNA Target Sites by PAR-CLIP', *Cell*, 141(1), pp. 129–141. doi: 10.1016/j.cell.2010.03.009.

Hambardzumyan, D. *et al.* (2011) 'Genetic modeling of gliomas in mice: new tools to tackle old problems', *Glia*. NIH Public Access, 59(8), p. 1155. doi: 10.1002/GLIA.21142.

Hamilton, J. D. *et al.* (2014) 'Glioblastoma Multiforme Metastasis Outside the CNS: Three Case Reports and Possible Mechanisms of Escape', *Journal of Clinical Oncology*, 32(22), pp. e80–e84. doi: 10.1200/JCO.2013.48.7546.

Han, T. *et al.* (2013) 'How does cancer cell metabolism affect tumor

migration and invasion?', *Cell Adhesion & Migration*, 7(5), pp. 395–403. doi: 10.4161/cam.26345.

Hanahan, D. and Weinberg, R. A. (2011) 'Hallmarks of cancer: the next generation.', *Cell*. Elsevier, 144(5), pp. 646–74. doi: 10.1016/j.cell.2011.02.013.

Harford-Wright, E., Bidère, N. and Gavard, J. (2016) 'β-escin selectively targets the glioblastoma-initiating cell population and reduces cell viability.', *Oncotarget*. Impact Journals, LLC, 7(41), pp. 66865–66879. doi: 10.18632/oncotarget.11784.

Harryman, W. L. *et al.* (2016) 'The Cohesive Metastasis Phenotype in Human Prostate Cancer.', *Biochimica et biophysica acta*. NIH Public Access, 1866(2), pp. 221–231. doi: 10.1016/j.bbcan.2016.09.005.

Hashizume, R. *et al.* (1996) 'Expression of beta-catenin in normal breast tissue and breast carcinoma: a comparative study with epithelial cadherin and alpha-catenin.', *Histopathology*, 29(2), pp. 139–46. Available at: http://www.ncbi.nlm.nih.gov/pubmed/8872147 (Accessed: 21 July 2019).

Hattermann, K. *et al.* (2016) 'Stem cell markers in glioma progression and recurrence', *International Journal of Oncology*. Spandidos Publications, 49(5), pp. 1899–1910. doi: 10.3892/ijo.2016.3682.

Hatziapostolou, M., Polytarchou, C. and Iliopoulos, D. (2013) 'miRNAs link metabolic reprogramming to oncogenesis.', *Trends in endocrinology and metabolism: TEM*, 24(7), pp. 361–73. doi: 10.1016/j.tem.2013.03.002.

Hecker, T. P. *et al.* (2002) 'Focal adhesion kinase enhances signaling through the Shc/extracellular signal-regulated kinase pathway in anaplastic astrocytoma tumor biopsy samples.', *Cancer research*, 62(9), pp. 2699–707. Available at: http://www.ncbi.nlm.nih.gov/pubmed/11980671 (Accessed: 20 July 2019).

Hegerfeldt, Y. *et al.* (2002) 'Collective cell movement in primary melanoma explants: plasticity of cell-cell interaction, beta1-integrin function, and migration strategies.', *Cancer research*, 62(7), pp. 2125–30. Available at: http://www.ncbi.nlm.nih.gov/pubmed/11929834 (Accessed: 20 July 2019).

Hegi, M. E. *et al.* (2005) '*MGMT* Gene Silencing and Benefit from Temozolomide in Glioblastoma', *New England Journal of Medicine*. Massachusetts Medical Society , 352(10), pp. 997–1003. doi: 10.1056/NEJMoa043331.

Vander Heiden, M. G., Cantley, L. C. and Thompson, C. B. (2009) 'Understanding the Warburg effect: the metabolic requirements of cell proliferation.', *Science (New York, N.Y.)*, 324(5930), pp. 1029–33. doi: 10.1126/science.1160809.

Hermansen, S. K. *et al.* (2013) 'MiR-21 expression in the tumor cell compartment holds unfavorable prognostic value in gliomas', *Journal of Neuro-Oncology*, 111(1), pp. 71–81. doi: 10.1007/s11060-012-0992-3.

Hermansen, S. K. and Kristensen, B. W. (2013) 'MicroRNA biomarkers in glioblastoma.', *Journal of neuro-oncology*. United States, 114(1), pp. 13–

23. doi: 10.1007/s11060-013-1155-x.

Herms, A. *et al.* (2015) 'AMPK activation promotes lipid droplet dispersion on detyrosinated microtubules to increase mitochondrial fatty acid oxidation', *Nature communications*. Nature Publishing Group, 6, p. 7176.

Hirata, E. *et al.* (2012) 'In vivo fluorescence resonance energy transfer imaging reveals differential activation of Rho-family GTPases in glioblastoma cell invasion.', *Journal of cell science*. The Company of Biologists Ltd, 125(Pt 4), pp. 858–68. doi: 10.1242/jcs.089995.

Hoang-Minh, L. B. *et al.* (2018) 'Infiltrative and drug-resistant slow-cycling cells support metabolic heterogeneity in glioblastoma.', *The EMBO journal*. EMBO Press, 37(23), p. e98772. doi: 10.15252/embj.201798772.

Hoelzinger, D. B. *et al.* (2005) 'Gene expression profile of glioblastoma multiforme invasive phenotype points to new therapeutic targets.', *Neoplasia (New York, N.Y.)*, 7(1), pp. 7–16. doi: 10.1593/neo.04535.

Holubarsch, C. J. F. *et al.* (2007) 'A double-blind randomized multicentre clinical trial to evaluate the efficacy and safety of two doses of etomoxir in comparison with placebo in patients with moderate congestive heart failure: the ERGO (etomoxir for the recovery of glucose oxidation) study', *Clinical Science*, 113(4), pp. 205–212. doi: 10.1042/CS20060307.

Horská, A. and Barker, P. B. (2010) 'Imaging of brain tumors: MR spectroscopy and metabolic imaging.', *Neuroimaging clinics of North America*. NIH Public Access, 20(3), pp. 293–310. doi:

10.1016/j.nic.2010.04.003.

Hou, L. C. *et al.* (2006) 'Recurrent glioblastoma multiforme: a review of natural history and management options.', *Neurosurgical focus*, 20(4), p. E5. Available at: http://www.ncbi.nlm.nih.gov/pubmed/16709036 (Accessed: 16 May 2019).

Hresko, R. C. and Mueckler, M. (2005) 'mTOR.RICTOR is the Ser473 kinase for Akt/protein kinase B in 3T3-L1 adipocytes.', *The Journal of biological chemistry*, 280(49), pp. 40406–16. doi: 10.1074/jbc.M508361200.

Hsu, M. *et al.* (2000) 'Cadherin repertoire determines partner-specific gap junctional communication during melanoma progression.', *Journal of cell science*, 113 (Pt 9), pp. 1535–42. Available at: http://www.ncbi.nlm.nih.gov/pubmed/10751145 (Accessed: 21 July 2019).

Huang, D. *et al.* (2015) 'miR-340 suppresses glioblastoma multiforme.', *Oncotarget*, 6(11), pp. 9257–70. Available at: http://www.pubmedcentral.nih.gov/articlerender.fcgi?artid=4496215&tool=pmcentrez&rendertype=abstract (Accessed: 4 June 2016).

Huang, J. *et al.* (2016) 'A phase I study to repurpose disulfiram in combination with temozolomide to treat newly diagnosed glioblastoma after chemoradiotherapy', *Journal of Neuro-Oncology*, 128(2), pp. 259–266. doi: 10.1007/s11060-016-2104-2.

Huang, Shaosong *et al.* (2019) 'Flot2 targeted by miR-449 acts as a prognostic biomarker in glioma', *Artificial Cells, Nanomedicine, and*

Biotechnology. Taylor & Francis, 47(1), pp. 250–255. doi: 10.1080/21691401.2018.1549062.

Huber, W. *et al.* (2015) 'Orchestrating high-throughput genomic analysis with Bioconductor.', *Nature methods*, 12(2), pp. 115–21. doi: 10.1038/nmeth.3252.

Hughes, C. S., Postovit, L. M. and Lajoie, G. A. (2010) 'Matrigel: A complex protein mixture required for optimal growth of cell culture', *PROTEOMICS*, 10(9), pp. 1886–1890. doi: 10.1002/pmic.200900758.

Huntzinger, E. and Izaurralde, E. (2011) 'Gene silencing by microRNAs: contributions of translational repression and mRNA decay.', *Nature reviews. Genetics*. Nature Publishing Group, a division of Macmillan Publishers Limited. All Rights Reserved., 12(2), pp. 99–110. Available at: http://dx.doi.org/10.1038/nrg2936 (Accessed: 15 July 2014).

Huse, J. T. *et al.* (2009) 'The PTEN-regulating microRNA miR-26a is amplified in high-grade glioma and facilitates gliomagenesis in vivo.', *Genes & development*, 23(11), pp. 1327–37. Available at: http://www.pubmedcentral.nih.gov/articlerender.fcgi?artid=2701585&tool=pmcentrez&rendertype=abstract (Accessed: 26 March 2016).

Huszthy, P. C. *et al.* (2012) 'In vivo models of primary brain tumors: pitfalls and perspectives.', *Neuro-oncology*, 14(8), pp. 979–93. doi: 10.1093/neuonc/nos135.

Hutter-Schmid, B., Kniewallner, K. M. and Humpel, C. (2015) 'Organotypic

brain slice cultures as a model to study angiogenesis of brain vessels', *Frontiers in Cell and Developmental Biology*, 3. doi: 10.3389/fcell.2015.00052.

Hynes, Richard O (2002) 'Integrins: bidirectional, allosteric signaling machines.', *Cell*, 110(6), pp. 673–87. doi: 10.1016/s0092-8674(02)00971-6.

Hynes, Richard O. (2002) 'Integrins: Bidirectional, Allosteric Signaling Machines', *Cell*. Cell Press, 110(6), pp. 673–687. doi: 10.1016/S0092-8674(02)00971-6.

Hyrup, B. and Nielsen, P. E. (1996) 'Peptide nucleic acids (PNA): synthesis, properties and potential applications.', *Bioorganic & medicinal chemistry*, 4(1), pp. 5–23. Available at: http://www.ncbi.nlm.nih.gov/pubmed/8689239 (Accessed: 30 May 2016).

Iacob, G. and Dinca, E. B. (2009) 'Current data and strategy in glioblastoma multiforme.', *Journal of medicine and life*. Carol Davila - University Press, 2(4), pp. 386–93. Available at: /pmc/articles/PMC3019011/?report=abstract (Accessed: 7 July 2016).

Ikeda, M. *et al.* (2008) 'Characterization of four mammalian 3-hydroxyacyl-CoA dehydratases involved in very long-chain fatty acid synthesis', *FEBS Letters*, 582(16), pp. 2435–2440. doi: 10.1016/j.febslet.2008.06.007.

Inazu, M. *et al.* (2013) 'Functional expression of choline transporter-like protein 1 (CTL1) in small cell lung carcinoma cells: A target molecule for

lung cancer therapy', *Pharmacological Research*, 76, pp. 119–131. doi: 10.1016/j.phrs.2013.07.011.

Inda, M.-D.-M., Bonavia, R. and Seoane, J. (2014) 'Glioblastoma multiforme: a look inside its heterogeneous nature.', *Cancers*, 6(1), pp. 226–39. doi: 10.3390/cancers6010226.

Irizarry, R. A. *et al.* (2003) 'Exploration, normalization, and summaries of high density oligonucleotide array probe level data.', *Biostatistics (Oxford, England)*, 4(2), pp. 249–64. doi: 10.1093/biostatistics/4.2.249.

Isakovic, A. *et al.* (2007) 'Dual antiglioma action of metformin: cell cycle arrest and mitochondria-dependent apoptosis', *Cellular and Molecular Life Sciences*, 64(10), pp. 1290–1302. doi: 10.1007/s00018-007-7080-4.

Ishiguro, N. *et al.* (2008) 'Decreased biosynthesis of lung surfactant constituent phosphatidylcholine due to inhibition of choline transporter by gefitinib in lung alveolar cells.', *Pharmaceutical research*, 25(2), pp. 417–27. doi: 10.1007/s11095-007-9362-9.

Ishihara, H. *et al.* (2008) 'Endothelial Cell Barrier Impairment Induced by Glioblastomas and Transforming Growth Factor β $_2$ Involves Matrix Metalloproteinases and Tight Junction Proteins', *Journal of Neuropathology & Experimental Neurology*. Narnia, 67(5), pp. 435–448. doi: 10.1097/NEN.0b013e31816fd622.

Itkonen, H. M. *et al.* (2017) 'Lipid degradation promotes prostate cancer cell survival.', *Oncotarget*. Impact Journals, LLC, 8(24), pp. 38264–38275.

doi: 10.18632/oncotarget.16123.

Iwadate, Y. (2016) 'Epithelial-mesenchymal transition in glioblastoma progression.', *Oncology letters*. Spandidos Publications, 11(3), pp. 1615–1620. doi: 10.3892/ol.2016.4113.

Izquierdo-Garcia, J. L. *et al.* (2015) 'Metabolic Reprogramming in Mutant IDH1 Glioma Cells', *PLOS ONE*. Edited by I. Ulasov. Woodhead Pub, 10(2), p. e0118781. doi: 10.1371/journal.pone.0118781.

Jacobs, V. L. *et al.* (2011) 'Current review of in vivo GBM rodent models: emphasis on the CNS-1 tumour model.', *ASN neuro*, 3(3), p. e00063. doi: 10.1042/AN20110014.

Jacobsen, A. *et al.* (2013) 'Analysis of microRNA-target interactions across diverse cancer types.', *Nature structural & molecular biology*. NIH Public Access, 20(11), pp. 1325–32. doi: 10.1038/nsmb.2678.

Janas, M. M. *et al.* (2012) 'Alternative RISC assembly: binding and repression of microRNA-mRNA duplexes by human Ago proteins.', *RNA (New York, N.Y.)*. Cold Spring Harbor Laboratory Press, 18(11), pp. 2041–55. doi: 10.1261/rna.035675.112.

Jarc, E. *et al.* (2018) 'Lipid droplets induced by secreted phospholipase A2 and unsaturated fatty acids protect breast cancer cells from nutrient and lipotoxic stress', *Biochimica et Biophysica Acta (BBA)-Molecular and Cell Biology of Lipids*. Elsevier, 1863(3), pp. 247–265.

JASPARS, L. H. *et al.* (1996) 'EXTRACELLULAR MATRIX AND β1 INTEGRIN

EXPRESSION IN NODAL AND EXTRANODAL T-CELL LYMPHOMAS', *The Journal of Pathology*, 178(1), pp. 36–43. doi: 10.1002/(SICI)1096-9896(199601)178:1<36::AID-PATH426>3.0.CO;2-S.

Jensen, S. S. *et al.* (2016) 'Establishment and Characterization of a Tumor Stem Cell-Based Glioblastoma Invasion Model', *PLOS ONE*. Edited by I. Ulasov, 11(7), p. e0159746. doi: 10.1371/journal.pone.0159746.

Jeon, S.-M., Chandel, N. S. and Hay, N. (2012) 'AMPK regulates NADPH homeostasis to promote tumour cell survival during energy stress', *Nature*, 485(7400), pp. 661–665. doi: 10.1038/nature11066.

Jepsen, R. K. *et al.* (2016) 'Intra-tumor heterogeneity of microRNA-92a, microRNA-375 and microRNA-424 in colorectal cancer', *Experimental and Molecular Pathology*, 100(1), pp. 125–131. doi: 10.1016/j.yexmp.2015.12.004.

Ji, Q. *et al.* (2013) 'Resveratrol Inhibits Invasion and Metastasis of Colorectal Cancer Cells via MALAT1 Mediated Wnt/β-Catenin Signal Pathway', *PLoS ONE*. Edited by I. U. Agoulnik. Public Library of Science, 8(11), p. e78700. doi: 10.1371/journal.pone.0078700.

Ji, Q. *et al.* (2014) 'Long non-coding RNA MALAT1 promotes tumour growth and metastasis in colorectal cancer through binding to SFPQ and releasing oncogene PTBP2 from SFPQ/PTBP2 complex', *British Journal of Cancer*. Nature Publishing Group, 111(4), pp. 736–748. doi: 10.1038/bjc.2014.383.

Jia, Z.-H. *et al.* (2017) 'Phosphorylation of STAT3 at Tyr705 regulates MMP-

9 production in epithelial ovarian cancer', *PLOS ONE*. Edited by A. Ahmad. Public Library of Science, 12(8), p. e0183622. doi: 10.1371/journal.pone.0183622.

Jiao, Y. *et al.* (2012) 'Frequent ATRX, CIC, FUBP1 and IDH1 mutations refine the classification of malignant gliomas.', *Oncotarget*, 3(7), pp. 709–22. doi: 10.18632/oncotarget.588.

Jin, H. Y. *et al.* (2015) 'Transfection of microRNA Mimics Should Be Used with Caution.', *Frontiers in genetics*. Frontiers Media SA, 6, p. 340. doi: 10.3389/fgene.2015.00340.

Jin, L. *et al.* (2015) 'Glutamate Dehydrogenase 1 Signals through Antioxidant Glutathione Peroxidase 1 to Regulate Redox Homeostasis and Tumor Growth', *Cancer Cell*, 27(2), pp. 257–270. doi: 10.1016/j.ccell.2014.12.006.

Jin, W. *et al.* (2012) 'Small RNA Sequencing Reveals MicroRNAs That Modulate Angiotensin II Effects in Vascular Smooth Muscle Cells', *Journal of Biological Chemistry*. American Society for Biochemistry and Molecular Biology, 287(19), pp. 15672–15683. doi: 10.1074/jbc.M111.322669.

Jin, Y. *et al.* (2013) 'Evaluating the microRNA targeting sites by luciferase reporter gene assay.', *Methods in molecular biology (Clifton, N.J.)*. NIH Public Access, 936, pp. 117–27. doi: 10.1007/978-1-62703-083-0_10.

Johnson, B. *et al.* (2014) 'Mutational analysis reveals the origin and therapy-driven evolution of recurrent glioma', *science.sciencemag.org*.

Available at: https://science.sciencemag.org/content/343/6167/189.short (Accessed: 27 July 2019).

Jones, J. E. C. *et al.* (2017) 'Inhibition of Acetyl-CoA Carboxylase 1 (ACC1) and 2 (ACC2) Reduces Proliferation and De Novo Lipogenesis of EGFRvIII Human Glioblastoma Cells', *PLOS ONE*. Edited by M. Jekabsons. Public Library of Science, 12(1), p. e0169566. doi: 10.1371/journal.pone.0169566.

Jong, C. J., Azuma, J. and Schaffer, S. (2012) 'Mechanism underlying the antioxidant activity of taurine: prevention of mitochondrial oxidant production', *Amino Acids*, 42(6), pp. 2223–2232. doi: 10.1007/s00726-011-0962-7.

Jung, S. *et al.* (2001) 'Tracking the invasiveness of human astrocytoma cells by using green fluorescent protein in an organotypical brain slice model', *Journal of Neurosurgery*, 94(1), pp. 80–89. doi: 10.3171/jns.2001.94.1.0080.

Jung, S. *et al.* (2002) 'Brain tumor invasion model system using organotypic brain-slice culture as an alternative to in vivo model', *Journal of Cancer Research and Clinical Oncology*, 128(9), pp. 469–476. doi: 10.1007/s00432-002-0366-x.

Justus, C. R. *et al.* (2014) 'In vitro Cell Migration and Invasion Assays Video Link', *In vitro Cell Migration and Invasion Assays. J. Vis. Exp*, (88). doi: 10.3791/51046.

Kaibuchi, K., Kuroda, S. and Amano, M. (1999) 'Regulation of the Cytoskeleton and Cell Adhesion by the Rho Family GTPases in Mammalian Cells', *Annual Review of Biochemistry*, 68(1), pp. 459–486. doi: 10.1146/annurev.biochem.68.1.459.

Kalluri, R. and Weinberg, R. A. (2009) 'The basics of epithelial-mesenchymal transition.', *The Journal of clinical investigation*. American Society for Clinical Investigation, 119(6), pp. 1420–8. doi: 10.1172/JCI39104.

Kalmar, G. B. *et al.* (1994) 'Primary structure and expression of a human CTP:phosphocholine cytidylyltransferase.', *Biochimica et biophysica acta*, 1219(2), pp. 328–34. doi: 10.1016/0167-4781(94)90056-6.

Kamphorst, J. J. *et al.* (2011) 'Liquid Chromatography–High Resolution Mass Spectrometry Analysis of Fatty Acid Metabolism', *Analytical Chemistry*, 83(23), pp. 9114–9122. doi: 10.1021/ac202220b.

Kantarjian, H. *et al.* (2002) 'Hematologic and cytogenetic responses to imatinib mesylate in chronic myelogenous leukemia.', *The New England journal of medicine*, 346(9), pp. 645–52. doi: 10.1056/NEJMoa011573.

Karginov, F. V *et al.* (2007) 'A biochemical approach to identifying microRNA targets.', *Proceedings of the National Academy of Sciences of the United States of America*. National Academy of Sciences, 104(49), pp. 19291–6. doi: 10.1073/pnas.0709971104.

Kartha, R. V and Subramanian, S. (2014) 'Competing endogenous RNAs

(ceRNAs): new entrants to the intricacies of gene regulation.', *Frontiers in genetics*, 5, p. 8. doi: 10.3389/fgene.2014.00008.

Kast, R. E., Karpel-Massler, G. and Halatsch, M.-E. (2014) 'CUSP9* treatment protocol for recurrent glioblastoma: aprepitant, artesunate, auranofin, captopril, celecoxib, disulfiram, itraconazole, ritonavir, sertraline augmenting continuous low dose temozolomide.', *Oncotarget*. Impact Journals, LLC, 5(18), pp. 8052–82. doi: 10.18632/oncotarget.2408.

Katakowski, M. *et al.* (2013) 'Exosomes from marrow stromal cells expressing miR-146b inhibit glioma growth.', *Cancer letters*. Ireland, 335(1), pp. 201–204. doi: 10.1016/j.canlet.2013.02.019.

Kato, M. *et al.* (2007) 'Distinct structural mechanisms for inhibition of pyruvate dehydrogenase kinase isoforms by AZD7545, dichloroacetate, and radicicol.', *Structure (London, England : 1993)*. Elsevier, 15(8), pp. 992–1004. doi: 10.1016/j.str.2007.07.001.

Kato, Y. *et al.* (2013) 'Acidic extracellular microenvironment and cancer.', *Cancer cell international*. BioMed Central, 13(1), p. 89. doi: 10.1186/1475-2867-13-89.

Katoh, K. *et al.* (2001) 'Rho-Kinase–Mediated Contraction of Isolated Stress Fibers', *The Journal of Cell Biology*, 153(3), pp. 569–584. doi: 10.1083/jcb.153.3.569.

Kaur, B. *et al.* (2005) 'Hypoxia and the hypoxia-inducible-factor pathway in glioma growth and angiogenesis.', *Neuro-oncology*, 7(2), pp. 134–53.

doi: 10.1215/S1152851704001115.

Kefas, B. *et al.* (2008) 'microRNA-7 inhibits the epidermal growth factor receptor and the Akt pathway and is down-regulated in glioblastoma.', *Cancer research*, 68(10), pp. 3566–72. Available at: http://cancerres.aacrjournals.org/content/68/10/3566.full (Accessed: 17 March 2016).

Kefas, B. *et al.* (2009) 'The neuronal microRNA miR-326 acts in a feedback loop with notch and has therapeutic potential against brain tumors.', *The Journal of neuroscience : the official journal of the Society for Neuroscience*. United States, 29(48), pp. 15161–15168. doi: 10.1523/JNEUROSCI.4966-09.2009.

Kefas, B. *et al.* (2010) 'Pyruvate kinase M2 is a target of the tumor-suppressive microRNA-326 and regulates the survival of glioma cells.', *Neuro-oncology*, 12(11), pp. 1102–12. doi: 10.1093/neuonc/noq080.

Kennedy, J. A. *et al.* (2000) 'Effect of perhexiline and oxfenicine on myocardial function and metabolism during low-flow ischemia/reperfusion in the isolated rat heart.', *Journal of cardiovascular pharmacology*, 36(6), pp. 794–801. Available at: http://www.ncbi.nlm.nih.gov/pubmed/11117381 (Accessed: 20 March 2019).

Kennedy, J. A., Unger, S. A. and Horowitz, J. D. (1996) 'Inhibition of carnitine palmitoyltransferase-1 in rat heart and liver by perhexiline and

amiodarone.', *Biochemical pharmacology*, 52(2), pp. 273–80. Available at: http://www.ncbi.nlm.nih.gov/pubmed/8694852 (Accessed: 20 March 2019).

Kesanakurti, D. *et al.* (2012) 'Functional cooperativity by direct interaction between PAK4 and MMP-2 in the regulation of anoikis resistance, migration and invasion in glioma', *Cell Death & Disease*. Nature Publishing Group, 3(12), pp. e445–e445. doi: 10.1038/cddis.2012.182.

Khalil, A. A. *et al.* (2017) 'Collective invasion in ductal and lobular breast cancer associates with distant metastasis', *Clinical & Experimental Metastasis*. Springer, 34(6–7), pp. 421–429. doi: 10.1007/s10585-017-9858-6.

Khalil, A. A. and Friedl, P. (2010) 'Determinants of leader cells in collective cell migration', *Integrative Biology*. Narnia, 2(11–12), p. 568. doi: 10.1039/c0ib00052c.

Khan, A. A. *et al.* (2009) 'Transfection of small RNAs globally perturbs gene regulation by endogenous microRNAs', *Nature Biotechnology*, 27(6), pp. 549–555. doi: 10.1038/nbt.1543.

Khandekar, M. J., Cohen, P. and Spiegelman, B. M. (2011) 'Molecular mechanisms of cancer development in obesity', *Nature Reviews Cancer*, 11(12), pp. 886–895. doi: 10.1038/nrc3174.

Kichukova, T. M. *et al.* (2017) 'Profiling of Circulating Serum MicroRNAs in Children with Autism Spectrum Disorder using Stem-loop qRT-PCR Assay',

Folia Medica, 59(1), pp. 43–52. doi: 10.1515/folmed-2017-0009.

Kim, H. *et al.* (2010) 'Integrative genome analysis reveals an oncomir/oncogene cluster regulating glioblastoma survivorship.', *Proceedings of the National Academy of Sciences of the United States of America*, 107(5), pp. 2183–8. Available at: http://www.pubmedcentral.nih.gov/articlerender.fcgi?artid=2836668&tool=pmcentrez&rendertype=abstract (Accessed: 4 April 2016).

Kim, K.-H. *et al.* (2001) 'Potential Mechanisms for the Inhibition of Tumor Cell Growth by Manganese Superoxide Dismutase', *Antioxidants & Redox Signaling*. Mary Ann Liebert, Inc. , 3(3), pp. 361–373. doi: 10.1089/15230860152409013.

Kimura, K. *et al.* (1996) 'Regulation of myosin phosphatase by Rho and Rho-associated kinase (Rho-kinase)', *Science (New York, N.Y.)*, 273(5272), pp. 245–8. Available at: http://www.ncbi.nlm.nih.gov/pubmed/8662509 (Accessed: 19 May 2019).

KIRBY, K. S. (1956) 'A new method for the isolation of ribonucleic acids from mammalian tissues.', *The Biochemical journal*, 64(3), pp. 405–8. Available at: http://www.pubmedcentral.nih.gov/articlerender.fcgi?artid=1199750&tool=pmcentrez&rendertype=abstract (Accessed: 6 August 2016).

Kleihues, P. and Ohgaki, H. (1999) 'Primary and secondary glioblastomas: From concept to clinicaldiagnosis', *Neuro-Oncology*, 1(1), pp. 44–51.

Available at: http://neuro-oncology.oxfordjournals.org/content/1/1/44.abstract?ijkey=c912d1776436b257f83d4039d938833463ed2462&keytype2=tf_ipsecsha (Accessed: 29 November 2015).

Klink, B. *et al.* (2013) 'A Novel, Diffusely Infiltrative Xenograft Model of Human Anaplastic Oligodendroglioma with Mutations in FUBP1, CIC, and IDH1', *PLoS ONE*. Edited by I. Ulasov, 8(3), p. e59773. doi: 10.1371/journal.pone.0059773.

Kloosterhof, N. K. *et al.* (2011) 'Isocitrate dehydrogenase-1 mutations: a fundamentally new understanding of diffuse glioma?', *The Lancet. Oncology*, 12(1), pp. 83–91. doi: 10.1016/S1470-2045(10)70053-X.

Knyazev, E. N. *et al.* (2016) 'Plasma Levels of hsa-miR-619-5p and hsa-miR-1184 Differ in Prostatic Benign Hyperplasia and Cancer', *Bulletin of Experimental Biology and Medicine*, 161(1), pp. 108–111. doi: 10.1007/s10517-016-3357-7.

Kohe, S. *et al.* (2017) 'Immunohistochemical staining of lipid droplets with adipophilin in paraffin-embedded glioma tissue identifies an association between lipid droplets and tumour grade', *Journal of Histology and Histopathology*, 4(1), p. 4. doi: 10.7243/2055-091X-4-4.

Kondoh, H. *et al.* (2007) 'Protection from oxidative stress by enhanced glycolysis; a possible mechanism of cellular immortalization.', *Histology and histopathology*, 22(1), pp. 85–90. Available at:

http://www.ncbi.nlm.nih.gov/pubmed/17128414 (Accessed: 7 June 2016).

Koo, S. *et al.* (2012) 'Serial selection for invasiveness increases expression of miR-143/miR-145 in glioblastoma cell lines.', *BMC cancer*. BioMed Central, 12(1), p. 143. Available at: http://bmccancer.biomedcentral.com/articles/10.1186/1471-2407-12-143 (Accessed: 4 June 2016).

Kosaka, T. *et al.* (2006) 'Analysis of epidermal growth factor receptor gene mutation in patients with non-small cell lung cancer and acquired resistance to gefitinib', *Clinical Cancer Research*, 12(19), pp. 5764–5769. doi: 10.1158/1078-0432.CCR-06-0714.

Koshy, M. *et al.* (2012) 'Improved survival time trends for glioblastoma using the SEER 17 population-based registries.', *Journal of neuro-oncology*, 107(1), pp. 207–12. Available at: http://www.pubmedcentral.nih.gov/articlerender.fcgi?artid=4077033&tool=pmcentrez&rendertype=abstract (Accessed: 5 March 2016).

Kostoulas, G. *et al.* (1999) 'Stimulation of angiogenesis through cathepsin B inactivation of the tissue inhibitors of matrix metalloproteinases.', *FEBS letters*, 455(3), pp. 286–90. Available at: http://www.ncbi.nlm.nih.gov/pubmed/10437790 (Accessed: 12 May 2019).

Kraus, A. C. *et al.* (2002) 'In vitro chemo- and radio-resistance in small cell lung cancer correlates with cell adhesion and constitutive activation of AKT and MAP kinase pathways', *Oncogene*, 21(57), pp. 8683–8695. doi:

10.1038/sj.onc.1205939.

Krause, M. R. and Regen, S. L. (2014) 'The Structural Role of Cholesterol in Cell Membranes: From Condensed Bilayers to Lipid Rafts', *Accounts of Chemical Research*, 47(12), pp. 3512–3521. doi: 10.1021/ar500260t.

Kubiatowski, T. *et al.* (2001) 'Association of increased phosphatidylinositol 3-kinase signaling with increased invasiveness and gelatinase activity in malignant gliomas', *Journal of Neurosurgery*, 95(3), pp. 480–488. doi: 10.3171/jns.2001.95.3.0480.

Kuhlmann, J. D. *et al.* (2014) 'Circulating U2 Small Nuclear RNA Fragments as a Novel Diagnostic Tool for Patients with Epithelial Ovarian Cancer', *Clinical Chemistry*, 60(1), pp. 206–213. doi: 10.1373/clinchem.2013.213066.

Kuhn, D. E. *et al.* (2008) 'Experimental validation of miRNA targets.', *Methods (San Diego, Calif.)*. NIH Public Access, 44(1), pp. 47–54. doi: 10.1016/j.ymeth.2007.09.005.

Kuleshov, M. V *et al.* (2016) 'Enrichr: a comprehensive gene set enrichment analysis web server 2016 update.', *Nucleic acids research*. Oxford University Press, 44(W1), pp. W90-7. doi: 10.1093/nar/gkw377.

Kumar, P. *et al.* (2007) 'Transvascular delivery of small interfering RNA to the central nervous system.', *Nature*, 448(7149), pp. 39–43. doi: 10.1038/nature05901.

Kung, C.-P. and Raab-Traub, N. (2008) 'Epstein-Barr virus latent

membrane protein 1 induces expression of the epidermal growth factor receptor through effects on Bcl-3 and STAT3.', *Journal of virology*, 82(11), pp. 5486–93. Available at: http://jvi.asm.org/content/82/11/5486 (Accessed: 4 April 2016).

Kunigal, S. *et al.* (2006) 'SPARC-induced migration of glioblastoma cell lines via uPA-uPAR signaling and activation of small GTPase RhoA.', *International journal of oncology*. NIH Public Access, 29(6), pp. 1349–57. Available at: http://www.ncbi.nlm.nih.gov/pubmed/17088972 (Accessed: 22 July 2019).

Kuo, W.-T. *et al.* (2015) 'Bioinformatic Interrogation of 5p-arm and 3p-arm Specific miRNA Expression Using TCGA Datasets.', *Journal of clinical medicine*, 4(9), pp. 1798–814. doi: 10.3390/jcm4091798.

Laberge, R.-M. *et al.* (2013) 'Mitochondrial DNA damage induces apoptosis in senescent cells.', *Cell death & disease*. Macmillan Publishers Limited, 4, p. e727. doi: 10.1038/cddis.2013.199.

Lafitte, F. *et al.* (2001) 'Multiple glioblastomas: CT and MR features', *European Radiology*. Springer-Verlag, 11(1), pp. 131–136. doi: 10.1007/s003300000538.

Lai, Y.-H. *et al.* (2018) 'MiR-31-5p-ACOX1 Axis Enhances Tumorigenic Fitness in Oral Squamous Cell Carcinoma Via the Promigratory Prostaglandin E2.', *Theranostics*. Ivyspring International Publisher, 8(2), pp. 486–504. doi: 10.7150/thno.22059.

Lakowicz, J. R. (1988) 'Principles of frequency-domain fluorescence

spectroscopy and applications to cell membranes.', *Sub-cellular biochemistry*. United States, 13, pp. 89–126. doi: 10.1007/978-1-4613-9359-7_3.

Lamouille, S., Xu, J. and Derynck, R. (2014) 'Molecular mechanisms of epithelial-mesenchymal transition.', *Nature reviews. Molecular cell biology*. NIH Public Access, 15(3), pp. 178–96. doi: 10.1038/nrm3758.

Lan, F. *et al.* (2015) 'miR-144-3p exerts anti-tumor effects in glioblastoma by targeting c-Met.', *Journal of neurochemistry*, 135(2), pp. 274–86. Available at: http://www.ncbi.nlm.nih.gov/pubmed/26250785 (Accessed: 17 May 2016).

Langbein, S. *et al.* (2006) 'Expression of transketolase TKTL1 predicts colon and urothelial cancer patient survival: Warburg effect reinterpreted', *British Journal of Cancer*, 94(4), pp. 578–585. doi: 10.1038/sj.bjc.6602962.

Lara-Velazquez, M. *et al.* (2019) 'The Study of Brain Tumor Stem Cell Migration.', *Methods in molecular biology (Clifton, N.J.)*. NIH Public Access, 1869, pp. 93–104. doi: 10.1007/978-1-4939-8805-1_9.

Larsson, O. (1996) 'HMG-CoA reductase inhibitors: role in normal and malignant cells.', *Critical reviews in oncology/hematology*, 22(3), pp. 197–212. Available at: http://www.ncbi.nlm.nih.gov/pubmed/8793275 (Accessed: 27 July 2019).

Lazo, P. A. (1981) 'Amino acids and glucose utilization by different metabolic pathways in ascites-tumour cells.', *European journal of*

biochemistry / FEBS, 117(1), pp. 19–25. Available at: http://www.ncbi.nlm.nih.gov/pubmed/6790281 (Accessed: 12 March 2016).

Lee, H. K. *et al.* (2013) 'Mesenchymal stem cells deliver synthetic microRNA mimics to glioma cells and glioma stem cells and inhibit their cell migration and self-renewal.', *Oncotarget*, 4(2), pp. 346–61. doi: 10.18632/oncotarget.868.

Lee, J. *et al.* (2006) 'Tumor stem cells derived from glioblastomas cultured in bFGF and EGF more closely mirror the phenotype and genotype of primary tumors than do serum-cultured cell lines', *Cancer Cell*, 9(5), pp. 391–403. doi: 10.1016/j.ccr.2006.03.030.

Lee, K. S. *et al.* (2013) 'Immunohistochemical classification of primary and secondary glioblastomas.', *Korean journal of pathology*. Korean Society of Pathologists and Korean Society for Cytopathology, 47(6), pp. 541–8. doi: 10.4132/KoreanJPathol.2013.47.6.541.

Lee, Y. *et al.* (2003) 'The nuclear RNase III Drosha initiates microRNA processing.', *Nature*, 425(6956), pp. 415–9. Available at: http://dx.doi.org/10.1038/nature01957 (Accessed: 17 February 2015).

Lee, Y. *et al.* (2004) 'MicroRNA genes are transcribed by RNA polymerase II.', *The EMBO journal*, 23(20), pp. 4051–60. doi: 10.1038/sj.emboj.7600385.

Lee, Y. *et al.* (2017) 'Randomized Phase II Study of Afatinib Plus

Simvastatin Versus Afatinib Alone in Previously Treated Patients with Advanced Nonadenocarcinomatous Non-small Cell Lung Cancer', *Cancer Research and Treatment*, 49(4), pp. 1001–1011. doi: 10.4143/crt.2016.546.

Lehmann, S. *et al.* (2017) 'Hypoxia Induces a HIF-1-Dependent Transition from Collective-to-Amoeboid Dissemination in Epithelial Cancer Cells', *Current Biology*, 27(3), pp. 392–400. doi: 10.1016/j.cub.2016.11.057.

Lei, C.-J. *et al.* (2016) 'Effect of co-transfection of miR-520c-3p and miR-132 on proliferation and apoptosis of hepatocellular carcinoma Huh7', *Asian Pacific Journal of Tropical Medicine*, 9(9), pp. 898–902. doi: https://doi.org/10.1016/j.apjtm.2016.07.015.

van der Leij, F. R. *et al.* (2000) 'Genomics of the Human Carnitine Acyltransferase Genes', *Molecular Genetics and Metabolism*. Academic Press, 71(1–2), pp. 139–153. doi: 10.1006/MGME.2000.3055.

Leins, A. *et al.* (2003) 'Expression of tenascin-C in various human brain tumors and its relevance for survival in patients with astrocytoma', *Cancer*, 98(11), pp. 2430–2439. doi: 10.1002/cncr.11796.

Lemmon, M. A. and Schlessinger, J. (2010) 'Cell signaling by receptor tyrosine kinases.', *Cell*, 141(7), pp. 1117–34. Available at: http://www.pubmedcentral.nih.gov/articlerender.fcgi?artid=2914105&tool=pmcentrez&rendertype=abstract (Accessed: 10 July 2014).

Lenting, K. *et al.* (2017) 'Glioma: experimental models and reality.', *Acta*

neuropathologica. Springer, 133(2), pp. 263–282. doi: 10.1007/s00401-017-1671-4.

Leung, A. K. L. and Sharp, P. A. (2010a) 'MicroRNA functions in stress responses.', *Molecular cell*, 40(2), pp. 205–15. doi: 10.1016/j.molcel.2010.09.027.

Leung, A. K. L. and Sharp, P. A. (2010b) 'MicroRNA functions in stress responses.', *Molecular cell*, 40(2), pp. 205–15. doi: 10.1016/j.molcel.2010.09.027.

Levin, V. A. *et al.* (2002) 'Randomized phase II study of temozolomide (TMZ) with and without the matrix metalloprotease (MMP) inhibitor prinomastat in patients (pts) with glioblastoma multiforme (GBM) following best surgery and radiation therapy', in *ASCO 2002 Annual Conference*. Available at: https://virtualtrials.com/newsarticle.cfm?item=1663.

Levin, V. A. *et al.* (2006) 'Randomized, double-blind, placebo-controlled trial of marimastat in glioblastoma multiforme patients following surgery and irradiation★', *Journal of Neuro-Oncology*, 78(3), pp. 295–302. doi: 10.1007/s11060-005-9098-5.

Levin, V. A. *et al.* (2012) 'Protein and phosphoprotein levels in glioma and adenocarcinoma cell lines grown in normoxia and hypoxia in monolayer and three-dimensional cultures', *Proteome Science*. BioMed Central, 10(1), p. 5. doi: 10.1186/1477-5956-10-5.

Lewis, B. P., Burge, C. B. and Bartel, D. P. (2005) 'Conserved Seed Pairing, Often Flanked by Adenosines, Indicates that Thousands of Human Genes are MicroRNA Targets', *Cell*, 120(1), pp. 15–20. doi: 10.1016/j.cell.2004.12.035.

Lewis, W. H. (1934) 'On the locomotion of the polymorphonuclear neutrophiles of the rat in autoplasma cultures', *Bull. Johns Hopkins Hosp*.

Li, C. *et al.* (2016) 'miR-133b inhibits glioma cell proliferation and invasion by targeting Sirt1.', *Oncotarget*. Impact Journals, LLC, 7(24), pp. 36247–36254. doi: 10.18632/oncotarget.9198.

Li, P. *et al.* (2017) 'MALAT1 Is Associated with Poor Response to Oxaliplatin-Based Chemotherapy in Colorectal Cancer Patients and Promotes Chemoresistance through EZH2.', *Molecular cancer therapeutics*. American Association for Cancer Research, 16(4), pp. 739–751. doi: 10.1158/1535-7163.MCT-16-0591.

Li, W.-Q. *et al.* (2015) 'miR-27a suppresses the clonogenic growth and migration of human glioblastoma multiforme cells by targeting BTG2.', *International journal of oncology*, 46(4), pp. 1601–8. doi: 10.3892/ijo.2015.2843.

Li, X.-T. *et al.* (2015) 'miR-494-3p Regulates Cellular Proliferation, Invasion, Migration, and Apoptosis by PTEN/AKT Signaling in Human Glioblastoma Cells.', *Cellular and molecular neurobiology*, 35(5), pp. 679–87. Available

at:
http://www.pubmedcentral.nih.gov/articlerender.fcgi?artid=4477718&tool=pmcentrez&rendertype=abstract (Accessed: 4 June 2016).

Li, X. *et al.* (2015) 'Two mature products of MIR-491 coordinate to suppress key cancer hallmarks in glioblastoma', *Oncogene*, 34(13), pp. 1619–1628. doi: 10.1038/onc.2014.98.

Li, Xin *et al.* (2014) 'A Systematic In Silico Mining of the Mechanistic Implications and Therapeutic Potentials of Estrogen Receptor (ER)-α in Breast Cancer', *PLoS ONE*. Edited by W. Xu. Public Library of Science, 9(3), p. e91894. doi: 10.1371/journal.pone.0091894.

Li, Yiming *et al.* (2009) 'MicroRNA-21 targets LRRFIP1 and contributes to VM-26 resistance in glioblastoma multiforme.', *Brain research*, 1286, pp. 13–8. Available at: http://www.ncbi.nlm.nih.gov/pubmed/19559015 (Accessed: 28 May 2016).

Li, Yunqing *et al.* (2009) 'MicroRNA-34a inhibits glioblastoma growth by targeting multiple oncogenes.', *Cancer research*, 69(19), pp. 7569–76. Available at: http://www.pubmedcentral.nih.gov/articlerender.fcgi?artid=2756313&tool=pmcentrez&rendertype=abstract (Accessed: 13 March 2016).

Li, Y. *et al.* (2013) 'miR-146b-5p inhibits glioma migration and invasion by targeting MMP16.', *Cancer letters*. Ireland, 339(2), pp. 260–269. doi: 10.1016/j.canlet.2013.06.018.

Li, Y. *et al.* (2016) 'MicroRNA-132 cause apoptosis of glioma cells through blockade of the SREBP-1c metabolic pathway related to SIRT1', *Biomedicine & Pharmacotherapy*, 78, pp. 177–184. doi: 10.1016/j.biopha.2016.01.022.

Li, Y., Zong, W.-X. and Ding, W.-X. (2017) 'Recycling the danger via lipid droplet biogenesis after autophagy', *Autophagy*. Taylor & Francis, 13(11), pp. 1995–1997. doi: 10.1080/15548627.2017.1371394.

Li, Z. and Rana, T. M. (2014) 'Therapeutic targeting of microRNAs: current status and future challenges', *Nature Reviews Drug Discovery*. Nature Publishing Group, 13(8), pp. 622–638. doi: 10.1038/nrd4359.

Li, Z. and Vance, D. E. (2008) 'Phosphatidylcholine and choline homeostasis.', *Journal of lipid research*. American Society for Biochemistry and Molecular Biology, 49(6), pp. 1187–94. doi: 10.1194/jlr.R700019-JLR200.

Liao, C., Chen, W. and Wang, J. (2019) 'MicroRNA-20a Regulates Glioma Cell Proliferation, Invasion, and Apoptosis by Targeting CUGBP Elav-Like Family Member 2', *World Neurosurgery*, 121, pp. e519–e527. doi: 10.1016/j.wneu.2018.09.155.

Lidar, Z. *et al.* (2004) 'Convection-enhanced delivery of paclitaxel for the treatment of recurrent malignant glioma: a phase I/II clinical study.', *Journal of neurosurgery*, 100(3), pp. 472–9. Available at: http://www.ncbi.nlm.nih.gov/pubmed/15035283 (Accessed: 28 May 2016).

Liegl, B. *et al.* (2008) 'Heterogeneity of kinase inhibitor resistance mechanisms in GIST', *The Journal of Pathology*, 216(1), pp. 64–74. doi: 10.1002/path.2382.

Ligon, K. L. *et al.* (2004) 'The oligodendroglial lineage marker OLIG2 is universally expressed in diffuse gliomas.', *Journal of neuropathology and experimental neurology*, 63(5), pp. 499–509. Available at: http://www.ncbi.nlm.nih.gov/pubmed/15198128 (Accessed: 4 February 2019).

Lim, L. P. *et al.* (2005) 'Microarray analysis shows that some microRNAs downregulate large numbers of target mRNAs', *Nature*, 433(7027), pp. 769–773. doi: 10.1038/nature03315.

Lim, S. H. *et al.* (2015) 'A randomised, double-blind, placebo-controlled multi-centre phase III trial of XELIRI/FOLFIRI plus simvastatin for patients with metastatic colorectal cancer', *British Journal of Cancer*, 113(10), pp. 1421–1426. doi: 10.1038/bjc.2015.371.

Lin, H. *et al.* (2017) 'Fatty acid oxidation is required for the respiration and proliferation of malignant glioma cells.', *Neuro-oncology*. Oxford University Press, 19(1), pp. 43–54. doi: 10.1093/neuonc/now128.

Lin, S. and Gregory, R. I. (2015) 'MicroRNA biogenesis pathways in cancer', *Nature Reviews Cancer*. Nature Publishing Group, 15(6), pp. 321–333. doi: 10.1038/nrc3932.

Lindon, J. C. *et al.* (2003) 'Contemporary issues in toxicology the role of

metabonomics in toxicology and its evaluation by the COMET project.', *Toxicology and applied pharmacology*, 187(3), pp. 137–46. Available at: http://www.ncbi.nlm.nih.gov/pubmed/12662897 (Accessed: 24 July 2019).

Ling, N. *et al.* (2013) 'microRNA-155 regulates cell proliferation and invasion by targeting FOXO3a in glioma.', *Oncology reports*. Greece, 30(5), pp. 2111–2118. doi: 10.3892/or.2013.2685.

Lintz, M., Muñoz, A. and Reinhart-King, C. A. (2017) 'The Mechanics of Single Cell and Collective Migration of Tumor Cells.', *Journal of biomechanical engineering*. American Society of Mechanical Engineers, 139(2), p. 0210051. doi: 10.1115/1.4035121.

Liu, H.-L. *et al.* (2010) 'Blood-brain barrier disruption with focused ultrasound enhances delivery of chemotherapeutic drugs for glioblastoma treatment.', *Radiology*, 255(2), pp. 415–25. doi: 10.1148/radiol.10090699.

Liu, J. *et al.* (2005) 'MicroRNA-dependent localization of targeted mRNAs to mammalian P-bodies', *Nature Cell Biology*. Nature Publishing Group, 7(7), pp. 719–723. doi: 10.1038/ncb1274.

Liu, J. *et al.* (2013) 'Phosphoglycerate dehydrogenase induces glioma cells proliferation and invasion by stabilizing forkhead box M1', *Journal of Neuro-Oncology*, 111(3), pp. 245–255. doi: 10.1007/s11060-012-1018-x.

Liu, N. and Olson, E. N. (2010) 'MicroRNA regulatory networks in cardiovascular development.', *Developmental cell*. NIH Public Access, 18(4), pp. 510–25. doi: 10.1016/j.devcel.2010.03.010.

Liu, Q. *et al.* (2015) 'miR-155 Regulates Glioma Cells Invasion and Chemosensitivity by p38 Isforms In Vitro.', *Journal of cellular biochemistry*, 116(7), pp. 1213–21. doi: 10.1002/jcb.25073.

Liu, S., Sun, J. and Lan, Q. (2013) 'TGF-β-induced miR10a/b expression promotes human glioma cell migration by targeting PTEN', *Molecular Medicine Reports*. Spandidos Publications, 8(6), pp. 1741–1746. Available at: http://www.spandidos-publications.com/mmr/8/6/1741/abstract (Accessed: 4 June 2016).

Liu, X. *et al.* (2013) 'Poly(amido amine) is an ideal carrier of miR-7 for enhancing gene silencing effects on the EGFR pathway in U251 glioma cells.', *Oncology reports*. Greece, 29(4), pp. 1387–1394. doi: 10.3892/or.2013.2283.

Liu, Y. (2006) 'Fatty acid oxidation is a dominant bioenergetic pathway in prostate cancer', *Prostate Cancer and Prostatic Diseases*, 9(3), pp. 230–234. doi: 10.1038/sj.pcan.4500879.

Liu, Y. *et al.* (2009) 'The expression and significance of HIF-1alpha and GLUT-3 in glioma.', *Brain research*, 1304, pp. 149–54. doi: 10.1016/j.brainres.2009.09.083.

Liu, Y. *et al.* (2012) 'MiR-218 reverses high invasiveness of glioblastoma cells by targeting the oncogenic transcription factor LEF1.', *Oncology reports*. Greece, 28(3), pp. 1013–1021. doi: 10.3892/or.2012.1902.

Liu, Y., Duan, N. and Duan, S. (2018) 'MiR-29a Inhibits Glioma Tumorigenesis through a Negative Feedback Loop of TRAF4/Akt Signaling', *BioMed Research International*. Hindawi, 2018, pp. 1–8. doi: 10.1155/2018/2461363.

Liu, Z. *et al.* (2014) 'miR-7 inhibits glioblastoma growth by simultaneously interfering with the PI3K/ATK and Raf/MEK/ERK pathways', *International Journal of Oncology*. Spandidos Publications, 44(5), pp. 1571–1580. Available at: http://www.spandidos-publications.com/ijo/44/5/1571/abstract (Accessed: 17 March 2016).

Liu, Z. *et al.* (2017) 'MicroRNA-153 regulates glutamine metabolism in glioblastoma through targeting glutaminase', *Tumor Biology*, 39(2), p. 101042831769142. doi: 10.1177/1010428317691429.

Löffler, D. *et al.* (2007) 'Interleukin-6 dependent survival of multiple myeloma cells involves the Stat3-mediated induction of microRNA-21 through a highly conserved enhancer.', *Blood*, 110(4), pp. 1330–3. Available at: http://www.ncbi.nlm.nih.gov/pubmed/17496199 (Accessed: 4 April 2016).

Lohr, J. G. *et al.* (2014) 'Widespread Genetic Heterogeneity in Multiple Myeloma: Implications for Targeted Therapy', *Cancer Cell*, 25(1), pp. 91–101. doi: 10.1016/j.ccr.2013.12.015.

Louis, D. N. *et al.* (2007) 'The 2007 WHO classification of tumours of the central nervous system.', *Acta neuropathologica*, 114(2), pp. 97–109.

Available at: http://www.pubmedcentral.nih.gov/articlerender.fcgi?artid=1929165&tool=pmcentrez&rendertype=abstract (Accessed: 11 July 2014).

Louis, D. N. *et al.* (2016) 'The 2016 World Health Organization Classification of Tumors of the Central Nervous System: a summary.', *Acta neuropathologica*, 131(6), pp. 803–20. doi: 10.1007/s00401-016-1545-1.

Lu, K. V *et al.* (2012) 'VEGF inhibits tumor cell invasion and mesenchymal transition through a MET/VEGFR2 complex.', *Cancer cell*. NIH Public Access, 22(1), pp. 21–35. doi: 10.1016/j.ccr.2012.05.037.

Lu, S. C. (2009) 'Regulation of glutathione synthesis.', *Molecular aspects of medicine*. NIH Public Access, 30(1–2), pp. 42–59. doi: 10.1016/j.mam.2008.05.005.

Lu, W. *et al.* (2010) 'Metabolomic Analysis via Reversed-Phase Ion-Pairing Liquid Chromatography Coupled to a Stand Alone Orbitrap Mass Spectrometer', *Analytical Chemistry*, 82(8), pp. 3212–3221. doi: 10.1021/ac902837x.

Lu, W. *et al.* (2017) 'Metabolite Measurement: Pitfalls to Avoid and Practices to Follow', *Annual Review of Biochemistry*, 86(1), pp. 277–304. doi: 10.1146/annurev-biochem-061516-044952.

Lu, Z. J. *et al.* (2011) 'The effect of miR-7 on behavior and global protein expression in glioma cell lines.', *Electrophoresis*, 32(24), pp. 3612–20. Available at: http://www.ncbi.nlm.nih.gov/pubmed/22120825 (Accessed:

3 April 2016).

Luan, W. *et al.* (2015) 'PKM2 promotes glucose metabolism and cell growth in gliomas through a mechanism involving a let-7a/c-Myc/hnRNPA1 feedback loop.', *Oncotarget*, 6(15), pp. 13006–18. Available at: http://www.pubmedcentral.nih.gov/articlerender.fcgi?artid=4536995&tool=pmcentrez&rendertype=abstract (Accessed: 24 November 2015).

Luchman, H. A. *et al.* (2012) 'An in vivo patient-derived model of endogenous IDH1-mutant glioma', *Neuro-Oncology*, 14(2), pp. 184–191. doi: 10.1093/neuonc/nor207.

Lun, M. *et al.* (2011) 'The natural history of extracranial metastasis from glioblastoma multiforme', *Journal of Neuro-Oncology*, 105(2), pp. 261–273. doi: 10.1007/s11060-011-0575-8.

Lunt, S. Y. and Vander Heiden, M. G. (2011) 'Aerobic Glycolysis: Meeting the Metabolic Requirements of Cell Proliferation', *Annual Review of Cell and Developmental Biology*, 27(1), pp. 441–464. doi: 10.1146/annurev-cellbio-092910-154237.

Lykidis, A., Murti, K. G. and Jackowski, S. (1998) 'Cloning and characterization of a second human CTP:phosphocholine cytidylyltransferase.', *The Journal of biological chemistry*, 273(22), pp. 14022–9. Available at: http://www.ncbi.nlm.nih.gov/pubmed/9593753 (Accessed: 27 January 2019).

Machová, E. *et al.* (2009) 'Detection of choline transporter-like 1 protein

CTL1 in neuroblastoma × glioma cells and in the CNS, and its role in choline uptake', *Journal of Neurochemistry*. John Wiley & Sons, Ltd (10.1111), 110(4), pp. 1297–1309. doi: 10.1111/j.1471-4159.2009.06218.x.

Madhavan, M. *et al.* (2001) 'Cadherins as Predictive Markers of Nodal Metastasis in Breast Cancer', *Modern Pathology*, 14(5), pp. 423–427. doi: 10.1038/modpathol.3880329.

Majewski, N. *et al.* (2004) 'Hexokinase-Mitochondria Interaction Mediated by Akt Is Required to Inhibit Apoptosis in the Presence or Absence of Bax and Bak', *Molecular Cell*, 16(5), pp. 819–830. doi: 10.1016/j.molcel.2004.11.014.

Mäkelä, T. P. *et al.* (1992) 'Alternative forms of Max as enhancers or suppressors of Myc-ras cotransformation.', *Science (New York, N.Y.)*, 256(5055), pp. 373–7. Available at: http://www.ncbi.nlm.nih.gov/pubmed/1566084 (Accessed: 24 March 2016).

Malzkorn, B. *et al.* (2010) 'Identification and functional characterization of microRNAs involved in the malignant progression of gliomas.', *Brain pathology (Zurich, Switzerland)*. Switzerland, 20(3), pp. 539–550. doi: 10.1111/j.1750-3639.2009.00328.x.

Manchester, K. L. (1995) 'Value of A260/A280 ratios for measurement of purity of nucleic acids.', *BioTechniques*, 19(2), pp. 208–10. Available at:

http://www.ncbi.nlm.nih.gov/pubmed/8527139 (Accessed: 6 August 2016).

Manser, E. *et al.* (1994) 'A brain serine/threonine protein kinase activated by Cdc42 and Rac1', *Nature*. Nature Publishing Group, 367(6458), pp. 40–46. doi: 10.1038/367040a0.

Marabita, F. *et al.* (2016) 'Normalization of circulating microRNA expression data obtained by quantitative real-time RT-PCR.', *Briefings in bioinformatics*. Oxford University Press, 17(2), pp. 204–12. doi: 10.1093/bib/bbv056.

Markovic, D. S. *et al.* (2009) 'Gliomas induce and exploit microglial MT1-MMP expression for tumor expansion', *Proceedings of the National Academy of Sciences*, 106(30), pp. 12530–12535. doi: 10.1073/pnas.0804273106.

Marrone, K. A. *et al.* (2018) 'A Randomized Phase II Study of Metformin plus Paclitaxel/Carboplatin/Bevacizumab in Patients with Chemotherapy-Naïve Advanced or Metastatic Nonsquamous Non-Small Cell Lung Cancer.', *The oncologist*. AlphaMed Press, 23(7), pp. 859–865. doi: 10.1634/theoncologist.2017-0465.

Martin-McGill, K. J. *et al.* (2017) 'Ketogenic diets as an adjuvant therapy in glioblastoma (the KEATING trial): study protocol for a randomised pilot study.', *Pilot and feasibility studies*. BioMed Central, 3, p. 67. doi: 10.1186/s40814-017-0209-9.

Martinez-Sanchez, A. and Murphy, C. L. (2013) 'MicroRNA Target

Identification—Experimental Approaches', *Biology*. Multidisciplinary Digital Publishing Institute (MDPI), 2(1), p. 189. doi: 10.3390/BIOLOGY2010189.

Masson, N. and Ratcliffe, P. J. (2014) 'Hypoxia signaling pathways in cancer metabolism: the importance of co-selecting interconnected physiological pathways.', *Cancer & metabolism*, 2(1), p. 3. doi: 10.1186/2049-3002-2-3.

Masui, K. *et al.* (2013) 'mTOR complex 2 controls glycolytic metabolism in glioblastoma through FoxO acetylation and upregulation of c-Myc.', *Cell metabolism*, 18(5), pp. 726–39. Available at: http://www.pubmedcentral.nih.gov/articlerender.fcgi?artid=3840163&tool=pmcentrez&rendertype=abstract (Accessed: 24 February 2016).

Mathiisen, T. M. *et al.* (2010) 'The perivascular astroglial sheath provides a complete covering of the brain microvessels: An electron microscopic 3D reconstruction', *Glia*, 58(9), pp. 1094–1103. doi: 10.1002/glia.20990.

Mathupala, S. P. (2009) 'Delivery of small-interfering RNA (siRNA) to the brain.', *Expert opinion on therapeutic patents*, 19(2), pp. 137–40. doi: 10.1517/13543770802680195.

Mathupala, S. P., Ko, Y. H. and Pedersen, P. L. (2006) 'Hexokinase II: cancer's double-edged sword acting as both facilitator and gatekeeper of malignancy when bound to mitochondria.', *Oncogene*, 25(34), pp. 4777–86. doi: 10.1038/sj.onc.1209603.

Maus, A. and Peters, G. J. (2017) 'Glutamate and α-ketoglutarate: key

players in glioma metabolism', *Amino Acids*. Springer Vienna, 49(1), pp. 21–32. doi: 10.1007/s00726-016-2342-9.

Mazurek, S. *et al.* (2005) 'Pyruvate kinase type M2 and its role in tumor growth and spreading', *Seminars in Cancer Biology*, 15(4), pp. 300–308. doi: 10.1016/j.semcancer.2005.04.009.

McCall, M. N. and Almudevar, A. (2012) 'Affymetrix GeneChip microarray preprocessing for multivariate analyses.', *Briefings in bioinformatics*, 13(5), pp. 536–46. doi: 10.1093/bib/bbr072.

McGarry, J. D. and Brown, N. F. (1997) 'The Mitochondrial Carnitine Palmitoyltransferase System - From Concept to Molecular Analysis', *European Journal of Biochemistry*. John Wiley & Sons, Ltd (10.1111), 244(1), pp. 1–14. doi: 10.1111/j.1432-1033.1997.00001.x.

Mei, J., Bachoo, R. and Zhang, C.-L. (2011) 'MicroRNA-146a inhibits glioma development by targeting Notch1.', *Molecular and cellular biology*. United States, 31(17), pp. 3584–3592. doi: 10.1128/MCB.05821-11.

Meister, G. (2013) 'Argonaute proteins: functional insights and emerging roles.', *Nature reviews. Genetics*. Nature Publishing Group, a division of Macmillan Publishers Limited. All Rights Reserved., 14(7), pp. 447–59. Available at: http://dx.doi.org/10.1038/nrg3462 (Accessed: 6 July 2015).

Meister, G. and Tuschl, T. (2004) 'Mechanisms of gene silencing by double-stranded RNA.', *Nature*, 431(7006), pp. 343–9. Available at: http://dx.doi.org/10.1038/nature02873 (Accessed: 3 November 2015).

Mejia, N. R. and MacKenzie, R. E. (1988) 'NAD-dependent methylenetetrahydrofolate dehydrogenase-methenyltetrahydrofolate cyclohydrolase in transformed cells is a mitochondrial enzyme.', *Biochemical and biophysical research communications*, 155(1), pp. 1–6. doi: 10.1016/s0006-291x(88)81040-4.

Melone, M. A. B. *et al.* (2018) 'The carnitine system and cancer metabolic plasticity.', *Cell death & disease*. Nature Publishing Group, 9(2), p. 228. doi: 10.1038/s41419-018-0313-7.

Mendoza, M. C., Er, E. E. and Blenis, J. (2011) 'The Ras-ERK and PI3K-mTOR pathways: cross-talk and compensation.', *Trends in biochemical sciences*, 36(6), pp. 320–8. Available at: http://www.pubmedcentral.nih.gov/articlerender.fcgi?artid=3112285&tool=pmcentrez&rendertype=abstract (Accessed: 1 January 2015).

Menei, P. *et al.* (2004) 'Stereotaxic implantation of 5-fluorouracil-releasing microspheres in malignant glioma.', *Cancer*, 100(2), pp. 405–10. Available at: http://www.ncbi.nlm.nih.gov/pubmed/14716778 (Accessed: 28 May 2016).

Menzie, J., Prentice, H. and Wu, J.-Y. (2013) 'Neuroprotective Mechanisms of Taurine against Ischemic Stroke.', *Brain sciences*. Multidisciplinary Digital Publishing Institute (MDPI), 3(2), pp. 877–907. doi: 10.3390/brainsci3020877.

Merzak, A., Koocheckpour, S. and Pilkington, G. J. (1994) 'CD44 mediates

human glioma cell adhesion and invasion in vitro.', *Cancer research*, 54(15), pp. 3988–92. Available at: http://www.ncbi.nlm.nih.gov/pubmed/7518347 (Accessed: 13 May 2019).

Messali, A., Villacorta, R. and Hay, J. W. (2014) 'A review of the economic burden of glioblastoma and the cost effectiveness of pharmacologic treatments.', *PharmacoEconomics*, 32(12), pp. 1201–12. doi: 10.1007/s40273-014-0198-y.

Meyer, M. *et al.* (2015) 'Single cell-derived clonal analysis of human glioblastoma links functional and genomic heterogeneity.', *Proceedings of the National Academy of Sciences of the United States of America*, 112(3), pp. 851–6. doi: 10.1073/pnas.1320611111.

Michel, V. *et al.* (2006) 'Choline transport for phospholipid synthesis.', *Experimental biology and medicine (Maywood, N.J.)*, 231(5), pp. 490–504. Available at: http://www.ncbi.nlm.nih.gov/pubmed/16636297 (Accessed: 11 January 2019).

Michelakis, E. D. *et al.* (2010) 'Metabolic modulation of glioblastoma with dichloroacetate.', *Science translational medicine*, 2(31), p. 31ra34. doi: 10.1126/scitranslmed.3000677.

Michlewski, G. and Cáceres, J. F. (2010) 'Antagonistic role of hnRNP A1 and KSRP in the regulation of let-7a biogenesis.', *Nature structural & molecular biology*, 17(8), pp. 1011–8. doi: 10.1038/nsmb.1874.

Mihaylova, M. M. *et al.* (2011) 'Class IIa histone deacetylases are hormone-

activated regulators of FOXO and mammalian glucose homeostasis.', *Cell*, 145(4), pp. 607–21. Available at: http://www.pubmedcentral.nih.gov/articlerender.fcgi?artid=3117637&tool=pmcentrez&rendertype=abstract (Accessed: 28 February 2016).

Mili, S. and Steitz, J. A. (2004) 'Evidence for reassociation of RNA-binding proteins after cell lysis: implications for the interpretation of immunoprecipitation analyses.', *RNA (New York, N.Y.)*. Cold Spring Harbor Laboratory Press, 10(11), pp. 1692–4. doi: 10.1261/rna.7151404.

Minniti, G. *et al.* (2010) 'Patterns of failure and comparison of different target volume delineations in patients with glioblastoma treated with conformal radiotherapy plus concomitant and adjuvant temozolomide.', *Radiotherapy and oncology : journal of the European Society for Therapeutic Radiology and Oncology*, 97(3), pp. 377–81. doi: 10.1016/j.radonc.2010.08.020.

Misale, S. *et al.* (2012) 'Emergence of KRAS mutations and acquired resistance to anti-EGFR therapy in colorectal cancer', *Nature*, 486(7404), pp. 532–536. doi: 10.1038/nature11156.

Mitchison, T. (2011) 'Intravital imaging proposal', *Elsevier*. Available at: https://www.sciencedirect.com/science/article/pii/S0092867411013341 (Accessed: 22 July 2019).

Mohanam, Sanjeeva *et al.* (2001) 'Down-regulation of cathepsin B expression impairs the invasive and tumorigenic potential of human

glioblastoma cells', *Oncogene*, 20(28), pp. 3665–3673. doi: 10.1038/sj.onc.1204480.

Mohanam, S *et al.* (2001) 'Stable transfection of urokinase-type plasminogen activator antisense construct modulates invasion of human glioblastoma cells.', *Clinical cancer research : an official journal of the American Association for Cancer Research*, 7(8), pp. 2519–26. Available at: http://www.ncbi.nlm.nih.gov/pubmed/11489835 (Accessed: 12 May 2019).

Molina, J. R. *et al.* (2010) 'Invasive Glioblastoma Cells Acquire Stemness and Increased Akt Activation', *Neoplasia*. Elsevier, 12(6), pp. 453-IN5. doi: 10.1593/NEO.10126.

Montana, V. and Sontheimer, H. (2011) 'Bradykinin promotes the chemotactic invasion of primary brain tumors.', *The Journal of neuroscience : the official journal of the Society for Neuroscience*. Society for Neuroscience, 31(13), pp. 4858–67. doi: 10.1523/JNEUROSCI.3825-10.2011.

Moon, Y.-A. and Horton, J. D. (2003) 'Identification of Two Mammalian Reductases Involved in the Two-carbon Fatty Acyl Elongation Cascade', *Journal of Biological Chemistry*, 278(9), pp. 7335–7343. doi: 10.1074/jbc.M211684200.

Moreno, M. *et al.* (2017) 'GPR56/ADGRG1 Inhibits Mesenchymal Differentiation and Radioresistance in Glioblastoma', *Cell Reports*, 21(8), pp. 2183–2197. doi: 10.1016/j.celrep.2017.10.083.

Morton, J. J. *et al.* (2016) 'Humanized Mouse Xenograft Models: Narrowing the Tumor–Microenvironment Gap', *Cancer Research*, 76(21), pp. 6153–6158. doi: 10.1158/0008-5472.CAN-16-1260.

Moser, K. V. *et al.* (2003) 'Brain capillaries and cholinergic neurons persist in organotypic brain slices in the absence of blood flow', *European Journal of Neuroscience*, 18(1), pp. 85–94. doi: 10.1046/j.1460-9568.2003.02728.x.

Moss, M. L. and Lambert, M. H. (2002) 'Shedding of membrane proteins by ADAM family proteases.', *Essays in biochemistry*, 38, pp. 141–53. Available at: http://www.ncbi.nlm.nih.gov/pubmed/12463167 (Accessed: 20 July 2019).

Mueller, S. C. *et al.* (1999) 'A Novel Protease-docking Function of Integrin at Invadopodia', *Journal of Biological Chemistry*, 274(35), pp. 24947–24952. doi: 10.1074/jbc.274.35.24947.

Mukherjee, J. *et al.* (2006) 'ENU administration causes genomic instability along with single nucleotide polymorphisms in p53 during gliomagenesis: T11TS administration demonstrated in vivo apoptosis of these genetically altered tumor cells', *Cancer Biology & Therapy*, 5(2), pp. 156–164. doi: 10.4161/cbt.5.2.2313.

Mullarky, E. *et al.* (2011) 'PHGDH amplification and altered glucose metabolism in human melanoma', *Pigment Cell & Melanoma Research*, 24(6), pp. 1112–1115. doi: 10.1111/j.1755-148X.2011.00919.x.

Muller, F. L. *et al.* (2012) 'Passenger deletions generate therapeutic vulnerabilities in cancer', *Nature*, 488(7411), pp. 337–342. doi: 10.1038/nature11331.

Munoz, J. L. *et al.* (2013) 'Delivery of Functional Anti-miR-9 by Mesenchymal Stem Cell-derived Exosomes to Glioblastoma Multiforme Cells Conferred Chemosensitivity.', *Molecular therapy. Nucleic acids*, 2, p. e126. doi: 10.1038/mtna.2013.60.

Munoz, J. L. *et al.* (2015) 'Temozolomide resistance in glioblastoma occurs by miRNA-9-targeted PTCH1, independent of sonic hedgehog level.', *Oncotarget*, 6(2), pp. 1190–201. doi: 10.18632/oncotarget.2778.

Nabeshima, K. *et al.* (1999) 'Cohort migration of carcinoma cells: differentiated colorectal carcinoma cells move as coherent cell clusters or sheets.', *Histology and histopathology*, 14(4), pp. 1183–97. doi: 10.14670/HH-14.1183.

Nabeshima, K. *et al.* (2000) 'Front-cell-specific expression of membrane-type 1 matrix metalloproteinase and gelatinase A during cohort migration of colon carcinoma cells induced by hepatocyte growth factor/scatter factor.', *Cancer research*, 60(13), pp. 3364–9. Available at: http://www.ncbi.nlm.nih.gov/pubmed/10910039 (Accessed: 22 July 2019).

Naganuma, T. and Kihara, A. (2014) 'Two modes of regulation of the fatty acid elongase ELOVL6 by the 3-ketoacyl-CoA reductase KAR in the fatty acid elongation cycle.', *PloS one*. Public Library of Science, 9(7), p. e101823.

doi: 10.1371/journal.pone.0101823.

Nakada, M. *et al.* (2005) 'EphB2/R-Ras Signaling Regulates Glioma Cell Adhesion, Growth, and Invasion', *The American Journal of Pathology*, 167(2), pp. 565–576. doi: 10.1016/S0002-9440(10)62998-7.

Nam, L. *et al.* (2018) 'Drug Delivery Nanosystems for the Localized Treatment of Glioblastoma Multiforme.', *Materials (Basel, Switzerland)*. Multidisciplinary Digital Publishing Institute (MDPI), 11(5). doi: 10.3390/ma11050779.

Ng, P. C. *et al.* (2015) 'Comparative MiRNA Expressional Profiles and Molecular Networks in Human Small Bowel Tissues of Necrotizing Enterocolitis and Spontaneous Intestinal Perforation.', *PloS one*. Public Library of Science, 10(8), p. e0135737. doi: 10.1371/journal.pone.0135737.

Nicholson, J. K., Lindon, J. C. and Holmes, E. (1999) '"Metabonomics": understanding the metabolic responses of living systems to pathophysiological stimuli via multivariate statistical analysis of biological NMR spectroscopic data', *Xenobiotica*. Taylor & Francis, 29(11), pp. 1181–1189. doi: 10.1080/004982599238047.

Nilsson, R. *et al.* (2014) 'Metabolic enzyme expression highlights a key role for MTHFD2 and the mitochondrial folate pathway in cancer', *Nature Communications*, 5(1), p. 3128. doi: 10.1038/ncomms4128.

Niwa, R. *et al.* (2002) 'Control of actin reorganization by Slingshot, a family

of phosphatases that dephosphorylate ADF/cofilin.', *Cell*, 108(2), pp. 233–46. Available at: http://www.ncbi.nlm.nih.gov/pubmed/11832213 (Accessed: 19 December 2017).

Noble, W. S. (2009) 'How does multiple testing correction work?', *Nature biotechnology*. NIH Public Access, 27(12), pp. 1135–7. doi: 10.1038/nbt1209-1135.

Noguchi, T., Inoue, H. and Tanaka, T. (1986) 'The M1- and M2-type isozymes of rat pyruvate kinase are produced from the same gene by alternative RNA splicing.', *The Journal of biological chemistry*, 261(29), pp. 13807–12. Available at: http://www.ncbi.nlm.nih.gov/pubmed/3020052 (Accessed: 4 April 2016).

Noushmehr, H. *et al.* (2010) 'Identification of a CpG island methylator phenotype that defines a distinct subgroup of glioma.', *Cancer cell*. NIH Public Access, 17(5), pp. 510–22. doi: 10.1016/j.ccr.2010.03.017.

Nowell, P. C. (1976) 'The clonal evolution of tumor cell populations.', *Science (New York, N.Y.)*, 194(4260), pp. 23–8. Available at: http://www.ncbi.nlm.nih.gov/pubmed/959840 (Accessed: 13 August 2016).

O'Neil, D., Glowatz, H. and Schlumpberger, M. (2013) 'Ribosomal RNA depletion for efficient use of RNA-seq capacity.', *Current protocols in molecular biology / edited by Frederick M. Ausubel ... [et al.]*, Chapter 4, p. Unit 4.19. doi: 10.1002/0471142727.mb0419s103.

Ogawa, K. *et al.* (1989) 'Distribution of collagen Type IV in brain tumors: An immunohistochemical study', *Journal of Neuro-Oncology*. Kluwer Academic Publishers, 7(4), pp. 357–366. doi: 10.1007/BF02147093.

Ohgaki, H. *et al.* (2004) 'Genetic pathways to glioblastoma: a population-based study.', *Cancer research*, 64(19), pp. 6892–9. Available at: http://cancerres.aacrjournals.org/content/64/19/6892.abstract?ijkey=bc3228808376a43b8caaa852a0be1a49d9963182&keytype2=tf_ipsecsha (Accessed: 29 February 2016).

Ohgaki, H. and Kleihues, P. (2005a) 'Epidemiology and etiology of gliomas', *Acta Neuropathologica*, 109(1), pp. 93–108. Available at: http://www.ncbi.nlm.nih.gov/pubmed/15685439 (Accessed: 8 January 2016).

Ohgaki, H. and Kleihues, P. (2005b) 'Population-based studies on incidence, survival rates, and genetic alterations in astrocytic and oligodendroglial gliomas.', *Journal of neuropathology and experimental neurology*, 64(6), pp. 479–89. Available at: http://www.ncbi.nlm.nih.gov/pubmed/15977639 (Accessed: 5 March 2016).

Ohgaki, H. and Kleihues, P. (2009) 'Genetic alterations and signaling pathways in the evolution of gliomas.', *Cancer science*, 100(12), pp. 2235–41. Available at: http://www.ncbi.nlm.nih.gov/pubmed/19737147 (Accessed: 17 February 2016).

Ohgaki, H. and Kleihues, P. (2011) 'Genetic profile of astrocytic and

oligodendroglial gliomas.', *Brain tumor pathology*, 28(3), pp. 177–83. doi: 10.1007/s10014-011-0029-1.

Ohgaki, H. and Kleihues, P. (2013) 'The definition of primary and secondary glioblastoma.', *Clinical cancer research : an official journal of the American Association for Cancer Research*, 19(4), pp. 764–72. Available at: http://clincancerres.aacrjournals.org/content/19/4/764.long (Accessed: 12 December 2015).

Ohnishi, T. *et al.* (no date) 'A novel model of glioma cell invasion using organotypic brain slice culture', *AACR*. Available at: http://cancerres.aacrjournals.org/content/58/14/2935.short (Accessed: 22 July 2019).

Okegawa, T. *et al.* (2017) 'Intratumor Heterogeneity in Primary Kidney Cancer Revealed by Metabolic Profiling of Multiple Spatially Separated Samples within Tumors.', *EBioMedicine*. Elsevier, 19, pp. 31–38. doi: 10.1016/j.ebiom.2017.04.009.

Olofsson, S.-O. *et al.* (2009) 'Lipid droplets as dynamic organelles connecting storage and efflux of lipids', *Biochimica et Biophysica Acta (BBA)-Molecular and Cell Biology of Lipids*. Elsevier, 1791(6), pp. 448–458.

Omar Zaki, S. S. *et al.* (2019) 'The influence of serum-supplemented culture media in a transwell migration assay', *Cell Biology International*. John Wiley & Sons, Ltd, p. cbin.11122. doi: 10.1002/cbin.11122.

Omoto, K. *et al.* (2018) 'False-positive inflammatory change mimicking

glioblastoma multiforme under 5-aminolevulinic acid-guided surgery: A case report.', *Surgical neurology international*, 9, p. 49. doi: 10.4103/sni.sni_473_17.

Ornell, K. *et al.* (2015) 'Abstract 3124: Synergistic modulation of microRNAs for treatment of glioblastoma cancer initiating cells', *Cancer Research*, 75(15 Supplement), pp. 3124–3124. doi: 10.1158/1538-7445.AM2015-3124.

Ørom, U. A. and Lund, A. H. (2007) 'Isolation of microRNA targets using biotinylated synthetic microRNAs', *Methods*, 43(2), pp. 162–165. doi: 10.1016/j.ymeth.2007.04.007.

Ostrom, Q. T. *et al.* (2013a) 'CBTRUS statistical report: Primary brain and central nervous system tumors diagnosed in the United States in 2006-2010.', *Neuro-oncology*, 15 Suppl 2, pp. ii1-56. Available at: http://www.pubmedcentral.nih.gov/articlerender.fcgi?artid=3798196&tool=pmcentrez&rendertype=abstract (Accessed: 13 January 2016).

Ostrom, Q. T. *et al.* (2013b) 'CBTRUS statistical report: Primary brain and central nervous system tumors diagnosed in the United States in 2006-2010.', *Neuro-oncology*, 15 Suppl 2, pp. ii1-56. doi: 10.1093/neuonc/not151.

Owen, O. E., Kalhan, S. C. and Hanson, R. W. (2002) 'The Key Role of Anaplerosis and Cataplerosis for Citric Acid Cycle Function', *Journal of Biological Chemistry*, 277(34), pp. 30409–30412. doi:

10.1074/jbc.R200006200.

PAGE and DL (1987) 'Diagnostic Histopathology of the Breast', *Churchill Livingstone*. Edinburge London Merbourne and New York, pp. 219–223. Available at: https://ci.nii.ac.jp/naid/10012013115/ (Accessed: 22 July 2019).

Palecek, S. P. *et al.* (1997) 'Integrin-ligand binding properties govern cell migration speed through cell-substratum adhesiveness', *Nature*, 385(6616), pp. 537–540. doi: 10.1038/385537a0.

Pallan, P. S. *et al.* (2011) 'Unexpected origins of the enhanced pairing affinity of 2'-fluoro-modified RNA.', *Nucleic acids research*, 39(8), pp. 3482–95. doi: 10.1093/nar/gkq1270.

Pandyra, A. A. *et al.* (2015) 'Genome-wide RNAi analysis reveals that simultaneous inhibition of specific mevalonate pathway genes potentiates tumor cell death.', *Oncotarget*. Impact Journals, LLC, 6(29), pp. 26909–21. doi: 10.18632/oncotarget.4817.

Pannuru, P. *et al.* (2014) 'miR-let-7f-1 regulates SPARC mediated cisplatin resistance in medulloblastoma cells.', *Cellular signalling*. England, 26(10), pp. 2193–2201. doi: 10.1016/j.cellsig.2014.06.014.

Papagiannakopoulos, T. *et al.* (2012) 'Pro-neural miR-128 is a glioma tumor suppressor that targets mitogenic kinases.', *Oncogene*, 31(15), pp. 1884–95. Available at: http://www.pubmedcentral.nih.gov/articlerender.fcgi?artid=4160048&tool

=pmcentrez&rendertype=abstract (Accessed: 17 March 2016).

Paraskevopoulou, M. D. *et al.* (2013) 'DIANA-microT web server v5.0: service integration into miRNA functional analysis workflows.', *Nucleic acids research*, 41(Web Server issue), pp. W169-73. doi: 10.1093/nar/gkt393.

Park, J.-E. *et al.* (2011) 'Dicer recognizes the 5' end of RNA for efficient and accurate processing', *Nature*, 475(7355), pp. 201–205. doi: 10.1038/nature10198.

Park, Jun Hyoung *et al.* (2016) 'Fatty Acid Oxidation-Driven Src Links Mitochondrial Energy Reprogramming and Oncogenic Properties in Triple-Negative Breast Cancer.', *Cell reports*. NIH Public Access, 14(9), pp. 2154–2165. doi: 10.1016/j.celrep.2016.02.004.

Park, Jun Hyoung *et al.* (2016) 'Fatty Acid Oxidation-Driven Src Links Mitochondrial Energy Reprogramming and Oncogenic Properties in Triple-Negative Breast Cancer', *Cell Reports*. Cell Press, 14(9), pp. 2154–2165. doi: 10.1016/J.CELREP.2016.02.004.

Parkinson, J. F. *et al.* (2008) 'Variation of O(6)-methylguanine-DNA methyltransferase (MGMT) promoter methylation in serial samples in glioblastoma.', *Journal of neuro-oncology*, 87(1), pp. 71–8. doi: 10.1007/s11060-007-9486-0.

Patel, A. P. *et al.* (2014) 'Single-cell RNA-seq highlights intratumoral heterogeneity in primary glioblastoma.', *Science (New York, N.Y.)*. American Association for the Advancement of Science, 344(6190), pp.

1396–401. doi: 10.1126/science.1254257.

Patel, K. *et al.* (2014) 'The LKB1-salt-inducible kinase pathway functions as a key gluconeogenic suppressor in the liver', *Nature Communications*, 5(1), p. 4535. doi: 10.1038/ncomms5535.

Patti, G. J., Yanes, O. and Siuzdak, G. (2012) 'Innovation: Metabolomics: the apogee of the omics trilogy.', *Nature reviews. Molecular cell biology*. NIH Public Access, 13(4), pp. 263–9. doi: 10.1038/nrm3314.

Patton, J. G. *et al.* (2015) 'Biogenesis, delivery, and function of extracellular RNA.', *Journal of extracellular vesicles*, 4, p. 27494. Available at: http://www.pubmedcentral.nih.gov/articlerender.fcgi?artid=4553266&tool=pmcentrez&rendertype=abstract (Accessed: 30 May 2016).

Paule, M. R. and White, R. J. (2000) 'Survey and summary: transcription by RNA polymerases I and III.', *Nucleic acids research*, 28(6), pp. 1283–98. Available at: http://www.pubmedcentral.nih.gov/articlerender.fcgi?artid=111039&tool=pmcentrez&rendertype=abstract (Accessed: 27 June 2016).

Paulus, W. *et al.* (1996) 'Diffuse brain invasion of glioma cells requires beta 1 integrins.', *Laboratory investigation; a journal of technical methods and pathology*, 75(6), pp. 819–26. Available at: http://www.ncbi.nlm.nih.gov/pubmed/8973477 (Accessed: 20 July 2019).

Pedersen, P.-H. *et al.* (1995) 'Migratory patterns oflac-z transfected human glioma cells in the rat brain', *International Journal of Cancer*. John Wiley &

Sons, Ltd, 62(6), pp. 767–771. doi: 10.1002/ijc.2910620620.

Pegg, A. E. (1990) 'Mammalian O6-Alkylguanine-DNA Alkyltransferase: Regulation and Importance in Response to Alkylating Carcinogenic and Therapeutic Agents', *Cancer Res.*, 50(19), pp. 6119–6129. Available at: http://cancerres.aacrjournals.org/content/50/19/6119?ijkey=22a00b440434eef480b944f3d6dc542180863c3e&keytype2=tf_ipsecsha (Accessed: 13 August 2016).

Peltier, H. J. and Latham, G. J. (2008) 'Normalization of microRNA expression levels in quantitative RT-PCR assays: identification of suitable reference RNA targets in normal and cancerous human solid tissues.', *RNA (New York, N.Y.)*. Cold Spring Harbor Laboratory Press, 14(5), pp. 844–52. doi: 10.1261/rna.939908.

Pencheva, N. *et al.* (2017) 'Identification of a Druggable Pathway Controlling Glioblastoma Invasiveness', *Cell Reports*, 20(1), pp. 48–60. doi: 10.1016/j.celrep.2017.06.036.

Peng, B. *et al.* (2014) 'MicroRNA218 inhibits glioma migration and invasion via inhibiting glioma-associated oncogene homolog 1 expression at N terminus', *Tumor Biology*, 35(4), pp. 3831–3837. doi: 10.1007/s13277-013-1507-3.

Peschiaroli, A. *et al.* (2013) 'miR-143 regulates hexokinase 2 expression in cancer cells.', *Oncogene*. Macmillan Publishers Limited, 32(6), pp. 797–802. doi: 10.1038/onc.2012.100.

Peter, I. D., Linet, M. S. and Heineman, E. F. (1995) 'Etiology of Brain Tumors in Adults', *Epidemiologic Reviews*, 17(2), pp. 382–414. doi: 10.1093/oxfordjournals.epirev.a036200.

Peveling-Oberhag, J. *et al.* (2014) 'MicroRNA Profiling of Laser-Microdissected Hepatocellular Carcinoma Reveals an Oncogenic Phenotype of the Tumor Capsule.', *Translational oncology*. Neoplasia Press, 7(6), pp. 672–80. doi: 10.1016/j.tranon.2014.09.003.

Pfaff, M., Du, X. and Ginsberg, M. H. (1999) 'Calpain cleavage of integrin beta cytoplasmic domains.', *FEBS letters*, 460(1), pp. 17–22. doi: 10.1016/s0014-5793(99)01250-8.

Phan, L. M., Yeung, S.-C. J. and Lee, M.-H. (2014) 'Cancer metabolic reprogramming: importance, main features, and potentials for precise targeted anti-cancer therapies.', *Cancer biology & medicine*, 11(1), pp. 1–19. doi: 10.7497/j.issn.2095-3941.2014.01.001.

Piccirillo, S. G. M. *et al.* (2012) 'Fluorescence-guided surgical sampling of glioblastoma identifies phenotypically distinct tumour-initiating cell populations in the tumour mass and margin.', *British journal of cancer*, 107(3), pp. 462–8. doi: 10.1038/bjc.2012.271.

Di Pietro, E. *et al.* (2002) 'Mitochondrial NAD-dependent methylenetetrahydrofolate dehydrogenase-methenyltetrahydrofolate cyclohydrolase is essential for embryonic development.', *Molecular and cellular biology*, 22(12), pp. 4158–66. doi: 10.1128/mcb.22.12.4158-

4166.2002.

Pishvaian, M. J. *et al.* (1999) 'Cadherin-11 is expressed in invasive breast cancer cell lines.', *Cancer research*, 59(4), pp. 947–52. Available at: http://www.ncbi.nlm.nih.gov/pubmed/10029089 (Accessed: 21 July 2019).

Pistollato, F. *et al.* (2010) 'Intratumoral hypoxic gradient drives stem cells distribution and MGMT expression in glioblastoma.', *Stem cells (Dayton, Ohio)*, 28(5), pp. 851–62. doi: 10.1002/stem.415.

Piwecka, M. *et al.* (2015) 'Comprehensive analysis of microRNA expression profile in malignant glioma tissues.', *Molecular oncology*. Wiley-Blackwell, 9(7), pp. 1324–40. doi: 10.1016/j.molonc.2015.03.007.

Polette, M. *et al.* (1998) 'Association of fibroblastoid features with the invasive phenotype in human bronchial cancer cell lines.', *Clinical & experimental metastasis*, 16(2), pp. 105–12. Available at: http://www.ncbi.nlm.nih.gov/pubmed/9514091 (Accessed: 20 July 2019).

Pollard, S. M. *et al.* (2009) 'Glioma Stem Cell Lines Expanded in Adherent Culture Have Tumor-Specific Phenotypes and Are Suitable for Chemical and Genetic Screens', *Cell Stem Cell*, 4(6), pp. 568–580. doi: 10.1016/j.stem.2009.03.014.

Pontén, J. and Macintyre, E. H. (2009) 'Long Term Culture of Normal and Neoplastic Human Glia', *Acta Pathologica Microbiologica Scandinavica*. John Wiley & Sons, Ltd (10.1111), 74(4), pp. 465–486. doi: 10.1111/j.1699-0463.1968.tb03502.x.

Possemato, R. *et al.* (2011) 'Functional genomics reveals serine synthesis is essential in PHGDH-amplified breast cancer', *Nature*. NIH Public Access, 476(7360), p. 346. doi: 10.1038/NATURE10350.

Potter, D. A. *et al.* (1998) 'Calpain Regulates Actin Remodeling during Cell Spreading', *The Journal of Cell Biology*, 141(3), pp. 647–662. doi: 10.1083/jcb.141.3.647.

Price, N. T. *et al.* (2002) 'A Novel Brain-Expressed Protein Related to Carnitine Palmitoyltransferase I', *Genomics*. Academic Press, 80(4), pp. 433–442. doi: 10.1006/GENO.2002.6845.

Purow, B. (2011) 'The elephant in the room: do microRNA-based therapies have a realistic chance of succeeding for brain tumors such as glioblastoma?', *Journal of neuro-oncology*. United States, 103(3), pp. 429–436. doi: 10.1007/s11060-010-0449-5.

Qiu, G. *et al.* (2016) 'Dysregulation of MALAT1 and miR-619-5p as a prognostic indicator in advanced colorectal carcinoma.', *Oncology letters*. Spandidos Publications, 12(6), pp. 5036–5042. doi: 10.3892/ol.2016.5312.

Qu, Q. *et al.* (2016) 'Fatty acid oxidation and carnitine palmitoyltransferase I: emerging therapeutic targets in cancer', *Cell Death & Disease*, 7(5), pp. e2226–e2226. doi: 10.1038/cddis.2016.132.

Rabinowitz, J. D. and Kimball, E. (2007) 'Acidic Acetonitrile for Cellular Metabolome Extraction from *Escherichia coli*', *Analytical Chemistry*, 79(16), pp. 6167–6173. doi: 10.1021/ac070470c.

Raizer, J. J. *et al.* (2014) 'Economics of Malignant Gliomas: A Critical Review.', *Journal of oncology practice / American Society of Clinical Oncology*, 11(1), pp. e59-65. doi: 10.1200/JOP.2012.000560.

Rambold, A. S., Cohen, S. and Lippincott-Schwartz, J. (2015) 'Fatty acid trafficking in starved cells: regulation by lipid droplet lipolysis, autophagy, and mitochondrial fusion dynamics', *Developmental cell*. Elsevier, 32(6), pp. 678–692.

Ramírez, C. M. *et al.* (2013) 'MicroRNA 33 Regulates Glucose Metabolism', *Molecular and Cellular Biology*. American Society for Microbiology Journals, 33(15), pp. 2891–2902. doi: 10.1128/MCB.00016-13.

Ramos-Montoya, A. *et al.* (2006) 'Pentose phosphate cycle oxidative and nonoxidative balance: A new vulnerable target for overcoming drug resistance in cancer.', *International journal of cancer*, 119(12), pp. 2733–41. doi: 10.1002/ijc.22227.

Rao, S. A. M. *et al.* (2013) 'miR-219-5p inhibits receptor tyrosine kinase pathway by targeting EGFR in glioblastoma.', *PloS one*. United States, 8(5), p. e63164. doi: 10.1371/journal.pone.0063164.

Rao, S. A. M., Santosh, V. and Somasundaram, K. (2010) 'Genome-wide expression profiling identifies deregulated miRNAs in malignant astrocytoma.', *Modern pathology : an official journal of the United States and Canadian Academy of Pathology, Inc*, 23(10), pp. 1404–17. doi: 10.1038/modpathol.2010.135.

Rao, S. S. *et al.* (2013) 'Glioblastoma Behaviors in Three-Dimensional Collagen-Hyaluronan Composite Hydrogels', *ACS Applied Materials & Interfaces*, 5(19), pp. 9276–9284. doi: 10.1021/am402097j.

Rao, S. S. *et al.* (2014) 'Toward 3D Biomimetic Models to Understand the Behavior of Glioblastoma Multiforme Cells', *Tissue Engineering Part B: Reviews*, 20(4), pp. 314–327. doi: 10.1089/ten.teb.2013.0227.

Ratheiser, K. *et al.* (1991) 'Inhibition by etomoxir of carnitine palmitoyltransferase I reduces hepatic glucose production and plasma lipids in non-insulin-dependent diabetes mellitus.', *Metabolism: clinical and experimental*, 40(11), pp. 1185–90. Available at: http://www.ncbi.nlm.nih.gov/pubmed/1943747 (Accessed: 22 March 2019).

Rathod, S. S. *et al.* (2014) 'Tumor suppressive miRNA-34a suppresses cell proliferation and tumor growth of glioma stem cells by targeting Akt and Wnt signaling pathways.', *FEBS open bio*, 4, pp. 485–95. Available at: http://www.sciencedirect.com/science/article/pii/S2211546314000503 (Accessed: 19 March 2016).

Raychaudhuri, M. *et al.* (2012) 'Intratumoral Heterogeneity of MicroRNA Expression in Breast Cancer', *The Journal of Molecular Diagnostics*, 14(4), pp. 376–384. doi: 10.1016/j.jmoldx.2012.01.016.

Reczko, M. *et al.* (2012) 'Functional microRNA targets in protein coding sequences.', *Bioinformatics (Oxford, England)*, 28(6), pp. 771–6. doi:

10.1093/bioinformatics/bts043.

Regen, C. M. and Horwitz, A. F. (1992) 'Dynamics of beta 1 integrin-mediated adhesive contacts in motile fibroblasts', *The Journal of Cell Biology*, 119(5), pp. 1347–1359. doi: 10.1083/jcb.119.5.1347.

Rehmsmeier, M. *et al.* (2004) 'Fast and effective prediction of microRNA/target duplexes.', *RNA (New York, N.Y.)*, 10(10), pp. 1507–17. Available at: http://www.pubmedcentral.nih.gov/articlerender.fcgi?artid=1370637&tool=pmcentrez&rendertype=abstract (Accessed: 15 February 2016).

Reifenberger, G. *et al.* (2012) 'Predictive impact of MGMT promoter methylation in glioblastoma of the elderly.', *International journal of cancer*, 131(6), pp. 1342–50. doi: 10.1002/ijc.27385.

Rempel, S. A. *et al.* (1994) 'Cathepsin B expression and localization in glioma progression and invasion.', *Cancer research*, 54(23), pp. 6027–31. Available at: http://www.ncbi.nlm.nih.gov/pubmed/7954439 (Accessed: 12 May 2019).

Ren, X.-R. *et al.* (2015) 'Perhexiline promotes HER3 ablation through receptor internalization and inhibits tumor growth', *Breast Cancer Research*. BioMed Central, 17(1), p. 20. doi: 10.1186/s13058-015-0528-9.

Ren, Y., Kang, C.-S., *et al.* (2010) 'Co-delivery of as-miR-21 and 5-FU by poly(amidoamine) dendrimer attenuates human glioma cell growth in vitro.', *Journal of biomaterials science. Polymer edition*, 21(3), pp. 303–14.

Available at: http://www.ncbi.nlm.nih.gov/pubmed/20178687 (Accessed: 28 May 2016).

Ren, Y., Zhou, X., *et al.* (2010) 'MicroRNA-21 inhibitor sensitizes human glioblastoma cells U251 (PTEN-mutant) and LN229 (PTEN-wild type) to taxol.', *BMC cancer*. BioMed Central, 10(1), p. 27. Available at: http://bmccancer.biomedcentral.com/articles/10.1186/1471-2407-10-27 (Accessed: 21 March 2016).

Reuss, D. E. *et al.* (2015) 'IDH mutant diffuse and anaplastic astrocytomas have similar age at presentation and little difference in survival: a grading problem for WHO', *Acta Neuropathologica*, 129(6), pp. 867–873. doi: 10.1007/s00401-015-1438-8.

Ricard, C. and Debarbieux, F. C. (2014) 'Six-color intravital two-photon imaging of brain tumors and their dynamic microenvironment', *Frontiers in Cellular Neuroscience*, 8. doi: 10.3389/fncel.2014.00057.

Ridley, A. J. *et al.* (1992) 'The small GTP-binding protein rac regulates growth factor-induced membrane ruffling.', *Cell*, 70(3), pp. 401–10. Available at: http://www.ncbi.nlm.nih.gov/pubmed/1643658 (Accessed: 19 May 2019).

Ridley, A. J. *et al.* (2003) 'Cell Migration: Integrating Signals from Front to Back', *Science*, 302(5651), pp. 1704–1709. doi: 10.1126/science.1092053.

Riemenschneider, M. J. *et al.* (2005) 'In Situ Analysis of Integrin and Growth Factor Receptor Signaling Pathways in Human Glioblastomas

Suggests Overlapping Relationships with Focal Adhesion Kinase Activation', *The American Journal of Pathology*. Elsevier, 167(5), pp. 1379–1387. doi: 10.1016/S0002-9440(10)61225-4.

Righi, V. *et al.* (2009) '^{1} H HR-MAS and genomic analysis of human tumor biopsies discriminate between high and low grade astrocytomas', *NMR in Biomedicine*, 22(6), pp. 629–637. doi: 10.1002/nbm.1377.

Rinaldi, M. *et al.* (2016) 'ROS and Brain Gliomas: An Overview of Potential and Innovative Therapeutic Strategies', *International Journal of Molecular Sciences*, 17(6), p. 984. doi: 10.3390/ijms17060984.

Rintoul, R. C. and Sethi, T. (2001) 'The role of extracellular matrix in small-cell lung cancer', *The Lancet Oncology*. Elsevier, 2(7), pp. 437–442. doi: 10.1016/S1470-2045(00)00421-6.

Ritchie, M. E. *et al.* (2015) 'limma powers differential expression analyses for RNA-sequencing and microarray studies', *Nucleic Acids Research*, pp. gkv007-. doi: 10.1093/nar/gkv007.

Ritchie, W. *et al.* (2009) 'Conserved Expression Patterns Predict microRNA Targets', *PLoS Computational Biology*. Edited by U. Ohler. Public Library of Science, 5(9), p. e1000513. doi: 10.1371/journal.pcbi.1000513.

Ritchie, W., Flamant, S. and Rasko, J. E. J. (2009) 'Predicting microRNA targets and functions: traps for the unwary', *Nature Methods*. Nature Publishing Group, 6(6), pp. 397–398. doi: 10.1038/nmeth0609-397.

Ritchie, W. and Rasko, J. E. J. (2014) 'Refining microRNA target predictions:

Sorting the wheat from the chaff', *Biochemical and Biophysical Research Communications*. Academic Press, 445(4), pp. 780–784. doi: 10.1016/J.BBRC.2014.01.181.

Rohatgi, R. *et al.* (1999) 'The interaction between N-WASP and the Arp2/3 complex links Cdc42-dependent signals to actin assembly.', *Cell*, 97(2), pp. 221–31. doi: 10.1016/s0092-8674(00)80732-1.

Ross, J. L. *et al.* (2017) '5-Aminolevulinic Acid Guided Sampling of Glioblastoma Microenvironments Identifies Pro-Survival Signaling at Infiltrative Margins', *Scientific Reports*, 7(1), p. 15593. doi: 10.1038/s41598-017-15849-w.

Ross, S. A. and Davis, C. D. (2014) 'The emerging role of microRNAs and nutrition in modulating health and disease.', *Annual review of nutrition*. United States, 34, pp. 305–336. doi: 10.1146/annurev-nutr-071813-105729.

Roussos, E. T., Condeelis, J. S. and Patsialou, A. (2011) 'Chemotaxis in cancer', *Nature Reviews Cancer 2011 11:8*. Nature Publishing Group, 11(8), p. 573. doi: 10.1038/nrc3078.

Ru, P. *et al.* (2016) 'Feedback Loop Regulation of SCAP/SREBP-1 by miR-29 Modulates EGFR Signaling-Driven Glioblastoma Growth.', *Cell reports*. NIH Public Access, 16(6), pp. 1527–1535. doi: 10.1016/j.celrep.2016.07.017.

Russell, W. L. *et al.* (1979) 'Specific-locus test shows ethylnitrosourea to

be the most potent mutagen in the mouse.', *Proceedings of the National Academy of Sciences of the United States of America*. National Academy of Sciences, 76(11), pp. 5818–9. doi: 10.1073/pnas.76.11.5818.

Salajegheh, A. *et al.* (2015) 'Modulatory role of *miR-205* in angiogenesis and progression of thyroid cancer', *Journal of Molecular Endocrinology*. BioScientifica, 55(3), pp. 183–196. doi: 10.1530/JME-15-0182.

Salhia, B. *et al.* (2008) 'The Guanine Nucleotide Exchange Factors Trio, Ect2, and Vav3 Mediate the Invasive Behavior of Glioblastoma', *The American Journal of Pathology*, 173(6), pp. 1828–1838. doi: 10.2353/ajpath.2008.080043.

Salvo, T. G. Di *et al.* (2015) 'Right ventricular long noncoding RNA expression in human heart failure', *http://dx.doi.org/10.1086/679721*. University of Chicago PressChicago, IL.

Sambrook, J. and Russell, D. W. (2006) 'Purification of nucleic acids by extraction with phenol:chloroform.', *CSH protocols*, 2006(1), p. pdb.prot4455-. doi: 10.1101/pdb.prot4455.

Sampetrean, O. *et al.* (2011) 'Invasion Precedes Tumor Mass Formation in a Malignant Brain Tumor Model of Genetically Modified Neural Stem Cells', *Neoplasia*, 13(9), pp. 784-IN3. doi: 10.1593/neo.11624.

Sánchez-Ávila, N. *et al.* (2009) 'Fast, sensitive and highly discriminant gas chromatography–mass spectrometry method for profiling analysis of fatty acids in serum', *Journal of Chromatography A*, 1216(40), pp. 6864–6872.

doi: 10.1016/j.chroma.2009.08.045.

Santandreu, F. M. *et al.* (2008) 'Differences in mitochondrial function and antioxidant systems between regions of human glioma.', *Cellular physiology and biochemistry : international journal of experimental cellular physiology, biochemistry, and pharmacology*, 22(5–6), pp. 757–68. doi: 10.1159/000185559.

Sanzey, M. *et al.* (2015) 'Comprehensive Analysis of Glycolytic Enzymes as Therapeutic Targets in the Treatment of Glioblastoma', *PLOS ONE*. Edited by M. G. Castro, 10(5), p. e0123544. doi: 10.1371/journal.pone.0123544.

Sazani, P., Astriab-Fischer, A. and Kole, R. (2003) 'Effects of base modifications on antisense properties of 2'-O-methoxyethyl and PNA oligonucleotides.', *Antisense & nucleic acid drug development*, 13(3), pp. 119–28. doi: 10.1089/108729003768247583.

Schafer, Z. T. *et al.* (2009) 'Antioxidant and oncogene rescue of metabolic defects caused by loss of matrix attachment.', *Nature*. NIH Public Access, 461(7260), pp. 109–13. doi: 10.1038/nature08268.

Scherer, H. J. (1938) 'Structural Development in Gliomas', *The American Journal of Cancer*. American Association for Cancer Research Journals, 34(3), pp. 333–351. doi: 10.1158/ajc.1938.333.

Schmidt-Schweda, S. and Holubarsch, C. (2000) 'First clinical trial with etomoxir in patients with chronic congestive heart failure.', *Clinical science (London, England : 1979)*. Portland Press Limited, 99(1), pp. 27–35. doi:

10.1042/CS0990027.

Schroeder, A. *et al.* (2006) 'The RIN: an RNA integrity number for assigning integrity values to RNA measurements.', *BMC molecular biology*, 7, p. 3. doi: 10.1186/1471-2199-7-3.

Schultz-Cherry, S. *et al.* (1995) 'Regulation of Transforming Growth Factor-β Activation by Discrete Sequences of Thrombospondin 1', *Journal of Biological Chemistry*, 270(13), pp. 7304–7310. doi: 10.1074/jbc.270.13.7304.

Schultz-Cherry, S., Lawler, J. and Murphy-Ullrich, J. E. (1994) 'The type 1 repeats of thrombospondin 1 activate latent transforming growth factor-beta.', *The Journal of biological chemistry*, 269(43), pp. 26783–8. Available at: http://www.ncbi.nlm.nih.gov/pubmed/7929414 (Accessed: 22 July 2019).

Schwartz, K. A. *et al.* (2018) 'Investigating the Ketogenic Diet As Treatment for Primary Aggressive Brain Cancer: Challenges and Lessons Learned.', *Frontiers in nutrition*. Frontiers Media SA, 5, p. 11. doi: 10.3389/fnut.2018.00011.

Scorsetti, M. *et al.* (2015) 'Multimodality therapy approaches, local and systemic treatment, compared with chemotherapy alone in recurrent glioblastoma.', *BMC cancer*, 15, p. 486. doi: 10.1186/s12885-015-1488-2.

Seckl, M. J. *et al.* (2017) 'Multicenter, Phase III, Randomized, Double-Blind, Placebo-Controlled Trial of Pravastatin Added to First-Line Standard

Chemotherapy in Small-Cell Lung Cancer (LUNGSTAR)', *Journal of Clinical Oncology*, 35(14), pp. 1506–1514. doi: 10.1200/JCO.2016.69.7391.

Seidel, S., Garvalov, B. K. and Acker, T. (2015) 'Isolation and Culture of Primary Glioblastoma Cells from Human Tumor Specimens', in *Methods in molecular biology (Clifton, N.J.)*, pp. 263–275. doi: 10.1007/978-1-4939-1785-3_19.

Seliger, C., Ricci, C., *et al.* (2016) 'Diabetes, use of antidiabetic drugs, and the risk of glioma.', *Neuro-oncology*. Oxford University Press, 18(3), pp. 340–9. doi: 10.1093/neuonc/nov100.

Seliger, C., Meyer, A.-L., *et al.* (2016) 'Metformin inhibits proliferation and migration of glioblastoma cells independently of TGF-β2', *Cell Cycle*, 15(13), pp. 1755–1766. doi: 10.1080/15384101.2016.1186316.

Seliger, C., Meier, C. R., *et al.* (2016) 'Statin use and risk of glioma: population-based case–control analysis', *European Journal of Epidemiology*, 31(9), pp. 947–952. doi: 10.1007/s10654-016-0145-7.

Seliger, C. *et al.* (2019) 'Use of metformin and survival of patients with high-grade glioma', *International Journal of Cancer*. John Wiley & Sons, Ltd, 144(2), pp. 273–280. doi: 10.1002/ijc.31783.

Seliger, C. and Hau, P. (2018) 'Drug Repurposing of Metabolic Agents in Malignant Glioma.', *International journal of molecular sciences*. Multidisciplinary Digital Publishing Institute (MDPI), 19(9). doi: 10.3390/ijms19092768.

Sen, S., Ng, W. P. and Kumar, S. (2012) 'Contributions of talin-1 to glioma cell-matrix tensional homeostasis.', *Journal of the Royal Society, Interface*. The Royal Society, 9(71), pp. 1311–7. doi: 10.1098/rsif.2011.0567.

Seol, H. J. *et al.* (2009) 'The Guanine Nucleotide Exchange Factor SWAP-70 Modulates the Migration and Invasiveness of Human Malignant Glioma Cells', *Translational Oncology*, 2(4), pp. 300-IN1. doi: 10.1593/tlo.09172.

Sesen, J. *et al.* (2015) 'Metformin Inhibits Growth of Human Glioblastoma Cells and Enhances Therapeutic Response', *PLOS ONE*. Edited by M. M. Alonso, 10(4), p. e0123721. doi: 10.1371/journal.pone.0123721.

Shah, N. P. *et al.* (2002) 'Multiple BCR-ABL kinase domain mutations confer polyclonal resistance to the tyrosine kinase inhibitor imatinib (STI571) in chronic phase and blast crisis chronic myeloid leukemia.', *Cancer cell*, 2(2), pp. 117–25. Available at: http://www.ncbi.nlm.nih.gov/pubmed/12204532 (Accessed: 27 July 2019).

Shao, W. *et al.* (2014) 'Malignancy-associated metabolic profiling of human glioma cell lines using 1H NMR spectroscopy.', *Molecular cancer*. BioMed Central, 13, p. 197. doi: 10.1186/1476-4598-13-197.

Sharbati, Jutta *et al.* (2015) 'Small molecule and RNAi induced phenotype transition of expanded and primary colonic epithelial cells', *Scientific Reports, Published online: 30 July 2015; | doi:10.1038/srep12681*. Nature Publishing Group, 5, pp. 1012–21. doi: 10.1038/SREP12681.

She, X. *et al.* (2014) 'miR-128 and miR-149 enhance the chemosensitivity

of temozolomide by Rap1B-mediated cytoskeletal remodeling in glioblastoma.', *Oncology reports*, 32(3), pp. 957–64. doi: 10.3892/or.2014.3318.

Shen, L. *et al.* (2015) 'MicroRNA-199a-3p suppresses glioma cell proliferation by regulating the AKT/mTOR signaling pathway.', *Tumour biology : the journal of the International Society for Oncodevelopmental Biology and Medicine*, 36(9), pp. 6929–38. Available at: http://www.pubmedcentral.nih.gov/articlerender.fcgi?artid=4644202&tool=pmcentrez&rendertype=abstract (Accessed: 27 March 2016).

Shen, Z. (2011) 'Genomic instability and cancer: an introduction.', *Journal of molecular cell biology*, 3(1), pp. 1–3. doi: 10.1093/jmcb/mjq057.

Shi, C. *et al.* (2018) 'miR-29s function as tumor suppressors in gliomas by targeting TRAF4 and predict patient prognosis', *Cell Death & Disease*. Nature Publishing Group, 9(11), p. 1078. doi: 10.1038/S41419-018-1092-X.

Shi, L. *et al.* (2010) 'MiR-125b is critical for the suppression of human U251 glioma stem cell proliferation.', *Brain research*. Netherlands, 1312, pp. 120–126. doi: 10.1016/j.brainres.2009.11.056.

Shi, L. *et al.* (2014) 'miR-125b inhibitor may enhance the invasion-prevention activity of temozolomide in glioblastoma stem cells by targeting PIAS3.', *BioDrugs : clinical immunotherapeutics, biopharmaceuticals and gene therapy*. New Zealand, 28(1), pp. 41–54. doi: 10.1007/s40259-013-

0053-2.

Shi, Z. *et al.* (2013) 'AC1MMYR2, an inhibitor of dicer-mediated biogenesis of Oncomir miR-21, reverses epithelial-mesenchymal transition and suppresses tumor growth and progression.', *Cancer research*, 73(17), pp. 5519–31. doi: 10.1158/0008-5472.CAN-13-0280.

Shimizu, S., Narita, M. and Tsujimoto, Y. (1999) 'Bcl-2 family proteins regulate the release of apoptogenic cytochrome c by the mitochondrial channel VDAC.', *Nature*. Macmillan Magazines Ltd., 399(6735), pp. 483–7. doi: 10.1038/20959.

Shimoyama, Y. *et al.* (1989) 'Cadherin cell-adhesion molecules in human epithelial tissues and carcinomas.', *Cancer research*. American Association for Cancer Research, 49(8), pp. 2128–33. Available at: http://www.ncbi.nlm.nih.gov/pubmed/2702654 (Accessed: 22 July 2019).

Shin, C.-S. *et al.* (2017) 'The glutamate/cystine xCT antiporter antagonizes glutamine metabolism and reduces nutrient flexibility', *Nature Communications*. Nature Publishing Group, 8(1), p. 15074. doi: 10.1038/ncomms15074.

Shin, J. *et al.* (2017) 'Restoration of miR-29b exerts anti-cancer effects on glioblastoma', *Cancer Cell International*. BioMed Central, 17(1), p. 104. doi: 10.1186/s12935-017-0476-9.

Shinawi, T. *et al.* (2013) 'DNA methylation profiles of long- and short-term glioblastoma survivors.', *Epigenetics*. Landes Bioscience, 8(2), pp. 149–56.

doi: 10.4161/epi.23398.

Shkurnikov, M. Y. *et al.* (2017) 'Plasma Level of hsa-miR-619-5p microRNA Is Associated with Prostatic Cancer Dissemination beyond the Capsule', *Bulletin of Experimental Biology and Medicine*, 163(4), pp. 475–477. doi: 10.1007/s10517-017-3831-x.

Shyu, P. J. *et al.* (2018) 'Dropping in on lipid droplets: insights into cellular stress and cancer.', *Bioscience reports*, 38(5). doi: 10.1042/BSR20180764.

Siebzehnrubl, F. A. *et al.* (2013) 'The ZEB1 pathway links glioblastoma initiation, invasion and chemoresistance', *EMBO Molecular Medicine*. John Wiley & Sons, Ltd, 5(8), pp. 1196–1212. doi: 10.1002/emmm.201302827.

Silber, J. *et al.* (2012) 'miR-34a repression in proneural malignant gliomas upregulates expression of its target PDGFRA and promotes tumorigenesis.', *PloS one*, 7(3), p. e33844. Available at: http://www.pubmedcentral.nih.gov/articlerender.fcgi?artid=3313940&tool=pmcentrez&rendertype=abstract (Accessed: 19 March 2016).

Silbergeld, D. L. and Chicoine, M. R. (1997) 'Isolation and characterization of human malignant glioma cells from histologically normal brain.', *Journal of neurosurgery*, 86(3), pp. 525–31. doi: 10.3171/jns.1997.86.3.0525.

da Silva, R. P. *et al.* (2009) 'Creatine synthesis: hepatic metabolism of guanidinoacetate and creatine in the rat in vitro and in vivo.', *American journal of physiology. Endocrinology and metabolism*. American Physiological Society, 296(2), pp. E256-61. doi:

10.1152/ajpendo.90547.2008.

Singh, R. *et al.* (2009) 'Autophagy regulates lipid metabolism', *Nature*. Nature Publishing Group, 458(7242), p. 1131.

Singh, S., Narang, A. S. and Mahato, R. I. (2011) 'Subcellular Fate and Off-Target Effects of siRNA, shRNA, and miRNA', *Pharmaceutical Research*, 28(12), pp. 2996–3015. doi: 10.1007/s11095-011-0608-1.

Skalsky, R. L. and Cullen, B. R. (2011) 'Reduced expression of brain-enriched microRNAs in glioblastomas permits targeted regulation of a cell death gene.', *PloS one*. United States, 6(9), p. e24248. doi: 10.1371/journal.pone.0024248.

Skinner, M. D. *et al.* (2014) 'Disulfiram Efficacy in the Treatment of Alcohol Dependence: A Meta-Analysis', *PLoS ONE*. Edited by J. Laks, 9(2), p. e87366. doi: 10.1371/journal.pone.0087366.

Slotte, J. P. and Ramstedt, B. (2007) 'The functional role of sphingomyelin in cell membranes', *European Journal of Lipid Science and Technology*. John Wiley & Sons, Ltd, 109(10), pp. 977–981. doi: 10.1002/ejlt.200700024.

Small, E. M. and Olson, E. N. (2011) 'Pervasive roles of microRNAs in cardiovascular biology.', *Nature*. NIH Public Access, 469(7330), pp. 336–42. doi: 10.1038/nature09783.

Smilenov, L. B. *et al.* (1999) 'Focal Adhesion Motility Revealed in Stationary Fibroblasts', *Science*, 286(5442), pp. 1172–1174. doi: 10.1126/science.286.5442.1172.

Smyth, G. K. (2004) 'Linear models and empirical bayes methods for assessing differential expression in microarray experiments.', *Statistical applications in genetics and molecular biology*, 3, p. Article3. doi: 10.2202/1544-6115.1027.

Solaro, R. J. (2000) 'Myosin light chain phosphatase: a Cinderella of cellular signaling.', *Circulation research*, 87(3), pp. 173–5. Available at: http://www.ncbi.nlm.nih.gov/pubmed/10926864 (Accessed: 19 May 2019).

Song, L.-B. *et al.* (2009) 'The polycomb group protein Bmi-1 represses the tumor suppressor PTEN and induces epithelial-mesenchymal transition in human nasopharyngeal epithelial cells.', *The Journal of clinical investigation*, 119(12), pp. 3626–36. Available at: http://www.pubmedcentral.nih.gov/articlerender.fcgi?artid=2786794&tool=pmcentrez&rendertype=abstract (Accessed: 4 April 2016).

Song, L. *et al.* (2010) 'miR-218 inhibits the invasive ability of glioma cells by direct downregulation of IKK-beta.', *Biochemical and biophysical research communications*. United States, 402(1), pp. 135–140. doi: 10.1016/j.bbrc.2010.10.003.

Sørensen, L. B. *et al.* (2003) 'Polymorphic hydroxylation of perhexiline in vitro.', *British journal of clinical pharmacology*, 55(6), pp. 635–8. Available at: http://www.ncbi.nlm.nih.gov/pubmed/12814462 (Accessed: 20 March 2019).

Sottoriva, A. *et al.* (2013) 'Intratumor heterogeneity in human glioblastoma

reflects cancer evolutionary dynamics.', *Proceedings of the National Academy of Sciences of the United States of America*, 110(10), pp. 4009–14. doi: 10.1073/pnas.1219747110.

Spurway, T. D. *et al.* (1997) 'The flux control coefficient of carnitine palmitoyltransferase I on palmitate beta-oxidation in rat hepatocyte cultures.', *The Biochemical journal*, 323 (Pt 1), pp. 119–22. Available at: http://www.ncbi.nlm.nih.gov/pubmed/9173869 (Accessed: 20 March 2019).

Srivastava, N. K. *et al.* (2009) 'In vitro, high-resolution 1H and 31P NMR based analysis of the lipid components in the tissue, serum, and CSF of the patients with primary brain tumors: one possible diagnostic view.', *NMR in Biomedicine*, 23(2), p. n/a-n/a. doi: 10.1002/nbm.1427.

Stenvang, J. *et al.* (2008) 'The utility of LNA in microRNA-based cancer diagnostics and therapeutics.', *Seminars in cancer biology*, 18(2), pp. 89–102. doi: 10.1016/j.semcancer.2008.01.004.

Stenvang, J. *et al.* (2012) 'Inhibition of microRNA function by antimiR oligonucleotides.', *Silence*. BioMed Central, 3(1), p. 1. doi: 10.1186/1758-907X-3-1.

Stieber, D. *et al.* (2014) 'Glioblastomas are composed of genetically divergent clones with distinct tumourigenic potential and variable stem cell-associated phenotypes.', *Acta neuropathologica*, 127(2), pp. 203–19. doi: 10.1007/s00401-013-1196-4.

Stipanuk, M. H. and Ueki, I. (2011) 'Dealing with methionine/homocysteine sulfur: cysteine metabolism to taurine and inorganic sulfur.', *Journal of inherited metabolic disease*. NIH Public Access, 34(1), pp. 17–32. doi: 10.1007/s10545-009-9006-9.

Straub, B. K. *et al.* (2013) 'Adipophilin/perilipin-2 as a lipid droplet-specific marker for metabolically active cells and diseases associated with metabolic dysregulation.', *Histopathology*. England, 62(4), pp. 617–631. doi: 10.1111/his.12038.

Stummer, W. *et al.* (2006) 'Fluorescence-guided surgery with 5-aminolevulinic acid for resection of malignant glioma: a randomised controlled multicentre phase III trial.', *The Lancet. Oncology*, 7(5), pp. 392–401. doi: 10.1016/S1470-2045(06)70665-9.

Stupp, R. *et al.* (2009) 'Effects of radiotherapy with concomitant and adjuvant temozolomide versus radiotherapy alone on survival in glioblastoma in a randomised phase III study: 5-year analysis of the EORTC-NCIC trial', *The Lancet Oncology*, 10(5), pp. 459–466. doi: 10.1016/S1470-2045(09)70025-7.

Stupp, R. *et al.* (2010) 'Phase I/IIa study of cilengitide and temozolomide with concomitant radiotherapy followed by cilengitide and temozolomide maintenance therapy in patients with newly diagnosed glioblastoma.', *Journal of clinical oncology : official journal of the American Society of Clinical Oncology*. American Society of Clinical Oncology, 28(16), pp.

2712–8. doi: 10.1200/JCO.2009.26.6650.

Stupp, R. *et al.* (2014) 'Cilengitide combined with standard treatment for patients with newly diagnosed glioblastoma with methylated MGMT promoter (CENTRIC EORTC 26071-22072 study): a multicentre, randomised, open-label, phase 3 trial', *The Lancet Oncology*, 15(10), pp. 1100–1108. doi: 10.1016/S1470-2045(14)70379-1.

Suman, P. *et al.* (2012) 'AP-1 Transcription Factors, Mucin-Type Molecules and MMPs Regulate the IL-11 Mediated Invasiveness of JEG-3 and HTR-8/SVneo Trophoblastic Cells', *PLoS ONE*. Edited by S. Yenugu. Public Library of Science, 7(1), p. e29745. doi: 10.1371/journal.pone.0029745.

Svec, D. *et al.* (2015) 'How good is a PCR efficiency estimate: Recommendations for precise and robust qPCR efficiency assessments', *Biomolecular Detection and Quantification*, 3, pp. 9–16. doi: 10.1016/j.bdq.2015.01.005.

Swanton, C. (2014) 'Editor's choice: Cancer evolution: the final frontier of precision medicine?', *Annals of Oncology*. Available at: https://www.ncbi.nlm.nih.gov/pmc/articles/PMC4433531/ (Accessed: 27 July 2019).

Swietach, P., Vaughan-Jones, R. D. and Harris, A. L. (2007) 'Regulation of tumor pH and the role of carbonic anhydrase 9', *Cancer and Metastasis Reviews*, 26(2), pp. 299–310. doi: 10.1007/s10555-007-9064-0.

Sztalryd, C. and Kimmel, A. R. (2014) 'Perilipins: lipid droplet coat proteins

adapted for tissue-specific energy storage and utilization, and lipid cytoprotection', *Biochimie*. Elsevier, 96, pp. 96–101.

Taddei, M. L. *et al.* (2014) 'Mesenchymal to amoeboid transition is associated with stem-like features of melanoma cells.', *Cell communication and signaling : CCS*. BioMed Central, 12, p. 24. doi: 10.1186/1478-811X-12-24.

Tan, J. S. Y. *et al.* (2014) 'Recent Advances in Understanding Proteins Involved in Lipid Droplet Formation, Growth and Fusion', *Journal of Genetics and Genomics*, 41(5), pp. 251–259. doi: https://doi.org/10.1016/j.jgg.2014.03.003.

Tarling, E. J., de Aguiar Vallim, T. Q. and Edwards, P. A. (2013) 'Role of ABC transporters in lipid transport and human disease.', *Trends in endocrinology and metabolism: TEM*. NIH Public Access, 24(7), pp. 342–50. doi: 10.1016/j.tem.2013.01.006.

Teoh, S. T. and Lunt, S. Y. (2018) 'Metabolism in cancer metastasis: bioenergetics, biosynthesis, and beyond', *Wiley Interdisciplinary Reviews: Systems Biology and Medicine*. John Wiley & Sons, Ltd, 10(2), p. e1406. doi: 10.1002/wsbm.1406.

Teplyuk, N. M. *et al.* (2016) 'Therapeutic potential of targeting microRNA-10b in established intracranial glioblastoma: first steps toward the clinic.', *EMBO molecular medicine*, 8(3), pp. 268–87. doi: 10.15252/emmm.201505495.

Tester, A. M. *et al.* (2000) 'MMP-9 secretion and MMP-2 activation distinguish invasive and metastatic sublines of a mouse mammary carcinoma system showing epithelial-mesenchymal transition traits.', *Clinical & experimental metastasis*, 18(7), pp. 553–60. Available at: http://www.ncbi.nlm.nih.gov/pubmed/11688960 (Accessed: 20 July 2019).

The Cancer Genome Atlas Research Network (2008) 'Comprehensive genomic characterization defines human glioblastoma genes and core pathways.', *Nature*, 455(7216), pp. 1061–8. Available at: http://www.pubmedcentral.nih.gov/articlerender.fcgi?artid=2671642&tool=pmcentrez&rendertype=abstract (Accessed: 10 July 2014).

Thiery, J. P. (2002) 'Epithelial–mesenchymal transitions in tumour progression', *Nature Reviews Cancer*. Nature Publishing Group, 2(6), pp. 442–454. doi: 10.1038/nrc822.

Thomas, T. W. and DiMilla, P. A. (2000) 'Spreading and motility of human glioblastoma cells on sheets of silicone rubber depend on substratum compliance', *Medical & Biological Engineering & Computing*, 38(3), pp. 360–370. doi: 10.1007/BF02347059.

Thomson, D. W., Bracken, C. P. and Goodall, G. J. (2011) 'Experimental strategies for microRNA target identification.', *Nucleic acids research*. Oxford University Press, 39(16), pp. 6845–53. doi: 10.1093/nar/gkr330.

Thon, N., Kreth, S. and Kreth, F.-W. (2013) 'Personalized treatment strategies in glioblastoma: MGMT promoter methylation status.',

OncoTargets and therapy. Dove Press, 6, pp. 1363–72. doi: 10.2147/OTT.S50208.

Tirinato, L. *et al.* (2017) 'An Overview of Lipid Droplets in Cancer and Cancer Stem Cells.', *Stem cells international*. United States, 2017, p. 1656053. doi: 10.1155/2017/1656053.

Torsvik, A. *et al.* (2014) 'U-251 revisited: genetic drift and phenotypic consequences of long-term cultures of glioblastoma cells', *Cancer Medicine*, 3(4), pp. 812–824. doi: 10.1002/cam4.219.

Tran, B. and Rosenthal, M. A. (2010) 'Survival comparison between glioblastoma multiforme and other incurable cancers.', *Journal of clinical neuroscience : official journal of the Neurosurgical Society of Australasia*, 17(4), pp. 417–21. Available at: http://www.ncbi.nlm.nih.gov/pubmed/20167494 (Accessed: 28 February 2016).

Tugnoli, V. *et al.* (2001) 'Characterization of lipids from human brain tissues by multinuclear magnetic resonance spectroscopy', *Biopolymers*, 62(6), pp. 297–306. doi: 10.1002/bip.10005.

Turke, A. B. *et al.* (2010) 'Preexistence and Clonal Selection of MET Amplification in EGFR Mutant NSCLC', *Cancer Cell*, 17(1), pp. 77–88. doi: 10.1016/j.ccr.2009.11.022.

Turley, E. A. *et al.* (1993) 'Ras-Transformed Cells Express Both CD44 and RHAMM Hyaluronan Receptors: Only RHAMM Is Essential for Hyaluronan-

Promoted Locomotion', *Experimental Cell Research*, 207(2), pp. 277–282. doi: 10.1006/excr.1993.1194.

Tymoczko, J. L. and Stryer, L. (2002) 'Carbon Atoms of Degraded Amino Acids Emerge as Major Metabolic Intermediates', in Berg J M (ed.) *Biochemistry*. 5th edn. New York: W. H. Freeman, pp. 2223–2232. doi: 10.1007/s00726-011-0962-7.

Ueland, P. M. (2011) 'Choline and betaine in health and disease', *Journal of Inherited Metabolic Disease*, 34(1), pp. 3–15. doi: 10.1007/s10545-010-9088-4.

Uhm, J. H. *et al.* (1999) 'Vitronectin, a glioma-derived extracellular matrix protein, protects tumor cells from apoptotic death.', *Clinical cancer research : an official journal of the American Association for Cancer Research*, 5(6), pp. 1587–94. Available at: http://www.ncbi.nlm.nih.gov/pubmed/10389948 (Accessed: 19 May 2019).

Ulanet, D. B. *et al.* (2014) 'Mesenchymal Phenotype Predisposes Lung Cancer Cells to Impaired Proliferation and Redox Stress in Response to Glutaminase Inhibition', *PLoS ONE*. Edited by P. G. Petronini, 9(12), p. e115144. doi: 10.1371/journal.pone.0115144.

Ulrich, T. A., de Juan Pardo, E. M. and Kumar, S. (2009) 'The Mechanical Rigidity of the Extracellular Matrix Regulates the Structure, Motility, and Proliferation of Glioma Cells', *Cancer Research*, 69(10), pp. 4167–4174. doi: 10.1158/0008-5472.CAN-08-4859.

Utsuki, S. *et al.* (2002) *Relationship between the expression of E-, N-cadherins and beta-catenin and tumor grade in astrocytomas*, *Journal of Neuro-Oncology*. Available at: https://link.springer.com/content/pdf/10.1023%2FA%3A1015720220602.pdf (Accessed: 12 May 2019).

Utsuki, S. *et al.* (2007) 'Histological examination of false positive tissue resection using 5-aminolevulinic acid-induced fluorescence guidance.', *Neurologia medico-chirurgica*. Japan, 47(5), pp. 210–214. doi: 10.2176/nmc.47.210.

Valster, A. *et al.* (2005) 'Cell migration and invasion assays', *Methods*, 37(2), pp. 208–215. doi: 10.1016/j.ymeth.2005.08.001.

Vedhachalam, C. *et al.* (2007) 'Mechanism of ATP-binding Cassette Transporter A1-mediated Cellular Lipid Efflux to Apolipoprotein A-I and Formation of High Density Lipoprotein Particles', *Journal of Biological Chemistry*, 282(34), pp. 25123–25130. doi: 10.1074/jbc.M704590200.

Vejnar, C. E. and Zdobnov, E. M. (2012) 'MiRmap: comprehensive prediction of microRNA target repression strength.', *Nucleic acids research*. Oxford University Press, 40(22), pp. 11673–83. doi: 10.1093/nar/gks901.

Vella, S. *et al.* (2016) 'Perhexiline maleate enhances antitumor efficacy of cisplatin in neuroblastoma by inducing over-expression of NDM29 ncRNA', *Scientific Reports*. Nature Publishing Group, 5(1), p. 18144. doi: 10.1038/srep18144.

Velpula, K. K. *et al.* (2013) 'Combined Targeting of PDK1 and EGFR Triggers Regression of Glioblastoma by Reversing the Warburg Effect', *Cancer Research*, 73(24), pp. 7277–7289. doi: 10.1158/0008-5472.CAN-13-1868.

Verbeek, B. *et al.* (2008) 'O6-Methylguanine-DNA methyltransferase inactivation and chemotherapy.', *British medical bulletin*, 85(1), pp. 17–33. doi: 10.1093/bmb/ldm036.

Verhaak, R. G. W. *et al.* (2010) 'Integrated genomic analysis identifies clinically relevant subtypes of glioblastoma characterized by abnormalities in PDGFRA, IDH1, EGFR, and NF1.', *Cancer cell*, 17(1), pp. 98–110. doi: 10.1016/j.ccr.2009.12.020.

Verschueren, H., De Baetselier, P. and Bereiter-Hahn, J. (1991) 'Dynamic morphology of metastatic mouse T-lymphoma cells invading through monolayers of 10T½ cells', *Cell Motility and the Cytoskeleton*, 20(3), pp. 203–214. doi: 10.1002/cm.970200304.

Victor, B. C. *et al.* (2011) 'Inhibition of cathepsin B activity attenuates extracellular matrix degradation and inflammatory breast cancer invasion.', *Breast cancer research : BCR*, 13(6), p. R115. doi: 10.1186/bcr3058.

Villa, G. R. *et al.* (2016) 'An LXR-Cholesterol Axis Creates a Metabolic Co-Dependency for Brain Cancers', *Cancer Cell*, 30(5), pp. 683–693. doi: 10.1016/j.ccell.2016.09.008.

Visani, M. *et al.* (2013) 'Definition of miRNAs expression profile in glioblastoma samples: the relevance of non-neoplastic brain reference.',

PloS one. United States, 8(1), p. e55314. doi: 10.1371/journal.pone.0055314.

Völker, H.-U. *et al.* (2008) 'Expression of Transketolase-like 1 and Activation of Akt in Grade IV Glioblastomas Compared With Grades II and III Astrocytic Gliomas', *American Journal of Clinical Pathology*, 130(1), pp. 50–57. doi: 10.1309/6H9844AMMET82DBJ.

Vrablic, A. S. *et al.* (2001) 'Altered mitochondrial function and overgeneration of reactive oxygen species precede the induction of apoptosis by 1-O-octadecyl-2-methyl-rac-glycero-3-phosphocholine in p53-defective hepatocytes.', *FASEB journal : official publication of the Federation of American Societies for Experimental Biology*, 15(10), pp. 1739–44. Available at: http://www.ncbi.nlm.nih.gov/pubmed/11481221 (Accessed: 16 January 2019).

de Vries, N. A. *et al.* (2010) 'Rapid and Robust Transgenic High-Grade Glioma Mouse Models for Therapy Intervention Studies', *Clinical Cancer Research*, 16(13), pp. 3431–3441. doi: 10.1158/1078-0432.CCR-09-3414.

Wachsberger, P. R. *et al.* (2007) 'VEGF Trap in Combination With Radiotherapy Improves Tumor Control in U87 Glioblastoma', *International Journal of Radiation Oncology*Biology*Physics*, 67(5), pp. 1526–1537. doi: 10.1016/j.ijrobp.2006.11.011.

Wallimann, T. *et al.* (1992) 'Intracellular compartmentation, structure and function of creatine kinase isoenzymes in tissues with high and fluctuating

energy demands: the "phosphocreatine circuit" for cellular energy homeostasis.', *The Biochemical journal*, 281 (Pt 1), pp. 21–40. Available at: http://www.ncbi.nlm.nih.gov/pubmed/1731757 (Accessed: 27 January 2019).

Wang, B. M. (1989) 'Flow cytometric analysis of the effect of activated macrophages on alveolar cell carcinoma of lung in vitro.', *Zhonghua bing li xue za zhi = Chinese journal of pathology*, 18(3), pp. 207–10. Available at: http://www.ncbi.nlm.nih.gov/pubmed/2561474 (Accessed: 24 July 2019).

Wang, D. *et al.* (2000) 'p125 focal adhesion kinase promotes malignant astrocytoma cell proliferation in vivo.', *Journal of cell science*, 113 Pt 23, pp. 4221–30. Available at: http://www.ncbi.nlm.nih.gov/pubmed/11069767 (Accessed: 20 July 2019).

Wang, G. *et al.* (2013) 'Differential phosphofructokinase-1 isoenzyme patterns associated with glycolytic efficiency in human breast cancer and paracancer tissues.', *Oncology letters*. Spandidos Publications, 6(6), pp. 1701–1706. doi: 10.3892/ol.2013.1599.

Wang, H. *et al.* (2015) 'The challenges and the promise of molecular targeted therapy in malignant gliomas.', *Neoplasia (New York, N.Y.)*, 17(3), pp. 239–55. doi: 10.1016/j.neo.2015.02.002.

Wang, K. *et al.* (2015) 'MiR-27a regulates Wnt/beta-catenin signaling through targeting SFRP1 in glioma.', *Neuroreport*, 26(12), pp. 695–702. doi: 10.1097/WNR.0000000000000410.

Wang, L. *et al.* (2013) 'Astrocytes Directly Influence Tumor Cell Invasion and Metastasis In Vivo', *PLoS ONE*. Edited by G. Qin. Public Library of Science, 8(12), p. e80933. doi: 10.1371/journal.pone.0080933.

Wang, L. *et al.* (2014) 'MiR-143 acts as a tumor suppressor by targeting N-RAS and enhances temozolomide-induced apoptosis in glioma.', *Oncotarget*, 5(14), pp. 5416–27. Available at: http://www.pubmedcentral.nih.gov/articlerender.fcgi?artid=4170647&tool=pmcentrez&rendertype=abstract (Accessed: 4 June 2016).

Wang, M. *et al.* (2003) 'The expression of matrix metalloproteinase-2 and -9 in human gliomas of different pathological grades.', *Brain tumor pathology*, 20(2), pp. 65–72. Available at: http://www.ncbi.nlm.nih.gov/pubmed/14756443 (Accessed: 12 May 2019).

Wang, W. *et al.* (2013) 'Regulation of epidermal growth factor receptor signaling by plasmid-based microRNA-7 inhibits human malignant gliomas growth and metastasis in vivo.', *Neoplasma*. Slovakia, 60(3), pp. 274–283. doi: 10.4149/neo_2013_036.

Wang, W. *et al.* (2016) 'Alteration of the Metabolome Profile in Endothelial Cells by Overexpression of miR-143/145', *Journal of Microbiology and Biotechnology*, 26(3), pp. 572–578. doi: 10.4014/jmb.1507.07103.

Wang, X.-R. *et al.* (2013) 'Overexpressed let-7a inhibits glioma cell malignancy by directly targeting K-ras, independently of PTEN.', *Neuro-oncology*, 15(11), pp. 1491–501. doi: 10.1093/neuonc/not107.

Wang, Z. *et al.* (2015) 'Oncogenic miR-20a and miR-106a enhance the invasiveness of human glioma stem cells by directly targeting TIMP-2.', *Oncogene*. England, 34(11), pp. 1407–1419. doi: 10.1038/onc.2014.75.

Warburg, O. (1956) 'On the Origin of Cancer Cells', *Science*, 123(3191), pp. 309–314. doi: 10.1126/science.123.3191.309.

Ward, N. P. *et al.* (2017) 'Complex I inhibition augments dichloroacetate cytotoxicity through enhancing oxidative stress in VM-M3 glioblastoma cells.', *PloS one*. Public Library of Science, 12(6), p. e0180061. doi: 10.1371/journal.pone.0180061.

Wasserfallen, J.-B. *et al.* (2005) 'Cost of temozolomide therapy and global care for recurrent malignant gliomas followed until death.', *Neuro-oncology*, 7(2), pp. 189–95. doi: 10.1215/S1152851704000687.

Watanabe, Y., Tomita, M. and Kanai, A. (2007) 'Computational Methods for MicroRNA Target Prediction', in *Methods in enzymology*, pp. 65–86. doi: 10.1016/S0076-6879(07)27004-1.

Watkins, S. *et al.* (2014) 'Disruption of astrocyte–vascular coupling and the blood–brain barrier by invading glioma cells', *Nature Communications*, 5(1), p. 4196. doi: 10.1038/ncomms5196.

Wear, M. A., Schafer, D. A. and Cooper, J. A. (2000) 'Actin dynamics: Assembly and disassembly of actin networks', *Current Biology*, 10(24), pp. R891–R895. doi: 10.1016/S0960-9822(00)00845-9.

Webster, R. J. *et al.* (2009) 'Regulation of epidermal growth factor receptor

signaling in human cancer cells by microRNA-7.', *The Journal of biological chemistry*, 284(9), pp. 5731–41. Available at: http://www.ncbi.nlm.nih.gov/pubmed/19073608 (Accessed: 3 April 2016).

Welch, M. R. and Grommes, C. (2013) 'Retrospective analysis of the effects of steroid therapy and antidiabetic medication on survival in diabetic glioblastoma patients', *CNS Oncology*, 2(3), pp. 237–246. doi: 10.2217/cns.13.12.

Weller, M. *et al.* (2003) 'Neuro-Oncology Working Group 01 trial of nimustine plus teniposide versus nimustine plus cytarabine chemotherapy in addition to involved-field radiotherapy in the first-line treatment of malignant glioma.', *Journal of clinical oncology : official journal of the American Society of Clinical Oncology*, 21(17), pp. 3276–84. Available at: http://www.ncbi.nlm.nih.gov/pubmed/12947063 (Accessed: 28 May 2016).

Westermark, B., Pontén, J. and Hugosson, R. (1973) 'Determinants for the establishment of permanent tissue culture lines from human gliomas.', *Acta pathologica et microbiologica Scandinavica. Section A, Pathology*, 81(6), pp. 791–805. Available at: http://www.ncbi.nlm.nih.gov/pubmed/4359449 (Accessed: 22 July 2019).

White, C. C. *et al.* (2003) 'Fluorescence-based microtiter plate assay for glutamate–cysteine ligase activity', *Analytical Biochemistry*. Academic Press, 318(2), pp. 175–180. doi: 10.1016/S0003-2697(03)00143-X.

Wick, W. *et al.* (2014) 'MGMT testing--the challenges for biomarker-based

glioma treatment.', *Nature reviews. Neurology*. Nature Publishing Group, a division of Macmillan Publishers Limited. All Rights Reserved., 10(7), pp. 372–85. doi: 10.1038/nrneurol.2014.100.

Wiegand, G. and Remington, S. J. (1986) 'Citrate Synthase: Structure, Control, and Mechanism', *Annual Review of Biophysics and Biophysical Chemistry*, 15(1), pp. 97–117. doi: 10.1146/annurev.bb.15.060186.000525.

Wöhrer, A. *et al.* (2009) 'The Austrian Brain Tumour Registry: a cooperative way to establish a population-based brain tumour registry.', *Journal of neuro-oncology*, 95(3), pp. 401–11. Available at: http://www.ncbi.nlm.nih.gov/pubmed/19562257 (Accessed: 7 February 2016).

Wolf, A., Agnihotri, S., Munoz, D., *et al.* (2011) 'Developmental profile and regulation of the glycolytic enzyme hexokinase 2 in normal brain and glioblastoma multiforme', *Neurobiology of Disease*, 44(1), pp. 84–91. doi: 10.1016/j.nbd.2011.06.007.

Wolf, A., Agnihotri, S., Micallef, J., *et al.* (2011) 'Hexokinase 2 is a key mediator of aerobic glycolysis and promotes tumor growth in human glioblastoma multiforme.', *The Journal of experimental medicine*, 208(2), pp. 313–26. Available at: http://www.pubmedcentral.nih.gov/articlerender.fcgi?artid=3039857&tool=pmcentrez&rendertype=abstract (Accessed: 10 May 2016).

Wolf, K. *et al.* (2003) 'Compensation mechanism in tumor cell migration', *The Journal of Cell Biology*, 160(2), pp. 267–277. doi: 10.1083/jcb.200209006.

Wolins, N. E., Brasaemle, D. L. and Bickel, P. E. (2006) 'A proposed model of fat packaging by exchangeable lipid droplet proteins', *FEBS letters*. Wiley Online Library, 580(23), pp. 5484–5491.

Wolins, N. E., Rubin, B. and Brasaemle, D. L. (2001) 'TIP47 associates with lipid droplets', *Journal of Biological Chemistry*. ASBMB, 276(7), pp. 5101–5108.

Wong, K. *et al.* (2011) 'Characterization of a human tumorsphere glioma orthotopic model using magnetic resonance imaging.', *Journal of neuro-oncology*. Springer, 104(2), pp. 473–81. doi: 10.1007/s11060-010-0517-x.

Wong, N. and Wang, X. (2015) 'miRDB: an online resource for microRNA target prediction and functional annotations.', *Nucleic acids research*. Oxford University Press, 43(Database issue), pp. D146-52. doi: 10.1093/nar/gku1104.

Wong, S. T. S. *et al.* (2012) 'MicroRNA-21 inhibition enhances in vitro chemosensitivity of temozolomide-resistant glioblastoma cells.', *Anticancer research*. Greece, 32(7), pp. 2835–2841.

Wright, H. J. *et al.* (2017) 'CDCP1 drives triple-negative breast cancer metastasis through reduction of lipid-droplet abundance and stimulation of

fatty acid oxidation', *Proceedings of the National Academy of Sciences*. National Academy of Sciences, p. 201703791. doi: 10.1073/PNAS.1703791114.

Wu, C. *et al.* (2009) 'Combinatorial control of suicide gene expression by tissue-specific promoter and microRNA regulation for cancer therapy.', *Molecular therapy : the journal of the American Society of Gene Therapy*. The American Society of Gene & Cell Therapy, 17(12), pp. 2058–66. Available at: http://dx.doi.org/10.1038/mt.2009.225 (Accessed: 28 May 2016).

Wu, D. *et al.* (2011) 'MicroRNA-7 regulates glioblastoma cell invasion via targeting focal adhesion kinase expression.', *Chinese medical journal*, 124(17), pp. 2616–21. Available at: http://www.ncbi.nlm.nih.gov/pubmed/22040413 (Accessed: 3 April 2016).

Wu, N. *et al.* (2013) 'MiR-125b acts as an oncogene in glioblastoma cells and inhibits cell apoptosis through p53 and p38MAPK-independent pathways', *British Journal of Cancer*, 109(11), pp. 2853–2863. doi: 10.1038/bjc.2013.672.

Wu, Z. *et al.* (2013) 'Increased expression of microRNA-9 predicts an unfavorable prognosis in human glioma.', *Molecular and cellular biochemistry*, 384(1–2), pp. 263–8. Available at: http://www.ncbi.nlm.nih.gov/pubmed/24122417 (Accessed: 24 March 2016).

Xia, H. *et al.* (2009) 'microRNA-146b inhibits glioma cell migration and invasion by targeting MMPs', *Brain Research*, 1269, pp. 158–165. doi: 10.1016/j.brainres.2009.02.037.

Xia, S. *et al.* (2016) 'Tumor microenvironment tenascin-C promotes glioblastoma invasion and negatively regulates tumor proliferation', *Neuro-Oncology*, 18(4), pp. 507–517. doi: 10.1093/neuonc/nov171.

Xia, X. *et al.* (2015) 'MicroRNA-1908 functions as a glioblastoma oncogene by suppressing PTEN tumor suppressor pathway.', *Molecular cancer*. BioMed Central, 14(1), p. 154. doi: 10.1186/s12943-015-0423-0.

Xie, Q. *et al.* (2014) 'MicroRNA-221 targeting PI3-K/Akt signaling axis induces cell proliferation and BCNU resistance in human glioblastoma.', *Neuropathology : official journal of the Japanese Society of Neuropathology*. Australia, 34(5), pp. 455–464. doi: 10.1111/neup.12129.

Xie, T. *et al.* (2004) 'Stat3 activation regulates the expression of matrix metalloproteinase-2 and tumor invasion and metastasis', *Oncogene*. Nature Publishing Group, 23(20), pp. 3550–3560. doi: 10.1038/sj.onc.1207383.

Xu, T. *et al.* (2019) 'MicroRNA-940 inhibits glioma progression by blocking mitochondrial folate metabolism through targeting of MTHFD2.', *American journal of cancer research*. e-Century Publishing Corporation, 9(2), pp. 250–269. Available at: http://www.ncbi.nlm.nih.gov/pubmed/30906627 (Accessed: 23 July 2019).

Xu, W. *et al.* (2011) 'Oncometabolite 2-hydroxyglutarate is a competitive

inhibitor of α-ketoglutarate-dependent dioxygenases.', *Cancer cell*, 19(1), pp. 17–30. doi: 10.1016/j.ccr.2010.12.014.

Xue, H. *et al.* (2016) 'MicroRNA-584-3p, a novel tumor suppressor and prognostic marker, reduces the migration and invasion of human glioma cells by targeting hypoxia-induced ROCK1', *Oncotarget*. Impact Journals, 7(4), pp. 4785–4805. doi: 10.18632/oncotarget.6735.

Yamada, K. M. and Cukierman, E. (2007) 'Modeling Tissue Morphogenesis and Cancer in 3D', *Cell*, 130(4), pp. 601–610. doi: 10.1016/j.cell.2007.08.006.

Yamamoto, M., Sawaya, R., Mohanam, S., Bindal, A. K., *et al.* (1994) 'Expression and localization of urokinase-type plasminogen activator in human astrocytomas in vivo.', *Cancer research*, 54(14), pp. 3656–61. Available at: http://www.ncbi.nlm.nih.gov/pubmed/8033079 (Accessed: 12 May 2019).

Yamamoto, M., Sawaya, R., Mohanam, S., Rao, V. H., *et al.* (1994) 'Expression and localization of urokinase-type plasminogen activator receptor in human gliomas.', *Cancer research*, 54(18), pp. 5016–20. Available at: http://www.ncbi.nlm.nih.gov/pubmed/8069869 (Accessed: 12 May 2019).

Yamashita, Y. *et al.* (2017) 'Differences in elongation of very long chain fatty acids and fatty acid metabolism between triple-negative and hormone receptor-positive breast cancer.', *BMC cancer*. BioMed Central, 17(1), p.

589. doi: 10.1186/s12885-017-3554-4.

Yamazaki, N. *et al.* (1996) 'Isolation and characterization of cDNA and genomic clones encoding human muscle type carnitine palmitoyltransferase I', *Biochimica et Biophysica Acta (BBA) - Gene Structure and Expression*. Elsevier, 1307(2), pp. 157–161. doi: 10.1016/0167-4781(96)00069-3.

Yan, C. *et al.* (2014) 'The mTOR Inhibitor Rapamycin Synergizes with a Fatty Acid Synthase Inhibitor to Induce Cytotoxicity in ER/HER2-Positive Breast Cancer Cells', *PLoS ONE*. Edited by D. Calvisi, 9(5), p. e97697. doi: 10.1371/journal.pone.0097697.

Yan, W. *et al.* (2011) 'Identification of MMP-9 specific microRNA expression profile as potential targets of anti-invasion therapy in glioblastoma multiforme.', *Brain research*. Netherlands, 1411, pp. 108–115. doi: 10.1016/j.brainres.2011.07.002.

Yanae, M. *et al.* (2011) 'Statin-induced apoptosis via the suppression of ERK1/2 and Akt activation by inhibition of the geranylgeranyl-pyrophosphate biosynthesis in glioblastoma', *Journal of Experimental & Clinical Cancer Research*, 30(1), p. 74. doi: 10.1186/1756-9966-30-74.

Yang, C.-S. *et al.* (2015) 'Fatty acid synthase inhibition engages a novel caspase-2 regulatory mechanism to induce ovarian cancer cell death', *Oncogene*, 34(25), pp. 3264–3272. doi: 10.1038/onc.2014.271.

Yang, F. *et al.* (2015) 'MiR-221/222 promote human glioma cell invasion and angiogenesis by targeting TIMP2.', *Tumour biology : the journal of the*

International Society for Oncodevelopmental Biology and Medicine. Netherlands, 36(5), pp. 3763–3773. doi: 10.1007/s13277-014-3017-3.

Yang, G. *et al.* (2011) 'MiR-106a inhibits glioma cell growth by targeting E2F1 independent of p53 status.', *Journal of molecular medicine (Berlin, Germany)*. Germany, 89(10), pp. 1037–1050. doi: 10.1007/s00109-011-0775-x.

Yang, H. W. *et al.* (2012) 'Cooperative activation of PI3K by Ras and Rho family small GTPases.', *Molecular cell*, 47(2), pp. 281–90. Available at: http://www.sciencedirect.com/science/article/pii/S1097276512003905 (Accessed: 9 March 2016).

Yang, J. *et al.* (2016) 'PFKL/miR-128 axis regulates glycolysis by inhibiting AKT phosphorylation and predicts poor survival in lung cancer.', *American journal of cancer research*, 6(2), pp. 473–85. Available at: http://www.pubmedcentral.nih.gov/articlerender.fcgi?artid=4859674&tool=pmcentrez&rendertype=abstract (Accessed: 21 May 2016).

Yang, K. and Han, X. (2016) 'Lipidomics: Techniques, Applications, and Outcomes Related to Biomedical Sciences', *Trends in Biochemical Sciences*, 41(11), pp. 954–969. doi: 10.1016/j.tibs.2016.08.010.

Yang, L., Venneti, S. and Nagrath, D. (2017) 'Glutaminolysis: A Hallmark of Cancer Metabolism', *Annual Review of Biomedical Engineering*, 19(1), pp. 163–194. doi: 10.1146/annurev-bioeng-071516-044546.

Yang, M.-H. *et al.* (2015) 'MALAT1 promotes colorectal cancer cell

proliferation/migration/invasion via PRKA kinase anchor protein 9', *Biochimica et Biophysica Acta (BBA) - Molecular Basis of Disease*. Elsevier, 1852(1), pp. 166–174. doi: 10.1016/J.BBADIS.2014.11.013.

Yang, N. (2015) 'An overview of viral and nonviral delivery systems for microRNA.', *International journal of pharmaceutical investigation*. Medknow Publications, 5(4), pp. 179–81. doi: 10.4103/2230-973X.167646.

Yang, X. M. and MacKenzie, R. E. (1993) 'NAD-dependent methylenetetrahydrofolate dehydrogenase-methenyltetrahydrofolate cyclohydrolase is the mammalian homolog of the mitochondrial enzyme encoded by the yeast MIS1 gene', *Biochemistry*, 32(41), pp. 11118–11123. doi: 10.1021/bi00092a022.

Yang, Y. *et al.* (2011) 'Influence of chondroitin sulfate and hyaluronic acid on structure, mechanical properties, and glioma invasion of collagen I gels', *Biomaterials*, 32(31), pp. 7932–7940. doi: 10.1016/j.biomaterials.2011.07.018.

Yao, C.-H. *et al.* (2018) 'Identifying off-target effects of etomoxir reveals that carnitine palmitoyltransferase I is essential for cancer cell proliferation independent of β-oxidation', *PLOS Biology*. Edited by J. Locasale. Public Library of Science, 16(3), p. e2003782. doi: 10.1371/journal.pbio.2003782.

Yao, Y. *et al.* (2015) 'MiR-449a exerts tumor-suppressive functions in human glioblastoma by targeting Myc-associated zinc-finger protein.', *Molecular oncology*. Wiley-Blackwell, 9(3), pp. 640–56. doi:

10.1016/j.molonc.2014.11.003.

Yerli, H. *et al.* (2007) 'Evaluation of cerebral glioma grade by using normal side creatine as an internal reference in multi-voxel 1H-MR spectroscopy.', *Diagnostic and interventional radiology (Ankara, Turkey)*, 13(1), pp. 3–9. Available at: http://www.ncbi.nlm.nih.gov/pubmed/17354186 (Accessed: 16 January 2019).

Yi, R. *et al.* (2003) 'Exportin-5 mediates the nuclear export of pre-microRNAs and short hairpin RNAs.', *Genes & development*. Cold Spring Harbor Laboratory Press, 17(24), pp. 3011–6. doi: 10.1101/gad.1158803.

Yin, D. *et al.* (2013) 'miR-34a functions as a tumor suppressor modulating EGFR in glioblastoma multiforme.', *Oncogene*, 32(9), pp. 1155–63. doi: 10.1038/onc.2012.132.

Yoo, B. H. *et al.* (2004) '2'-O-methyl-modified phosphorothioate antisense oligonucleotides have reduced non-specific effects in vitro.', *Nucleic acids research*, 32(6), pp. 2008–16. doi: 10.1093/nar/gkh516.

Yoshida, D. *et al.* (2002) 'Tracking cell invasion of human glioma cells and suppression by anti-matrix metalloproteinase agent in rodent brain-slice model', *Brain Tumor Pathology*, 19(2), pp. 69–76. doi: 10.1007/BF02478930.

Yoshida, T. *et al.* (2012) 'CD44 in human glioma correlates with histopathological grade and cell migration', *Pathology International*, 62(7), pp. 463–470. doi: 10.1111/j.1440-1827.2012.02823.x.

Yu, L. *et al.* (2017) 'The Glycolytic Switch in Tumors: How Many Players Are Involved?', *Journal of Cancer*. Ivyspring International Publisher, 8(17), pp. 3430–3440. doi: 10.7150/jca.21125.

Yu, Z. *et al.* (2015) 'Metformin and temozolomide act synergistically to inhibit growth of glioma cells and glioma stem cells <i>in vitro</i> and <i>in vivo</i&gt';, *Oncotarget*, 6(32), pp. 32930–43. doi: 10.18632/oncotarget.5405.

Yuan, M. *et al.* (2012) 'A positive/negative ion–switching, targeted mass spectrometry–based metabolomics platform for bodily fluids, cells, and fresh and fixed tissue', *Nature Protocols*, 7(5), pp. 872–881. doi: 10.1038/nprot.2012.024.

Yumura, S., Mori, H. and Fukui, Y. (1984) 'Localization of actin and myosin for the study of ameboid movement in Dictyostelium using improved immunofluorescence', *The Journal of Cell Biology*, 99(3), pp. 894–899. doi: 10.1083/jcb.99.3.894.

Zagzag, D. *et al.* (2008) 'Hypoxia- and Vascular Endothelial Growth Factor-Induced Stromal Cell-Derived Factor-1α/CXCR4 Expression in Glioblastomas', *The American Journal of Pathology*, 173(2), pp. 545–560. doi: 10.2353/ajpath.2008.071197.

Zamecnik, J. (2005) 'The extracellular space and matrix of gliomas', *Acta Neuropathologica*, 110(5), pp. 435–442. doi: 10.1007/s00401-005-1078-5.

Zeisel, S. H. *et al.* (1989) 'Effect of choline deficiency on S-adenosylmethionine and methionine concentrations in rat liver.', *The Biochemical journal*. Portland Press Ltd, 259(3), pp. 725–9. Available at: http://www.ncbi.nlm.nih.gov/pubmed/2730584 (Accessed: 27 January 2019).

Zeng, L. *et al.* (2003) 'PTPα regulates integrin-stimulated FAK autophosphorylation and cytoskeletal rearrangement in cell spreading and migration', *The Journal of Cell Biology*, 160(1), pp. 137–146. doi: 10.1083/jcb.200206049.

Zhai, H. *et al.* (2011) 'Annexin A2 promotes glioma cell invasion and tumor progression.', *The Journal of neuroscience : the official journal of the Society for Neuroscience*. NIH Public Access, 31(40), pp. 14346–60. doi: 10.1523/JNEUROSCI.3299-11.2011.

Zhang, F. *et al.* (2011) 'In Vivo MRI Tracking of Cell Invasion and Migration in a Rat Glioma Model', *Molecular Imaging and Biology*, 13(4), pp. 695–701. doi: 10.1007/s11307-010-0401-2.

Zhang, F. *et al.* (2015) 'Elevated STAT3 Signaling-Mediated Upregulation of MMP-2/9 Confers Enhanced Invasion Ability in Multidrug-Resistant Breast Cancer Cells.', *International journal of molecular sciences*. Multidisciplinary Digital Publishing Institute (MDPI), 16(10), pp. 24772–90. doi: 10.3390/ijms161024772.

Zhang, M. *et al.* (2008) 'Nestin and CD133: valuable stem cell-specific

markers for determining clinical outcome of glioma patients', *Journal of Experimental & Clinical Cancer Research*. BioMed Central, 27(1), p. 85. doi: 10.1186/1756-9966-27-85.

Zhang, Y. *et al.* (2014) 'Multiple receptor tyrosine kinases converge on microRNA-134 to control KRAS, STAT5B, and glioblastoma.', *Cell death and differentiation*, 21(5), pp. 720–34. doi: 10.1038/cdd.2013.196.

Zhang, Y., Wang, Z. and Gemeinhart, R. A. (2013) 'Progress in microRNA delivery.', *Journal of controlled release : official journal of the Controlled Release Society*, 172(3), pp. 962–74. doi: 10.1016/j.jconrel.2013.09.015.

Zhang, Z. *et al.* (2017) 'Novel copper complexes as potential proteasome inhibitors for cancer treatment', *Molecular Medicine Reports*, 15(1), pp. 3–11. doi: 10.3892/mmr.2016.6022.

Zhao, S., Yang, G., *et al.* (2013) 'MiR-106a is an independent prognostic marker in patients with glioblastoma.', *Neuro-oncology*, 15(6), pp. 707–17. doi: 10.1093/neuonc/not001.

Zhao, S., Liu, H., *et al.* (2013a) 'miR-143 inhibits glycolysis and depletes stemness of glioblastoma stem-like cells.', *Cancer letters*, 333(2), pp. 253–60. Available at: http://www.sciencedirect.com/science/article/pii/S0304383513000852 (Accessed: 16 May 2016).

Zhao, S., Liu, H., *et al.* (2013b) 'miR-143 inhibits glycolysis and depletes stemness of glioblastoma stem-like cells.', *Cancer letters*, 333(2), pp. 253–

60. doi: 10.1016/j.canlet.2013.01.039.

Zheng, J. (2012) 'Energy metabolism of cancer: Glycolysis versus oxidative phosphorylation (Review).', *Oncology letters*, 4(6), pp. 1151–1157. doi: 10.3892/ol.2012.928.

Zhou, X. *et al.* (2010a) 'Downregulation of miR-21 inhibits EGFR pathway and suppresses the growth of human glioblastoma cells independent of PTEN status.', *Laboratory investigation; a journal of technical methods and pathology*, 90(2), pp. 144–55. Available at: http://www.ncbi.nlm.nih.gov/pubmed/20048743 (Accessed: 17 February 2016).

Zhou, X. *et al.* (2010b) 'Downregulation of miR-21 inhibits EGFR pathway and suppresses the growth of human glioblastoma cells independent of PTEN status.', *Laboratory investigation; a journal of technical methods and pathology*. United States and Canadian Academy of Pathology, Inc., 90(2), pp. 144–55. Available at: http://dx.doi.org/10.1038/labinvest.2009.126 (Accessed: 17 February 2016).

Zhou, Y. xin *et al.* (2015) 'miR-132 can inhibit glioma cells invasion and migration by target MMP16 in vitro', *OncoTargets and Therapy*. Dove Press, 8, p. 3211. doi: 10.2147/OTT.S79282.

Zimmermann, D. R. and Dours-Zimmermann, M. T. (2008) 'Extracellular matrix of the central nervous system: from neglect to challenge', *Histochemistry and Cell Biology*, 130(4), pp. 635–653. doi:

10.1007/s00418-008-0485-9.

Zitvogel, L. *et al.* (2016) 'Mouse models in oncoimmunology', *Nature Reviews Cancer*, 16(12), pp. 759–773. doi: 10.1038/nrc.2016.91.

Zong, H., Verhaak, R. G. W. and Canoll, P. (2012) 'The cellular origin for malignant glioma and prospects for clinical advancements.', *Expert review of molecular diagnostics*, 12(4), pp. 383–94. Available at: http://www.pubmedcentral.nih.gov/articlerender.fcgi?artid=3368274&tool=pmcentrez&rendertype=abstract (Accessed: 5 March 2016).

Zook, B. C., Simmens, S. J. and Jones, R. V. (2000) 'Evaluation of ENU-Induced Gliomas in Rats: Nomenclature, Immunochemistry, and Malignancy', *Toxicologic Pathology*, 28(1), pp. 193–201. doi: 10.1177/019262330002800124.